

Copyright

by

Aaron Webb

2021

The Dissertation Committee for Aaron Webb

certifies that this is the approved version of the following dissertation:

**A Deep Learning Approach to Differential Measurements of
Higgs - Top Interactions in Multilepton Final States using
the ATLAS Detector at the LHC**

Committee:

Peter Onyisi, Supervisor

Timothy Andeen

Can Kilic

James Scott

**A Deep Learning Approach to Differential Measurements of
Higgs - Top Interactions in Multilepton Final States using
the ATLAS Detector at the LHC**

by

Aaron Webb, B.S.

DISSERTATION

Presented to the Faculty of the Graduate School of
The University of Texas at Austin
in Partial Fulfillment
of the Requirements
for the Degree of

DOCTOR OF PHILOSOPHY

THE UNIVERSITY OF TEXAS AT AUSTIN

August 2021

Dedicated to something

Acknowledgments

I wish to thank

A Deep Learning Approach to Differential Measurements of Higgs - Top Interactions in Multilepton Final States using the ATLAS Detector at the LHC

Publication No. _____

Aaron Webb, Ph.D.
The University of Texas at Austin, 2021

Supervisor: Peter Onyisi

Several theories Beyond the Standard Model predict a modification of the momentum spectrum of the Higgs Boson, without a significantly altered rate of Higgs produced in association with top quark pairs ($t\bar{t}H$). This provides a physical observable that can be used to search for new physics based on data collected by the LHC. This thesis presents techniques and preliminary results for a differential measurement of the Higgs transverse momentum in $t\bar{t}H$ events with multiple leptons in the final state, using data collected at an energy of $\sqrt{s} = 13$ TeV by the ATLAS detector at the LHC.

Because of the challenges inherent in reconstructing the Higgs in multilepton final states, a deep learning approach is used to predict of the Higgs. The regressed Higgs p_T spectrum is fit to data for events with two same-sign leptons and three leptons in the final state, in order to extract normalization factors for high ($p_T(H) > 150$ GeV) and low ($p_T(H) < 150$ GeV) momentum $t\bar{t}H$ events. Preliminary results are presented for 80 fb^{-1} of data, with projected results shown for 140 fb^{-1} .

This thesis also details a measurement of $WZ +$ heavy flavor production, a significant background to $t\bar{t}H$ that is poorly understood. This study targets events with three leptons and one or two jets in the final state, using 140 fb^{-1} of $\sqrt{s} = 13$ TeV data. A measured cross-section of $X \pm X \text{ fb}$ ($X \pm X \text{ fb}$) is observed for $WZ + b$ ($WZ + c$) with 1 associated jet and $X \pm X \text{ fb}$ ($X \pm X \text{ fb}$) for $WZ + b$ ($WZ + c$) with 2 assoicated jets.

Table of Contents

Acknowledgments	v
Abstract	vi
List of Tables	xi
List of Figures	xiv
Part I Introduction	1
0.1 Introduction	2
Part II Theoretical Motivation	4
0.2 The Standard Model and the Higgs Boson	5
0.2.1 The Forces and Particles of the Standard Model	5
0.2.2 The Higgs Mechanism	7
0.2.2.1 The Higgs Field	8
0.2.2.2 Electroweak Symmetry Breaking	9
0.2.3 $t\bar{t}H$ Production	11
0.2.4 $WZ +$ Heavy Flavor Production	13
0.2.5 Extensions to the Standard Model	14
Part III The LHC and the ATLAS Detector	18
0.3 The LHC	19
0.4 The ATLAS Detector	21
0.4.1 Inner Detector	22

0.4.2	Calorimeters	23
0.4.3	Muon Spectrometer	24
0.4.4	Trigger System	24
Part IV	Measurement of WZ + Heavy Flavor	26
0.5	Introduction	27
0.6	Data and Monte Carlo Samples	28
0.6.1	Data Samples	28
0.6.2	Monte Carlo Samples	28
0.7	Object Reconstruction	29
0.8	Event Selection and Signal Region Definitions	31
0.8.1	Event Preselection	32
0.8.2	Fit Regions	32
0.8.3	Non-Prompt Lepton Estimation	33
0.9	tZ Separation Multivariate Analysis	35
0.10	Systematic Uncertainties	36
0.11	Results	39
0.11.1	Fit Procedure	39
0.11.2	Results of the Simultaneous Fit	40
0.11.3	Inclusive 1-2 Jet Fit	43
0.11.4	Alternate tZ Inclusive Fit	46
0.11.4.1	tZ Inclusive Fit	46
0.11.4.2	Floating tZ	46
0.12	Conclusion	47
Part V	Differential Studies of t<bar>t}H Multilepton</bar>	48
0.13	Data and Monte Carlo Samples	49
0.13.1	Data Samples	49
0.13.2	Monte Carlo Samples	49
0.14	Object Reconstruction	51
0.15	Higgs Momentum Reconstruction	52

0.15.1	Physics Object Truth Matching	53
0.15.2	b-jet Identification	53
0.15.2.1	2lSS Channel	54
0.15.2.2	3l Channel	59
0.15.3	Higgs Reconstruction	62
0.15.3.1	2lSS Channel	63
0.15.3.2	3l Semi-leptonic Channel	67
0.15.3.3	3l Fully-leptonic Channel	71
0.15.4	p_T Prediction	75
0.15.4.1	2lSS Channel	76
0.15.4.2	3l Semi-leptonic Channel	78
0.15.4.3	3l Fully-leptonic Channel	81
0.15.5	3l Decay Mode	83
0.16	Signal Region Definitions	85
0.16.1	Pre-MVA Event Selection	85
0.16.2	Event MVA	89
0.16.3	Signal Region Definitions	96
0.17	Systematic Uncertainties	97
0.18	Results	100
0.18.1	Results - 79.8 fb^{-1}	101
0.18.2	Projected Results - 139 fb^{-1}	105
Part VI	Conclusion	109
Appendices		111
.1	Non-prompt lepton MVA	112
.2	Supplementary WZ + Heavy Flavor Studies	114
.2.1	Non-prompt CR Modelling	114
.2.2	tZ Interference Studies	118
.2.3	Alternate tZ Inclusive Fit	119
.2.3.1	tZ Inclusive Fit	119
.2.3.2	Floating tZ	120

.3	Supplementary $t\bar{t}H$ Differential Analysis Studies	120
.3.1	Higgs Reconstruction Model Details	120
.3.1.1	b-jet Identification Features - 2lSS	120
.3.1.2	b-jet Identification Features - 3l	124
.3.1.3	Higgs Reconstruction Features - 2lSS	129
.3.1.4	Higgs Reconstruction Features - 3lS	134
.3.1.5	Higgs Reconstruction Features - 3lF	139
.3.2	Background Rejection MVA Details	143
.3.2.1	Background Rejection MVA Features - 2lSS	143
.3.2.2	Background Rejection MVA Features - 3l	147
.3.3	Truth Level Studies	152
.3.4	Alternate b-jet Identification Algorithm	153
.3.5	Binary Classification of the Higgs p_T	154
.3.6	Impact of Alternative Jet Selection	156

List of Tables

1	Summary of the predominant SM Higgs ($m_H = 125$ GeV) branching ratios. Particles with a star imply off-shell decays.	13
2	The configurations used for event generation of signal and background processes, including the event generator, matrix element (ME) order, parton shower algorithm, and parton distribution function (PDF).	29
3	c -jet and light-flavor jet rejections corresponding to each b -tagging Working Point by b -jet efficiency, evaluated on $t\bar{t}$ events.	31
4	A list of the regions used in the fit and the selection used for each.	33
5	Sources of systematic uncertainty considered in the analysis.	37
6	Summary of theoretical uncertainties for normalization of MC predictions in the analysis.	39
7	Normalization factors and cross-sections extracted from the fit for each of the fiducial regions considered	41
8	Summary of the most significant sources of systematic uncertainty on the measurement of $WZ + b$ with exactly one associated jet.	42
9	Summary of the most significant sources of systematic uncertainty on the measurement of $WZ + c$ with exactly one associated jet.	42
10	Summary of the most significant sources of systematic uncertainty on the measurement of $WZ + b$ with 2 associated jets.	43
11	Summary of the most significant sources of systematic uncertainty on the measurement of $WZ + c$ with 2 associated jets.	43
12	Summary of the most significant sources of systematic uncertainty on the measurement of $WZ + b$ with one or two associated jets.	45
13	Summary of the most significant sources of systematic uncertainty on the measurement of $WZ + b$ with exactly one associated jet.	46
14	The configurations used for event generation of signal and background processes, including the event generator, matrix element (ME) order, parton shower algorithm, and parton distribution functin (PDF).	49
15	Input features used in the b -jet identification algorithm for the 2LSS channel	55

16	Accuracy of the NN in identifying b-jets from tops in 2lSS events, overall and split by the number of b-tagged jets in the event, compared to the accuracy of taking the two highest b-tagged jets.	58
17	Input features for the b-jet identification algorithm in the 3l channel.	59
18	Accuracy of the NN in identifying b-jets from tops, compared to the naive method of taking the highest b-tagged jets.	62
19	Input features used to identify the Higgs decay products in 2lSS events	64
20	Input features used to identify the Higgs decay products in 3l semi-leptonic events	68
22	Input features used to identify the Higgs decay products in 3l fully leptonic events	72
23	Input features for reconstructing the Higgs p_T spectrum for 2lSS events	76
24	Input features for reconstructing the Higgs p_T spectrum for 3lS events	79
25	Input features for reconstructing the Higgs p_T spectrum for 3lF events	81
26	Input features used to distinguish semi-leptonic and fully-leptonic Higgs decays in the 3l channel.	84
27	Yields of the 2lSS preselection region	86
29	Yields of the 3l preselection region.	88
32	Cutoff values on background rejection MVA score applied to signal regions.	96
33	Selection applied to define the three signal regions used in the fit. . .	97
34	Sources of systematic uncertainty considered in the analysis. Some of the systematic uncertainties are split into several components, as indicated by the number in the rightmost column.	98
35	Normalization factors - with statistical and systematic uncertainties - derived from the fit over fake control regions for each source of non-prompt leptons considered.	99
36	Summary of theoretical uncertainties for MC predictions in the analysis.	100
37	Best fit μ values for $t\bar{t}H$ high p_T and $t\bar{t}H$ low p_T , where $\mu = \sigma_{\text{obs}}/\sigma_{\text{pred}}$	102
38	Summary of the most significant sources of systematic uncertainty on the measurement of $t\bar{t}H$ high p_T	103
39	Summary of the most significant sources of systematic uncertainty on the measurement of $t\bar{t}H$ low p_T	103
40	Best fit μ values for $t\bar{t}H$ high p_T and $t\bar{t}H$ low p_T , where $\mu = \sigma_{\text{obs}}/\sigma_{\text{pred}}$	106
41	Summary of the most significant sources of systematic uncertainty on the measurement of $t\bar{t}H$ high p_T	107

42	Summary of the most significant sources of systematic uncertainty on the measurement of $t\bar{t}H$ low p_T	107
43	A table of the variables used in the training of <code>PromptLeptonVeto</code> . .	113
44	Summary of the most significant sources of systematic uncertainty on the measurement of $WZ + b$ with exactly one associated jet.	120
45	Accuracy of the NN in identifying b -jets from tops in 2LSS events for the alternate categorical method compared to the nominal method. .	154

List of Figures

0.2.1 A summary of the particles of the Standard Model, including their mass, charge and spin, with the fermions listed on the left, and the bosons on the right. [?]	6
0.2.2 The value of the Higgs potential, $V(\Phi)$ as a function of Φ , for the case that $\mu^2 < 0$ [?].	8
0.2.3 Diagram of a Higgs boson produced via gluon-gluon fusion.	11
0.2.4 Diagram of a Higgs boson produced in association with a pair of top quarks.	12
0.2.5 Example Feynman diagrams of $WZ +$ heavy flavor production	14
0.2.6 Above diagram is the leading order correction to the Higgs mass via a top quark loop, and below is the stop squark loop, coming from a supersymmetric extension of the SM, that provides a potential cancellation of the top diagram.	15
0.2.7 The momentum spectrum of the Higgs boson produced via top-quarks with (red) and without (blue) the presence of dimension-six operators.	16
0.2.8 Feynman diagrams of $t\bar{t}H$ production with (a) two same-sign leptons and (b) three leptons in the final state.	17
0.3.1 A summary of the accelerator chain used to feed protons into the LHC [?].	20
0.4.1 Cutaway view of the ATLAS detector, with labels of its major components [?].	21
0.4.2 Cutaway view of the Inner Detector [?].	22
0.4.3 Cutaway view of the calorimeter system of the ATLAS detector [?].	23
0.9.1 Distribution of the BDT response for $WZ+b$ (blue) and tZ (orange) events, for both training and testing samples.	36
0.11.1 Post-fit summary of the fit regions.	40
0.11.2 Correlations between the various measured components of WZ .	41
0.11.3 Post-fit summary of the fit regions.	44

0.15.1	Input features for top2lSS training. The signal in blue represents events where both jet candidates are truth b-jets from top decays, and the orange is all other combinations. Each are scaled to the same number of events. (a) shows the DL1r working point of leading jet, (b) shows the p_T of the leading jet, (c) shows the ΔR of the two jets, (d) the invariant mass of lepton 1 and jet 1, (e) the ΔR of lepton 0 and jet 0, and (f) the p_T of both jets, both leptons, and the E_T^{miss}	56
0.15.2	Data/MC comparisons of input features for top2lSS training for 79.8 fb^{-1} of data. (a) shows the DL1r working point of leading jet, (b) shows the p_T of the leading jet, (c) shows the ΔR of the two jets, (d) the invariant mass of lepton 1 and jet 1, (e) the ΔR of lepton 0 and jet 0, and (f) the p_T of both jets, both leptons, and the E_T^{miss}	57
0.15.3	Results of the b-jet identification algorithm for the 2lSS channel, showing (a) the output score of the NN for correct and incorrect combinations of jets. (b) the ROC curve of the output, showing background rejection as a function of signal efficiency	58
0.15.4	Input features for top3l training. The signal in blue represents events where both jet candidates are truth b-jets from top decays, and the orange is all other combinations. Scaled to the same number of events. (a) show the DL1r WP of jet 0, (b) the p_T of jet 0, (c) ΔR between jet 0 and jet 1, (d) the invariant mass of lepton 1 and jet 1, (e) ΔR between lepton 0 and jet 0, and (f) ΔR between lepton 0 and jet 1	60
0.15.5	Data/MC comparisons of input features for top3l training for 79.8 fb^{-1} of data. (a) show the DL1r WP of jet 0, (b) the p_T of jet 0, (c) ΔR between jet 0 and jet 1, (d) the invariant mass of lepton 1 and jet 1, (e) ΔR between lepton 0 and jet 0, and (f) ΔR between lepton 0 and jet 1	61
0.15.6	Results of the b-jet identification algorithm for the 3l channel, showing (a) the output score of the NN for correct and incorrect combinations of jets. (b) the ROC curve of the output, showing background rejection as a function of signal efficiency	62
0.15.7	Input features for higgs2lSS training. The signal in blue represents events where both jet candidates are truth b-jets from top decays, and the orange is all other combinations. Scaled to the same number of events. (a) shows the invariant mass of the two jet candidates and the lepton candidate, (b) the invariant mass of jet 0 and the lepton candidate, (c) ΔR between the jet candidates, (d) ΔR between jet 0 + jet 1 and the lepton candidate, (e) ΔR between the lepton from the top and the leading b-jet, (f) the p_T of jet 0	65

0.15.8	Data/MC comparisons of input features for higgs2lSS training for 79.8 fb^{-1} of data. (a) shows the invariant mass of the two jet candidates and the lepton candidate, (b) the invariant mass of jet 0 and the lepton candidate, (c) ΔR between the jet candidates, (d) ΔR between jet 0 + jet 1 and the lepton candidate, (e) ΔR between the lepton from the top and the leading b-jet, (f) the p_T of jet 0.	66
0.15.9	Result of the Higgs reconstruction algorithm in the 2lSS channel, showing (a) the output score of the NN for correct and incorrect combinations of jets scaled to an equal number of events, and (b) the ROC curve of the output, showing background rejection as a function of signal efficiency	67
0.15.10	Input features for higgs3lS training. The signal in blue represents events where both jet candidates are truth b-jets from top decays, and the orange is all other combinations. Scaled to the same number of events.	69
0.15.11	Data/MC comparisons of input features for higgs3lS training for 79.8 fb^{-1} of data.	70
0.15.12	Results of the Higgs reconstruction algorithm in the 3lS channel, showing (a) the output score of the NN for correct and incorrect combinations of jets, scaled to an equal number of entries., (b) the ROC curve of the output, showing background rejection as a function of signal efficiency	71
0.15.13	Input features for higgs3lF training. The signal in blue represents events where both jet candidates are truth b-jets from top decays, and the orange is all other combinations. Scaled to the same number of events.	73
0.15.14	Data/MC comparisons of input features for higgs3lF training for 79.8 fb^{-1} of data.	74
0.15.15(a)	(a) the output score of the NN for correct and incorrect combinations of jets. (a) the ROC curve of the output, showing background rejection as a function of signal efficiency	75
0.15.16	The regressed Higgs momentum spectrum as a function of the truth p_T for 2lSS $t\bar{t}H$ events in (a) a scatterplot, where the color of each point represents the log of the point density, based on Gaussian Kernal Density Estimation, and (b) a histogram where each column has been normalized to one.	77
0.15.17(a)	(a) shows the reconstructed Higgs p_T for 2lSS events with truth $p_T > 150 \text{ GeV}$ and $< 150 \text{ GeV}$, while (b) shows the ROC curve for those two sets of events.	78

0.15.1	The regressed Higgs momentum spectrum as a function of the truth p_T for 3lS $t\bar{t}H$ events in (a) a scatterplot, where the color of each point represents the log of the point density, based on Gaussian Kernal Density Estimation, and (b) a histogram where each column has been normalized to one.	80
0.15.19	81
0.15.20	The regressed Higgs momentum spectrum as a function of the truth p_T for 3lF $t\bar{t}H$ events in (a) a scatterplot, where the color of each point represents the log of the point density, based on Gaussian Kernal Density Estimation, and (b) a histogram where each column has been normalized to one.	82
0.15.21a	(a) shows the reconstructed Higgs p_T for 3lF events with truth $p_T > 150$ GeV and < 150 GeV, while (b) shows the ROC curve for those two sets of events.	83
0.15.21b	(a) shows the output of the decay separation NN for Semi-leptonic (blue) and Fully-leptonic (orange) 3l events, scaled to equal area. (b) shows the ROC curve for those two sets of events.	85
0.16.1	Data/MC comparisons of the 2lSS pre-selection region. (a) and (b) show the p_T of leptons 0 and 1, (c) shows the invariant mass of lepton 0 and 1, (d) shows the jet multiplicity, (e) the b-tagged jet multiplicity, and (f) the missing transverse energy.	87
0.16.2	Data/MC comparisons of the 3l pre-selection region. (a) and (b) show the p_T of leptons 0 and 1, (c) shows the invariant mass of lepton 0 and 1, (d) shows the jet multiplicity, (e) the b-tagged jet multiplicity, and (f) the missing transverse energy.	89
0.16.3	Output BDT scores of training and testing data for signal (blue) and background (orange) for 2lSS events with (a) high regressed Higgs p_T and (b) low regressed Higgs p_T . (b) and (d) show the ROC curve for the 2lSS high and low p_T models, respectively.	92
0.16.4	Output BDT scores of training and testing data for signal (blue) and background (orange) for 3lS events with (a) high regressed Higgs p_T and (b) low regressed Higgs p_T . (b) and (d) show the ROC curve for the 3lS high and low p_T models, respectively.	93
0.16.5	Output BDT scores of training and testing data for signal (blue) and background (orange) for 3lF events with (a) high regressed Higgs p_T and (b) low regressed Higgs p_T . (b) and (d) show the ROC curve for the 3lF high and low p_T models, respectively.	94
0.16.6	Output score of the high p_T BDTs in the (a) 2lSS, (b) 3lS, and (c) 3lF channels	95
0.16.7	Output score of the low p_T BDTs in the (a) 2lSS, (b) 3lS, and (c) 3lF channels	95

0.18.1	Post-fit distributions of the reconstructed Higgs p_T in the three signal regions, (a) 2lSS, (b) 3lS, and (c) 3lF, for 79.8 fb^{-1} of MC	101
0.18.2	Post-fit summary of the yields in each signal region.	102
0.18.3	Impact of systematic uncertainties on the measurement of high p_T (left) and low p_T (right) $t\bar{t}H$ events	104
0.18.4	Blinded post-fit distributions of the reconstructed Higgs p_T in the three signal regions, (a) 2lSS, (b) 3lS, and (c) 3lF, for 139 fb^{-1} of data	105
0.18.5	Post-fit summary of fit.	106
0.18.6	Impact of systematic uncertainties on the measurement of high p_T (left) and low p_T (right) $t\bar{t}H$ events	108
.1.1	Distribution of the PLV BDT discriminant for (a) electrons and (b) muons	113
.1.2	ROC curves for the PLV as well as the performance of the standard FixedCutTight WP for (left) electrons and (right) muons	114
.2.1	Comparisons between the data and MC distributions of the p_T of the lepton originating from the W-candidate in the Z+jets CR for each of the 1-jet b-tag working point regions	115
.2.2	Comparisons between the data and MC distributions of the p_T of the lepton originating from the W-candidate in the Z+jets CR for each of the 2-jet b-tag working point regions	116
.2.3	Comparisons between the data and MC distributions of the p_T of the OS lepton in the $t\bar{t}$ CR for each of the 1-jet b-tag working point regions	117
.2.4	Comparisons between the data and MC distributions of the p_T of the OS lepton in the $t\bar{t}$ CR for each of the 2-jet b-tag working point regions	118
.3.1	Input features for top2lSS	121
.3.2	Input features for top2lSS	122
.3.3	Input features for top2lSS	123
.3.4	Input features for top3l	125
.3.5	Input features for top3l	126
.3.6	Input features for top3l	127
.3.7	Input features for top3l	128
.3.8	Input features for higgs2lSS	130
.3.9	Input features for higgs2lSS	131
.3.10	Input features for higgs2lSS	132
.3.11	Input features for higgs2lSS	133

.3.12 Input features for higgs3lS	135
.3.13 Input features for higgs3lS	136
.3.14 Input features for higgs3lS	137
.3.15 Input features for higgs3lS	138
.3.16 Input features for higgs3lF	140
.3.17 Input features for higgs3lF	141
.3.18 Input features for higgs3lF	142
.3.19 Input features for sigBkg2lSS	144
.3.20 Input features for sigBkg2lSS	145
.3.21 Input features for sigBkg2lSS	146
.3.22 Input features for sigBkg3l	148
.3.23 Input features for sigBkg3l	149
.3.24 Input features for sigBkg3l	150
.3.25 Input features for sigBkg3l	151
.3.26 The regressed Higgs momentum spectrum as a function of the truth p_T for 2lSS $t\bar{t}H$ events in (a) a scatterplot, where the color of each point represents the log of the point density, based on Gaussian Kernel Density Estimation, and (b) a histogram where each column has been normalized to one.	152
.3.27 (a) shows the reconstructed Higgs p_T for 2lSS events with truth $p_T > 150$ GeV and < 150 GeV, while (b) shows the ROC curve for those two sets of events.	153
.3.28 Output distribution of the NN score for the binary high/low p_T separation model in the 2lSS channel.	154
.3.29 Output distribution of the NN score for the binary high/low p_T separation model in the 3lS channel.	155
.3.30 Output distribution of the NN score for the binary high/low p_T separation model in the 3lS channel.	155
.3.31 Output of the model designed to predict the Higgs momentum in the 2lSS channel, with the jet p_T cutoff used is raised to 20 GeV.	156
.3.32 Output of the model designed to predict the Higgs momentum in the 2lSS channel, with the jet p_T cutoff used is raised to 25 GeV.	157

Part I

Introduction

0.1 Introduction

Particle physics is an attempt to describe the fundamental building blocks of the universe and their interactions. The Standard Model (SM) - our best current theory of fundamental particle physics - does a remarkable job of that. All known fundamental particles and (almost) all of the forces underlying their interactions can be explained by the SM, and the predictions from this theory agree with experiment to an incredibly precise degree. This is especially true since the Higgs Boson, the last piece of the SM predicted decades before, was finally discovered at the Large Hadron Collider (LHC) in 2012 [?].

Despite the success of the SM, there remains significant work to be done. For one, the SM is incomplete: it fails to provide a description of gravity, to give an explanation for the observation of Dark Matter, or to provide a mechanism for neutrinos to gain mass. Further, a Higgs Boson with a mass of around 125 GeV, as observed at the LHC, gives rise to what is known a hierarchy problem - such a low mass Higgs requires a seemingly unnatural level of “fine tuning” that is unexplained by the SM.

A promising avenue for addressing these problems is to study the properties of the Higgs Boson and the way it interacts with other particles, in part simply because these interactions have not been measured before. Its interactions with the Top Quark are a particularly promising place to look. Because the Higgs Field is responsible for allowing particle to acquire mass, the strength of a particle’s interaction with the Higgs Boson is proportional to its mass. As the most massive of the fundamental particles, the Top Quark has the strongest coupling to the Higgs Boson, meaning any new physics in the Higgs sector is likely to present itself most prominantly in its interaction with the Top Quark.

These interactions can be measured by directly by studying the production of a Higgs Boson in association with a pair of Top Quarks ($t\bar{t}H$). While studies have been done measuring the overall rate of $t\bar{t}H$ production, there are several theories of physics Beyond the Standard Model (BSM) that would affect the kinematics of $t\bar{t}H$ production without altering its overall rate. This dissertation attempts to make a differential measurement of the kinematics of the Higgs Boson in $t\bar{t}H$ events in order to search for these BSM effects.

The proton-proton collision data collected by the ATLAS detector at the LHC from 2015-2018 provides the opportunity to make this measurement for the first time. The unprecedented energy achieved by the LHC during this period greatly increase the rate at which $t\bar{t}H$ events are produced, and the large amount of data collected provides the necessary statistics for a differential measurement to be performed.

A study of $t\bar{t}H$ events with multiple leptons in the final state is performed, using 139 fb^{-1} of data from proton-proton collisions at an energy $\sqrt{s} = 13 \text{ TeV}$ collected by the ATLAS detector from 2015-2018. Events are separated into channels based on the number of light leptons in the final state - either two same-sign leptons, or three leptons. A deep neural network is used to reconstruct the momentum of the

Higgs Boson in each event. This momentum spectrum is fit to data for each analysis channel in order to search for evidence of these BSM effects.

An additional study of WZ produced in association with a heavy flavor jet (including both b-jets and charm jets) is also included. This process mimics the final state of ttH multilpeton events, making it an irreducible background for that analysis. However, this process is poorly understood, and difficult to simulate accurately, introducing large systematic uncertainties for analyses that include it as a background. A measurement of WZ + heavy flavor in the fully leptonic decay mode is performed in an attempt to reduce this uncertainty.

This dissertation begins with a brief explanation of the SM, its limitations, and the theoretical motivation behind this work in Part II. This is followed by a description of the LHC and the ATLAS detector in Part III. Part IV details a measurement of WZ + heavy flavor. Studies of differential measurements of ttH are then described in Part V, and preliminary results are presented. Finally, the results of these studies are summarized in the conclusion, Part VI.

Part II

Theoretical Motivation

0.2 The Standard Model and the Higgs Boson

The Standard Model of particle physics (SM) is a Quantum Field Theory (QFT) describing the known fundamental particles and their interactions. It accounts for three of the four known fundamental force - electromagnetism, the weak nuclear force, and the strong nuclear force, but not gravity. Further, the SM describes a mechanism for combining the weak and electromagnetic forces into a singular interaction, known as the electroweak force. It is a non-Abelian gauge theory, invariant under the Lie Group $SU(3)_C \otimes SU(2)_L \otimes U(1)_Y$, where C refers to color charge, L, the helicity of the particle, and Y, the hypercharge.

0.2.1 The Forces and Particles of the Standard Model

The SM particles, summarized in Figure 0.2.1, can be classified into two general categories based on their spin: fermions, and bosons.

Standard Model of Elementary Particles

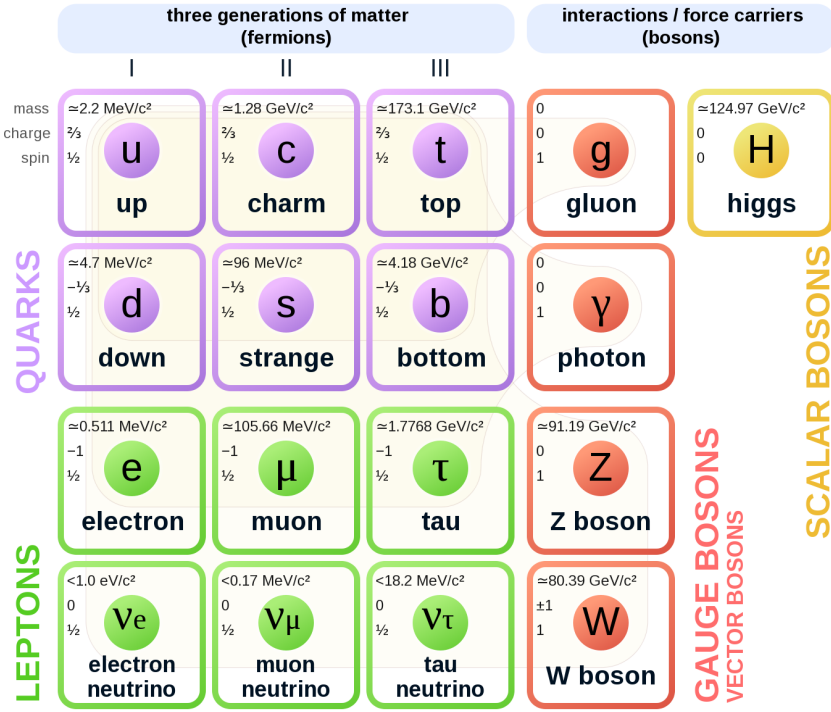


Figure 0.2.1: A summary of the particles of the Standard Model, including their mass, charge and spin, with the fermions listed on the left, and the bosons on the right. [?]

Fermions are particles with $\frac{1}{2}$ -integer spin, which according to the spin-statistics theorem, causes them to comply with the Pauli-exclusion principle. They can be separated into two groups, leptons and quarks, each of which consist of three generations of particles with increasing mass.

Leptons are fermions which interact via the electroweak force, but not the strong force. The three generation of leptons consist of the electron and electron neutrino, the muon and muon neutrino, the tau and tau neutrino. The quarks, by contrast, do interact via the strong force - which is to say they have color charge - in addition to the electroweak force. The three generations include the up and down quarks, the strange and charm quarks, and the top and bottom quarks.

Each of these generations form left-handed doublets invariant under $SU(2)$ transformations. For the leptons these doublets are:

$$\begin{pmatrix} e^- \\ \nu_e \end{pmatrix}_L, \begin{pmatrix} \mu^- \\ \nu_\mu \end{pmatrix}_L, \begin{pmatrix} \tau^- \\ \nu_\tau \end{pmatrix}_L \quad (0.2.1)$$

And for the quarks:

$$\begin{pmatrix} u \\ d \end{pmatrix}_L, \begin{pmatrix} s \\ c \end{pmatrix}_L, \begin{pmatrix} t \\ b \end{pmatrix}_L \quad (0.2.2)$$

For both leptons and quarks, the heavier generations can decay into the lighter generation of particles, while the first generation does not decay. Hence, ordinary matter generally consists of this first generation of fermions - electrons, up quarks, and down quarks. Each of these fermions has a corresponding anti-particle, which has an equal mass as its partner but opposite charge. The fermions acquire their mass via the Higgs Mechanism, except for the neutrinos, whose mass has been experimentally confirmed but is not accounted for in the SM.

Bosons, by contrast, have integer spin, and are therefore unconstrained by the Pauli-exclusion principle. The SM includes two kinds of bosons: Gauge bosons, which are spin-1 particles that mediate the interactions between the fermions, and a single scalar, i.e. spin-0, particle - the Higgs Boson. Of the gauge bosons, the W^+ , W^- and Z bosons - which are the mass eigenstates of the electroweak bosons - mediate the weak interaction, while the photon mediates the electric force, and the gluon mediates the strong force.

0.2.2 The Higgs Mechanism

A key feature of the SM is the gauge invariance of its Lagrangian. However, any terms added to the Lagrangian giving mass to the gauge bosons would violate this underlying symmetry of the theory. This presents a clear problem with the theory: The experimental observation that the W and Z bosons have mass seems to contradict the basic structure of the SM.

Rather than abandoning gauge invariance, an alternative way for particles to acquire mass beyond adding a simple mass term to the Lagrangian was theorized by Higgs, Englert and Brout in 1964 [?]. This procedure for introducing masses for the gauge bosons while preserving local gauge invariance, known as the Higgs mechanism, was incorporated into the electroweak theory by Weinberg in 1967 [?].

0.2.2.1 The Higgs Field

The Higgs mechanism introduces a complex scalar $SU(2)$ doublet, Φ , with the form:

$$\Phi = \begin{pmatrix} \phi^+ \\ \phi^0 \end{pmatrix}_L \quad (0.2.3)$$

This field introduces a scalar potential to the Lagrangian of the form:

$$V(\Phi) = \mu^2 |\Phi^\dagger \Phi| + \lambda (|\Phi^\dagger \Phi|)^2 \quad (0.2.4)$$

Where μ and λ are free parameters of the new field. This represents the most general potential allowed while preserving $SU(2)_L$ invariance and renormalizability. In the case that $\mu^2 < 0$, this potential takes the form shown in Figure 0.2.2.

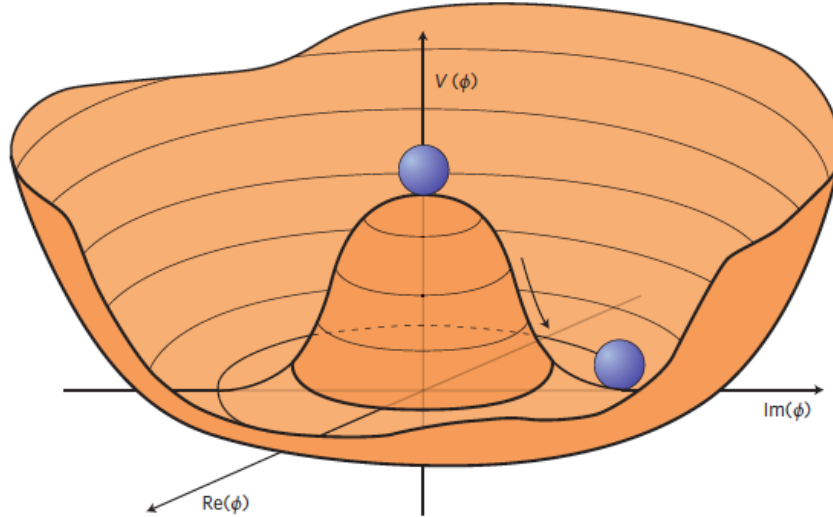


Figure 0.2.2: The value of the Higgs potential, $V(\Phi)$ as a function of Φ , for the case that $\mu^2 < 0$ [?].

The significant feature of this potential is that its minimum does not occur for a value of $\Phi = 0$. Instead, it is minimized when $|\Phi^\dagger \Phi| = -\mu^2/\lambda$. This means that in its ground state, the Higgs field takes on a non-zero value - referred to as a

vacuum expectation value (VEV). So while the Higgs potential is globally symmetric, about the minimum this symmetry is broken. Since the minimum is determined only by $\Phi^\dagger\Phi$, there is some ambiguity in the particular definition of the VEV, but it is generally represented as

$$\langle\Phi\rangle = \frac{1}{\sqrt{2}} \begin{pmatrix} 0 \\ v \end{pmatrix} \quad (0.2.5)$$

The full value of Φ can be written as

$$\langle\Phi\rangle = \frac{1}{\sqrt{2}} \begin{pmatrix} 0 \\ v + H/\sqrt{2} \end{pmatrix} \quad (0.2.6)$$

with v being the value of the VEV, and H being the real value of the scalar field.

0.2.2.2 Electroweak Symmetry Breaking

The Electroweak (EWK) interaction is described in the SM by a $SU(2)_L \otimes U(1)_Y$ gauge theory. This theory predicts three $SU(2)_L$ gauge boson, W_μ^1 , W_μ^2 , W_μ^3 , and a single $U(1)_Y$ gauge boson, B_μ . The couplings of these bosons to the Higgs field show up in the kinetic terms of the scalar field Φ in the Lagrangian:

$$(D_\mu\Phi)^\dagger(D^\mu\Phi) = |(\partial_\mu - \frac{ig}{2}W_\mu^a\sigma^a - \frac{ig'}{2}B_\mu Y)\Phi|^2 \quad (0.2.7)$$

Here D_μ represents the covariant derivative required to preserve gauge invariance, g and g' represent coupling constant of the gauge bosons, σ^a denotes the Pauli matrices of $SU(2)$, and Y represents the hypercharge of $U(1)$. The terms in this interaction which contribute to the masses of the gauge bosons can be written as:

$$\frac{1}{2}(0, v)(\frac{g}{2}W_\mu^a\sigma^a - \frac{g'}{2}B_\mu)^2 \begin{pmatrix} 0 \\ v \end{pmatrix} \quad (0.2.8)$$

Expanding these terms into the mass eigenstates of the electroweak interaction yields four physical gauge bosons, two charged and two neutral, which are linear combinations of the fields W_μ^1 , W_μ^2 , W_μ^3 , and B_μ :

$$\begin{aligned} W_\mu^\pm &= \frac{1}{\sqrt{2}}(W_\mu^1 \pm iW_\mu^2) \\ Z^\mu &= \frac{1}{\sqrt{(g^2 + g'^2)}}(-g'B_\mu + gW_\mu^3) \\ A^\mu &= \frac{1}{\sqrt{(g^2 + g'^2)}}(gB_\mu + g'W_\mu^3) \end{aligned} \quad (0.2.9)$$

And the masses of these fields are given by:

$$\begin{aligned} M_W^2 &= \frac{1}{4}g^2v^2 \\ M_Z^2 &= \frac{1}{4}(g^2 + g'^2)v^2 \\ M_A^2 &= 0 \end{aligned} \quad (0.2.10)$$

This produces exactly the particles we observe - three massive gauge bosons and a single massless photon. The massless photon represents the portion of the gauge symmetry, a single $U(1)$ of the electromagnetic force, that remains unbroken by the VEV.

Interactions with the Higgs field also lead to the generation of the fermion masses, which in the Lagrangian take the form:

$$-\lambda_\psi(\bar{\psi}_L \phi \psi_R + \bar{\psi}_R \phi^\dagger \psi_L) \quad (0.2.11)$$

After symmetry breaking has occurred and ϕ has taken on the value of the VEV as written in equation 0.2.5, the mass terms of the fermions become $\lambda_\psi v$. Written this way, the fermion masses are proportional to their Yukawa coupling to the VEV, λ_ψ .

Based on the equation 0.2.6, an additional mass term, $\mu^2 H^2$ arises from the potential $V(\Phi)$. This term can be understood as an excitation of the Higgs field, a scalar boson with mass $M_H = \mu$. This is the Higgs boson, which comes about as a natural prediction of electroweak symmetry breaking.

The fermions' Yukawa couplings to the VEV take the same form as the fermion's coupling to the Higgs boson - λ_ψ . Therefore, the strength of a fermion's interaction

with the Higgs is directly proportional to its mass. We now have a model that predicts a Higgs boson with mass $M_H = \mu$, which interacts with the fermions with coupling strength λ_ψ . Because μ and λ_ψ are free parameters of the theory, the mass of the Higgs boson and its interactions with the fermions must be measured experimentally.

0.2.3 $t\bar{t}H$ Production

The strength of a particles interaction with the Higgs, given by its Yukawa coupling, is proportionate to its mass. The top quark - as the heaviest known particle - has the strongest interaction, making this interaction particularly interesting to study. While several processes involve interactions between the Higgs and the top, some Higgs production modes include the top interaction only as a part of a loop diagram, such as the gluon-gluon fusion diagram shown in Figure 0.2.3. This process therefore only allows for an indirect probe of the Higgs-top Yukawa coupling, as the flavor of the quark in this diagram is not unique.

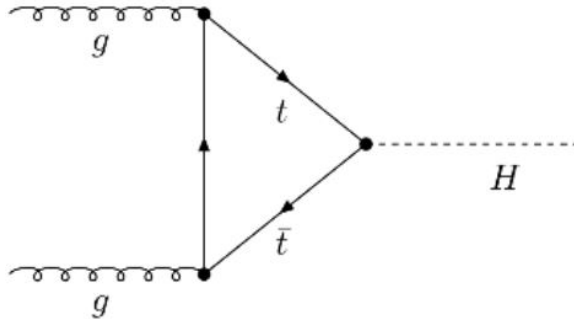


Figure 0.2.3: Diagram of a Higgs boson produced via gluon-gluon fusion.

Studying the Higgs produced in association with top quark pairs, $t\bar{t}H$, allows this interaction to be measured directly. This process, as shown in Figure 0.2.4, involves a unique coupling between the Higgs and the top, which can be identified by the top quark pair in the final state.

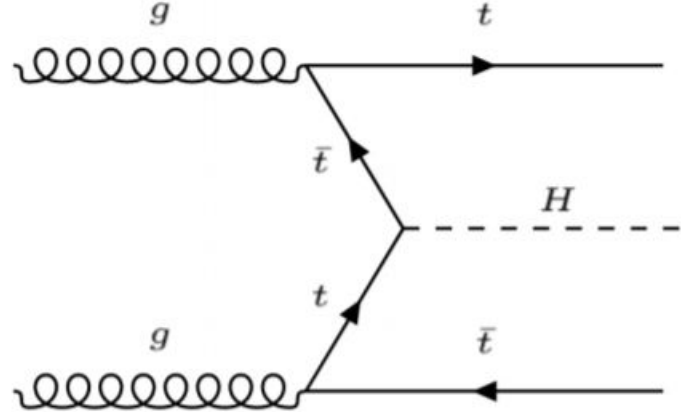


Figure 0.2.4: Diagram of a Higgs boson produced in association with a pair of top quarks.

The Higgs boson, as well as the top quarks, have very short lifetimes - on the order of 10^{-22} s and 10^{-25} s respectively - meaning they can only be observed via their decay products. Measuring this process is therefore a matter of identifying events with final states consistent with $t\bar{t}H$ production.

Studies of $t\bar{t}H$ production have been reported by the ATLAS collaboration for $H \rightarrow b\bar{b}$, $H \rightarrow \gamma\gamma$ and multilepton (encompassing $H \rightarrow W^+W^-$, $H \rightarrow ZZ$ and $H \rightarrow \tau^-\tau^+$, with $H \rightarrow ZZ \rightarrow 4l$ as a separate analysis) decay modes. While the branching ratio of $H \rightarrow W^+W^-$ is smaller than $H \rightarrow b\bar{b}$ (see Table 0.2.3), it produces a clearer signal, as $H \rightarrow b\bar{b}$ suffers from large $t\bar{t}$ backgrounds. On the other hand, $H \rightarrow \gamma\gamma$ produces the most easily identifiable signal, but has a much smaller branching ratio than $H \rightarrow W^+W^-$. Therefore, compared with other final states of $t\bar{t}H$, the $t\bar{t}H$ -ML channel is an attractive candidate for study, as it involves a good balance between statistical power and identifiability.

Decay Mode	Branching Ratio (%)
$H \rightarrow b\bar{b}$	58.2
$H \rightarrow WW^*$	21.4
$H \rightarrow gg$	8.19
$H \rightarrow \tau\tau$	6.27
$H \rightarrow c\bar{c}$	2.89
$H \rightarrow ZZ^*$	2.62
$H \rightarrow \gamma\gamma$	0.227

Table 1: Summary of the predominant SM Higgs ($m_H = 125$ GeV) branching ratios. Particles with a star imply off-shell decays.

Searches for $t\bar{t}H$ production typically target a measurement of the signal strength parameter, $\mu_{t\bar{t}H}$, which measures the ratio of the observed cross-section and the expected cross-section according to the SM.

$$\mu_{t\bar{t}H} = \frac{\sigma_{t\bar{t}H}^{\text{obs.}}}{\sigma_{t\bar{t}H}^{\text{SM}}} \quad (0.2.12)$$

$t\bar{t}H$ production was observed by ATLAS using up to 79.8 fb^{-1} of data collected at $\sqrt{s} = 13$ TeV, based on a combination of five Higgs decay modes: $b\bar{b}$, WW^* , $\tau^-\tau^+$, $\gamma\gamma$, and ZZ^* [?]. A significance of 5.8σ was observed, compared to a 4.9σ expected significance. Since then, two analyses have published updated results ($H \rightarrow \gamma\gamma$ and $H \rightarrow ZZ^* \rightarrow 4l$) with the full Run 2 dataset, representing 139 fb^{-1} . Studies are still ongoing in the remaining channels.

This thesis focuses on $t\bar{t}H$ events with multiple leptons in the final state, $t\bar{t}H - \text{ML}$, specifically targeting events with two same-sign leptons (2lSS) or three leptons (3l) in the final state. This includes $H \rightarrow W^+W^-$ events, where at least one of the W bosons decays leptonically.

0.2.4 WZ + Heavy Flavor Production

Part IV is dedicated to a measurement of WZ produced in association with a heavy flavor jet - namely, a charm or b-jet - in the fully leptonic channel. In the instance that both the W and Z bosons decay leptonically, this process produces a final state similar to $t\bar{t}H$, making it an irreducible background for $t\bar{t}H - \text{ML}$ specifically, and any analysis that includes multiple leptons and b-tagged jets in the final state more broadly.

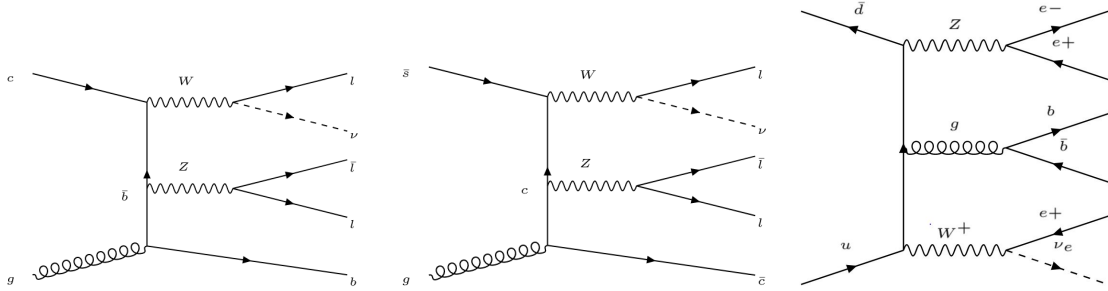


Figure 0.2.5: Example Feynman diagrams of $WZ + \text{heavy flavor}$ production

The b -jets produced in this process can be thought of in two different ways: either as originating from the quark “sea” of the initial state hadrons, or as the result of a gluon from one the colliding protons splitting into $b\bar{b}$ pairs. However, the heavy flavor contribution to the parton distribution function (PDF) of the proton is uncertain, and simulations of this process disagree depending on which of these two approaches one considers. This makes $WZ + \text{heavy flavor}$ difficult to accurately simulate, and introduces a large uncertainty for any analysis which includes it as a background, motivating a measurement of this process.

0.2.5 Extensions to the Standard Model

While the SM has been tested to great precision, particularly at the LHC, it is generally accepted that it is only valid up to a certain energy scale. It is assumed that above a certain energy, at the scale where something like a Grand Unified Theory (GUT) or quantum gravity become relevant, the SM will not be applicable. Further, there are several experimental observations that the SM fails to explain. For example, the SM predicts neutrinos to be massless, despite experimental observation to the contrary, and fails to explain the observation of dark matter and dark energy.

Another example, relevant to the Higgs sector, is known as the hierarchy problem: large quantum corrections to the Higgs mass from loop diagrams, such as those shown in Figure 0.2.6, are many orders of magnitude larger than the Higgs mass itself. The observed value of the Higgs mass therefore requires extremely precise cancellation between these corrections and the bare mass of the Higgs, a cancellation which seems unnatural and suggests something missing in our theoretical picture.

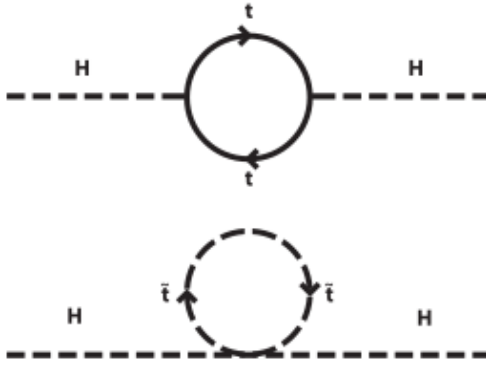


Figure 0.2.6: Above diagram is the leading order correction to the Higgs mass via a top quark loop, and below is the stop squark loop, coming from a supersymmetric extension of the SM, that provides a potential cancellation of the top diagram.

Because so many of the properties of the Higgs boson have not yet been studied, its interactions are a promising place to search for new physics that could resolve some of the limitations of the SM. As explained above, the interactions of the Higgs with the top quark, as in $t\bar{t}H$ production, are particularly interesting: As the most massive particle in the Standard Model, the top quark is the most strongly interacting with the Higgs. Therefore, any new physics effects are likely to be seen most prominently in this interaction.

These interactions can be measured directly by studying the production of a Higgs Boson in association with a pair of Top Quarks ($t\bar{t}H$). While this process has been observed by both the ATLAS [?] and CMS [?] collaborations, these analyses have focused on measuring the overall rate of $t\bar{t}H$ production. There are several theories of physics Beyond the Standard Model (BSM), however, that would affect the kinematics of $t\bar{t}H$ production without altering its overall rate [?].

An Effective Field Theory approach can be used to model the low energy effects of new, high energy physics, by parameterizing BSM effects as higher dimensional operators. These additional operators can then be added to the SM Lagrangian to write an effective Lagrangian that accounts for the effects of these higher energy physics. The lowest order of these that could contribute to Higgs-top couplings are dimension-six, as represented in Equation 0.2.13.

$$\mathcal{L}_{\text{eff}} = \mathcal{L}_{\text{SM}} + \frac{f}{\Lambda} \mathcal{O}^6 \quad (0.2.13)$$

Here Λ represents the energy scale of the new physics, and f is a Wilson coefficient which represents the strength of the effective coupling. An experimental observation of any non-zero value of f would be a sign of BSM physics.

The addition of these operators can be shown to modify the transverse momentum (p_T) spectrum of the Higgs Boson in Higg-top interactions, without effecting the overall rate of $t\bar{t}H$ production [?]. The possible impact of these higher order effects on the Higgs p_T spectrum are shown in Figure 0.2.7.

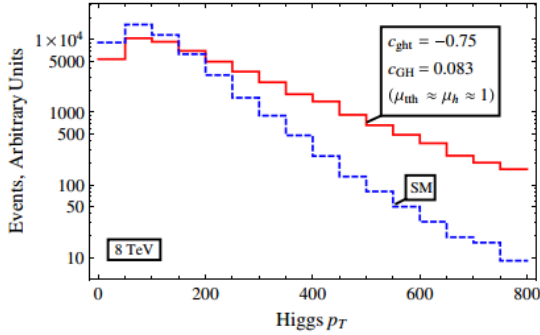


Figure 0.2.7: The momentum spectrum of the Higgs boson produced via top-quarks with (red) and without (blue) the presence of dimension-six operators.

This provides a clear, physics observable that could be used to search for evidence of BSM physics. The energy and luminosity produced by the LHC now make such a measurement possible. Reconstructing the momentum spectrum of the Higgs in $t\bar{t}H$ events therefore provides a means to search for new physics in the Higgs sector.

Reconstructing the Higgs is a particular challenge in the multilepton channels of $t\bar{t}H$, due to an ambiguity arising from multiple sources of missing energy. In the $H \rightarrow \gamma\gamma$ channel, the kinematics of the Higgs can be fully reconstructed from the two photons. The same is true of $H \rightarrow bb$, though with the additional challenge of identifying which two of the four b-quarks in the final state originated from the Higgs. By contrast, the two channels (2lSS and 3l) targeted by this analysis include at least one neutrino originating from the Higgs decay.

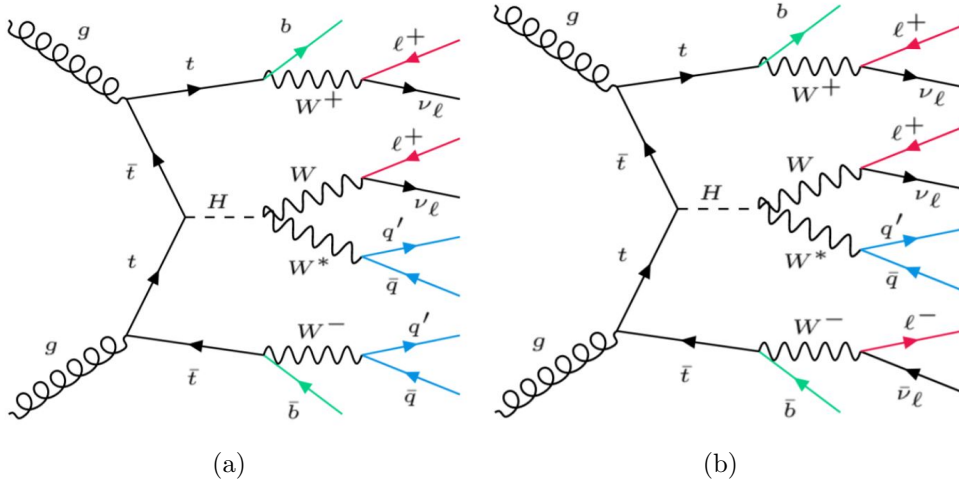


Figure 0.2.8: Feynman diagrams of $t\bar{t}H$ production with (a) two same-sign leptons and (b) three leptons in the final state.

Neutrinos are not detected by ATLAS; instead, their presence is inferred from missing transverse energy in the detector, E_{miss}^T . The two channels targeted here include not just a neutrino from the Higgs decay, but at least one additional neutrino from the decay of the top-quarks. This makes disentangling the contribution of the Higgs decay to E_{miss}^T , and thereby fully reconstructing the Higgs, impossible.

This challenge motivates the use of more sophisticated machine learning techniques when attempting to perform differential measurements of the Higgs p_T spectrum in the multi-lepton channels of $t\bar{t}H$.

Part III

The LHC and the ATLAS Detector

0.3 The LHC

The Large Hadron Collider (LHC) is a particle accelerator consisting of a 27 km ring, designed to collide protons at high energy. Located outside of Geneva, Switzerland and buried about 100 m underground, it consists of a ring of superconducting magnets which are used to accelerate opposing beams of protons - or lead ions - which collide at the center of one of the various detectors located around the LHC ring which record the result of these collisions. These detectors include two general purpose detectors, ATLAS and CMS, which are designed to make precision measurements of a broad range of physics phenomenon, and two more specialized experiments, LHCb and ALICE, which are optimized to study b-quarks and heavy-ion physics, respectively.

The LHC first began running in 2009 at a proton-proton center of mass energy of $\sqrt{s} = 8$ TeV. It operated at this energy from 2009 to 2012, known as Run 1, and data collected during this period was used in discovering the Higgs Boson. The LHC began running again in 2015, and collected data at an increased energy of $\sqrt{s} = 13$ TeV until 2018, a period referred to as Run 2.

The LHC consists of a chain of accelerators, which accelerate the protons to higher and higher energies until they are injected into the main ring. This process is summarized in figure 0.3.1. Protons extracted from a tank of ionized hydrogen are fed into a linear accelerator, LINAC2, where they reach an energy of 50 MeV. From there, they enter a series of three separate circular accelerators, before being injected into the main accelerator ring at an energy of 450 GeV. Within the main ring protons are separated into two separate beams moving in opposite directions, and their energy is increased to their full collision energy. Radiofrequency cavities are used to accelerate these particles and sort them into bunches. From 2015-2018, these bunches consisted of around 100 billion protons each with an energy of 6.5 TeV per proton, which collided at a rate of 40 MHz, or every 25 ns.

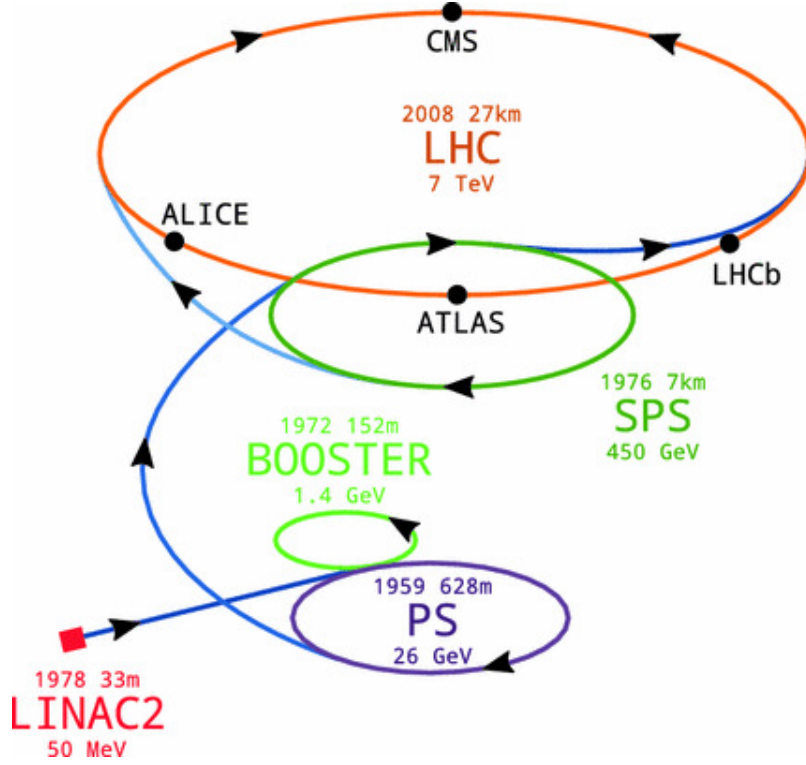


Figure 0.3.1: A summary of the accelerator chain used to feed protons into the LHC [?].

Because these proton bunches consist of a large number of particles, each bunch crossing consists of not just one, but several direct proton-proton collisions. The number of interactions that occur per bunch crossing, μ , is known as pileup. During Run 2, the average pileup for bunch crossings was around $\langle \mu \rangle = 35$, with values typically ranging between 10 and 70.

The amount of data collected by the LHC is measured in terms of luminosity, which is the ratio of the number of events detected per unit time, $\frac{dN}{dt}$, and the interaction cross-section, σ .

$$\mathcal{L} = \frac{1}{\sigma} \frac{dN}{dt} \quad (0.3.1)$$

The design luminosity of the LHC is $10^{34} \text{ cm}^{-2}\text{s}^{-1}$, however the LHC has achieved a luminosity of over $2 \times 10^{34} \text{ cm}^{-2}\text{s}^{-1}$. The total luminosity is then this instantaneous luminosity integrated over time.

$$\mathcal{L}_{\text{int}} = \int \mathcal{L} dt \quad (0.3.2)$$

The integrated luminosity collected by the ATLAS detector as of the end of 2018 is around 140 fb^{-1} , exceeding the expected integrated luminosity of 100 fb^{-1} .

0.4 The ATLAS Detector

ATLAS (a not terribly natural acronym for “A Toroidal LHC Apparatus”) is a general purpose detector designed to maximize the detection efficiency of all physics objects, including leptons, jets, and photons. This means it is capable of measuring all SM particles, with the exception of neutrinos, the presence of which can be inferred based on missing transverse momentum. The detector measures 44 m long, and 25 m tall.

The ATLAS detector consists of multiple concentric layers, each of which serves a different purpose in reconstructing collisions. At the very center of the detector is the interaction point where the proton beams of the LHC collide.

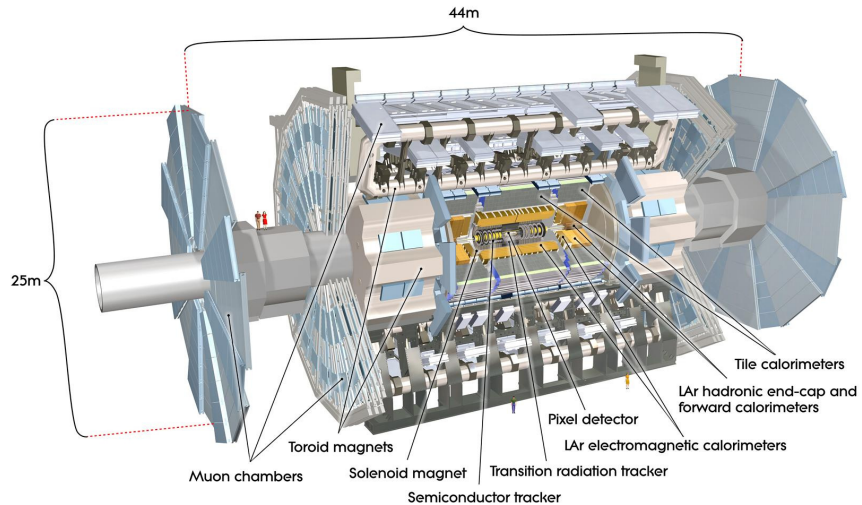


Figure 0.4.1: Cutaway view of the ATLAS detector, with labels of its major components [?].

0.4.1 Inner Detector

Just surrounding the interaction point is the Inner Detector, designed to track the path of charged particles moving through the detector. An inner solenoid surrounding the Inner Detector is used to produce a magnetic field of 2 T. This large magnetic field causes the path of charged particles moving through the Inner Detector to bend. Because this magnetic field is uniform and well known, it can be used in conjunction with the curvature of a particle's path to measure its charge and momentum.

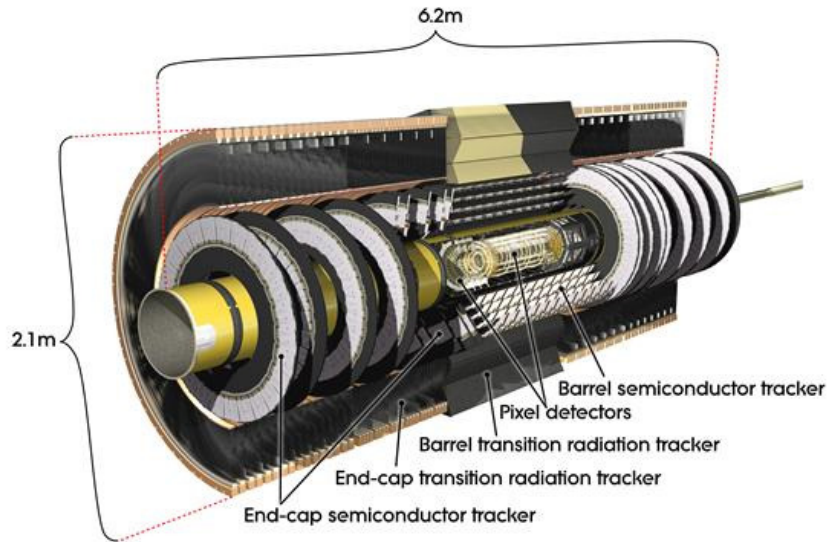


Figure 0.4.2: Cutaway view of the Inner Detector [?].

The Inner Detector consists of three components - the Pixel Detector, the Semiconductor Tracker (SCT), and the Transition Radiation Tracker (TRT). The Pixel Detector is the innermost of these, beginning just 33.25 mm away from the beam line. It consists of three silicon layers along the barrel, as well as three endcap layers, covering a range of $|\eta| < 2.5$.

The Semiconductor Tracker (SCT) is similar to the Pixel detector, but uses long strips of silicon rather than small pixels to cover a larger spatial area. It includes over 6 million readout strips, allowing the position of charged particles to be measured to an accuracy of 17 μm .

The outermost component of the inner detector, the TRT consists of around 300,000 straw tubes filled with ionizable gas, which produces current through a wire in the center of each tube when a charged particle passes through. Between these straws are layers of material designed to produce transition radiation from

ultrarelativistic particles as they pass through each material boundary, amplifying the signal. The position uncertainty in the TRT is higher than the other two, on the order of 200 μm , but covering a much larger area.

0.4.2 Calorimeters

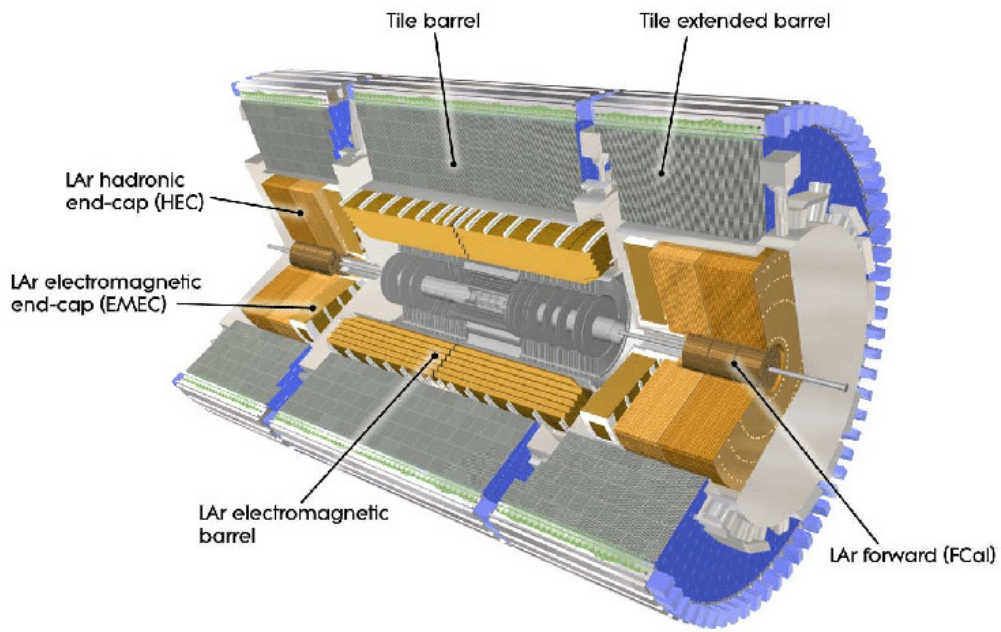


Figure 0.4.3: Cutaway view of the calorimeter system of the ATLAS detector [?].

Situated outside the Inner Detector are two concentric calorimeters. The inner calorimeter uses liquid argon (LAr) to measure the energy of particles that interact electromagnetically, which includes photons and any charged particle. The LAr calorimeter is made of heavy metals, primarily lead and copper, which causes electromagnetically interacting particles to shower, depositing their energy in the detector. The showering of the high energy particles that pass through the calorimeter cause the liquid argon to ionize, and the ionized electrons are detected by electronic readouts. The LAr calorimeter consists of around 180,000 readout channels.

The outer calorimeter measures the energy from particles that pass through the EM calorimeter, and measures the energy of particles that interact via the strong force. This is primarily hadrons. It is composed of steel plates designed to cause

hadronic showering and around 500,000 scintillating tiles as the active material. The signals from the hadronic calorimeter are read out by photomultiplier tubes (PMTs).

0.4.3 Muon Spectrometer

Because muons are heavier than electrons and photons, and do not interact via the strong force, they generally pass through the detector without being stopped by the calorimeters. The outermost components of the detector are designed specifically to measure the energy and momentum of muons produced in the LHC. The muon spectrometer consists of tracking and triggering systems. The largest of the subdetectors, it extends from the outside of the calorimeter system, about a 4.25 m radius from the beam line, to a radius of 11 m. This large detector system is necessary to accurately measure the momentum of muons, which is essential not only for measurements involving the muons themselves, but also to accurately estimate the missing energy in each event.

Two large toroidal magnets within the muon system generate a large magnetic field which covers an area 26 m long with a radius of 10 m. Because the area covered by this magnet system is so large, a uniform magnetic field like the one produced in the Inner Detector is impractical. Instead, the magnetic field that exists in the muon spectrometer ranges between 2 T and 8 T, and is much less uniform. The path of the muons passing through the spectrometer is bent by this field, allowing their charge to be determined.

1200 tracking chambers are placed in the muon system in order to precisely measure the tracks of muons with high spatial resolution. The path of the muons are tracked by Monitored Drift Tubes, which are drift chambers formed by aluminum tubes and filled with ionizing gas. These tubes produce a multi-layer spatial resolution on the order of 50 μm .

0.4.4 Trigger System

Because of the high collision rate and large amount of data collected by the various subdetectors, ATLAS produces far more data than can actually be stored. Each event produces around 25 Mb of raw data, which multiplied by the bunch crossing rate of 40 MHz, comes out to around a petabyte of data every second. The information from every event cannot practically be stored, therefore a sophisticated trigger system is employed in real time to determine whether events are sufficiently interesting to be worth storing.

The trigger system in ATLAS involves multiple levels, each of which select out which events move on to the next level of scrutiny. The level-1 trigger uses hardware information from the calorimeters and muon spectrometer to select events that contain candidates for particles commonly used in analysis, such as energetic

leptons and jets. The level-1 trigger reduces the rate of events from 40 MHz to around 100 kHz.

Events that pass the level-1 trigger move to the High-Level Trigger (HLT). The HLT takes place outside of the detector in software, and looks for properties such as a large amount of missing transverse energy, well defined leptons, and multiple high energy jets. Events that pass the HLT are stored and used for analysis. Because the specifics of the HLT are determined by software rather than hardware, the thresholds can be changed throughout the run of the detector in response to run conditions such as changes to pileup and luminosity. After the HLT is applied, the event rate is reduced to around 1000 per second, which are recorded for analysis.

Part IV

Measurement of WZ + Heavy Flavor

0.5 Introduction

The production of WZ in association with a heavy flavor jet represents an important background for many major analyses. This includes any process with multiple leptons and b-jets in the final state, such as $t\bar{t}H$, $t\bar{t}W$, and $t\bar{t}Z$. While precise measurements have been made of inclusive WZ production [?], $WZ +$ heavy flavor remains poorly understood. This is largely because the QCD processes involved in the production of the b-jet make it difficult to simulate accurately. This introduces a large uncertainty for analyses that include this process as a background.

We perform a study of the fully leptonic decay mode of this channel; that is, events where both the W and Z decay leptonically. Because WZ has no associated jets at leading order, while the major backgrounds for this channel tend to have high jet multiplicity, events with more than two jets are rejected. This gives a final state signature of three leptons and one or two jets.

Events that meet a preselection criteria are sorted into regions based on the b-tagging score of their associated jets. This is done to separate $WZ +$ b-jet events from $WZ +$ charm and $WZ +$ light jets. These regions are fit to data in order to make a more accurate estimate of the contribution of $WZ +$ heavy-flavor, where heavy-flavor jets include b-jets and charm jets. The full Run-2 dataset collected by the ATLAS detector, representing 139 fb^{-1} of data from pp collisions at $\sqrt{s} = 13 \text{ TeV}$, is used for this study.

The fiducial volume at particle level is defined based on the number of stable leptons and jets in each event. Three light leptons with total charge ± 1 and one or two associated jets are required. Only leptons which do not originate from hadron or τ decays are considered. The phase space definitions use dressed kinematics of the final state particles. Leptons are dressed by summing the momentum of photons within a cone of $\Delta R < 0.1$ of the lepton to correct the leptons energy. Particle level jets are reconstructed using the anti- k_t algorithm with a radius of $R = 0.4$. The kinematic selection applied to these objects is summarized below:

- Three light leptons with total charge ± 1 , $|\eta| < 2.5$
- OS lepton with $p_T > 10 \text{ GeV}$, SS leptons with $p_T > 20 \text{ GeV}$
- One OSSF lepton pair with $|M(l\bar{l}) - 91.2 \text{ GeV}| < 10 \text{ GeV}$
- One or two associated truth jets with $p_T > 25 \text{ GeV}$, $|\eta| < 2.5$, $R < 0.4$

The result of the fit is used to extract the cross-section in this fiducial region for $WZ + b$ and $WZ + c$ with one associated jet, and $WZ + b$ and $WZ + c$ with two associated jets, where the number and flavor of the jets is determined at particle level. Events with both charm and b-jets are counted as $WZ + b$. The analysis reports a cross-section measurement of $WZ + b$ and $WZ +$ charm, along with their correlations, for both 1-jet and 2-jet exclusive regions.

Section 0.6 details the data and Monte Carlo (MC) samples used in the analysis. The reconstruction of various physics objects is described in Section 0.7. Section 0.8 describes the event selection applied to these samples, along the definitions of the various regions used in the fit. The multivariate analysis techniques used to separate the tZ background from WZ + heavy flavor are described in Section 0.9. Section 0.17 describes the various sources of systematic uncertainties considered in the fit. Finally, the results of the analysis are summarized in Section 0.18, followed by a brief conclusion in Section 0.12.

0.6 Data and Monte Carlo Samples

0.6.1 Data Samples

This study uses a sample of proton-proton collision data collected by the ATLAS detector from 2015 through 2018 at an energy of $\sqrt{s} = 13$ TeV, which represents an integrated luminosity of 139 fb^{-1} [?]. This data set was collected with a bunch-crossing rate of 25 ns. All data used in this analysis was verified by data quality checks [?].

0.6.2 Monte Carlo Samples

Several different generators were used to produce Monte Carlo simulations of the signal and background processes. For all samples, the response of the ATLAS detector is simulated using GEANT4 [?]. The WZ signal samples are simulated using Sherpa 2.2.2 [?]. Specific information about the Monte Carlo samples being used can be found in Table 14.

Table 2: The configurations used for event generation of signal and background processes, including the event generator, matrix element (ME) order, parton shower algorithm, and parton distribution function (PDF).

Process	Event generator	ME order	Parton Shower	PDF
WZ, ZZ, WW	SHERPA 2.2.2	MEPS NLO	SHERPA	CT10 [?]
tZ	MG5_AMC [?]	NLO	PYTHIA 8	CTEQ6L1
tW	MG5_AMC (SHERPA 2.1.1)	NLO (LO multileg)	PYTHIA 8 (SHERPA)	NNPDF 3.0 NLO (NNPDF 3.0 NLO)
t <bar>t}(Z/γ^* → ll)</bar>	MG5_AMC	NLO	PYTHIA 8	NNPDF 3.0 NLO
tH	MG5_AMC (MG5_AMC)	NLO (NLO)	PYTHIA 8 (HERWIG++) [?]	NNPDF 3.0 NLO [?] (CT10 [?])
tHqb	MG5_AMC	LO	PYTHIA 8	CT10
tHW	MG5_AMC (SHERPA 2.1.1)	NLO (LO multileg)	HERWIG++ (SHERPA)	CT10 (NNPDF 3.0 NLO)
tWZ	MG5_AMC	NLO	PYTHIA 8	NNPDF 2.3 LO
t <bar>t}t, t<bar>t>t<bar>t}</bar></bar></bar>	MG5_AMC	LO	PYTHIA 8	NNPDF 2.3 LO [?]
t <bar>t}W⁺W⁻</bar>	MG5_AMC	LO	PYTHIA 8	NNPDF 2.3 LO
t <bar>t}</bar>	POWHEG-BOX v2 [?]	NLO	PYTHIA 8	NNPDF 3.0 NLO
t <bar>t}\gamma</bar>	MG5_AMC	LO	PYTHIA 8	NNPDF 2.3 LO
s-, t-channel, Wt single top	POWHEG-BOX v1 [?]	NLO	PYTHIA 6	CT10
qqVV, VVV				
Z → l ⁺ l ⁻	SHERPA 2.2.1	MEPS NLO	SHERPA	NNPDF 3.0 NLO

0.7 Object Reconstruction

All regions defined in this analysis share a common lepton, jet, and overall event preselection. The selection applied to each physics object is detailed here; the event preselection, and the selection used to define the various fit regions, is described in Section 0.8.

All events are required to be selected by dilepton triggers. The p_T thresholds of the dilepton trigger on two electrons were 12 GeV in 2015, 17 GeV in 2016, and 24 GeV in 2017 and 2018, while for the dimuon triggers the p_T thresholds on the leading (sub-leading) muon were 18 GeV (8 GeV) in 2015, and 22 GeV (8 GeV) in 2016–2018. For the electron+muon triggers, the p_T thresholds on the electron (muon) were 17 GeV (14 GeV) for all datasets.

Electron candidates are reconstructed from energy clusters in the electromagnetic calorimeter that are associated with charged particle tracks reconstructed in the inner detector [?]. Electron candidates are required to have $p_T > 10$ GeV and

$|\eta_{\text{cluster}}| < 2.47$. Candidates in the transition region between different electromagnetic calorimeter components, $1.37 < |\eta_{\text{cluster}}| < 1.52$, are rejected. A multivariate likelihood discriminant combining shower shape and track information is used to distinguish real electrons from hadronic showers (fake electrons). To further reduce the non-prompt electron contribution, the track is required to be consistent with originating from the primary vertex; requirements are imposed on the transverse impact parameter significance ($|d_0|/\sigma_{d_0} < 5$) and the longitudinal impact parameter ($|\Delta z_0 \sin \theta_\ell| < 0.5$ mm). Electron candidates are required to pass the TIGHTLH identification requirement detailed in [?].

Muon candidates are reconstructed by combining inner detector tracks with track segments or full tracks in the muon spectrometer [?]. Muon candidates are required to have $p_T > 10$ GeV and $|\eta| < 2.5$. The longitudinal impact parameter is the same for both electrons and muons, while muons are required to pass a slightly tighter transverse impact parameter selection, $|d_0|/\sigma_{d_0} < 3$. Muons are also required to pass Medium ID requirements, as detailed in [?]. Leptons are additionally required to pass a non-prompt BDT selection, described in detail in [?]. Optimized working points and scale factors for this BDT are taken from that analysis.

Jets are reconstructed from calibrated topological clusters built from energy deposits in the calorimeters using the anti- k_t algorithm [?], as well as information from the inner tracking detector, with a radius parameter $R = 0.4$. Jets with energy contributions likely arising from noise or detector effects are removed from consideration, and only jets satisfying $p_T > 25$ GeV and $|\eta| < 2.5$ are used in this analysis. For jets with $p_T < 60$ GeV and $|\eta| < 2.4$, a jet-track association algorithm is used to confirm that the jet originates from the selected primary vertex, in order to reject jets arising from pileup collisions [?].

In order to make a measurement of $WZ +$ heavy flavor it is necessary to distinguish these events from $WZ +$ light jets. For this purpose, the DL1r b-tagging algorithm is used to distinguish heavy flavor jets from lighter ones [?]. The DL1r algorithm uses jet kinematics, particularly jet vertex information, as input for a neural network which assigns each jet a score designed to reflect how likely that jet is to have originated from a b-quark.

From the output of the BDT, calibrated working points (WPs) are developed based on the efficiency of truth b-jets at particular values of the DL1r algorithm. The working points used in this analysis are summarized in Table 3.

WP b-jet eff.	Rejection	
	c-jet	light jet
85%	2.6	29
77%	4.9	130
70%	9.4	390
60%	27	1300

Table 3: c-jet and light-flavor jet rejections corresponding to each b-tagging Working Point by b-jet efficiency, evaluated on $t\bar{t}$ events.

As shown in table 3, a tighter WP will accept fewer b-jets, but reject a higher fraction of charm and light jets. Generally, analyses that include b-jets will use a fixed working point, for example, requiring that a jet pass the 70% threshold. By instead treating these working point as bins, e.g. events with jets that fall between the 85% and 77% WPs fall into one bin, while events with jets passing the 60% WP fall into another, additional information can be gained. This analysis uses each of these working points to form orthogonal regions in order to provide separation between $WZ + b$, $WZ + c$, and $WZ + \text{light}$.

Missing transverse momentum (E_T^{miss}) is used as part of the event selection. The missing transverse momentum vector is defined as the negative of the vector of the transverse momenta of all reconstructed physics objects as well as remaining unclustered energy, the latter of which is estimated from low- p_T tracks associated with the primary vertex but not assigned to a hard object, with object definitions taken from [?]. Light leptons considered in the E_T^{miss} reconstruction are required to have $p_T > 10$ GeV, while jets are required to have $p_T > 20$ GeV.

To avoid double counting objects and remove leptons originating from decays of hadrons, overlap removal is performed in the following order: any electron candidate within $\Delta R = 0.1$ of another electron candidate with higher p_T is removed; any electron candidate within $\Delta R = 0.1$ of a muon candidate is removed; any jet within $\Delta R = 0.2$ of an electron candidate is removed; if a muon candidate and a jet lie within $\Delta R = \min(0.4, 0.04 + 10[\text{GeV}] / p_T(\text{muon}))$ of each other, the jet is kept and the muon is removed if the jet has at least three associated tracks, otherwise the jet is removed and the muon is kept. This algorithm is applied to the preselected objects.

0.8 Event Selection and Signal Region Definitions

Events are required to pass a preselection described in Section 0.8.1. Those that pass this preselection are divided into various fit regions described in Section 0.8.2, based on the number of jets in the event, and the b-tag score of those jets.

0.8.1 Event Preselection

Events are required to include exactly three reconstructed light leptons passing the requirement described in 0.7, which have a total charge of ± 1 . As the opposite sign lepton is found to be prompt the vast majority of the time [?], it is required to have $p_T > 10$ GeV, while the same sign leptons are required to have $p_T > 20$ GeV to reduce the contribution of non-prompt leptons.

The invariant mass of at least one pair of opposite sign, same flavor leptons is required to fall within 10 GeV of the mass of the Z boson, 91.2 GeV. Events where one of the opposite sign pairs have an invariant mass less than 12 GeV are rejected in order to suppress low mass resonances.

An additional requirement is placed on the missing transverse energy, $E_T^{\text{miss}} \geq 20$ GeV. The transverse mass of the W candidate, defined as $\sqrt{2p_T^{\text{lep}} E_T^{\text{miss}} * (1 - \cos(\phi_{\text{lep}} - \phi_{E_T^{\text{miss}}}))}$, is required to be greater than 30 GeV. Here E_T^{miss} is the missing transverse energy, and the lepton considered is the lepton not included in the Z-candidate.

Events are required to have exactly one or two reconstructed. Events with more than two jets are rejected in order to reduce the contribution of backgrounds such as $t\bar{t}Z$ and $t\bar{t}W$, which tend to have higher jet multiplicity.

The WZ events are split into WZ + b, WZ + c, and WZ + light based on the truth flavor of the associated jet in the event, as determined by the presence of a b- or c-hadron within $R = 0.3$ of the jet. In this ordering b-jet supersedes charm, which supersedes light. That is, WZ + light events contain no charm and no b jets at truth level, WZ + c contain at least one truth charm and no b-jets, and WZ + b contains at least one truth b-jet.

0.8.2 Fit Regions

Once preselection has been applied, the remaining events are categorized into one of twelve orthogonal regions. The regions used in the fit are summarized in Table 4.

Table 4: A list of the regions used in the fit and the selection used for each.

Region	Selection
1j, $j_{85\%}$	$N_{\text{jets}} = 1, n_{\text{Jets_DL1r_85}} = 0$
1j, 85%-77%	$N_{\text{jets}} = 1, n_{\text{Jets_DL1r_85}} = 1, n_{\text{Jets_DL1r_77}} = 0$
1j, 77%-70%	$N_{\text{jets}} = 1, n_{\text{Jets_DL1r_77}} = 1, n_{\text{Jets_DL1r_70}} = 0$
1j, 70%-60%	$N_{\text{jets}} = 1, n_{\text{Jets_DL1r_70}} = 1, n_{\text{Jets_DL1r_60}} = 0$
1j, $\zeta_{60\%}$	$N_{\text{jets}} = 1, n_{\text{Jets_DL1r_60}} = 1, tZ \text{ BDT } \zeta < 0.12$
1j tZ CR	$N_{\text{jets}} = 1, n_{\text{Jets_DL1r_60}} = 1, tZ \text{ BDT } \zeta > 0.12$
2j, $j_{85\%}$	$N_{\text{jets}} = 2, n_{\text{Jets_DL1r_85}} = 0$
2j, 85%-77%	$N_{\text{jets}} = 2, n_{\text{Jets_DL1r_85}} = 1, n_{\text{Jets_DL1r_77}} = 0$
2j, 77%-70%	$N_{\text{jets}} = 2, n_{\text{Jets_DL1r_77}} = 1, n_{\text{Jets_DL1r_70}} = 0$
2j, 70%-60%	$N_{\text{jets}} = 2, n_{\text{Jets_DL1r_70}} = 1, n_{\text{Jets_DL1r_60}} = 0$
2j, $\zeta_{60\%}$	$N_{\text{jets}} = 2, n_{\text{Jets_DL1r_60}} = 1, tZ \text{ BDT } \zeta < 0.12$
2j tZ CR	$N_{\text{jets}} = 2, n_{\text{Jets_DL1r_60}} = 1, tZ \text{ BDT } \zeta > 0.12$

The working points discussed in Section 0.7 are used to separate events into fit regions based on the highest working point reached by a jet in each event. Because the background composition differs significantly based on the number of b-jets, events are further subdivided into 1-jet and 2-jet regions in order to minimize the impact of background uncertainties.

An unfolding procedure is performed to account for differences in the number of reconstructed jets compared to the number of truth jets in each event. In order to account for migration of WZ+1-jet and WZ+2-jet events between the 1-jet and 2-jet bins at reco level, the signal samples are separated based on the number of truth jets. Events with 0 jets or more than 3 jets at truth level, yet fall within one of the categories listed in Table 4, are categorized as WZ + other, and treated as background. The composition of the number of truth jets in each reco jet bin is taken from MC, with uncertainties in these estimates described in detail in Section 0.17.

An additional tZ control region is created based on the BDT described in Section 0.9. The region with 1-jet passing the 60% working point is split in two - a signal enriched region of events with a BDT score greater than 0.12, and a tZ control region including events with less than 0.12. This cutoff is optimized for significance of WZ + b.

0.8.3 Non-Prompt Lepton Estimation

Two processes that act as sources of non-prompt leptons appear in the analysis: $t\bar{t}$ and Z+jet production both produce two prompt leptons, but can meet the selec-

tion of this analysis when an additional non-prompt lepton appears in the event. The contribution of these processes is estimated with Monte Carlo simulations, which are validated using non-prompt enriched regions. These validation regions are used to derive correction factors and uncertainties for the non-prompt contribution.

$t\bar{t}$ events can produce two prompt leptons from the decay of each of the tops. These top decays produce two b-quarks, the decay of which can produce additional non-prompt leptons, which occasionally pass the event preselection. In order to validate that the Monte Carlo accurately simulates this process accurately, the MC prediction in a non-prompt $t\bar{t}$ enriched validation region is compared to data.

The $t\bar{t}$ validation region is similar to the preselection region - three leptons meeting the criteria described in Section 0.8 are required, and the requirements on E_T^{miss} remain the same. However, the selection requiring that a lepton pair form a Z-candidate are reversed. Events where the invariant mass of any two opposite sign, same flavor leptons falls within 10 GeV of 91.2 GeV are rejected. This ensures the $t\bar{t}$ validation region is orthogonal to the preselection region.

Further, because the jet multiplicity of $t\bar{t}$ events tends to be higher than WZ + jets, the number of jets in each event is required to be greater than 1. As b-jets are almost invariably produced from top decays, at least one b-tagged jet passing the 70% DL1r WP in each event is required.

Data is compared to MC predictions in the region for a variety of kinematic variable, as well as various b-tag WPs. A constant normalization discrepancy between data and MC predictions of approximately 10% is found, which is accounted for by applying a constant correction factor of 0.9 to the $t\bar{t}$ MC prediction. Once this correction factor has been applied, no significant modelling discrepancies, either in terms of shape or overall yield, are found in any of the kinematic distributions considered. As data and MC are found to agree within 20% for each of the b-tag WPs considered, a 20% systematic uncertainty on the $t\bar{t}$ prediction is included for the analysis.

Similar to $t\bar{t}$, a Z+jets validation region is produced in order to validate the MC predictions. The lepton requirements remain the same as the preselection region. Because no neutrinos are present for this process, the E_T^{miss} cut is reversed, requiring $E_T^{\text{miss}} > 30$ GeV. This also ensures this validation region is orthogonal to the preselection region. Further, the number of jets in each event is required to be greater than or equal to one.

While there is general agreement between data and MC, the shape of the p_T spectrum of the lepton from the W candidate is found to differ. This is the lepton not included in the Z-candidate, and in the case of Z+jets, this lepton is most often the non-prompt lepton. To account for this discrepancy, a variable correction factor is applied to Z+jets. χ^2 minimization of the W lepton p_T spectrum is performed to derive a correction factor.

The systematic uncertainty in the Z + jets prediction is evaluated by comparing data to MC for each of the continuous b-tag WPs. For each of the regions considered,

the data falls within 25% of the MC prediction once this correction factor has been applied. Therefore, a 25% systematic uncertainty is applied to Z + jets in the analysis.

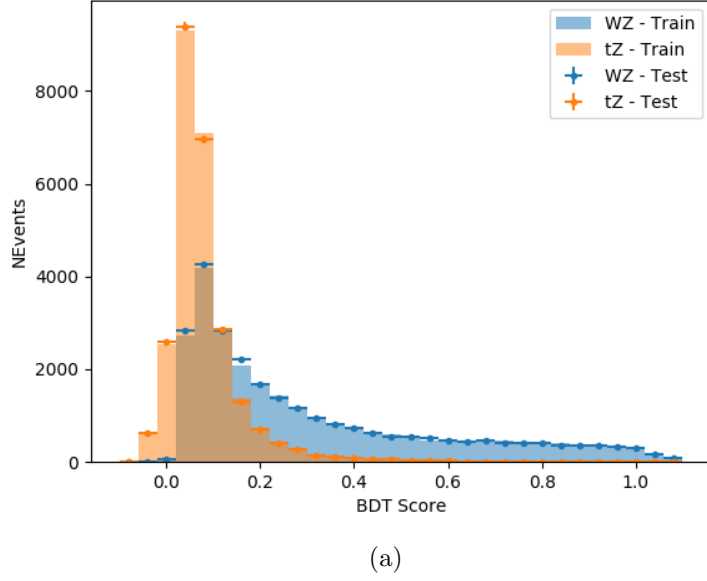
0.9 tZ Separation Multivariate Analysis

An important process to consider in this analysis is tZ: the top almost always decays into a W boson and b-quark, and when both the W and Z decay leptonically, this gives three leptons and a heavy flavor jet in the final state. Because tZ can produce a final state identical to the signal, it represents a predominant background in the most signal enriched regions. That is, the region with one jet passing the 60% DL1r WP. Therefore, a boosted decision tree (BDT) algorithm is trained using XGBoost [?] to separate WZ + heavy flavor from tZ using kinematic quantities. The result of this BDT is used to create a tZ enriched region in the fit, reducing its impact on the measurement of WZ + heavy flavor.

The kinematic variables used as inputs to train this BDT include the invariant mass of the reconstructed top candidate, the p_T of each of the leptons and associated jets, the invariant mass of each combination of lepton pairs, E_T^{miss} , the distance between each combination of leptons, $\Delta R(l\bar{l})$, and the distance between each lepton and the jet, $\Delta R(lj)$.

Here the top candidate is reconstructed based on the procedure described in section 6.1 of [?]. Broadly, the mass of the top quark candidate is reconstructed from the jet, the lepton not included in the Z-candidate, and a reconstructed neutrino. In the case that there is one jet in the event, there is only possible b-jet candidate. For events with two jets, the jet with the highest DL1r score is used.

The training samples included only events meeting the requirements of the 1-jet, $\geq 60\%$ region, i.e. passing all the selection described in section 0.8 and having exactly one jet which passes the tightest (60%) DL1r working point. A sample of 20,000 background (tZ) and signal (WZ+b) Monte Carlo events are used to train the BDT. And additional 5,000 events are reserved for testing the model, in order to prevent over-fitting. A total of 750 decision trees with a maximum depth of 6 branches are used to build the model. These parameters are chosen empirically, by training several models with different parameters and selecting the one that gave the best separation for the test sample. The results of the BDT training are shown in figure 0.9.1.



(a)

Figure 0.9.1: Distribution of the BDT response for $\text{WZ} + \mathbf{b}$ (blue) and $t\bar{Z}$ (orange) events, for both training and testing samples.

A BDT score of 0.12 is selected as a cutoff, where events with scores higher than this form a signal enriched region, and events with scores lower than this form a $t\bar{Z}$ control region. This cutoff is selected by varying the value of this cutoff in stat-only Asimov fits, and selecting the value that minimizes the statistical uncertainty on $\text{WZ} + \mathbf{b}$.

0.10 Systematic Uncertainties

The systematic uncertainties that are considered are summarized in Table 34. These are implemented in the fit either as a normalization factors or as a shape variation or both in the signal and background estimations. The numerical impact of each of these uncertainties is outlined in Section 0.18.

Table 5: Sources of systematic uncertainty considered in the analysis.

Systematic uncertainty	Components
Luminosity	1
Pileup reweighting	1
Physics Objects	
Electron	6
Muon	15
Jet energy scale	28
Jet energy resolution	8
Jet vertex fraction	1
Jet flavor tagging	131
E_T^{miss}	3
Total (Experimental)	194
Signal Modeling	
Shape modelling	3
Renormalization and factorization scales	5
nJet Migration	5
Background Modeling	
Cross section	15
Renormalization and factorization scales	12
Total (Signal and background modeling)	35
Total (Overall)	230

The uncertainty in the combined 2015–2018 integrated luminosity is 1.7% [?], obtained using the LUCID-2 detector [?] for the primary luminosity measurements.

The experimental uncertainties are related to the reconstruction and identification of light leptons and b-tagging of jets, and to the reconstruction of E_T^{miss} . The sources which contribute to the uncertainty in the jet energy scale (JES) [?] are decomposed into uncorrelated components and treated as independent sources of uncertainty in the analysis. A similar approach is used for the jet energy resolution (JER) uncertainty.

The uncertainties in the b-tagging efficiencies measured in dedicated calibration analyses [?] are also decomposed into uncorrelated components. The large number of components for b-tagging is due to the calibration of the distribution of the MVA discriminant for each individual WP bin.

The fit involves varying the overall normalization of signal templates over the regions described in Section 0.8.2, which are defined by the flavor and number of associ-

ated jets at truth-level. The modelling of these template shapes therefore significantly impacts the final result. Additional signal uncertainties, probing the shape of the signal templates as well as the rate of migrations between the number of truth-jets and reconstructed jets, are estimated by comparing estimates from the nominal Sherpa WZ samples with alternative WZ samples generated with POWHEG+PYTHIA8. Separate systematics are included in the fit for WZ + b , WZ + c and WZ + light, where the distribution among each of the fit regions is varied based on the prediction of the Powheg sample.

A similar approach is taken to account for uncertainties in migrations between the number of reco and truth jets. The fraction of events with 1 truth jet which fall into the 1 jet bin versus the 2 jet bin at reco level is compared for Sherpa and Powheg. The same is done for events with 2 truth jets. A systematic is included where events are shifted between the 1-jet and 2-jet regions based on the differences between these two shapes. This is done independently for each of the WZ + b , WZ + c , and WZ + light templates.

Additional systematics are included to account for the uncertainty in the contamination of 0 jet and 3 or more jet events (as defined at truth level) in the 1 and 2 reco jet bins. Because these events fall outside the scope of this measurement, these events are included as a background. As such, a normalization, rather than a shape, uncertainty is applied for this background. The number of WZ events with 0-jets and ≥ 3 -jets in the reconstructed 1-jet and 2-jet regions are compared for Sherpa and Powheg, and these differences are taken as separate normalization systematics on the yield of WZ+0-jet and WZ+ ≥ 3 -jet events.

Theoretical uncertainties applied to MC background predictions, including cross section, PDF, and scale uncertainties are taken from theory calculations, with the exception of non-prompt and diboson backgrounds. The cross-section uncertainty on tZ is taken from [?]. Derivation of the non-prompt background uncertainties, Z+jets and $t\bar{t}$, are explained in Section 0.8.3. These normalization uncertainties are chosen so as to account for the complete uncertainty in the non-prompt contribution, and therefore no additional modelling uncertainties are considered for Z+jets and $t\bar{t}$.

Due to its importance as a background, additional modelling uncertainties are considered for tZ. Alternative tZ samples with variations in scale and shower modelling are included as systematics. The other VV + heavy flavor processes (namely VV+b and VV+charm, which primarily consist of ZZ events) are also poorly understood, because these processes involve the same physics as WZ + heavy flavor, and have also not been measured. Therefore, a conservative 50% uncertainty is applied to those samples. While this uncertainty is large, it is found to have little impact on the significance of the final result.

The theory uncertainties applied to the MC estimates are summarized in Table 36.

Process	X-section [%]
WZ	QCD Scale: $^{+3.7}_{-3.4}$ PDF($+\alpha_S$): ± 3.1
tZ	X-sec: ± 15.2
t \bar{t} H (aMC@NLO+Pythia8)	QCD Scale: $^{+5.8}_{-9.2}$ PDF($+\alpha_S$): ± 3.6
t \bar{t} Z (aMC@NLO+Pythia8)	QCD Scale: $^{+9.6}_{-11.3}$ PDF($+\alpha_S$): ± 4
t \bar{t} W (aMC@NLO+Pythia8)	QCD Scale: $^{+12.9}_{-11.5}$ PDF($+\alpha_S$): ± 3.4
VV + b/charm (Sherpa 2.2.1)	± 50
VV + light (Sherpa 2.2.1)	± 6
t \bar{t}	± 20
Z + jets	± 25
Others	± 50

Table 6: Summary of theoretical uncertainties for normalization of MC predictions in the analysis.

0.11 Results

0.11.1 Fit Procedure

A maximum-likelihood fit is performed over the total yields in the various fit regions described in Section 0.8 in order to extract the best-fit value of the WZ + b and WZ + c jet contributions for events with both 1 and 2 associated jets.

Because the fit regions are defined by the number of associated jets at reco-level, the signal is split into separate samples based on the number of truth jets in order to account for differences in the number of truth jets compared to the number of reco-jets. The WZ + b, WZ + c and WZ + light contributions are separated into independent samples based on the number of truth jets in each event. WZ + 1 truth-jet and WZ + 2 truth-jets are treated as signal samples, while WZ + 0 truth-jets and WZ + $>=3$ truth-jets are treated as an additional background.

A maximum likelihood fit to data is performed simultaneously in the regions described in Section 0.8, summarized in figure 0.11.1. The six signal templates, which include WZ + b 1-jet, WZ + c 1-jet, WZ + light 1-jet, WZ + b 2-jets, WZ + c 2-jets, WZ + light 2-jets, are allowed to float, while the remaining background contributions are held fixed. Normalization factors for each of these templates are extracted from the fit. A simultaneous fit is performed over all 1-jet and 2-jet regions.

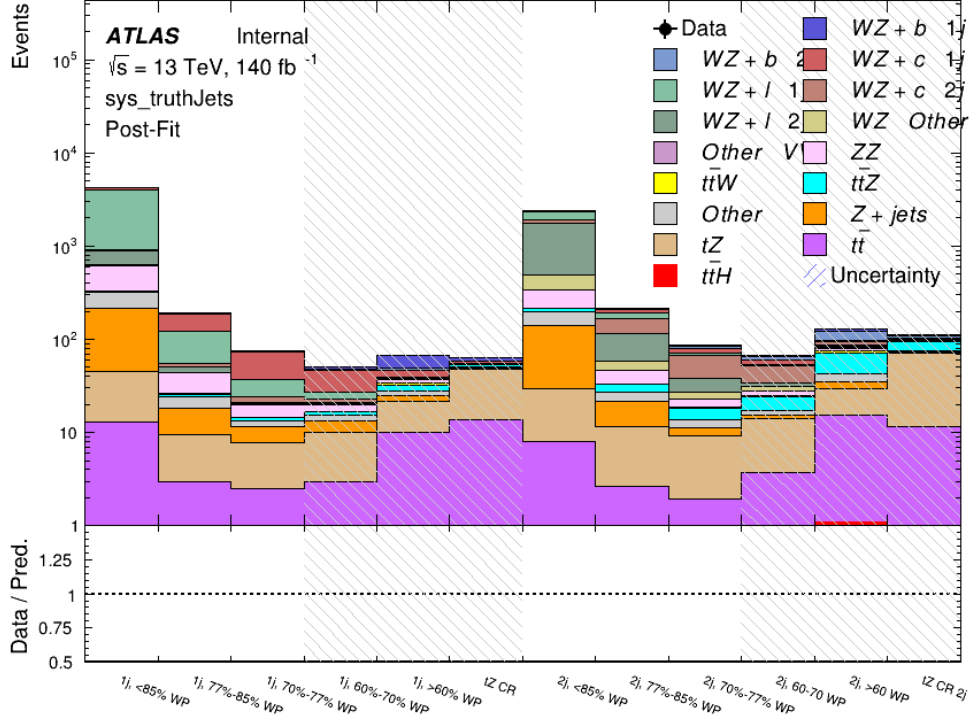


Figure 0.11.1: Post-fit summary of the fit regions.

Several alternative fit strategies are reported as well, including a measurement of $WZ + 1$ or 2 jets inclusively, a fit where tZ is allowed to float, and a case where tZ is included as part of the signal.

As described in Section 0.17, there are 230 systematic uncertainties that are considered as NPs in the fit. These NPs are constrained by Gaussian or log-normal probability density functions. The latter are used for normalisation factors to ensure that they are always positive. The expected number of signal and background events are functions of the likelihood. The prior for each NP is added as a penalty term, decreasing the likelihood as it is shifted away from its nominal value.

0.11.2 Results of the Simultaneous Fit

The results of the fit to an Asimov dataset for the fiducial regions considered, including both the normalization factors as well as the expected cross-sections, along with their uncertainties, are summarized in Table 7.

Process	μ	σ
WZ + b - 1-jet	$1.00^{+0.47}_{-0.43}(\text{stat})^{+0.32}_{-0.27}(\text{sys})$	$1.74^{+0.82}_{-0.75}(\text{stat})^{+0.53}_{-0.48}(\text{sys}) \text{ fb}$
WZ + c - 1-jet	$1.00^{+0.18}_{-0.17}(\text{stat})^{+0.19}_{-0.17}(\text{sys})$	$14.6^{+2.5}_{-2.3}(\text{stat})^{+2.6}_{-2.3}(\text{sys}) \text{ fb}$
WZ + b - 2-jet	$1.00^{+0.53}_{-0.51}(\text{stat})^{+0.39}_{-0.34}(\text{sys})$	$2.5^{+1.3}_{-1.3}(\text{stat})^{+0.95}_{-0.83}(\text{sys}) \text{ fb}$
WZ + c - 2-jet	$1.00^{+0.25}_{-0.24}(\text{stat})^{+0.32}_{-0.27}(\text{sys})$	$12.7^{+3.3}_{-3.2}(\text{stat})^{+3.9}_{-3.4}(\text{sys}) \text{ fb}$

Table 7: Normalization factors and cross-sections extracted from the fit for each of the fiducial regions considered

An expected significance of 2.0σ is observed for WZ + b with 1-jet, and 1.7σ for WZ + \bar{b} with two jets. A summary of the correlations between these various measurements is shown in Figure 0.11.2.

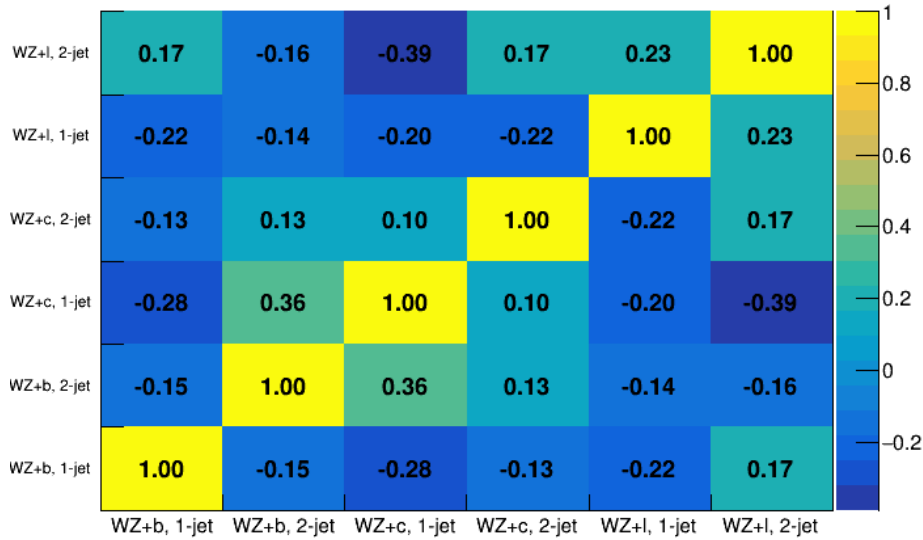


Figure 0.11.2: Correlations between the various measured components of WZ.

The impact of each NP is calculated by performing the fit with the parameter of interest held fixed, varied from its fitted value by its uncertainty, and calculating $\Delta\mu$ relative to the baseline fit. The impact of the most significant sources of systematic uncertainties on WZ + b and WZ + c with one associated jet are summarized in Table 8-9.

Uncertainty Source	$\Delta\sigma/\sigma_{\text{nominal}}$	
Jet Energy Scale	0.14	-0.15
WZ + light, 1-jet cross-section	0.12	-0.14
WZ + c, 1-jet cross-section	-0.09	0.11
tZ Modelling (shower tune)	-0.07	0.08
Other Diboson + b cross-section	-0.07	0.07
tZ cross-section	-0.06	0.08
Jet Energy Resolution	-0.07	0.07
WZ + b 1j/2j Migration	0.08	-0.07
Luminosity	-0.06	0.07
Flavor tagging	0.05	0.05
t̄t cross-section	-0.05	0.05
Total Systematic Uncertainty	0.28	0.33

Table 8: Summary of the most significant sources of systematic uncertainty on the measurement of WZ + b with exactly one associated jet.

Uncertainty Source	$\Delta\sigma/\sigma_{\text{nominal}}$	
WZ + c 1j/2j migration	0.12	-0.09
Flavor Tagging	0.09	0.08
WZ + b, 1-jet cross-section	-0.04	0.05
Luminosity	-0.04	0.04
Jet Energy Resolution	0.04	0.04
WZ + b, 2-jet cross-section	0.04	-0.03
WZ cross-section - QCD scale	-0.04	0.04
Jet Energy Scaling	0.04	0.02
WZ cross-section - PDF	-0.03	0.03
WZ + light, 1-jet cross-section	0.03	-0.03
total	0.19	0.17

Table 9: Summary of the most significant sources of systematic uncertainty on the measurement of WZ + c with exactly one associated jet.

The impact of the most significant systematic uncertainties on the 2-jet fiducial regions are summarized in Table 10-11.

Uncertainty Source	$\Delta\sigma/\sigma_{\text{nominal}}$	
WZ + c 2-jet cross-section	-0.13	0.16
WZ + l 2-jet cross-section	0.12	-0.09
ttZ cross-section - QCD scale	-0.10	0.13
Luminosity	-0.11	0.12
WZ + b 1-jet cross-section	-0.11	0.10
Jet Energy Scale	-0.11	0.11
tZ cross-section	-0.11	0.11
WtZ cross-section	-0.07	0.07
Flavor tagging	0.05	0.05
Other VV + b cross-section	-0.05	0.05
Total	0.36	0.37

Table 10: Summary of the most significant sources of systematic uncertainty on the measurement of WZ + b with 2 associated jets.

Uncertainty Source	$\Delta\sigma/\sigma_{\text{nominal}}$	
WZ + c 1j/2j migration	-0.17	0.25
Flavor Tagging	0.14	0.13
WZ + b, 1-jet cross-section	-0.09	0.09
Jet Energy Scale	0.06	0.08
Jet Energy Resolution	0.05	0.05
WZ >=3j/2j migration	-0.04	0.04
WZ + c 2j/1j migration	-0.04	0.04
WZ cross-section - QCD scale	-0.04	0.04
WZ + light modelling	0.04	-0.03
Luminosity	-0.03	0.03
total	0.27	0.32

Table 11: Summary of the most significant sources of systematic uncertainty on the measurement of WZ + c with 2 associated jets.

0.11.3 Inclusive 1-2 Jet Fit

An alternative fit is performed which combines the WZ + 1-jet and WZ + 2-jet samples rather than fitting them independently. This is done primarily as a cross-check of the nominal analysis, to see if measuring 1-jet and 2-jet events separately and combining them gives drastically different results than measuring them together.

For this study, three signal templates, WZ + b, WZ + c and WZ + light, are fit to data, and the systematics accounting for migrations between 1-jet and 2-jet bins are removed. All other background and nuisance parameters remain the same as the nominal fit.

The measured μ value for WZ + b is $\mu = 1.00^{+0.30}_{-0.29}(\text{stat})^{+0.25}_{-0.23}(\text{sys})$, with a significance of 2.8σ , and the uncertainty on WZ + c is $\mu = 1.00 \pm 0.12(\text{stat}) \pm 0.13(\text{sys})$. This is compared to combined uncertainty of $\mu = 1.00^{+0.32}_{-0.30}(\text{stat})^{+0.24}_{-0.23}(\text{sys})$ for WZ + b when 1-jet and 2-jet events are measured separately and then combined.

A post-fit summary plot of the fit regions is shown in Figure 0.11.3:

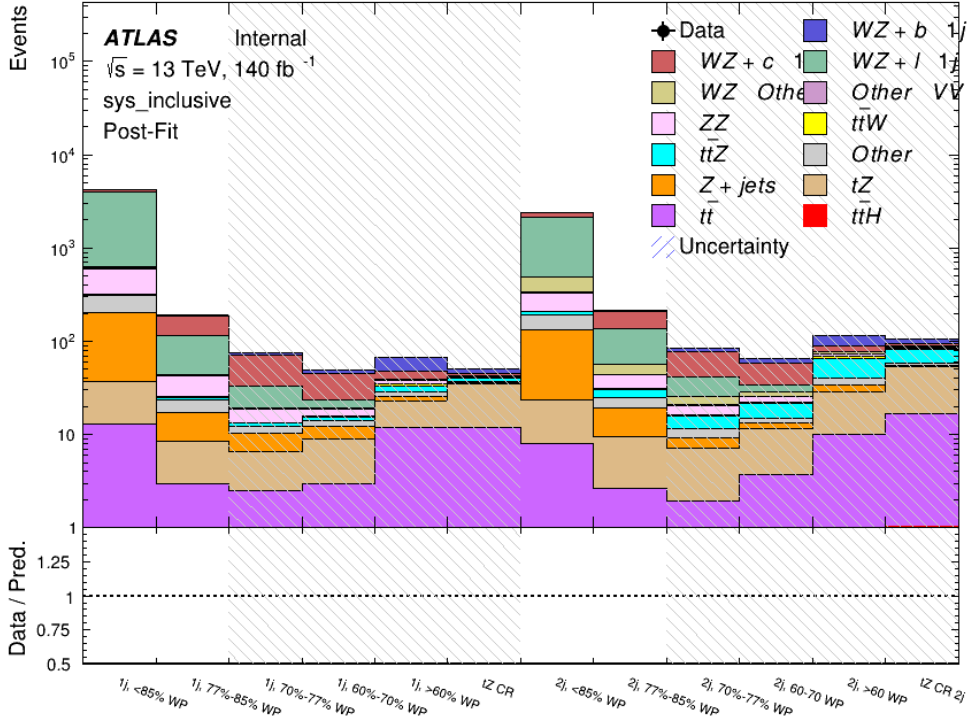


Figure 0.11.3: Post-fit summary of the fit regions.

The impact of the most significant sources of systematic uncertainties on the measurement of WZ + b is summarized in Table 12.

Uncertainty Source	$\Delta\mu$	
WZ + light cross-section	0.13	-0.12
WZ + c cross-section	-0.10	0.12
Jet Energy Scale	0.08	0.13
tZ cross-section	-0.10	0.10
Jet Energy Resolution	-0.10	0.10
Luminosity	-0.08	0.09
Other Diboson + b cross-section	-0.07	0.07
Flavor tagging	0.05	0.05
t <bar>t</bar>	-0.05	0.05
WZ cross-section - QCD scale	-0.04	0.03
Total Systematic Uncertainty	0.28	0.32

Table 12: Summary of the most significant sources of systematic uncertainty on the measurement of $WZ + b$ with one or two associated jets.

0.11.4 Alternate tZ Inclusive Fit

0.11.4.1 tZ Inclusive Fit

While tZ is often considered as a distinct process form WZ + b, this could also be considered part of the signal. Alternative studies are performed where, using the same framework as the nominal analysis, a measurement of WZ + b is performed that includes tZ as part of WZ+b.

Because of this change, the tZ CR is no longer necessary, and only the five pseudo-continuous b-tag regions are used in the fit. Further, systematics related to the tZ cross-section are removed from the fit, as they are now encompassed by the normalization measurement of WZ + b. All other systematic uncertainties are carried over from the nominal analysis.

An expected WZ + b cross-section of $4.1^{+0.78}_{-0.74}(\text{stat})^{+0.53}_{-0.52}(\text{sys}) \text{ fb}$ is extracted from the fit, with an expected significance of 4.0σ .

The impact of the predominate systematics are summarized in Table 44.

Uncertainty Source	$\Delta\mu$	
WZ + light cross-section	0.08	-0.08
Jet Energy Scale	-0.06	0.08
Luminosity	-0.05	0.06
WZ + c cross-section	-0.04	0.05
Other Diboson + b cross-section	-0.04	0.04
WZ cross-section - QCD scale	-0.04	0.03
t̄ cross-section	-0.03	0.03
Jet Energy Resolution	-0.03	0.03
Flavor tagging	-0.03	0.03
Z+jets cross section	-0.02	0.02
Total Systematic Uncertainty	-0.15	0.16

Table 13: Summary of the most significant sources of systematic uncertainty on the measurement of WZ + b with exactly one associated jet.

0.11.4.2 Floating tZ

In order to quantify the impact of the tZ uncertainty on the fit, an alternate fit strategy is used where the tZ normalization is allowed to float. This normalization factor replaces the cross-section uncertainty on tZ, and all other parameters of the fit remain the same.

An uncertainty of 17% on the normalization of tZ is extracted from the fit, compared to a theory uncertainty of 15% applied to the tZ cross-section. The measured uncertainties on WZ remain the same.

0.12 Conclusion

A measurement of WZ + heavy flavor is performed using 140 fb^{-1} of $\sqrt{s} = 13$ TeV proton-proton collision data collected by the ATLAS detector at the LHC. The expected cross-section of WZ + b with 1-jet is $1.74^{+0.82}_{-0.75}(\text{stat})^{+0.53}_{-0.48}(\text{sys}) \text{ fb}$, and $14.6 \pm 2.5(\text{stat}) \pm 2.3(\text{sys}) \text{ fb}$ for WZ + c, with a correlation of -0.22 between them. An expected significance of 2.0 is observed for WZ + b in this region.

For the 2-jet regions, an expected significance of 1.7 is observed for WZ + b, with an expected cross-section of $2.5^{+1.3}_{-1.3}(\text{stat})^{+0.95}_{-0.83}(\text{sys}) \text{ fb}$. For WZ + c, a cross-section of $12.7 \pm 3.2(\text{stat}) \pm 2.7(\text{sys}) \text{ fb}$ is expected for 2-jet events. A correlation of -0.26 is observed for WZ + b and WZ + c.

This section will be include final results once unblinded.

Part V

Differential Studies of $t\bar{t}H$

Multilepton

0.13 Data and Monte Carlo Samples

0.13.1 Data Samples

The study uses proton-proton collision data collected by the ATLAS detector from 2015 through 2018, which represents an integrated luminosity of 139 fb^{-1} [?] and an energy of $\sqrt{s} = 13 \text{ TeV}$. All data used in this analysis was included in one of the Good Run Lists verified by Data Quality checks [?].

0.13.2 Monte Carlo Samples

Several Monte Carlo (MC) generators were used to simulate both signal and background processes. For all of these, the effects of the ATLAS detector are simulated in GEANT4 [?]. The specific event generator used for each of these MC samples is listed in Table 14. A Higgs mass of 125 GeV is assumed in all simulations.

Table 14: The configurations used for event generation of signal and background processes, including the event generator, matrix element (ME) order, parton shower algorithm, and parton distribution function (PDF).

Process	Event generator	ME order	Parton Shower	PDF
$t\bar{t}H$	MG5_AMC	NLO	PYTHIA 8	NNPDF 3.0 NLO [?]
	(MG5_AMC)	(NLO)	(HERWIG++)	(CT10 [?])
$t\bar{t}W$	MG5_AMC	NLO	PYTHIA 8	NNPDF 3.0 NLO
	(SHERPA 2.1.1)	(LO multileg)	(SHERPA)	(NNPDF 3.0 NLO)
$t\bar{t}(Z/\gamma^* \rightarrow ll)$	MG5_AMC	NLO	PYTHIA 8	NNPDF 3.0 NLO
VV	SHERPA 2.2.2	MEPS NLO	SHERPA	CT10
$t\bar{t}$	POWHEG-BOX v2 [?]	NLO	PYTHIA 8	NNPDF 3.0 NLO
$t\bar{t}\gamma$	MG5_AMC	LO	PYTHIA 8	NNPDF 2.3 LO
tZ	MG5_AMC	LO	PYTHIA 6	CTEQ6L1
$tHqb$	MG5_AMC	LO	PYTHIA 8	CT10
tHW	MG5_AMC	NLO	HERWIG++	CT10
	(SHERPA 2.1.1)	(LO multileg)	(SHERPA)	(NNPDF 3.0 NLO)
tWZ	MG5_AMC	NLO	PYTHIA 8	NNPDF 2.3 LO
$t\bar{t}t, t\bar{t}t\bar{t}$	MG5_AMC	LO	PYTHIA 8	NNPDF 2.3 LO
$t\bar{t}W^+W^-$	MG5_AMC	LO	PYTHIA 8	NNPDF 2.3 LO
s-, t-channel, Wt single top	POWHEG-BOX v1 [?]	NLO	PYTHIA 6	CT10
$qqVV, VVV$				
$Z \rightarrow l^+l^-$	SHERPA 2.2.1	MEPS NLO	SHERPA	NNPDF 3.0 NLO

The signal sample ($t\bar{t}H$) is modelled at NLO with POWHEG-BOX v2 using the NNPDF2.0 parton distribution function (PDF) [?]. Parton showering and hadronisation were modelled with PYTHIA 8.2 [?]. The $t\bar{t}H$ sample is normalized to a cross-section of 507^{+35}_{-50} fb based on NLO calculations. Uncertainties are based on varying the QCD factorisation and renormalisation scale, as well as uncertainties in the PDF and α_s .

The $t\bar{t}W$ background is simulated using Sherpa 2.2.1 with the NNPDF3.0 NLO PDF. The matrix element is calculated with up to one additional parton at NLO, and up to two at LO. As explained in detail in [?], the $t\bar{t}W$ contribution predicted by MC is found disagree significantly with what is observed in data. While an effort is currently being undertaken to measure $t\bar{t}W$ more accurately, the approached used by the 79.8 fb^{-1} $t\bar{t}H$ analysis is used here: A normalization factor of 1.68 is applied to the MC estimate of $t\bar{t}W$ and additional systematic uncertainties on $t\bar{t}W$ are included to account for this modelling descrepancy, as outlined in Section 0.17.

The $t\bar{t}(Z/\gamma^*)$ process is simulated with the MADGRAPH5_AMC@NLO generator, using NNPDF3.0. Diboson processes are generated with SHERPA 2.2.2 at NLO precision for one extra parton, and at LO for up to three extra partons.

The “fake”, or non-prompt, background comes primarily from leptons originating from hadron decays, leptons with missidentified charge, and photon conversions. While the main $t\bar{t}H$ analysis is currently refining a data-driven approach for estimating the contribution of events with non-prompt leptons, at the time of this note this strategy has not been completely developed for the full Run-2 dataset. Therefore, the non-prompt contribution is estimated with MC, while applying normalization corrections and systematic uncertainties derived from data driven techniques developed for the 79.8 fb^{-1} $t\bar{t}H/t\bar{t}W$ analysis [?].

The primary contribution to the non-prompt lepton background is from $t\bar{t}$ production, with $V+jets$ and single-top as much smaller sources. Estimation of this background is done primarily using an inclusive $t\bar{t}$ sample, with corrections applied based on data driven methods. This sample is generated using POWHEG, with PYTHIA8 performing the parton shower and fragmentation. Likelihood fits over several control regions enriched with these non-prompt backgrounds are fit to data in order to derive normalization factors for these backgrounds. The specific normalization factors and uncertainties applied to the non-prompt contributions are listed in Section 0.17.

Other processes, such as tH , tZ , $t\bar{t}WW$ and $t\bar{t}t\bar{t}$, are expected to make minor contributions to the total background. The generators and setting used for these backgrounds are summarized in Table 14.

0.14 Object Reconstruction

All analysis channels considered in this note share a common object selection for leptons and jets, as well as a shared trigger selection. Events are required to be selected by dilepton triggers. The p_T thresholds of the dilepton trigger on two electrons were 12 GeV in 2015, 17 GeV in 2016, and 24 GeV in 2017 and 2018, while for the dimuon triggers the p_T thresholds on the leading (sub-leading) muon were 18 GeV (8 GeV) in 2015, and 22 GeV (8 GeV) in 2016–2018. For the electron+muon triggers, the p_T thresholds on the electron (muon) were 17 GeV (14 GeV) for all datasets.

Electron candidates are reconstructed from energy clusters in the electromagnetic calorimeter that are associated with charged particle tracks reconstructed in the inner detector [?]. Electron candidates are required to have $p_T > 10$ GeV and $|\eta_{\text{CLUSTER}}| < 2.47$. Candidates in the transition region between different electromagnetic calorimeter components, $1.37 < |\eta_{\text{CLUSTER}}| < 1.52$, are rejected. A multivariate likelihood discriminant combining shower shape and track information is used to distinguish prompt electrons from nonprompt leptons, such as those originating from hadronic showers.

To further reduce the non-prompt contribution, the track of each electron is required to originate from the primary vertex; requirements are imposed on the transverse impact parameter significance ($|d_0|/\sigma_{d_0}$) and the longitudinal impact parameter ($|\Delta z_0 \sin \theta_\ell|$). Muon candidates are reconstructed by combining inner detector tracks with track segments or full tracks in the muon spectrometer [?]. Muon candidates are required to have $p_T > 10$ GeV and $|\eta| < 2.5$.

All leptons are required to pass a non-prompt BDT selection developed by the main $t\bar{t}H/t\bar{t}W$ analysis, described in detail in [?]. Optimized working points and scale factors for this BDT are taken from that analysis. This BDT and the WPs used are summarized in Appendix .1,

Jets are reconstructed from calibrated topological clusters built from energy deposits in the calorimeters [?], using the anti- k_t algorithm with a radius parameter $R = 0.4$. Particle Flow, or PFlow, jets are used in the analysis, which are hadronic objects reconstructed using information from both the tracker and the calorimeter. Jets with energy contributions likely arising from noise or detector effects are removed from consideration [?], and only jets satisfying $p_T > 25$ GeV and $|\eta| < 2.5$ are used in this analysis. For jets with $p_T < 60$ GeV and $|\eta| < 2.4$, a jet-track association algorithm is used to confirm that the jet originates from the selected primary vertex, in order to reject jets arising from pileup collisions [?].

Each analysis channel used in this analysis includes b-jets in the final state. These are identified using the DL1r b-tagging algorithm, which uses jet vertex and kinematic information to distinguish heavy and light flavored jets. These features are used as inputs to a neural network, the output of which is used to form calibrated working points (WPs) based on how likely a jet is to have originated from a b-quark. This analysis uses the 70% DL1r WP - implying an efficiency of 70% for truth b-jets - for selecting b-tagged jets.

Because all $t\bar{t}H - ML$ channels considered include multiple neutrinos, missing transverse energy (E_T^{miss}) is present in each event. The missing transverse momentum vector is defined as the inverse of the sum of the transverse momenta of all reconstructed physics objects as well as remaining unclustered energy, the latter of which is estimated from low- p_T tracks associated with the primary vertex but not assigned to a hard object [?].

To avoid double counting objects and remove leptons originating from decays of hadrons, overlap removal is performed in the following order: any electron candidate within $\Delta R = 0.1$ of another electron candidate with higher p_T is removed; any electron candidate within $\Delta R = 0.1$ of a muon candidate is removed; any jet within $\Delta R = 0.2$ of an electron candidate is removed; if a muon candidate and a jet lie within $\Delta R = \min(0.4, 0.04 + 10[\text{GeV}] / p_T(\text{muon}))$ of each other, the jet is kept and the muon is removed if the jet has three or more tracks, otherwise the muon is kept and the jet is removed.

0.15 Higgs Momentum Reconstruction

Reconstructing the momentum of the Higgs boson is a particular challenge for channels with leptons in the final state: Because all channels include at least two neutrinos in the final state, the Higgs can never be fully reconstructed. However, the momentum spectrum can be well predicted by a neural network when provided with the kinematics of the Higgs Boson decay products - as verified by studies detailed in Appendix .3.3. With this in mind, several layers of MVAs are used to reconstruction the Higgs momentum:

The first layer is a model designed to select which jets are most likely to be the b-jets that came from the top decay, detailed in Section 0.15.2. As described in Section 0.15.3, the kinematics of these jets and possible Higgs decay products are fed into the second layer, which is designed to identify the decay products of the Higgs Boson itself. The kinematics of the particles this layer identifies as most likely to have originated from the Higgs decay are then fed into yet another neural-network, which predicts the momentum of the Higgs (0.15.4). For the 3l channel, because the Higgs can decay into either one lepton and two jets or two leptons, an additional MVA is used to determine the decay mode of the Higgs boson in the 3l channel (0.15.5).

Models are trained on Monte Carlo simulations of $t\bar{t}H$ events generated using MG5_AMC. For all of these models, the Keras neural network framework, with Tensorflow 2.0 as the backend [?], is used, and the number of hidden layers and nodes are determined using grid search optimization. Each neural network uses the LeakyReLU activation function, a learning rate of 0.01, and the Adam optimization algorithm, as alternatives are found to either decrease or have no impact on performance. Batch normalization is applied after each layer in order to stabilize the

model and decrease training time. For the classification algorithms (b-jet matching, Higgs reconstruction, and $3l$ decay identification) binary-cross entropy is used as the loss function, while the p_T reconstruction algorithm uses MSE.

The specific inputs features used for each model are arrived at through a process of trial and error - features considered potentially useful are tried, and those that are found to increase performance are included. While each model includes a relatively large number of features, some using upwards of 30, this inclusive approach is found to maximize the performance of each model while decreasing the variance compared to a reduced number of inputs. Each input feature is validated by comparing MC simulations to 79.8 fb^{-1} of data, with the full set of features shown in Section .3.

0.15.1 Physics Object Truth Matching

Machine Learning algorithms are trained to identify the decay products of the Higgs Boson using MC simulations of $t\bar{t}H$ events. The kinematics of the reconstructed physics objects, as well as event level variables such the jet multiplicity and missing energy, used as inputs, with the parent ID taken from the truth record used to label the data. The objects considered include light leptons and jets.

Reconstructed physics objects are matched to particle level objects in the Monte Carlo, in order to identify the parent particle of these reconstructed objects. Reconstructed jets are matched to truth jets based on the requirements that the reco jet and truth jet fall within $\Delta R < 0.4$, and the two objects have a p_T that agrees within 10%. Truth level and reco level leptons are required to have the same flavor, a $\Delta R < 0.1$, and p_T that agree within 10%. Events where no match can be found between the particle level decay products and the reconstructed objects are not included in training.

Leptons considered as possible Higgs and top decay candidates are required to pass the selection described in Section 0.14. For jets, however, it is found that a large fraction that originate from either the top decay or the Higgs decay fall outside the selection described in Section 0.14. Specifically, jets from the Higgs decay tend to be soft, with 32% having $p_T < 25 \text{ GeV}$. Therefore jets with $p_T < 15 \text{ GeV}$ are considered as possible candidates in the models described below. By contrast, less than 5% of the jets originating from the Higgs fall below this p_T threshold. The jets are found to be well modeled even down to this low p_T threshold, as shown in Section 0.16.1. The impact of using different p_T selection for the jet candidates is considered in detail in Section .3.6. The overlap removal selection is not applied to the objects considered in the models.

0.15.2 b-jet Identification

Including the kinematics of the b-jets that originate from the top decay is found to improve the identification of the Higgs decay products, and improve the

accuracy with which the Higgs momentum can be reconstructed. Because these b-jets are reconstructed by the detector with high efficiency (just over 90% of the time), and can be identified relatively consistently, the first step in reconstructing the Higgs is selecting the b-jets from the top decay.

Exactly two b-jets are expected in the final state of $t\bar{t}H - ML$ events. However, in both the 3l and 2lSS channels, only one or more b-tagged jets are required (where the 70% DL1r b-tag working point is used). Therefore, for events which have exactly one, or more than two, b-tagged jets, deciding which combination of jets correspond to the top decay is non-trivial. Further, events with 1 b-tagged jet represent just over half of all $t\bar{t}H - ML$ events. Of those, both b-jets are reconstructed by the detector 75% of the time. Therefore, rather than adjusting the selection to require exactly 2 b-tagged jets, and losing more than half of the signal events, a neural network is used to predict which pair of jets is most likely to correspond to truth b-jets.

Once the network is trained, kinematic variables for all possible pairings of jets are fed into the model, and the pair of jets with the highest output score are taken to be b-jets in successive steps of the analysis.

An alternate approach is considered, where information about all jets in each event are used as the feature set, and the model is tasked with identifying which two originated from the top decay. While this approach is found to underperform the nominal approach, and therefore not used in the analysis, the results are documented in Appendix .3.4.

0.15.2.1 2lSS Channel

For the 2lSS channel, the input features shown in Table 15 are used for training. Here j_0 and j_1 are the two jet candidates, while l_0 and l_1 are the two leptons in the event, both ordered by p_T . jet DL1r is an integer corresponding to the calibrated b-tagging working points reached by each jet, where 5 represents the tightest working point and 1 represents the loosest. The variables nJets DL1r 60% and nJets DL1r 85% represent the number of jets in the event passing the 60% and 85% b-tag working points, respectively.

jet p_T 0	jet p_T 1	Lepton p_T 0
Lepton p_T 1	jet η 0	jet η 1
$\Delta R(j_0)(j_1)$	$M(j_0 j_1)$	$\Delta R(l_0)(j_0)$
$\Delta R(l_0)(j_1)$	$\Delta R(l_1)(j_0)$	$\Delta R(l_1)(j_1)$
$M(l_0 j_0)$	$M(l_0 j_1)$	$M(l_1 j_0)$
$M(l_1 j_1)$	jet DL1r 0	jet DL1r 1
nJets OR DL1r 85	nJets OR DL1r 60	$\Delta R(j_0 l_0)(j_1 l_1)$
$\Delta R(j_0 l_1)(j_1 l_0)$	$p_T(j_0 j_1 l_0 l_1 E_T^{\text{miss}})$	$M(j_0 j_1 l_0 l_1 E_T^{\text{miss}})$
$\Delta\phi(j_0)(E_T^{\text{miss}})$	$\Delta\phi(j_1)(E_T^{\text{miss}})$	HT jets
nJets	E_T^{miss}	

Table 15: Input features used in the b-jet identification algorithm for the 2lSS channel

As there are far more incorrect combinations than correct ones, by a factor of more than 20:1, the training set is resampled to reduce the fraction of incorrect combinations. A random sample of 5 million incorrect entries are used for training, along with around 1 million correct entries. 10% of the dataset is set aside for testing, leaving around 5 million datapoints for training.

The difference between the distributions for a few of these features for the "correct" (i.e. both jets are truth b-jets), and "incorrect" combinations are shown in Figure 0.15.1. The correct and incorrect contributions are scaled to the same integral, so as to better demonstrate the differences in the distributions.

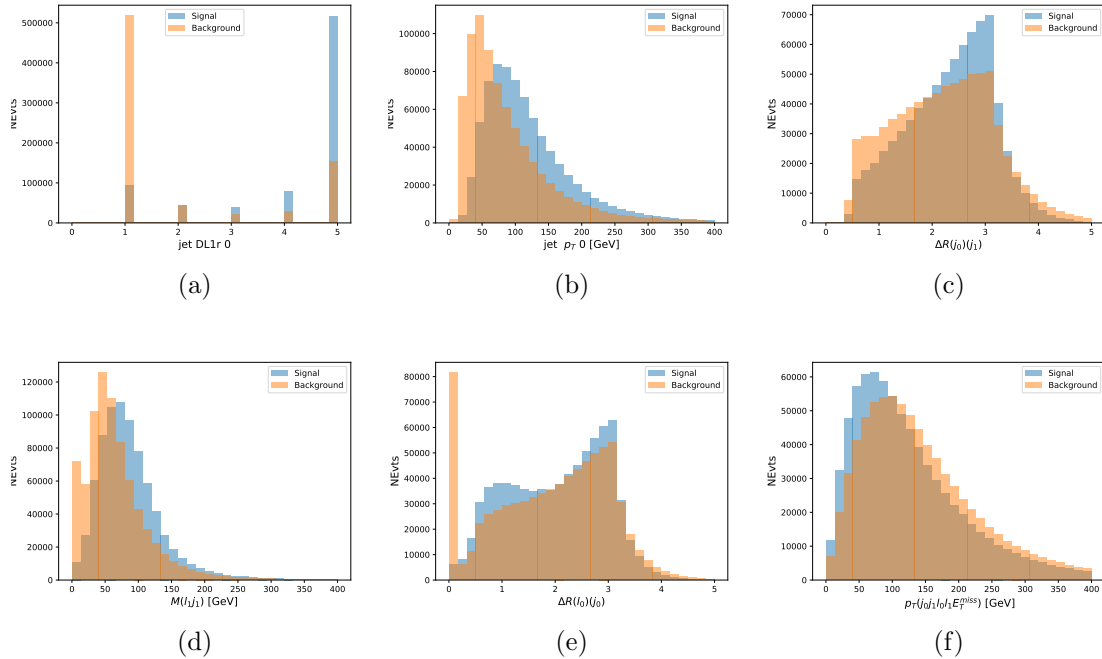


Figure 0.15.1: Input features for top2lSS training. The signal in blue represents events where both jet candidates are truth b-jets from top decays, and the orange is all other combinations. Each are scaled to the same number of events. (a) shows the DL1r working point of leading jet, (b) shows the p_T of the leading jet, (c) shows the ΔR of the two jets, (d) the invariant mass of lepton 1 and jet 1, (e) the ΔR of lepton 0 and jet 0, and (f) the p_T of both jets, both leptons, and the E_T^{miss} .

The modeling of these inputs is validated against data, with Figure 0.15.2 showing good general agreement between data and MC. Plots for the complete list of features can be found in Appendix .3.

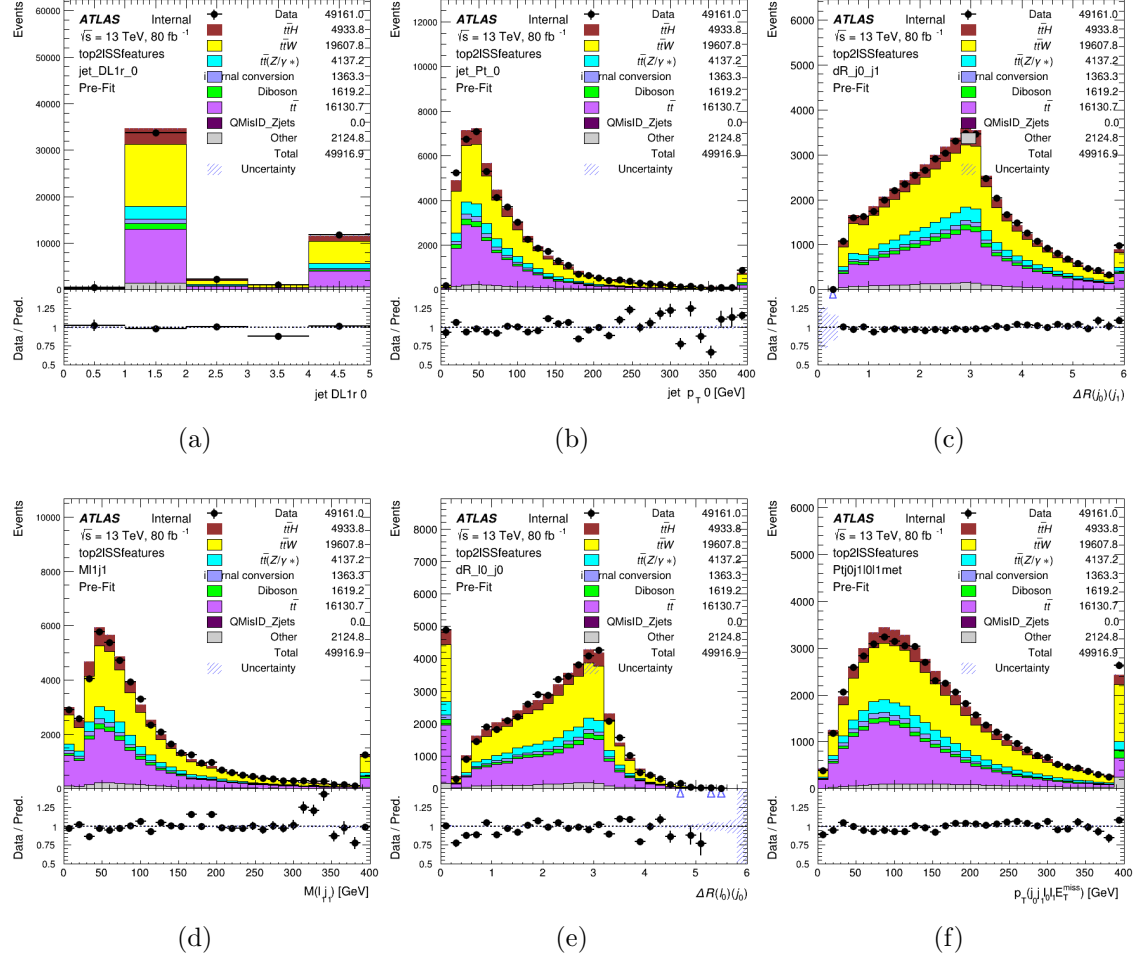


Figure 0.15.2: Data/MC comparisons of input features for top2lSS training for 79.8 fb^{-1} of data. (a) shows the DL1r working point of leading jet, (b) shows the p_T of the leading jet, (c) shows the ΔR of the two jets, (d) the invariant mass of lepton 1 and jet 1, (e) the ΔR of lepton 0 and jet 0, and (f) the p_T of both jets, both leptons, and the E_T^{miss} .

Based on the results of grid search evaluation, the optimal architecture is found to include 5 hidden layers with 40 nodes each. No regularizer or dropout is added to the network, as overfitting is found to not be an issue. The output score distribution as well as the ROC curve for the trained model are shown in Figure 0.15.2.1. The model is found to identify the correct pairing of jets for 73% of 2lSS signal events on test data.

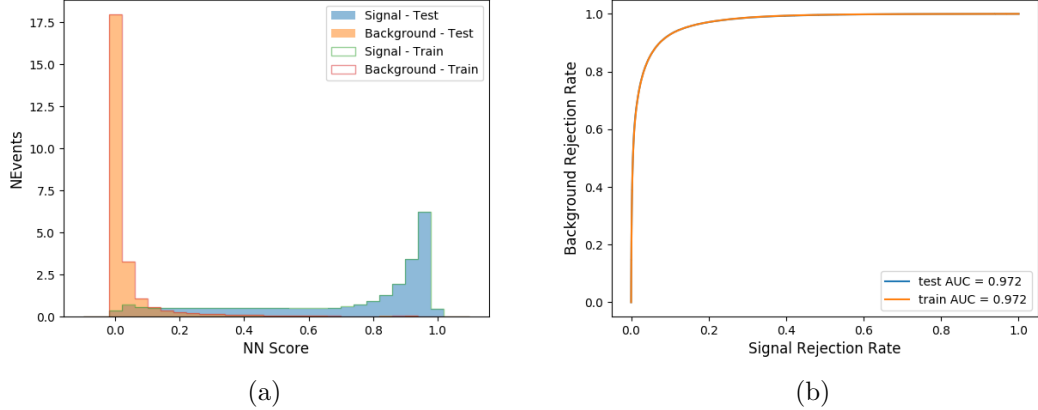


Figure 0.15.3: Results of the b-jet identification algorithm for the 2lSS channel, showing (a) the output score of the NN for correct and incorrect combinations of jets. (b) the ROC curve of the output, showing background rejection as a function of signal efficiency

For point of comparison, a "naive" approach to identifying b-jets is used as well: The two jets which pass the highest DL1r b-tag working point are assumed to be the b-jets from the top decay. In the case that multiple jets meet the same b-tag working point, the jet with higher p_T is used. This method identifies the correct jet pair 65% of the time.

The accuracy of the model for different b-tagged jet multiplicities, compared to this naive approach, is shown in Table 16.

b-jet Selection	Neural Network	Naive
1 b-jet	58.6%	42.1%
2 b-jets	88.4%	87.1%
≥ 3 b-jets	61.7%	53.3%
Overall	73.9%	67.2%

Table 16: Accuracy of the NN in identifying b-jets from tops in 2lSS events, overall and split by the number of b-tagged jets in the event, compared to the accuracy of taking the two highest b-tagged jets.

This suggests that when there are exactly two b-tagged jets in an event, little is gained by using this more sophisticated approach, while for events with 1 or ≥ 3 b-tagged jets, the model does provide significant improvements.

0.15.2.2 3l Channel

The input features used in the 3l channel are listed in Table 17, with the same naming convention as the 2lSS channel.

jet p_T 0	jet p_T 1	jet η 0
jet η 1	Lepton p_T 0	Lepton p_T 1
Lepton p_T 2	$\Delta R(j_0)(j_1)$	$M(j_0 j_1)$
$\Delta R(l_0)(j_0)$	$\Delta R(l_1)(j_0)$	$\Delta R(l_2)(j_0)$
$\Delta R(l_0)(j_1)$	$\Delta R(l_1)(j_1)$	$\Delta R(l_2)(j_1)$
$M(l_0 j_0)$	$M(l_1 j_0)$	$M(l_2 j_0)$
$M(l_0 j_1)$	$M(l_1 j_1)$	$M(l_2 j_1)$
$\Delta R(j_0 l_0)(j_1 l_1)$	$\Delta R(j_0 l_0)(j_1 l_2)$	$\Delta R(j_0 l_1)(j_1 l_0)$
$\Delta R(j_0 l_2)(j_1 l_0)$	jet DL1r 0	jet DL1r 1
$p_T(j_0 j_1 l_0 l_1 l_2 E_T^{\text{miss}})$	$M(t j_0 j_1 l_0 l_1 l_2 E_T^{\text{miss}})$	$\Delta \phi(j_0)(E_T^{\text{miss}})$
$\Delta \phi(j_1)(E_T^{\text{miss}})$	HT Lepton	HT jets
nJets	E_T^{miss}	nJets OR DL1r 85
nJets OR DL1r 60		

Table 17: Input features for the b-jet identification algorithm in the 3l channel.

A few of these features are shown in Figure 0.15.4, comparing the distributions for correct and incorrect combinations of jets.

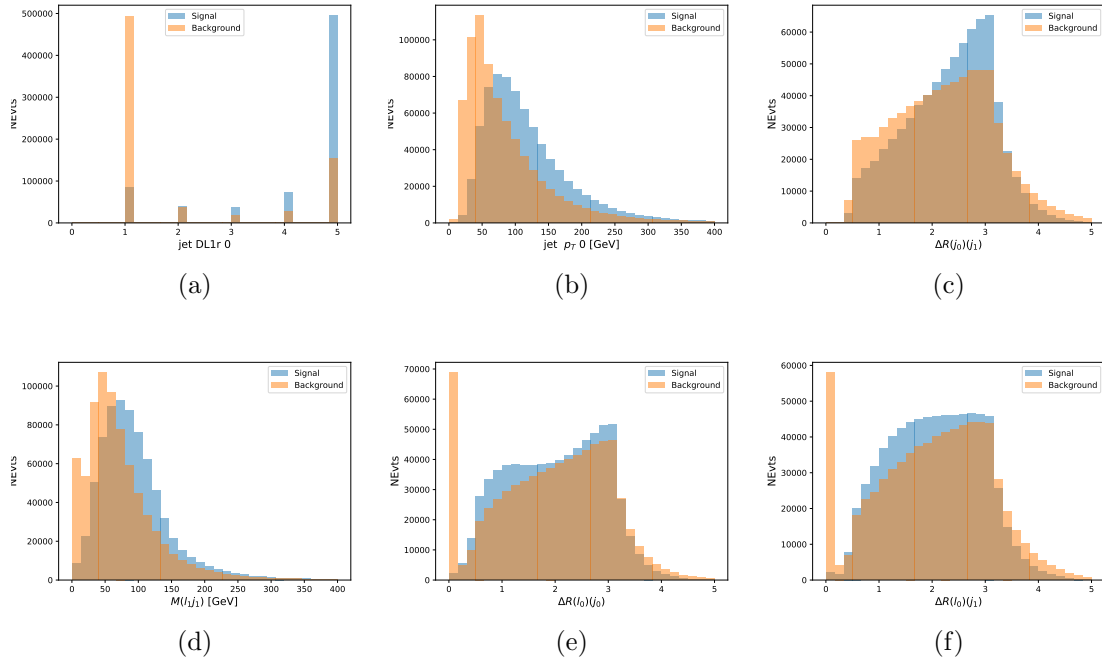


Figure 0.15.4: Input features for top3l training. The signal in blue represents events where both jet candidates are truth b-jets from top decays, and the orange is all other combinations. Scaled to the same number of events. (a) show the DL1r WP of jet 0, (b) the p_T of jet 0, (c) ΔR between jet 0 and jet 1, (d) the invariant mass of lepton 1 and jet 1, (e) ΔR between lepton 0 and jet 0, and (f) ΔR between lepton 0 and jet 1

The modeling of these inputs is validated against data, with Figure 0.15.5 showing good general agreement between data and MC.

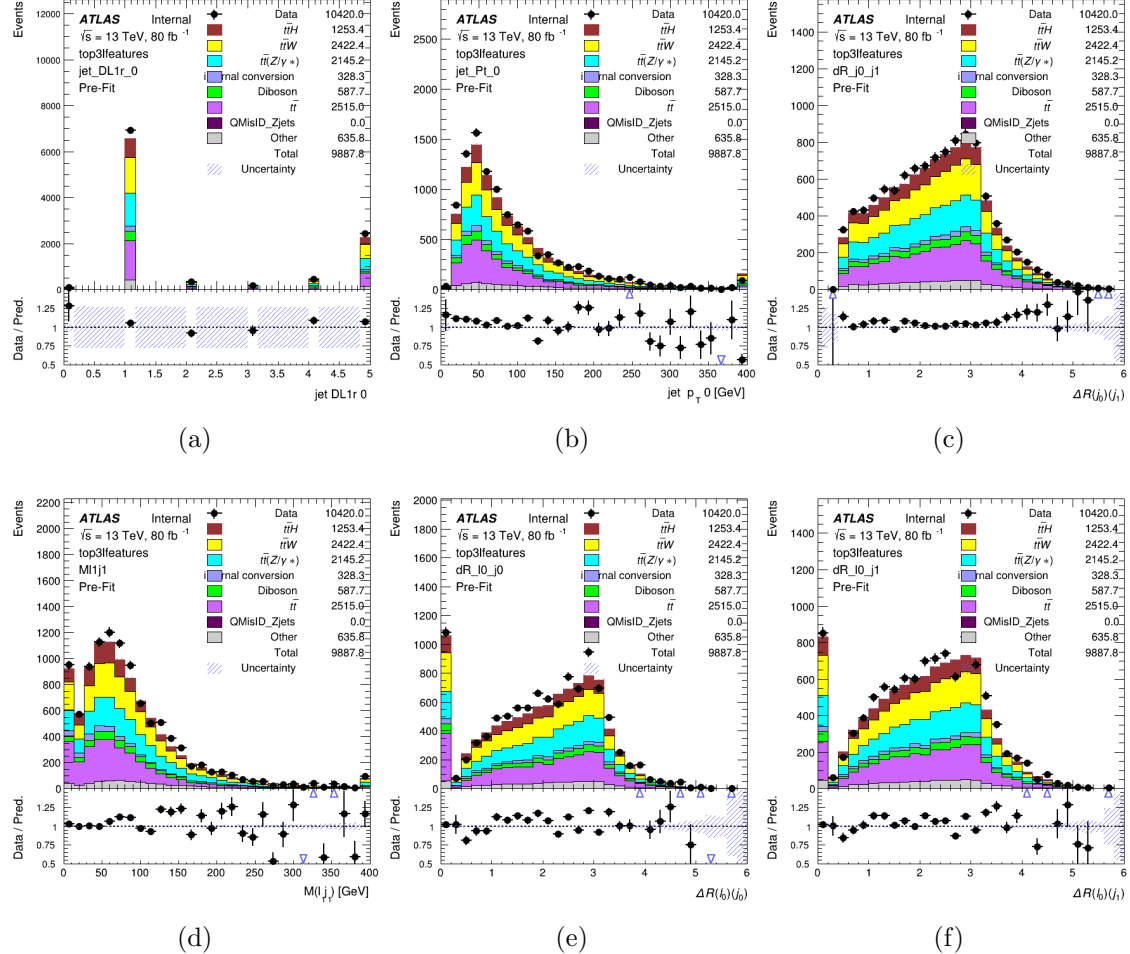


Figure 0.15.5: Data/MC comparisons of input features for top3l training for 79.8 fb^{-1} of data. (a) show the DL1r WP of jet 0, (b) the p_T of jet 0, (c) ΔR between jet 0 and jet 1, (d) the invariant mass of lepton 1 and jet 1, (e) ΔR between lepton 0 and jet 0, and (f) ΔR between lepton 0 and jet 1

Again, the dataset is downsized to reduce the ratio of correct and incorrect combination from 20:1, to 5:1. Around 7 million events are used for training, with 10% set aside for testing. Based on the results of grid search evaluation, the optimal architecture is found to include 5 hidden layers with 60 nodes each. The output score distribution as well as the ROC curve for the trained model are shown in Figure 0.15.2.2.

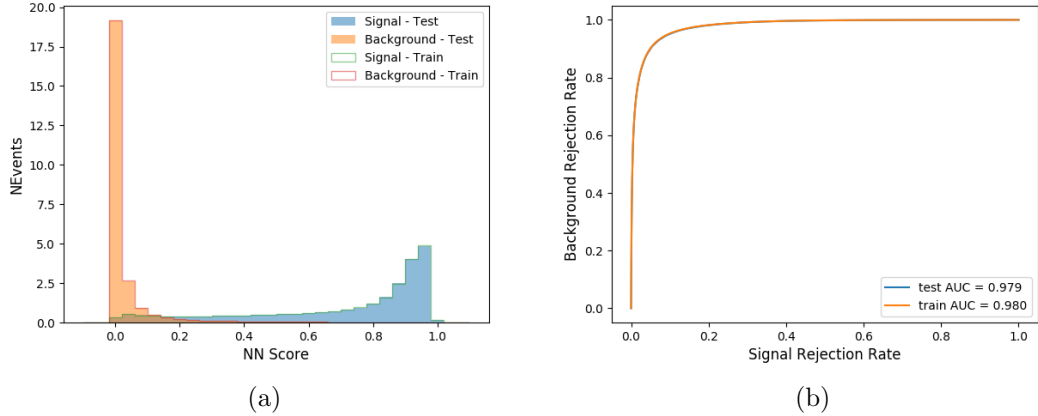


Figure 0.15.6: Results of the b-jet identification algorithm for the 3l channel, showing (a) the output score of the NN for correct and incorrect combinations of jets. (b) the ROC curve of the output, showing background rejection as a function of signal efficiency

This procedure is found to identify the correct pairing of jets for nearly 80% of 3l signal events. The accuracy of the model is summarized in Table 18, once again compared to the naive approach described above.

Table 18: Accuracy of the NN in identifying b-jets from tops, compared to the naive method of taking the highest b-tagged jets.

	NN	Naive
1 b-jet	69.0%	48.9%
2 b-jets	89.6%	88.3%
≥ 3 b-jets	55.7%	52.3%
Overall	79.8%	70.2%

0.15.3 Higgs Reconstruction

Techniques similar to the b-jet identification algorithms are employed to select the decay products of the Higgs: kinematics of all possible combinations of reconstructed objects are fed into a neural network to determine which of those is most likely to be the decay products of the Higgs.

Again separate models are used for the 2lSS and 3l channels, while the 3l channel has now been split into two: $t\bar{t}H$ events with three leptons in the final state include both instances where the Higgs decays into a lepton (and a neutrino) and a pair of jets, and instances where the Higgs decays to two leptons (and two neutrinos which are not reconstructed).

3l events are therefore categorized as either semi-leptonic (3lS) or fully-leptonic (3lF). In the semi-leptonic case the reconstructed decay products consist of two jets and a single lepton. For the fully-leptonic case, the decay products include 2 of the three leptons associated with the event. For training these models, events are separated into these two categories using truth level information. A separate MVA, described in Section 0.15.5, is used to make this distinction at reconstructed level, and determine which model to use.

For all channels, the models described in Section 0.15.2 are used to identify b-jet candidates, whose kinematics are used as additional input features to help identify the Higgs decay products. These jets are not considered as possible candidates for the Higgs decay, justified by the fact that these models are found to misidentify jets from the Higgs decay as jets from the top decay less than 1% of the time.

0.15.3.1 2lSS Channel

For the 2lSS channel, the Higgs decay products include one light lepton and two jets. The neural network is trained on the kinematics of different combinations of leptons and jets, as well as the b-jets identified in Section 0.15.2, with the specific input features listed in Table 19.

Lepton p_T H	Lepton p_T T	jet p_T 0
jet p_T 1	top p_T 0	top p_T 1
top η 0	top η 1	jet η 0
jet η 1	jet Phi 0	jet Phi 1
Lepton η H	Lepton η T	$\Delta R(j_0)(j_1)$
$\Delta R(l_H)(j_0)$	$\Delta R(l_H)(j_1)$	$M(j_0 j_1)$
$M(l_H j_0)$	$M(l_H j_1)$	$\Delta R(l_H)(b_0)$
$\Delta R(l_H)(b_1)$	$\Delta R(l_T)(b_0)$	$\Delta R(l_T)(b_1)$
$\Delta R(j_0 j_1)(l_H)$	$\Delta R(j_0 j_1)(l_T)$	$\Delta R(j_0 j_1)(b_0)$
$\Delta R(j_0 j_1)(b_1)$	$\Delta R(j_0)(b_0)$	$\Delta R(j_0)(b_1)$
$\Delta R(j_1)(b_0)$	$\Delta R(j_1)(b_1)$	$M(j_0 j_1 l_H)$
$p_T(j_0 j_1 l_H l_T b_0 b_1 E_T^{\text{miss}})$	b-jet Reco Score	E_T^{miss}
nJets	HT jets	

Table 19: Input features used to identify the Higgs decay products in 2LSS events

Here j_0 and j_1 , and l_H are the jet and lepton decay candidates, respectively. The other lepton in the event is labeled l_T , as it is assumed to have come from the decay of one of the top quarks. b_0 and b_1 are the two b-jets identified by the b-jet identification algorithm. The b-jet Reco Score is the output of the b-jet reconstruction algorithm.

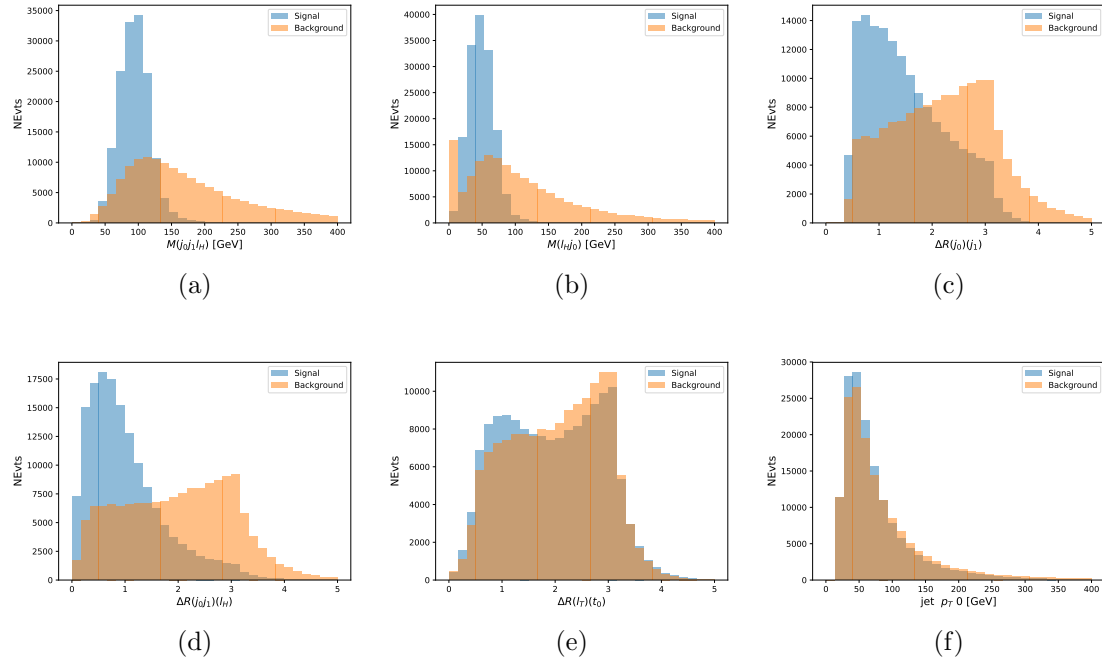


Figure 0.15.7: Input features for higgs2lSS training. The signal in blue represents events where both jet candidates are truth b-jets from top decays, and the orange is all other combinations. Scaled to the same number of events. (a) shows the invariant mass of the two jet candidates and the lepton candidate, (b) the invariant mass of jet 0 and the lepton candidate, (c) ΔR between the jet candidates, (d) ΔR between jet 0 + jet 1 and the lepton candidate, (e) ΔR between the lepton from the top and the leading b-jet, (f) the p_T of jet 0.

The modeling of these inputs is validated against data, with Figure 0.15.2 showing good general agreement between data and MC. Plots for the complete list of features can be found in Section .3.

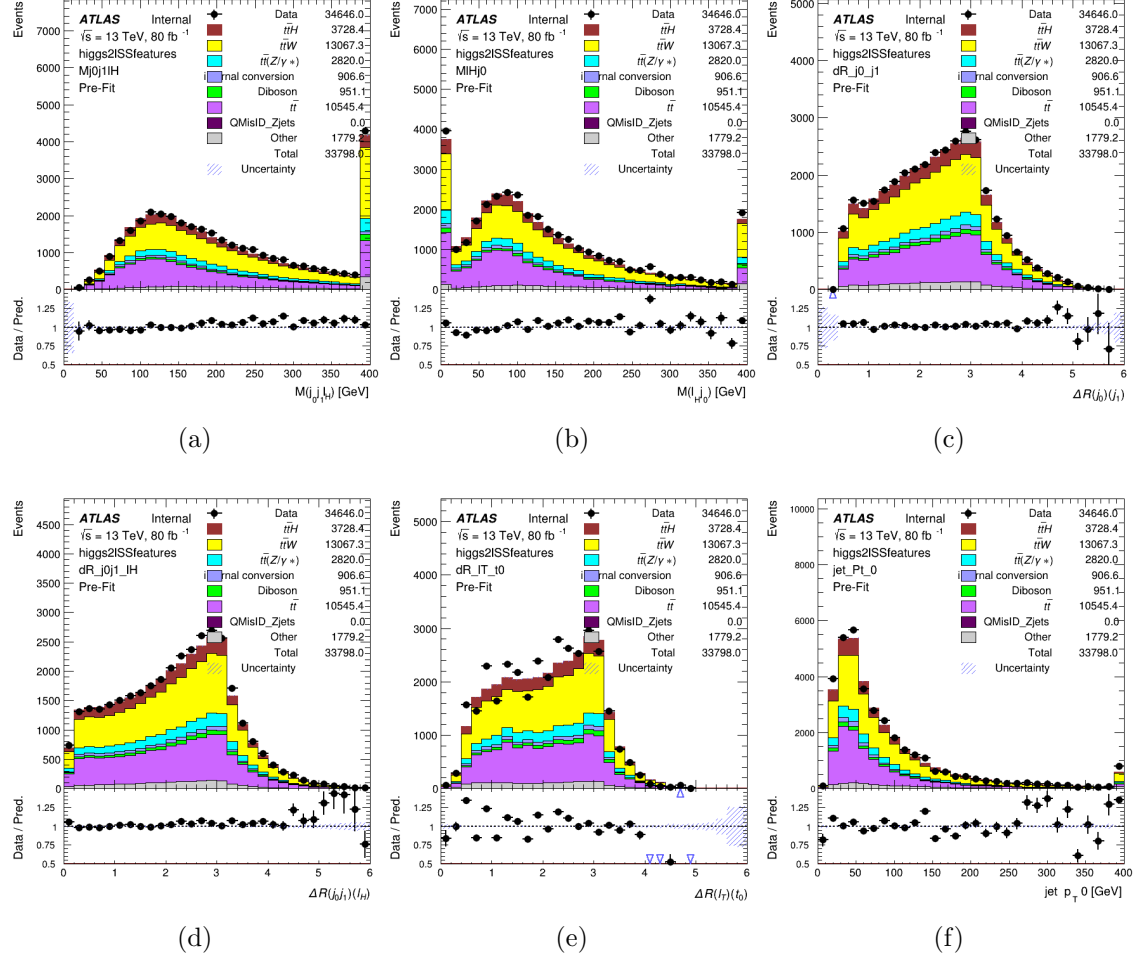


Figure 0.15.8: Data/MC comparisons of input features for higgs2lSS training for 79.8 fb^{-1} of data. (a) shows the invariant mass of the two jet candidates and the lepton candidate, (b) the invariant mass of jet 0 and the lepton candidate, (c) ΔR between the jet candidates, (d) ΔR between jet 0 + jet 1 and the lepton candidate, (e) ΔR between the lepton from the top and the leading b-jet, (f) the p_T of jet 0.

A neural network consisting of 7 hidden layers with 60 nodes each is trained on around 2 million events, with an additional 200,000 reserved for testing the model. In order to compensate for the large number of incorrect combinations, these have been downsampled such that the correct combinations represent over 10% of the training set. The output of the NN is summarized in Figure 0.15.3.1.

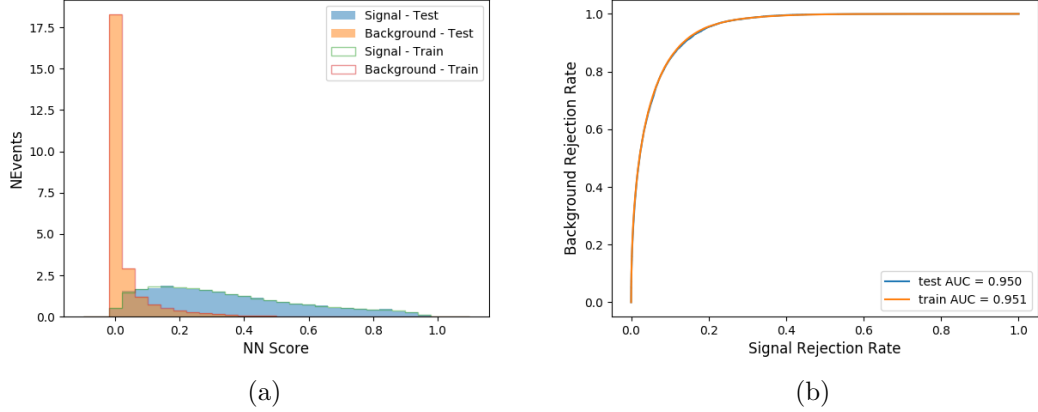


Figure 0.15.9: Result of the Higgs reconstruction algorithm in the 2lSS channel, showing (a) the output score of the NN for correct and incorrect combinations of jets scaled to an equal number of events, and (b) the ROC curve of the output, showing background rejection as a function of signal efficiency

The neural network identifies the correct combination 55% of the time. It identifies the correct lepton 85% of the time, and selects the correct lepton and at least one of the correct jets 81% of the time.

0.15.3.2 3l Semi-leptonic Channel

For 3l $t\bar{t}H$ where the Higgs decay semi-leptonically, the decay products include one of the three leptons and two jets. In this case, the other two leptons originated from the decay of the tops, meaning the opposite-sign (OS) lepton cannot have come from the Higgs. This leaves only the two same-sign (SS) leptons as possible Higgs decay products.

Lepton p_T H	Lepton p_T T_0	Lepton p_T T_1
jet p_T 0	jet p_T 1	top p_T 0
top p_T 1	jet η 0	jet η 1
jet ϕ 0	jet ϕ 1	$\Delta R(j_0)(j_1)$
$M(j_0 j_1)$	$\Delta R(l_H)(j_0)$	$\Delta R(l_H)(j_1)$
$\Delta R(j_0 j_1)(l_H)$	$\Delta R(j_0 j_1)(l_{T_1})$	$\Delta R(l_{T_0})(l_{T_1})$
$\Delta R(l_H)(l_{T_1})$	$M(j_0 j_1 l_{T_0})$	$M(j_0 j_1 l_{T_1})$
$M(j_0 j_1 l_H)$	$\Delta R(j_0 j_1 l_H)(l_{T_0})$	$\Delta R(j_0 j_1 l_H)(l_{T_1})$
$\Delta\phi(j_0 j_1 l_H)(E_T^{\text{miss}})$	$p_T(j_0 j_1 l_H l_{T_0} l_{T_1} b_0 b_1 E_T^{\text{miss}})$	$M(j_0 j_1 b_0)$
$M(j_0 j_1 b_1)$	$\Delta R(l_{T_0})(b_0)$	$\Delta R(l_{T_0})(b_1)$
$\Delta R(l_{T_1})(b_0)$	$\Delta R(l_{T_1})(b_1)$	$\Delta R(j_0)(b_0)$
$\Delta R(j_0)(b_1)$	$\Delta R(j_1)(b_0)$	$\Delta R(j_1)(b_1)$
b-jet Reco Score	E_T^{miss}	HT jets
nJets		

Table 20: Input features used to identify the Higgs decay products in 3l semi-leptonic events

Here j_0 and j_1 , and l_H are the jet and lepton decay candidates, respectively. The other two leptons in the event are labeled as l_{T_0} and l_{T_1} . b_0 and b_1 are the two b-jets identified by the b-jet identification algorithm. The b-jet Reco Score is the output of the b-jet identification algorithm.

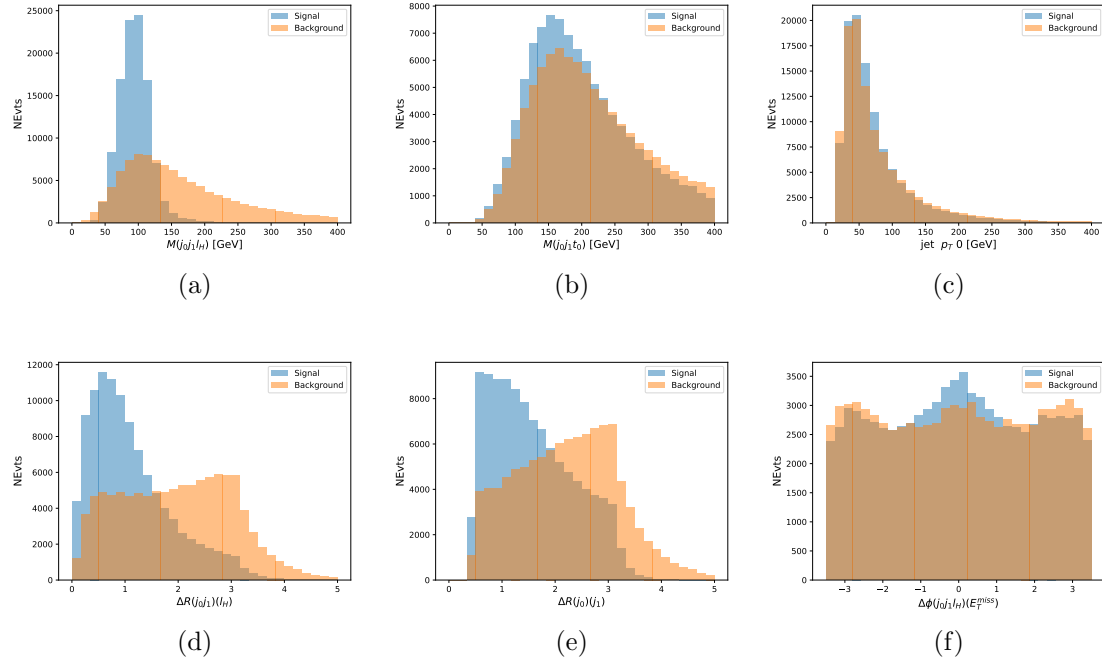


Figure 0.15.10: Input features for higgs3lS training. The signal in blue represents events where both jet candidates are truth b-jets from top decays, and the orange is all other combinations. Scaled to the same number of events.

The modeling of these inputs is validated against data, with Figure 0.15.11 showing good general agreement between data and MC. Plots for the complete list of features can be found in appendix .3.1.

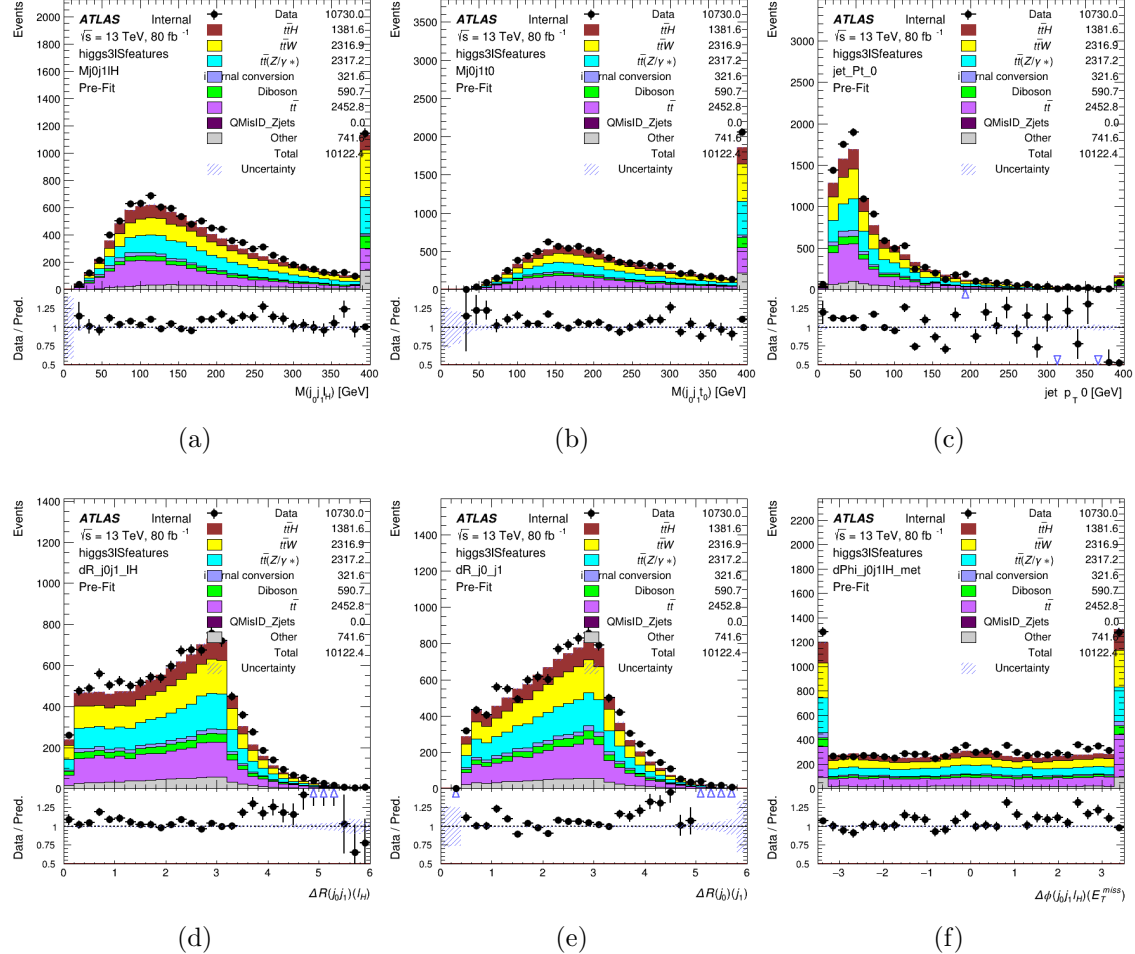


Figure 0.15.11: Data/MC comparisons of input features for higgs3lS training for 79.8 fb^{-1} of data.

A neural network of 7 hidden layers with 70 nodes each is trained on 1.8 million events. Once again, incorrect combinations are downsampled, such that the correct combinations are around 10% of the training set. 10% of the dataset is reserved for testing. The output of the NN is summarized in Figure 0.15.3.2.

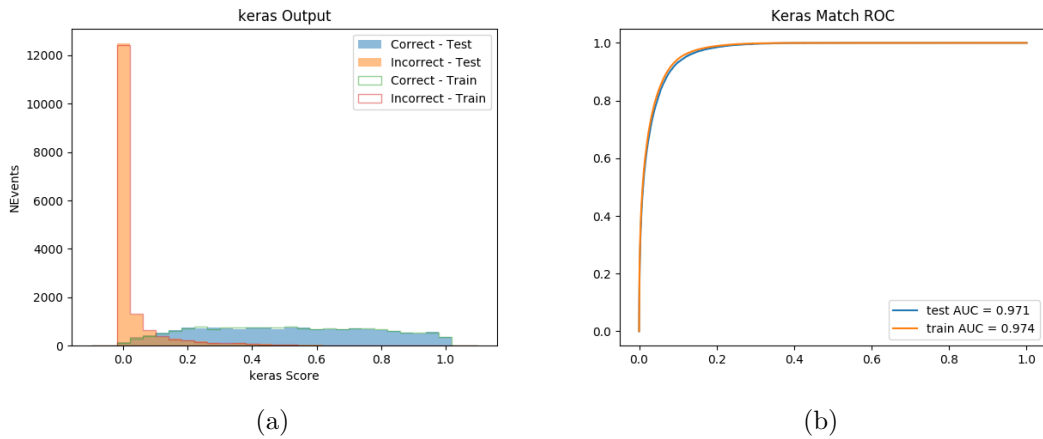


Figure 0.15.12: Results of the Higgs reconstruction algorithm in the 3LS channel, showing (a) the output score of the NN for correct and incorrect combinations of jets, scaled to an equal number of entries., (b) the ROC curve of the output, showing background rejection as a function of signal efficiency

The neural network identifies the correct combination 64% of the time. It identifies the correct lepton 85% of the time, and selects the correct lepton and at least one of the correct jets 83% of the time.

0.15.3.3 3l Fully-leptonic Channel

In the fully-leptonic 3l case, the goal is identify which two of the three leptons originated from the Higgs decay. Since one of these two must be the OS lepton, this problem is reduced to determining which of the two SS leptons originated from the Higgs. The kinematics of both possibilities are used for training; one where the SS lepton from the Higgs is correctly labeled, and one where it is not.

Lepton $p_T H_1$	Lepton $p_T H_0$	Lepton $p_T T$
top $p_T 0$	top $p_T 1$	$\Delta\phi(l_{H_1})(E_T^{\text{miss}})$
$\Delta\phi(l_T)(E_T^{\text{miss}})$	$M(l_{H_0} l_{H_1})$	$M(l_{H_1} l_T)$
$M(l_{H_0} l_T)$	$\Delta R(l_{H_0})(l_{H_1})$	$\Delta R(l_{H_1})(l_T)$
$\Delta R(l_{H_0})(l_T)$	$\Delta R(l_{H_0} l_{H_1})(l_T)$	$\Delta R(l_{H_0} l_T)(l_{H_1})$
$\Delta R(l_{H_0} l_{H_1})(b_0)$	$\Delta R(l_{H_0} l_{H_1})(b_1)$	$\Delta R(l_{H_0} b_0)$
$M(l_{H_0} b_0)$	$\Delta R(l_{H_0} b_1)$	$M(l_{H_0} b_1)$
$\Delta R(l_{H_1} b_0)$	$M(l_{H_1} b_0)$	$\Delta R(l_{H_1} b_1)$
$M(l_{H_1} b_1)$	E_T^{miss}	b-jet Reco Score

Table 21: Input features used to identify the Higgs decay products in 3lF events

Table 22: Input features used to identify the Higgs decay products in 3l fully leptonic events

Here l_{H_0} and l_{H_1} are the Higgs decay candidates. The other lepton in the event is labeled l_T . b_0 and b_1 are the two b-jets identified by the b-jet identification algorithm. The b-jet Reco Score is the output of the Higgs reconstruction algorithm.

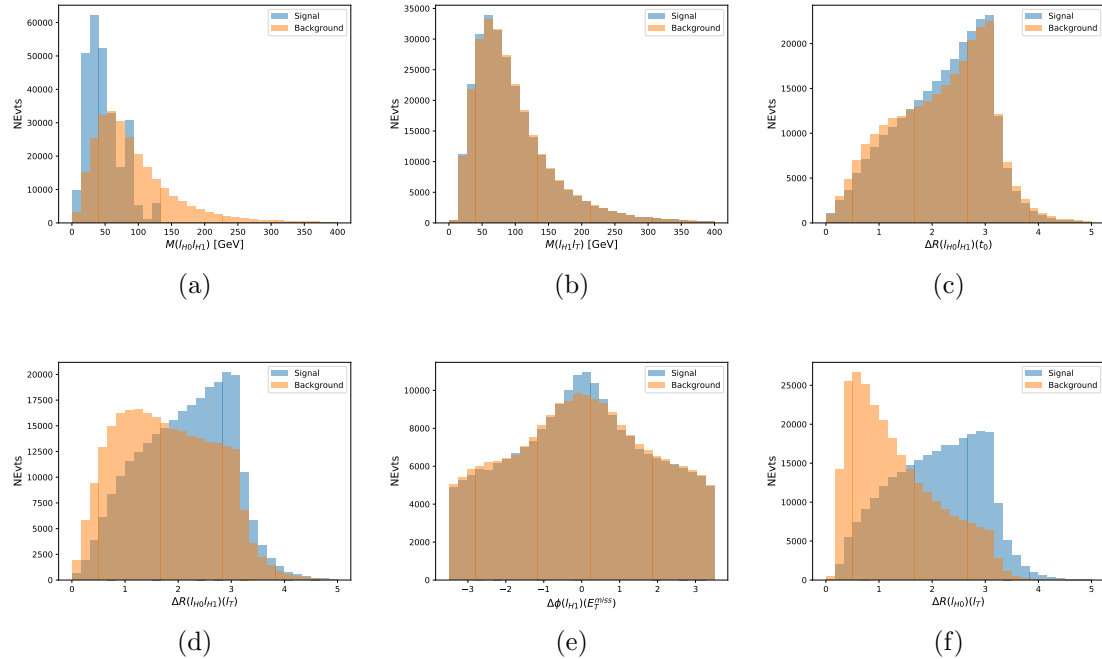


Figure 0.15.13: Input features for higgs3lF training. The signal in blue represents events where both jet candidates are truth b-jets from top decays, and the orange is all other combinations. Scaled to the same number of events.

The modeling of these inputs is validated against data, with Figure 0.15.14 showing good general agreement between data and MC. Plots for the complete list of features can be found in Section .3.

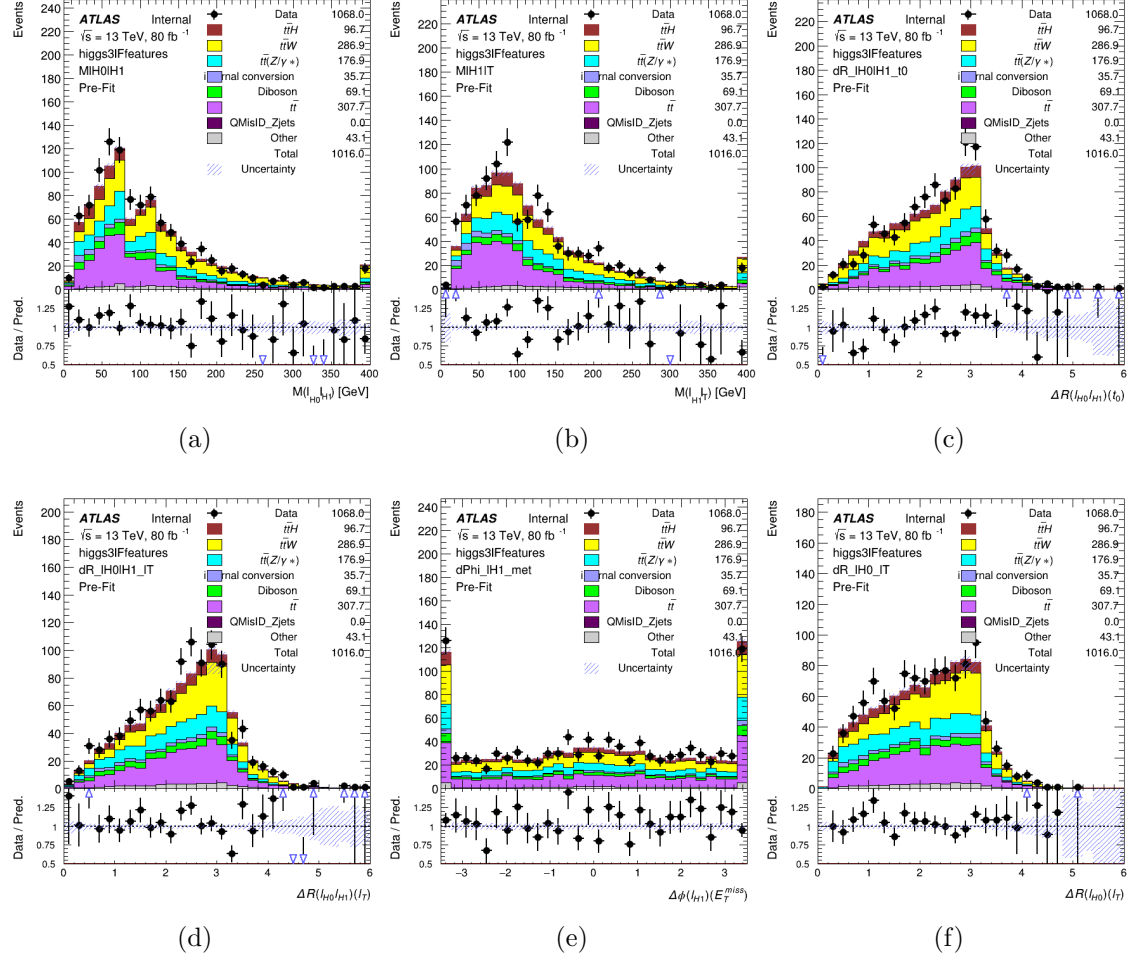


Figure 0.15.14: Data/MC comparisons of input features for higgs3lF training for 79.8 fb^{-1} of data.

A neural network consisting of 5 nodes and 60 hidden units is trained on 800,000 events, with 10% of the dataset reserved for testing. The output of the model is summarized in Figure 0.15.3.3.

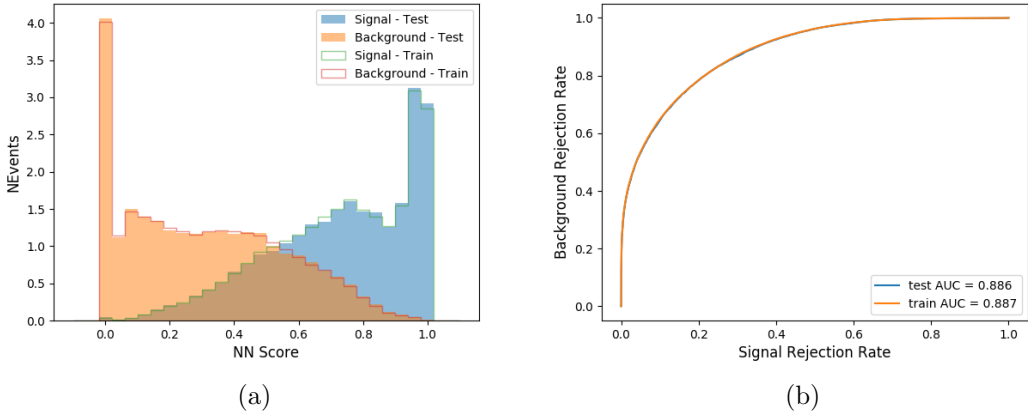


Figure 0.15.15: (a) the output score of the NN for correct and incorrect combinations of jets. (a) the ROC curve of the output, showing background rejection as a function of signal efficiency

The correct lepton is identified by the model for 80% of events in the testing data set.

0.15.4 p_T Prediction

Once the most probable decay products have been identified, their kinematics are used as inputs to a regression model which attempts to predict the momentum of the Higgs Boson. Once again, a DNN is used. Input variables representing the b-jets and leptons not from the Higgs decay are included as well, as these are found to improve performance. The truth p_T of the Higgs, as predicted by MC, are used as labels. Separate models are built for each channel - 2lSS, 3l Semi-leptonic and 3l Fully-leptonic.

As a two-bin fit is targeted for the final result, some metrics evaluating the performance of the models aim to show how well it distinguished between "high p_T " and "low p_T " events. A cutoff point of 150 GeV is used to define these two categories.

Because the analysis uses a two bin fit of the Higgs p_T , the momentum reconstruction could be treated as a binary classification problem, rather than a regression problem. This approach is explored in detail in Section .3.5, and is found not to provide any significant increase in sensitivity. The regression approach is used because it provides more flexibility for future analyses, as it is independent of the cutoff between high and low p_T , as well as the number of bins. Further, a regression allows the output of the neural network to be more clearly understood, as it can be directly compared to a physics observable.

0.15.4.1 2lSS Channel

The input variables listed in Table 23 are used to predict the Higgs p_T in the 2lSS channel. Here j_0 and j_1 are the two jets identified as Higgs decay products. The lepton identified as originating from the Higgs is labeled l_H , while the other lepton is labeled l_T , as it is assumed to have come from the decay of one of the top quarks. b_0 and b_1 are the two b-jets identified by the b-jet identification algorithm. The Higgs Reco Score and b-jet Reco Score are the outputs of the Higgs reconstruction algorithm, and the b-jet identification algorithm, respectively.

HT	$M(j_0 j_1)$	$M(j_0 j_1 l_H)$
$M(l_H j_0)$	$M(l_H j_1)$	$p_T(b_0 b_1)$
$p_T(j_0 j_1 l_H)$	$\Delta\phi(j_0 j_1 l_H)(E_T^{\text{miss}})$	$\Delta R(j_0)(j_1)$
$\Delta R(j_0 j_1)(l_H)$	$\Delta R(j_0 j_1 l_H)(l_T)$	$\Delta R(j_0 j_1 l_H)(b_0)$
$\Delta R(j_0 j_1 l_H)(b_1)$	$\Delta R(l_H)(j_0)$	$\Delta R(l_H)(b_0)$
$\Delta R(l_H)(b_1)$	$\Delta R(l_T)(b_0)$	$\Delta R(l_T)(b_1)$
$\Delta R(b_0)(b_1)$	Higgs Reco Score	jet η 0
jet η 1	jet Φ 0	jet Φ 1
jet p_T 0	jet p_T 1	Lepton η H
Lepton ϕ H	Lepton p_T H	Lepton p_T T
E_T^{miss}	nJets	b-jet Reco Score
b-jet p_T 0	b-jet p_T 1	

Table 23: Input features for reconstructing the Higgs p_T spectrum for 2lSS events

The optimal neural network architecture for this channel is found to consist of 7 hidden layers with 60 nodes each. The input data set includes 1.2 million events, 10% of which is used for testing, the other 90% for training. Training is found to converge after around 150 epochs.

To evaluate the performance of the model, the predicted p_T spectrum is compared to the truth Higgs p_T in Figure 0.15.16. In order to visualize the model performance more clearly, in (a) of that figure, the color of each point is determined by Kernel Density Estimation (KDE). The color shown represents the logarithm of the output from KDE, to counteract the large number of low p_T events. For that same reason, each column of the histogram shown in (b) of Figure 0.15.16 is normalized to unity. This plot therefore demonstrates what the model predicts for each slice of truth p_T .

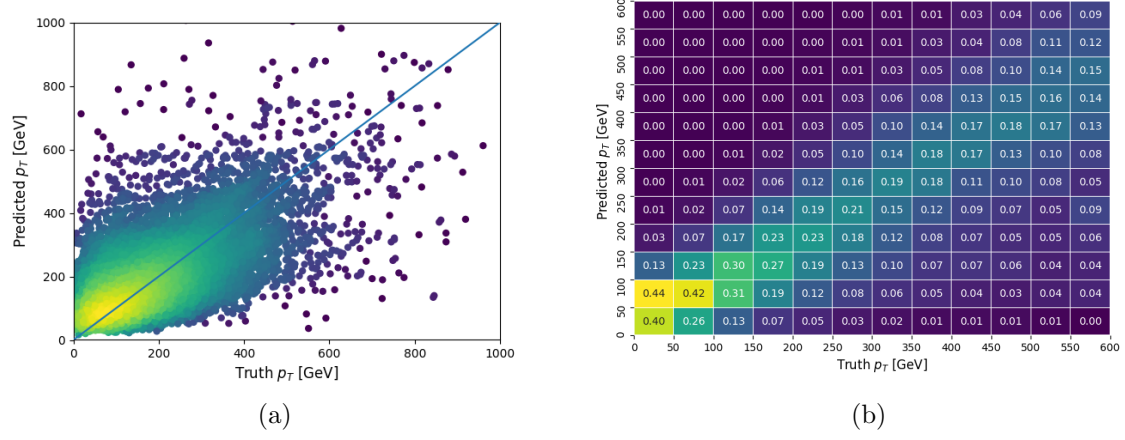


Figure 0.15.16: The regressed Higgs momentum spectrum as a function of the truth p_T for 2lSS $t\bar{t}H$ events in (a) a scatterplot, where the color of each point represents the log of the point density, based on Gaussian Kernal Density Estimation, and (b) a histogram where each column has been normalized to one.

We are also interested in how well the model distinguishes between events with $p_T < 150$ GeV and > 150 GeV. Figure 0.15.17 demonstrates the NN output for high and low p_T events based on this cutoff.

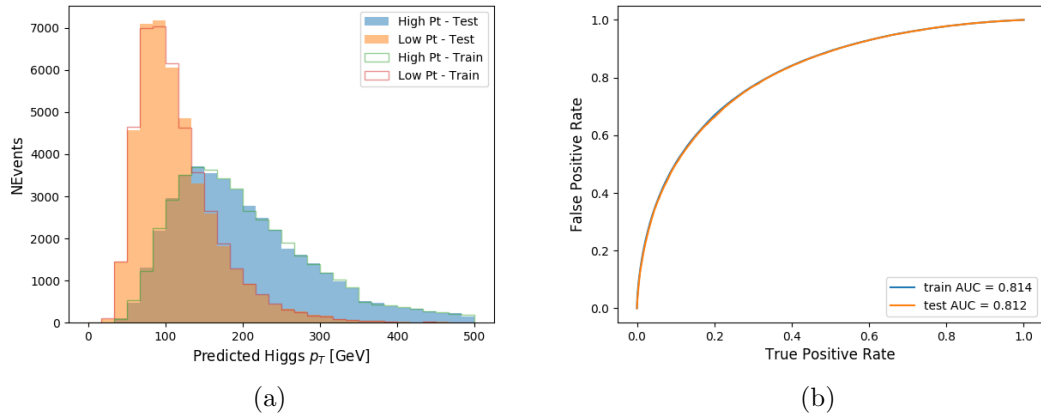


Figure 0.15.17: (a) shows the reconstructed Higgs p_T for 2lSS events with truth $p_T > 150$ GeV and < 150 GeV, while (b) shows the ROC curve for those two sets of events.

0.15.4.2 3l Semi-leptonic Channel

The following input features are used to predict the Higgs p_T for events in the 3lS channel:

HT jets	MET	$M(j_0 j_1)$
$M(j_0 j_1 l_H)$	$M(j_0 j_1 l_{T0})$	$M(j_0 j_1 l_{T1})$
$M(j_0 j_1 b_0)$	$M(j_0 j_1 b_1)$	$M(b_0 l_{T0})$
$M(b_0 l_{T1})$	$M(b_1 l_{T0})$	$M(b_1 l_{T1})$
$\Delta\phi(j_0 j_1 l_H)(E_T^{\text{miss}})$	$\Delta R(j_0)(j_1)$	$\Delta R(j_0 j_1)(l_H)$
$\Delta R(j_0 j_1)(l_{T1})$	$\Delta R(j_0 j_1)(b_0)$	$\Delta R(j_0 j_1)(b_1)$
$\Delta R(j_0 j_1 l_H)(l_{T0})$	$\Delta R(j_0 j_1 l_H)(l_{T1})$	$\Delta R(j_0 j_1 l_H)(b_0)$
$\Delta R(j_0 j_1 l_H)(b_1)$	$\Delta R(l_H)(j_0)$	$\Delta R(l_H)(j_1)$
$\Delta R(l_H)(l_{T1})$	$\Delta R(l_{T0})(l_{T1})$	$\Delta R(l_{T0})(b_0)$
$\Delta R(l_{T0})(b_1)$	$\Delta R(l_{T1})(b_0)$	$\Delta R(l_{T1})(b_1)$
Higgs Reco Score	jet η 0	jet η 1
jet ϕ 0	jet ϕ 1	jet p_T 0
jet p_T 1	Lepton η H	Lepton ϕ H
Lepton p_T H	Lepton p_T T0	Lepton p_T T1
nJets	b-jet Reco Score	b-jet p_T 0
	b-jet p_T 1	

Table 24: Input features for reconstructing the Higgs p_T spectrum for 3LS events

Again, j_0 and j_1 are the two jets identified as Higgs decay products, ordered by p_T . The lepton identified as originating from the Higgs is labeled l_H , while the other two leptons are labeled l_{T0} and l_{T1} . b_0 and b_1 are the two b-jets identified by the b-jet identification algorithm. The Higgs Reco Score and b-jet Reco Score are the outputs of the Higgs reconstruction algorithm, and the b-jet identification algorithm, respectively.

The optimal neural network architecture for this channel is found to consist of 7 hidden layers with 80 nodes each. The input data set includes one million events, 10% of which is used for testing, the other 90% for training. Training is found to converge after around 150 epochs.

To evaluate the performance of the model, the predicted p_T spectrum is compared to the truth Higgs p_T in Figure 0.15.18. Once again, (a) of 0.15.18 shows a scatterplots of predicted vs truth p_T , where the color of each point corresponds to the log of the relative KDE at that point. Each column of the histogram in (b) is normalized to unity, to better demonstrate the output of the NN for each slice of truth p_T .

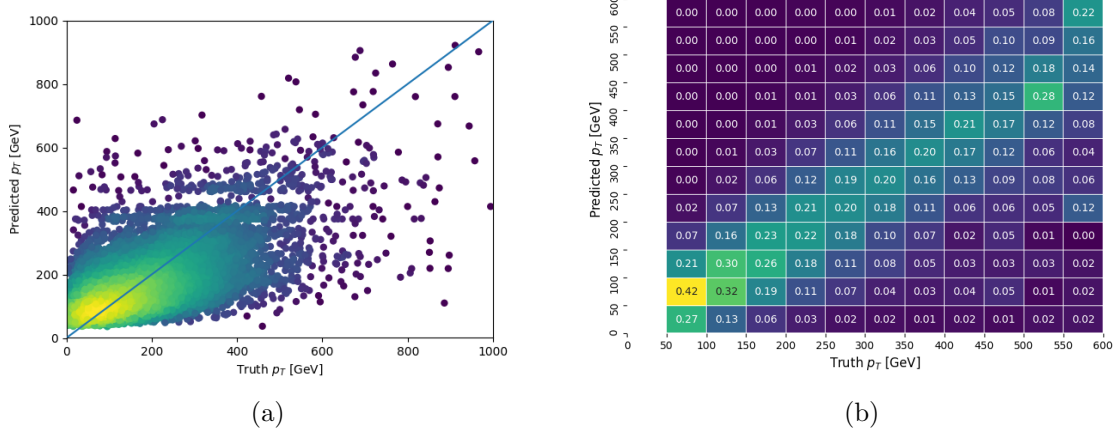


Figure 0.15.18: The regressed Higgs momentum spectrum as a function of the truth p_T for 3lS $t\bar{t}H$ events in (a) a scatterplot, where the color of each point represents the log of the point density, based on Gaussian Kernel Density Estimation, and (b) a histogram where each column has been normalized to one.

Figure 0.15.19 shows (a) the output of the NN for events with truth p_T less than and greater than 150 GeV and (b) the ROC curve demonstrating how well the NN distinguishes high and low p_T events.

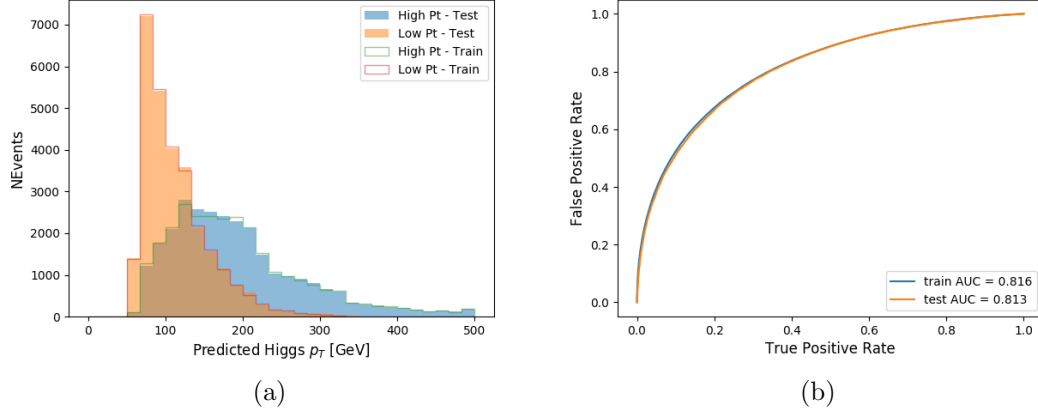


Figure 0.15.19: (

a) shows the reconstructed Higgs p_T for 3lS events with truth $p_T > 150$ GeV and < 150 GeV, while (b) shows the ROC curve for those two sets of events.

0.15.4.3 3l Fully-leptonic Channel

The features listed in 25 are used to construct a model for predictin the Higgs p_T for 3lF events.

HT	$M(l_{H0}l_{H1})$	$M(l_{H0}l_T)$
$M(l_{H0}b_0)$	$M(l_{H0}b_1)$	$M(l_{H1}l_T)$
$M(l_{H1}b_0)$	$M(l_{H1}b_1)$	$\Delta R(l_{H0})(l_{H1})$
$\Delta R(l_{H0})(l_T)$	$\Delta R(l_{H0}l_{H1})(l_T)$	$\Delta R(l_{H0}l_T)(l_{H1})$
$\Delta R(l_{H1})(l_T)$	$\Delta R(l_{H0}b_0)$	$\Delta R(l_{H0}b_1)$
$\Delta R(l_{H1}b_1)$	$\Delta R(l_{H1}b_0)$	Higgs Reco Score
Lepton η H_0	Lepton η H_1	Lepton η T
Lepton p_T H_0	Lepton p_T H_1	Lepton p_T T
E_T^{miss}	b-jet Reco Score	b-jet p_T 0
b-jet p_T 1		

Table 25: Input features for reconstructing the Higgs p_T spectrum for 3lF events

l_{H0} and l_{H1} respresent the two leptons identified by the Higgs reconstruction

model as originating from the Higgs, while l_T is the other lepton in the event. The Higgs Reco Score and b-jet Reco Score are the outputs of the Higgs reconstruction algorithm, and b-jet identification algorithm, respectively.

The optimal neural network architecture for this channel is found to consist of 5 hidden layers with 40 nodes each. The input data set includes 400,000 events, 10% of which is used for testing, the other 90% for training. Training is found to converge after around 150 epochs.

The predicted transverse momentum, as a function of the truth p_T , is shown in Figure 0.15.20.

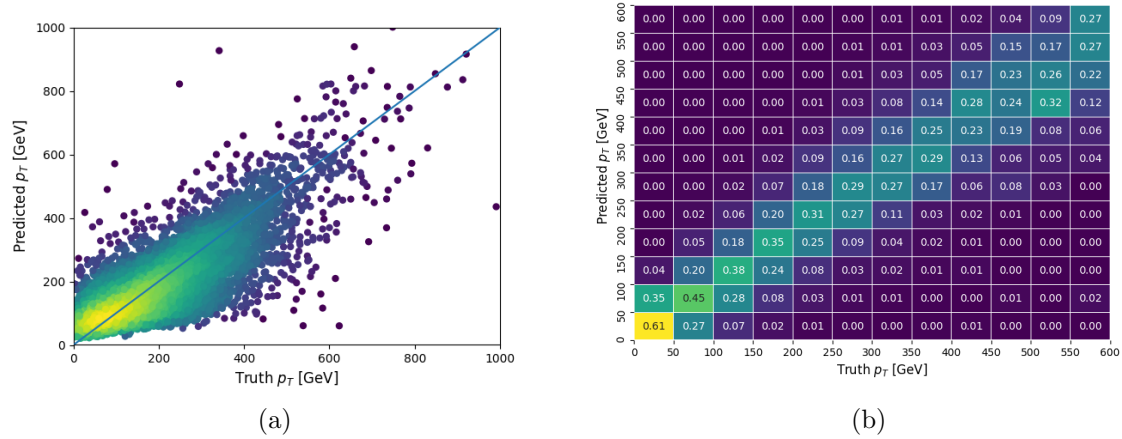


Figure 0.15.20: The regressed Higgs momentum spectrum as a function of the truth p_T for 3lF $t\bar{t}H$ events in (a) a scatterplot, where the color of each point represents the log of the point density, based on Gaussian Kernel Density Estimation, and (b) a histogram where each column has been normalized to one.

When split into high and low p_T , based on a cutoff of 150 GeV, the

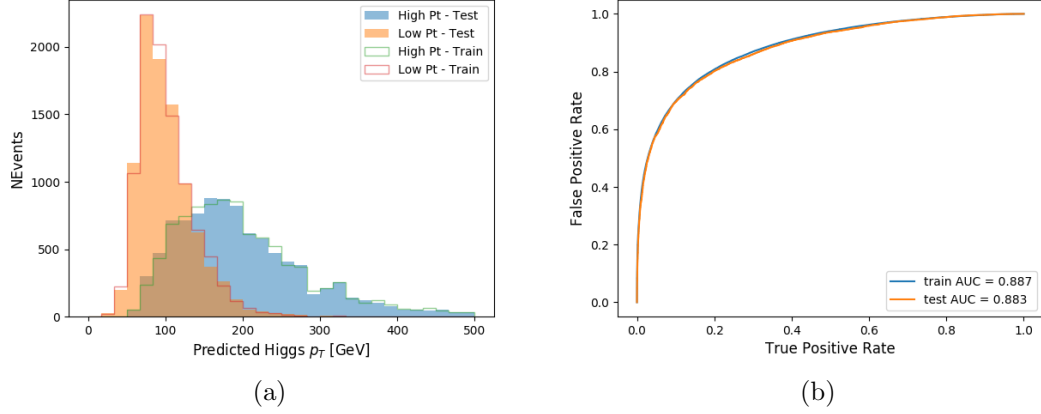


Figure 0.15.21: (a) shows the reconstructed Higgs p_T for 3lF events with truth $p_T > 150$ GeV and < 150 GeV, while (b) shows the ROC curve for those two sets of events.

0.15.5 3l Decay Mode

In the 3l channel, there are two possible ways for the Higgs to decay, both involving intermediate W boson pairs: Either both W bosons decay leptonically, in which case the reconstructed decay consists of two leptons (referred as the fully-leptonic 3l channel), or one W decays leptonically and the other hadronically, giving two jets and one lepton in the final state (referred to as the semi-leptonic 3l channel). In order to accurately reconstruct the Higgs, it is necessary to identify which of these decays took place for each 3l event.

The kinematics of each event, along with the output scores of the Higgs and top reconstruction algorithms, are used to distinguish these two possible decay modes. The particular inputs used are listed in Table 26.

HT jets	$M(l_0 t_0)$	$M(l_0 t_1)$
$M(l_1 t_0)$	$M(l_1 t_1)$	$M(l_0 l_1)$
$M(l_0 l_2)$	$M(l_1 l_2)$	$\Delta R(l_0 t_0)$
$\Delta R(l_0 t_1)$	$\Delta R(l_1 t_0)$	$\Delta R(l_1 t_1)$
$\Delta R(l_0 l_1)$	$\Delta R(l_0 l_2)$	$\Delta R(l_1 l_2)$
Lepton η 0	Lepton η 1	Lepton η 2
Lepton ϕ 0	Lepton ϕ 1	Lepton ϕ 2
Lepton p_T 0	Lepton p_T 1	Lepton p_T 2
E_T^{miss}	nJets	nJets OR DL1r 60
nJets OR DL1r 85	score3lF	score3lS
topScore	total charge	

Table 26: Input features used to distinguish semi-leptonic and fully-leptonic Higgs decays in the 3l channel.

Here l_0 is the opposite charge lepton, l_1 and l_2 are the two SS leptons order by ΔR from lepton 0. score3lF and score3lS are the outputs of the 3lS and 3lF Higgs reconstruction algorithms, while topScore is the output of the b-jet identification algorithm.

A neural network with 5 hidden layers, each with 50 nodes, is trained to distinguish these two decay modes. The output of the model is summarized in Figure 0.15.22.

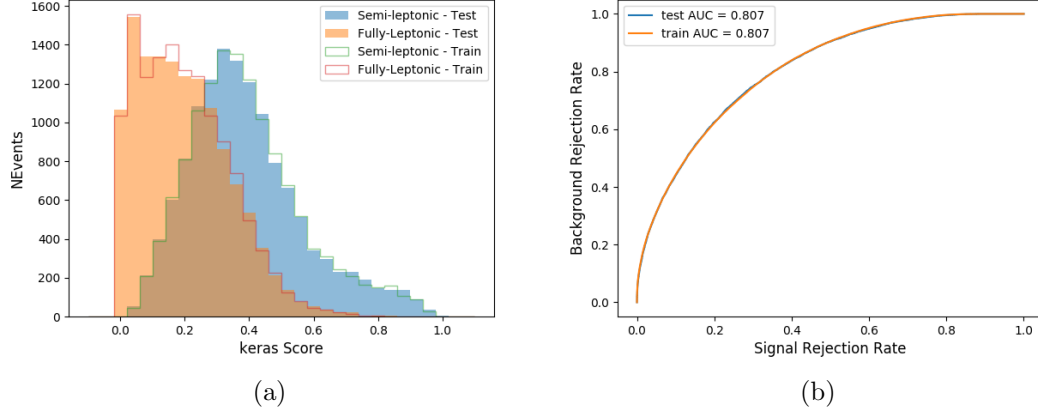


Figure 0.15.22: (a) shows the output of the decay separation NN for Semi-leptonic (blue) and Fully-leptonic (orange) 3l events, scaled to equal area. (b) shows the ROC curve for those two sets of events.

A cutoff of 0.23 is determined to be optimal for separating 3lS and 3lF in the fit.

0.16 Signal Region Definitions

Events are divided into two channels based on the number of leptons in the final state: one with two same-sign leptons, the other with three leptons. The 3l channel includes events where two leptons originated from the Higgs boson as well as events where only one of the leptons originated from the Higgs. This motivates splitting the 3l channel into semi-leptonic, and fully leptonic channels, after an event preselection has been applied.

0.16.1 Pre-MVA Event Selection

A preselection is applied to define orthogonal analysis channels based on the number of leptons in each event. For the 2lSS channel, the following preselection is used:

- Two very tight, same-charge, light leptons with $p_T > 20$ GeV
- ≥ 4 reconstructed jets, ≥ 1 b-tagged jets

- No reconstructed tau candidates

The event yield after the 2lSS preselection has been applied, for MC and data at 79.8 fb^{-1} , is shown in Table 0.16.1.

Process	Yield
t̄tH high p _T	41 ± 5
t̄tH low p _T	71 ± 8
t̄tW	450 ± 70
t̄t(Z/γ*)	91 ± 11
t̄tl̄l low mass	10 ± 6
Rare Top	20 ± 12
VV	42 ± 22
tZ	10 ± 5
QMisID	44.7 ± 2.7
Fakes int. conv	47 ± 26
Fakes ext. conv	46 ± 44
Fakes HF e	45 ± 23
Fakes HF μ	250 ± 50
Three top	2.2 ± 1.1
Four top	5.64 ± 0.31
t̄tWW	10.9 ± 0.6
tW	0.0 ± 0.0
WtZ	9.1 ± 0.8
VVV	0.30 ± 0.05
VH	0.6 ± 1.0
Total	1170 ± 120
Data	1108

Table 27: Yields of the 2lSS preselection region

Figure 0.16.1. Good general agreement is found.

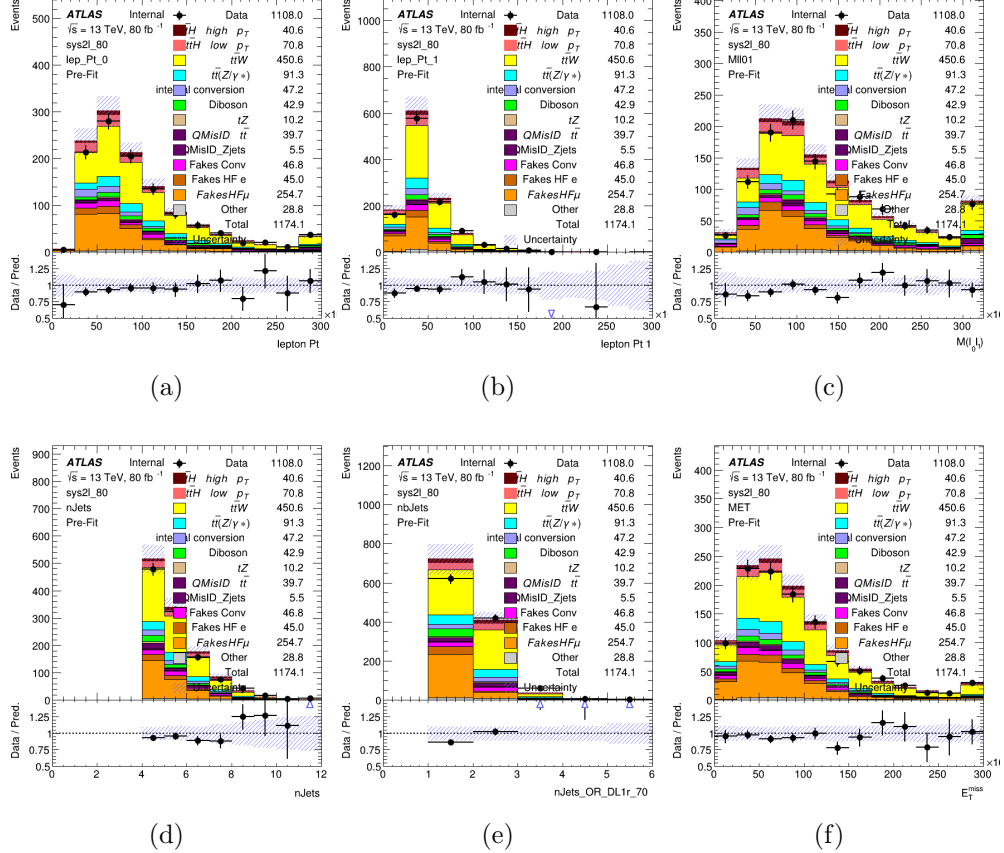


Figure 0.16.1: Data/MC comparisons of the 2lSS pre-selection region. (a) and (b) show the p_T of leptons 0 and 1, (c) shows the invariant mass of lepton 0 and 1, (d) shows the jet multiplicity, (e) the b-tagged jet multiplicity, and (f) the missing transverse energy.

For the 3l channel, the following selection is applied:

- Three light leptons with total charge ± 1
- Same charge leptons are required to be very tight, with $p_T > 20$ GeV
- Opposite charge lepton must be loose, with $p_T > 10$ GeV
- ≥ 2 reconstructed jets, ≥ 1 b-tagged jets
- No reconstructed tau candidates

- $|M(l^+l^-) - 91.2 \text{ GeV}| > 10 \text{ GeV}$ for all opposite-charge, same-flavor lepton pairs

The event yield after the 3l preselection has been applied, for MC and data at 79.8 fb^{-1} , is shown in Table 0.16.1.

Process	Yield
t̄tH high p _T	20.5 ± 2.3
t̄tH low p _T	33.6 ± 3.8
t̄tW	138 ± 18
t̄tZ/γ	80 ± 9
t̄tlllowmass	3.5 ± 2.0
rareTop	22 ± 12
VV	39 ± 19
tZ	9.2 ± 4.5
QMisID	1.8 ± 0.6
Fakes int. conv	31 ± 17
Fakes ext. conv	14 ± 11
Fakes HF e	20 ± 10
Fakes HF μ	102 ± 22
Three top	0.96 ± 0.48
Four top	6.17 ± 0.35
t̄tWW	5.46 ± 0.33
tW	0.0 ± 0.0
WtZ	8.7 ± 0.6
VVV	0.81 ± 0.11
VH	0.0 ± 0.0
Total	512 ± 48
Data	535

Table 28: Yields of the 3l preselection region.

Table 29: Yields of the 3l preselection region.

Comparisons of kinematic distributions for data and MC in this region are shown in Figure 0.16.2.

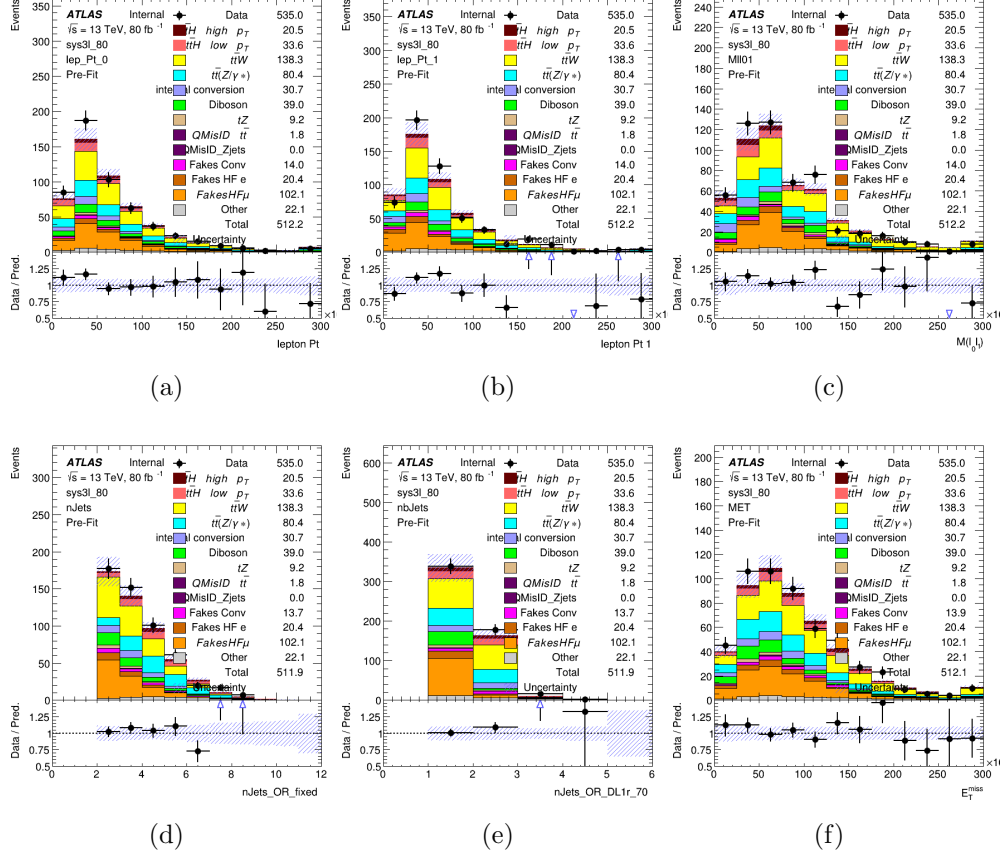


Figure 0.16.2: Data/MC comparisons of the 3l pre-selection region. (a) and (b) show the p_T of leptons 0 and 1, (c) shows the invariant mass of lepton 0 and 1, (d) shows the jet multiplicity, (e) the b-tagged jet multiplicity, and (f) the missing transverse energy.

0.16.2 Event MVA

Separate multi-variate analysis techniques (MVAs) are used in order to distinguish signal events from background for each analysis channel - 2lSS, 3l semi-leptonic (3lS), and 3l fully leptonic (3lF). Here events with three leptons are split into 3lS and 3lF based on the model described in 0.15.5. In particular, Boosted Decision Tree (BDT) algorithms are produced with XGBoost [?] are trained using the kinematics of signal and background events derived from Monte Carlo simulations. Events are weighted in the BDT training by the weight of each Monte Carlo event.

Because the background composition differs for events with a high reconstructed Higgs p_T compared to events with low reconstructed Higgs p_T , separate MVAs are produced for high and low p_T regions. This is found to provide better significance than attempting to build an inclusive model, as demonstrated in appendix .3.2. A cutoff of 150 GeV is used. This gives a total of 6 background rejection MVAs - explicitly, 2lSS high p_T , 2lSS low p_T , 3lS high p_T , 3lS low p_T , 3lF high p_T , and 3lF low p_T .

The following features are used in both the high and low p_T 2lSS BDTs:

HT	$M(\text{lep}, \bar{E}_T^{\text{miss}})$	$M(l_0 l_1)$
binHiggs p_T 2lSS	$\Delta R(l_0)(l_1)$	diLepton type
higgsRecoScore	jet η 0	jet η 1
jet ϕ 0	jet ϕ 1	jet p_T 0
jet p_T 1	Lepton η 0	Lepton η 1
Lepton ϕ 0	Lepton ϕ 1	Lepton p_T 0
Lepton p_T 1	\bar{E}_T^{miss}	$\min \Delta R(l_0)(\text{jet})$
$\min \Delta R(l_1)(\text{jet})$	$\min \Delta R(\text{Lepton})(\text{bjet})$	mjjMax frwdJet
nJets	nJets OR DL1r 60	nJets OR DL1r 70
nJets OR DL1r 85	topRecoScore	

Table 30: Input features used to distinguish signal and background events in the 2lSS channel.

While for each of the 3l BDTs, the features listed below are used for training:

$M(\text{lep}, E_T^{\text{miss}})$	$M(l_0 l_1)$	$M(l_0 l_1 l_2)$
$M(l_0 l_2)$	$M(l_1 l_2)$	binHiggs p_T 3lF
binHiggs p_T 3lS	$\Delta R(l_0)(l_1)$	$\Delta R(l_0)(l_2)$
$\Delta R(l_1)(l_2)$	decayScore	higgsRecoScore3lF
higgsRecoScore3lS	jet η 0	jet η 1
jet ϕ 0	jet ϕ 1	jet p_T 0
jet p_T 1	Lepton η 0	Lepton η 1
Lepton η 2	Lepton ϕ 0	Lepton ϕ 1
Lepton ϕ 2	Lepton p_T 0	Lepton p_T 1
Lepton p_T 2	E_T^{miss}	min $\Delta R(l_0)(\text{jet})$
min $\Delta R(l_1)(\text{jet})$	min $\Delta R(l_2)(\text{jet})$	min $\Delta R(\text{Lepton})(\text{bjet})$
mjjMax frwdJet	nJets	nJets OR DL1r 60
nJets OR DL1r 70	nJets OR DL1r 85	topScore

Table 31: Input features used to distinguish signal and background events in the 3l channel.

Modelling of each of these input features is verified in Appendix .3.2 by comparing data and MC for 79.8 fb^{-1} . The BDTs are produced with a maximum tree depth of 6, using AUC as the target loss function. The BDT response distribution and ROC curve for each model is shown in Figures 0.16.3-0.16.5.

2lSS

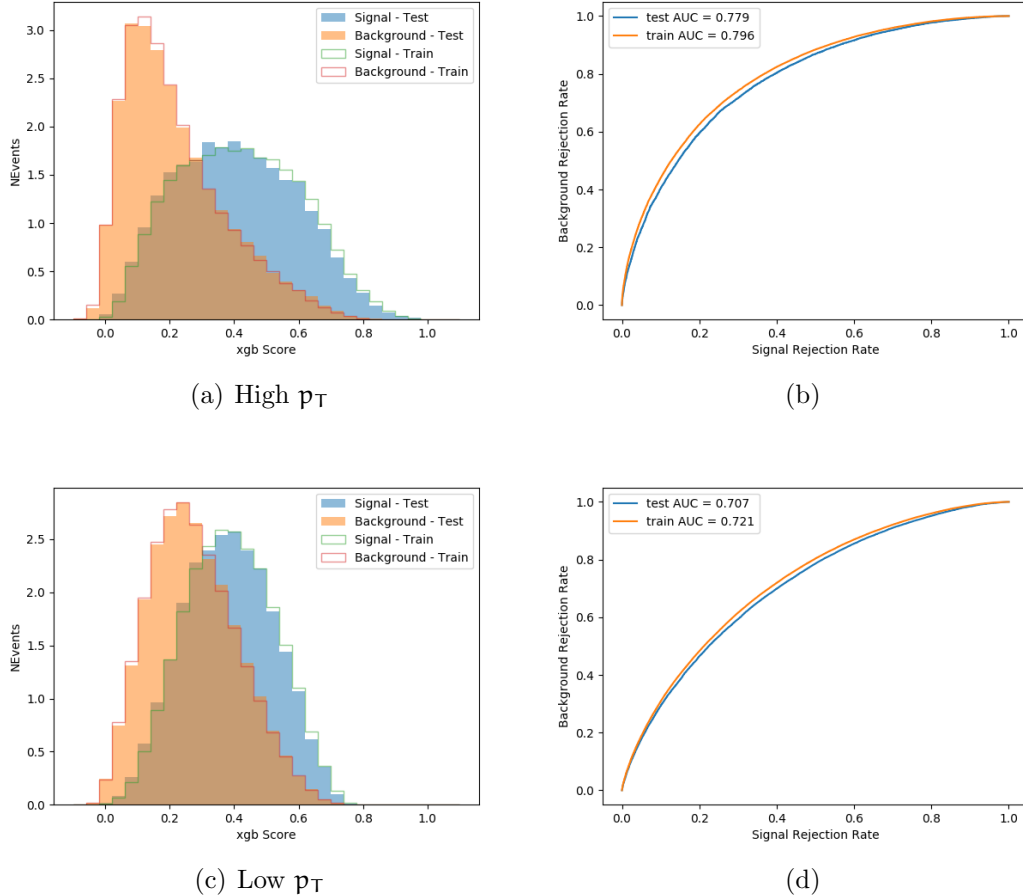


Figure 0.16.3: Output BDT scores of training and testing data for signal (blue) and background (orange) for 2lSS events with (a) high regressed Higgs p_T and (b) low regressed Higgs p_T . (b) and (d) show the ROC curve for the 2lSS high and low p_T models, respectively.

3l - Semileptonic

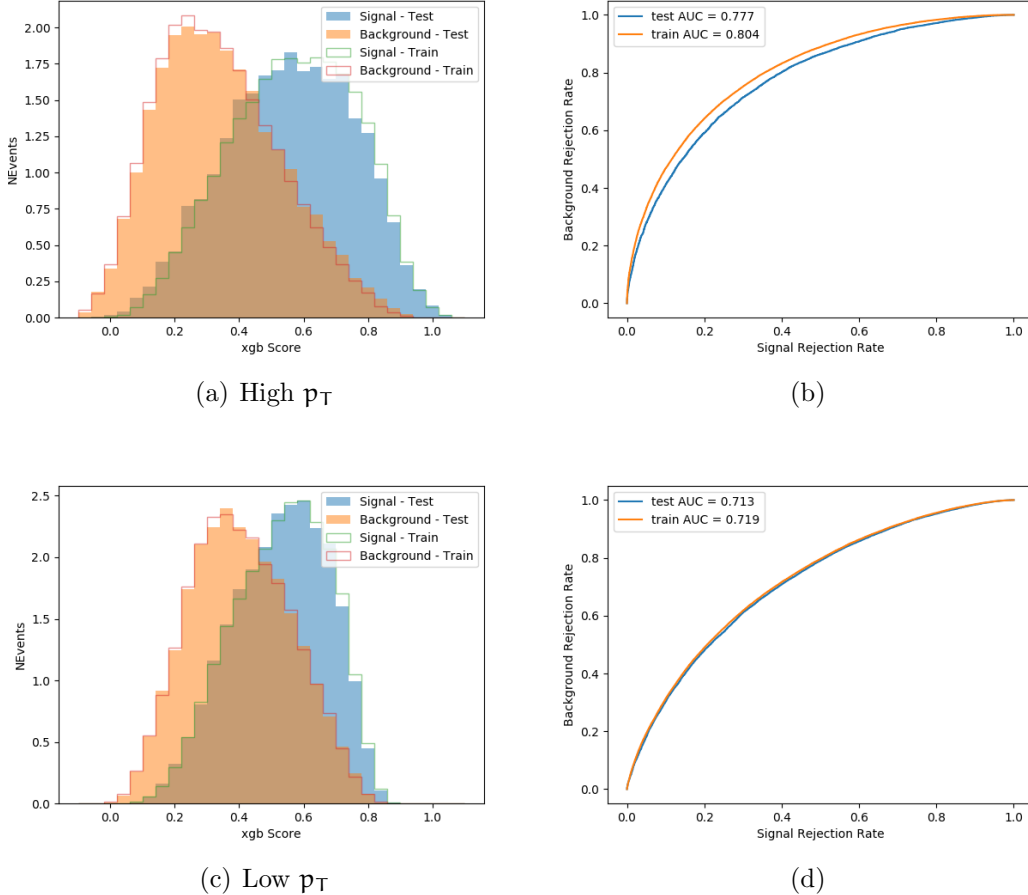


Figure 0.16.4: Output BDT scores of training and testing data for signal (blue) and background (orange) for 3lS events with (a) high regressed Higgs p_T and (b) low regressed Higgs p_T . (b) and (d) show the ROC curve for the 3lS high and low p_T models, respectively.

3l - Fully Leptonic

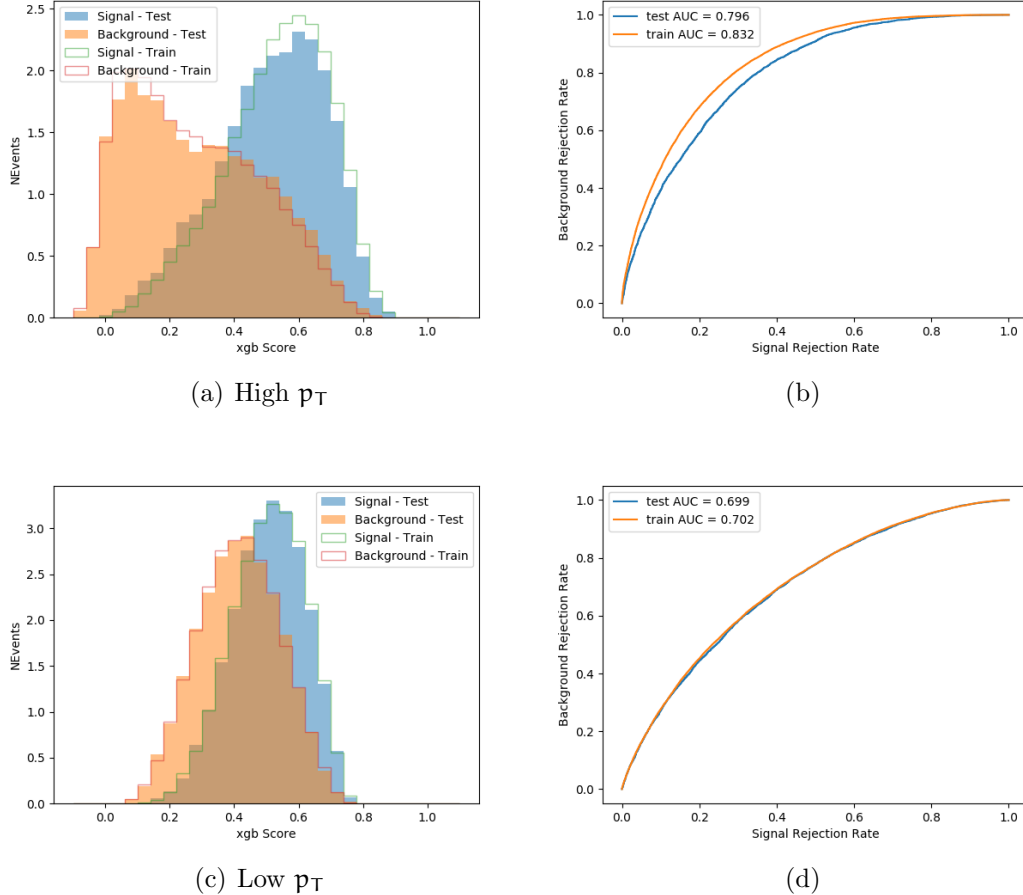


Figure 0.16.5: Output BDT scores of training and testing data for signal (blue) and background (orange) for 3lF events with (a) high regressed Higgs p_T and (b) low regressed Higgs p_T . (b) and (d) show the ROC curve for the 3lF high and low p_T models, respectively.

Output distributions of each MVA, comparing MC predictions to data at 79.8 fb^{-1} are shown in figures 0.16.6-0.16.2.

High p_T Background Rejection BDTs

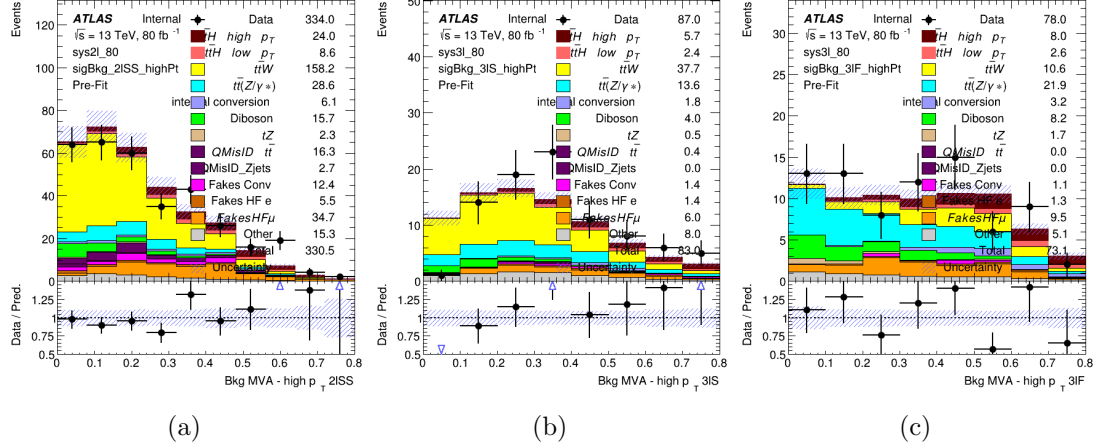


Figure 0.16.6: Output score of the high p_T BDTs in the (a) 2lSS, (b) 3lS, and (c) 3lF channels

Low p_T Background Rejection BDTs

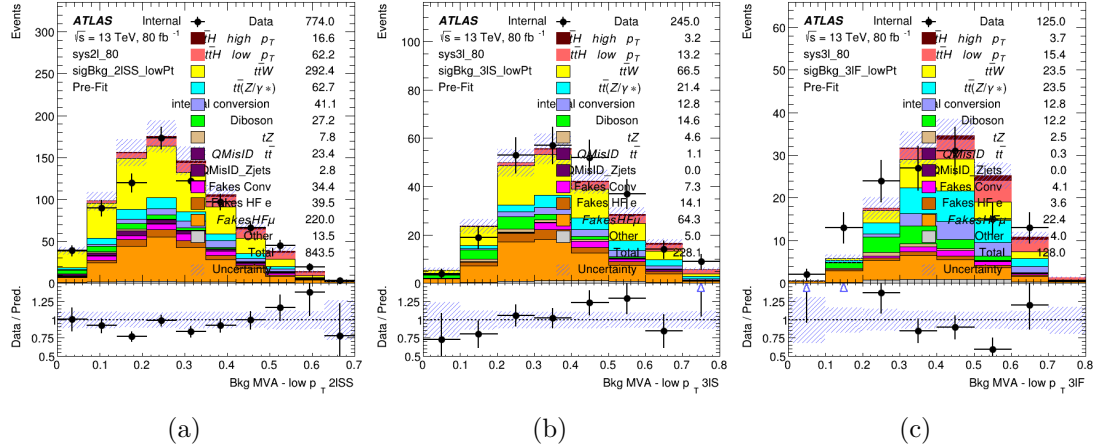


Figure 0.16.7: Output score of the low p_T BDTs in the (a) 2lSS, (b) 3lS, and (c) 3lF channels

0.16.3 Signal Region Definitions

Once pre-selection has been applied, channels are further refined based on the MVAs described above. The output of the model described in Section 0.15.5 is used to separate the three channel into two - Semi-leptonic and Fully-leptonic - based on the predicted decay mode of the Higgs boson. This leaves three orthogonal signal regions - 2lSS, 3lS, and 3lF.

For each event, depending on the number of leptons as well as whether the p_T of the Higgs is predicted to be high (> 150 GeV) or low (< 150 GeV), a cut on the appropriate background rejection MVA is applied. The particular cut values, listed in Table 32, are determined by maximizing S/\sqrt{B} in each region.

Channel	BDT Score
2lSS high p_T	0.36
2lSS low p_T	0.34
3lS high p_T	0.51
3lS low p_T	0.43
3lF high p_T	0.33
3lF low p_T	0.41

Table 32: Cutoff values on background rejection MVA score applied to signal regions.

The event preselection and MVA selection listed in Table 32 are used define the three signal regions used in the fit. These signal region definitions are summarized in Table 33.

Region	Selection
2LS	Two same charge tight leptons with $p_T > 20$ GeV $N_{\text{jets}} \geq 4$, $N_{\text{b-jets}} \geq 1$ b-tagged jets Zero τ_{had} $H_{p_T}^{\text{pred}} > 150$ GeV and BDT score > 0.36 or $H_{p_T}^{\text{pred}} < 150$ GeV and BDT score > 0.34
3LS	Three light leptons with total charge ± 1 Two tight SS leptons, $p_T > 20$ GeV One loose OS lepton, $p_T > 10$ GeV $N_{\text{jets}} \geq 2$, $N_{\text{b-jets}} \geq 1$ b-tagged jets Zero τ_{had} $ M(l^+l^-) - 91.2 \text{ GeV} > 10$ GeV for all OSSF lepton pairs Decay NN Score < 0.23 $H_{p_T}^{\text{pred}} > 150$ GeV and BDT score > 0.51 or $H_{p_T}^{\text{pred}} < 150$ GeV and BDT score > 0.43
3LF	Three light leptons with total charge ± 1 Two tight SS leptons, $p_T > 20$ GeV One loose OS lepton, $p_T > 10$ GeV $N_{\text{jets}} \geq 2$, $N_{\text{b-jets}} \geq 1$ b-tagged jets Zero τ_{had} $ M(l^+l^-) - 91.2 \text{ GeV} > 10$ GeV for all OSSF lepton pairs Decay NN Score > 0.23 $H_{p_T}^{\text{pred}} > 150$ GeV and BDT score > 0.33 or $H_{p_T}^{\text{pred}} < 150$ GeV and BDT score > 0.41

Table 33: Selection applied to define the three signal regions used in the fit.

0.17 Systematic Uncertainties

The systematic uncertainties that are considered are summarized in Table 34. These are implemented in the fit either as a normalization factors or as a shape variation or both in the signal and background estimations. The numerical impact of each of these uncertainties is outlined in section 0.18.

Table 34: Sources of systematic uncertainty considered in the analysis. Some of the systematic uncertainties are split into several components, as indicated by the number in the rightmost column.

Systematic uncertainty	Components
Luminosity	1
Pileup reweighting	1
Physics Objects	
Electron	6
Muon	15
Jet energy scale and resolution	28
Jet vertex fraction	1
Jet flavor tagging	131
E_T^{miss}	3
Total (Experimental)	186
Background Modeling	
Cross section	24
Renormalization and factorization scales	10
Parton shower and hadronization model	2
Shower tune	4
Total (Signal and background modeling)	40
Background Modeling	
Cross section	24
Renormalization and factorization scales	10
Parton shower and hadronization model	2
Shower tune	4
Total (Signal and background modeling)	40
Total (Overall)	226

The uncertainty in the combined integrated luminosity is derived from a calibration of the luminosity scale using x-y beam-separation scans performed for 13 TeV proton-proton data [?], [?].

The experimental uncertainties are related to the reconstruction and identification of light leptons and b-tagging of jets, and to the reconstruction of E_T^{miss} .

The sources which contribute to the uncertainty in the jet energy scale [?] are decomposed into uncorrelated components and treated as independent sources in the analysis. This method decomposes the uncertainties into 30 nuisance parameters

included in the fit. A similar method is used to account for jet energy resolution (JER) uncertainties, and 8 JER uncertainty components are included as NPs in the fit.

The uncertainties in the b-tagging efficiencies measured in dedicated calibration analyses [?] are also decomposed into uncorrelated components. The large number of components for b-tagging is due to the calibration of the distribution of the BDT discriminant for each of the b-tag Working Points considered in the analysis.

As mentioned in Section 0.13.2, a normalization corrections and uncertainties on the estimates of non-prompt leptons backgrounds are derived using data driven techniques, described in detail in [?]. These are derived from a likelihood fit over various non-prompt enriched control regions, targeting several sources of non-prompt light leptons separately: external conversion electrons, internal conversion electrons, electrons from heavy flavor decays, and muons from heavy flavor decays.

The normalization factor and uncertainty applied to each source of non-prompt leptons is summarized in Table 0.17

Processss	Normalization Factor
NF_e^{ExtCO}	1.70 ± 0.51
NF_e^{IntCO}	0.75 ± 0.26
NF_e^{HF}	1.09 ± 0.32
NF_{μ}^{HF}	1.28 ± 0.17

Table 35: Normalization factors - with statistical and systematic uncertainties - derived from the fit over fake control regions for each source of non-prompt leptons considered.

In addition to those derived from the control regions, several additional uncertainties are assigned to the non-prompt lepton background. An additional 25% uncertainty on material conversions is assigned, based on the comparison between data and MC in a region where a loose electron fails the photon conversion veto. A shape uncertainty of 15% (6%) is assigned to the HF non-prompt electron (muon) background based on a comparison between data and MC where the second leading electron (muon) is only required to be loose. As the contribution from light non-prompt leptons is small, about 10% percent of the contribution from HF non-prompt leptons, it is derived from the agreement between data and simulation in a LF enriched region at low values of the non-prompt lepton BDT. The resulting uncertainty is 100%, and is taken to be uncorrelated between internal and material conversions.

Theoretical uncertainties applied to MC predictions, including cross section, PDF, and scale uncertainties are taken from theory calculations for the predominate prompt backgrounds. Following the nominal $t\bar{t}H - \text{ML}$ analysis, a 50% uncertainty

is applied to Diboson to account for the large uncertainty in estimating $VV + \text{heavy flavor}$. The other “rare” background processes - including tZ , rare top processes, $ttWW$, WtZ , VVV , $tHjb$ and WtH - are assigned an overall 50% normalization uncertainty as well. The theory uncertainties applied to the MC estimates are summarized in Table 36.

Process	X-section [%]
$t\bar{t} H$ (aMC@NLO+Pythia8)	QCD Scale: $^{+5.8}_{-9.2}$ PDF($+\alpha_S$): ± 3.6
$t\bar{t} Z$ (aMC@NLO+Pythia8)	QCD Scale: $^{+9.6}_{-11.3}$ PDF($+\alpha_S$): ± 4
$t\bar{t} W$ (aMC@NLO+Pythia8)	QCD Scale: $^{+12.9}_{-11.5}$ PDF($+\alpha_S$): ± 3.4
$tHjb$ (aMC@NLO+Pythia8)	QCD Scale: $^{+6.5}_{-14.9}$ PDF($+\alpha_S$): ± 3.7
WtH (aMC@NLO+Pythia8)	QCD Scale: $^{+5.0}_{-6.7}$ PDF($+\alpha_S$): ± 6.3
VV (Sherpa 2.2.1)	± 50
Others	± 50

Table 36: Summary of theoretical uncertainties for MC predictions in the analysis.

Additional uncertainties to account for $t\bar{t}W$ mismodelling are also applied. These include a “Generator” uncertainty, based on a comparison between the nominal Sherpa 2.2.5 sample, and the formerly used aMC@NLO sample, and an “Extra radiation” uncertainty, which includes renormalisation and factorisation scale variations of the Sherpa 2.2.5 sample.

0.18 Results

A maximum likelihood fit is performed simultaneously over the reconstructed Higgs p_T spectrum in the three signal regions, $2lSS$, $3lS$, and $3lF$. The signal is split into high and low p_T samples, based on whether the truth p_T of the Higgs is above or below 150 GeV. The parameters $\mu_{t\bar{t}H \text{ high } p_T}$ and $\mu_{t\bar{t}H \text{ low } p_T}$, where $\mu = \sigma_{\text{observed}}/\sigma_{\text{SM}}$, are extracted from the fit, signifying the difference between the observed value and the theory prediction. Unblinded results are shown for the 79.8 fb^{-1} data set, as well as MC only projections of results using the full Run-2, 139 fb^{-1} dataset.

As described in Section 0.17, there are 229 systematic uncertainties that are considered as NPs in the fit. These NP s are constrained by Gaussian or log-normal

probability density functions. The latter are used for normalisation factors to ensure that they are always positive. The expected number of signal and background events are functions of the likelihood. The prior for each NP is added as a penalty term, decreasing the likelihood as it is shifted away from its nominal value.

0.18.1 Results - 79.8 fb⁻¹

As the data collected from 2015–2017 has been unblinded for $t\bar{t}H$ –ML channels, representing 79.8 fb^{-1} , those events are unblinded. The predicted Higgs p_T spectrum is fit to data simultaneously in each of the three signal regions shown in Figure 0.18.1.

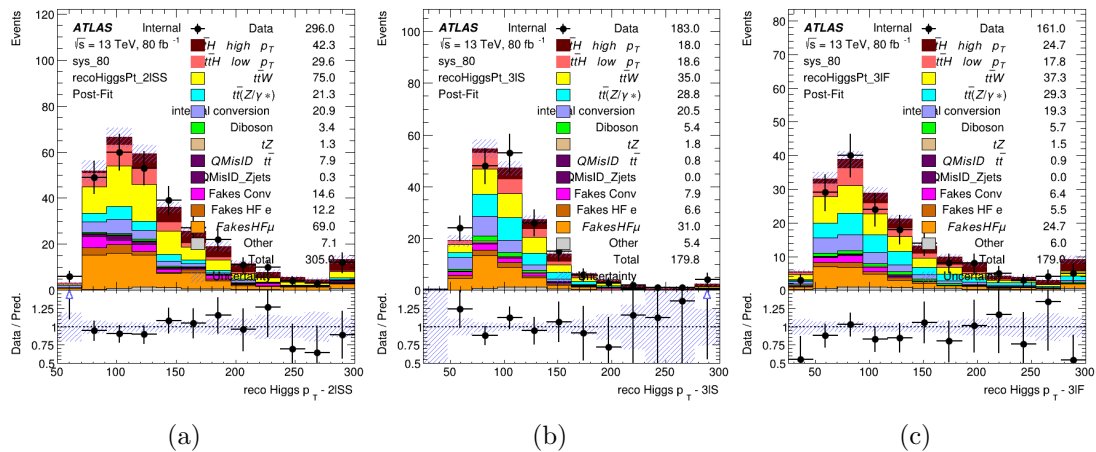


Figure 0.18.1: Post-fit distributions of the reconstructed Higgs p_T in the three signal regions, (a) 2lSS, (b) 3lS, and (c) 3lF, for 79.8 fb^{-1} of MC

A post-fit summary of the fitted regions is shown in Figure 0.18.2.

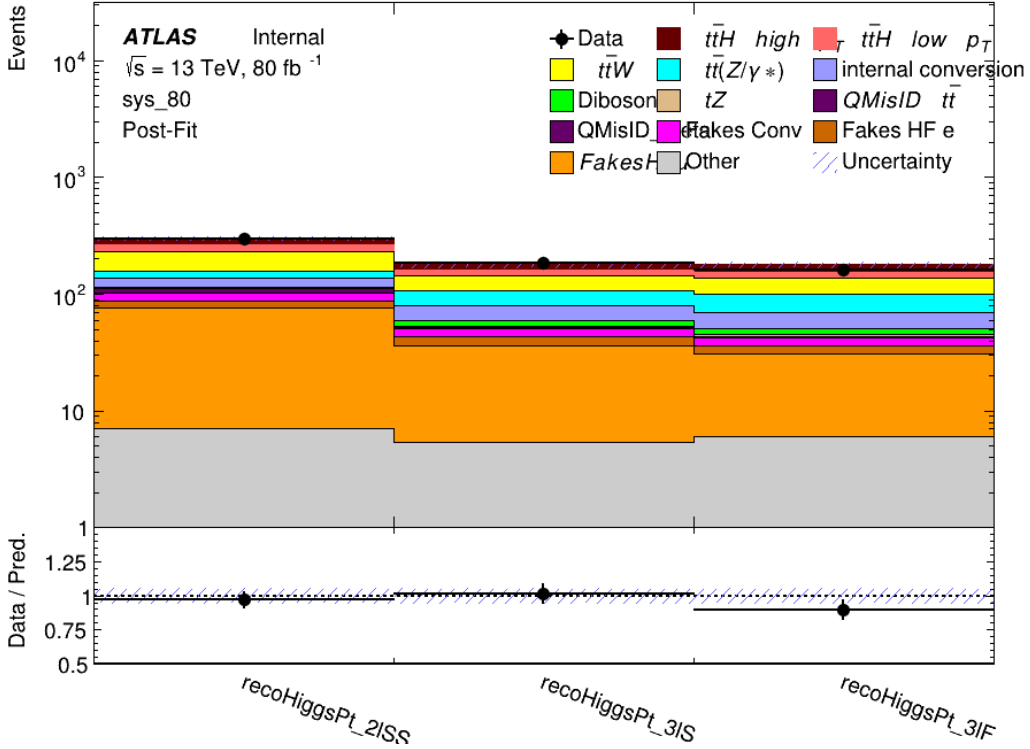


Figure 0.18.2: Post-fit summary of the yields in each signal region.

The measured μ values for high and low p_T Higgs production obtained from the fit are shown in 37. A significance of 1.7σ is observed for $t\bar{t}H$ high p_T , and 2.1σ is measured for $t\bar{t}H$ low p_T .

$$\mu_{t\bar{t}H \text{ high } p_T} = 2.1^{+0.62}_{-0.59}(\text{stat})^{+0.40}_{-0.43}(\text{sys})$$

$$\mu_{t\bar{t}H \text{ low } p_T} = 0.83^{+0.39}_{-0.40}(\text{stat})^{+0.51}_{-0.53}(\text{sys})$$

Table 37: Best fit μ values for $t\bar{t}H$ high p_T and $t\bar{t}H$ low p_T , where $\mu = \sigma_{\text{obs}}/\sigma_{\text{pred}}$

The most prominent sources of systematic uncertainty, as measured by their impact on $\mu_{t\bar{t}H \text{ high } p_T}$, are summarized in Table 38.

Uncertainty Source	$\Delta\mu$	
Jet Energy Scale	0.25	0.23
$t\bar{t}H$ cross-section (QCD scale)	-0.11	0.21
Luminosity	-0.13	0.14
Flavor Tagging	0.14	0.13
$t\bar{t}W$ cross-section (QCD scale)	-0.12	0.11
Higgs Branching Ratio	-0.1	0.11
$t\bar{t}H$ cross-section (PDF)	-0.07	0.08
Electron ID	-0.06	0.06
Non-prompt Muon Normalization	-0.05	0.06
$t\bar{t}Z$ cross-section (QCD scale)	-0.05	0.05
Diboson cross-section	-0.05	0.05
Fake muon modelling	-0.04	0.04
Total	0.40	0.43

Table 38: Summary of the most significant sources of systematic uncertainty on the measurement of $t\bar{t}H$ high p_T .

The most significant sources of uncertainty on the measurement of $t\bar{t}H$ - low p_T are shown in Table 39.

Uncertainty Source	$\Delta\mu$	
Internal Conversions	-0.26	0.26
Luminosity	-0.16	0.17
Non-prompt Muon Normalization	-0.16	0.16
$t\bar{t}W$ cross-section (QCD scale)	-0.17	0.15
Jet Energy Scal	0.15	0.15
Non-prompt Electron Modelling	-0.13	0.14
Flavor Tagging	0.13	0.13
Non-prompt Muon Modelling	-0.12	0.13
Non-prompt Electron Normalization	-0.11	0.11
$t\bar{t}Z$ cross-section (QCD scale)	-0.08	0.09
Diboson Cross-section	-0.07	0.07
Total	0.51	0.53

Table 39: Summary of the most significant sources of systematic uncertainty on the measurement of $t\bar{t}H$ low p_T .

The ranking and impact of those nuisance parameters with the largest contribution to the overall uncertainty is shown in Figure 0.18.3.

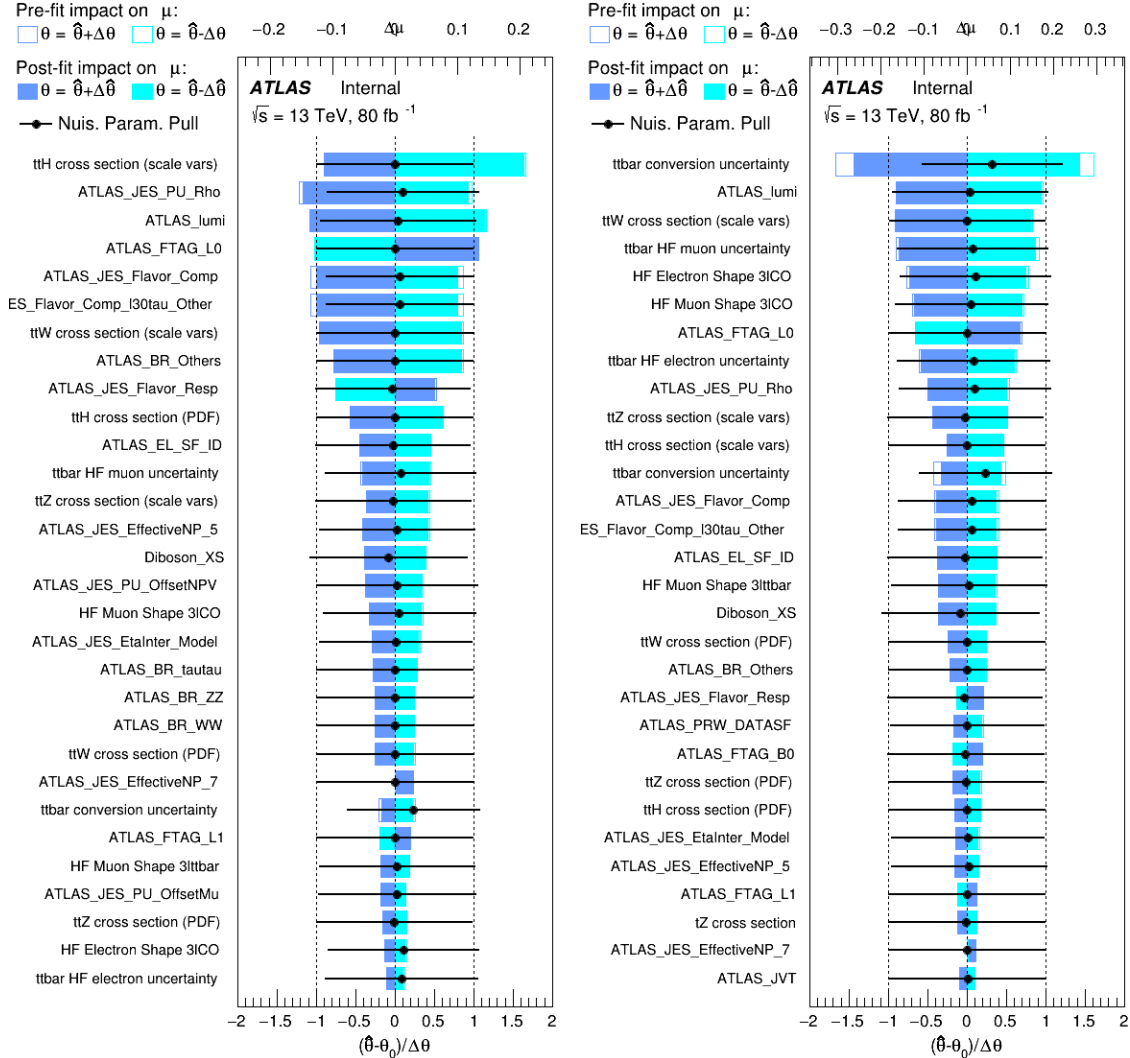


Figure 0.18.3: Impact of systematic uncertainties on the measurement of high p_T (left) and low p_T (right) $t\bar{t}H$ events

0.18.2 Projected Results - 139 fb^{-1}

As data collected in 2018 has not yet been unblinded for $t\bar{t}H - \text{ML}$ at the time of this note, data from that year remains blinded. Instead, an Asimov fit is performed - with the MC prediction being used both as the SM prediction as well as the data in the fit - in order to give expected results.

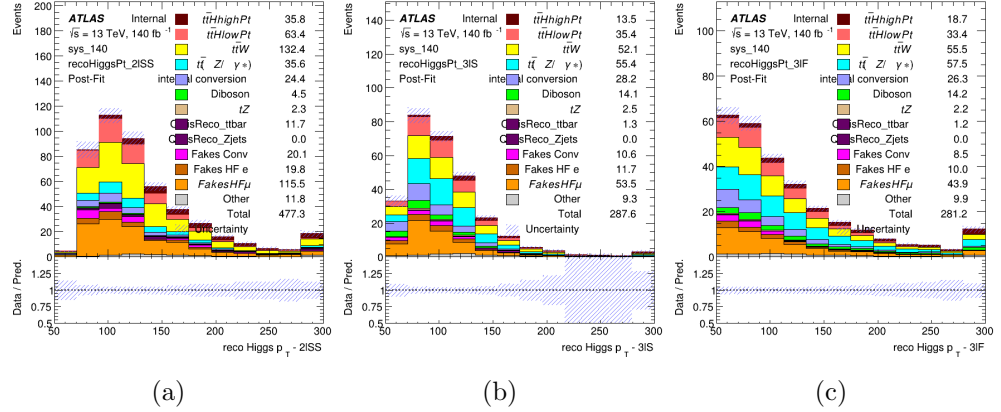


Figure 0.18.4: Blinded post-fit distributions of the reconstructed Higgs p_T in the three signal regions, (a) 2lSS, (b) 3lS, and (c) 3lF, for 139 fb^{-1} of data

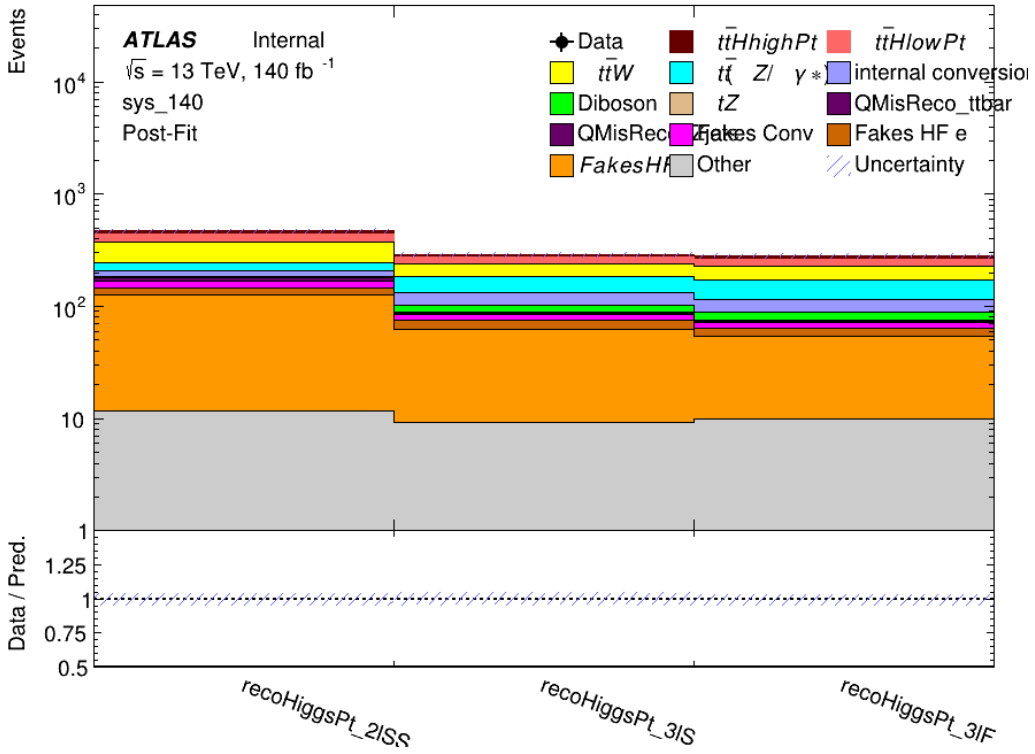


Figure 0.18.5: Post-fit summary of fit.

Projected uncertainties on the μ values extracted from the fit for high and low p_T Higgs are shown in 40. A significance of 2.0σ is expected for $t\bar{t}H$ high p_T , and a projected significance 2.3σ is extracted for $t\bar{t}H$ low p_T .

$$\mu_{t\bar{t}H \text{ high } p_T} = 1.00^{+0.45}_{-0.43}(\text{stat})^{+0.30}_{-0.31}(\text{sys})$$

$$\mu_{t\bar{t}H \text{ low } p_T} = 1.00^{+0.29}_{-0.30}(\text{stat})^{+0.48}_{-0.50}(\text{sys})$$

Table 40: Best fit μ values for $t\bar{t}H$ high p_T and $t\bar{t}H$ low p_T , where $\mu = \sigma_{\text{obs}}/\sigma_{\text{pred}}$

The most prominent sources of systematic uncertainty, as measured by their impact on $\mu_{t\bar{t}H \text{ high } p_T}$, are summarized in Table 41.

Uncertainty Source	$\Delta\mu$	
Jet Energy Scale	0.19	0.17
$t\bar{t}W$ Cross-section (QCD Scale)	-0.12	0.11
Luminosity	-0.1	0.11
Flavor Tagging	0.1	0.1
$t\bar{t}H$ Cross-section (QCD Scale)	-0.05	0.1
$t\bar{t}Z$ Cross-section (QCD Scale)	-0.05	0.06
Non-prompt Muon Normalization	-0.05	0.05
Higgs Branching Ratio	-0.05	0.05
Diboson Cross-section	-0.04	0.05
Non-prompt Muon Modelling	-0.04	0.04
$t\bar{t}H$ Cross-section (PDF)	-0.03	0.04
Electron ID	-0.04	0.04
$t\bar{t}W$ Cross-section (PDF)	-0.03	0.03
Total	0.30	0.31

Table 41: Summary of the most significant sources of systematic uncertainty on the measurement of $t\bar{t}H$ high p_T .

The most significant sources of systematic uncertainty on $t\bar{t}H$ low p_T are summarized in Table 42.

Uncertainty Source	$\Delta\mu$	
Internal Conversions	-0.18	0.2
Jet Energy Scale	0.19	0.16
Non-prompt Muon Normalization	-0.16	0.17
Luminosity	-0.15	0.17
$t\bar{t}W$ Cross-section (QCD Scale)	-0.17	0.15
Non-prompt Electron Modelling	-0.13	0.14
Non-prompt Muon Modelling	-0.13	0.13
Flavor Tagging	0.13	0.12
Non-prompt Electron Normalization	-0.1	0.11
$t\bar{t}Z$ Cross-section (QCD Scale)	-0.07	0.09
$t\bar{t}H$ Cross-section (QCD Scale)	-0.05	0.1
Total	0.48	0.50

Table 42: Summary of the most significant sources of systematic uncertainty on the measurement of $t\bar{t}H$ low p_T .

The ranking and impact of those nuisance parameters with the largest contribution to the overall uncertainty is shown in Figure 0.18.6.

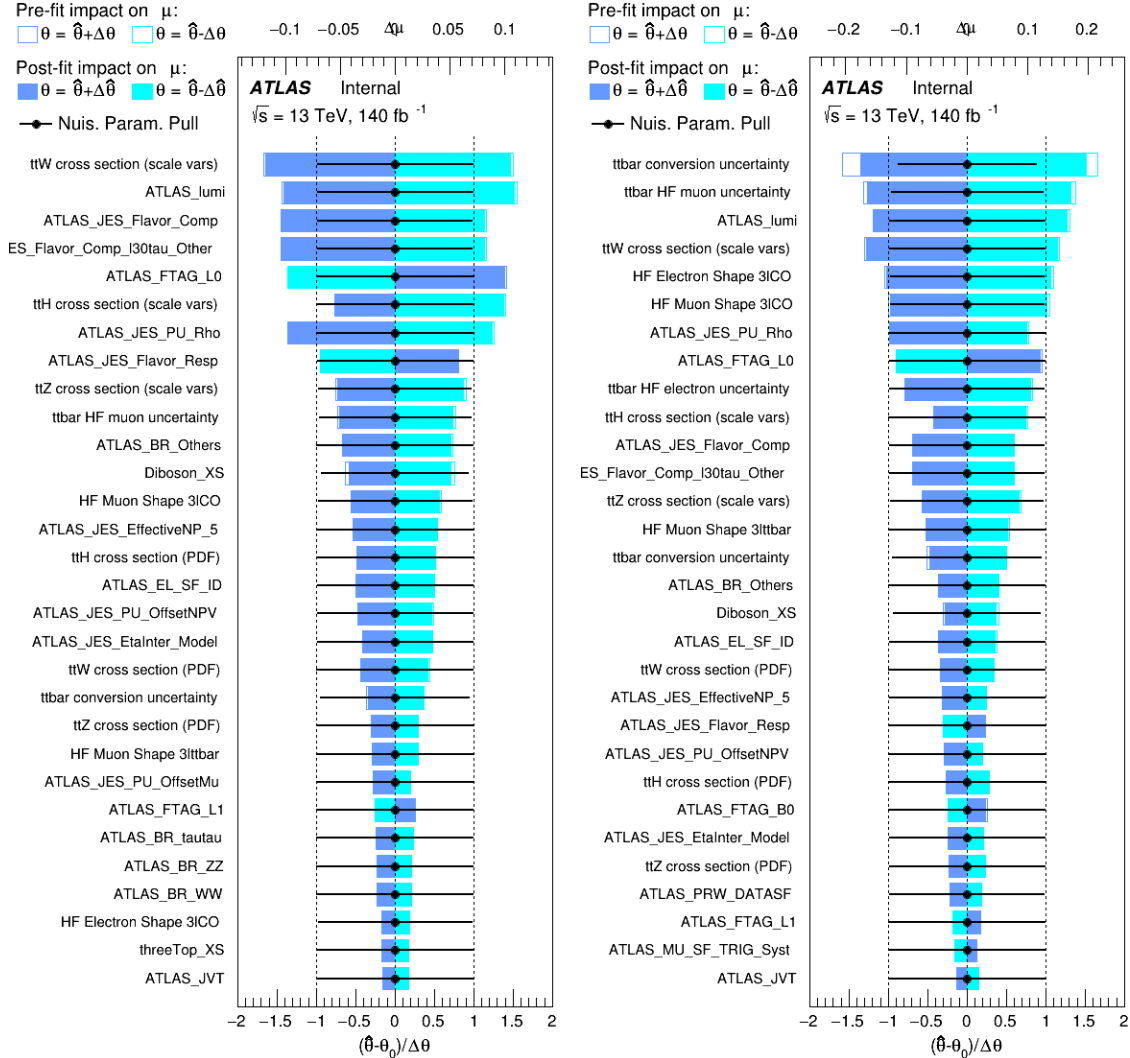


Figure 0.18.6: Impact of systematic uncertainties on the measurement of high p_T (left) and low p_T (right) $t\bar{t}H$ events

Part VI

Conclusion

A method of employing machine learning techniques in order to reconstruct the momentum spectrum of the Higgs boson produced in association with top quark pairs has been presented for events with multiple leptons in the final state. Preliminary results for using these techniques to perform differential measurements in this channel have been presented: Using 80 fb^{-1} of data, normalization factors of $\mu_{t\bar{t}H \text{ high } p_T} = 2.1^{+0.62}_{-0.59}(\text{stat})^{+0.40}_{-0.43}(\text{sys})$ and $\mu_{t\bar{t}H \text{ low } p_T} = 0.83^{+0.39}_{-0.40}(\text{stat})^{+0.51}_{-0.53}(\text{sys})$ are measured for events with Higgs $p_T > 150 \text{ GeV}$ and $< 150 \text{ GeV}$, respectively. Projected results for 139 fb^{-1} of data give sensitivity of $\mu_{t\bar{t}H \text{ high } p_T} = 1.00^{+0.45}_{-0.43}(\text{stat})^{+0.30}_{-0.31}(\text{sys})$ and $\mu_{t\bar{t}H \text{ low } p_T} = 1.00^{+0.29}_{-0.30}(\text{stat})^{+0.48}_{-0.50}(\text{sys})$.

Appendices

.1 Non-prompt lepton MVA

A lepton MVA has been developed to better reject non-prompt leptons than standard cut based selections based upon impact parameter, isolation and PID. The name of this MVA is `PromptLeptonVeto`. The full set of studies and detailed explanation can be found in [?].

The decays of W and Z bosons are commonly selected by the identification of one or two electrons or muons. The negligible lifetimes of these bosons mean that the leptons produced in the decay originate from the interaction vertex and are thus labelled “prompt”. Analyses using these light leptons impose strict reconstruction quality, isolation and impact parameter requirements to remove “fake” leptons. A significant source of the fake light leptons are non-prompt leptons produced in decays of hadrons that contain bottom (**b**) or charm (**c**) quarks. Such hadrons typically have microscopically significant lifetimes that can be detected experimentally.

These non-prompt leptons can also pass the tight selection criteria. In analyses that involve top (**t**) quarks, which decay almost exclusively into a W boson and a **b** quark, non-prompt leptons from the semileptonic decay of bottom and charm hadrons can be a significant source of background events. This is particularly the case in the selection of same-sign dilepton and multilepton final states.

The main idea is to identify non-prompt light leptons using lifetime information associated with a track jet that matches the selected light lepton. This lifetime information is computed using tracks contained within the jet. Typically, lepton lifetime is determined using the impact parameter of the track reconstructed by the inner tracking detector which is matched to the reconstructed lepton. Using additional reconstructed charged particle tracks increases the precision of identifying the displaced decay vertex of bottom or charm hadrons that produced a non-prompt light lepton. The MVA also includes information related to the isolation of the lepton to reject non-prompt leptons.

`PromptLeptonVeto` is a gradient boosted BDT. The training of the BDT is performed on leptons selected from the POWHEG+PYTHIA6 non-allhad $t\bar{t}$ MC sample. Eight variables are used to train the BDT in order to discriminate between prompt and non-prompt leptons. The track jets that are matched to the non-prompt leptons correspond to jets initiated by **b** or **c** quarks, and may contain a displaced vertex. Consequently, three of the selected variables are used to identify **b**-tag jets by standard ATLAS flavour tagging algorithms. Two variables use the relationship between the track jet and lepton: the ratio of the lepton p_T with respect to the track jet p_T and ΔR between the lepton and the track jet axis. Finally three additional variables test whether the reconstructed lepton is isolated: the number of tracks collected by the track jet and the lepton track and calorimeter isolation variables. Table 43 describes the variables used to train the BDT algorithm. The choice of input variables has been extensively discussed with Egamma, Muon, Tracking, and Flavour Tagging CP groups.

The output distribution of the BDT is shown in Figure .1.

Variable	Description
N_{track} in track jet	Number of tracks collected by the track jet
$\text{IP2 log}(P_b/P_{\text{light}})$	Log-likelihood ratio between the b and light jet hypotheses with the IP2D algorithm
$\text{IP3 log}(P_b/P_{\text{light}})$	Log-likelihood ratio between the b and light jet hypotheses with the IP3D algorithm
$N_{\text{TrkAtVtx}} \text{ SV} + \text{JF}$	Number of tracks used in the secondary vertex found by the SV1 algorithm in addition to the number of tracks from secondary vertices found by the JetFitter algorithm with at least two tracks
$p_T^{\text{lepton}}/p_T^{\text{track jet}}$	The ratio of the lepton p_T and the track jet p_T
$\Delta R(\text{lepton}, \text{track jet})$	ΔR between the lepton and the track jet axis
$p_T^{\text{VarCone30}}/p_T$	Lepton track isolation, with track collecting radius of $\Delta R < 0.3$
$E_T^{\text{TopoCone30}}/p_T$	Lepton calorimeter isolation, with topological cluster collecting radius of $\Delta R < 0.3$

Table 43: A table of the variables used in the training of `PromptLeptonVeto`.

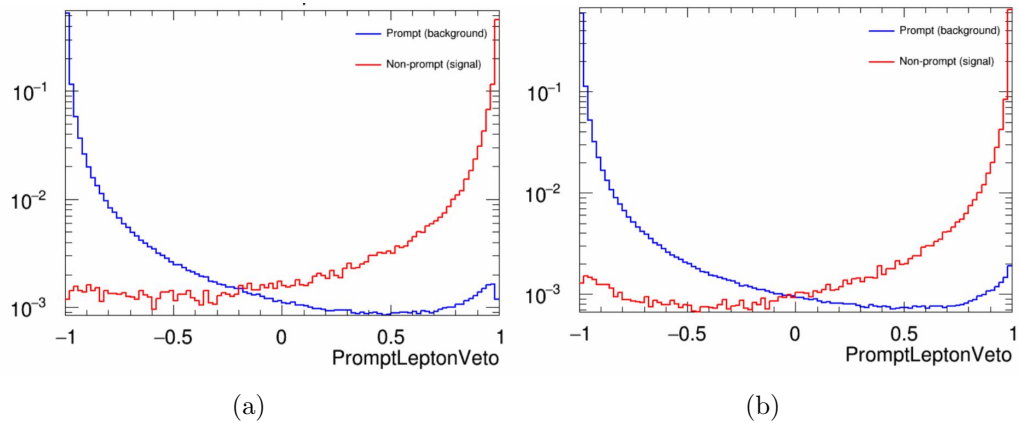


Figure .1.1: Distribution of the PLV BDT discriminant for (a) electrons and (b) muons

The ROC curve for the BDT response, compared to the standard `FixedCutTight` WP, is shown in figure .1, which shows a clear improvement when using this alternative training.

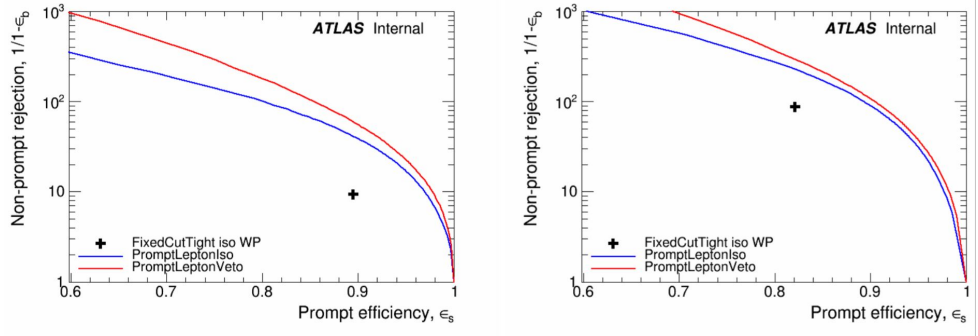


Figure .1.2: ROC curves for the PLV as well as the performance of the standard FixedCutTight WP for (left) electrons and (right) muons

A cutoff value of -0.7 for electrons and -0.5 for muons are chosen as the WPs for this MVA, based on an optimisation of S/\sqrt{B} performed in the preselection regions of the $t\bar{t}H$ – ML analysis, which have a signature similar to that of this analysis.

The efficiency of the tight `PromptLeptonVeto` working point is measured using the tag and probe method with $Z \rightarrow \ell^+\ell^-$ events. Such calibration are performed by analysers from this analysis in communication with the Egamma and Muon combined performance groups. The scale factor are approximately 0.92 for $10 < p_T < 15$ GeV, and averaging at 0.98 to 0.99 for higher p_T leptons. An extra systematic is applied to muons within $\Delta R < 0.6$ of a calorimeter jet, since there is a strong dependence on the scale factor due to the presence of these jets. For electrons, the dominant systematics is coming from pile-up dependence. Overall the systematics are a maximum of 3% at low p_T and decreasing at a function of p_T .

.2 Supplementary WZ + Heavy Flavor Studies

.2.1 Non-prompt CR Modelling

In order to further validate the modeling in each of the non-prompt CRs, additional kinematic plots are made in the Z+jets CR and $t\bar{t}$ CR in each of the continuous b-tag regions, after the correction factors detailed in Section 0.8.3 have been applied.

In the case of the Z+jets CR, the p_T spectrum of the lepton originating from the W candidate is shown, as this is the distribution used to extract the scale factor applied to Z+jets. These plots are shown in Figures .2.1 and .2.2.

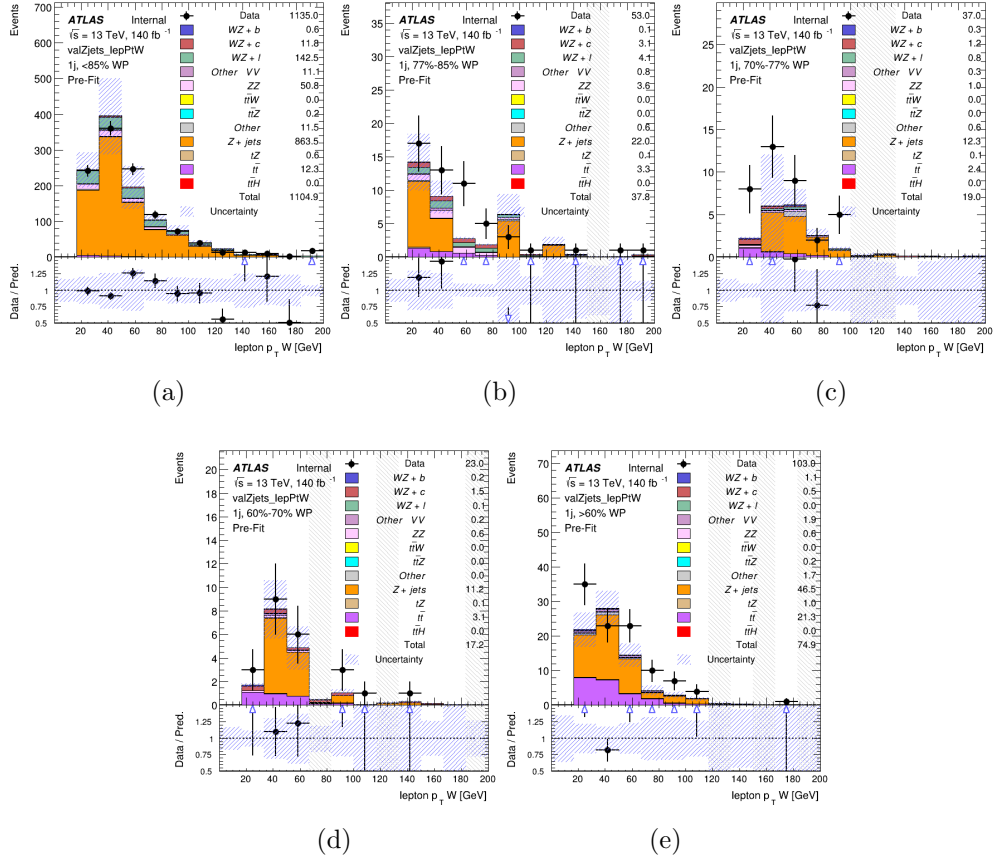


Figure .2.1: Comparisons between the data and MC distributions of the p_T of the lepton originating from the W-candidate in the Z+jets CR for each of the 1-jet b-tag working point regions

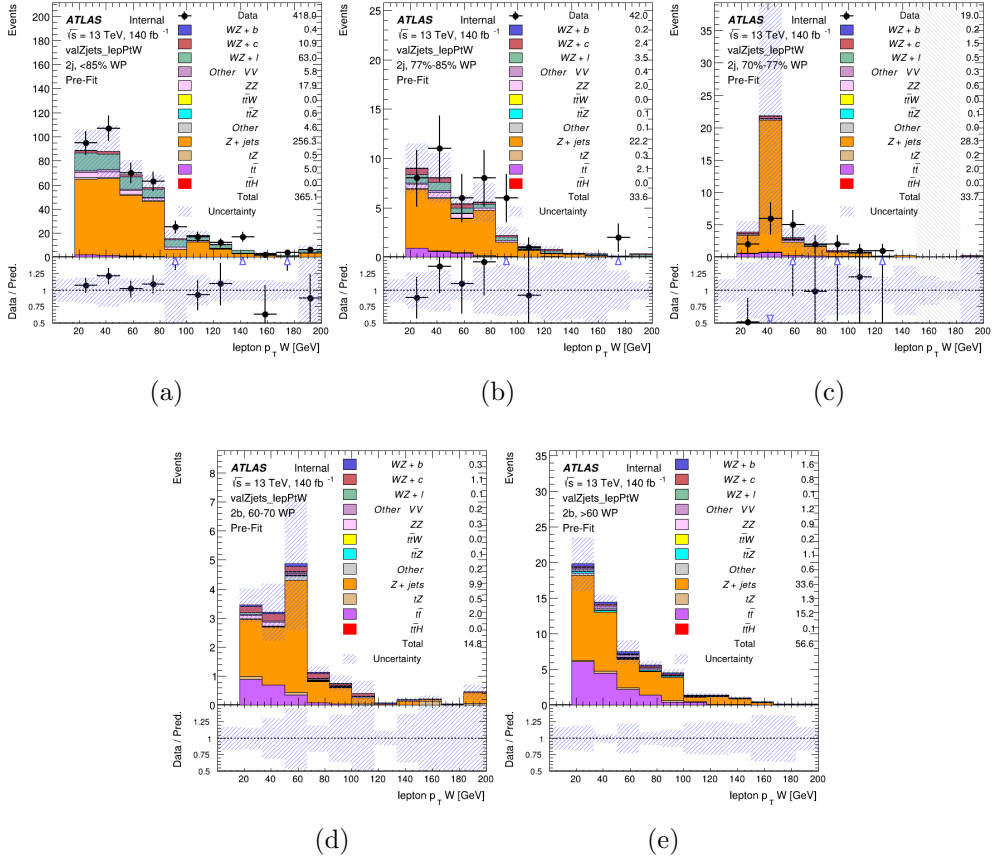


Figure .2.2: Comparisons between the data and MC distributions of the p_T of the lepton originating from the W-candidate in the Z+jets CR for each of the 2-jet b-tag working point regions

The same is shown for the $t\bar{t}$ CR, but the p_T of the OS lepton is used instead as a representation of the modeling, as the lepton from the W is not well defined for $t\bar{t}$ events. These plots are shown in Figures .2.3 and .2.4.

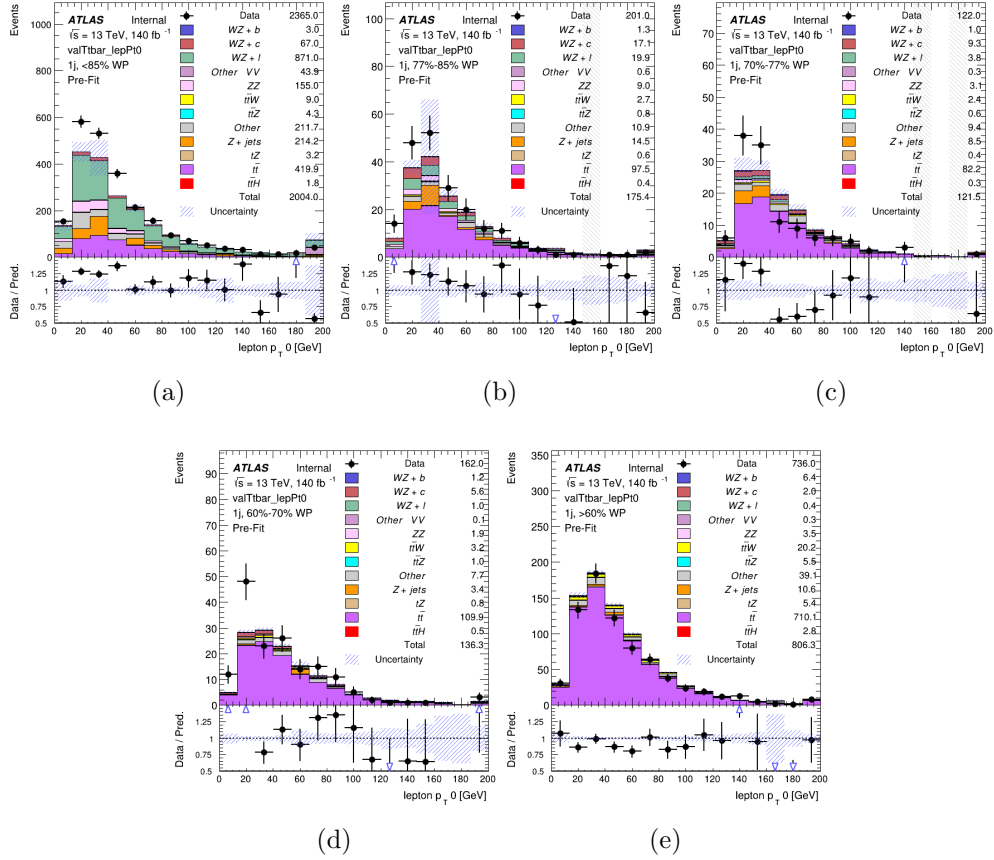


Figure .2.3: Comparisons between the data and MC distributions of the p_T of the OS lepton in the $t\bar{t}$ CR for each of the 1-jet b-tag working point regions

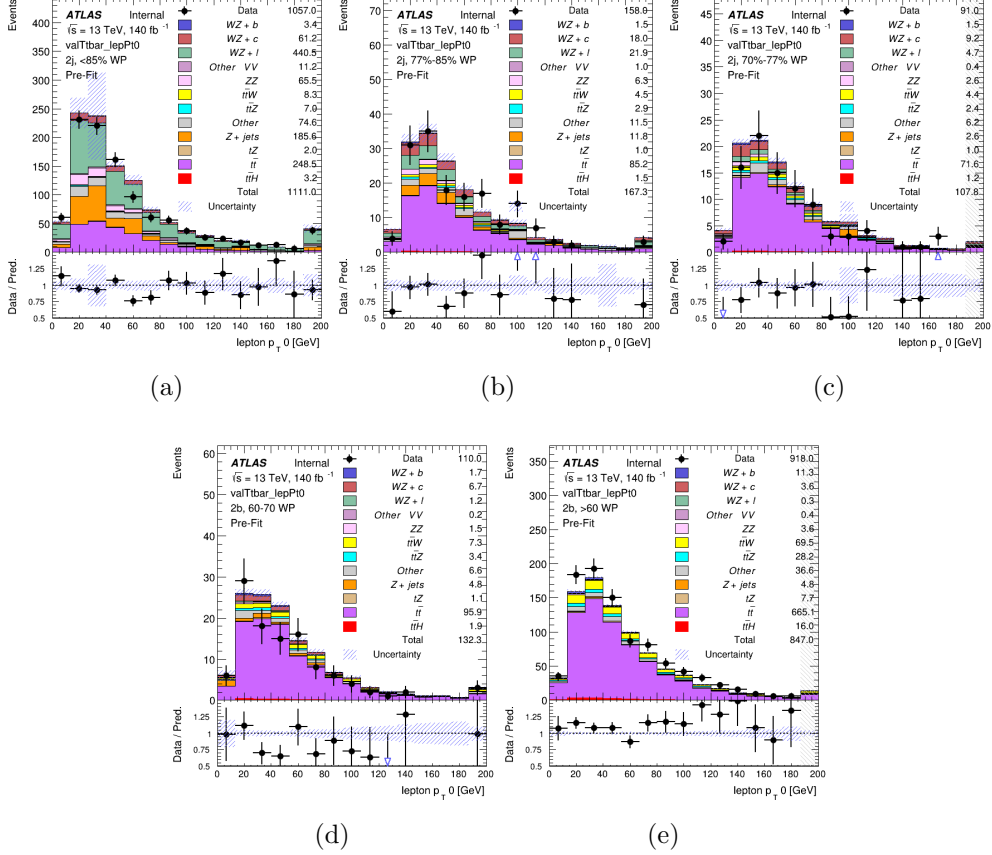


Figure .2.4: Comparisons between the data and MC distributions of the p_T of the OS lepton in the $t\bar{t}$ CR for each of the 2-jet b-tag working point regions

2.2 tZ Interference Studies

Because it includes an on-shell Z boson as well as a b-jet and W from the top decay, tZ production represents an identical final state to WZ + b-jet. This implies the possibility of matrix level interference between these two processes not accounted for in the Monte Carlo simulations, which consider the two processes independently. Truth level studies are performed in order to estimate the impact of these interference effects.

In order to estimate the matrix level interference effects between tZ and WZ + b-jet, two different sets of simulations are produced using MADGRAPH 5 [?] - one which simulates these two processes independently, and another where they are

produced simultaneously, such that interference effects are present. These two sets of samples are then compared, and the difference between them can be taken to represent any interference effects.

MadGraph simulations of 10,000 tZ and 10,000 WZ + b events are produced, along with 20,000 events where both are present, in the fiducial region where three leptons and at least one jet are produced.

A selection mimicking the preselection used in the main analysis is applied to the samples: The SS leptons are required to have $p_T > 20$ GeV, and > 10 GeV is required for the OS lepton. The associated b-jet is required to have $p_T > 25$ GeV, and all physics objects are required to fall in a range of $|\eta| < 2.5$.

The overall cross-section with and without intereferece effects agree within error, and no significant differences in the kinematic distributions are seen. It is therefore concluded that interference effects do not significantly impact the results.

.2.3 Alternate tZ Inclusive Fit

.2.3.1 tZ Inclusive Fit

While tZ is often considered as a distinct process form WZ + b, this could also be considered part of the signal. Alternative studies are performed where, using the same framework as the nominal analysis, a measurement of WZ + b is performed that includes tZ as part of WZ+b.

Because of this change, the tZ CR is no longer necessary, and only the five pseudo-continuous b-tag regions are used in the fit. Further, systematics related to the tZ cross-section are removed from the fit, as they are now encompassed by the normalization measurement of WZ + b. All other systematic uncertainties are carried over from the nominal analysis.

An expected WZ + b cross-section of $4.1^{+0.78}_{-0.74}(\text{stat})^{+0.53}_{-0.52}(\text{sys})$ fb is extracted from the fit, with an expected significance of 4.0σ .

The impact of the predominate systematics are summarized in Table 44.

Uncertainty Source	$\Delta\mu$	
WZ + light cross-section	0.08	-0.08
Jet Energy Scale	-0.06	0.08
Luminosity	-0.05	0.06
WZ + c cross-section	-0.04	0.05
Other Diboson + b cross-section	-0.04	0.04
WZ cross-section - QCD scale	-0.04	0.03
t̄t cross-section	-0.03	0.03
Jet Energy Resolution	-0.03	0.03
Flavor tagging	-0.03	0.03
Z+jets cross section	-0.02	0.02
Total Systematic Uncertainty	-0.15	0.16

Table 44: Summary of the most significant sources of systematic uncertainty on the measurement of WZ + b with exactly one associated jet.

.2.3.2 Floating tZ

In order to quantify the impact of the tZ uncertainty on the fit, an alternate fit strategy is used where the tZ normalization is allowed to float. This normalization factor replaces the cross-section uncertainty on tZ, and all other parameters of the fit remain the same.

An uncertainty of 17% on the normalization of tZ is extracted from the fit, compared to a theory uncertainty of 15% applied to the tZ cross-section. The measured uncertainties on WZ remain the same.

3 Supplementary t̄tH Differential Analysis Studies

The following section provides details of the various MVAs as well as a few studies performed in support of this analysis, exploring alternate decisions and strategies.

.3.1 Higgs Reconstruction Model Details

.3.1.1 b-jet Identification Features - 2lSS

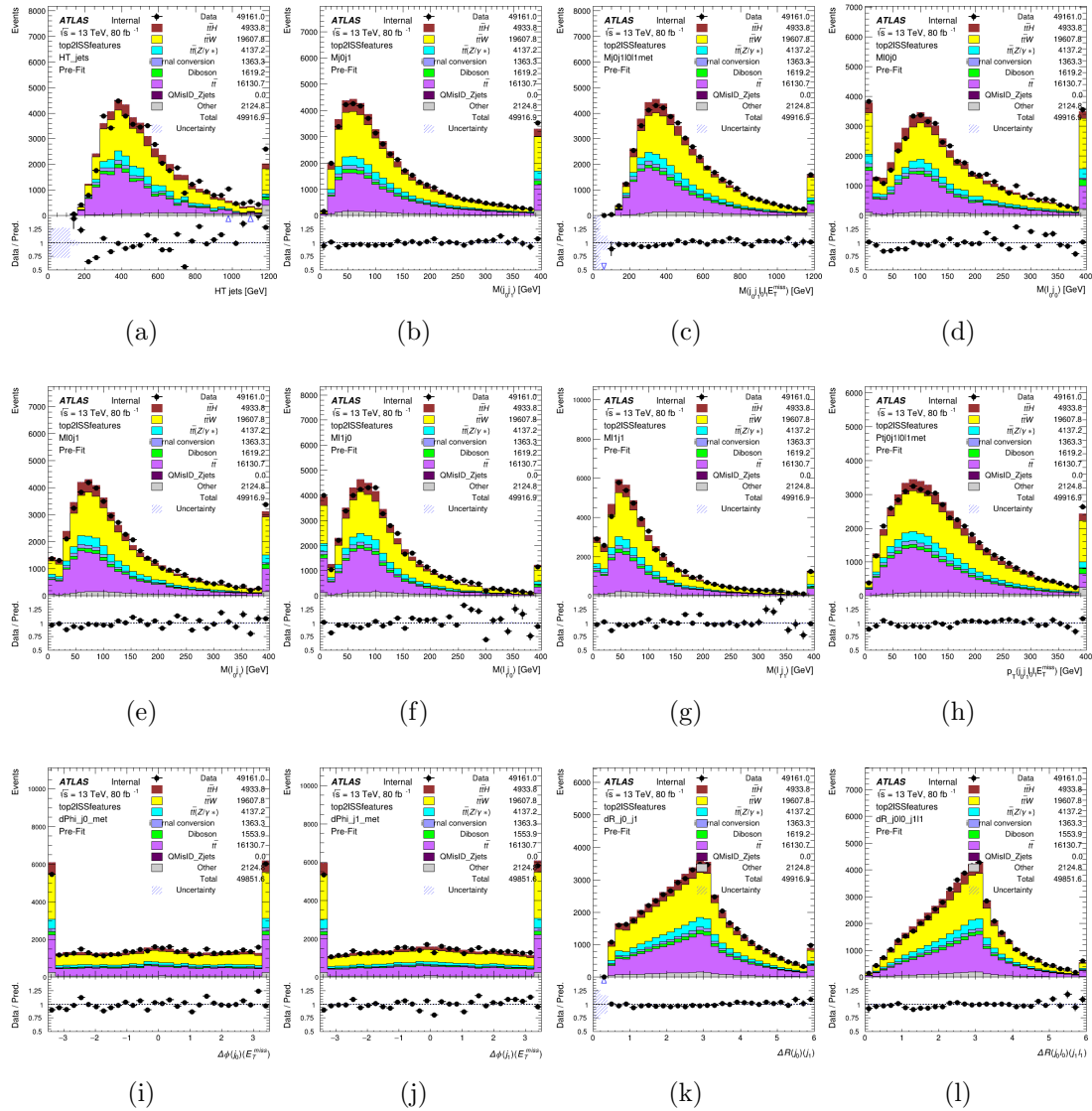


Figure .3.1: Input features for top2lSS

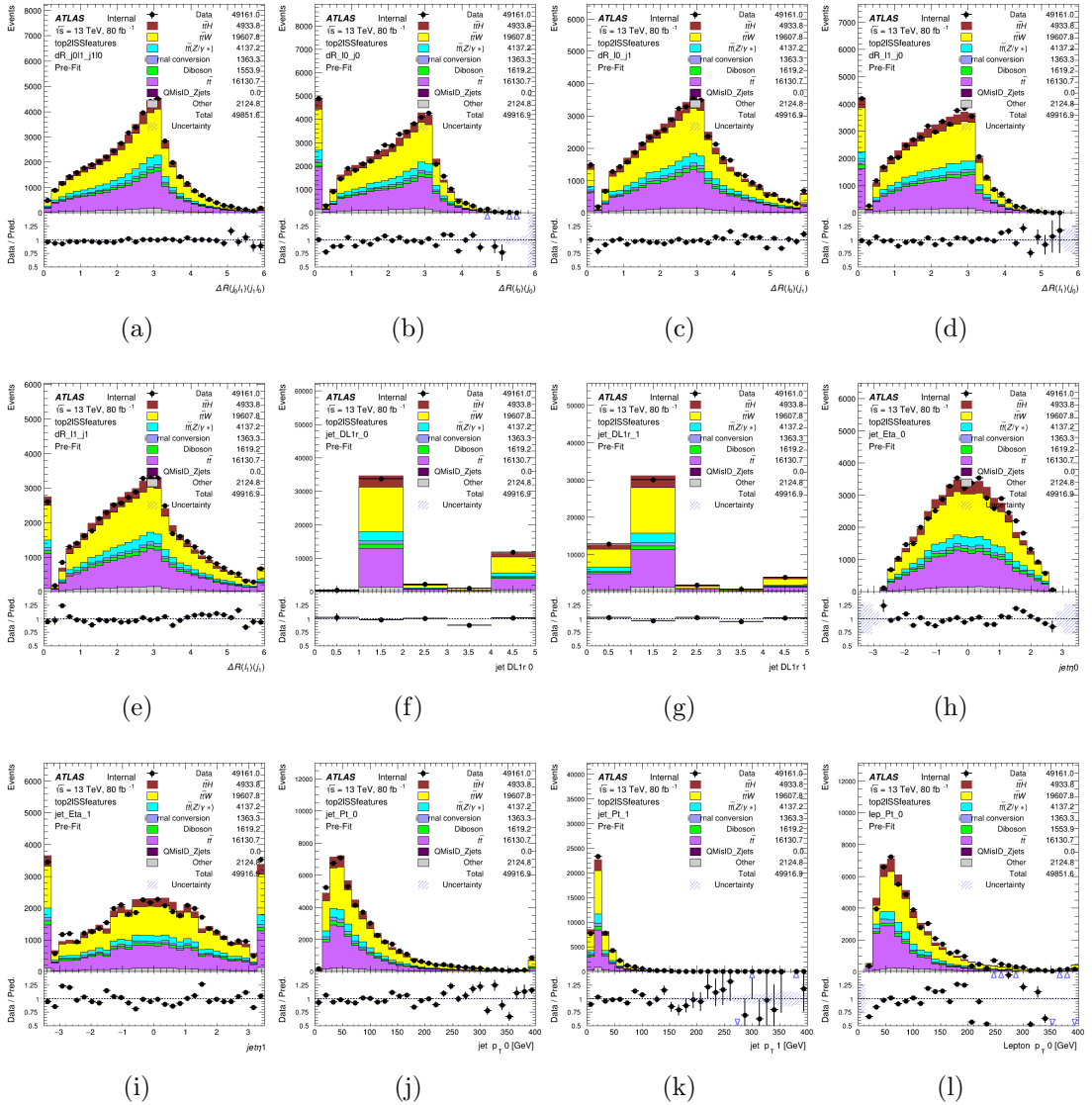


Figure .3.2: Input features for top2lSS

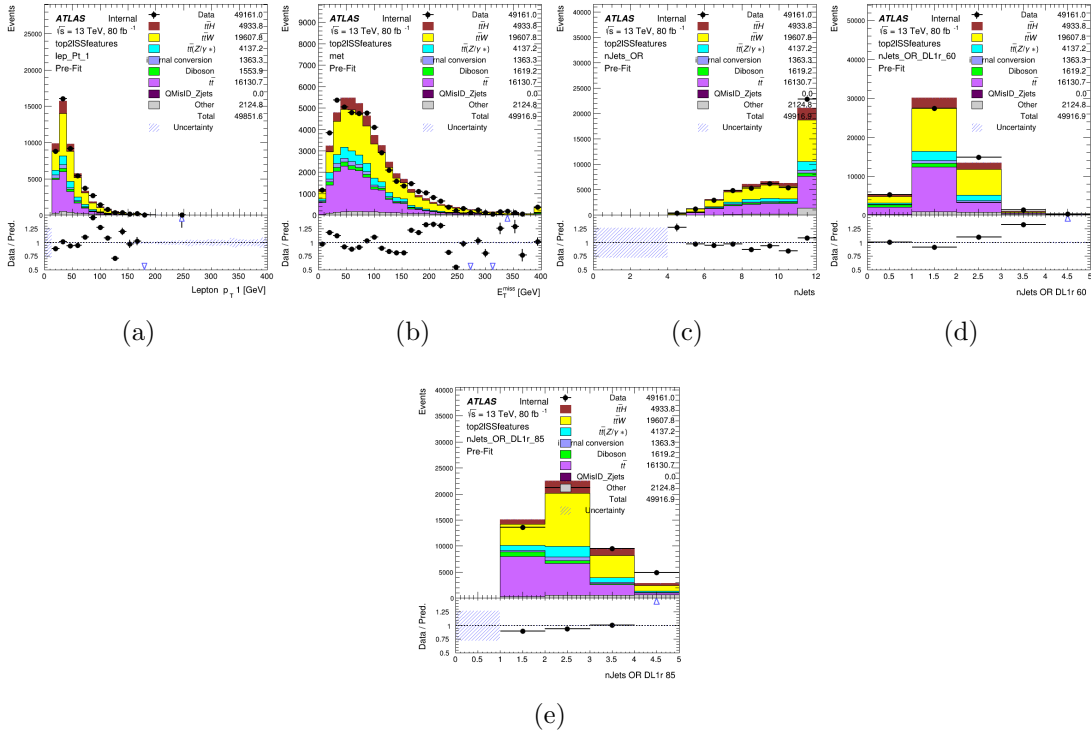


Figure .3.3: Input features for top2lSS

.3.1.2 b-jet Identification Features - 3l

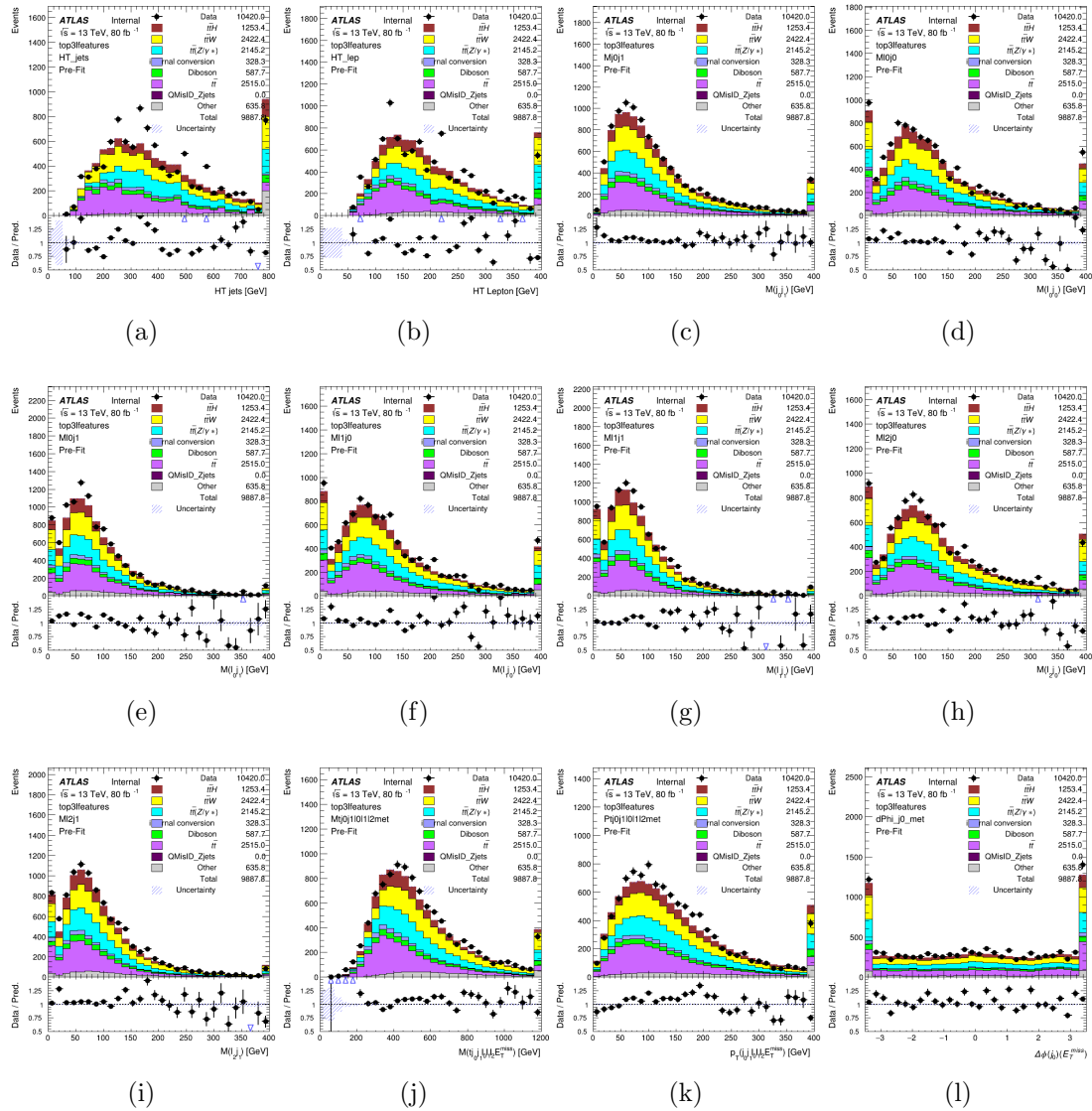


Figure .3.4: Input features for top3l

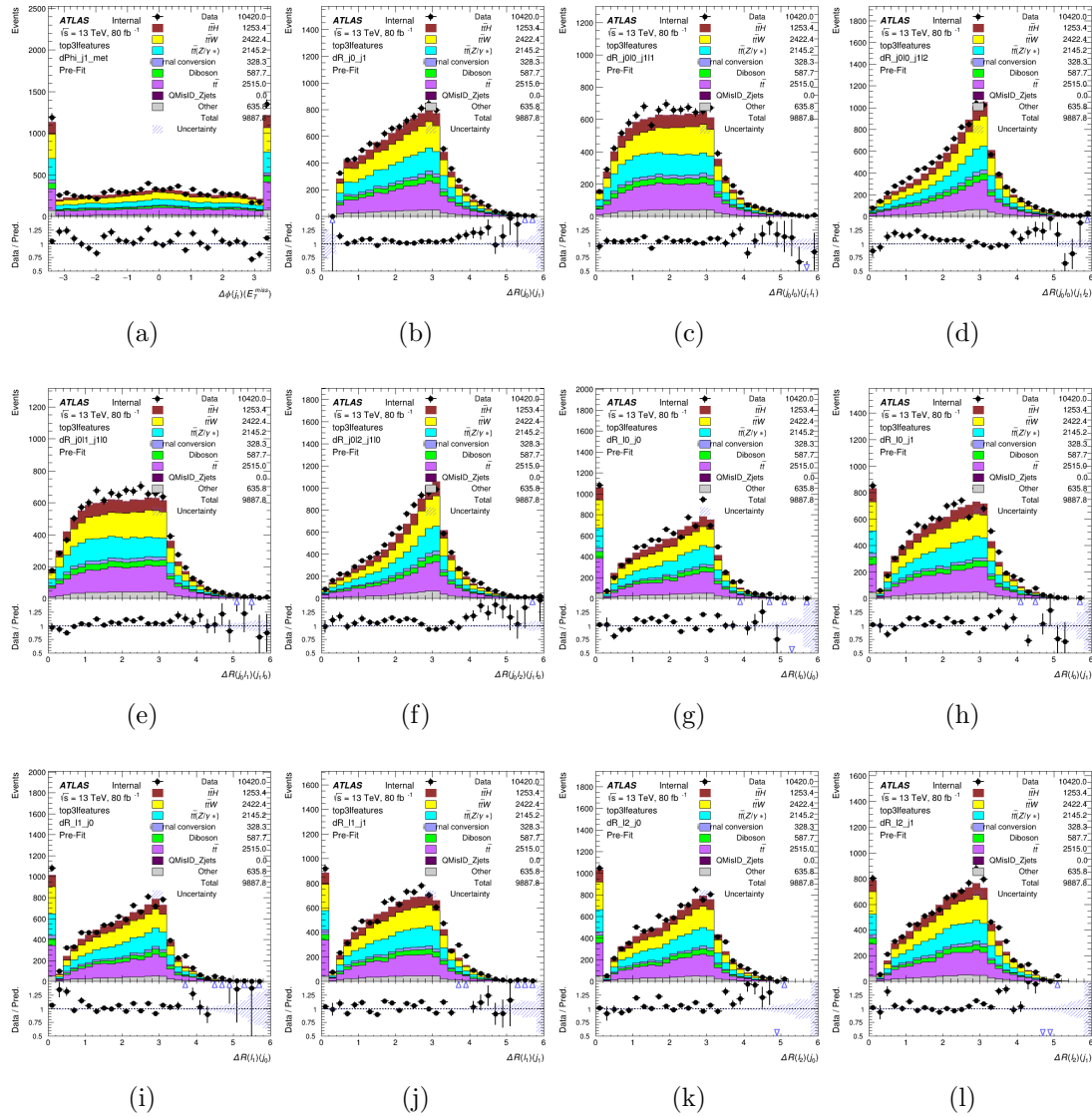


Figure 3.5: Input features for top3l

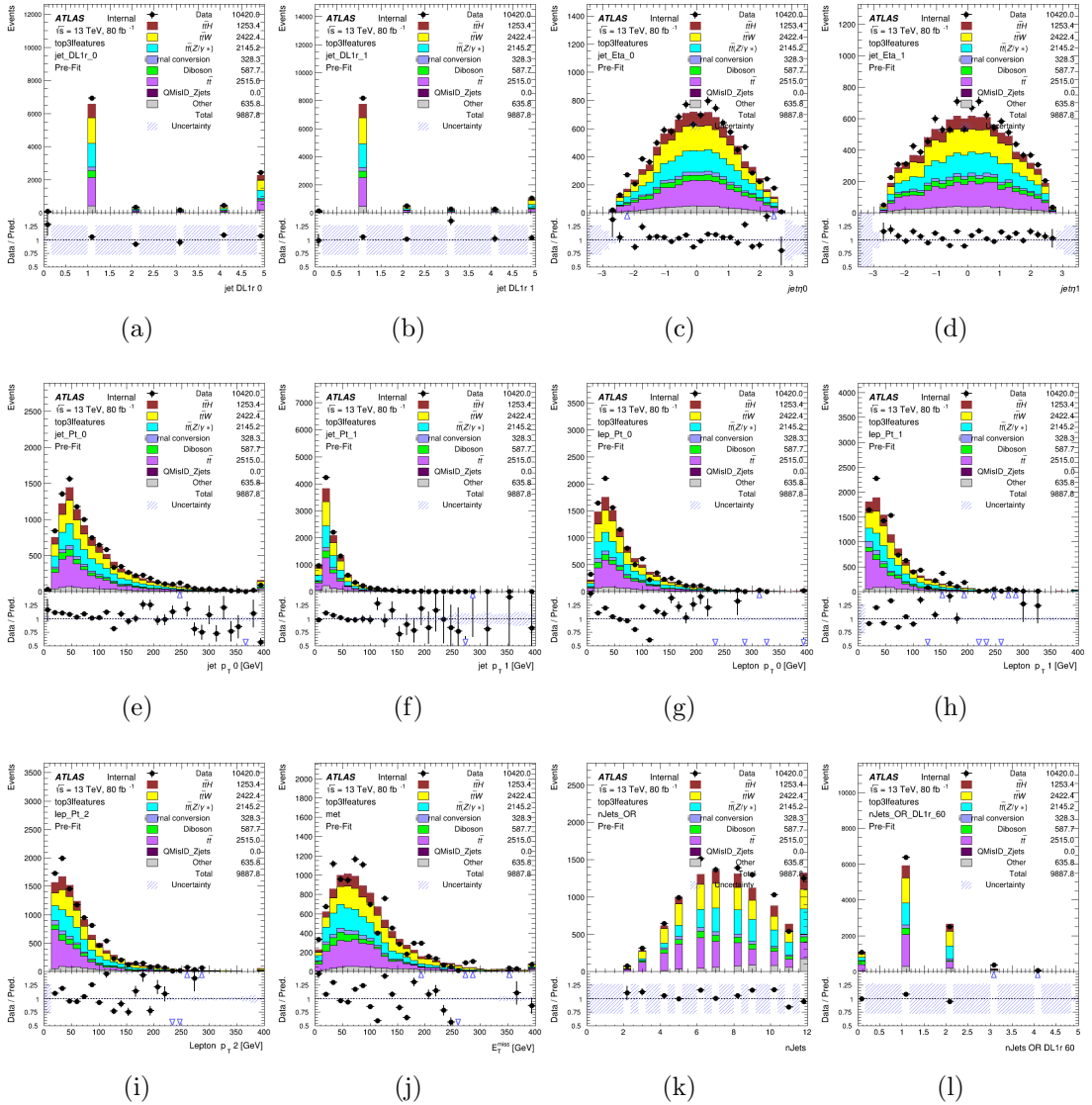
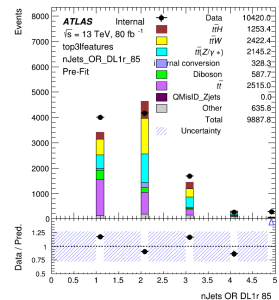


Figure 3.6: Input features for top3l



(a)

Figure .3.7: Input features for top3l

.3.1.3 Higgs Reconstruction Features - 2lSS

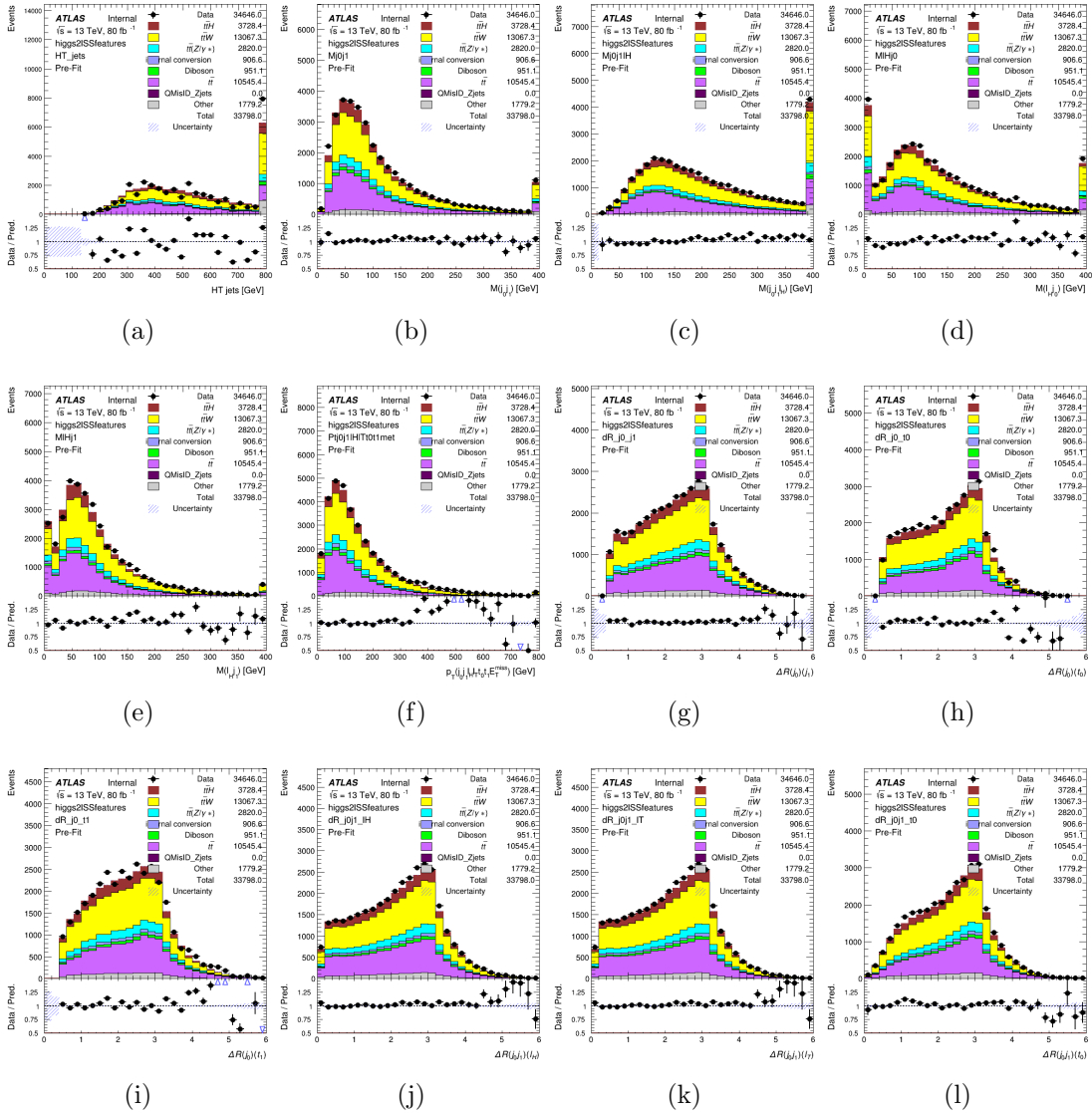


Figure .3.8: Input features for higgs2lSS

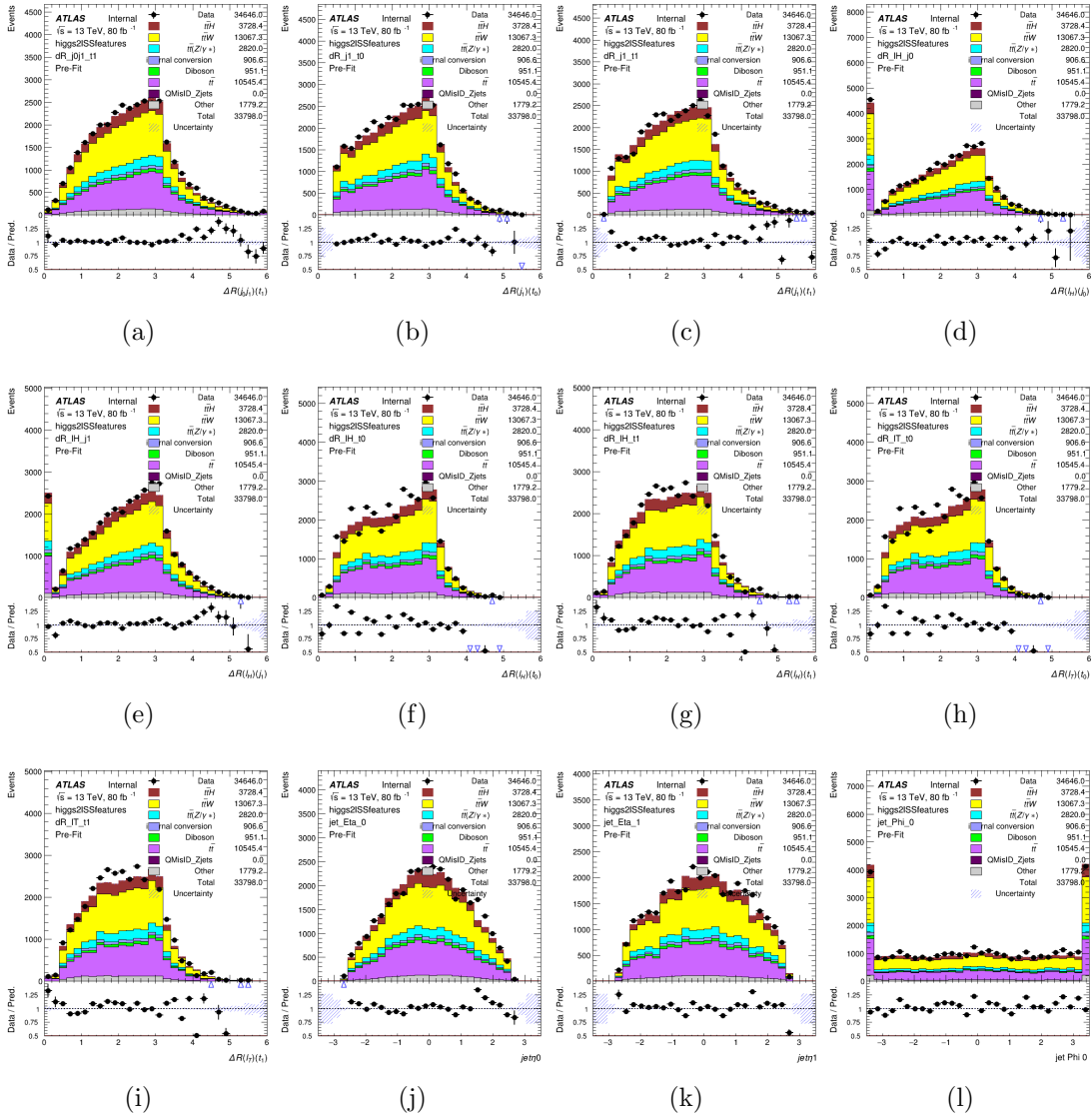


Figure .3.9: Input features for higgs2lSS

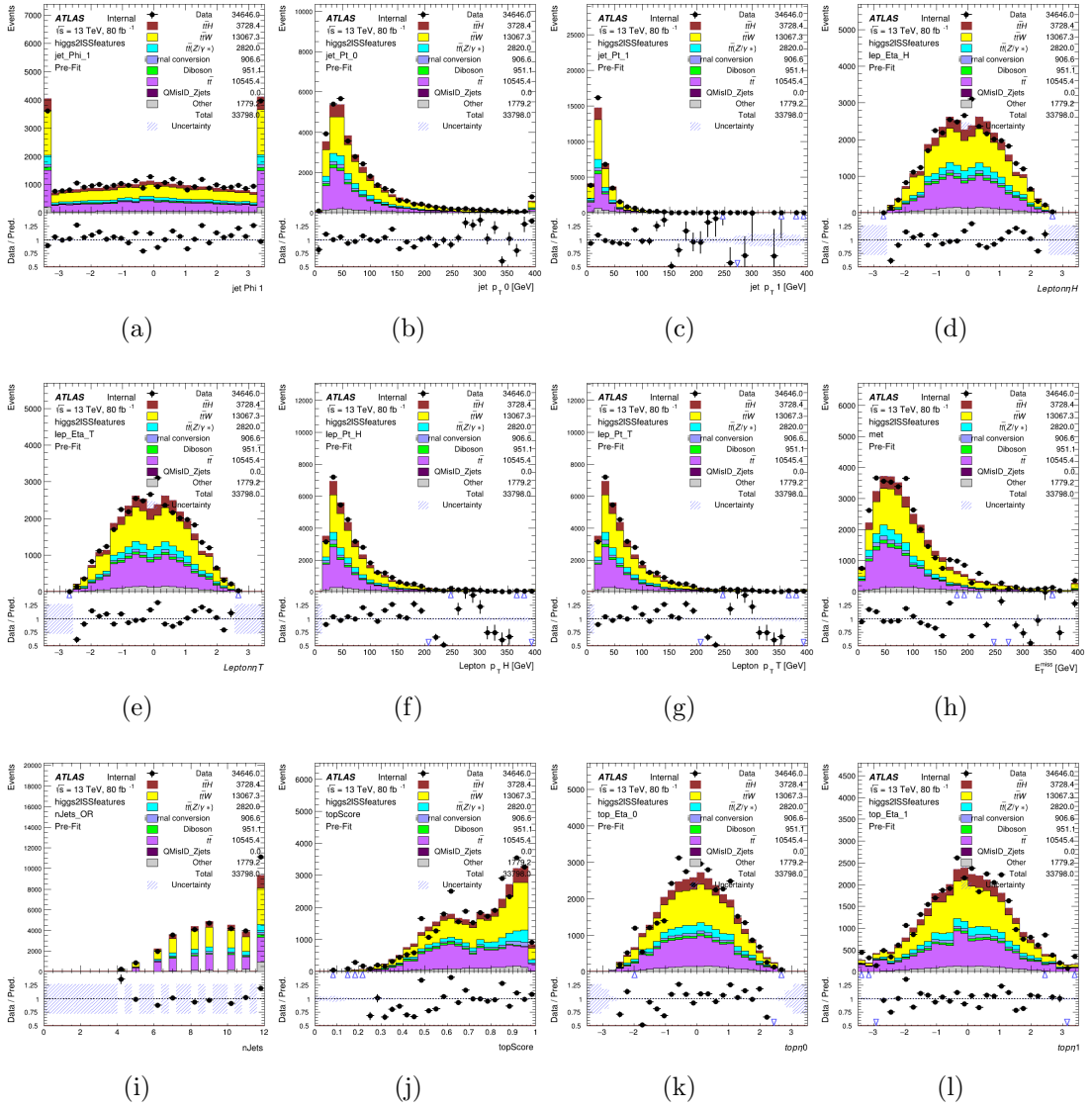


Figure .3.10: Input features for higgs2lSS

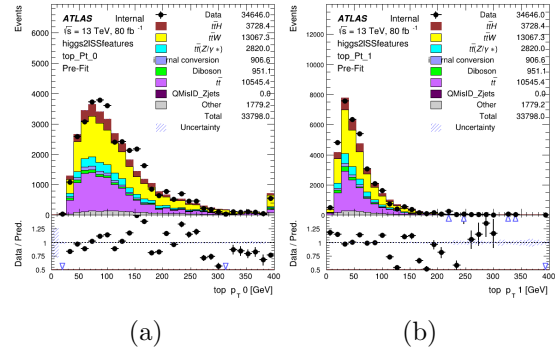


Figure .3.11: Input features for higgs2lSS

.3.1.4 Higgs Reconstruction Features - 3lS

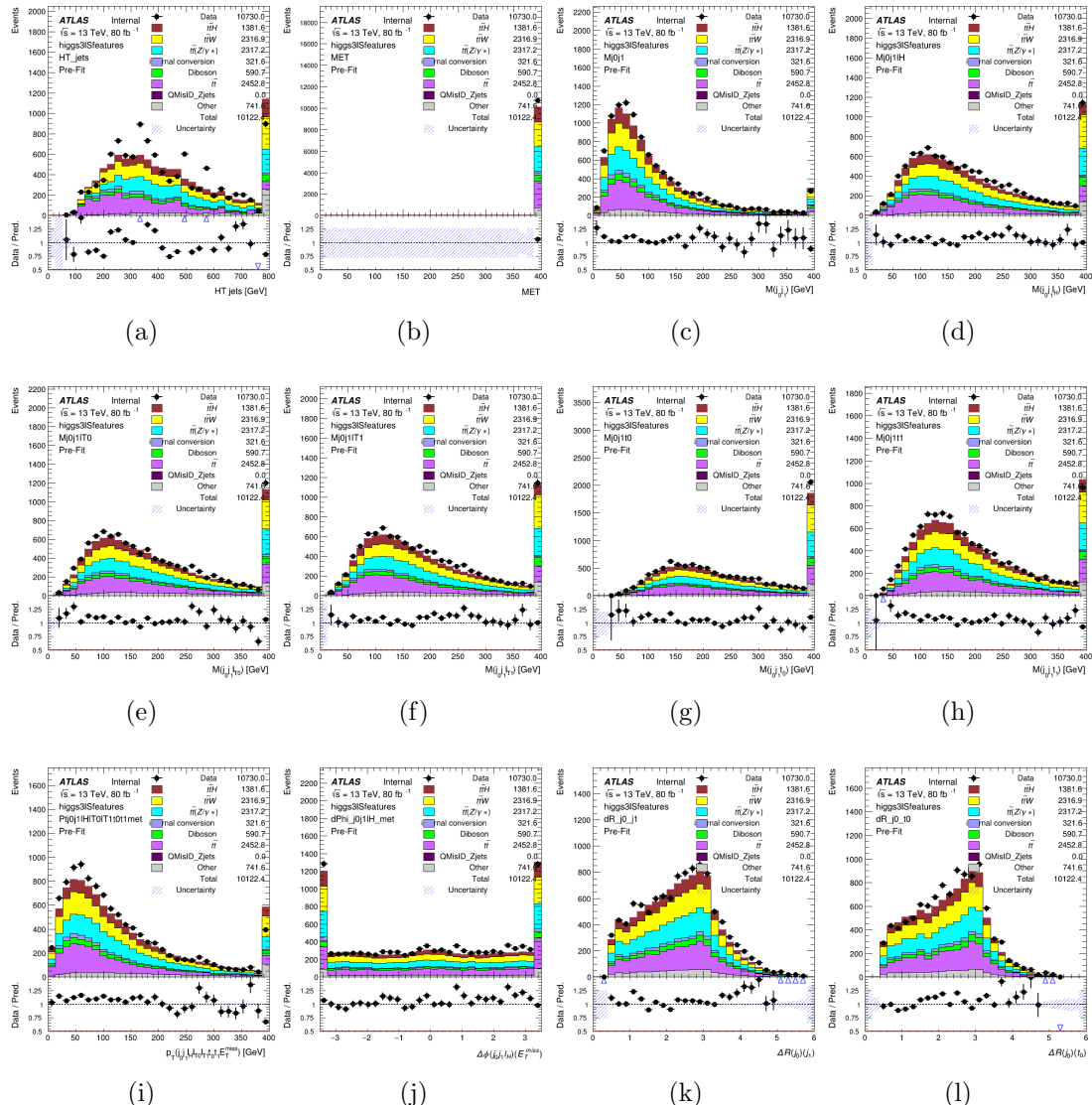


Figure .3.12: Input features for higgs3lS

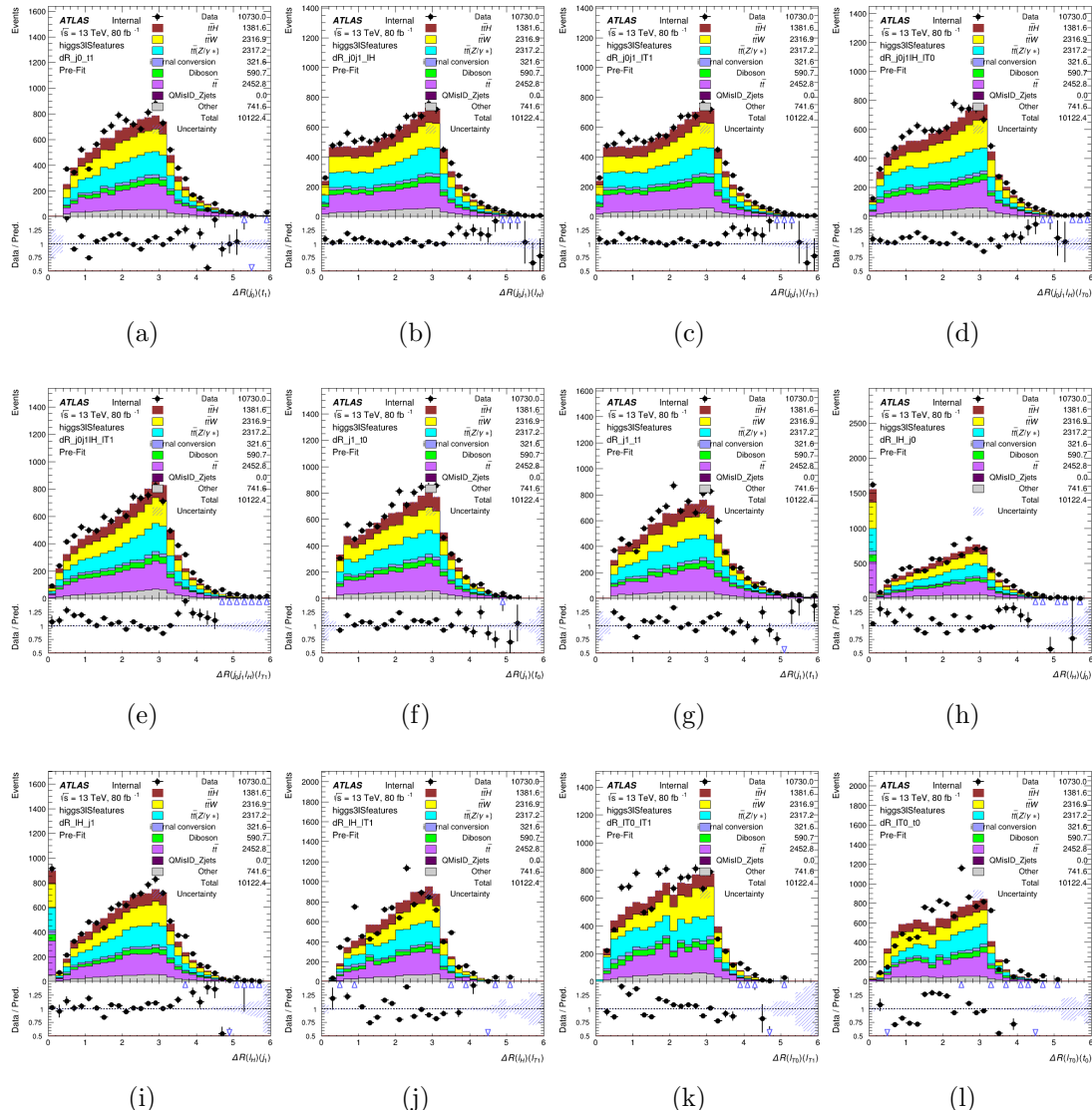


Figure .3.13: Input features for higgs3lS

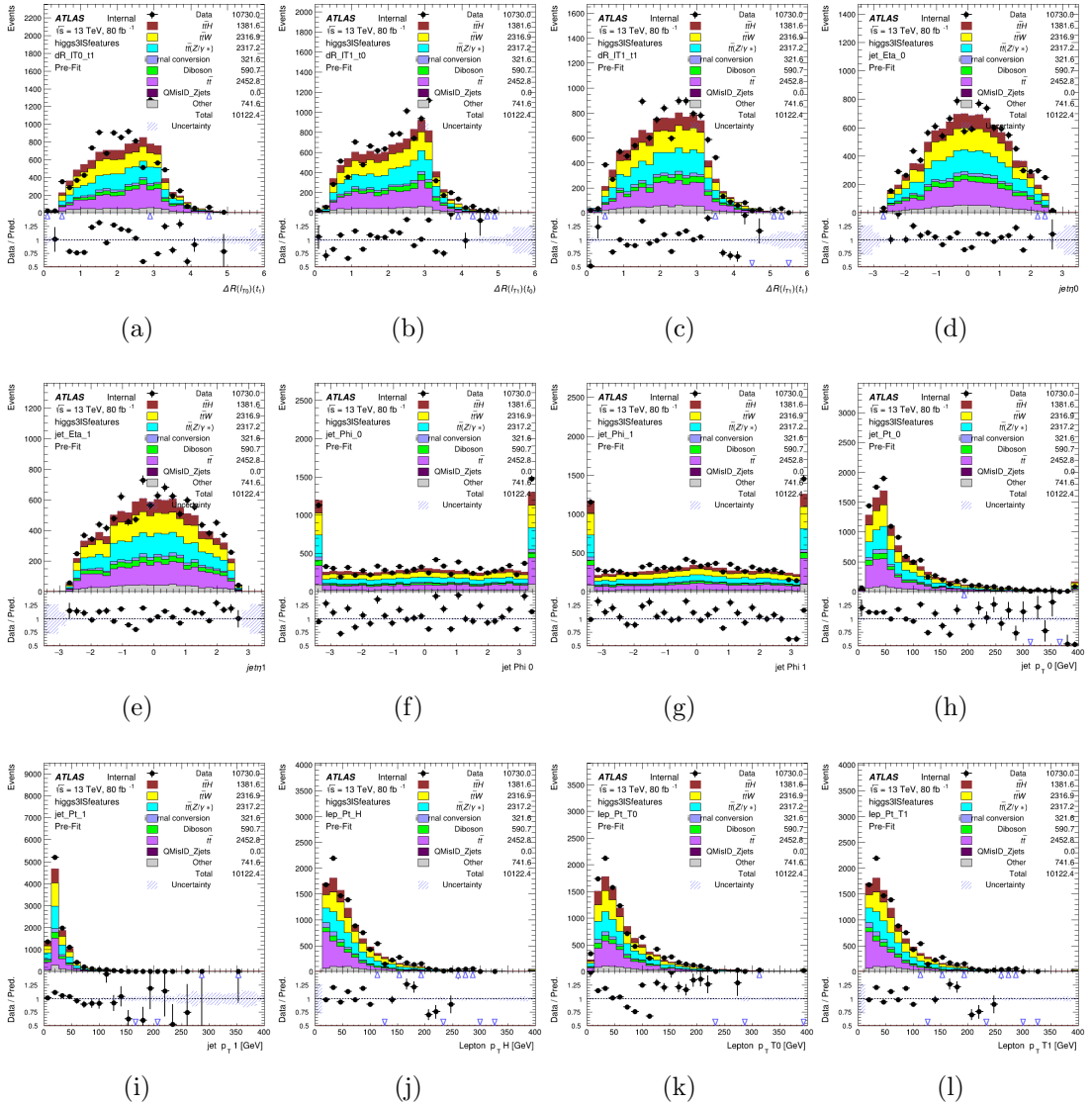


Figure .3.14: Input features for higgs3IS

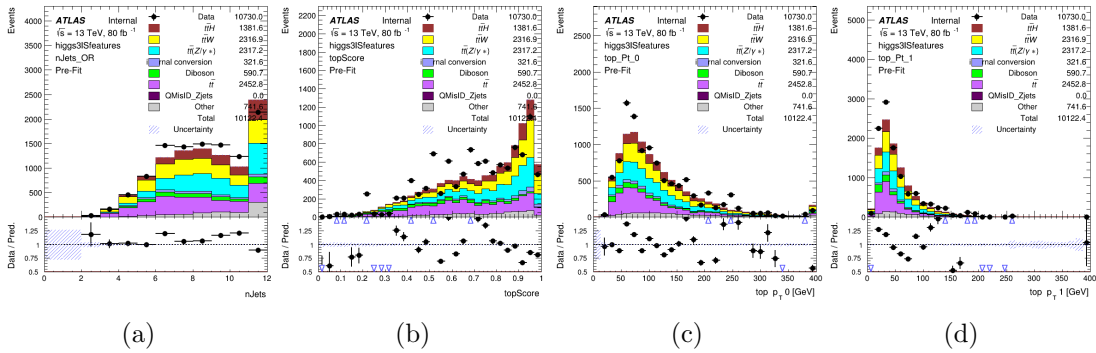


Figure .3.15: Input features for higgs3IS

.3.1.5 Higgs Reconstruction Features - 3lF

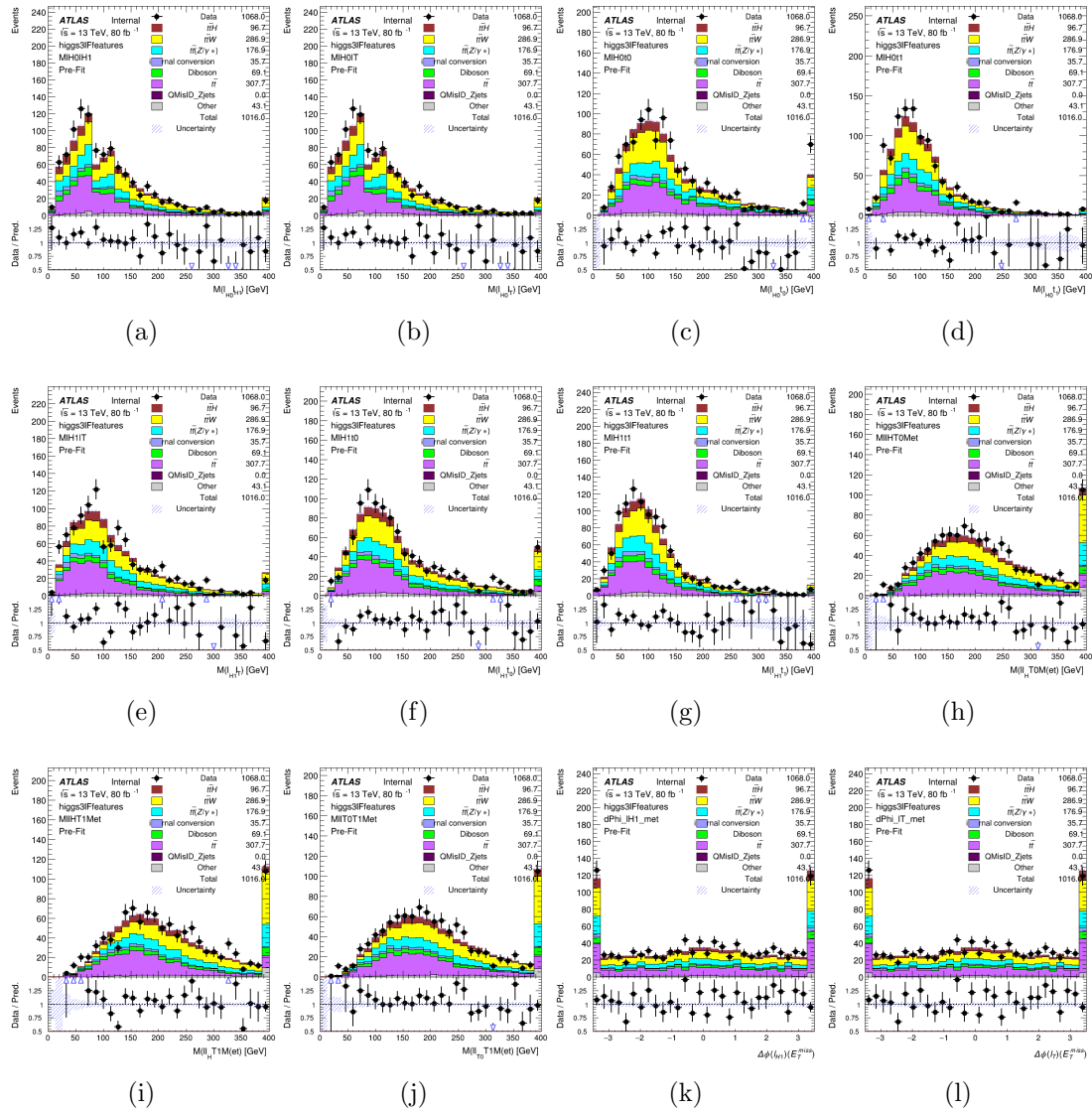


Figure .3.16: Input features for higgs3lF

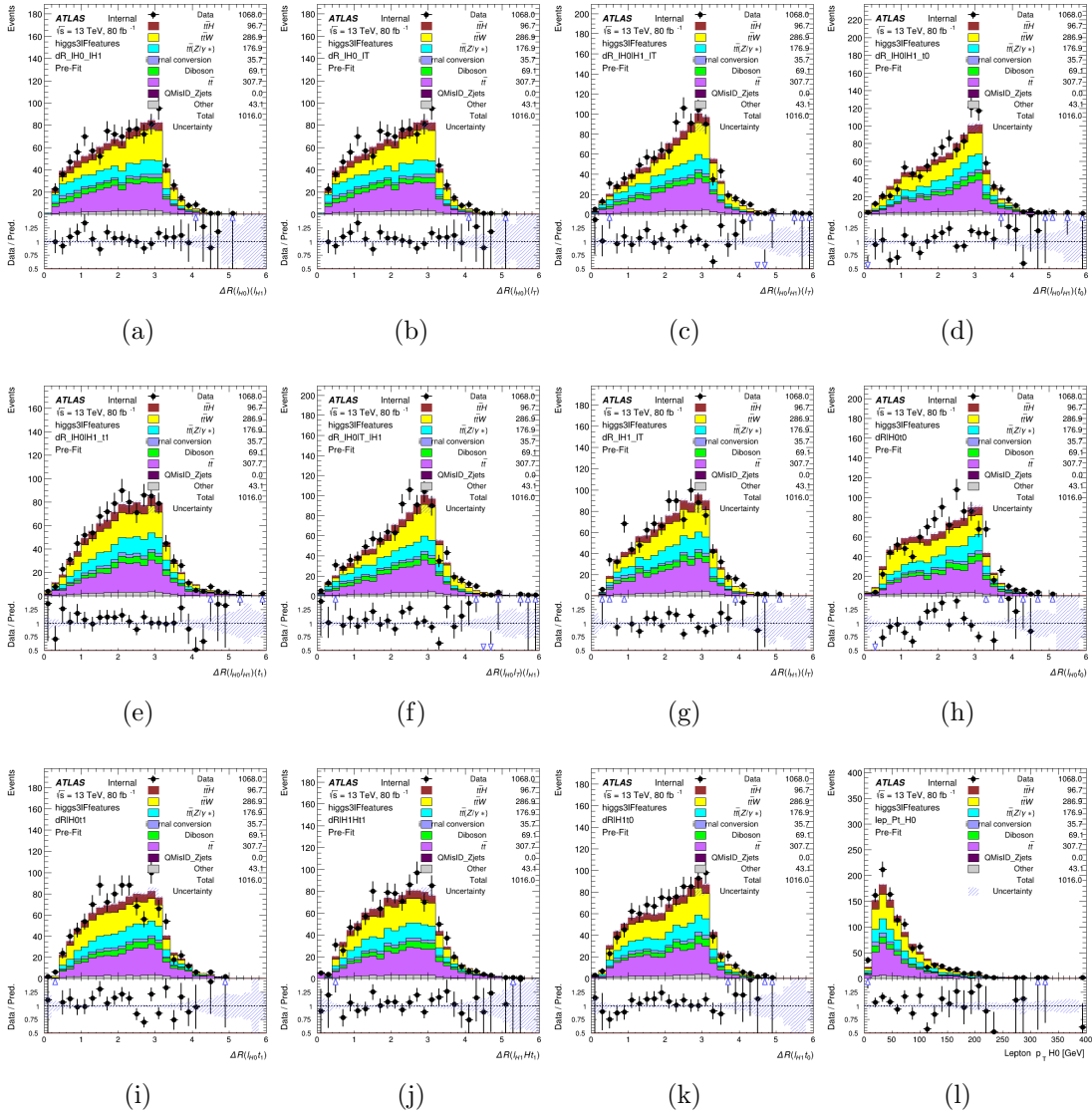


Figure .3.17: Input features for higgs3lF

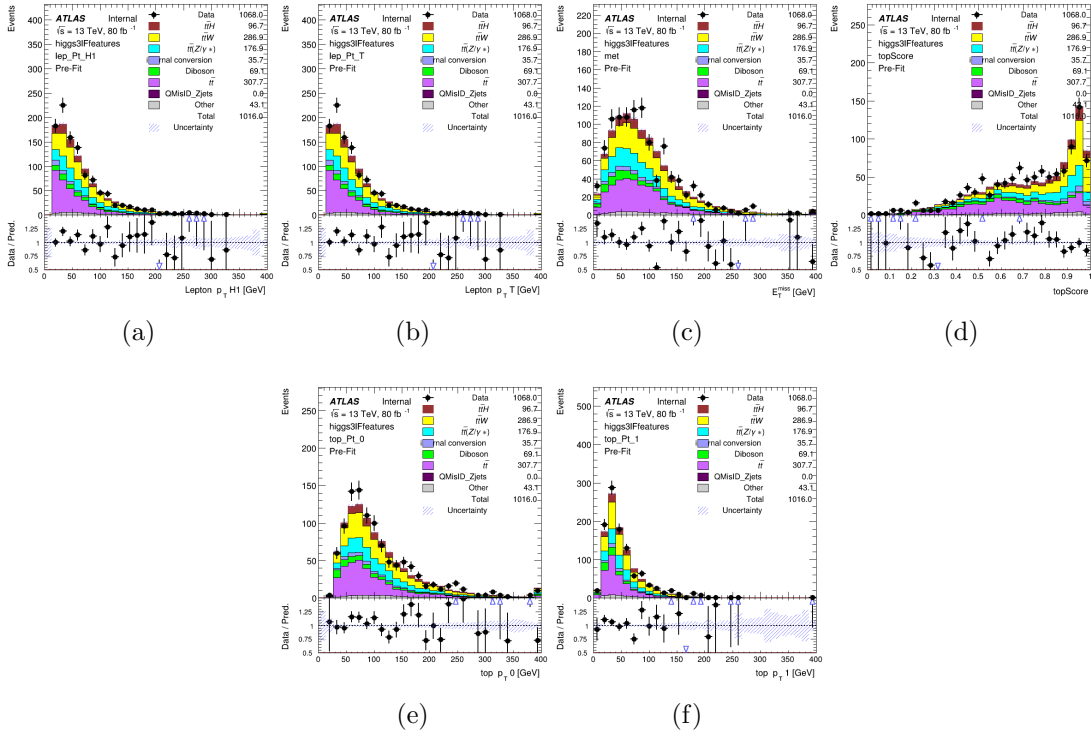


Figure .3.18: Input features for higgs3LF

.3.2 Background Rejection MVA Details

.3.2.1 Background Rejection MVA Features - 2lSS

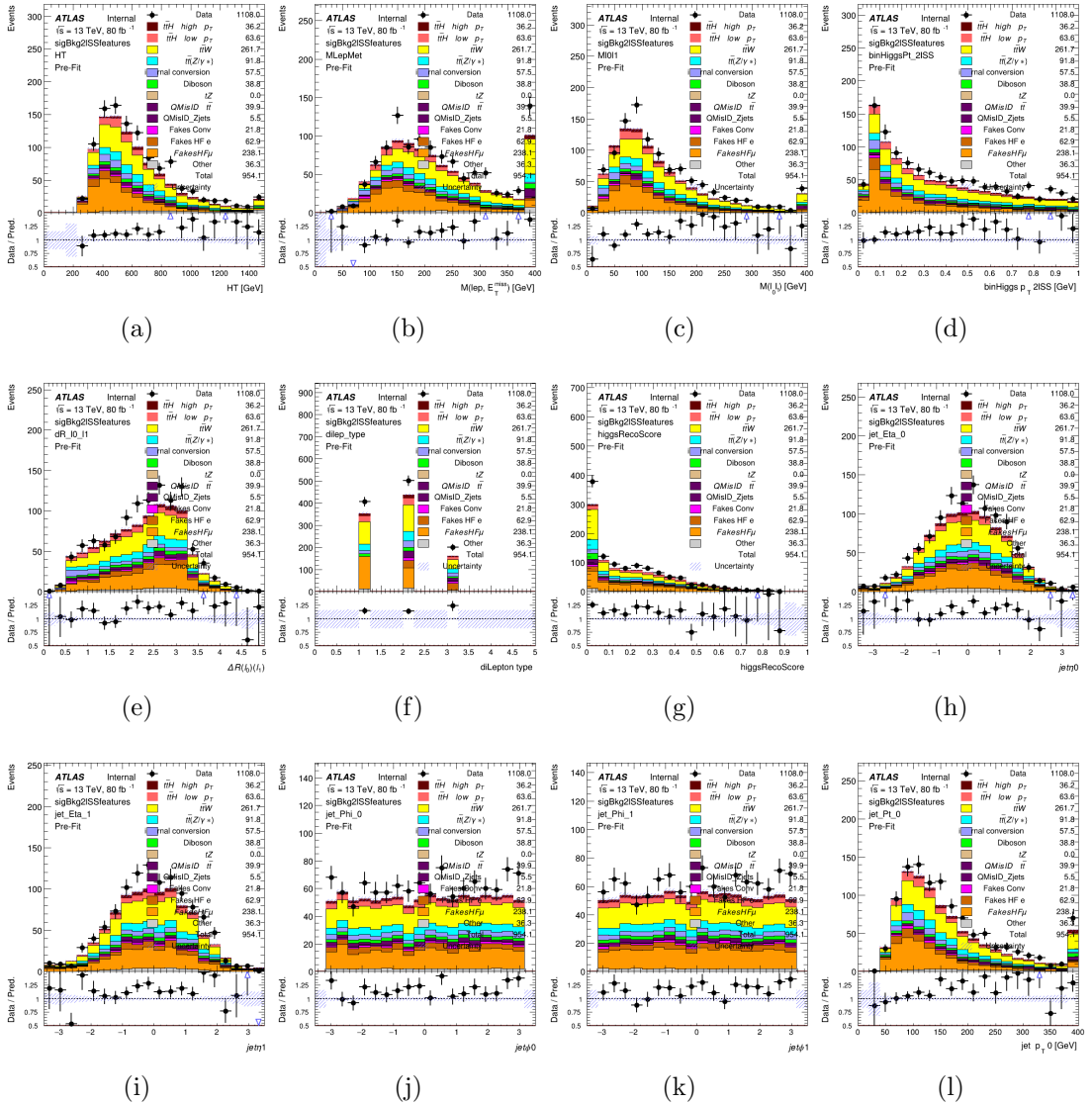


Figure .3.19: Input features for sigBkg2lSS

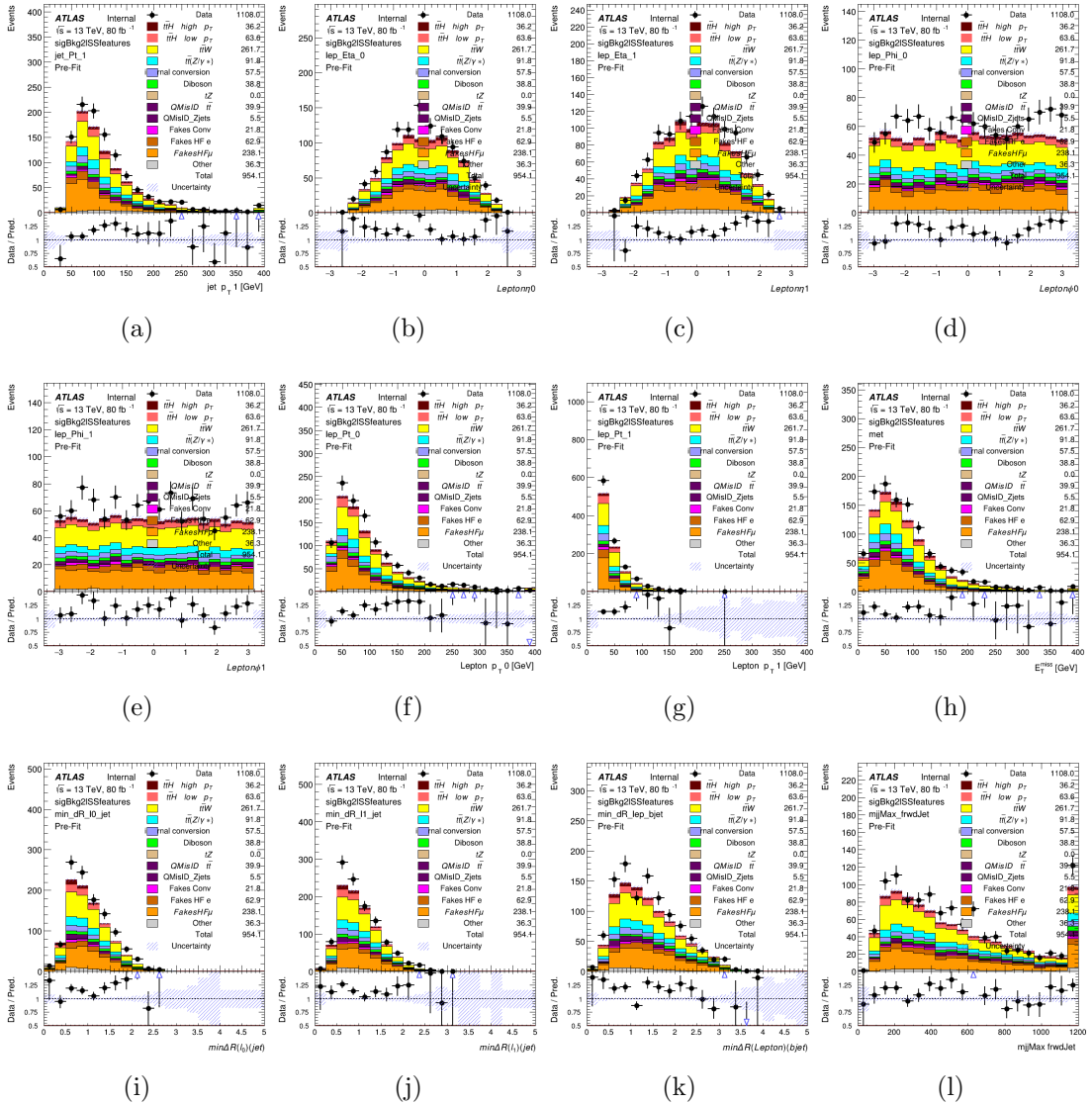


Figure .3.20: Input features for `sigBkg2lSS`

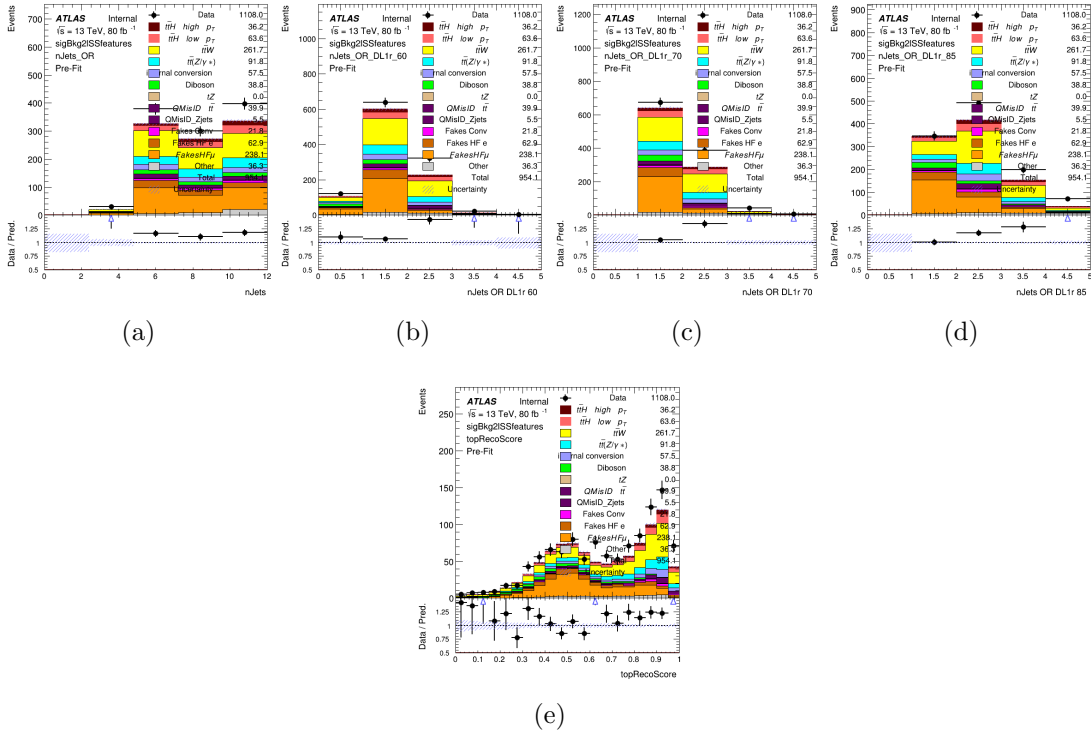


Figure .3.21: Input features for sigBkg2lSS

.3.2.2 Background Rejection MVA Features - 3l

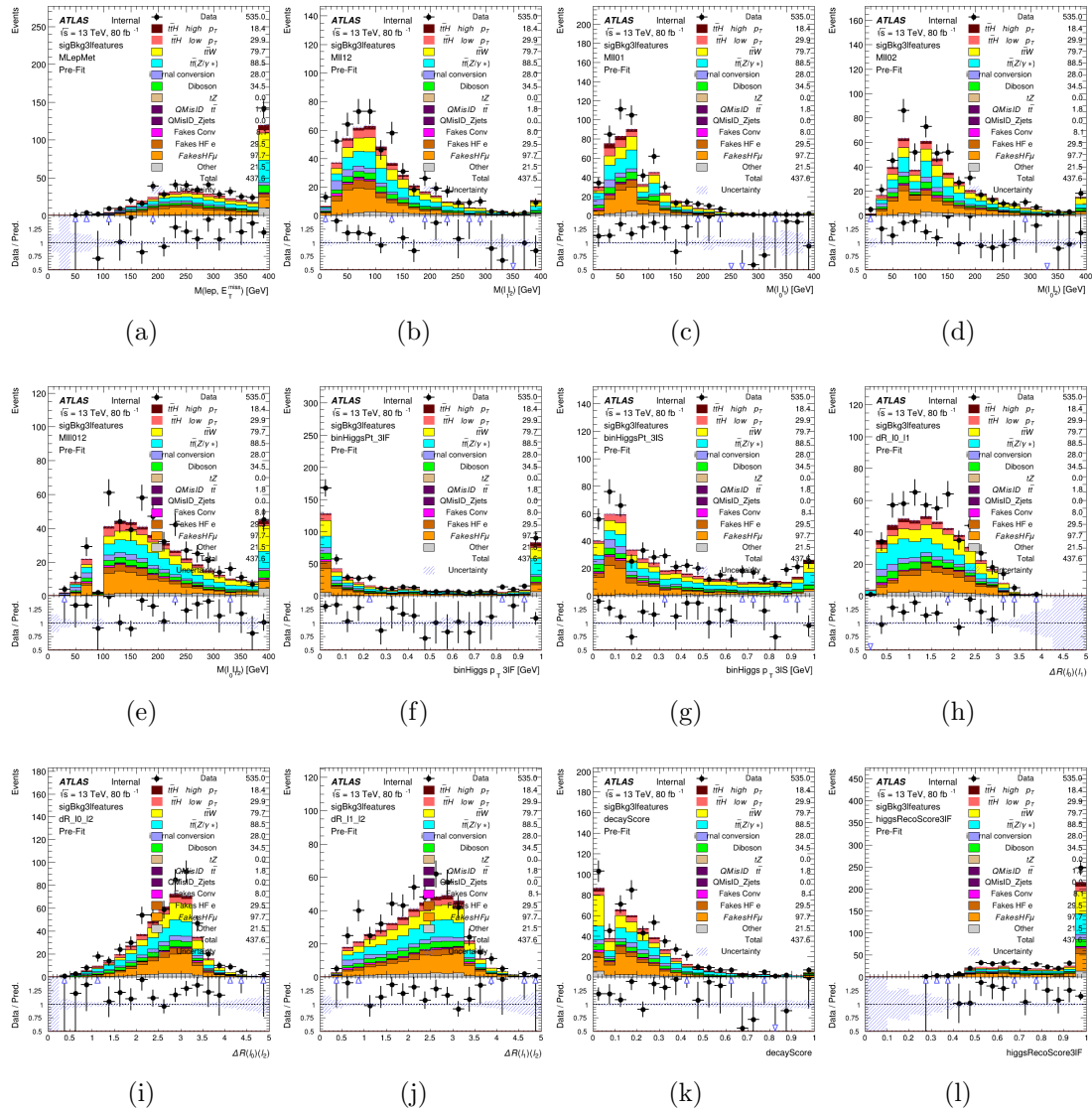


Figure .3.22: Input features for sigBkg3l

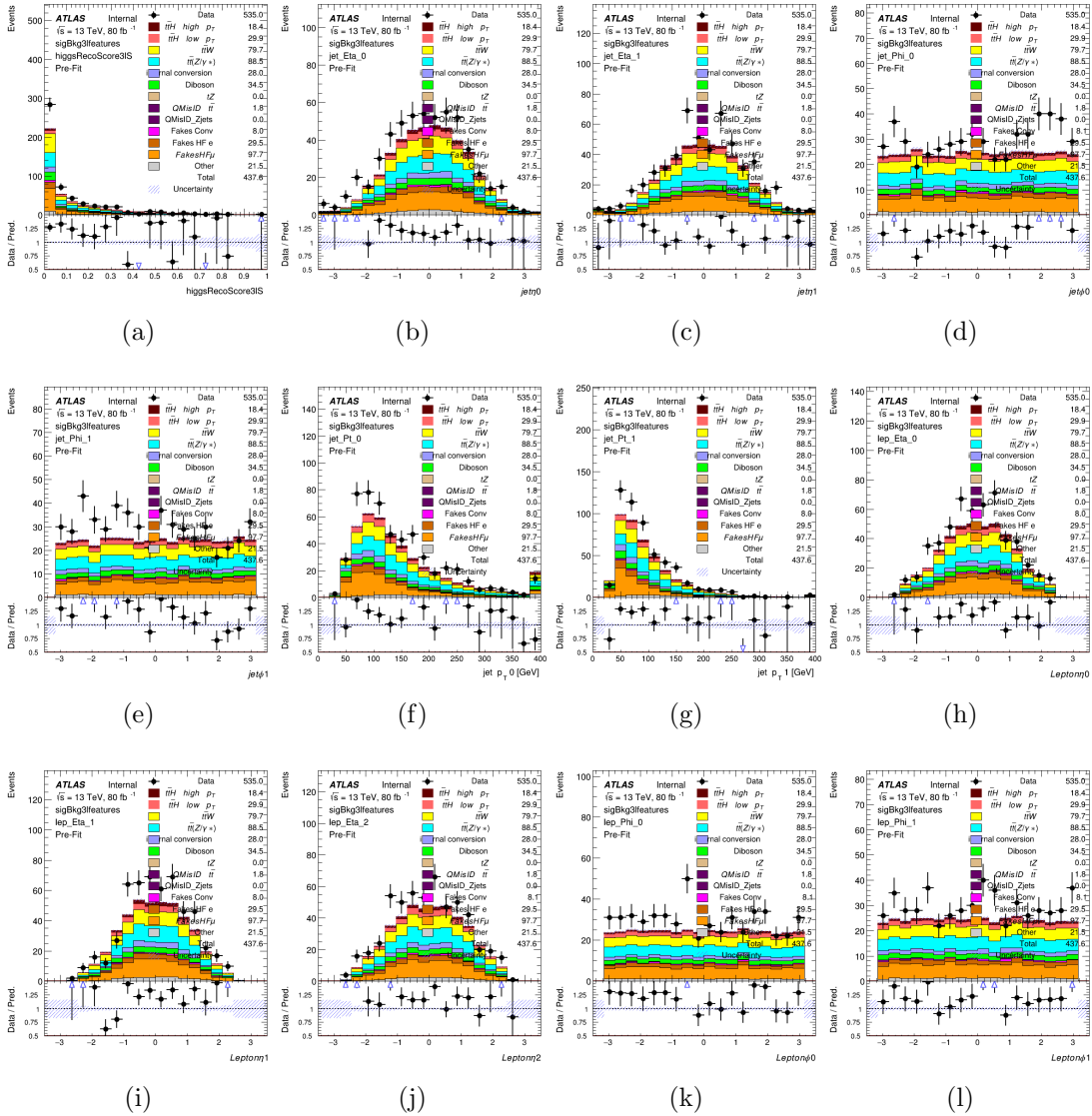


Figure .3.23: Input features for sigBkg3l

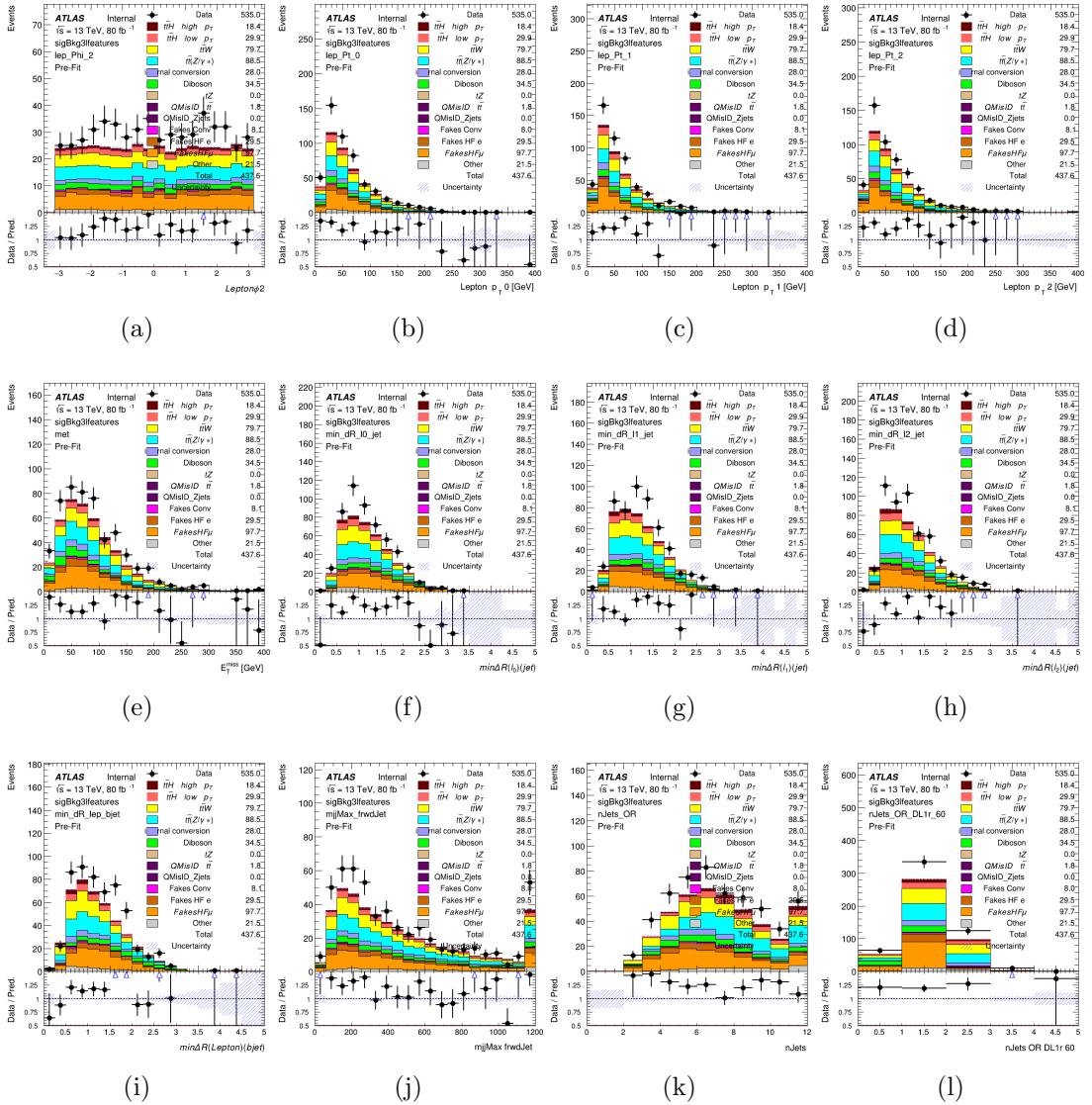


Figure .3.24: Input features for sigBkg3l

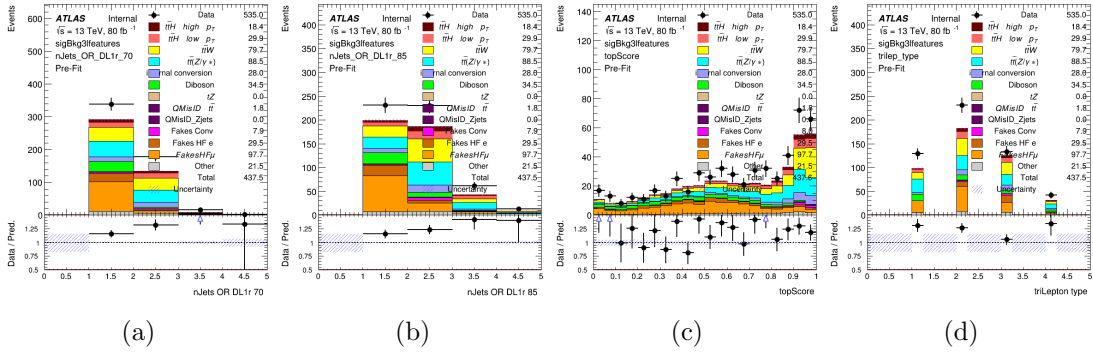


Figure .3.25: Input features for sigBkg3l

3.3 Truth Level Studies

Attempts to identify the decay products of the Higgs are motivated by the ability to reconstruct the Higgs momentum based on their kinematics. In order to demonstrate that this is the case, the kinematics of reconstructed objects that are truth matched to the Higgs decay are used as inputs to a neural network which is designed to predict the momentum of the Higgs. This is done in the 2lSS channel, as it proves to be the most challenging for p_T reconstruction.

Only leptons and jets which are truth matched to the Higgs are used as inputs for the model; events where the lepton and both jets are not reconstructed are not included. The model uses the same feature set and network architecture as the p_T prediction model used in the main analysis, as described in Section 0.15.4.1.

The results of the model are summarized below:

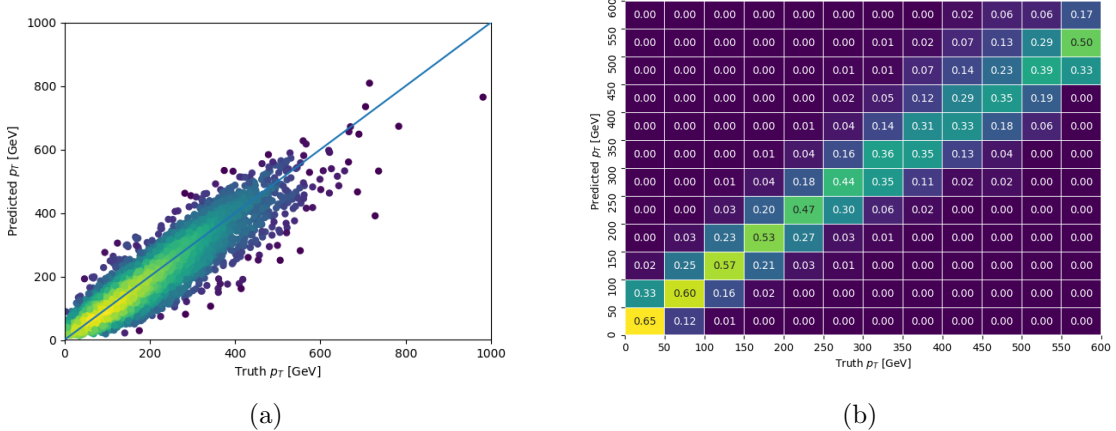


Figure .3.26: The regressed Higgs momentum spectrum as a function of the truth p_T for 2lSS $t\bar{t}H$ events in (a) a scatterplot, where the color of each point represents the log of the point density, based on Gaussian Kernel Density Estimation, and (b) a histogram where each column has been normalized to one.

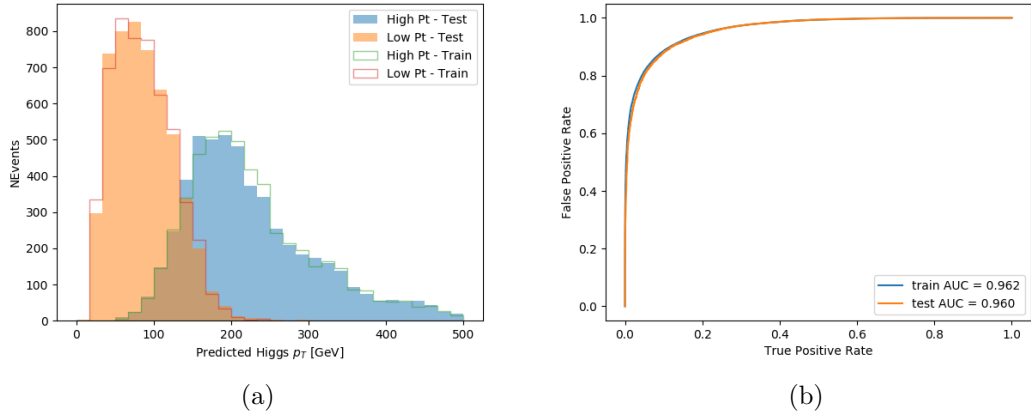


Figure .3.27: (a) shows the reconstructed Higgs p_T for 2lSS events with truth $p_T > 150$ GeV and < 150 GeV, while (b) shows the ROC curve for those two sets of events.

Based on the performance of the model, as shown Figures .3.26 and .3.27, the Higgs momentum can be reconstructed with fairly high precision when its decay products are correctly identified.

.3.4 Alternate b-jet Identification Algorithm

The nominal analysis reconstructs the b-jets by considering different combinations of jets, and asking a neural network to determine whether each combination consists of b-jets from top quark decays. An alternate approach would be to give the neural network about all of the jets in an event at once, and train it to select which two are most likely to be the b-jets from top decay. It was hypothesized that this could perform better than considering each combination independently, as the neural network could consider the event as a whole. While this is not found to be the case, these studies are documented here as a point of interest and comparison.

For these studies, the kinematics of the 10 highest p_T jets in each event are used for training. This includes the vast majority of truth b-jets. Specifically the p_T , η , ϕ , E , and DL1r score of each jet are used. For events with fewer than 10 jets, these values are substituted with 0. The p_T , η , ϕ , and E of the leptons and E_T^{miss} are included as well. Categorical cross entropy is used as the loss function.

Table 45: Accuracy of the NN in identifying b-jets from tops in 2lSS events for the alternate categorical method compared to the nominal method.

Channel	Categorical	Nominal
2lSS	70.6%	73.9%
3l	76.1%	79.8%

.3.5 Binary Classification of the Higgs p_T

A two bin fit of the Higgs momentum is used because statistics are insufficient for any finer resolution. This means separating high and low p_T events is sufficient for this analysis. As such, rather than attempting the reconstruct the full Higgs p_T spectrum, a binary classification approach is explored.

A model is built to determine whether $t\bar{t}H$ events include a high p_T (>150 GeV) or low p_T (<150 GeV) Higgs Boson. While this is now a classification model, it uses the same input features described in section 0.15.4. Binary crossentropy is used as the loss function.

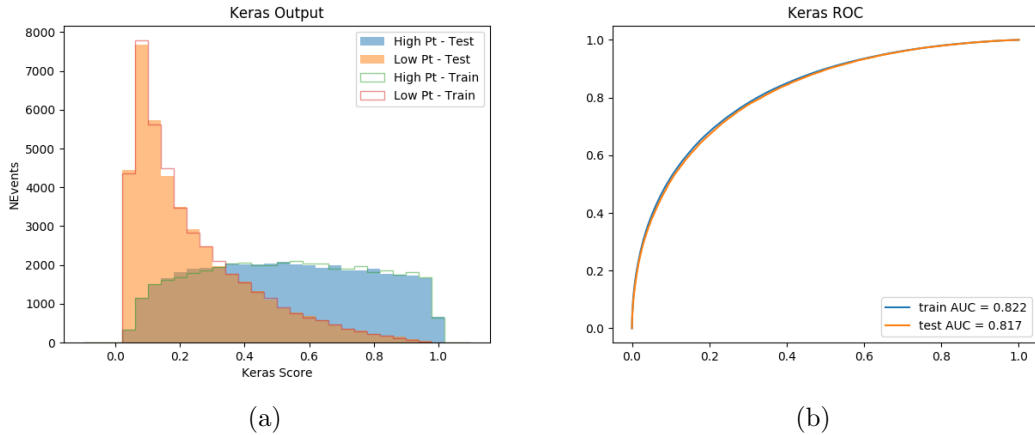


Figure .3.28: Output distribution of the NN score for the binary high/low p_T separation model in the 2lSS channel.

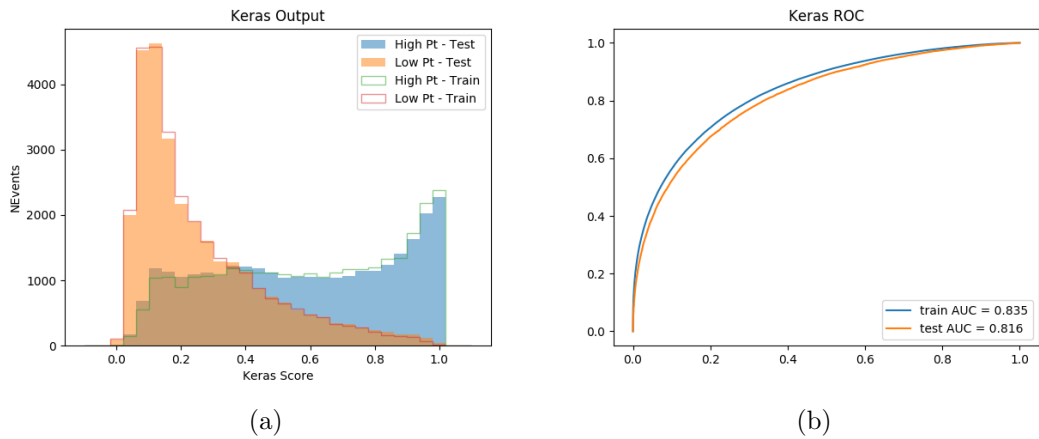


Figure .3.29: Output distribution of the NN score for the binary high/low p_T separation model in the 3lS channel.

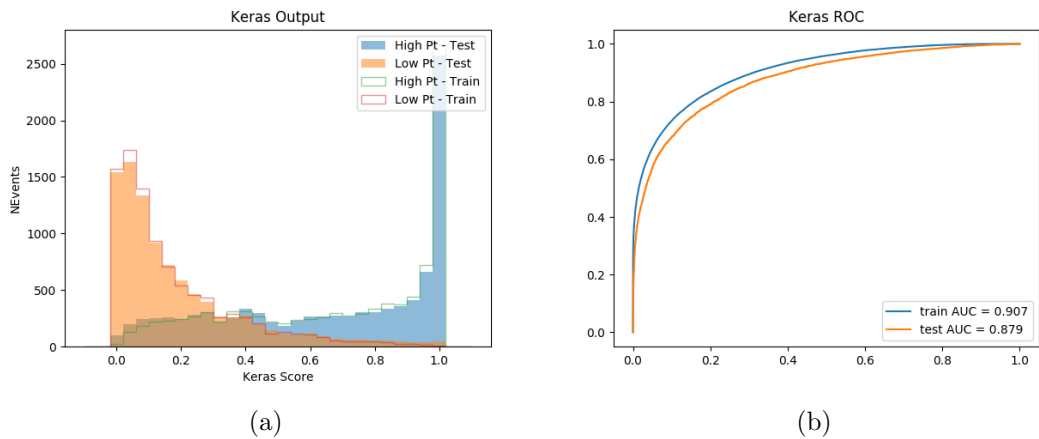


Figure .3.30: Output distribution of the NN score for the binary high/low p_T separation model in the 3lS channel.

3.6 Impact of Alternative Jet Selection

A relatively low p_T threshold of 15 GeV is used to determine jet candidates, as the jets originating from the Higgs decay are found to fall between 15 and 25 GeV a large fraction of the time. The impact of different jet p_T cuts on our ability to reconstruct the Higgs p_T is explored here.

The models are retrained in the 2lSS channel with the same parameters as those used in the nominal analysis, but the jet p_T threshold is altered. The performance of the Higgs p_T prediction models for jet p_T cuts of 20 and 25 GeV are shown below.

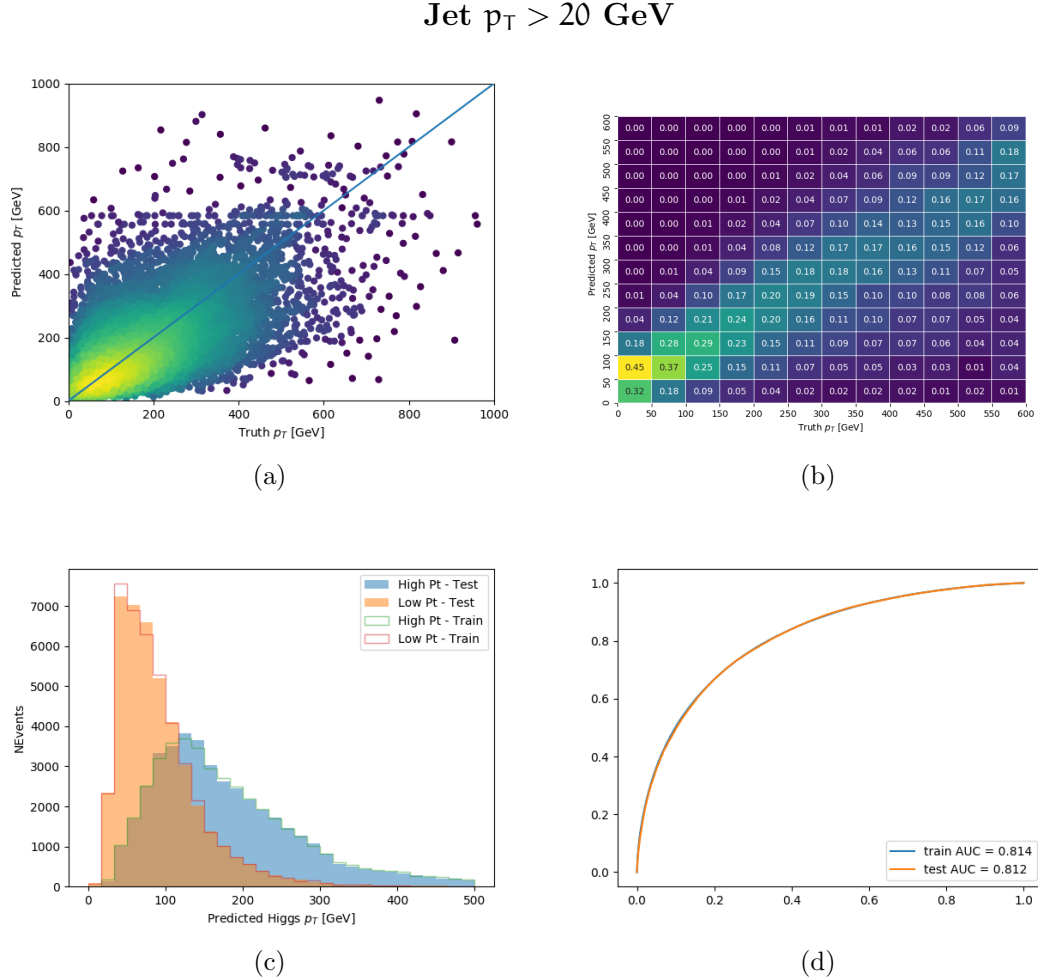


Figure .3.31: Output of the model designed to predict the Higgs momentum in the 2lSS channel, with the jet p_T cutoff used is raised to 20 GeV.

Jet $p_T > 25$ GeV

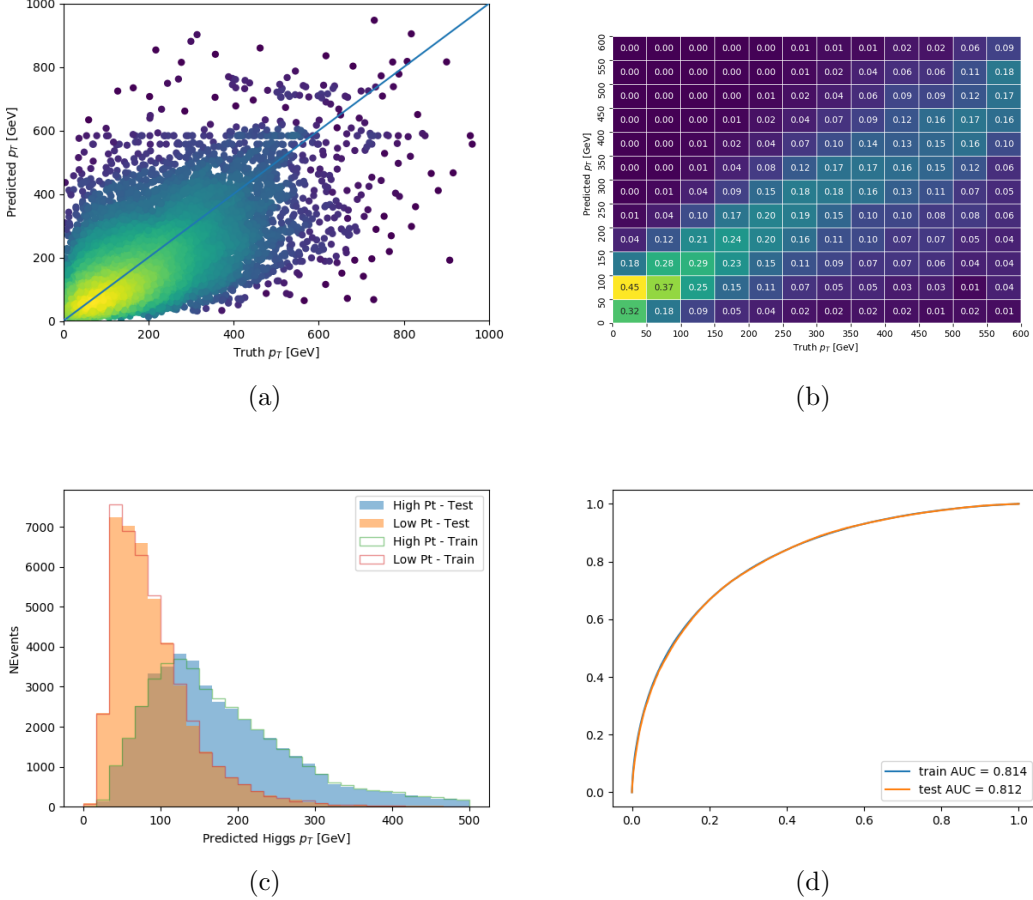


Figure .3.32: Output of the model designed to predict the Higgs momentum in the 2lSS channel, with the jet p_T cutoff used is raised to 25 GeV.

Bibliography

- [1]
- [2]
- [3] Detector and technology.
- [4] The top quark and higgs boson masses and the stability of the electroweak vacuum. *Physics Letters B*, 716.
- [5] Evidence for the associated production of the Higgs boson and a top quark pair with the ATLAS detector. Technical Report ATLAS-CONF-2017-077, CERN, Geneva, Nov 2017.
- [6] Luminosity determination in pp collisions at $\sqrt{s} = 13$ TeV using the ATLAS detector at the LHC. 6 2019.
- [7] P. Speckmayer A. Hoecker. TMVA 4 Toolkit for Multivariate Data Analysis with ROOT. *arXiv:physics/0703039*, 2013.
- [8] S. Agostinelli et al. GEANT4: A Simulation toolkit. *Nucl. Instrum. Meth.*, A506:250–303, 2003.
- [9] J. Alwall et al. The automated computation of tree-level and next-to-leading order differential cross sections, and their matching to parton shower simulations. *JHEP*, 07:079, 2014.
- [10] C. Amsler. The Review of Particle Physics. *Physics Letters B*, 667, 2008.
- [11] ATLAS and CMS Collaborations. Combination of ATLAS and CMS results on the mass of the top quark using up to 4.9 fb^{-1} of data. ATLAS-CONF-2012-095, 2012.
- [12] ATLAS and CMS Collaborations. Combination of ATLAS and CMS top-quark pair cross-section measurements using proton–proton collisions at $\sqrt{s} = 7 \text{ TeV}$. ATLAS-CONF-2012-134, 2012.
- [13] ATLAS and CMS Collaborations. Combination of ATLAS and CMS results on the mass of the top-quark using up to 4.9 fb^{-1} of $\sqrt{s} = 7 \text{ TeV}$ LHC data. ATLAS-CONF-2013-102, 2013.

- [14] ATLAS and CMS Collaborations. Combination of single top-quark cross-sections measurements in the t-channel at $\sqrt{s} = 8$ TeV with the ATLAS and CMS experiments. ATLAS-CONF-2013-098, 2013.
- [15] ATLAS and CMS Collaborations. Combination of the ATLAS and CMS measurements of the W -boson polarization in top-quark decays. ATLAS-CONF-2013-033, 2013.
- [16] ATLAS and CMS Collaborations. Combination of ATLAS and CMS $t\bar{t}$ charge asymmetry measurements using LHC proton–proton collisions at $\sqrt{s} = 7$ TeV. ATLAS-CONF-2014-012, 2014.
- [17] ATLAS and CMS Collaborations. Combination of ATLAS and CMS top quark pair cross section measurements in the $e\mu$ final state using proton–proton collisions at $\sqrt{s} = 8$ TeV. ATLAS-CONF-2014-054, 2014.
- [18] ATLAS and CMS Collaborations. Combination of cross-section measurements for associated production of a single top-quark and a W boson at $\sqrt{s} = 8$ TeV with the ATLAS and CMS experiments. ATLAS-CONF-2014-052, 2014.
- [19] ATLAS and CMS Collaborations. Jet energy scale uncertainty correlations between ATLAS and CMS. ATL-PHYS-PUB-2014-020, 2014.
- [20] ATLAS and CMS Collaborations. Combined Measurement of the Higgs Boson Mass in $p\bar{p}$ Collisions at $\sqrt{s} = 7$ and 8 TeV with the ATLAS and CMS Experiments. *Phys. Rev. Lett.*, 114:191803, 2015.
- [21] ATLAS and CMS Collaborations. Combined Measurement of the Higgs Boson Mass in $p\bar{p}$ Collisions at $\sqrt{s} = 7$ and 8 TeV with the ATLAS and CMS Experiments. *Phys. Rev. Lett.*, 114:191803, 2015.
- [22] ATLAS and CMS Collaborations. Jet energy scale uncertainty correlations between ATLAS and CMS at $\sqrt{s} = 8$ TeV. ATL-PHYS-PUB-2015-049, 2015.
- [23] ATLAS and CMS Collaborations. Measurements of the Higgs boson production and decay rates and constraints on its couplings from a combined ATLAS and CMS analysis of the LHC $p\bar{p}$ collision data at $\sqrt{s} = 7$ and 8 TeV. ATLAS-CONF-2015-044, 2015.
- [24] ATLAS and CMS Collaborations. A search for R-parity violating decays of the top squark in four-jet final states with the ATLAS experiment at $\sqrt{s} = 13$ TeV. ATLAS-CONF-2016-022, 2016.

- [25] ATLAS and CMS Collaborations. Combination of cross-section measurements for associated production of a single top-quark and a W boson at $\sqrt{s} = 8$ TeV with the ATLAS and CMS experiments. ATLAS-CONF-2016-023, 2016.
- [26] ATLAS and CMS Collaborations. Combination of results from the ATLAS and CMS experiments on anomalous triple gauge couplings from ZZ production in $p\bar{p}$ collisions at a center-of-mass energy of 7 TeV at the LHC. ATLAS-CONF-2016-036, 2016.
- [27] ATLAS and CMS Collaborations. Measurements of the Higgs boson production and decay rates and constraints on its couplings from a combined ATLAS and CMS analysis of the LHC $p\bar{p}$ collision data at $\sqrt{s} = 7$ and 8 TeV. *JHEP*, 08:045, 2016.
- [28] ATLAS and CMS Collaborations. Measurements of the Higgs boson production and decay rates and constraints on its couplings from a combined ATLAS and CMS analysis of the LHC $p\bar{p}$ collision data at $\sqrt{s} = 7$ and 8 TeV. *JHEP*, 08:045, 2016.
- [29] ATLAS and CMS Collaborations. Combination of inclusive and differential $t\bar{t}$ charge asymmetry measurements using ATLAS and CMS data at $\sqrt{s} = 7$ TeV and 8 TeV. *JHEP*, 2017.
- [30] ATLAS and CMS Collaborations. Combination of inclusive and differential $t\bar{t}$ charge asymmetry measurements using ATLAS and CMS data at $\sqrt{s} = 7$ TeV and 8 TeV. *JHEP*, 2017.
- [31] ATLAS, CDF, CMS and DO Collaborations. First combination of Tevatron and LHC measurements of the top-quark mass. ATLAS-CONF-2014-008, 2014.
- [32] ATLAS, CMS and LHCb Collaborations. Search for the rare decays $B_{(S)}^0 \rightarrow \mu^+ \mu^-$ at the LHC with the ATLAS, CMS and LHCb experiments. ATLAS-CONF-2012-061, 2012.
- [33] ATLAS Collaboration. ATLAS Computing Acknowledgements. ATL-GEN-PUB-2016-002.
- [34] ATLAS Collaboration. ATLAS Detector and Physics Performance : Technical Design Report 2. 1999.
- [35] ATLAS Collaboration. The ATLAS Experiment at the CERN Large Hadron Collider. *JINST*, 3:S08003, 2008.

- [36] ATLAS Collaboration. A method for discovering heavy particles decaying into single boosted jets with substructure using the k_\perp algorithm. ATL-PHYS-PUB-2009-076, 2009.
- [37] ATLAS Collaboration. ATLAS searches for MSSM Higgs bosons decaying into SUSY cascades. ATL-PHYS-PUB-2009-079, 2009.
- [38] ATLAS Collaboration. ATLAS Sensitivity to the Standard Model Higgs in the HW and HZ Channels at High Transverse Momenta. ATL-PHYS-PUB-2009-088, 2009.
- [39] ATLAS Collaboration. Background Estimation for Inclusive SUSY Searches - The Tiles Method. ATL-PHYS-PUB-2009-077, 2009.
- [40] ATLAS Collaboration. Data-Driven Determination of $t\bar{t}$ Background to Supersymmetry Searches in ATLAS. ATL-PHYS-PUB-2009-083, 2009.
- [41] ATLAS Collaboration. Discovery Potential for Supersymmetry with b-jet Final States with the ATLAS detector. ATL-PHYS-PUB-2009-075, 2009.
- [42] ATLAS Collaboration. Expected performance of the ATLAS detector in GMSB models with τ final states. ATL-PHYS-PUB-2009-089, 2009.
- [43] ATLAS Collaboration. Measuring WZ longitudinal polarization with the ATLAS detector. ATL-PHYS-PUB-2009-078, 2009.
- [44] ATLAS Collaboration. Prospects for associated single top quark production cross section measurements in the dilepton decay mode with ATLAS. ATL-PHYS-PUB-2009-001, 2009.
- [45] ATLAS Collaboration. Prospects for measuring top pair production in the dilepton channel with early ATLAS data at $\sqrt{s} = 10$ TeV. ATL-PHYS-PUB-2009-086, 2009.
- [46] ATLAS Collaboration. Prospects for Supersymmetry and Univeral Extra Dimensions discovery based on inclusive searches at a 10 TeV centre-of-mass energy with the ATLAS detector . ATL-PHYS-PUB-2009-084, 2009.
- [47] ATLAS Collaboration. Prospects for the Top Pair Production Cross-section at $\sqrt{s} = 10$ TeV in the Single Lepton Channel in ATLAS. ATL-PHYS-PUB-2009-087, 2009.
- [48] ATLAS Collaboration. Reconstruction of High-Mass $t\bar{t}$ Resonances in the Lepton+Jets Channel. ATL-PHYS-PUB-2009-081, 2009.
- [49] ATLAS Collaboration. Search for highly-excited string states with ATLAS. ATL-PHYS-PUB-2009-011, 2009.

- [50] ATLAS Collaboration. Searching for Supersymmetry with two same-sign leptons, multi-jets plus missing transverse energy in ATLAS at $\sqrt{s} = 10$ TeV. ATL-PHYS-PUB-2009-085, 2009.
- [51] ATLAS Collaboration. The Impact of Inner Detector Misalignments on Selected Physics Processes. ATL-PHYS-PUB-2009-080, 2009.
- [52] ATLAS Collaboration. Triggering on Long-Lived Neutral Particles in the ATLAS Detector. ATL-PHYS-PUB-2009-082, 2009.
- [53] ATLAS Collaboration. A first measurement of the differential cross-section for the $J/\psi \rightarrow \mu^+\mu^-$ resonance and the non-prompt to prompt J/ψ cross section ratio with $p\bar{p}$ collisions at $\sqrt{s} = 7$ TeV in ATLAS. ATLAS-CONF-2010-062, 2010.
- [54] ATLAS Collaboration. Alignment Performance of the ATLAS Inner Detector Tracking System in 7 TeV proton–proton collisions at the LHC. ATLAS-CONF-2010-067, 2010.
- [55] ATLAS Collaboration. Angular correlations between charged particles from proton–proton collisions at $\sqrt{s} = 900$ GeV and $\sqrt{s} = 7$ TeV measured with ATLAS detector. ATLAS-CONF-2010-082, 2010.
- [56] ATLAS Collaboration. ATLAS Calorimeter Response to Single Isolated Hadrons and Estimation of the Calorimeter Jet Scale Uncertainty. ATLAS-CONF-2010-052, 2010.
- [57] ATLAS Collaboration. ATLAS High Level Calorimeter Trigger Software Performance for First LHC Collision Events. ATLAS-CONF-2010-030, 2010.
- [58] ATLAS Collaboration. ATLAS Monte Carlo tunes for MC09. ATL-PHYS-PUB-2010-002, 2010.
- [59] ATLAS Collaboration. ATLAS Muon Trigger Performance in cosmic rays and $p\bar{p}$ collisions at $\sqrt{s} = 900$ GeV. ATLAS-CONF-2010-013, 2010.
- [60] ATLAS Collaboration. ATLAS Sensitivity Prospects for Higgs Boson Production at the LHC Running at 7, 8 or 9 TeV. ATL-PHYS-PUB-2010-015, 2010.
- [61] ATLAS Collaboration. ATLAS Sensitivity Prospects for Higgs Boson Production at the LHC Running at 7 TeV. ATL-PHYS-PUB-2010-009, 2010.
- [62] ATLAS Collaboration. ATLAS sensitivity prospects to W' and Z' in the decay channels $W' \rightarrow \ell\nu$ and $Z' \rightarrow \ell^+\ell^-$ at $\sqrt{s} = 7$ TeV. ATL-PHYS-PUB-2010-007, 2010.

- [63] ATLAS Collaboration. Azimuthal Decorrelations in Dijet Events at $\sqrt{s} = 7$ TeV. ATLAS-CONF-2010-083, 2010.
- [64] ATLAS Collaboration. Background studies for top-pair production in lepton plus jets final states in $\sqrt{s} = 7$ TeV ATLAS data. ATLAS-CONF-2010-087, 2010.
- [65] ATLAS Collaboration. Background studies to searches for long-lived stopped particles decaying out-of-time with LHC collisions. ATLAS-CONF-2010-071, 2010.
- [66] ATLAS Collaboration. Calibrating the b-Tag Efficiency and Mistag Rate of the SV0 b-Tagging Algorithm in 3 pb^{-1} of Data with the ATLAS Detector. ATLAS-CONF-2010-099, 2010.
- [67] ATLAS Collaboration. Characterization of Interaction-Point Beam Parameters Using the pp Event-Vertex Distribution Reconstructed in the ATLAS Detector at the LHC. ATLAS-CONF-2010-027, 2010.
- [68] ATLAS Collaboration. Charged particle multiplicities in pp interactions at $\sqrt{s} = 0.9$ and 7 TeV in a diffractive limited phase-space measured with the ATLAS detector at the LHC and new PYTHIA6 tune. ATLAS-CONF-2010-031, 2010.
- [69] ATLAS Collaboration. Charged particle multiplicities in pp interactions at $\sqrt{s} = 2.36$ TeV measured with the ATLAS detector at the LHC. ATLAS-CONF-2010-047, 2010.
- [70] ATLAS Collaboration. Charged-particle multiplicities in pp interactions at $\sqrt{s} = 900$ GeV measured with the ATLAS detector at the LHC. *Phys. Lett. B*, 688:21, 2010.
- [71] ATLAS Collaboration. Charged particle multiplicities in pp interactions for track $p_T > 100$ MeV at $\sqrt{s} = 0.9$ and 7 TeV measured with the ATLAS detector at the LHC. ATLAS-CONF-2010-046, 2010.
- [72] ATLAS Collaboration. Charged particle multiplicities in pp interactions at $\sqrt{s} = 7$ TeV measured with the ATLAS detector at the LHC. ATLAS-CONF-2010-024, 2010.
- [73] ATLAS Collaboration. Commissioning of the ATLAS Muon Spectrometer with cosmic rays. *Eur. Phys. J. C*, 70:875, 2010.
- [74] ATLAS Collaboration. Commissioning of the ATLAS Tau-Lepton Reconstruction Using 900 GeV Minimum-Bias Data. ATLAS-CONF-2010-012, 2010.

- [75] ATLAS Collaboration. Cut-based Identification of Hadronic τ Decays in Early ATLAS Data. ATL-PHYS-PUB-2010-001, 2010.
- [76] ATLAS Collaboration. $D^{(*)}$ mesons reconstruction in $p\bar{p}$ collisions at $\sqrt{s} = 7$ TeV. ATLAS-CONF-2010-034, 2010.
- [77] ATLAS Collaboration. Data-driven background estimation for the $H \rightarrow \tau^+\tau^- \rightarrow \ell\tau_h$ search at $\sqrt{s} = 7$ TeV with the ATLAS detector. ATLAS-CONF-2010-096, 2010.
- [78] ATLAS Collaboration. Data-Quality Requirements and Event Cleaning for Jets and Missing Transverse Energy Reconstruction with the ATLAS Detector in Proton–Proton Collisions at a Center-of-Mass Energy of $\sqrt{s} = 7$ TeV. ATLAS-CONF-2010-038, 2010.
- [79] ATLAS Collaboration. Discovery Potential of $A/H \rightarrow \tau^+\tau^- \rightarrow \ell h$ in ATLAS. ATL-PHYS-PUB-2010-011, 2010.
- [80] ATLAS Collaboration. Drift Time Measurement in the ATLAS Liquid Argon Electromagnetic Calorimeter using Cosmic Muons. *Eur. Phys. J. C*, 70:755, 2010.
- [81] ATLAS Collaboration. Early supersymmetry searches in channels with jets and missing transverse momentum with the ATLAS detector. ATLAS-CONF-2010-065, 2010.
- [82] ATLAS Collaboration. Early supersymmetry searches in events with missing transverse energy and b-jets with the ATLAS detector. ATLAS-CONF-2010-079, 2010.
- [83] ATLAS Collaboration. Early supersymmetry searches with jets, missing transverse momentum and one or more leptons with the ATLAS Detector. ATLAS-CONF-2010-066, 2010.
- [84] ATLAS Collaboration. Electron and photon reconstruction and identification in ATLAS: expected performance at high energy and results at 900 GeV. ATLAS-CONF-2010-005, 2010.
- [85] ATLAS Collaboration. Estimating Track Momentum Resolution in Minimum Bias Events using Simulation and K_S^0 in $\sqrt{s} = 900$ GeV Collision Data. ATLAS-CONF-2010-009, 2010.
- [86] ATLAS Collaboration. Evidence for prompt photon production in $p\bar{p}$ collisions at $\sqrt{s} = 7$ TeV with the ATLAS detector. ATLAS-CONF-2010-077, 2010.

- [87] ATLAS Collaboration. Expected event distributions for early top pair candidates in ATLAS at $\sqrt{s} = 7$ TeV. ATL-PHYS-PUB-2010-012, 2010.
- [88] ATLAS Collaboration. Expected Sensitivity in Light Charged Higgs Boson Searches for $H^+ \rightarrow \tau^+ \nu$ and $H^+ \rightarrow c\bar{s}$ in Early LHC Data at the ATLAS Experiment. ATL-PHYS-PUB-2010-006, 2010.
- [89] ATLAS Collaboration. Extraction of the prompt muon component in inclusive muons produced at $\sqrt{s} = 7$ TeV. ATLAS-CONF-2010-075, 2010.
- [90] ATLAS Collaboration. First look at the JetProb b-tagging algorithm in the 900 GeV collision data with the ATLAS detector. ATLAS-CONF-2010-010, 2010.
- [91] ATLAS Collaboration. First observation of the $J/\psi \rightarrow \mu^+\mu^-$ resonance in ATLAS pp collisions at $\sqrt{s} = 7$ TeV. ATLAS-CONF-2010-045, 2010.
- [92] ATLAS Collaboration. First tuning of HERWIG/JIMMY to ATLAS data. ATL-PHYS-PUB-2010-014, 2010.
- [93] ATLAS Collaboration. High- p_T dijet angular distributions in pp interactions at $\sqrt{s} = 7$ TeV measured with the ATLAS detector at the LHC. ATLAS-CONF-2010-074, 2010.
- [94] ATLAS Collaboration. Identification of muon candidates in pp collisions at $\sqrt{s} = 900$ GeV with the ATLAS Detector. ATLAS-CONF-2010-015, 2010.
- [95] ATLAS Collaboration. Impact parameter-based b-tagging algorithms in the 7 TeV collision data with the ATLAS detector: the TrackCounting and Jet-Probe algorithms. ATLAS-CONF-2010-041, 2010.
- [96] ATLAS Collaboration. In-situ pseudorapidity intercalibration to evaluate jet energy scale uncertainty and calorimeter performance in the forward region. ATLAS-CONF-2010-055, 2010.
- [97] ATLAS Collaboration. Inputs to Jet Reconstruction and Calibration with the ATLAS Detector Using Proton–Proton Collisions at $\sqrt{s} = 900$ GeV. ATLAS-CONF-2010-016, 2010.
- [98] ATLAS Collaboration. Jet Energy Resolution and Selection Efficiency Relative to Track Jets from In-situ Techniques with the ATLAS Detector Using Proton–Proton Collisions at a Center of Mass Energy $\sqrt{s} = 7$ TeV. ATLAS-CONF-2010-054, 2010.
- [99] ATLAS Collaboration. Jet energy scale and its systematic uncertainty for jets produced in proton–proton collisions at $\sqrt{s} = 7$ TeV and measured with the ATLAS detector. ATLAS-CONF-2010-056, 2010.

- [100] ATLAS Collaboration. Jet kinematic distributions in proton–proton collisions at $\sqrt{s} = 900$ GeV with the ATLAS detector. ATLAS-CONF-2010-001, 2010.
- [101] ATLAS Collaboration. J/ψ Performance of the ATLAS Inner Detector. ATLAS-CONF-2010-078, 2010.
- [102] ATLAS Collaboration. Kinematic Distributions of K_S^0 and Λ^0 decays in collision data at $\sqrt{s} = 7$ TeV. ATLAS-CONF-2010-033, 2010.
- [103] ATLAS Collaboration. Luminosity Determination Using the ATLAS Detector. ATLAS-CONF-2010-060, 2010.
- [104] ATLAS Collaboration. Mapping the material in the ATLAS Inner Detector using secondary hadronic interactions in 7 TeV collisions. ATLAS-CONF-2010-058, 2010.
- [105] ATLAS Collaboration. Measurement of differential cross section and fragmentation of jets from tracks in proton–proton collisions at center-of-mass energy $\sqrt{s} = 7$ TeV with the ATLAS detector. ATLAS-CONF-2010-049, 2010.
- [106] ATLAS Collaboration. Measurement of dijet production with a jet veto in $p\bar{p}$ collisions at $\sqrt{s} = 7$ TeV using the ATLAS detector. ATLAS-CONF-2010-085, 2010.
- [107] ATLAS Collaboration. Measurement of jet production in proton–proton collisions at 7 TeV centre-of-mass energy with the ATLAS Detector. ATLAS-CONF-2010-050, 2010.
- [108] ATLAS Collaboration. Measurement of the missing transverse momentum based on tracks in proton–proton collisions at $\sqrt{s} = 900$ GeV centre-of-mass energy with the ATLAS detector. ATLAS-CONF-2010-020, 2010.
- [109] ATLAS Collaboration. Measurement of the Rate of Collisions from Satellite Bunches for the April-May 2010 LHC Luminosity Calibration. ATLAS-CONF-2010-102, 2010.
- [110] ATLAS Collaboration. Measurement of the $W \rightarrow \ell\nu$ and $Z/\gamma^* \rightarrow \ell\ell$ production cross sections in proton–proton collisions at $\sqrt{s} = 7$ TeV with the ATLAS detector. *JHEP*, 12:060, 2010.
- [111] ATLAS Collaboration. Measurement of the $W \rightarrow \ell\nu$ production cross-section and observation of $Z \rightarrow \ell\ell$ production in proton–proton collisions at $\sqrt{s} = 7$ TeV with the ATLAS detector. ATLAS-CONF-2010-051, 2010.

- [112] ATLAS Collaboration. Measurement of the $Z \rightarrow \ell\ell$ production cross section in proton–proton collisions at $\sqrt{s} = 7$ TeV with the ATLAS detector. ATLAS-CONF-2010-076, 2010.
- [113] ATLAS Collaboration. Measurement of Ξ, Ω baryons and $K^*(890)$ meson production at $\sqrt{s} = 7$ TeV. ATLAS-CONF-2010-032, 2010.
- [114] ATLAS Collaboration. Measurements of multijet production cross sections in proton–proton collisions at 7 TeV center-of-mass energy with the ATLAS Detector. ATLAS-CONF-2010-084, 2010.
- [115] ATLAS Collaboration. Muon Performance in Minimum Bias $p\bar{p}$ Collision Data at $\sqrt{s} = 7$ TeV with ATLAS. ATLAS-CONF-2010-036, 2010.
- [116] ATLAS Collaboration. Muon Reconstruction Performance. ATLAS-CONF-2010-064, 2010.
- [117] ATLAS Collaboration. Observation of a Centrality-Dependent Dijet Asymmetry in Lead–Lead Collisions at $\sqrt{s_{NN}} = 2.76$ TeV with the ATLAS Detector at the LHC. *Phys. Rev. Lett.*, 105:252303, 2010.
- [118] ATLAS Collaboration. Observation of Energetic Jets in $p\bar{p}$ Collisions at $\sqrt{s} = 7$ TeV using the ATLAS Experiment at the LHC. ATLAS-CONF-2010-043, 2010.
- [119] ATLAS Collaboration. Observation of inclusive electrons in the ATLAS experiment at $\sqrt{s} = 7$ TeV. ATLAS-CONF-2010-073, 2010.
- [120] ATLAS Collaboration. Observation of the Background from W -jets to the $H \rightarrow WW^{(*)} \rightarrow \ell\nu\ell\nu$ Search with the ATLAS detector at $\sqrt{s} = 7$ TeV. ATLAS-CONF-2010-092, 2010.
- [121] ATLAS Collaboration. Observation of $W \rightarrow \ell\nu$ and $Z \rightarrow \ell\ell$ production in proton–proton collisions at $\sqrt{s} = 7$ TeV with the ATLAS detector. ATLAS-CONF-2010-044, 2010.
- [122] ATLAS Collaboration. Observation of $W \rightarrow \tau\nu_\tau$ Decays with the ATLAS Experiment. ATLAS-CONF-2010-097, 2010.
- [123] ATLAS Collaboration. Performance of Impact Parameter-Based b -tagging Algorithms with the ATLAS Detector using Proton–Proton Collisions at $\sqrt{s} = 7$ TeV. ATLAS-CONF-2010-091, 2010.
- [124] ATLAS Collaboration. Performance of primary vertex reconstruction in proton–proton collisions at $\sqrt{s} = 7$ TeV in the ATLAS experiment. ATLAS-CONF-2010-069, 2010.

- [125] ATLAS Collaboration. Performance of the ATLAS detector using first collision data. *JHEP*, 09:056, 2010.
- [126] ATLAS Collaboration. Performance of the ATLAS electromagnetic calorimeter for $\pi^0 \rightarrow \gamma\gamma$ and $\eta \rightarrow \gamma\gamma$ events. ATLAS-CONF-2010-006, 2010.
- [127] ATLAS Collaboration. Performance of the ATLAS Inner Detector Trigger algorithms in pp collisions at $\sqrt{s} = 900$ GeV. ATLAS-CONF-2010-014, 2010.
- [128] ATLAS Collaboration. Performance of the ATLAS jet trigger with pp collisions at $\sqrt{s} = 900$ GeV. ATLAS-CONF-2010-028, 2010.
- [129] ATLAS Collaboration. Performance of the ATLAS Muon Trigger in pp collisions at $\sqrt{s} = 7$ TeV. ATLAS-CONF-2010-095, 2010.
- [130] ATLAS Collaboration. Performance of the ATLAS Secondary Vertex b-tagging Algorithm in 7 TeV Collision Data. ATLAS-CONF-2010-042, 2010.
- [131] ATLAS Collaboration. Performance of the ATLAS Secondary Vertex b-tagging Algorithm in 900 GeV Collision Data. ATLAS-CONF-2010-004, 2010.
- [132] ATLAS Collaboration. Performance of the ATLAS Silicon Pattern Recognition Algorithm in Data and Simulation at $\sqrt{s} = 7$ TeV. ATLAS-CONF-2010-072, 2010.
- [133] ATLAS Collaboration. Performance of the ATLAS tau trigger in pp collisions at $\sqrt{s} = 7$ TeV. ATLAS-CONF-2010-090, 2010.
- [134] ATLAS Collaboration. Performance of the ATLAS tau trigger in pp collisions at $\sqrt{s} = 900$ GeV. ATLAS-CONF-2010-021, 2010.
- [135] ATLAS Collaboration. Performance of the Electron and Photon Trigger in pp Collisions at $\sqrt{s} = 900$ GeV. ATLAS-CONF-2010-022, 2010.
- [136] ATLAS Collaboration. Performance of the Minimum Bias Trigger in pp collisions at $\sqrt{s} = 7$ TeV. ATLAS-CONF-2010-068, 2010.
- [137] ATLAS Collaboration. Performance of the Minimum Bias Trigger in pp Collisions at $\sqrt{s} = 900$ GeV. ATLAS-CONF-2010-025, 2010.
- [138] ATLAS Collaboration. Performance of the Missing Transverse Energy Reconstruction and Calibration in Proton–Proton Collisions at a Center-of-Mass Energy of $\sqrt{s} = 7$ TeV with the ATLAS Detector. ATLAS-CONF-2010-057, 2010.

- [139] ATLAS Collaboration. Performance of the missing transverse energy reconstruction in minimum bias collisions at center-of-mass energy of $\sqrt{s} = 7$ TeV with the ATLAS detector. ATLAS-CONF-2010-039, 2010.
- [140] ATLAS Collaboration. Performance of the missing transverse energy reconstruction in minimum bias events at \sqrt{s} of 900 GeV and 2.36 TeV with the ATLAS detector. ATLAS-CONF-2010-008, 2010.
- [141] ATLAS Collaboration. Performances of the Atlas Jet Trigger from the Early $\sqrt{s} = 7$ TeV Data. ATLAS-CONF-2010-094, 2010.
- [142] ATLAS Collaboration. $\phi(1020)$ -meson production in $\sqrt{s} = 900$ GeV collision data. ATLAS-CONF-2010-023, 2010.
- [143] ATLAS Collaboration. Photon Conversions at $\sqrt{s} = 900$ GeV measured with the ATLAS Detector. ATLAS-CONF-2010-007, 2010.
- [144] ATLAS Collaboration. Preliminary studies for the measurement of the inclusive muon spectrum in $p\bar{p}$ collisions at $\sqrt{s} = 7$ TeV with the ATLAS detector. ATLAS-CONF-2010-035, 2010.
- [145] ATLAS Collaboration. Probing the response of the ATLAS electromagnetic calorimeter and material upstream with energy flow from $\sqrt{s} = 7$ TeV minimum bias events. ATLAS-CONF-2010-037, 2010.
- [146] ATLAS Collaboration. Properties and internal structure of jets produced in proton–proton collisions at $\sqrt{s} = 900$ GeV. ATLAS-CONF-2010-018, 2010.
- [147] ATLAS Collaboration. Properties of Jets and Inputs to Jet Reconstruction and Calibration with the ATLAS Detector Using Proton–Proton Collisions at $\sqrt{s} = 7$ TeV. ATLAS-CONF-2010-053, 2010.
- [148] ATLAS Collaboration. Properties of tracks in jets observed in proton–proton collisions at $\sqrt{s} = 7$ TeV in the ATLAS detector. ATLAS-CONF-2010-061, 2010.
- [149] ATLAS Collaboration. Prospects for early $t\bar{t}$ resonance searches in ATLAS. ATL-PHYS-PUB-2010-008, 2010.
- [150] ATLAS Collaboration. Prospects for Higgs boson searches using the $H \rightarrow WW^{(*)} \rightarrow l\nu l\nu$ decay mode with the ATLAS detector at 10 TeV. ATL-PHYS-PUB-2010-005, 2010.
- [151] ATLAS Collaboration. Prospects for Supersymmetry discovery based on inclusive searches at a 7 TeV centre-of-mass energy with the ATLAS detector. ATL-PHYS-PUB-2010-010, 2010.

- [152] ATLAS Collaboration. Prospects for the Measurement of the Top-Quark Mass using the Template Method with early ATLAS Data. ATL-PHYS-PUB-2010-004, 2010.
- [153] ATLAS Collaboration. Readiness of the ATLAS liquid argon calorimeter for LHC collisions. *Eur. Phys. J. C*, 70:723, 2010.
- [154] ATLAS Collaboration. Readiness of the ATLAS Tile Calorimeter for LHC collisions. *Eur. Phys. J. C*, 70:1193, 2010.
- [155] ATLAS Collaboration. Reconstruction of hadronic tau candidates in QCD events at ATLAS with 7 TeV proton–proton collisions. ATLAS-CONF-2010-059, 2010.
- [156] ATLAS Collaboration. Reconstruction of jets from tracks in proton–proton collisions at centre-of-mass energy $\sqrt{s} = 900$ GeV with the ATLAS detector. ATLAS-CONF-2010-002, 2010.
- [157] ATLAS Collaboration. Response of the ATLAS calorimeters to single isolated hadrons produced in proton–proton collisions at a center-of-mass energy of $\sqrt{s} = 900$ GeV. ATLAS-CONF-2010-017, 2010.
- [158] ATLAS Collaboration. Search for high-mass states with electron plus missing transverse energy using the ATLAS Detector at $\sqrt{s} = 7$ TeV. ATLAS-CONF-2010-089, 2010.
- [159] ATLAS Collaboration. Search for new particles decaying into dijets in proton–proton collisions at $\sqrt{s} = 7$ TeV with the ATLAS detector. ATLAS-CONF-2010-080, 2010.
- [160] ATLAS Collaboration. Search for New Particles in Two-Jet Final States in 7 TeV Proton–Proton Collisions with the ATLAS Detector at the LHC. *Phys. Rev. Lett.*, 105:161801, 2010.
- [161] ATLAS Collaboration. Search for new physics in multi-body final states at high invariant masses with ATLAS. ATLAS-CONF-2010-088, 2010.
- [162] ATLAS Collaboration. Search for top pair candidate events in ATLAS at $\sqrt{s} = 7$ TeV. ATLAS-CONF-2010-063, 2010.
- [163] ATLAS Collaboration. Soft muon tagging and $D^*\mu$ reconstruction in 7 TeV collisions with ATLAS. ATLAS-CONF-2010-100, 2010.
- [164] ATLAS Collaboration. Strategy to Search for Single-Top Events using early Data of the ATLAS Detector at the LHC. ATL-PHYS-PUB-2010-003, 2010.

- [165] ATLAS Collaboration. Studies of Diffractive Enhanced Minimum Bias Events in ATLAS. ATLAS-CONF-2010-048, 2010.
- [166] ATLAS Collaboration. Study of the Material Budget in the ATLAS Inner Detector with K_S^0 decays in collision data at $\sqrt{s} = 900$ GeV. ATLAS-CONF-2010-019, 2010.
- [167] ATLAS Collaboration. Tau Reconstruction and Identification Performance in ATLAS. ATLAS-CONF-2010-086, 2010.
- [168] ATLAS Collaboration. The ATLAS Inner Detector commissioning and calibration. *Eur. Phys. J. C*, 70:787, 2010.
- [169] ATLAS Collaboration. The ATLAS missing E_T trigger performance with initial LHC runs at $\sqrt{s} = 900$ GeV. ATLAS-CONF-2010-026, 2010.
- [170] ATLAS Collaboration. The ATLAS Simulation Infrastructure. *Eur. Phys. J. C*, 70:823, 2010.
- [171] ATLAS Collaboration. The simulation principle and performance of the ATLAS fast calorimeter simulation FastCaloSim. ATL-PHYS-PUB-2010-013, 2010.
- [172] ATLAS Collaboration. Track-based underlying event measurements in $p\bar{p}$ collisions at $\sqrt{s} = 900$ GeV and 7 TeV with the ATLAS Detector at the LHC. ATLAS-CONF-2010-029, 2010.
- [173] ATLAS Collaboration. Track-based underlying event measurements in $p\bar{p}$ collisions at $\sqrt{s} = 900$ GeV and 7 TeV with the ATLAS Detector at the LHC. ATLAS-CONF-2010-081, 2010.
- [174] ATLAS Collaboration. Tracking Results and Comparison to Monte Carlo simulation at $\sqrt{s} = 900$ GeV. ATLAS-CONF-2010-011, 2010.
- [175] ATLAS Collaboration. Tracking Studies for b-tagging with 7 TeV Collision Data with the ATLAS Detector. ATLAS-CONF-2010-040, 2010.
- [176] ATLAS Collaboration. Tracking Studies for b-tagging with 7 TeV Collision Data with the ATLAS Detector. ATLAS-CONF-2010-070, 2010.
- [177] ATLAS Collaboration. Tracking studies for b-tagging with 900 GeV collision data with the ATLAS detector. ATLAS-CONF-2010-003, 2010.
- [178] ATLAS Collaboration. Update of the search for new particles decaying into dijets in proton–proton collisions at $\sqrt{s} = 7$ TeV with the ATLAS detector. ATLAS-CONF-2010-093, 2010.

- [179] ATLAS Collaboration. A combined measurement of the top quark pair production cross-section using dilepton and single-lepton final states. ATLAS-CONF-2011-040, 2011.
- [180] ATLAS Collaboration. A measurement of the ATLAS muon reconstruction and trigger efficiency using J/ψ decays. ATLAS-CONF-2011-021, 2011.
- [181] ATLAS Collaboration. A measurement of the total W^\pm and Z/γ^* cross sections in the e and μ decay channels and of their ratios in pp collisions at $\sqrt{s} = 7$ TeV with the ATLAS detector. ATLAS-CONF-2011-041, 2011.
- [182] ATLAS Collaboration. A Search for a light charged Higgs boson decaying to $c\bar{s}$ in pp collisions at $\sqrt{s} = 7$ TeV with the ATLAS detector. ATLAS-CONF-2011-094, 2011.
- [183] ATLAS Collaboration. A search for Flavour Changing Neutral Currents in Top Quark Decays $t \rightarrow qZ$ at $\sqrt{s} = 7$ TeV in 0.70 fb^{-1} of pp collision data collected with the ATLAS Detector. ATLAS-CONF-2011-154, 2011.
- [184] ATLAS Collaboration. A Search for Lepton-Jets with Muons in pp Collisions at $\sqrt{s} = 7$ TeV in the ATLAS Detector. ATLAS-CONF-2011-076, 2011.
- [185] ATLAS Collaboration. A Search for Light CP-odd Higgs Bosons Decaying to $\mu^+\mu^-$ in ATLAS. ATLAS-CONF-2011-020, 2011.
- [186] ATLAS Collaboration. A Search for New High-Mass Phenomena Producing Top Quarks with the ATLAS Experiment. ATLAS-CONF-2011-070, 2011.
- [187] ATLAS Collaboration. A search for new physics in dijet mass and angular distributions in pp collisions at $\sqrt{s} = 7$ TeV measured with the ATLAS detector. *New J. Phys.*, 13:053044, 2011.
- [188] ATLAS Collaboration. A Search for Randall-Sundrum Gravitons Decaying to Photon Pairs in $\sqrt{s} = 7$ TeV pp Collisions. ATLAS-CONF-2011-044, 2011.
- [189] ATLAS Collaboration. A Search for $t\bar{t}$ Resonances in the Dilepton Channel in 1.04 fb^{-1} of pp collisions at $\sqrt{s} = 7$ TeV with the ATLAS experiment. ATLAS-CONF-2011-123, 2011.
- [190] ATLAS Collaboration. A Search for $t\bar{t}$ Resonances in the Lepton Plus Jets Channel using 200 pb^{-1} of pp Collisions at $\sqrt{s} = 7$ TeV. ATLAS-CONF-2011-087, 2011.

- [191] ATLAS Collaboration. Alignment of the ATLAS Inner Detector Tracking System with 2010 LHC proton–proton collisions at $\sqrt{s} = 7$ TeV. ATLAS-CONF-2011-012, 2011.
- [192] ATLAS Collaboration. An extrapolation to a larger fiducial volume of the measurement of the $W \rightarrow \ell\nu$ charge asymmetry in proton–proton collisions at $\sqrt{s} = 7$ TeV with the ATLAS detector: Graphical comparison between ATLAS, CMS and LHCb. ATLAS-CONF-2011-129, 2011.
- [193] ATLAS Collaboration. ATLAS Calorimeter Response to Single Isolated Hadrons and Estimation of the Calorimeter Jet Scale Uncertainty. ATLAS-CONF-2011-028, 2011.
- [194] ATLAS Collaboration. ATLAS Muon Momentum Resolution in the First Pass Reconstruction of the 2010 $p\bar{p}$ Collision Data at $\sqrt{s} = 7$ TeV. ATLAS-CONF-2011-046, 2011.
- [195] ATLAS Collaboration. ATLAS top physics potential as a function of LHC integrated luminosity. ATL-PHYS-PUB-2011-004, 2011.
- [196] ATLAS Collaboration. ATLAS tunes of PYTHIA 6 and Pythia 8 for MC11. ATL-PHYS-PUB-2011-009, 2011.
- [197] ATLAS Collaboration. b-Jet Tagging Efficiency Calibration using the *System8* Method. ATLAS-CONF-2011-143, 2011.
- [198] ATLAS Collaboration. Calibrating the b-Tag Efficiency and Mistag Rate in 35 pb^{-1} of Data with the ATLAS Detector. ATLAS-CONF-2011-089, 2011.
- [199] ATLAS Collaboration. Calibration of the ATLAS Transition Radiation Tracker. ATLAS-CONF-2011-006, 2011.
- [200] ATLAS Collaboration. Calorimeter response to isolated particles identified using resonances in proton–proton collisions at $\sqrt{s} = 7$ TeV with the ATLAS detector. ATLAS-CONF-2011-019, 2011.
- [201] ATLAS Collaboration. Central charged-particle multiplicities in $p\bar{p}$ interactions with $|\eta| < 0.8$ and $p_T > 0.5$ and 1 GeV measured with the ATLAS detector at the LHC. ATLAS-CONF-2010-101, 2011.
- [202] ATLAS Collaboration. Centrality dependence of Jet Yields and Jet Fragmentation in Lead–Lead Collisions at $\sqrt{s_{\text{NN}}} = 2.76$ TeV with the ATLAS detector at the LHC. ATLAS-CONF-2011-075, 2011.
- [203] ATLAS Collaboration. Charged-particle multiplicities in $p\bar{p}$ interactions measured with the ATLAS detector at the LHC. *New J. Phys.*, 13:053033, 2011.

- [204] ATLAS Collaboration. Close-by Jet Effects on Jet Energy Scale Calibration in pp Collisions at $\sqrt{s} = 7 \text{ TeV}$ with the ATLAS detector. ATLAS-CONF-2011-062, 2011.
- [205] ATLAS Collaboration. Combination of Higgs Boson Searches with up to 4.9 fb^{-1} of pp Collision Data Taken at $\sqrt{s} = 7 \text{ TeV}$ with the ATLAS Experiment at the LHC. ATLAS-CONF-2011-163, 2011.
- [206] ATLAS Collaboration. Combined exclusion reach of searches for squarks and gluinos using final states with jets, missing transverse momentum, and zero or one lepton, with the ATLAS detector in $\sqrt{s} = 7 \text{ TeV}$ proton–proton collisions. ATLAS-CONF-2011-064, 2011.
- [207] ATLAS Collaboration. Combined Standard Model Higgs Boson Searches in pp Collisions at $\sqrt{s} = 7 \text{ TeV}$ with the ATLAS Experiment at the LHC. ATLAS-CONF-2011-112, 2011.
- [208] ATLAS Collaboration. Combined Standard Model Higgs boson searches with up to 2.3 fb^{-1} of pp collision data at $\sqrt{s} = 7 \text{ TeV}$ at the LHC. ATLAS-CONF-2011-157, 2011.
- [209] ATLAS Collaboration. Commissioning of the ATLAS high performance b-tagging algorithms in the 7 TeV collision data. ATLAS-CONF-2011-102, 2011.
- [210] ATLAS Collaboration. Comparison of $D^{(*)}$ meson production cross sections with FONLL and GM-VFNS predictions. ATL-PHYS-PUB-2011-012, 2011.
- [211] ATLAS Collaboration. Comparisons of the measured inclusive jet cross section to a selection of NLO QCD predictions, and a study of the parton content of the calculations. ATL-PHYS-PUB-2011-005, 2011.
- [212] ATLAS Collaboration. Compiled measurements of the inclusive isolated prompt photon cross section in pp collisions at $\sqrt{s} = 7 \text{ TeV}$ with the ATLAS detector. ATL-PHYS-PUB-2011-013, 2011.
- [213] ATLAS Collaboration. Constraining the gauge-mediated Supersymmetry breaking model in final states with two leptons, jets and missing transverse momentum with the ATLAS experiment at $\sqrt{s} = 7 \text{ TeV}$. ATLAS-CONF-2011-156, 2011.
- [214] ATLAS Collaboration. Constraints on Anomalous $\mu^+ \mu^+$ and Like-sign Top Quark Pair Production. ATLAS-CONF-2011-139, 2011.
- [215] ATLAS Collaboration. Data-driven estimation of the background to charged Higgs boson searches hadronically-decaying τ final states in ATLAS. ATLAS-CONF-2011-051, 2011.

- [216] ATLAS Collaboration. dE/dx measurement in the ATLAS Pixel Detector and its use for particle identification. ATLAS-CONF-2011-016, 2011.
- [217] ATLAS Collaboration. Determination of the ATLAS jet energy measurement uncertainty using photon-jet events in proton–proton collisions at $\sqrt{s} = 7$ TeV. ATLAS-CONF-2011-031, 2011.
- [218] ATLAS Collaboration. Determination of the muon reconstruction efficiency in ATLAS at the Z resonance in proton–proton collisions at $\sqrt{s} = 7$ TeV. ATLAS-CONF-2011-008, 2011.
- [219] ATLAS Collaboration. Determination of the Top-Quark Mass from the $t\bar{t}$ Cross Section Measurement in $p\bar{p}$ Collisions at $\sqrt{s} = 7$ TeV with the ATLAS detector. ATLAS-CONF-2011-054, 2011.
- [220] ATLAS Collaboration. Di-muon composition in ATLAS at 7 TeV. ATLAS-CONF-2011-003, 2011.
- [221] ATLAS Collaboration. Expected electron performance in the ATLAS experiment. ATL-PHYS-PUB-2011-006, 2011.
- [222] ATLAS Collaboration. Expected photon performance in the ATLAS experiment. ATL-PHYS-PUB-2011-007, 2011.
- [223] ATLAS Collaboration. Further ATLAS tunes of PYTHIA 6 and Pythia 8. ATL-PHYS-PUB-2011-014, 2011.
- [224] ATLAS Collaboration. Further investigations of ATLAS Sensitivity to Higgs Boson Production in different assumed LHC scenarios. ATL-PHYS-PUB-2011-001, 2011.
- [225] ATLAS Collaboration. Higgs Boson Searches using the $H \rightarrow WW^{(*)} \rightarrow \ell\nu\ell\nu$ Decay Mode with the ATLAS Detector at 7 TeV. ATLAS-CONF-2011-005, 2011.
- [226] ATLAS Collaboration. In-situ jet energy scale and jet shape corrections for multiple interactions in the first ATLAS data at the LHC. ATLAS-CONF-2011-030, 2011.
- [227] ATLAS Collaboration. In-situ pseudorapidity intercalibration for evaluation of jet energy scale uncertainty using dijet events in proton–proton collisions at $\sqrt{s} = 7$ TeV. ATLAS-CONF-2011-014, 2011.
- [228] ATLAS Collaboration. Inclusive search for same-sign dilepton signatures in $p\bar{p}$ collisions at $\sqrt{s} = 7$ TeV with the ATLAS detector. *JHEP*, 10:107, 2011.

- [229] ATLAS Collaboration. Interpretation of same-sign dilepton events at ATLAS with a simplified SUSY model. ATLAS-CONF-2011-091, 2011.
- [230] ATLAS Collaboration. Invariant mass distribution of jet pairs produced in association with a leptonically decaying W boson using 1.02 fb^{-1} of ATLAS data. ATLAS-CONF-2011-097, 2011.
- [231] ATLAS Collaboration. Invariant mass distribution of jet pairs produced in association with one lepton and missing transverse energy at the ATLAS experiment. ATLAS-CONF-2011-069, 2011.
- [232] ATLAS Collaboration. Jet energy scale and its systematic uncertainty in proton-proton collisions at $\sqrt{s} = 7 \text{ TeV}$ with ATLAS 2010 data. ATLAS-CONF-2011-032, 2011.
- [233] ATLAS Collaboration. Jet Shapes in ATLAS and Monte Carlo modeling. ATL-PHYS-PUB-2011-010, 2011.
- [234] ATLAS Collaboration. Light-quark and Gluon Jets in ATLAS: Calorimeter Response, Jet Energy Scale Systematics, and Sample Characterization. ATLAS-CONF-2011-053, 2011.
- [235] ATLAS Collaboration. Limits on the production of the Standard Model Higgs Boson in pp collisions at $\sqrt{s} = 7 \text{ TeV}$ with the ATLAS detector. *Eur. Phys. J. C*, 71:1728, 2011.
- [236] ATLAS Collaboration. Luminosity determination in pp collisions at $\sqrt{s} = 7 \text{ TeV}$ using the ATLAS detector at the LHC. *Eur. Phys. J. C*, 71:1630, 2011.
- [237] ATLAS Collaboration. Luminosity determination in pp collisions at $\sqrt{s} = 7 \text{ TeV}$ using the ATLAS detector at the LHC. *Eur. Phys. J. C*, 71:1630, 2011.
- [238] ATLAS Collaboration. Luminosity Determination in pp Collisions at $\sqrt{s} = 7 \text{ TeV}$ using the ATLAS Detector in 2011. ATLAS-CONF-2011-116, 2011.
- [239] ATLAS Collaboration. Measurement of $D^{(*)}$ meson production cross sections in pp collisions at $\sqrt{s} = 7 \text{ TeV}$ with the ATLAS detector. ATLAS-CONF-2011-017, 2011.
- [240] ATLAS Collaboration. Measurement of Dijet Azimuthal Decorrelations in pp Collisions at $\sqrt{s} = 7 \text{ TeV}$. *Phys. Rev. Lett.*, 106:172002, 2011.
- [241] ATLAS Collaboration. Measurement of dijet production with a jet veto in pp collisions at $\sqrt{s} = 7 \text{ TeV}$ using the ATLAS detector. ATLAS-CONF-2011-038, 2011.

- [242] ATLAS Collaboration. Measurement of dijet production with a veto on additional central jet activity in pp collisions at $\sqrt{s} = 7$ TeV using the ATLAS detector. *JHEP*, 09:053, 2011.
- [243] ATLAS Collaboration. Measurement of elliptic flow and higher-order flow coefficients with the ATLAS detector in $\sqrt{s_{\text{NN}}} = 2.76$ TeV Pb+Pb collisions. ATLAS-CONF-2011-074, 2011.
- [244] ATLAS Collaboration. Measurement of hadronic tau decay identification efficiency using $W \rightarrow \tau\nu$ events. ATLAS-CONF-2011-093, 2011.
- [245] ATLAS Collaboration. Measurement of hard double-partonic interactions in $W \rightarrow l\nu + 2$ jet events using the ATLAS detector at the LHC. ATLAS-CONF-2011-160, 2011.
- [246] ATLAS Collaboration. Measurement of inclusive jet and dijet cross sections in proton–proton collision data at 7 TeV centre-of-mass energy using the ATLAS detector. ATLAS-CONF-2011-047, 2011.
- [247] ATLAS Collaboration. Measurement of inclusive jet and dijet cross sections in proton–proton collisions at 7 TeV centre-of-mass energy with the ATLAS detector. *Eur. Phys. J. C*, 71:1512, 2011.
- [248] ATLAS Collaboration. Measurement of Inclusive Two-Particle Angular Correlations in Proton–Proton Collisions at $\sqrt{s} = 900$ GeV and 7 TeV. ATLAS-CONF-2011-055, 2011.
- [249] ATLAS Collaboration. Measurement of Jet Mass and Substructure for Inclusive Jets in $\sqrt{s} = 7$ TeV pp Collisions with the ATLAS Experiment. ATLAS-CONF-2011-073, 2011.
- [250] ATLAS Collaboration. Measurement of multi-jet cross-sections in proton–proton collisions at 7 TeV center-of-mass energy. ATLAS-CONF-2011-043, 2011.
- [251] ATLAS Collaboration. Measurement of multi-jet cross sections in proton–proton collisions at a 7 TeV center-of-mass energy. *Eur. Phys. J. C*, 71:1763, 2011.
- [252] ATLAS Collaboration. Measurement of spin correlation in $t\bar{t}$ production from pp collisions at $\sqrt{s} = 7$ TeV using the ATLAS detector. ATLAS-CONF-2011-117, 2011.
- [253] ATLAS Collaboration. Measurement of $t\bar{t}$ production in the all-hadronic channel in 1.02 fb^{-1} of pp collisions at $\sqrt{s} = 7$ TeV with the ATLAS detector. ATLAS-CONF-2011-140, 2011.

- [254] ATLAS Collaboration. Measurement of the average B lifetime in inclusive $B \rightarrow J/\psi X \rightarrow \mu^+\mu^-X$ decays with the ATLAS detector. ATLAS-CONF-2011-145, 2011.
- [255] ATLAS Collaboration. Measurement of the b -jet production cross section using muons in jets with ATLAS in $p\bar{p}$ collisions at $\sqrt{s} = 7$ TeV. ATLAS-CONF-2011-057, 2011.
- [256] ATLAS Collaboration. Measurement of the B_d^0 and B_s^0 lifetimes in the decay modes $B_d^0 \rightarrow J/\psi K^{*0}$ and $B_s^0 \rightarrow J/\psi \phi$ in ATLAS. ATLAS-CONF-2011-092, 2011.
- [257] ATLAS Collaboration. Measurement of the backgrounds to the $H \rightarrow \gamma\gamma$ search and reappraisal of its sensitivity with 37 pb^{-1} of data recorded by the ATLAS detector. ATLAS-CONF-2011-004, 2011.
- [258] ATLAS Collaboration. Measurement of the centrality dependence of charged particle spectra and R_{CP} in lead–lead collisions at $\sqrt{s_{NN}} = 2.76$ TeV with the ATLAS detector at the LHC. ATLAS-CONF-2011-079, 2011.
- [259] ATLAS Collaboration. Measurement of the centrality dependence of J/ψ yields and observation of Z production in lead–lead collisions with the ATLAS detector at the LHC. *Phys. Lett. B*, 697:294, 2011.
- [260] ATLAS Collaboration. Measurement of the charge asymmetry in top quark pair production in $p\bar{p}$ collisions at $\sqrt{s} = 7$ TeV using the ATLAS detector. ATLAS-CONF-2011-106, 2011.
- [261] ATLAS Collaboration. Measurement of the differential cross-sections of inclusive, prompt and non-prompt J/ψ production in proton–proton collisions at $\sqrt{s} = 7$ TeV. *Nucl. Phys. B*, 850:387, 2011.
- [262] ATLAS Collaboration. Measurement of the inclusive and dijet cross-sections of b -jets in $p\bar{p}$ collisions at $\sqrt{s} = 7$ TeV with the ATLAS detector. *Eur. Phys. J. C*, 71:1846, 2011.
- [263] ATLAS Collaboration. Measurement of the inclusive and dijet cross sections of b -jets in $p\bar{p}$ collisions at $\sqrt{s} = 7$ TeV with the ATLAS detector. ATLAS-CONF-2011-056, 2011.
- [264] ATLAS Collaboration. Measurement of the inclusive isolated prompt photon cross-section in $p\bar{p}$ collisions at $\sqrt{s} = 7$ TeV using 35 pb^{-1} of ATLAS data. *Phys. Lett. B*, 706:150, 2011.

- [265] ATLAS Collaboration. Measurement of the inclusive isolated prompt photon cross section in pp collisions at $\sqrt{s} = 7 \text{ TeV}$ with the ATLAS detector. *Phys. Rev. D*, 83:052005, 2011.
- [266] ATLAS Collaboration. Measurement of the inclusive isolated prompt photon cross-section in pp collisions at $\sqrt{s} = 7 \text{ TeV}$ with the ATLAS detector using 35 pb^{-1} . ATLAS-CONF-2011-058, 2011.
- [267] ATLAS Collaboration. Measurement of the inclusive $t\bar{t}\gamma$ cross section at $\sqrt{s} = 7 \text{ TeV}$ with the ATLAS detector. ATLAS-CONF-2011-153, 2011.
- [268] ATLAS Collaboration. Measurement of the inelastic proton–proton cross-section at $\sqrt{s} = 7 \text{ TeV}$ with the ATLAS detector. *Nature Commun.*, 2:463, 2011.
- [269] ATLAS Collaboration. Measurement of the Inelastic Proton–Proton Cross Section at $\sqrt{s} = 7 \text{ TeV}$ with the ATLAS Detector. ATLAS-CONF-2011-002, 2011.
- [270] ATLAS Collaboration. Measurement of the jet fragmentation function and transverse profile in proton–proton collisions at a center-of-mass energy of 7 TeV with the ATLAS detector. *Eur. Phys. J. C*, 71:1795, 2011.
- [271] ATLAS Collaboration. Measurement of the Mis-identification Probability of τ Leptons from Hadronic Jets and from Electrons. ATLAS-CONF-2011-113, 2011.
- [272] ATLAS Collaboration. Measurement of the production cross section for W -bosons in association with jets in pp collisions at $\sqrt{s} = 7 \text{ TeV}$ with the ATLAS detector. *Phys. Lett. B*, 698:325, 2011.
- [273] ATLAS Collaboration. Measurement of the production cross section for W -bosons in association with jets in pp collisions using 33 pb^{-1} of data at $\sqrt{s} = 7 \text{ TeV}$ with the ATLAS detector. ATLAS-CONF-2011-060, 2011.
- [274] ATLAS Collaboration. Measurement of the production cross section for Z/γ^* in association with jets in pp collisions at $\sqrt{s} = 7 \text{ TeV}$ with the ATLAS detector. ATLAS-CONF-2011-001, 2011.
- [275] ATLAS Collaboration. Measurement of the production cross section for Z/γ^* in association with jets in pp collisions at $\sqrt{s} = 7 \text{ TeV}$ with the ATLAS Detector. ATLAS-CONF-2011-042, 2011.
- [276] ATLAS Collaboration. Measurement of the t-channel Single top-Quark Production Cross Section in 0.70 fb^{-1} of pp Collisions at $\sqrt{s} = 7 \text{ TeV}$ collected with the ATLAS detector. ATLAS-CONF-2011-101, 2011.

- [277] ATLAS Collaboration. Measurement of the $t\bar{t}$ production cross-section in pp collisions at $\sqrt{s} = 7$ TeV using kinematic information of lepton+jets events. ATLAS-CONF-2011-121, 2011.
- [278] ATLAS Collaboration. Measurement of the top quark charge in pp collisions at $\sqrt{s} = 7$ TeV in the ATLAS experiment. ATLAS-CONF-2011-141, 2011.
- [279] ATLAS Collaboration. Measurement of the Top-Quark Mass from 2011 ATLAS Data using the Template Method. ATLAS-CONF-2011-120, 2011.
- [280] ATLAS Collaboration. Measurement of the Top-Quark Mass using the Template Method in pp Collisions at $\sqrt{s} = 7$ TeV with the ATLAS detector. ATLAS-CONF-2011-033, 2011.
- [281] ATLAS Collaboration. Measurement of the top quark pair cross-section with ATLAS in pp collisions at $\sqrt{s} = 7$ TeV in the single-lepton channel using b -tagging. ATLAS-CONF-2011-035, 2011.
- [282] ATLAS Collaboration. Measurement of the top quark pair production cross-section based on a statistical combination of measurements of dilepton and single-lepton final states at $\sqrt{s} = 7$ TeV with the ATLAS detector. ATLAS-CONF-2011-108, 2011.
- [283] ATLAS Collaboration. Measurement of the top-quark pair production cross-section in pp collisions at $\sqrt{s} = 7$ TeV in dilepton final states with ATLAS. ATLAS-CONF-2011-100, 2011.
- [284] ATLAS Collaboration. Measurement of the top quark pair production cross section in pp collisions at $\sqrt{s} = 7$ TeV in $\mu + \tau$ final states with ATLAS. ATLAS-CONF-2011-119, 2011.
- [285] ATLAS Collaboration. Measurement of the top quark-pair production cross section with ATLAS in pp collisions at $\sqrt{s} = 7$ TeV. *Eur. Phys. J. C*, 71:1577, 2011.
- [286] ATLAS Collaboration. Measurement of the top quark pair production cross section with ATLAS in pp collisions at $\sqrt{s} = 7$ TeV in dilepton final states. ATLAS-CONF-2011-034, 2011.
- [287] ATLAS Collaboration. Measurement of the transverse momentum distribution of Z/γ^* bosons in proton–proton collisions at $\sqrt{s} = 7$ TeV with the ATLAS detector. *Phys. Lett. B*, 705:415, 2011.
- [288] ATLAS Collaboration. Measurement of the $\Upsilon(1S)$ Production Cross-Section in pp Collisions at $\sqrt{s} = 7$ TeV in ATLAS. *Phys. Lett. B*, 705:9, 2011.

- [289] ATLAS Collaboration. Measurement of the W boson polarisation in top quark decays in 0.70 fb^{-1} of pp collisions at $\sqrt{s} = 7 \text{ TeV}$ with the ATLAS detector. ATLAS-CONF-2011-122, 2011.
- [290] ATLAS Collaboration. Measurement of the W -boson polarisation in top quark decays in pp collision data at $\sqrt{s} = 7 \text{ TeV}$ using the ATLAS detector. ATLAS-CONF-2011-037, 2011.
- [291] ATLAS Collaboration. Measurement of the W charge asymmetry in the $W \rightarrow \mu\nu$ decay mode in pp collisions at $\sqrt{s} = 7 \text{ TeV}$ with the ATLAS detector. *Phys. Lett. B*, 701:31, 2011.
- [292] ATLAS Collaboration. Measurement of the $W^\pm Z$ Production Cross-Section in Proton–Proton Collisions at $\sqrt{s} = 7 \text{ TeV}$ with the ATLAS Detector. ATLAS-CONF-2011-084, 2011.
- [293] ATLAS Collaboration. Measurement of the $W^\pm Z$ Production Cross Section in Proton–Proton Collisions at $\sqrt{s} = 7 \text{ TeV}$ with the ATLAS Detector. ATLAS-CONF-2011-099, 2011.
- [294] ATLAS Collaboration. Measurement of the W^+W^- Cross Section in $\sqrt{s} = 7 \text{ TeV}$ pp Collisions with ATLAS. *Phys. Rev. Lett.*, 107:041802, 2011.
- [295] ATLAS Collaboration. Measurement of the W^+W^- production cross section in proton–proton collisions at $\sqrt{s} = 7 \text{ TeV}$ with the ATLAS detector. ATLAS-CONF-2011-015, 2011.
- [296] ATLAS Collaboration. Measurement of the W^+W^- production cross section in proton–proton collisions at $\sqrt{s} = 7 \text{ TeV}$ with the ATLAS detector. ATLAS-CONF-2011-110, 2011.
- [297] ATLAS Collaboration. Measurement of the $Z \rightarrow \tau\tau$ cross section with the ATLAS detector. *Phys. Rev. D*, 84:112006, 2011.
- [298] ATLAS Collaboration. Measurement of the ZZ Production Cross Section in Proton–Proton Collisions at $\sqrt{s} = 7 \text{ TeV}$ with the ATLAS Detector. ATLAS-CONF-2011-107, 2011.
- [299] ATLAS Collaboration. Measurement of underlying event characteristics using charged particles in pp collisions at $\sqrt{s} = 900 \text{ GeV}$ and 7 TeV with the ATLAS detector. *Phys. Rev. D*, 83:112001, 2011.
- [300] ATLAS Collaboration. Measurement of underlying event characteristics using charged particles in pp collisions at $\sqrt{s} = 900 \text{ GeV}$ and 7 TeV with the ATLAS detector in a limited phase space. ATLAS-CONF-2011-009, 2011.

- [301] ATLAS Collaboration. Measurement of $W\gamma$ and $Z\gamma$ production at $\sqrt{s} = 7$ TeV with the ATLAS Detector. ATLAS-CONF-2011-013, 2011.
- [302] ATLAS Collaboration. Measurement of $W\gamma$ and $Z\gamma$ production in proton–proton collisions at $\sqrt{s} = 7$ TeV with the ATLAS detector. *JHEP*, 09:072, 2011.
- [303] ATLAS Collaboration. Measurements of underlying-event properties using neutral and charged particles in $p\bar{p}$ collisions at $\sqrt{s} = 900$ GeV and $\sqrt{s} = 7$ TeV with the ATLAS detector at the LHC. *Eur. Phys. J. C*, 71:1636, 2011.
- [304] ATLAS Collaboration. Measurements of W Boson Yields in Pb+Pb collisions at 2.76 TeV/nucleon via Single Muons with the ATLAS Detector. ATLAS-CONF-2011-078, 2011.
- [305] ATLAS Collaboration. Muon reconstruction efficiency in reprocessed 2010 LHC proton–proton collision data recorded with the ATLAS detector. ATLAS-CONF-2011-063, 2011.
- [306] ATLAS Collaboration. New ATLAS event generator tunes to 2010 data. ATL-PHYS-PUB-2011-008, 2011.
- [307] ATLAS Collaboration. Non-collision backgrounds as measured by the ATLAS detector during the 2010 proton–proton run. ATLAS-CONF-2011-137, 2011.
- [308] ATLAS Collaboration. Observation of leading ϕ -mesons in high p_T jets with the ATLAS detector at $\sqrt{s} = 7$ TeV. ATLAS-CONF-2011-146, 2011.
- [309] ATLAS Collaboration. Observation of t-channel Single Top-Quark Production in $p\bar{p}$ Collisions at $\sqrt{s} = 7$ TeV with the ATLAS detector. ATLAS-CONF-2011-088, 2011.
- [310] ATLAS Collaboration. Observation of the B_d^0 and B_s^0 mesons in the decays $B_d^0 \rightarrow J/\psi K^{*0}$ and $B_s \rightarrow J/\psi \phi$ in ATLAS. ATLAS-CONF-2011-050, 2011.
- [311] ATLAS Collaboration. Observation of the B^\pm meson in the decay $B^\pm \rightarrow J/\psi(\mu^+\mu^-)K^\pm$ in ATLAS. ATLAS-CONF-2010-098, 2011.
- [312] ATLAS Collaboration. Observation of the $\chi_{c1}(1P)$ and $\chi_{c2}(1P)$ charmonium states in $\sqrt{s} = 7$ TeV $p\bar{p}$ collisions at the ATLAS experiment. ATLAS-CONF-2011-136, 2011.
- [313] ATLAS Collaboration. Observation of the decay $B_d^0 \rightarrow J/\psi(\mu^+\mu^-)K_s^0(\pi^+\pi^-)$ with the ATLAS experiment at the LHC. ATLAS-CONF-2011-105, 2011.

- [314] ATLAS Collaboration. Observation of the decay $\Lambda_b^0 \rightarrow J/\psi(\mu^+\mu^-)\Lambda^0(p^+\pi^-)$ with the ATLAS experiment at the LHC. ATLAS-CONF-2011-124, 2011.
- [315] ATLAS Collaboration. Observation of the process $Z \rightarrow \tau\tau \rightarrow e\mu + 4\nu$ with the ATLAS Detector. ATLAS-CONF-2011-045, 2011.
- [316] ATLAS Collaboration. Observation of $Z \rightarrow \tau_h\tau_l$ Decays with the ATLAS detector. ATLAS-CONF-2011-010, 2011.
- [317] ATLAS Collaboration. Particle Identification Performance of the ATLAS Transition Radiation Tracker. ATLAS-CONF-2011-128, 2011.
- [318] ATLAS Collaboration. Performance of the ATLAS transverse energy triggers with initial LHC runs at $\sqrt{s} = 7$ TeV. ATLAS-CONF-2011-072, 2011.
- [319] ATLAS Collaboration. Performance of the Electron and Photon Trigger in pp Collisions at $\sqrt{s} = 7$ TeV with the ATLAS Detector at the LHC. ATLAS-CONF-2011-114, 2011.
- [320] ATLAS Collaboration. Performance of the Reconstruction and Identification of Hadronic Tau Decays with ATLAS. ATLAS-CONF-2011-152, 2011.
- [321] ATLAS Collaboration. Physics potential of Z' and W' searches with the ATLAS Detector as a function of the LHC center-of-mass energy. ATL-PHYS-PUB-2011-002, 2011.
- [322] ATLAS Collaboration. Probing the jet energy measurement at the TeV-scale using the multi-jet balance technique in proton–proton collisions at $\sqrt{s} = 7$ TeV with the ATLAS detector. ATLAS-CONF-2011-029, 2011.
- [323] ATLAS Collaboration. Procedure for the LHC Higgs boson search combination in summer 2011. ATL-PHYS-PUB-2011-011, 2011.
- [324] ATLAS Collaboration. Properties of jets measured from tracks in proton–proton collisions at center-of-mass energy $\sqrt{s} = 7$ TeV with the ATLAS detector. *Phys. Rev. D*, 84:054001, 2011.
- [325] ATLAS Collaboration. Rapidity Gap Cross Sections in pp Interactions at $\sqrt{s} = 7$ TeV. ATLAS-CONF-2011-059, 2011.
- [326] ATLAS Collaboration. Reconstructed jet multiplicities from the top-quark pair decays and associated jets in pp collisions at $\sqrt{s} = 7$ TeV measured with the ATLAS detector at the LHC. ATLAS-CONF-2011-142, 2011.
- [327] ATLAS Collaboration. Reconstruction and Calibration of Missing Transverse Energy and Performance in Z and W events in ATLAS Proton–Proton Collisions at $\sqrt{s} = 7$ TeV. ATLAS-CONF-2011-080, 2011.

- [328] ATLAS Collaboration. Reconstruction, Energy Calibration, and Identification of Hadronically Decaying Tau Leptons in the ATLAS Experiment. ATLAS-CONF-2011-077, 2011.
- [329] ATLAS Collaboration. Search for a charged Higgs boson decaying via $H^+ \rightarrow \tau_{lep} + \nu$ in $t\bar{t}$ events with one or two light leptons in the final state using 1.03 fb^{-1} of pp collision data recorded at $\sqrt{s} = 7 \text{ TeV}$ with the ATLAS detector. ATLAS-CONF-2011-151, 2011.
- [330] ATLAS Collaboration. Search for a fermiophobic Higgs boson in the diphoton channel with the ATLAS detector. ATLAS-CONF-2011-149, 2011.
- [331] ATLAS Collaboration. Search for a heavy gauge boson decaying to a charged lepton and a neutrino in 1 fb^{-1} of pp collisions at $\sqrt{s} = 7 \text{ TeV}$ using the ATLAS detector. *Phys. Lett. B*, 705:28, 2011.
- [332] ATLAS Collaboration. Search for a heavy neutral particle decaying into an electron and a muon pair using $L = 0.87 \text{ fb}^{-1}$ of ATLAS data. ATLAS-CONF-2011-109, 2011.
- [333] ATLAS Collaboration. Search for a heavy neutral particle decaying into an electron and a muon using 1 fb^{-1} of ATLAS data. *Eur. Phys. J. C*, 71:1809, 2011.
- [334] ATLAS Collaboration. Search for a Heavy Particle Decaying into an Electron and a Muon with the ATLAS Detector in $\sqrt{s} = 7 \text{ TeV}$ pp Collisions at the LHC. *Phys. Rev. Lett.*, 106:251801, 2011.
- [335] ATLAS Collaboration. Search for a heavy Standard Model Higgs boson in the mass range 200–600 GeV in the channel $H \rightarrow ZZ \rightarrow \ell^+\ell^-\bar{q}\bar{q}$ using the ATLAS Detector. ATLAS-CONF-2011-150, 2011.
- [336] ATLAS Collaboration. Search for a Standard Model Higgs boson in the $H \rightarrow ZZ \rightarrow \ell^+\ell^-\nu\bar{\nu}$ decay channel with 2.05 fb^{-1} of ATLAS data. ATLAS-CONF-2011-148, 2011.
- [337] ATLAS Collaboration. Search for a Standard Model Higgs Boson in the $H \rightarrow ZZ \rightarrow \ell^+\ell^-\nu\bar{\nu}$ Decay Channel with the ATLAS Detector. *Phys. Rev. Lett.*, 107:221802, 2011.
- [338] ATLAS Collaboration. Search for a Standard Model Higgs boson in the Mass Range 200–600 GeV in the Channels $H \rightarrow ZZ \rightarrow \ell^+\ell^-\nu\bar{\nu}$ and $H \rightarrow ZZ \rightarrow \ell^+\ell^-\bar{q}\bar{q}$ with the ATLAS Detector. ATLAS-CONF-2011-026, 2011.

- [339] ATLAS Collaboration. Search for an excess of events with an identical flavour lepton pair and significant missing transverse momentum in $\sqrt{s} = 7$ TeV proton–proton collisions with the ATLAS detector. *Eur. Phys. J. C*, 71:1647, 2011.
- [340] ATLAS Collaboration. Search for Anomalous Missing E_T in $t\bar{t}$ events. ATLAS-CONF-2011-036, 2011.
- [341] ATLAS Collaboration. Search for Anomalous Production of Prompt Like-sign Muon Pairs. ATLAS-CONF-2011-126, 2011.
- [342] ATLAS Collaboration. Search for Charged Higgs Bosons in the $\tau + \text{jets}$ Final State in $t\bar{t}$ Decays with 1.03 fb^{-1} of pp Collision Data Recorded at $\sqrt{s} = 7$ TeV with the ATLAS Experiment. ATLAS-CONF-2011-138, 2011.
- [343] ATLAS Collaboration. Search for contact interactions in dimuon events from pp collisions at $\sqrt{s} = 7$ TeV with the ATLAS detector. *Phys. Rev. D*, 84:011101, 2011.
- [344] ATLAS Collaboration. Search for Dilepton Resonances in pp Collisions at $\sqrt{s} = 7$ TeV with the ATLAS Detector. *Phys. Rev. Lett.*, 107:272002, 2011.
- [345] ATLAS Collaboration. Search for Diphoton Events with Large Missing Transverse Energy in 7 TeV Proton–Proton Collisions with the ATLAS Detector. *Phys. Rev. Lett.*, 106:121803, 2011.
- [346] ATLAS Collaboration. Search for Diphoton Events with Large Missing Transverse Energy with 36 pb^{-1} of 7 TeV Proton–Proton Collision Data with the ATLAS Detector. *Eur. Phys. J. C*, 71:1744, 2011.
- [347] ATLAS Collaboration. Search for Doubly Charged Higgs Boson Production in Like-sign Muon Pairs in pp Collisions at $\sqrt{s} = 7$ TeV. ATLAS-CONF-2011-127, 2011.
- [348] ATLAS Collaboration. Search for FCNC Top Quark Processes at $\sqrt{s} = 7$ TeV with the ATLAS Detector. ATLAS-CONF-2011-061, 2011.
- [349] ATLAS Collaboration. Search for Fourth Generation Quarks Decaying to $W^+ q W^- \bar{q} \rightarrow \ell^+ \nu q \ell^- \nu \bar{q}$ in pp collisions at $\sqrt{s} = 7$ TeV with the ATLAS Detector. ATLAS-CONF-2011-022, 2011.
- [350] ATLAS Collaboration. Search for heavy long-lived charged particles with the ATLAS detector in pp collisions at $\sqrt{s} = 7$ TeV. *Phys. Lett. B*, 703:428, 2011.

- [351] ATLAS Collaboration. Search for heavy Majorana neutrino and W_R in dilepton plus jets events with the ATLAS detector in $p\bar{p}$ collisions at $\sqrt{s} = 7$ TeV. ATLAS-CONF-2011-115, 2011.
- [352] ATLAS Collaboration. Search for Higgs Boson Production in $p\bar{p}$ Collisions at $\sqrt{s} = 7$ TeV using the $H \rightarrow WW \rightarrow l\nu qq$ Decay Channel and the ATLAS Detector. ATLAS-CONF-2011-052, 2011.
- [353] ATLAS Collaboration. Search for high mass dilepton resonances in $p\bar{p}$ collisions at $\sqrt{s} = 7$ TeV with the ATLAS experiment. *Phys. Lett. B*, 700:163, 2011.
- [354] ATLAS Collaboration. Search for high-mass dilepton resonances in $p\bar{p}$ collisions at $\sqrt{s} = 7$ TeV with the ATLAS experiment. ATLAS-CONF-2011-083, 2011.
- [355] ATLAS Collaboration. Search for high-mass states with one lepton plus missing transverse momentum in proton–proton collisions at $\sqrt{s} = 7$ TeV with the ATLAS detector. *Phys. Lett. B*, 701:50, 2011.
- [356] ATLAS Collaboration. Search for high-mass states with one muon plus missing transverse momentum in proton–proton collisions at $\sqrt{s} = 7$ TeV with the ATLAS detector. ATLAS-CONF-2011-082, 2011.
- [357] ATLAS Collaboration. Search for massive colored scalars in four-jet final states in $\sqrt{s} = 7$ TeV proton–proton collisions with the ATLAS Detector. *Eur. Phys. J. C*, 71:1828, 2011.
- [358] ATLAS Collaboration. Search for massive long-lived highly ionising particles with the ATLAS detector at the LHC. *Phys. Lett. B*, 698:353, 2011.
- [359] ATLAS Collaboration. Search for Microscopic Black Holes in Multi-Jet Final States with the ATLAS Detector at $\sqrt{s} = 7$ TeV. ATLAS-CONF-2011-068, 2011.
- [360] ATLAS Collaboration. Search for neutral MSSM Higgs boson decaying to $\tau^+\tau^-$ pairs in proton–proton collisions at $\sqrt{s} = 7$ TeV with the ATLAS experiment. ATLAS-CONF-2011-024, 2011.
- [361] ATLAS Collaboration. Search for neutral MSSM Higgs bosons decaying to $\tau^+\tau^-$ pairs in proton–proton collisions at $\sqrt{s} = 7$ TeV with the ATLAS detector. *Phys. Lett. B*, 705:174, 2011.
- [362] ATLAS Collaboration. Search for neutral MSSM Higgs bosons decaying to $\tau^+\tau^-$ pairs in proton–proton collisions at $\sqrt{s} = 7$ TeV with the ATLAS detector. ATLAS-CONF-2011-132, 2011.

- [363] ATLAS Collaboration. Search for New Phenomena in Events with Four Charged Leptons. ATLAS-CONF-2011-144, 2011.
- [364] ATLAS Collaboration. Search for New Phenomena in Events with Three or more Charged Leptons. ATLAS-CONF-2011-158, 2011.
- [365] ATLAS Collaboration. Search for new phenomena in final states with large jet multiplicities and missing transverse momentum using $\sqrt{s} = 7$ TeV $p\bar{p}$ collisions with the ATLAS detector. *JHEP*, 11:099, 2011.
- [366] ATLAS Collaboration. Search for New Phenomena in Monojet plus Missing Transverse Momentum Final States using 1 fb^{-1} of $p\bar{p}$ Collisions at $\sqrt{s} = 7$ TeV with the ATLAS Detector. ATLAS-CONF-2011-096, 2011.
- [367] ATLAS Collaboration. Search for new phenomena with the monojet and missing transverse momentum signature using the ATLAS detector in $\sqrt{s} = 7$ TeV proton–proton collisions. *Phys. Lett. B*, 705:294, 2011.
- [368] ATLAS Collaboration. Search for New Physics in Dijet Mass Distributions in 0.81 fb^{-1} of $p\bar{p}$ Collisions at $\sqrt{s} = 7$ TeV. ATLAS-CONF-2011-095, 2011.
- [369] ATLAS Collaboration. Search for pair production of first or second generation leptoquarks in proton–proton collisions at $\sqrt{s} = 7$ TeV using the ATLAS detector at the LHC. *Phys. Rev. D*, 83:112006, 2011.
- [370] ATLAS Collaboration. Search for quark contact interactions in dijet angular distributions in $p\bar{p}$ collisions at $\sqrt{s} = 7$ TeV measured with the ATLAS detector. *Phys. Lett. B*, 694:327, 2011.
- [371] ATLAS Collaboration. Search for s-channel single top-quark production in $p\bar{p}$ collisions at $\sqrt{s} = 7$ TeV. ATLAS-CONF-2011-118, 2011.
- [372] ATLAS Collaboration. Search for squarks and gluinos using final states with jets and missing transverse momentum with the ATLAS detector in $\sqrt{s} = 7$ TeV proton–proton collisions. *Phys. Lett. B*, 701:186, 2011.
- [373] ATLAS Collaboration. Search for squarks and gluinos using final states with jets and missing transverse momentum with the ATLAS detector in $\sqrt{s} = 7$ TeV proton–proton collisions. ATLAS-CONF-2011-086, 2011.
- [374] ATLAS Collaboration. Search for stable hadronising squarks and gluinos with the ATLAS experiment at the LHC. *Phys. Lett. B*, 701:1, 2011.
- [375] ATLAS Collaboration. Search for strong gravity effects in same-sign dimuon final states. ATLAS-CONF-2011-065, 2011.

- [376] ATLAS Collaboration. Search for supersymmetric particles in events with lepton pairs and large missing transverse momentum in $\sqrt{s} = 7$ TeV proton–proton collisions with the ATLAS experiment. *Eur. Phys. J. C*, 71:1682, 2011.
- [377] ATLAS Collaboration. Search for supersymmetry in $p\bar{p}$ collisions at $\sqrt{s} = 7$ TeV in final states with missing transverse momentum and b -jets. *Phys. Lett. B*, 701:398, 2011.
- [378] ATLAS Collaboration. Search for supersymmetry in $p\bar{p}$ collisions at $\sqrt{s} = 7$ TeV in final states with missing transverse momentum, b -jets and no leptons with the ATLAS detector. ATLAS-CONF-2011-098, 2011.
- [379] ATLAS Collaboration. Search for supersymmetry in $p\bar{p}$ collisions at $\sqrt{s} = 7$ TeV in final states with missing transverse momentum, b -jets and one lepton with the ATLAS detector. ATLAS-CONF-2011-130, 2011.
- [380] ATLAS Collaboration. Search for Supersymmetry Using Final States with One Lepton, Jets, and Missing Transverse Momentum with the ATLAS Detector in $\sqrt{s} = 7$ TeV $p\bar{p}$ Collisions. *Phys. Rev. Lett.*, 106:131802, 2011.
- [381] ATLAS Collaboration. Search for supersymmetry with jets and missing transverse momentum: Additional model interpretations. ATLAS-CONF-2011-155, 2011.
- [382] ATLAS Collaboration. Search for supersymmetry with jets, missing transverse momentum and one lepton at $\sqrt{s} = 7$ TeV. ATLAS-CONF-2011-090, 2011.
- [383] ATLAS Collaboration. Search for $t\bar{t}$ production in the all-hadronic channel in ATLAS with $\sqrt{s} = 7$ TeV data. ATLAS-CONF-2011-066, 2011.
- [384] ATLAS Collaboration. Search for technihadrons in $p\bar{p}$ collisions at $\sqrt{s} = 7$ TeV with the ATLAS detector. ATLAS-CONF-2011-125, 2011.
- [385] ATLAS Collaboration. Search for the Higgs Boson in the Diphoton Channel with the ATLAS Detector using 209 pb^{-1} of 7 TeV Data taken in 2011. ATLAS-CONF-2011-085, 2011.
- [386] ATLAS Collaboration. Search for the Higgs boson in the diphoton final state with 38 pb^{-1} of data recorded by the ATLAS detector in proton–proton collisions at $\sqrt{s} = 7$ TeV. ATLAS-CONF-2011-025, 2011.
- [387] ATLAS Collaboration. Search for the Higgs Boson in the $H \rightarrow WW \rightarrow l\nu jj$ Decay Channel in $p\bar{p}$ Collisions at $\sqrt{s} = 7$ TeV with the ATLAS Detector. *Phys. Rev. Lett.*, 107:231801, 2011.

- [388] ATLAS Collaboration. Search for the Standard Model Higgs boson in the decay channel $H \rightarrow ZZ^{(*)} \rightarrow 4\ell$ with 4.8 fb^{-1} of pp collisions at $\sqrt{s} = 7 \text{ TeV}$. ATLAS-CONF-2011-162, 2011.
- [389] ATLAS Collaboration. Search for the Standard Model Higgs boson in the decay channel $H \rightarrow ZZ^{(*)} \rightarrow 4\ell$ with 40 pb^{-1} of pp collisions at $\sqrt{s} = 7 \text{ TeV}$. ATLAS-CONF-2011-048, 2011.
- [390] ATLAS Collaboration. Search for the Standard Model Higgs boson in the decay channel $H \rightarrow ZZ^{(*)} \rightarrow 4\ell$ with the ATLAS detector. *Phys. Lett. B*, 705:435, 2011.
- [391] ATLAS Collaboration. Search for the Standard Model Higgs boson in the decay channel $H \rightarrow ZZ^{(*)} \rightarrow 4\ell$ with the ATLAS detector. ATLAS-CONF-2011-131, 2011.
- [392] ATLAS Collaboration. Search for the Standard Model Higgs Boson in the Decay Mode $H \rightarrow \tau^+\tau^- \rightarrow \ell\ell + 4 \text{ Neutrinos}$ in Association with Jets in Proton–Proton Collisions at $\sqrt{s} = 7 \text{ TeV}$ with the ATLAS Detector. ATLAS-CONF-2011-133, 2011.
- [393] ATLAS Collaboration. Search for the Standard Model Higgs boson in the diphoton decay channel with 4.9 fb^{-1} of ATLAS data at $\sqrt{s} = 7 \text{ TeV}$. ATLAS-CONF-2011-161, 2011.
- [394] ATLAS Collaboration. Search for the Standard Model Higgs boson in the $H \rightarrow WW^{(*)} \rightarrow \ell\nu\ell\nu$ decay mode with the ATLAS Detector. ATLAS-CONF-2011-111, 2011.
- [395] ATLAS Collaboration. Search for the Standard Model Higgs boson in the $H \rightarrow WW^{(*)} \rightarrow \ell\nu\ell\nu$ decay mode using 1.7 fb^{-1} of data collected with the ATLAS detector at $\sqrt{s} = 7 \text{ TeV}$. ATLAS-CONF-2011-134, 2011.
- [396] ATLAS Collaboration. Search for the Standard Model Higgs boson in the two photon decay channel with the ATLAS detector at the LHC. *Phys. Lett. B*, 705:452, 2011.
- [397] ATLAS Collaboration. Search for the Standard Model Higgs boson produced in association with a vector boson and decaying to a b-quark pair with the ATLAS detector at the LHC. ATLAS-CONF-2011-103, 2011.
- [398] ATLAS Collaboration. Search for Wt associated production in dilepton final states with 0.70 fb^{-1} of $\sqrt{s} = 7 \text{ TeV}$ pp collision data in ATLAS. ATLAS-CONF-2011-104, 2011.

- [399] ATLAS Collaboration. Searches for Single Top-Quark Production with the ATLAS Detector in pp Collisions at $\sqrt{s} = 7 \text{ TeV}$. ATLAS-CONF-2011-027, 2011.
- [400] ATLAS Collaboration. Searches for TeV-gravity signatures in final states with leptons and jets with the ATLAS detector at $\sqrt{s} = 7 \text{ TeV}$. ATLAS-CONF-2011-147, 2011.
- [401] ATLAS Collaboration. Simple extrapolations for supersymmetry discovery limits at different LHC centre-of-mass energies and luminosities, based on inclusive searches with the ATLAS detector. ATL-PHYS-PUB-2011-003, 2011.
- [402] ATLAS Collaboration. Studies of the performance of the ATLAS detector using cosmic-ray muons. *Eur. Phys. J. C*, 71:1593, 2011.
- [403] ATLAS Collaboration. Studies of vector boson transverse momentum simulation in Monte Carlo event generators. ATL-PHYS-PUB-2011-015, 2011.
- [404] ATLAS Collaboration. Study of discriminating variables for charged Higgs boson searches in $t\bar{t}$ events with leptons, using 35 pb^{-1} of data from the ATLAS detector. ATLAS-CONF-2011-018, 2011.
- [405] ATLAS Collaboration. Study of jet shapes in inclusive jet production in pp collisions at $\sqrt{s} = 7 \text{ TeV}$ using the ATLAS detector. *Phys. Rev. D*, 83:052003, 2011.
- [406] ATLAS Collaboration. SUSY Searches at ATLAS in Multilepton Final States with Jets and Missing Transverse Energy. ATLAS-CONF-2011-039, 2011.
- [407] ATLAS Collaboration. Top Quark Pair Production Cross-section Measurement in ATLAS in the Single Lepton+Jets Channel without b-tagging. ATLAS-CONF-2011-023, 2011.
- [408] ATLAS Collaboration. Update of Background Studies in the Search for the Higgs Boson in the Diphoton Channel with the ATLAS detector at $\sqrt{s} = 7 \text{ TeV}$. ATLAS-CONF-2011-071, 2011.
- [409] ATLAS Collaboration. Update of the Combination of Higgs Boson Searches in 1.0 to 2.3 fb^{-1} of pp Collisions Data Taken at $\sqrt{s} = 7 \text{ TeV}$ with the ATLAS Experiment at the LHC. ATLAS-CONF-2011-135, 2011.
- [410] ATLAS Collaboration. Update of the Search for New Physics in the Dijet Mass Distribution in 163 pb^{-1} of pp Collisions at $\sqrt{s} = 7 \text{ TeV}$ Measured with the ATLAS Detector. ATLAS-CONF-2011-081, 2011.

- [411] ATLAS Collaboration. Update on the jet energy scale systematic uncertainty for jets produced in proton–proton collisions at $\sqrt{s} = 7$ TeV measured with the ATLAS detector. ATLAS-CONF-2011-007, 2011.
- [412] ATLAS Collaboration. Updated Luminosity Determination in $p\bar{p}$ Collisions at $\sqrt{s} = 7$ TeV using the ATLAS Detector. ATLAS-CONF-2011-011, 2011.
- [413] ATLAS Collaboration. Upper Limits on the Charge in Satellite Bunches for the October 2010 LHC Luminosity Calibration. ATLAS-CONF-2011-049, 2011.
- [414] ATLAS Collaboration. Validating the measurement of jet energies with the ATLAS detector using Z+jet events from proton–proton collisions at $\sqrt{s} = 7$ TeV. ATLAS-CONF-2011-159, 2011.
- [415] ATLAS Collaboration. Validation of the ATLAS jet energy scale uncertainties using tracks in proton–proton collisions at $\sqrt{s} = 7$ TeV. ATLAS-CONF-2011-067, 2011.
- [416] ATLAS Collaboration. *Phys. Lett. B*, 711:442, 2012.
- [417] ATLAS Collaboration. A general search for new phenomena with the ATLAS detector in $p\bar{p}$ collisions at $\sqrt{s} = 7$ TeV. ATLAS-CONF-2012-107, 2012.
- [418] ATLAS Collaboration. A measurement of the muon reconstruction efficiency in 2010 ATLAS data using J/ψ decays. ATLAS-CONF-2012-125, 2012.
- [419] ATLAS Collaboration. A measurement of the ratio of the W and Z cross sections with exactly one associated jet in $p\bar{p}$ collisions at $\sqrt{s} = 7$ TeV with ATLAS. *Phys. Lett. B*, 708:221, 2012.
- [420] ATLAS Collaboration. A Particle Consistent with the Higgs Boson Observed with the ATLAS Detector at the Large Hadron Collider. *Science*, 338:1576, 2012.
- [421] ATLAS Collaboration. A search for flavour changing neutral currents in top-quark decays in $p\bar{p}$ collision data collected with the ATLAS detector at $\sqrt{s} = 7$ TeV. *JHEP*, 09:139, 2012.
- [422] ATLAS Collaboration. A search for high mass resonances decaying to $\tau^+\tau^-$ in the ATLAS detector. ATLAS-CONF-2012-067, 2012.
- [423] ATLAS Collaboration. A search for $t\bar{t}$ resonances in lepton+jets events with highly boosted top quarks collected in $p\bar{p}$ collisions at $\sqrt{s} = 7$ TeV with the ATLAS detector. *JHEP*, 09:041, 2012.

- [424] ATLAS Collaboration. A Search for $t\bar{t}$ Resonances in the Lepton Plus Jets Channel using 2.05 fb^{-1} pp Collisions at $\sqrt{s} = 7 \text{ TeV}$. ATLAS-CONF-2012-029, 2012.
- [425] ATLAS Collaboration. A search for $t\bar{t}$ resonances in the lepton plus jets final state using 4.66 fb^{-1} of pp collisions at $\sqrt{s} = 7 \text{ TeV}$. ATLAS-CONF-2012-136, 2012.
- [426] ATLAS Collaboration. A search for $t\bar{t}$ resonances with the ATLAS detector in 2.05 fb^{-1} of proton–proton collisions at $\sqrt{s} = 7 \text{ TeV}$. *Eur. Phys. J. C*, 72:2083, 2012.
- [427] ATLAS Collaboration. A study of the material in the ATLAS inner detector using secondary hadronic interactions. *JINST*, 7:P01013, 2012.
- [428] ATLAS Collaboration. An update of combined measurements of the new Higgs-like boson with high mass resolution channels. ATLAS-CONF-2012-170, 2012.
- [429] ATLAS Collaboration. An update to the combined search for the Standard Model Higgs boson with the ATLAS detector at the LHC using up to 4.9 fb^{-1} of pp collision data at $\sqrt{s} = 7 \text{ TeV}$. ATLAS-CONF-2012-019, 2012.
- [430] ATLAS Collaboration. ATLAS measurements of the properties of jets for boosted particle searches. *Phys. Rev. D*, 86:072006, 2012.
- [431] ATLAS Collaboration. ATLAS measurements of the properties of jets for boosted particle searches. ATLAS-CONF-2012-044, 2012.
- [432] ATLAS Collaboration. ATLAS search for a heavy gauge boson decaying to a charged lepton and a neutrino in 4.7 fb^{-1} of pp collisions at $\sqrt{s} = 7 \text{ TeV}$. ATLAS-CONF-2012-086, 2012.
- [433] ATLAS Collaboration. ATLAS search for a heavy gauge boson decaying to a charged lepton and a neutrino in pp collisions at $\sqrt{s} = 7 \text{ TeV}$. *Eur. Phys. J. C*, 72:2241, 2012.
- [434] ATLAS Collaboration. b -jet tagging calibration on c -jets containing D^{*+} mesons. ATLAS-CONF-2012-039, 2012.
- [435] ATLAS Collaboration. Combined search for the Standard Model Higgs boson in pp collisions at $\sqrt{s} = 7 \text{ TeV}$ with the ATLAS detector. *Phys. Rev. D*, 86:032003, 2012.

- [436] ATLAS Collaboration. Combined search for the Standard Model Higgs boson using up to 4.9 fb^{-1} of pp collision data at $\sqrt{s} = 7 \text{ TeV}$ with the ATLAS detector at the LHC. *Phys. Lett. B*, 710:49, 2012.
- [437] ATLAS Collaboration. Constraining R-parity violating Minimal Supergravity with $\tilde{\tau}_1$ LSP in a four lepton final state with missing transverse momentum. ATLAS-CONF-2012-035, 2012.
- [438] ATLAS Collaboration. Coupling properties of the new Higgs-like boson observed with the ATLAS detector at the LHC. ATLAS-CONF-2012-127, 2012.
- [439] ATLAS Collaboration. Determination of the Strange-Quark Density of the Proton from ATLAS Measurements of the $W \rightarrow \ell\nu$ and $Z \rightarrow \ell\ell$ Cross Sections. *Phys. Rev. Lett.*, 109:012001, 2012.
- [440] ATLAS Collaboration. Determination of the tau energy scale and the associated systematic uncertainty in proton–proton collisions at $\sqrt{s} = 7 \text{ TeV}$ with the ATLAS detector at the LHC in 2011. ATLAS-CONF-2012-054, 2012.
- [441] ATLAS Collaboration. Determination of the Top Quark Mass with a Template Method in the All-Hadronic Decay Channel using 2.04 fb^{-1} of ATLAS Data. ATLAS-CONF-2012-030, 2012.
- [442] ATLAS Collaboration. Electron performance measurements with the ATLAS detector using the 2010 LHC proton–proton collision data. *Eur. Phys. J. C*, 72:1909, 2012.
- [443] ATLAS Collaboration. Evidence for the associated production of a W boson and a top quark in ATLAS at $\sqrt{s} = 7 \text{ TeV}$. *Phys. Lett. B*, 716:142, 2012.
- [444] ATLAS Collaboration. Forward-backward correlations and charged-particle azimuthal distributions in pp interactions using the ATLAS detector. *JHEP*, 07:019, 2012.
- [445] ATLAS Collaboration. Further search for supersymmetry at $\sqrt{s} = 7 \text{ TeV}$ in final states with jets, missing transverse momentum and isolated leptons with the ATLAS detector. *Phys. Rev. D*, 86:092002, 2012.
- [446] ATLAS Collaboration. Further search for supersymmetry at $\sqrt{s} = 7 \text{ TeV}$ in final states with jets, missing transverse momentum and one isolated lepton. ATLAS-CONF-2012-041, 2012.
- [447] ATLAS Collaboration. Future of the ATLAS heavy ion program. ATL-PHYS-PUB-2012-002, 2012.

- [448] ATLAS Collaboration. Hunt for new phenomena using large jet multiplicities and missing transverse momentum with ATLAS in 4.7 fb^{-1} of $\sqrt{s} = 7 \text{ TeV}$ proton–proton collisions. *JHEP*, 07:167, 2012.
- [449] ATLAS Collaboration. Hunt for new phenomena using large jet multiplicities and missing transverse momentum with ATLAS in $\mathcal{L} = 4.7 \text{ fb}^{-1}$ of $\sqrt{s} = 7 \text{ TeV}$ proton–proton collisions. ATLAS-CONF-2012-037, 2012.
- [450] ATLAS Collaboration. Identification and Tagging of Double b-hadron jets with the ATLAS Detector. ATLAS-CONF-2012-100, 2012.
- [451] ATLAS Collaboration. Improved electron reconstruction in ATLAS using the Gaussian Sum Filter-based model for bremsstrahlung. ATLAS-CONF-2012-047, 2012.
- [452] ATLAS Collaboration. Improved Luminosity Determination in pp Collisions at $\sqrt{s} = 7 \text{ TeV}$ using the ATLAS Detector at the LHC. ATLAS-CONF-2012-080, 2012.
- [453] ATLAS Collaboration. *In situ* jet pseudorapidity intercalibration of the ATLAS detector using dijet events in $\sqrt{s} = 7 \text{ TeV}$ proton–proton 2011 data. ATLAS-CONF-2012-124, 2012.
- [454] ATLAS Collaboration. Jet mass and substructure of inclusive jets in $\sqrt{s} = 7 \text{ TeV}$ pp collisions with the ATLAS experiment. *JHEP*, 05:128, 2012.
- [455] ATLAS Collaboration. K_s^0 and Λ production in pp interactions at $\sqrt{s} = 0.9$ and 7 TeV measured with the ATLAS detector at the LHC. *Phys. Rev. D*, 85:012001, 2012.
- [456] ATLAS Collaboration. Light-quark and gluon jets: calorimeter response, jet energy scale systematics and jet properties. ATLAS-CONF-2012-138, 2012.
- [457] ATLAS Collaboration. Measurement of $D^{*\pm}$ meson production in jets from pp collisions at $\sqrt{s} = 7 \text{ TeV}$ with the ATLAS detector. *Phys. Rev. D*, 85:052005, 2012.
- [458] ATLAS Collaboration. Measurement of event shapes at large momentum transfer with the ATLAS detector in pp collisions at $\sqrt{s} = 7 \text{ TeV}$. *Eur. Phys. J. C*, 72:2211, 2012.
- [459] ATLAS Collaboration. Measurement of high mass dijet production in pp collisions at $\sqrt{s} = 7 \text{ TeV}$ using the ATLAS detector. ATLAS-CONF-2012-021, 2012.

- [460] ATLAS Collaboration. Measurement of high \mathbf{p}_T isolated prompt photons in lead–lead collisions at $\sqrt{s_{NN}} = 2.76$ TeV with the ATLAS detector at the LHC. ATLAS-CONF-2012-051, 2012.
- [461] ATLAS Collaboration. Measurement of inclusive jet and dijet production in $\mathbf{p}\mathbf{p}$ collisions at $\sqrt{s} = 7$ TeV using the ATLAS detector. *Phys. Rev. D*, 86:014022, 2012.
- [462] ATLAS Collaboration. Measurement of inclusive jet charged particle fragmentation functions in Pb+Pb collisions at $\sqrt{s_{NN}} = 2.76$ TeV with the ATLAS detector. ATLAS-CONF-2012-115, 2012.
- [463] ATLAS Collaboration. Measurement of inclusive two-particle angular correlations in $\mathbf{p}\mathbf{p}$ collisions with the ATLAS detector at the LHC. *JHEP*, 05:157, 2012.
- [464] ATLAS Collaboration. Measurement of momentum imbalance in $Z \rightarrow \ell\ell +$ jet events in Lead–Lead collisions at $\sqrt{s_{NN}} = 2.76$ TeV with the ATLAS detector. ATLAS-CONF-2012-119, 2012.
- [465] ATLAS Collaboration. Measurement of reaction-plane correlations in Pb-Pb collisions at $\sqrt{s_{NN}} = 2.76$ TeV. ATLAS-CONF-2012-049, 2012.
- [466] ATLAS Collaboration. Measurement of $t\bar{t}$ production with a veto on additional central jet activity in $\mathbf{p}\mathbf{p}$ collisions at $\sqrt{s} = 7$ TeV using the ATLAS detector. *Eur. Phys. J. C*, 72:2043, 2012.
- [467] ATLAS Collaboration. Measurement of t-Channel Single Top-Quark Production in $\mathbf{p}\mathbf{p}$ Collisions at $\sqrt{s} = 8$ TeV with the ATLAS detector. ATLAS-CONF-2012-132, 2012.
- [468] ATLAS Collaboration. Measurement of τ polarization in $W \rightarrow \tau\nu$ decays with the ATLAS detector in $\mathbf{p}\mathbf{p}$ collisions at $\sqrt{s} = 7$ TeV. *Eur. Phys. J. C*, 72:2062, 2012.
- [469] ATLAS Collaboration. Measurement of Tau Polarization in $W \rightarrow \tau\nu$ Decays with the ATLAS Detector in $\mathbf{p}\mathbf{p}$ Collisions at $\sqrt{s} = 7$ TeV. ATLAS-CONF-2012-009, 2012.
- [470] ATLAS Collaboration. Measurement of the azimuthal anisotropy for charged particle production in $\sqrt{s_{NN}} = 2.76$ TeV lead–lead collisions with the ATLAS detector. *Phys. Rev. C*, 86:014907, 2012.
- [471] ATLAS Collaboration. Measurement of the azimuthal dependence of inclusive jet suppression in Pb+Pb collisions at $\sqrt{s_{NN}} = 2.76$ TeV with the ATLAS detector. ATLAS-CONF-2012-116, 2012.

- [472] ATLAS Collaboration. Measurement of the azimuthal ordering of charged hadrons with the ATLAS detector. *Phys. Rev. D*, 86:052005, 2012.
- [473] ATLAS Collaboration. Measurement of the b -hadron production cross section using decays to $D^{*+}\mu^-X$ final states in $p\bar{p}$ collisions at $\sqrt{s} = 7$ TeV with the ATLAS detector. *Nucl. Phys. B*, 864:341, 2012.
- [474] ATLAS Collaboration. Measurement of the b -tag Efficiency in a Sample of Jets Containing Muons with 5 fb^{-1} of data from the ATLAS detector. ATLAS-CONF-2012-043, 2012.
- [475] ATLAS Collaboration. Measurement of the centrality and pseudorapidity dependence of the integrated elliptic flow in lead–lead collisions at $\sqrt{s_{\text{NN}}} = 2.76$ TeV with the ATLAS detector. ATLAS-CONF-2012-117, 2012.
- [476] ATLAS Collaboration. Measurement of the centrality dependence of open heavy flavour production in lead–lead collisions at $\sqrt{s} = 2.76$ TeV with the ATLAS detector. ATLAS-CONF-2012-050, 2012.
- [477] ATLAS Collaboration. Measurement of the centrality dependence of the charged particle pseudorapidity distribution in lead–lead collisions at $\sqrt{s_{\text{NN}}} = 2.76$ TeV with the ATLAS detector. *Phys. Lett. B*, 710:363, 2012.
- [478] ATLAS Collaboration. Measurement of the charge asymmetry in dileptonic decays of top quark pairs in $p\bar{p}$ collisions at $\sqrt{s} = 7$ TeV using the ATLAS detector. ATLAS-CONF-2012-057, 2012.
- [479] ATLAS Collaboration. Measurement of the charge asymmetry in top quark pair production in $p\bar{p}$ collisions at $\sqrt{s} = 7$ TeV using the ATLAS detector. *Eur. Phys. J. C*, 72:2039, 2012.
- [480] ATLAS Collaboration. Measurement of the charged particle spectra in $\text{Pb}+\text{Pb}$ collisions at $\sqrt{s_{\text{NN}}} = 2.76$ TeV with the ATLAS detector at the LHC. ATLAS-CONF-2012-120, 2012.
- [481] ATLAS Collaboration. Measurement of the combined WW and WZ production cross section in the semileptonic final state in proton–proton collisions at $\sqrt{s} = 7$ TeV with the ATLAS detector. ATLAS-CONF-2012-157, 2012.
- [482] ATLAS Collaboration. Measurement of the correlation of jets with high p_T isolated prompt photons in lead–lead collisions at $\sqrt{s_{\text{NN}}} = 2.76$ TeV with the ATLAS detector at the LHC. ATLAS-CONF-2012-121, 2012.
- [483] ATLAS Collaboration. Measurement of the cross-section for b -jets produced in association with a Z boson at $\sqrt{s} = 7$ TeV with the ATLAS detector. *Phys. Lett. B*, 706:295, 2012.

- [484] ATLAS Collaboration. Measurement of the cross section for $t\bar{t}$ + jets production using a kinematic fit method with the ATLAS detector. ATLAS-CONF-2012-083, 2012.
- [485] ATLAS Collaboration. Measurement of the cross section for the production of a W boson in association with b-jets in pp collisions at $\sqrt{s} = 7$ TeV with the ATLAS detector. *Phys. Lett. B*, 707:418, 2012.
- [486] ATLAS Collaboration. Measurement of the cross section for top-quark pair production in pp collisions at $\sqrt{s} = 7$ TeV with the ATLAS detector using final states with two high- p_T leptons. *JHEP*, 05:059, 2012.
- [487] ATLAS Collaboration. Measurement of the cross-section for W boson production in association with b-jets in pp collisions at $\sqrt{s} = 7$ TeV with the ATLAS detector. ATLAS-CONF-2012-156, 2012.
- [488] ATLAS Collaboration. Measurement of the distributions of event-by-event flow harmonics in Pb-Pb collisions at $\sqrt{s_{NN}} = 2.76$ TeV. ATLAS-CONF-2012-114, 2012.
- [489] ATLAS Collaboration. Measurement of the elliptic flow with multi-particle cumulants in lead-lead collisions at $\sqrt{s_{NN}} = 2.76$ TeV with the ATLAS detector at the LHC. ATLAS-CONF-2012-118, 2012.
- [490] ATLAS Collaboration. Measurement of the flavour composition of dijet events in pp collisions at $\sqrt{s} = 7$ TeV with the ATLAS detector. ATLAS-CONF-2012-081, 2012.
- [491] ATLAS Collaboration. Measurement of the high-mass Drell-Yan differential cross-section in pp collisions at $\sqrt{s} = 7$ TeV with the ATLAS detector. ATLAS-CONF-2012-159, 2012.
- [492] ATLAS Collaboration. Measurement of the inclusive jet cross section in pp collisions at $\sqrt{s} = 2.76$ TeV and comparison to the inclusive jet cross section at $\sqrt{s} = 7$ TeV using the ATLAS detector. ATLAS-CONF-2012-128, 2012.
- [493] ATLAS Collaboration. Measurement of the inclusive W^\pm and Z/γ^* cross sections in the e and μ decay channels in pp collisions at $\sqrt{s} = 7$ TeV with the ATLAS detector. *Phys. Rev. D*, 85:072004, 2012.
- [494] ATLAS Collaboration. Measurement of the isolated diphoton cross section in pp collisions at $\sqrt{s} = 7$ TeV with the ATLAS detector. *Phys. Rev. D*, 85:012003, 2012.
- [495] ATLAS Collaboration. Measurement of the jet multiplicity in top-anti-top final states produced in 7 TeV proton-proton collisions with the ATLAS detector. ATLAS-CONF-2012-155, 2012.

- [496] ATLAS Collaboration. Measurement of the Λ_b^0 lifetime and mass in the ATLAS experiment. ATLAS-CONF-2012-055, 2012.
- [497] ATLAS Collaboration. Measurement of the Mistag Rate of b-tagging algorithms with 5 fb^{-1} of Data Collected by the ATLAS Detector. ATLAS-CONF-2012-040, 2012.
- [498] ATLAS Collaboration. Measurement of the polarisation of W bosons produced with large transverse momentum in pp collisions at $\sqrt{s} = 7 \text{ TeV}$ with the ATLAS experiment. *Eur. Phys. J. C*, 72:2001, 2012.
- [499] ATLAS Collaboration. Measurement of the production cross section for Z/γ^* in association with jets in pp collisions at $\sqrt{s} = 7 \text{ TeV}$ with the ATLAS detector. *Phys. Rev. D*, 85:032009, 2012.
- [500] ATLAS Collaboration. Measurement of the production cross section of an isolated photon associated with jets in proton–proton collisions at $\sqrt{s} = 7 \text{ TeV}$ with the ATLAS detector. *Phys. Rev. D*, 85:092014, 2012.
- [501] ATLAS Collaboration. Measurement of the pseudorapidity and transverse momentum dependence of the elliptic flow of charged particles in lead–lead collisions at $\sqrt{s_{\text{NN}}} = 2.76 \text{ TeV}$ with the ATLAS detector. *Phys. Lett. B*, 707:330, 2012.
- [502] ATLAS Collaboration. Measurement of the t-channel single top-quark and top-antiquark cross-sections and their ratio in pp collisions at $\sqrt{s} = 7 \text{ TeV}$. ATLAS-CONF-2012-056, 2012.
- [503] ATLAS Collaboration. Measurement of the t-channel single top-quark production cross section in pp collisions at $\sqrt{s} = 7 \text{ TeV}$ with the ATLAS detector. *Phys. Lett. B*, 717:330, 2012.
- [504] ATLAS Collaboration. Measurement of the $t\bar{t}$ production cross section in the all-hadronic channel in 4.7 fb^{-1} of pp collisions at $\sqrt{s} = 7 \text{ TeV}$ with the ATLAS detector. ATLAS-CONF-2012-031, 2012.
- [505] ATLAS Collaboration. Measurement of the $t\bar{t}$ production cross section in the final state with a hadronically decaying tau lepton and jets using the ATLAS detector. ATLAS-CONF-2012-032, 2012.
- [506] ATLAS Collaboration. Measurement of the top quark mass with the template method in the $t\bar{t} \rightarrow \text{lepton} + \text{jets}$ channel using ATLAS data. *Eur. Phys. J. C*, 72:2046, 2012.
- [507] ATLAS Collaboration. Measurement of the top quark pair cross section with ATLAS in pp collisions at $\sqrt{s} = 7 \text{ TeV}$ using final states with an electron or a muon and a hadronically decaying τ lepton. *Phys. Lett. B*, 717:89, 2012.

- [508] ATLAS Collaboration. Measurement of the top quark pair production cross section in pp collisions at $\sqrt{s} = 7 \text{ TeV}$ in dilepton final states with ATLAS. *Phys. Lett. B*, 707:459, 2012.
- [509] ATLAS Collaboration. Measurement of the top quark pair production cross section in the single-lepton channel with ATLAS in proton–proton collisions at 8 TeV using kinematic fits with b -tagging. ATLAS-CONF-2012-149, 2012.
- [510] ATLAS Collaboration. Measurement of the top quark pair production cross section with ATLAS in pp collisions at $\sqrt{s} = 7 \text{ TeV}$ in the single-lepton channel using semileptonic b decays. ATLAS-CONF-2012-131, 2012.
- [511] ATLAS Collaboration. Measurement of the top quark pair production cross-section with ATLAS in the single lepton channel. *Phys. Lett. B*, 711:244, 2012.
- [512] ATLAS Collaboration. Measurement of the total ZZ production cross section in the four-lepton channel using 4.7 fb^{-1} of ATLAS data. ATLAS-CONF-2012-026, 2012.
- [513] ATLAS Collaboration. Measurement of the total ZZ production cross section in the four-lepton channel using 5.8 fb^{-1} of ATLAS data at $\sqrt{s} = 8 \text{ TeV}$. ATLAS-CONF-2012-090, 2012.
- [514] ATLAS Collaboration. Measurement of the transverse momentum distribution of W bosons in pp collisions at $\sqrt{s} = 7 \text{ TeV}$ with the ATLAS detector. *Phys. Rev. D*, 85:012005, 2012.
- [515] ATLAS Collaboration. Measurement of the W boson polarization in top quark decays with the ATLAS detector. *JHEP*, 06:088, 2012.
- [516] ATLAS Collaboration. Measurement of the $W \rightarrow \tau\nu_\tau$ cross section in pp collisions at $\sqrt{s} = 7 \text{ TeV}$ with the ATLAS experiment. *Phys. Lett. B*, 706:276, 2012.
- [517] ATLAS Collaboration. Measurement of the WW cross section in $\sqrt{s} = 7 \text{ TeV}$ pp collisions with the ATLAS detector and limits on anomalous gauge couplings. *Phys. Lett. B*, 712:289, 2012.
- [518] ATLAS Collaboration. Measurement of the $W^\pm Z$ production cross section and limits on anomalous triple gauge couplings in proton–proton collisions at $\sqrt{s} = 7 \text{ TeV}$ with the ATLAS detector. *Phys. Lett. B*, 709:341, 2012.
- [519] ATLAS Collaboration. Measurement of the W^+W^- production cross section in proton–proton collisions at $\sqrt{s} = 7 \text{ TeV}$ with the ATLAS detector. ATLAS-CONF-2012-025, 2012.

- [520] ATLAS Collaboration. Measurement of the ZZ Production Cross Section and Limits on Anomalous Neutral Triple Gauge Couplings in Proton–Proton Collisions at $\sqrt{s} = 7$ TeV with the ATLAS Detector. *Phys. Rev. Lett.*, 108:041804, 2012.
- [521] ATLAS Collaboration. Measurement of the ZZ Production Cross Section in the $\ell^+\ell^-\nu\bar{\nu}$ channel in Proton–Proton Collisions at $\sqrt{s} = 7$ TeV with the ATLAS Detector. ATLAS-CONF-2012-027, 2012.
- [522] ATLAS Collaboration. Measurement of top quark polarisation in $t\bar{t}$ events with the ATLAS detector in proton–proton collisions at $\sqrt{s} = 7$ TeV. ATLAS-CONF-2012-133, 2012.
- [523] ATLAS Collaboration. Measurement of $W\gamma$ and $Z\gamma$ production cross sections in pp collisions at $\sqrt{s} = 7$ TeV and limits on anomalous triple gauge couplings with the ATLAS detector. *Phys. Lett. B*, 717:49, 2012.
- [524] ATLAS Collaboration. Measurement of $W^\pm Z$ production in proton–proton collisions at $\sqrt{s} = 7$ TeV with the ATLAS detector. *Eur. Phys. J. C*, 72:2173, 2012.
- [525] ATLAS Collaboration. Measurement of Z boson Production in Lead–Lead Collisions at $\sqrt{s_{NN}} = 2.76$ TeV with the ATLAS Detector. ATLAS-CONF-2012-052, 2012.
- [526] ATLAS Collaboration. Measurements of the electron and muon inclusive cross-sections in proton–proton collisions at $\sqrt{s} = 7$ TeV with the ATLAS detector. *Phys. Lett. B*, 707:438, 2012.
- [527] ATLAS Collaboration. Measurements of the photon identification efficiency with the ATLAS detector using 4.9 fb^{-1} of pp collision data collected in 2011. ATLAS-CONF-2012-123, 2012.
- [528] ATLAS Collaboration. Measurements of the pseudorapidity dependence of the total transverse energy in proton–proton collisions at $\sqrt{s} = 7$ TeV with ATLAS. *JHEP*, 11:033, 2012.
- [529] ATLAS Collaboration. Measuring the b -tag efficiency in a $t\bar{t}$ sample with 4.7 fb^{-1} of data from the ATLAS detector. ATLAS-CONF-2012-097, 2012.
- [530] ATLAS Collaboration. Observation and study of the Higgs boson candidate in the two photon decay channel with the ATLAS detector at the LHC. ATLAS-CONF-2012-168, 2012.
- [531] ATLAS Collaboration. Observation of a New χ_b State in Radiative Transitions to $\Upsilon(1S)$ and $\Upsilon(2S)$ at ATLAS. *Phys. Rev. Lett.*, 108:152001, 2012.

- [532] ATLAS Collaboration. Observation of a new particle in the search for the Standard Model Higgs boson with the ATLAS detector at the LHC. *Phys. Lett. B*, 716:1, 2012.
- [533] ATLAS collaboration. Observation of a new particle in the search for the Standard Model Higgs boson with the ATLAS detector at the LHC. *Physics Letters B*, 716, 2012.
- [534] ATLAS Collaboration. Observation of an excess of events in the search for the Standard Model Higgs boson in the $\gamma\gamma$ channel with the ATLAS detector. ATLAS-CONF-2012-091, 2012.
- [535] ATLAS Collaboration. Observation of an Excess of Events in the Search for the Standard Model Higgs Boson in the $H \rightarrow WW^{(*)} \rightarrow \ell\nu\ell\nu$ Channel with the ATLAS Detector. ATLAS-CONF-2012-098, 2012.
- [536] ATLAS Collaboration. Observation of an excess of events in the search for the Standard Model Higgs boson in the $H \rightarrow ZZ^{(*)} \rightarrow 4\ell$ channel with the ATLAS detector. ATLAS-CONF-2012-092, 2012.
- [537] ATLAS Collaboration. Observation of an Excess of Events in the Search for the Standard Model Higgs boson with the ATLAS detector at the LHC. ATLAS-CONF-2012-093, 2012.
- [538] ATLAS Collaboration. Observation of spin correlation in $t\bar{t}$ events from $p\bar{p}$ collisions at $\sqrt{s} = 7$ TeV using the ATLAS detector. *Phys. Rev. Lett.*, 108:212001, 2012.
- [539] ATLAS Collaboration. Observation of the B_c^\pm meson in the decay $B_c^\pm \rightarrow J/\psi(\mu^+\mu^-)\pi^\pm$ with the ATLAS detector at the LHC. ATLAS-CONF-2012-028, 2012.
- [540] ATLAS Collaboration. Performance of large-R jets and substructure reconstruction with the ATLAS detector. ATLAS-CONF-2012-065, 2012.
- [541] ATLAS Collaboration. Performance of Missing Transverse Momentum Reconstruction in ATLAS with 2011 Proton–Proton Collisions at $\sqrt{s} = 7$ TeV. ATLAS-CONF-2012-101, 2012.
- [542] ATLAS Collaboration. Performance of missing transverse momentum reconstruction in proton–proton collisions at $\sqrt{s} = 7$ TeV with ATLAS. *Eur. Phys. J. C*, 72:1844, 2012.
- [543] ATLAS Collaboration. Performance of the ATLAS Electron and Photon Trigger in $p\bar{p}$ Collisions at $\sqrt{s} = 7$ TeV in 2011. ATLAS-CONF-2012-048, 2012.

- [544] ATLAS Collaboration. Performance of the ATLAS Inner Detector Track and Vertex Reconstruction in High Pile-Up LHC Environment. ATLAS-CONF-2012-042, 2012.
- [545] ATLAS Collaboration. Performance of the ATLAS Minimum Bias and Forward Detector Triggers in 2011 Heavy Ion Run. ATLAS-CONF-2012-122, 2012.
- [546] ATLAS Collaboration. Performance of the ATLAS muon trigger in 2011. ATLAS-CONF-2012-099, 2012.
- [547] ATLAS Collaboration. Performance of the ATLAS Trigger System in 2010. *Eur. Phys. J. C*, 72:1849, 2012.
- [548] ATLAS Collaboration. Performance of the ATLAS Trigger System in 2010. *Eur. Phys. J. C*, 72:1849, 2012.
- [549] ATLAS Collaboration. Performance of the Reconstruction and Identification of Hadronic τ Decays in ATLAS with 2011 Data. ATLAS-CONF-2012-142, 2012.
- [550] ATLAS Collaboration. Physics at a High-Luminosity LHC with ATLAS. ATL-PHYS-PUB-2012-001, 2012.
- [551] ATLAS Collaboration. Physics at a High-Luminosity LHC with ATLAS (Update). ATL-PHYS-PUB-2012-004, 2012.
- [552] ATLAS Collaboration. Pile-up corrections for jets from proton–proton collisions at $\sqrt{s} = 7$ TeV in ATLAS in 2011. ATLAS-CONF-2012-064, 2012.
- [553] ATLAS Collaboration. Probing the measurement of jet energies with the ATLAS detector using photon+jet events in proton–proton collisions at $\sqrt{s} = 7$ TeV. ATLAS-CONF-2012-063, 2012.
- [554] ATLAS Collaboration. Probing the measurement of jet energies with the ATLAS detector using $Z + \text{jet}$ events from proton–proton collisions at $\sqrt{s} = 7$ TeV. ATLAS-CONF-2012-053, 2012.
- [555] ATLAS Collaboration. Rapidity gap cross sections measured with the ATLAS detector in pp collisions at $\sqrt{s} = 7$ TeV. *Eur. Phys. J. C*, 72:1926, 2012.
- [556] ATLAS Collaboration. Reconstruction of collinear final-state-radiation photons in Z decays to muons in $\sqrt{s} = 7$ TeV proton–proton collisions. ATLAS-CONF-2012-143, 2012.

- [557] ATLAS Collaboration. Search for a charged Higgs boson decaying via $H^\pm \rightarrow \tau\nu$ in $t\bar{t}$ events using 4.6 fb^{-1} of pp collision data at $\sqrt{s} = 7 \text{ TeV}$ with the ATLAS detector. ATLAS-CONF-2012-011, 2012.
- [558] ATLAS Collaboration. Search for a fermiophobic Higgs boson in the diphoton decay channel with 4.9 fb^{-1} of ATLAS data at $\sqrt{s} = 7 \text{ TeV}$. ATLAS-CONF-2012-013, 2012.
- [559] ATLAS Collaboration. Search for a fermiophobic Higgs boson in the diphoton decay channel with the ATLAS detector. *Eur. Phys. J. C*, 72:2157, 2012.
- [560] ATLAS Collaboration. Search for a heavy Standard Model Higgs boson in the channel $H \rightarrow ZZ \rightarrow \ell^+\ell^-\nu\bar{\nu}$ using the ATLAS detector. *Phys. Lett. B*, 707:27, 2012.
- [561] ATLAS Collaboration. Search for a heavy top quark partner in final states with two leptons with the ATLAS detector. ATLAS-CONF-2012-071, 2012.
- [562] ATLAS Collaboration. Search for a heavy top-quark partner in final states with two leptons with the ATLAS detector at the LHC. *JHEP*, 11:094, 2012.
- [563] ATLAS Collaboration. Search for a Higgs boson decaying to four photons through light CP-odd scalar coupling using 4.9 fb^{-1} of 7 TeV pp collision data taken with ATLAS detector at the LHC. ATLAS-CONF-2012-079, 2012.
- [564] ATLAS Collaboration. Search for a Higgs boson produced in association with a top-quark pair and decaying to $b\bar{b}$ in pp collisions at $\sqrt{s} = 7 \text{ TeV}$ using the ATLAS detector. ATLAS-CONF-2012-135, 2012.
- [565] ATLAS Collaboration. Search for a Light Higgs Boson Decaying to Long-Lived Weakly Interacting Particles in Proton-Proton Collisions at $\sqrt{s} = 7 \text{ TeV}$ with the ATLAS Detector. *Phys. Rev. Lett.*, 108:251801, 2012.
- [566] ATLAS Collaboration. Search for a standard model Higgs boson in the $H \rightarrow ZZ \rightarrow \ell^+\ell^-\nu\bar{\nu}$ decay channel using 4.7 fb^{-1} of $\sqrt{s} = 7 \text{ TeV}$ data with the ATLAS detector. *Phys. Lett. B*, 717:29, 2012.
- [567] ATLAS Collaboration. Search for a Standard Model Higgs boson in the $H \rightarrow ZZ \rightarrow \ell^+\ell^-\nu\bar{\nu}$ decay channel using 4.7 fb^{-1} of $\sqrt{s} = 7 \text{ TeV}$ data with the ATLAS Detector. ATLAS-CONF-2012-016, 2012.
- [568] ATLAS Collaboration. Search for a standard model Higgs boson in the mass range $200\text{--}600 \text{ GeV}$ in the $H \rightarrow ZZ \rightarrow \ell^+\ell^-\nu\bar{\nu}$ decay channel with the ATLAS detector. *Phys. Lett. B*, 717:70, 2012.

- [569] ATLAS Collaboration. Search for a Standard Model Higgs in the mass range 200–600 GeV in the channel $H \rightarrow ZZ \rightarrow \ell^+\ell^-q\bar{q}$ with the ATLAS detector. ATLAS-CONF-2012-017, 2012.
- [570] ATLAS Collaboration. Search for a supersymmetric partner of the top quark in final states with jets and missing transverse momentum at $\sqrt{s} = 7$ TeV with the ATLAS detector. ATLAS-CONF-2012-074, 2012.
- [571] ATLAS Collaboration. Search for a supersymmetric partner to the top quark in final states with jets and missing transverse momentum at $\sqrt{s} = 7$ TeV with the ATLAS detector. *Phys. Rev. Lett.*, 109:211802, 2012.
- [572] ATLAS Collaboration. Search for a supersymmetric top-quark partner in final states with two leptons in $\sqrt{s} = 8$ TeV pp collisions using 13 fb^{-1} of ATLAS data. ATLAS-CONF-2012-167, 2012.
- [573] ATLAS Collaboration. Search for anomalous production of prompt like-sign lepton pairs at $\sqrt{s} = 7$ TeV with the ATLAS detector. *JHEP*, 12:007, 2012.
- [574] ATLAS Collaboration. Search for anomalous production of prompt like-sign lepton pairs with the ATLAS detector. ATLAS-CONF-2012-069, 2012.
- [575] ATLAS Collaboration. Search for anomalous production of prompt like-sign muon pairs and constraints on physics beyond the standard model with the ATLAS detector. *Phys. Rev. D*, 85:032004, 2012.
- [576] ATLAS Collaboration. Search for anomaly-mediated supersymmetry breaking with the ATLAS detector based on a disappearing-track signature in pp collisions at $\sqrt{s} = 7$ TeV. *Eur. Phys. J. C*, 72:1993, 2012.
- [577] ATLAS Collaboration. Search for charged Higgs bosons decaying via $H^\pm \rightarrow \tau\nu$ in $t\bar{t}$ events using pp collision data at $\sqrt{s} = 7$ TeV with the ATLAS detector. *JHEP*, 06:039, 2012.
- [578] ATLAS Collaboration. Search for charged long-lived heavy particles with the ATLAS Experiment at the LHC. ATLAS-CONF-2012-022, 2012.
- [579] ATLAS Collaboration. Search for contact interactions in dilepton events from pp collisions at $\sqrt{s} = 7$ TeV with the ATLAS detector. *Phys. Lett. B*, 712:40, 2012.
- [580] ATLAS Collaboration. Search for dark matter and large extra dimensions in events with a photon and missing transverse momentum in pp collision data at $\sqrt{s} = 7$ TeV with the ATLAS detector. ATLAS-CONF-2012-085, 2012.

- [581] ATLAS Collaboration. Search for dark matter candidates and large extra dimensions in events with a jet and missing transverse momentum with the ATLAS detector. ATLAS-CONF-2012-084, 2012.
- [582] ATLAS Collaboration. Search for decays of stopped, long-lived particles from 7 TeV pp collisions with the ATLAS detector. *Eur. Phys. J. C*, 72:1965, 2012.
- [583] ATLAS Collaboration. Search for diphoton events with large missing transverse momentum in 1 fb^{-1} of 7 TeV proton–proton collision data with the ATLAS detector. *Phys. Lett. B*, 710:519, 2012.
- [584] ATLAS Collaboration. Search for Diphoton Events with Large Missing Transverse Momentum in 7 TeV pp Collision Data with the ATLAS Detector. ATLAS-CONF-2012-072, 2012.
- [585] ATLAS Collaboration. Search for diphoton events with large missing transverse momentum in 7 TeV proton–proton collision data with the ATLAS detector. *Phys. Lett. B*, 718:411, 2012.
- [586] ATLAS Collaboration. Search for direct chargino production in anomaly-mediated supersymmetry breaking models based on a disappearing-track signature, in pp collisions at $\sqrt{s} = 7 \text{ TeV}$ with the ATLAS detector at the LHC. ATLAS-CONF-2012-111, 2012.
- [587] ATLAS Collaboration. Search for direct production of charginos and neutralinos in events with three leptons and missing transverse momentum in 13.0 fb^{-1} of pp collisions at $\sqrt{s} = 8 \text{ TeV}$ with the ATLAS detector. ATLAS-CONF-2012-154, 2012.
- [588] ATLAS Collaboration. Search for direct production of charginos and neutralinos in events with three leptons and missing transverse momentum in $\sqrt{s} = 7 \text{ TeV}$ pp collisions with the ATLAS detector. ATLAS-CONF-2012-077, 2012.
- [589] ATLAS Collaboration. Search for direct sbottom pair production in events with missing transverse momentum and two b-jets in 12.8 fb^{-1} of pp collisions at $\sqrt{s} = 8 \text{ TeV}$ with the ATLAS Detector. ATLAS-CONF-2012-165, 2012.
- [590] ATLAS Collaboration. Search for direct slepton and gaugino production in final states with two leptons and missing transverse momentum with the ATLAS detector in pp collisions at $\sqrt{s} = 7 \text{ TeV}$. ATLAS-CONF-2012-076, 2012.
- [591] ATLAS Collaboration. Search for direct stop pair production in events with missing transverse momentum and two b-jets in 12.8 fb^{-1} of pp collisions at $\sqrt{s} = 8 \text{ TeV}$ with the ATLAS Detector. ATLAS-CONF-2013-001, 2012.

- [592] ATLAS Collaboration. Search for direct top squark pair production in final states with one isolated lepton, jets, and missing transverse momentum in $\sqrt{s} = 7$ TeV $p\bar{p}$ collisions using 4.7 fb^{-1} of ATLAS data. *Phys. Rev. Lett.*, 109:211803, 2012.
- [593] ATLAS Collaboration. Search for direct top squark pair production in final states with one isolated lepton, jets, and missing transverse momentum in $\sqrt{s} = 7$ TeV $p\bar{p}$ collisions using 4.7 fb^{-1} of ATLAS data. ATLAS-CONF-2012-073, 2012.
- [594] ATLAS Collaboration. Search for direct top squark pair production in final states with one isolated lepton, jets, and missing transverse momentum in $\sqrt{s} = 8$ TeV $p\bar{p}$ collisions using 13 fb^{-1} ATLAS data. ATLAS-CONF-2012-166, 2012.
- [595] ATLAS Collaboration. Search for Displaced Muon Jets from light Higgs boson decay in proton–proton collisions at $\sqrt{s} = 7$ TeV with the ATLAS detector. ATLAS-CONF-2012-089, 2012.
- [596] ATLAS Collaboration. Search for displaced vertices arising from decays of new heavy particles in 7 TeV $p\bar{p}$ collisions at ATLAS. *Phys. Lett. B*, 707:478, 2012.
- [597] ATLAS Collaboration. Search for doubly-charged Higgs bosons in like-sign dilepton final states at $\sqrt{s} = 7$ TeV with the ATLAS detector. *Eur. Phys. J. C*, 72:2244, 2012.
- [598] ATLAS Collaboration. Search for Down-Type Fourth Generation Quarks with the ATLAS Detector in Events with One Lepton and Hadronically Decaying W Bosons. *Phys. Rev. Lett.*, 109:032001, 2012.
- [599] ATLAS Collaboration. Search for events with large missing transverse momentum, jets, and at least two tau leptons in 7 TeV proton–proton collision data with the ATLAS detector. *Phys. Lett. B*, 714:180, 2012.
- [600] ATLAS Collaboration. Search for Events with Large Missing Transverse Momentum, Jets, and at Least Two Tau Leptons in 7 TeV Proton–Proton Collision Data with the ATLAS Detector. ATLAS-CONF-2012-002, 2012.
- [601] ATLAS Collaboration. Search for excited electrons and muons with 13 fb^{-1} of proton–proton collisions at $\sqrt{s} = 8$ TeV with the ATLAS detector. ATLAS-CONF-2012-146, 2012.
- [602] ATLAS Collaboration. Search for excited electrons and muons with 5 fb^{-1} of proton–proton collisions at $\sqrt{s} = 7$ TeV with the ATLAS detector. ATLAS-CONF-2012-008, 2012.

- [603] ATLAS Collaboration. Search for excited leptons in proton–proton collisions at $\sqrt{s} = 7$ TeV with the ATLAS detector. *Phys. Rev. D*, 85:072003, 2012.
- [604] ATLAS Collaboration. Search for exotic same-sign dilepton signatures (b' quark, $T_{5/3}$ and four top quarks production) in 4.7 fb^{-1} of $p\bar{p}$ collisions at $\sqrt{s} = 7$ TeV with the ATLAS detector. ATLAS-CONF-2012-130, 2012.
- [605] ATLAS Collaboration. Search for Extra Dimensions in the Diphoton Final State using 4.91 fb^{-1} of Proton–Proton Collisions recorded at $\sqrt{s} = 7$ TeV with the ATLAS Detector. ATLAS-CONF-2012-087, 2012.
- [606] ATLAS Collaboration. Search for extra dimensions using diphoton events in 7 TeV proton–proton collisions with the ATLAS detector. *Phys. Lett. B*, 710:538, 2012.
- [607] ATLAS Collaboration. Search for FCNC single top-quark production at $\sqrt{s} = 7$ TeV with the ATLAS detector. *Phys. Lett. B*, 712:351, 2012.
- [608] ATLAS Collaboration. Search for first generation scalar leptoquarks in $p\bar{p}$ collisions at $\sqrt{s} = 7$ TeV with the ATLAS detector. *Phys. Lett. B*, 709:158, 2012.
- [609] ATLAS Collaboration. Search for gluino-mediated scalar top and bottom quark production in final states with missing transverse energy and at least three b -jets with the ATLAS Detector. ATLAS-CONF-2012-058, 2012.
- [610] ATLAS Collaboration. Search for gluino pair production in final states with missing transverse momentum and at least three b -jets using 12.8 fb^{-1} of $p\bar{p}$ collisions at $\sqrt{s} = 8$ TeV with the ATLAS Detector. ATLAS-CONF-2012-145, 2012.
- [611] ATLAS Collaboration. Search for gluinos in events with two same-sign leptons, jets and missing transverse momentum with the ATLAS detector in $p\bar{p}$ collisions at $\sqrt{s} = 7$ TeV. *Phys. Rev. Lett.*, 108:241802, 2012.
- [612] ATLAS Collaboration. Search for gluinos in events with two same-sign leptons, jets and missing transverse momentum with the ATLAS detector in $p\bar{p}$ collisions at $\sqrt{s} = 7$ TeV. ATLAS-CONF-2012-004, 2012.
- [613] ATLAS Collaboration. Search for heavy neutrinos and right-handed W bosons in events with two leptons and jets in $p\bar{p}$ collisions at $\sqrt{s} = 7$ TeV with the ATLAS detector. *Eur. Phys. J. C*, 72:2056, 2012.
- [614] ATLAS Collaboration. Search for heavy vector-like quarks coupling to light quarks in proton–proton collisions at $\sqrt{s} = 7$ TeV with the ATLAS detector. *Phys. Lett. B*, 712:22, 2012.

- [615] ATLAS Collaboration. Search for high-mass dilepton resonances in 6.1 fb^{-1} of pp collisions at $\sqrt{s} = 8 \text{ TeV}$ with the ATLAS experiment. ATLAS-CONF-2012-129, 2012.
- [616] ATLAS Collaboration. Search for high-mass dilepton resonances with 5 fb^{-1} of pp collisions at $\sqrt{s} = 7 \text{ TeV}$ with the ATLAS experiment. ATLAS-CONF-2012-007, 2012.
- [617] ATLAS Collaboration. Search for high-mass resonances decaying to dilepton final states in pp collisions at $\sqrt{s} = 7 \text{ TeV}$ with the ATLAS detector. *JHEP*, 11:138, 2012.
- [618] ATLAS Collaboration. Search for lepton flavour violation in the $e\mu$ continuum with the ATLAS detector in $\sqrt{s} = 7 \text{ TeV}$ pp collisions at the LHC. *Eur. Phys. J. C*, 72:2040, 2012.
- [619] ATLAS Collaboration. Search for light scalar top quark pair production in final states with two leptons with the ATLAS detector in $\sqrt{s} = 7 \text{ TeV}$ proton–proton collisions. *Eur. Phys. J. C*, 72:2237, 2012.
- [620] ATLAS Collaboration. Search for light scalar top quark pair production in final states with two leptons with the ATLAS detector in $\sqrt{s} = 7 \text{ TeV}$ proton–proton collisions. ATLAS-CONF-2012-059, 2012.
- [621] ATLAS Collaboration. Search for light top squark pair production in final states with leptons and b -jets with the ATLAS detector in $\sqrt{s} = 7 \text{ TeV}$ proton–proton collisions. ATLAS-CONF-2012-070, 2012.
- [622] ATLAS Collaboration. Search for long-lived charginos in anomaly-mediated supersymmetry-breaking scenarios with the ATLAS detector using 4.7 fb^{-1} data of pp collisions at $\sqrt{s} = 7 \text{ TeV}$. ATLAS-CONF-2012-034, 2012.
- [623] ATLAS Collaboration. Search for long-lived, heavy particles in final states with a muon and multi-track displaced vertex in proton–proton collisions at $\sqrt{s} = 7 \text{ TeV}$ with the ATLAS detector. ATLAS-CONF-2012-113, 2012.
- [624] ATLAS Collaboration. Search for Magnetic Monopoles in $\sqrt{s} = 7 \text{ TeV}$ pp Collisions with the ATLAS Detector. *Phys. Rev. Lett.*, 109:261803, 2012.
- [625] ATLAS Collaboration. Search for magnetic monopoles in $\sqrt{s} = 7 \text{ TeV}$ pp collisions with the ATLAS detector. ATLAS-CONF-2012-062, 2012.
- [626] ATLAS Collaboration. Search for Majorana neutrino production in pp collisions at $\sqrt{s} = 7 \text{ TeV}$ in same-sign dimuon final states with the ATLAS detector. ATLAS-CONF-2012-139, 2012.

- [627] ATLAS Collaboration. Search for Massive Coloured Scalars with the ATLAS Detector in Four-Jet Final States using 4.6 fb^{-1} of $\sqrt{s} = 7 \text{ TeV}$ proton–proton collision data. ATLAS-CONF-2012-110, 2012.
- [628] ATLAS Collaboration. Search for neutral MSSM Higgs bosons in $\sqrt{s} = 7 \text{ TeV}$ pp collisions with the ATLAS detector. ATLAS-CONF-2012-094, 2012.
- [629] ATLAS Collaboration. Search for new particles decaying to ZZ using final states with leptons and jets with the ATLAS detector in $\sqrt{s} = 7 \text{ TeV}$ proton–proton collisions. *Phys. Lett. B*, 712:331, 2012.
- [630] ATLAS Collaboration. Search for New Phenomena in DijetMass and Angular Distributions using 4.8 fb^{-1} of pp Collisions at $\sqrt{s} = 7 \text{ TeV}$ collected by the ATLAS Detector. ATLAS-CONF-2012-038, 2012.
- [631] ATLAS Collaboration. Search for New Phenomena in Monojet plus Missing Transverse Momentum Final States using 10 fb^{-1} of pp Collisions at $\sqrt{s} = 8 \text{ TeV}$ with the ATLAS detector at the LHC. ATLAS-CONF-2012-147, 2012.
- [632] ATLAS Collaboration. Search for New Phenomena in $t\bar{t}$ Events With Large Missing Transverse Momentum in Proton–Proton Collisions at $\sqrt{s} = 7 \text{ TeV}$ with the ATLAS Detector. *Phys. Rev. Lett.*, 108:041805, 2012.
- [633] ATLAS Collaboration. Search for New Phenomena in the Dijet Mass Distribution updated using 13 fb^{-1} of pp Collisions at $\sqrt{s} = 8 \text{ TeV}$ collected by the ATLAS Detector. ATLAS-CONF-2012-148, 2012.
- [634] ATLAS Collaboration. Search for New Phenomena in the Dijet Mass Distribution using 5.8 fb^{-1} of pp Collisions at $\sqrt{s} = 8 \text{ TeV}$ collected by the ATLAS Detector. ATLAS-CONF-2012-088, 2012.
- [635] ATLAS Collaboration. Search for new phenomena in the $WW \rightarrow \ell\nu\ell'\nu'$ final state in pp collisions at $\sqrt{s} = 7 \text{ TeV}$ with the ATLAS detector. ATLAS-CONF-2012-068, 2012.
- [636] ATLAS Collaboration. Search for new phenomena using large jet multiplicities and missing transverse momentum with ATLAS in 5.8 fb^{-1} of $\sqrt{s} = 8 \text{ TeV}$ proton–proton collisions. ATLAS-CONF-2012-103, 2012.
- [637] ATLAS Collaboration. Search for new physics in the dijet mass distribution using 1 fb^{-1} of pp collision data at $\sqrt{s} = 7 \text{ TeV}$ collected by the ATLAS detector. *Phys. Lett. B*, 708:37, 2012.
- [638] ATLAS Collaboration. Search for pair-produced heavy quarks decaying to Wq in the two-lepton channel at $\sqrt{s} = 7 \text{ TeV}$ with the ATLAS detector. *Phys. Rev. D*, 86:012007, 2012.

- [639] ATLAS Collaboration. Search for Pair Production of a Heavy Up-Type Quark Decaying to a W Boson and a b Quark in the lepton + jets Channel with the ATLAS Detector. *Phys. Rev. Lett.*, 108:261802, 2012.
- [640] ATLAS Collaboration. Search for Pair Production of a New b' Quark that Decays into a Z Boson and a Bottom Quark with the ATLAS Detector. *Phys. Rev. Lett.*, 109:071801, 2012.
- [641] ATLAS Collaboration. Search for pair production of massive particles decaying into three quarks with the ATLAS detector in $\sqrt{s} = 7$ TeV $p\bar{p}$ collisions at the LHC. *JHEP*, 12:086, 2012.
- [642] ATLAS Collaboration. Search for physics beyond the Standard Model in events with a Z boson and large missing transverse momentum with the ATLAS detector. ATLAS-CONF-2012-046, 2012.
- [643] ATLAS Collaboration. Search for Production of Resonant States in the Photon-Jet Mass Distribution Using $p\bar{p}$ Collisions at $\sqrt{s} = 7$ TeV Collected by the ATLAS Detector. *Phys. Rev. Lett.*, 108:211802, 2012.
- [644] ATLAS Collaboration. Search for R-parity-violating supersymmetry in events with four or more leptons in $\sqrt{s} = 7$ TeV $p\bar{p}$ collisions with the ATLAS detector. *JHEP*, 12:124, 2012.
- [645] ATLAS Collaboration. Search for Resonances Decaying into Top Quark Pairs Using Fully Hadronic Decays in $p\bar{p}$ Collisions with ATLAS at $\sqrt{s} = 7$ TeV. ATLAS-CONF-2012-102, 2012.
- [646] ATLAS Collaboration. Search for resonant top plus jet production in $t\bar{t} +$ jets events with the ATLAS detector in $p\bar{p}$ collisions at $\sqrt{s} = 7$ TeV. *Phys. Rev. D*, 86:091103, 2012.
- [647] ATLAS Collaboration. Search for resonant WZ production in the $WZ \rightarrow \ell\nu\ell'\ell'$ channel in $\sqrt{s} = 7$ TeV $p\bar{p}$ collisions with the ATLAS detector. *Phys. Rev. D*, 85:112012, 2012.
- [648] ATLAS Collaboration. Search for resonant ZZ production in the $ZZ \rightarrow \ell\ell qq$ channel with the ATLAS detector using 7.2 fb^{-1} of $\sqrt{s} = 8$ TeV $p\bar{p}$ collision data. ATLAS-CONF-2012-150, 2012.
- [649] ATLAS Collaboration. Search for same-sign top-quark production and fourth-generation down-type quarks in $p\bar{p}$ collisions at $\sqrt{s} = 7$ TeV with the ATLAS detector. *JHEP*, 04:069, 2012.
- [650] ATLAS Collaboration. Search for scalar bottom pair production in final states with missing transverse momentum and two b -jets in $p\bar{p}$ collisions at $\sqrt{s} = 7$ TeV with the ATLAS Detector. ATLAS-CONF-2012-106, 2012.

- [651] ATLAS Collaboration. Search for Scalar Bottom Quark Pair Production with the ATLAS Detector in pp Collisions at $\sqrt{s} = 7 \text{ TeV}$. *Phys. Rev. Lett.*, 108:181802, 2012.
- [652] ATLAS Collaboration. Search for scalar top quark pair production in natural gauge mediated supersymmetry models with the ATLAS detector in pp collisions at $\sqrt{s} = 7 \text{ TeV}$. *Phys. Lett. B*, 715:44, 2012.
- [653] ATLAS Collaboration. Search for Scalar Top Quark Pair Production in Natural Gauge Mediated Supersymmetry Models with the ATLAS Detector in pp Collisions at $\sqrt{s} = 7 \text{ TeV}$. ATLAS-CONF-2012-036, 2012.
- [654] ATLAS Collaboration. Search for second generation scalar leptoquarks in pp collisions at $\sqrt{s} = 7 \text{ TeV}$ with the ATLAS detector. *Eur. Phys. J. C*, 72:2151, 2012.
- [655] ATLAS Collaboration. Search for Single Production of Vector-like Quarks Coupling to Light Generations in 4.64 fb^{-1} of ATLAS Data at $\sqrt{s} = 7 \text{ TeV}$. ATLAS-CONF-2012-137, 2012.
- [656] ATLAS Collaboration. Search for squarks and gluinos using final states with jets and missing transverse momentum with the ATLAS detector in $\sqrt{s} = 7 \text{ TeV}$ proton–proton collisions. *Phys. Lett. B*, 710:67, 2012.
- [657] ATLAS Collaboration. Search for squarks and gluinos with the ATLAS detector using final states with jets and missing transverse momentum and 4.7 fb^{-1} of $\sqrt{s} = 7 \text{ TeV}$ proton–proton collision data. ATLAS-CONF-2012-033, 2012.
- [658] ATLAS Collaboration. Search for squarks and gluinos with the ATLAS detector using final states with jets and missing transverse momentum at $\sqrt{s} = 8 \text{ TeV}$. ATLAS-CONF-2012-109, 2012.
- [659] ATLAS Collaboration. Search for strong gravity signatures in same-sign dimuon final states using the ATLAS detector at the LHC. *Phys. Lett. B*, 709:322, 2012.
- [660] ATLAS Collaboration. Search for supersymmetry at $\sqrt{s} = 7 \text{ TeV}$ in final states with large jet multiplicity, missing transverse momentum and one isolated lepton with the ATLAS detector. ATLAS-CONF-2012-140, 2012.
- [661] ATLAS Collaboration. Search for supersymmetry at $\sqrt{s} = 8 \text{ TeV}$ in final states with jets, missing transverse momentum and one isolated lepton. ATLAS-CONF-2012-104, 2012.

- [662] ATLAS Collaboration. Search for supersymmetry in events with at least one photon, one lepton, and large missing transverse momentum in proton–proton collision at a center-of-mass energy of 7 TeV with the ATLAS detector. ATLAS-CONF-2012-144, 2012.
- [663] ATLAS Collaboration. Search for supersymmetry in events with four or more leptons and missing transverse momentum in pp collisions at $\sqrt{s} = 7$ TeV with the ATLAS detector. ATLAS-CONF-2012-001, 2012.
- [664] ATLAS Collaboration. Search for supersymmetry in events with four or more leptons in 13.0 fb^{-1} pp collisions at $\sqrt{s} = 8$ TeV with the ATLAS detector. ATLAS-CONF-2012-153, 2012.
- [665] ATLAS Collaboration. Search for Supersymmetry in Events with Large Missing Transverse Momentum, Jets, and at Least One Tau Lepton in 7 TeV Proton–Proton Collision Data with the ATLAS Detector. *Eur. Phys. J. C*, 72:2215, 2012.
- [666] ATLAS Collaboration. Search for Supersymmetry in Events with Large Missing Transverse Momentum, Jets, and at Least One Tau Lepton in 7 TeV proton–proton Collision Data with the ATLAS Detector. ATLAS-CONF-2012-112, 2012.
- [667] ATLAS Collaboration. Search for supersymmetry in events with three leptons and missing transverse momentum in $\sqrt{s} = 7$ TeV pp collisions with the ATLAS detector. *Phys. Rev. Lett.*, 108:261804, 2012.
- [668] ATLAS Collaboration. Search for supersymmetry in events with three leptons and missing transverse momentum in $\sqrt{s} = 7$ TeV pp collisions with the ATLAS detector. ATLAS-CONF-2012-023, 2012.
- [669] ATLAS Collaboration. Search for supersymmetry in final states with jets, missing transverse momentum and a Z boson at $\sqrt{s} = 8$ TeV with the ATLAS detector. ATLAS-CONF-2012-152, 2012.
- [670] ATLAS Collaboration. Search for supersymmetry in final states with jets, missing transverse momentum and one isolated lepton in $\sqrt{s} = 7$ TeV pp collisions using 1 fb^{-1} of ATLAS data. *Phys. Rev. D*, 85:012006, 2012.
- [671] ATLAS Collaboration. Search for Supersymmetry in final states with two same-sign leptons, jets and missing transverse momentum with the ATLAS detector in pp collisions at $\sqrt{s} = 8$ TeV. ATLAS-CONF-2012-105, 2012.
- [672] ATLAS Collaboration. Search for supersymmetry in pp collisions at $\sqrt{s} = 7$ TeV in final states with missing transverse momentum and b-jets with the ATLAS detector. *Phys. Rev. D*, 85:112006, 2012.

- [673] ATLAS Collaboration. Search for Supersymmetry in pp Collisions at $\sqrt{s} = 7 \text{ TeV}$ in final states with missing transverse momentum and b -jets with the ATLAS detector. ATLAS-CONF-2012-003, 2012.
- [674] ATLAS Collaboration. Search for supersymmetry using events with three leptons, multiple jets, and missing transverse momentum in 13.0 fb^{-1} of pp collisions with the ATLAS detector at $\sqrt{s} = 8 \text{ TeV}$. ATLAS-CONF-2012-151, 2012.
- [675] ATLAS Collaboration. Search for supersymmetry using events with three leptons, multiple jets, and missing transverse momentum with the ATLAS detector. ATLAS-CONF-2012-108, 2012.
- [676] ATLAS Collaboration. Search for supersymmetry with jets, missing transverse momentum and at least one hadronically decaying τ lepton in proton–proton collisions at $\sqrt{s} = 7 \text{ TeV}$ with the ATLAS detector. *Phys. Lett. B*, 714:197, 2012.
- [677] ATLAS Collaboration. Search for supersymmetry with jets, missing transverse momentum and one or more τ leptons in proton–proton collisions at $\sqrt{s} = 7 \text{ TeV}$ with the ATLAS detector. ATLAS-CONF-2012-005, 2012.
- [678] ATLAS Collaboration. Search for $t\bar{b}$ resonances in proton–proton collisions at $\sqrt{s} = 7 \text{ TeV}$ with the ATLAS detector. *Phys. Rev. Lett.*, 109:081801, 2012.
- [679] ATLAS Collaboration. Search for $t\bar{t}Z$ production in the three lepton final state with 4.7 fb^{-1} of $\sqrt{s} = 7 \text{ TeV}$ pp collision data collected by the ATLAS detector. ATLAS-CONF-2012-126, 2012.
- [680] ATLAS Collaboration. Search for TeV-scale gravity signatures in final states with leptons and jets with the ATLAS detector at $\sqrt{s} = 7 \text{ TeV}$. *Phys. Lett. B*, 716:122, 2012.
- [681] ATLAS Collaboration. Search for the decay $B_s^0 \rightarrow \mu^+ \mu^-$ with the ATLAS detector. *Phys. Lett. B*, 713:387, 2012.
- [682] ATLAS Collaboration. Search for the decay $B_s^0 \rightarrow \mu^+ \mu^-$ with the ATLAS detector. ATLAS-CONF-2012-010, 2012.
- [683] ATLAS Collaboration. Search for the Higgs boson in the associated mode $W H \rightarrow WW^{(*)} \rightarrow \ell\nu\ell\nu\ell\nu$ with the ATLAS detector at $\sqrt{s} = 7 \text{ TeV}$. ATLAS-CONF-2012-078, 2012.

- [684] ATLAS Collaboration. Search for the Higgs boson in the $H \rightarrow WW \rightarrow \ell\nu jj$ decay channel at $\sqrt{s} = 7$ TeV with the ATLAS detector. *Phys. Lett. B*, 718:391, 2012.
- [685] ATLAS Collaboration. Search for the Higgs boson in the $H \rightarrow WW \rightarrow \ell\nu jj$ decay channel using 4.7 fb^{-1} of pp collisions at $\sqrt{s} = 7$ TeV with the ATLAS detector. ATLAS-CONF-2012-018, 2012.
- [686] ATLAS Collaboration. Search for the Higgs boson in the $H \rightarrow WW^{(*)} \rightarrow \ell^+\nu\ell^-\bar{\nu}$ decay channel in pp collisions at $\sqrt{s} = 7$ TeV with the ATLAS detector. *Phys. Rev. Lett.*, 108:111802, 2012.
- [687] ATLAS Collaboration. Search for the Standard Model Higgs boson in $H \rightarrow \tau^+\tau^-$ decays in proton–proton collisions with the ATLAS detector. ATLAS-CONF-2012-160, 2012.
- [688] ATLAS Collaboration. Search for the Standard Model Higgs boson in the decay channel $H \rightarrow ZZ^{(*)} \rightarrow 4\ell$ with 4.8 fb^{-1} of pp collision data at $\sqrt{s} = 7$ TeV with ATLAS. *Phys. Lett. B*, 710:383, 2012.
- [689] ATLAS Collaboration. Search for the Standard Model Higgs Boson in the Diphoton Decay Channel with 4.9 fb^{-1} of pp Collisions at $\sqrt{s} = 7$ TeV with ATLAS. *Phys. Rev. Lett.*, 108:111803, 2012.
- [690] ATLAS Collaboration. Search for the Standard Model Higgs boson in the $H \rightarrow \tau^+\tau^-$ decay mode in $\sqrt{s} = 7$ TeV pp collisions with ATLAS. *JHEP*, 09:070, 2012.
- [691] ATLAS Collaboration. Search for the Standard Model Higgs boson in the $H \rightarrow \tau^+\tau^-$ decay mode with 4.7 fb^{-1} of ATLAS data at $\sqrt{s} = 7$ TeV. ATLAS-CONF-2012-014, 2012.
- [692] ATLAS Collaboration. Search for the Standard Model Higgs boson in the $H \rightarrow WW^{(*)} \rightarrow \ell\nu\ell\nu$ decay mode with 4.7 fb^{-1} of ATLAS data at $\sqrt{s} = 7$ TeV. *Phys. Lett. B*, 716:62, 2012.
- [693] ATLAS Collaboration. Search for the Standard Model Higgs boson in the $H \rightarrow WW^{(*)} \rightarrow \ell\nu\ell\nu$ decay mode using Multivariate Techniques with 4.7 fb^{-1} of ATLAS data at $\sqrt{s} = 7$ TeV. ATLAS-CONF-2012-060, 2012.
- [694] ATLAS Collaboration. Search for the Standard Model Higgs boson in the $H \rightarrow WW^{(*)} \rightarrow \ell\nu\ell\nu$ decay mode with 4.7 fb^{-1} of ATLAS data at $\sqrt{s} = 7$ TeV. ATLAS-CONF-2012-012, 2012.

- [695] ATLAS Collaboration. Search for the Standard Model Higgs boson produced in association with a vector boson and decaying to a b-quark pair using up to 4.7 fb^{-1} of pp collision data at $\sqrt{s} = 7 \text{ TeV}$ with the ATLAS detector at the LHC. ATLAS-CONF-2012-015, 2012.
- [696] ATLAS Collaboration. Search for the Standard Model Higgs boson produced in association with a vector boson and decaying to a b-quark pair with the ATLAS detector. *Phys. Lett. B*, 718:369, 2012.
- [697] ATLAS Collaboration. Search for the Standard Model Higgs boson produced in association with a vector boson and decaying to bottom quarks with the ATLAS detector. ATLAS-CONF-2012-161, 2012.
- [698] ATLAS Collaboration. Search for top and bottom squarks from gluino pair production in final states with missing transverse energy and at least three b-jets with the ATLAS detector. *Eur. Phys. J. C*, 72:2174, 2012.
- [699] ATLAS Collaboration. Search for top-jet resonances in the lepton+jets channel of $t\bar{t} + \text{jets}$ events with the ATLAS detector in 4.7 fb^{-1} of pp collisions at $\sqrt{s} = 7 \text{ TeV}$. ATLAS-CONF-2012-096, 2012.
- [700] ATLAS Collaboration. Searches for Heavy Long-Lived Sleptons and R-hadrons with the ATLAS Detector in pp Collisions at $\sqrt{s} = 7 \text{ TeV}$. ATLAS-CONF-2012-075, 2012.
- [701] ATLAS Collaboration. Searches for supersymmetry with the ATLAS detector using final states with two leptons and missing transverse momentum in $\sqrt{s} = 7 \text{ TeV}$ proton–proton collisions. *Phys. Lett. B*, 709:137, 2012.
- [702] ATLAS Collaboration. Selection of jets produced in proton–proton collisions with the ATLAS detector using 2011 data. ATLAS-CONF-2012-020, 2012.
- [703] ATLAS Collaboration. Statistical combination of top quark pair production cross-section measurements using dilepton, single-lepton, and all-hadronic final states at $\sqrt{s} = 7 \text{ TeV}$ with the ATLAS detector. ATLAS-CONF-2012-024, 2012.
- [704] ATLAS Collaboration. Studies of the impact and mitigation of pile-up on large radius and groomed jets in ATLAS at $\sqrt{s} = 7 \text{ TeV}$. ATLAS-CONF-2012-066, 2012.
- [705] ATLAS Collaboration. Studies of Vector Boson Scattering with an Upgraded ATLAS Detector at a High-Luminosity LHC. ATL-PHYS-PUB-2012-005, 2012.
- [706] ATLAS Collaboration. Study of alignment-related systematic effects on the ATLAS Inner Detector track reconstruction. ATLAS-CONF-2012-141, 2012.

- [707] ATLAS Collaboration. Study of jets produced in association with a W boson in pp collisions at $\sqrt{s} = 7$ TeV with the ATLAS detector. *Phys. Rev. D*, 85:092002, 2012.
- [708] ATLAS Collaboration. Study of the channel $H \rightarrow Z^+Z^- \rightarrow \ell^+\ell^-q\bar{q}$ in the mass range $120 - 180$ TeV with the ATLAS Detector at $\sqrt{s} = 7$ TeV. ATLAS-CONF-2012-163, 2012.
- [709] ATLAS Collaboration. Summary of ATLAS Pythia 8 tunes. ATL-PHYS-PUB-2012-003, 2012.
- [710] ATLAS Collaboration. The underlying event in jet events at 7 TeV with the ATLAS experiment. ATLAS-CONF-2012-164, 2012.
- [711] ATLAS Collaboration. Time-dependent angular analysis of the decay $B_s^0 \rightarrow J/\psi \phi$ and extraction of $\Delta\Gamma_s$ and the CP-violating weak phase ϕ_s by ATLAS. *JHEP*, 12:072, 2012.
- [712] ATLAS Collaboration. Top-quark mass measurement in the $e\mu$ channel using the m_{T2} variable at ATLAS. ATLAS-CONF-2012-082, 2012.
- [713] ATLAS Collaboration. Transverse energy fluctuations in Pb+Pb collisions at $\sqrt{s_{NN}} = 2.76$ TeV with the ATLAS detector at the LHC. ATLAS-CONF-2012-045, 2012.
- [714] ATLAS Collaboration. Underlying event characteristics and their dependence on jet size of charged-particle jet events in pp collisions at $\sqrt{s} = 7$ TeV with the ATLAS detector. *Phys. Rev. D*, 86:072004, 2012.
- [715] ATLAS Collaboration. Update of the $H \rightarrow WW^{(*)} \rightarrow e\nu\mu\nu$ analysis with 13.0 fb^{-1} of $\sqrt{s} = 8$ TeV data collected with the ATLAS detector. ATLAS-CONF-2012-158, 2012.
- [716] ATLAS Collaboration. Updated ATLAS results on the signal strength of the Higgs-like boson for decays into WW and heavy fermion final states. ATLAS-CONF-2012-162, 2012.
- [717] ATLAS Collaboration. Updated results and measurements of properties of the new Higgs-like particle in the four lepton decay channel with the ATLAS detector. ATLAS-CONF-2012-169, 2012.
- [718] ATLAS Collaboration. $Z \rightarrow \tau\tau$ cross section measurement in proton–proton collisions at 7 TeV with the ATLAS experiment. ATLAS-CONF-2012-006, 2012.
- [719] ATLAS Collaboration. *Phys. Rev. D*, 88:079906, 2013.

- [720] ATLAS Collaboration. A Measurement of $W^\pm Z$ Production in Proton–Proton Collisions at $\sqrt{s} = 8$ TeV with the ATLAS Detector. ATLAS-CONF-2013-021, 2013.
- [721] ATLAS Collaboration. A search for heavy long-lived sleptons using 16 fb^{-1} of pp collisions at $\sqrt{s} = 8$ TeV with the ATLAS detector. ATLAS-CONF-2013-058, 2013.
- [722] ATLAS Collaboration. A search for high-mass ditau resonances decaying in the fully hadronic final state in pp collisions at $\sqrt{s} = 8$ TeV with the ATLAS detector. ATLAS-CONF-2013-066, 2013.
- [723] ATLAS Collaboration. A search for high-mass resonances decaying to $\tau^+\tau^-$ in pp collisions at $\sqrt{s} = 7$ TeV with the ATLAS detector. *Phys. Lett. B*, 719:242, 2013.
- [724] ATLAS Collaboration. A search for prompt lepton-jets in pp collisions at $\sqrt{s} = 7$ TeV with the ATLAS detector. *Phys. Lett. B*, 719:299, 2013.
- [725] ATLAS Collaboration. A search for $t\bar{t}$ resonances in lepton plus jets events with ATLAS using 14 fb^{-1} of proton–proton collisions at $\sqrt{s} = 8$ TeV. ATLAS-CONF-2013-052, 2013.
- [726] ATLAS Collaboration. A study of the sensitivity to the proton parton distributions of the inclusive photon production cross section in pp collisions at 7 TeV measured by the ATLAS experiment at the LHC. ATL-PHYS-PUB-2013-018, 2013.
- [727] ATLAS Collaboration. Angular Analysis of $B_d^0 \rightarrow K^{*0}\mu^+\mu^-$ with the ATLAS Experiment. ATLAS-CONF-2013-038, 2013.
- [728] ATLAS Collaboration. ATLAS B-physics studies at increased LHC luminosity, potential for CP-violation measurement in the $B_s^0 \rightarrow J/\psi\phi$ decay. ATL-PHYS-PUB-2013-010, 2013.
- [729] ATLAS Collaboration. ATLAS measurements of the 7 and 8 TeV cross sections for $Z \rightarrow 4\ell$ in pp collisions. ATLAS-CONF-2013-055, 2013.
- [730] ATLAS Collaboration. ATLAS search for new phenomena in dijet mass and angular distributions using pp collisions at $\sqrt{s} = 7$ TeV. *JHEP*, 01:029, 2013.
- [731] ATLAS Collaboration. Beyond-the-Standard-Model Higgs boson searches at a High-Luminosity LHC with ATLAS. ATL-PHYS-PUB-2013-016, 2013.
- [732] ATLAS Collaboration. Calibration of the b-tagging efficiency for c jets with the ATLAS detector using events with a W boson produced in association with a single c quark. ATLAS-CONF-2013-109, 2013.

- [733] ATLAS Collaboration. Characterisation and mitigation of beam-induced backgrounds observed in the ATLAS detector during the 2011 proton–proton run. *JINST*, 8:P07004, 2013.
- [734] ATLAS Collaboration. Combined coupling measurements of the Higgs-like boson with the ATLAS detector using up to 25 fb^{-1} of proton–proton collision data. ATLAS-CONF-2013-034, 2013.
- [735] ATLAS Collaboration. Combined measurements of the mass and signal strength of the Higgs-like boson with the ATLAS detector using up to 25 fb^{-1} of proton–proton collision data. ATLAS-CONF-2013-014, 2013.
- [736] ATLAS Collaboration. Comparison of selected ATLAS top pair differential cross section measurements to NLO QCD predictions. ATL-PHYS-PUB-2013-008, 2013.
- [737] ATLAS Collaboration. Cross-Section Measurement of $\psi(2S) \rightarrow J/\psi(\rightarrow \mu^+ \mu^-) \pi^+ \pi^-$ in $\sqrt{s} = 7 \text{ TeV}$ pp Collisions at ATLAS . ATLAS-CONF-2013-094, 2013.
- [738] ATLAS Collaboration. Determination of the tau energy scale and the associated systematic uncertainty in proton–proton collisions at $\sqrt{s} = 8 \text{ TeV}$ with the ATLAS detector at the LHC in 2012. ATLAS-CONF-2013-044, 2013.
- [739] ATLAS Collaboration. Differential cross sections of the Higgs boson measured in the diphoton decay channel with the ATLAS detector using 8 TeV proton–proton collision data. ATLAS-CONF-2013-072, 2013.
- [740] ATLAS Collaboration. Dynamics of isolated-photon and jet production in pp collisions at $\sqrt{s} = 7 \text{ TeV}$ with the ATLAS detector. ATLAS-CONF-2013-023, 2013.
- [741] ATLAS Collaboration. Dynamics of isolated-photon plus jet production in pp collisions at $\sqrt{s} = 7 \text{ TeV}$ with the ATLAS detector. *Nucl. Phys. B*, 875:483, 2013.
- [742] ATLAS Collaboration. Evidence for Higgs Boson Decays to the $\tau^+ \tau^-$ Final State with the ATLAS Detector. ATLAS-CONF-2013-108, 2013.
- [743] ATLAS Collaboration. Evidence for the spin-0 nature of the Higgs boson using ATLAS data. *Phys. Lett. B*, 726:120, 2013.
- [744] ATLAS Collaboration. Example ATLAS tunes of PYTHIA8, PYTHIA6 and POWHEG to an observable sensitive to Z boson transverse momentum. ATL-PHYS-PUB-2013-017, 2013.

- [745] ATLAS Collaboration. Expected pile-up values at the HL-LHC. ATL-UPGRADE-PUB-2013-014, 2013.
- [746] ATLAS Collaboration. Flavour tagged time dependent angular analysis of the $B_s^0 \rightarrow J/\psi \phi$ decay and extraction of $\Delta\Gamma_s$ and the weak phase ϕ_s in ATLAS. ATLAS-CONF-2013-039, 2013.
- [747] ATLAS Collaboration. Identification of Hadronic Decays of Tau Leptons in 2012 Data with the ATLAS Detector. ATLAS-CONF-2013-064, 2013.
- [748] ATLAS Collaboration. Improved luminosity determination in $p\bar{p}$ collisions at $\sqrt{s} = 7$ TeV using the ATLAS detector at the LHC. *Eur. Phys. J. C*, 73:2518, 2013.
- [749] ATLAS Collaboration. Inclusive cross sections of isolated prompt photons in $p\bar{p}$ collisions at $\sqrt{s} = 7$ TeV measured with the ATLAS detector using 4.7 fb^{-1} of data. ATLAS-CONF-2013-022, 2013.
- [750] ATLAS Collaboration. Jet Charge Studies with the ATLAS Detector Using $\sqrt{s} = 8$ TeV Proton–Proton Collision Data. ATLAS-CONF-2013-086, 2013.
- [751] ATLAS Collaboration. Jet energy measurement and systematic uncertainties using tracks for jets and for b-quark jets produced in proton–proton collisions at $\sqrt{s} = 7$ TeV in the ATLAS detector. ATLAS-CONF-2013-002, 2013.
- [752] ATLAS Collaboration. Jet energy measurement with the ATLAS detector in proton–proton collisions at $\sqrt{s} = 7$ TeV. *Eur. Phys. J. C*, 73:2304, 2013.
- [753] ATLAS Collaboration. Jet energy resolution in proton–proton collisions at $\sqrt{s} = 7$ TeV recorded in 2010 with the ATLAS detector. *Eur. Phys. J. C*, 73:2306, 2013.
- [754] ATLAS Collaboration. Jet energy resolution in proton–proton collisions at $\sqrt{s} = 7$ tev recorded in 2010 with the atlas detector. *The European Physical Journal C*, 73(3):2306, Mar 2013.
- [755] ATLAS Collaboration. Jet energy scale and its systematic uncertainty in proton–proton collisions at $\sqrt{s} = 7$ TeV with ATLAS 2011 data. ATLAS-CONF-2013-004, 2013.
- [756] ATLAS Collaboration. Limit on $B_s^0 \rightarrow \mu^+\mu^-$ branching fraction based on 4.9 fb^{-1} of integrated luminosity. ATLAS-CONF-2013-076, 2013.
- [757] ATLAS Collaboration. Luminosity Monitoring in ATLAS with MPX Detectors. ATLAS-CONF-2013-103, 2013.

- [758] ATLAS Collaboration. Measurement of angular correlations in Drell-Yan lepton pairs to probe Z/γ^* boson transverse momentum at $\sqrt{s} = 7$ TeV with the ATLAS detector. *Phys. Lett. B*, 720:32, 2013.
- [759] ATLAS Collaboration. Measurement of charged-particle event shape variables in inclusive $\sqrt{s} = 7$ TeV proton–proton interactions with the ATLAS detector. *Phys. Rev. D*, 88:032004, 2013.
- [760] ATLAS Collaboration. Measurement of χ_{c1} and χ_{c2} production with $\sqrt{s} = 7$ TeV $p\bar{p}$ collisions at ATLAS. ATLAS-CONF-2013-095, 2013.
- [761] ATLAS Collaboration. Measurement of δ rays in ATLAS silicon detectors. ATLAS-CONF-2013-005, 2013.
- [762] ATLAS Collaboration. Measurement of hard double-parton interactions in $W(\rightarrow \ell\nu) + 2$ jet events at $\sqrt{s} = 7$ TeV with the ATLAS detector. *New J. Phys.*, 15:033038, 2013.
- [763] ATLAS Collaboration. Measurement of isolated-photon pair production in $p\bar{p}$ collisions at $\sqrt{s} = 7$ TeV with the ATLAS detector. *JHEP*, 01:086, 2013.
- [764] ATLAS Collaboration. Measurement of jet shapes in top-quark pair events at $\sqrt{s} = 7$ TeV using the ATLAS detector. *Eur. Phys. J. C*, 73:2676, 2013.
- [765] ATLAS Collaboration. Measurement of k_T splitting scales in $W \rightarrow \ell\nu$ events at $\sqrt{s} = 7$ TeV with the ATLAS detector. *Eur. Phys. J. C*, 73:2432, 2013.
- [766] ATLAS Collaboration. Measurement of multi-jet cross-section ratios and determination of the strong coupling constant in proton–proton collisions at $\sqrt{s} = 7$ TeV with the ATLAS detector. ATLAS-CONF-2013-041, 2013.
- [767] ATLAS Collaboration. Measurement of the Azimuthal Angle Dependence of Inclusive Jet Yields in Pb+Pb Collisions at $\sqrt{s_{NN}} = 2.76$ TeV with the ATLAS detector. *Phys. Rev. Lett.*, 111:152301, 2013.
- [768] ATLAS Collaboration. Measurement of the centrality-dependence of inclusive jet production in p+Pb data at $\sqrt{s_{NN}} = 5.02$ TeV with the ATLAS detector. ATLAS-CONF-2013-105, 2013.
- [769] ATLAS Collaboration. Measurement of the centrality dependence of the charged particle pseudorapidity distribution in proton–lead collisions at $\sqrt{s_{NN}} = 5.02$ TeV with the ATLAS detector. ATLAS-CONF-2013-096, 2013.
- [770] ATLAS Collaboration. Measurement of the cross-section for associated production of a top quark and a W boson at $\sqrt{s} = 8$ TeV with the ATLAS detector. ATLAS-CONF-2013-100, 2013.

- [771] ATLAS Collaboration. Measurement of the cross-section for W boson production in association with b-jets in pp collisions at $\sqrt{s} = 7 \text{ TeV}$ with the ATLAS detector. *JHEP*, 06:084, 2013.
- [772] ATLAS Collaboration. Measurement of the differential cross-section of B^+ meson production in pp collisions at $\sqrt{s} = 7 \text{ TeV}$ at ATLAS. *JHEP*, 10:042, 2013.
- [773] ATLAS Collaboration. Measurement of the differential cross section of B^+ production in pp collisions at $\sqrt{s} = 7 \text{ TeV}$ at ATLAS. ATLAS-CONF-2013-008, 2013.
- [774] ATLAS Collaboration. Measurement of the distributions of event-by-event flow harmonics in lead-lead collisions at $\sqrt{s_{\text{NN}}} = 2.76 \text{ TeV}$ with the ATLAS detector at the LHC. *JHEP*, 11:183, 2013.
- [775] ATLAS Collaboration. Measurement of the flavour composition of dijet events in pp collisions at $\sqrt{s} = 7 \text{ TeV}$ with the ATLAS detector. *Eur. Phys. J. C*, 73:2301, 2013.
- [776] ATLAS Collaboration. Measurement of the forward-backward asymmetry of Z/γ^* bosons decaying into electron or muon pairs with the ATLAS detector at $\sqrt{s} = 7 \text{ TeV}$. ATLAS-CONF-2013-043, 2013.
- [777] ATLAS Collaboration. Measurement of the high-mass Drell-Yan differential cross-section in pp collisions at $\sqrt{s} = 7 \text{ TeV}$ with the ATLAS detector. *Phys. Lett. B*, 725:223, 2013.
- [778] ATLAS Collaboration. Measurement of the inclusive jet cross section in pp collisions at $\sqrt{s} = 7 \text{ TeV}$ and comparison to the inclusive jet cross section at $\sqrt{s} = 7 \text{ TeV}$ using the ATLAS detector. *Eur. Phys. J. C*, 73:2509, 2013.
- [779] ATLAS Collaboration. Measurement of the jet radius and transverse momentum dependence of inclusive jet suppression in lead-lead collisions at $\sqrt{s_{\text{NN}}} = 2.76 \text{ TeV}$ with the ATLAS detector. *Phys. Lett. B*, 719:220, 2013.
- [780] ATLAS Collaboration. Measurement of the Λ_b^0 lifetime and mass in the ATLAS experiment. *Phys. Rev. D*, 87:032002, 2013.
- [781] ATLAS Collaboration. Measurement of the parity violating asymmetry parameter α_b and the helicity amplitudes for the decay $\Lambda_b^0 \rightarrow J/\psi \Lambda^0$ in the ATLAS experiment. ATLAS-CONF-2013-071, 2013.

- [782] ATLAS Collaboration. Measurement of the production cross section of jets in association with a Z boson in pp collisions at $\sqrt{s} = 7 \text{ TeV}$ with the ATLAS detector. *JHEP*, 07:032, 2013.
- [783] ATLAS Collaboration. Measurement of the production cross section of prompt J/ψ mesons in association with a W^\pm boson in pp collisions at $\sqrt{s} = 7 \text{ TeV}$. ATLAS-CONF-2013-042, 2013.
- [784] ATLAS Collaboration. Measurement of the production of a W boson in association with a charm hadron in pp collisions at $\sqrt{s} = 7 \text{ TeV}$. ATLAS-CONF-2013-045, 2013.
- [785] ATLAS Collaboration. Measurement of the $t\bar{t}$ production cross-section in pp collisions at $\sqrt{s} = 8 \text{ TeV}$ using $e\mu$ events with b-tagged jets. ATLAS-CONF-2013-097, 2013.
- [786] ATLAS Collaboration. Measurement of the $t\bar{t}$ production cross section in the tau+jets channel using the ATLAS detector. *Eur. Phys. J. C*, 73:2328, 2013.
- [787] ATLAS Collaboration. Measurement of the top quark charge in pp collisions at $\sqrt{s} = 7 \text{ TeV}$ with the ATLAS detector. *JHEP*, 11:031, 2013.
- [788] ATLAS Collaboration. Measurement of the Top Quark Mass from $\sqrt{s} = 7 \text{ TeV}$ ATLAS Data using a 3-dimensional Template Fit. ATLAS-CONF-2013-046, 2013.
- [789] ATLAS Collaboration. Measurement of the Top Quark Mass in Dileptonic Top Quark Pair Decays with $\sqrt{s} = 7 \text{ TeV}$ ATLAS Data. ATLAS-CONF-2013-077, 2013.
- [790] ATLAS Collaboration. Measurement of the top quark pair production charge asymmetry in proton–proton collisions at $\sqrt{s} = 7 \text{ TeV}$ using the ATLAS detector. ATLAS-CONF-2013-078, 2013.
- [791] ATLAS Collaboration. Measurement of the total ZZ production cross section in proton–proton collisions at $\sqrt{s} = 8 \text{ TeV}$ in 20 fb^{-1} with the ATLAS detector. ATLAS-CONF-2013-020, 2013.
- [792] ATLAS Collaboration. Measurement of the $W \rightarrow \mu\nu$ charge asymmetry and its centrality dependence in Pb+Pb collisions at $\sqrt{s_{\text{NN}}} = 2.76 \text{ TeV}$ with the ATLAS detector. ATLAS-CONF-2013-106, 2013.
- [793] ATLAS Collaboration. Measurement of top quark pair differential cross-sections in the $\ell+\text{jets}$ channel in pp collisions at $\sqrt{s} = 7 \text{ TeV}$ using the ATLAS detector. ATLAS-CONF-2013-099, 2013.

- [794] ATLAS Collaboration. Measurement of Top Quark Polarization in Top-Antitop Events from Proton-Proton Collisions at $\sqrt{s} = 7$ TeV Using the ATLAS Detector. *Phys. Rev. Lett.*, 111:232002, 2013.
- [795] ATLAS Collaboration. Measurement of Upsilon production in 7 TeV pp collisions at ATLAS. *Phys. Rev. D*, 87:052004, 2013.
- [796] ATLAS Collaboration. Measurement of W^+W^- production in pp collisions at $\sqrt{s} = 7$ TeV with the ATLAS detector and limits on anomalous WWZ and $WW\gamma$ couplings. *Phys. Rev. D*, 87:112001, 2013.
- [797] ATLAS Collaboration. Measurement of Z Boson Production in Pb+Pb Collisions at $\sqrt{s_{NN}} = 2.76$ TeV with the ATLAS Detector. *Phys. Rev. Lett.*, 110:022301, 2013.
- [798] ATLAS Collaboration. Measurement of ZZ production in pp collisions at $\sqrt{s} = 7$ TeV and limits on anomalous ZZZ and ZZ γ couplings with the ATLAS detector. *JHEP*, 03:128, 2013.
- [799] ATLAS Collaboration. Measurement with the ATLAS detector of multi-particle azimuthal correlations in p+Pb collisions at $\sqrt{s_{NN}} = 5.02$ TeV. *Phys. Lett. B*, 725:60, 2013.
- [800] ATLAS Collaboration. Measurements of Higgs boson production and couplings in diboson final states with the ATLAS detector at the LHC. *Phys. Lett. B*, 726:88, 2013.
- [801] ATLAS Collaboration. Measurements of spin correlation in top-antitop events from proton-proton collisions at $\sqrt{s} = 7$ TeV using the ATLAS detector. ATLAS-CONF-2013-101, 2013.
- [802] ATLAS Collaboration. Measurements of the properties of the Higgs-like boson in the four lepton decay channel with the ATLAS detector using 25 fb^{-1} of proton-proton collision data. ATLAS-CONF-2013-013, 2013.
- [803] ATLAS Collaboration. Measurements of the properties of the Higgs-like boson in the two photon decay channel with the ATLAS detector using 25 fb^{-1} of proton-proton collision data. ATLAS-CONF-2013-012, 2013.
- [804] ATLAS Collaboration. Measurements of the properties of the Higgs-like boson in the $WW^{(*)} \rightarrow \ell\nu\ell\nu$ decay channel with the ATLAS detector using 25 fb^{-1} of proton-proton collision data. ATLAS-CONF-2013-030, 2013.
- [805] ATLAS Collaboration. Measurements of top quark pair relative differential cross-sections with ATLAS in pp collisions at $\sqrt{s} = 7$ TeV. *Eur. Phys. J. C*, 73:2261, 2013.

- [806] ATLAS Collaboration. Measurements of $W\gamma$ and $Z\gamma$ production in pp collisions at $\sqrt{s} = 7 \text{ TeV}$ with the ATLAS detector at the LHC. *Phys. Rev. D*, 87:112003, 2013.
- [807] ATLAS Collaboration. Monte Carlo generator comparisons to ATLAS measurements constraining QCD radiation in top anti-top final states. ATL-PHYS-PUB-2013-005, 2013.
- [808] ATLAS Collaboration. Multi-channel search for squarks and gluinos in $\sqrt{s} = 7 \text{ TeV}$ pp collisions with the ATLAS detector at the LHC. *Eur. Phys. J. C*, 73:2362, 2013.
- [809] ATLAS Collaboration. Observation of Associated Near-Side and Away-Side Long-Range Correlations in $\sqrt{s_{\text{NN}}} = 5.02 \text{ TeV}$ Proton–Lead Collisions with the ATLAS Detector. *Phys. Rev. Lett.*, 110:182302, 2013.
- [810] ATLAS Collaboration. Performance and Validation of Q-jets at the ATLAS Detector in pp Collisions at $\sqrt{s} = 8 \text{ TeV}$ in 2012. ATLAS-CONF-2013-087, 2013.
- [811] ATLAS Collaboration. Performance assumptions based on full simulation for an upgraded ATLAS detector at a High-Luminosity LHC. ATL-PHYS-PUB-2013-009, 2013.
- [812] ATLAS Collaboration. Performance assumptions for an upgraded ATLAS detector at a High-Luminosity LHC. ATL-PHYS-PUB-2013-004, 2013.
- [813] ATLAS Collaboration. Performance of boosted top quark identification in 2012 ATLAS data. ATLAS-CONF-2013-084, 2013.
- [814] ATLAS Collaboration. Performance of jet substructure techniques for large-R jets in proton–proton collisions at $\sqrt{s} = 7 \text{ TeV}$ using the ATLAS detector. *JHEP*, 09:076, 2013.
- [815] ATLAS Collaboration. Performance of Missing Transverse Momentum Reconstruction in ATLAS studied in Proton–Proton Collisions recorded in 2012 at $\sqrt{s} = 8 \text{ TeV}$. ATLAS-CONF-2013-082, 2013.
- [816] ATLAS Collaboration. Performance of pile-up subtraction for jet shapes in pp collisions at $\sqrt{s} = 8 \text{ TeV}$. ATLAS-CONF-2013-085, 2013.
- [817] ATLAS Collaboration. Performance of the ATLAS Minimum Bias and Forward Detector Triggers in $\text{p}+\text{Pb}$ collisions. ATLAS-CONF-2013-104, 2013.
- [818] ATLAS Collaboration. Performance of the ATLAS tau trigger in 2011. ATLAS-CONF-2013-006, 2013.

- [819] ATLAS Collaboration. Physics at a High-Luminosity LHC with ATLAS. ATL-PHYS-PUB-2013-007, 2013.
- [820] ATLAS Collaboration. Pile-up subtraction and suppression for jets in ATLAS. ATLAS-CONF-2013-083, 2013.
- [821] ATLAS Collaboration. Preliminary results on the muon reconstruction efficiency, momentum resolution, and momentum scale in ATLAS 2012 pp collision data. ATLAS-CONF-2013-088, 2013.
- [822] ATLAS Collaboration. Projections for measurements of Higgs boson cross sections, branching ratios and coupling parameters with the ATLAS detector at a HL-LHC. ATL-PHYS-PUB-2013-014, 2013.
- [823] ATLAS Collaboration. Prospects for benchmark Supersymmetry searches at the high luminosity LHC with the ATLAS Detector. ATL-PHYS-PUB-2013-011, 2013.
- [824] ATLAS Collaboration. Prospects for measurements of the HZZ vertex tensor structure in $H \rightarrow ZZ^* \rightarrow 4\ell$ decay channel with ATLAS. ATL-PHYS-PUB-2013-013, 2013.
- [825] ATLAS Collaboration. Search for a dijet resonance produced in association with a leptonically decaying W or Z boson with the ATLAS detector at $\sqrt{s} = 8$ TeV. ATLAS-CONF-2013-074, 2013.
- [826] ATLAS Collaboration. Search for a heavy narrow resonance decaying to $e\mu$, $e\tau$, or $\mu\tau$ with the ATLAS detector in $\sqrt{s} = 7$ TeV pp collisions at the LHC. *Phys. Lett. B*, 723:15, 2013.
- [827] ATLAS Collaboration. Search for a high-mass Higgs boson in the $H \rightarrow WW \rightarrow \ell\nu\ell\nu$ decay channel with the ATLAS detector using 21 fb^{-1} of proton-proton collision data. ATLAS-CONF-2013-067, 2013.
- [828] ATLAS Collaboration. Search for a light charged Higgs boson in the decay channel $H^+ \rightarrow c\bar{s}$ in $t\bar{t}$ events using pp collisions at $\sqrt{s} = 7$ TeV with the ATLAS detector. *Eur. Phys. J. C*, 73:2465, 2013.
- [829] ATLAS Collaboration. Search for anomalous production of events with same-sign dileptons and b jets in 14.3 fb^{-1} of pp collisions at $\sqrt{s} = 8$ TeV with the ATLAS detector. ATLAS-CONF-2013-051, 2013.
- [830] ATLAS Collaboration. Search for associated production of the Higgs boson in the $WH \rightarrow WWW^{(*)} \rightarrow \ell\nu\ell\nu\ell\nu$ and $ZH \rightarrow ZWW^{(*)} \rightarrow \ell\ell\ell\nu\ell\nu$ channels with the ATLAS detector at the LHC. ATLAS-CONF-2013-075, 2013.

- [831] ATLAS Collaboration. Search for charged Higgs bosons in the $\tau +$ jets final state with $p\bar{p}$ collision data recorded at $\sqrt{s} = 8$ TeV with the ATLAS experiment. ATLAS-CONF-2013-090, 2013.
- [832] ATLAS Collaboration. Search for charged Higgs bosons through the violation of lepton universality in $t\bar{t}$ events using $p\bar{p}$ collision data at $\sqrt{s} = 7$ TeV with the ATLAS experiment. *JHEP*, 03:076, 2013.
- [833] ATLAS Collaboration. Search for chargino and neutralino production in final states with one lepton, two b-jets consistent with a Higgs boson, and missing transverse momentum with the ATLAS detector in 20.3 fb^{-1} of $\sqrt{s} = 8$ TeV $p\bar{p}$ collisions. ATLAS-CONF-2013-093, 2013.
- [834] ATLAS Collaboration. Search for charginos nearly mass-degenerate with the lightest neutralino based on a disappearing-track signature in $p\bar{p}$ collisions at $\sqrt{s} = 8$ TeV with the ATLAS detector. ATLAS-CONF-2013-069, 2013.
- [835] ATLAS Collaboration. Search for charginos nearly mass degenerate with the lightest neutralino based on a disappearing-track signature in $p\bar{p}$ collisions at $\sqrt{s} = 8$ TeV with the ATLAS detector. *Phys. Rev. D*, 88:112006, 2013.
- [836] ATLAS Collaboration. Search for contact interactions and large extra dimensions in dilepton events from $p\bar{p}$ collisions at $\sqrt{s} = 7$ TeV with the ATLAS detector. *Phys. Rev. D*, 87:015010, 2013.
- [837] ATLAS Collaboration. Search for dark matter candidates and large extra dimensions in events with a jet and missing transverse momentum with the ATLAS detector. *JHEP*, 04:075, 2013.
- [838] ATLAS Collaboration. Search for dark matter candidates and large extra dimensions in events with a photon and missing transverse momentum in $p\bar{p}$ collision data at $\sqrt{s} = 7$ TeV with the ATLAS detector. *Phys. Rev. Lett.*, 110:011802, 2013.
- [839] ATLAS Collaboration. Search for dark matter pair production in events with a hadronically decaying W or Z boson and missing transverse momentum in $p\bar{p}$ collision data at $\sqrt{s} = 8$ TeV with the ATLAS detector. ATLAS-CONF-2013-073, 2013.
- [840] ATLAS Collaboration. Search for direct chargino production in anomaly-mediated supersymmetry breaking models based on a disappearing-track signature in $p\bar{p}$ collisions at $\sqrt{s} = 7$ TeV with the ATLAS detector. *JHEP*, 01:131, 2013.

- [841] ATLAS Collaboration. Search for direct production of charginos and neutralinos in events with three leptons and missing transverse momentum in 21 fb^{-1} of pp collisions at $\sqrt{s} = 8 \text{ TeV}$ with the ATLAS detector. ATLAS-CONF-2013-035, 2013.
- [842] ATLAS Collaboration. Search for direct production of charginos and neutralinos in events with three leptons and missing transverse momentum in $\sqrt{s} = 7 \text{ TeV}$ pp collisions with the ATLAS detector. *Phys. Lett. B*, 718:841, 2013.
- [843] ATLAS Collaboration. Search for direct production of the top squark in the all-hadronic $t\bar{t} + E_T^{\text{miss}}$ final state in 21 fb^{-1} of pp collisions at $\sqrt{s} = 8 \text{ TeV}$ with the ATLAS detector. ATLAS-CONF-2013-024, 2013.
- [844] ATLAS Collaboration. Search for direct slepton and gaugino production in final states with two leptons and missing transverse momentum with the ATLAS detector in pp collisions at $\sqrt{s} = 7 \text{ TeV}$. *Phys. Lett. B*, 718:879, 2013.
- [845] ATLAS Collaboration. Search for direct third-generation squark pair production in final states with missing transverse momentum and two b-jets in $\sqrt{s} = 8 \text{ TeV}$ pp collisions with the ATLAS detector. *JHEP*, 10:189, 2013.
- [846] ATLAS Collaboration. Search for direct third generation squark pair production in final states with Missing Transverse Momentum and two b-jets in $\sqrt{s} = 8 \text{ TeV}$ pp collisions with the ATLAS detector. ATLAS-CONF-2013-053, 2013.
- [847] ATLAS Collaboration. Search for direct top squark pair production in events with a Z boson, b-jets and missing transverse momentum in 21 fb^{-1} of proton–proton collisions at $\sqrt{s} = 8 \text{ TeV}$ with the ATLAS detector. ATLAS-CONF-2013-025, 2013.
- [848] ATLAS Collaboration. Search for direct top squark pair production in final states with one isolated lepton, jets, and missing transverse momentum in $\sqrt{s} = 8 \text{ TeV}$ pp collisions using 21 fb^{-1} of ATLAS data. ATLAS-CONF-2013-037, 2013.
- [849] ATLAS Collaboration. Search for direct top squark pair production in final states with two leptons in $\sqrt{s} = 8 \text{ TeV}$ pp collisions using 20 fb^{-1} of ATLAS data. ATLAS-CONF-2013-048, 2013.
- [850] ATLAS Collaboration. Search for displaced muonic lepton jets from light Higgs boson decay in proton–proton collisions at $\sqrt{s} = 7 \text{ TeV}$ with the ATLAS detector. *Phys. Lett. B*, 721:32, 2013.

- [851] ATLAS Collaboration. Search for electroweak production of supersymmetric particles in final states with at least two hadronically decaying taus and missing transverse momentum with the ATLAS detector in proton–proton collisions at $\sqrt{s} = 8$ TeV. ATLAS-CONF-2013-028, 2013.
- [852] ATLAS Collaboration. Search for excited electrons and muons in $\sqrt{s} = 8$ TeV proton–proton collisions with the ATLAS detector. *New J. Phys.*, 15:093011, 2013.
- [853] ATLAS Collaboration. Search for extra dimensions in diphoton events from proton–proton collisions recorded at $\sqrt{s} = 7$ TeV in the ATLAS detector at the LHC. *New J. Phys.*, 15:043007, 2013.
- [854] ATLAS Collaboration. Search for flavour changing neutral currents in top quark decays $t \rightarrow cH$, with $H \rightarrow \gamma\gamma$, and limit on the tch coupling with the ATLAS detector at the LHC. ATLAS-CONF-2013-081, 2013.
- [855] ATLAS Collaboration. Search for heavy top-like quarks decaying to a Higgs boson and a top quark in the lepton plus jets final state in pp collisions at $\sqrt{s} = 8$ TeV with the ATLAS detector. ATLAS-CONF-2013-018, 2013.
- [856] ATLAS Collaboration. Search for Higgs bosons in Two-Higgs-Doublet models in the $H \rightarrow WW \rightarrow e\nu\mu\nu$ channel with the ATLAS detector. ATLAS-CONF-2013-027, 2013.
- [857] ATLAS Collaboration. Search for high-mass dilepton resonances in 20 fb^{-1} of pp collisions at $\sqrt{s} = 8$ TeV with the ATLAS experiment. ATLAS-CONF-2013-017, 2013.
- [858] ATLAS Collaboration. Search for invisible decays of a Higgs boson produced in association with a Z boson in ATLAS. ATLAS-CONF-2013-011, 2013.
- [859] ATLAS Collaboration. Search for light top squark pair production in final states with leptons and b -jets with the ATLAS detector in $\sqrt{s} = 7$ TeV proton–proton collisions. *Phys. Lett. B*, 720:13, 2013.
- [860] ATLAS Collaboration. Search for long-lived, heavy particles in final states with a muon and a multi-track displaced vertex in proton–proton collisions at $\sqrt{s} = 8$ TeV with the ATLAS detector. ATLAS-CONF-2013-092, 2013.
- [861] ATLAS Collaboration. Search for long-lived, heavy particles in final states with a muon and multi-track displaced vertex in proton–proton collisions at $\sqrt{s} = 7$ TeV with the ATLAS detector. *Phys. Lett. B*, 719:280, 2013.
- [862] ATLAS Collaboration. Search for long-lived, multi-charged particles in pp collisions at $\sqrt{s} = 7$ TeV using the ATLAS detector. *Phys. Lett. B*, 722:305, 2013.

- [863] ATLAS Collaboration. Search for long-lived stopped gluino R-hadrons decaying out-of-time with LHC collisions in 2011 and 2012 using the ATLAS detector. ATLAS-CONF-2013-057, 2013.
- [864] ATLAS Collaboration. Search for long-lived stopped R-hadrons decaying out of time with pp collisions using the ATLAS detector. *Phys. Rev. D*, 88:112003, 2013.
- [865] ATLAS Collaboration. Search for massive particles decaying into multiple quarks with the ATLAS detector in $\sqrt{s} = 8$ TeV pp collisions. ATLAS-CONF-2013-091, 2013.
- [866] ATLAS Collaboration. Search for \mathcal{CP} violation in single top quark events in pp collisions at $\sqrt{s} = 7$ TeV with the ATLAS detector. ATLAS-CONF-2013-032, 2013.
- [867] ATLAS Collaboration. Search for microscopic black holes in a like-sign dimuon final state using large track multiplicity with the ATLAS detector. *Phys. Rev. D*, 88:072001, 2013.
- [868] ATLAS Collaboration. Search for new phenomena in events with three charged leptons at $\sqrt{s} = 7$ TeV with the ATLAS detector. *Phys. Rev. D*, 87:052002, 2013.
- [869] ATLAS Collaboration. Search for New Phenomena in Events with Three Charged Leptons at $\sqrt{s} = 8$ TeV with the ATLAS Detector. ATLAS-CONF-2013-070, 2013.
- [870] ATLAS Collaboration. Search for new phenomena in final states with large jet multiplicities and missing transverse momentum at $\sqrt{s} = 8$ TeV proton–proton collisions using the ATLAS experiment. *JHEP*, 10:130, 2013.
- [871] ATLAS Collaboration. Search for New Phenomena in the Photon+Jet Events Collected in Proton–Proton Collisions at $\sqrt{s} = 8$ TeV With the ATLAS Detector. ATLAS-CONF-2013-059, 2013.
- [872] ATLAS Collaboration. Search for new phenomena in the $WW \rightarrow \ell\nu\ell'\nu'$ final state in pp collisions at $\sqrt{s} = 7$ TeV with the ATLAS detector. *Phys. Lett. B*, 718:860, 2013.
- [873] ATLAS Collaboration. Search for new phenomena using final states with large jet multiplicities and missing transverse momentum with ATLAS in 20 fb^{-1} of $\sqrt{s} = 8$ TeV proton–proton collisions. ATLAS-CONF-2013-054, 2013.

- [874] ATLAS Collaboration. Search for non-pointing photons in the diphoton and E_T^{miss} final state in $\sqrt{s} = 7$ TeV proton–proton collisions using the ATLAS detector. ATLAS-CONF-2013-016, 2013.
- [875] ATLAS Collaboration. Search for nonpointing photons in the diphoton and E_T^{miss} final state in $\sqrt{s} = 7$ TeV proton–proton collisions using the ATLAS detector. *Phys. Rev. D*, 88:012001, 2013.
- [876] ATLAS Collaboration. Search for pair-produced massive coloured scalars in four-jet final states with the ATLAS detector in proton–proton collisions at $\sqrt{s} = 7$ TeV. *Eur. Phys. J. C*, 73:2263, 2013.
- [877] ATLAS Collaboration. Search for pair-produced top squarks decaying into charm quarks and the lightest neutralinos using 20.3 fb^{-1} of pp collisions at $\sqrt{s} = 8$ TeV with the ATLAS detector at the LHC. ATLAS-CONF-2013-068, 2013.
- [878] ATLAS Collaboration. Search for pair production of a heavy top-like quark decaying to a high- p_T W boson and a b quark in the lepton plus jets final state in pp collisions at $\sqrt{s} = 8$ TeV with the ATLAS detector. ATLAS-CONF-2013-060, 2013.
- [879] ATLAS Collaboration. Search for pair production of heavy top-like quarks decaying to a high- p_T W boson and a b quark in the lepton plus jets final state at $\sqrt{s} = 7$ TeV with the ATLAS detector. *Phys. Lett. B*, 718:1284, 2013.
- [880] ATLAS Collaboration. Search for pair production of new heavy quarks that decay to a Z boson and a third generation quark in pp collisions at $\sqrt{s} = 8$ TeV with the ATLAS detector. ATLAS-CONF-2013-056, 2013.
- [881] ATLAS Collaboration. Search for resonances decaying into top-quark pairs using fully hadronic decays in pp collisions with ATLAS at $\sqrt{s} = 7$ TeV. *JHEP*, 01:116, 2013.
- [882] ATLAS Collaboration. Search for resonant diboson production in the $WW/WZ \rightarrow \ell\nu jj$ decay channels with the ATLAS detector at $\sqrt{s} = 7$ TeV. *Phys. Rev. D*, 87:112006, 2013.
- [883] ATLAS Collaboration. Search for resonant $WZ \rightarrow \ell\nu\ell'\ell'$ production using $\sqrt{s} = 8$ TeV pp collisions with ATLAS. ATLAS-CONF-2013-015, 2013.
- [884] ATLAS Collaboration. Search for single b*-quark production with the ATLAS detector at $\sqrt{s} = 7$ TeV. *Phys. Lett. B*, 721:171, 2013.

- [885] ATLAS Collaboration. Search for single top-quark production via FCNC in strong interactions in $\sqrt{s} = 8$ TeV ATLAS data. ATLAS-CONF-2013-063, 2013.
- [886] ATLAS Collaboration. Search for squarks and gluinos in events with isolated leptons, jets and missing transverse momentum at $\sqrt{s} = 8$ TeV with the ATLAS detector. ATLAS-CONF-2013-062, 2013.
- [887] ATLAS Collaboration. Search for squarks and gluinos with the ATLAS detector in final states with jets and missing transverse momentum and 20.3 fb^{-1} of $\sqrt{s} = 8$ TeV proton–proton collision data. ATLAS-CONF-2013-047, 2013.
- [888] ATLAS Collaboration. Search for squarks and gluinos with the ATLAS detector in final states with jets and missing transverse momentum using 4.7 fb^{-1} of $\sqrt{s} = 7$ TeV proton–proton collision data. *Phys. Rev. D*, 87:012008, 2013.
- [889] ATLAS Collaboration. Search for strong production of supersymmetric particles in final states with missing transverse momentum and at least three b-jets using 20.1 fb^{-1} of pp collisions at $\sqrt{s} = 8$ TeV with the ATLAS Detector. ATLAS-CONF-2013-061, 2013.
- [890] ATLAS Collaboration. Search for strongly produced supersymmetric particles in decays with two leptons at $\sqrt{s} = 8$ TeV. ATLAS-CONF-2013-089, 2013.
- [891] ATLAS Collaboration. Search for strongly produced supersymmetric particles in final states with two same-sign leptons and jets with the ATLAS detector using 21 fb^{-1} of proton–proton collisions at $\sqrt{s} = 8$ TeV. ATLAS-CONF-2013-007, 2013.
- [892] ATLAS Collaboration. Search for Supersymmetry in Diphoton Events with Large Missing Transverse Momentum in 8 TeV pp Collision Data with the ATLAS Detector. ATLAS-CONF-2014-001, 2013.
- [893] ATLAS Collaboration. Search for supersymmetry in events with four or more leptons in 21 fb^{-1} of pp collisions at $\sqrt{s} = 8$ TeV with the ATLAS detector. ATLAS-CONF-2013-036, 2013.
- [894] ATLAS Collaboration. Search for Supersymmetry in Events with Large Missing Transverse Momentum, Jets, and at Least One Tau Lepton in 21 fb^{-1} of $\sqrt{s} = 8$ TeV Proton–Proton Collision Data with the ATLAS Detector. ATLAS-CONF-2013-026, 2013.

- [895] ATLAS Collaboration. Search for supersymmetry in events with photons, bottom quarks, and missing transverse momentum in proton–proton collisions at a centre-of-mass energy of 7 TeV with the ATLAS detector. *Phys. Lett. B*, 719:261, 2013.
- [896] ATLAS Collaboration. Search for $t\bar{t}$ resonances in the lepton plus jets final state with ATLAS using 4.7 fb^{-1} of pp collisions at $\sqrt{s} = 7 \text{ TeV}$. *Phys. Rev. D*, 88:012004, 2013.
- [897] ATLAS Collaboration. Search for $t\bar{t}\text{H}$ production in the $\text{H} \rightarrow \gamma\gamma$ channel at $\sqrt{s} = 8 \text{ TeV}$ with the ATLAS detector. ATLAS-CONF-2013-080, 2013.
- [898] ATLAS Collaboration. Search for the $b\bar{b}$ decay of the Standard Model Higgs boson in associated ($W/Z\text{H}$) production with the ATLAS detector. ATLAS-CONF-2013-079, 2013.
- [899] ATLAS Collaboration. Search for the neutral Higgs bosons of the Minimal Supersymmetric Standard Model in pp collisions at $\sqrt{s} = 7 \text{ TeV}$ with the ATLAS detector. *JHEP*, 02:095, 2013.
- [900] ATLAS Collaboration. Search for the Standard Model Higgs boson in $\text{H} \rightarrow \mu^+\mu^-$ decays with the ATLAS detector. ATLAS-CONF-2013-010, 2013.
- [901] ATLAS Collaboration. Search for the Standard Model Higgs boson in the $\text{H} \rightarrow Z\gamma$ decay mode with pp collisions at $\sqrt{s} = 7$ and 8 TeV . ATLAS-CONF-2013-009, 2013.
- [902] ATLAS Collaboration. Search for third generation scalar leptoquarks in pp collisions at $\sqrt{s} = 7 \text{ TeV}$ with the ATLAS detector. *JHEP*, 06:033, 2013.
- [903] ATLAS Collaboration. Search for Type III Seesaw Model Heavy Fermions in Events with Four Charged Leptons using 5.8 fb^{-1} of $\sqrt{s} = 8 \text{ TeV}$ data with the ATLAS Detector. ATLAS-CONF-2013-019, 2013.
- [904] ATLAS Collaboration. Search for $W' \rightarrow t\bar{b}$ in proton–proton collisions at a centre-of-mass energy of $\sqrt{s} = 8 \text{ TeV}$ with the ATLAS detector. ATLAS-CONF-2013-050, 2013.
- [905] ATLAS Collaboration. Search for WH production with a light Higgs boson decaying to prompt electron-jets in proton–proton collisions at $\sqrt{s} = 7 \text{ TeV}$ with the ATLAS detector. *New J. Phys.*, 15:043009, 2013.
- [906] ATLAS Collaboration. Searches for direct scalar top pair production in final states with two leptons using the stransverse mass variable and a multivariate analysis technique in $\sqrt{s} = 8 \text{ TeV}$ pp collisions using 20.3 fb^{-1} of ATLAS data. ATLAS-CONF-2013-065, 2013.

- [907] ATLAS Collaboration. Searches for direct-slepton pair and chargino pair production in final states with two opposite-sign leptons, missing transverse momentum and no jets in 20 fb^{-1} of pp collisions at $\sqrt{s} = 8 \text{ TeV}$ with the ATLAS detector. ATLAS-CONF-2013-049, 2013.
- [908] ATLAS Collaboration. Searches for heavy long-lived sleptons and R-Hadrons with the ATLAS detector in pp collisions at $\sqrt{s} = 7 \text{ TeV}$. *Phys. Lett. B*, 720:277, 2013.
- [909] ATLAS Collaboration. Searches for Supersymmetry at the high luminosity LHC with the ATLAS Detector. ATL-PHYS-PUB-2013-002, 2013.
- [910] ATLAS Collaboration. Sensitivity of ATLAS at HL-LHC to flavour changing neutral currents in top quark decays $t \rightarrow cH$, with $H \rightarrow \gamma\gamma$. ATL-PHYS-PUB-2013-012, 2013.
- [911] ATLAS Collaboration. Sensitivity to New Phenomena via Higgs Couplings with the ATLAS Detector at a High-Luminosity LHC. ATL-PHYS-PUB-2013-015, 2013.
- [912] ATLAS Collaboration. Single hadron response measurement and calorimeter jet energy scale uncertainty with the ATLAS detector at the LHC. *Eur. Phys. J. C*, 73:2305, 2013.
- [913] ATLAS Collaboration. Studies for the development of the Inner Detector trigger algorithms at ATLAS. ATL-DAQ-PUB-2013-002, 2013.
- [914] ATLAS Collaboration. Studies of Sensitivity to New Dilepton and Ditop Resonances with an Upgraded ATLAS Detector at a High-Luminosity LHC. ATL-PHYS-PUB-2013-003, 2013.
- [915] ATLAS Collaboration. Studies of the ATLAS potential for Higgs self-coupling measurements at a High Luminosity LHC. ATL-PHYS-PUB-2013-001, 2013.
- [916] ATLAS Collaboration. Studies of Vector Boson Scattering And Triboson Production with an Upgraded ATLAS Detector at a High-Luminosity LHC. ATL-PHYS-PUB-2013-006, 2013.
- [917] ATLAS Collaboration. Study of the spin of the Higgs-like boson in the two photon decay channel using 20.7 fb^{-1} of pp collisions collected at $\sqrt{s} = 8 \text{ TeV}$ with the ATLAS detector. ATLAS-CONF-2013-029, 2013.
- [918] ATLAS Collaboration. Study of the spin of the new boson with up to 25 fb^{-1} of ATLAS data. ATLAS-CONF-2013-040, 2013.

- [919] ATLAS Collaboration. Study of the spin properties of the Higgs-like boson in the $H \rightarrow WW^{(*)} \rightarrow e\nu\mu\nu$ channel with 21 fb^{-1} of $\sqrt{s} = 8 \text{ TeV}$ data collected with the ATLAS detector. ATLAS-CONF-2013-031, 2013.
- [920] ATLAS Collaboration. TeV-scale jet energy calibration using multijet events including close-by jet effects at the ATLAS experiment. ATLAS-CONF-2013-003, 2013.
- [921] ATLAS Collaboration. Transverse momentum, rapidity, and centrality dependence of inclusive charged-particle production in $\sqrt{s_{NN}} = 5.02 \text{ TeV}$ $p+p$ collisions measured by the ATLAS experiment. ATLAS-CONF-2013-107, 2013.
- [922] ATLAS Collaboration. Triggers for displaced decays of long-lived neutral particles in the ATLAS detector. *JINST*, 8:P07015, 2013.
- [923] ATLAS Collaboration. *Phys. Lett. B*, 734:406, 2014.
- [924] ATLAS Collaboration. *JHEP*, 01:109, 2014.
- [925] ATLAS Collaboration. A general search for new phenomena with the ATLAS detector in $p+p$ collisions at $\sqrt{s} = 8 \text{ TeV}$. ATLAS-CONF-2014-006, 2014.
- [926] ATLAS Collaboration. A Leakage Current-based Measurement of the Radiation Damage in the ATLAS Pixel Detector. ATL-INDET-PUB-2014-004, 2014.
- [927] ATLAS Collaboration. A measurement of single hadron response using data at $\sqrt{s} = 8 \text{ TeV}$ with the ATLAS detector. ATL-PHYS-PUB-2014-002, 2014.
- [928] ATLAS Collaboration. A measurement of the ratio of the production cross sections for W and Z bosons in association with jets with the ATLAS detector. *Eur. Phys. J. C*, 74:3168, 2014.
- [929] ATLAS Collaboration. A measurement of the ratio of the production cross sections for W and Z bosons in association with jets with the ATLAS detector. ATLAS-CONF-2014-034, 2014.
- [930] ATLAS Collaboration. A neural network clustering algorithm for the ATLAS silicon pixel detector. *JINST*, 9:P09009, 2014.
- [931] ATLAS Collaboration. A search for resonant Higgs-pair production in the $b\bar{b}b\bar{b}$ final state in $p+p$ collisions at $\sqrt{s} = 8 \text{ TeV}$. ATLAS-CONF-2014-005, 2014.

- [932] ATLAS Collaboration. A study of Standard Model Higgs boson production in the decay mode $H \rightarrow b\bar{b}$ in association with a W or Z boson for High Luminosity LHC Running. ATL-PHYS-PUB-2014-011, 2014.
- [933] ATLAS Collaboration. Alignment of the ATLAS Inner Detector and its Performance in 2012. ATLAS-CONF-2014-047, 2014.
- [934] ATLAS Collaboration. ATLAS interpretation of the combined measurements of coupling properties of the Higgs boson in terms of its production cross sections. ATL-PHYS-PUB-2014-009, 2014.
- [935] ATLAS Collaboration. ATLAS Pixel IBL: Stave Quality Assurance. ATL-INDET-PUB-2014-006, 2014.
- [936] ATLAS Collaboration. ATLAS Pythia 8 tunes to 7 TeV data. ATL-PHYS-PUB-2014-021, 2014.
- [937] ATLAS Collaboration. b -tagging in dense environments. ATL-PHYS-PUB-2014-014, 2014.
- [938] ATLAS Collaboration. Basic ATLAS TRT performance studies of Run 1. ATL-INDET-PUB-2014-001, 2014.
- [939] ATLAS Collaboration. Calibration of b -tagging using dileptonic top pair events in a combinatorial likelihood approach with the ATLAS experiment. ATLAS-CONF-2014-004, 2014.
- [940] ATLAS Collaboration. Calibration of the performance of b -tagging for c and light-flavour jets in the 2012 ATLAS data. ATLAS-CONF-2014-046, 2014.
- [941] ATLAS Collaboration. Centrality and rapidity dependence of inclusive jet production in $\sqrt{s_{NN}} = 5.02$ TeV proton–lead collisions with the ATLAS detector. ATLAS-CONF-2014-024, 2014.
- [942] ATLAS Collaboration. Centrality, rapidity and p_T dependence of isolated prompt photon production in lead–lead collisions at $\sqrt{s_{NN}} = 2.76$ TeV with the ATLAS detector at the LHC. ATLAS-CONF-2014-026, 2014.
- [943] ATLAS Collaboration. Charged hadron production in $p+Pb$ collisions at $\sqrt{s_{NN}} = 5.02$ TeV measured at high transverse momentum by the ATLAS experiment. ATLAS-CONF-2014-029, 2014.
- [944] ATLAS Collaboration. Common Framework Implementation for the Track-Based Alignment of the ATLAS Detector. ATL-SOFT-PUB-2014-003, 2014.
- [945] ATLAS Collaboration. Comparison of Monte Carlo generator predictions for bottom and charm hadrons in the decays of top quarks and the fragmentation of high p_T jets. ATL-PHYS-PUB-2014-008, 2014.

- [946] ATLAS Collaboration. Comparison of Monte Carlo generator predictions for gap fraction and jet multiplicity observables in $t\bar{t}$ events. ATL-PHYS-PUB-2014-005, 2014.
- [947] ATLAS Collaboration. Comparison of the response of the ATLAS detector to electromagnetic processes in data at 8 TeV and simulation using different GEANT4 setups. ATL-PHYS-PUB-2014-003, 2014.
- [948] ATLAS Collaboration. Comprehensive measurements of t-channel single top-quark production cross sections at $\sqrt{s} = 7$ TeV with the ATLAS detector. *Phys. Rev. D*, 90:112006, 2014.
- [949] ATLAS Collaboration. Constraints on New Phenomena via Higgs Boson Coupling Measurements with the ATLAS Detector. ATLAS-CONF-2014-010, 2014.
- [950] ATLAS Collaboration. Determination of the off-shell Higgs boson signal strength in the high-mass ZZ final state with the ATLAS detector. ATLAS-CONF-2014-042, 2014.
- [951] ATLAS Collaboration. Determination of the top-quark pole mass using $t\bar{t}+1$ -jet events collected with the ATLAS experiment in 7 TeV pp collisions. ATLAS-CONF-2014-053, 2014.
- [952] ATLAS Collaboration. Differential top–antitop production cross-section measurements in pp collisions at $\sqrt{s} = 7$ TeV as a function of pseudo-top-quark observables in the single-lepton channel using the ATLAS detector. ATLAS-CONF-2014-059, 2014.
- [953] ATLAS Collaboration. Electron and photon energy calibration with the ATLAS detector using LHC Run 1 data. *Eur. Phys. J. C*, 74:3071, 2014.
- [954] ATLAS Collaboration. Electron efficiency measurements with the ATLAS detector using the 2012 LHC proton–proton collision data. ATLAS-CONF-2014-032, 2014.
- [955] ATLAS Collaboration. Electron reconstruction and identification efficiency measurements with the ATLAS detector using the 2011 LHC proton–proton collision data. *Eur. Phys. J. C*, 74:2941, 2014.
- [956] ATLAS Collaboration. Electron reconstruction and identification efficiency measurements with the ATLAS detector using the 2011 LHC proton-proton collision data. *Eur. Phys. J. C*, 74(7):2941, 2014.
- [957] ATLAS Collaboration. Estimation of non-prompt and fake lepton backgrounds in final states with top quarks produced in proton–proton collisions at $\sqrt{s} = 8$ TeV with the ATLAS Detector. ATLAS-CONF-2014-058, 2014.

- [958] ATLAS Collaboration. Evidence for Electroweak Production of $W^\pm W^\pm jj$ in pp Collisions at $\sqrt{s} = 8$ TeV with the ATLAS Detector. *Phys. Rev. Lett.*, 113:141803, 2014.
- [959] ATLAS Collaboration. Evidence for Higgs-Boson Yukawa couplings in the $H \rightarrow \tau\tau$ decay mode with the ATLAS detector. ATLAS-CONF-2014-061, 2014.
- [960] ATLAS Collaboration. Evidence for the associated production of a vector boson (W, Z) and top quark pair in the dilepton and trilepton channels in pp collision data at $\sqrt{s} = 8$ TeV collected by the ATLAS detector at the LHC. ATLAS-CONF-2014-038, 2014.
- [961] ATLAS Collaboration. Evidence of the electroweak production of $W^\pm W^\pm jj$ in pp collisions at $\sqrt{s} = 8$ TeV with the ATLAS detector. ATLAS-CONF-2014-013, 2014.
- [962] ATLAS Collaboration. Fiducial and differential cross sections of Higgs boson production measured in the four-lepton decay channel in pp collisions at $\sqrt{s} = 8$ TeV with the ATLAS detector. *Phys. Lett. B*, 738:234, 2014.
- [963] ATLAS Collaboration. Flavor Tagging with Track-Jets in Boosted Topologies with the ATLAS Detector. ATL-PHYS-PUB-2014-013, 2014.
- [964] ATLAS Collaboration. Flavour tagged time-dependent angular analysis of the $B_s^0 \rightarrow J/\psi \phi$ decay and extraction of $\Delta\Gamma_s$ and the weak phase ϕ_s in ATLAS. *Phys. Rev. D*, 90:052007, 2014.
- [965] ATLAS Collaboration. HL-LHC projections for signal and background yield measurements of the $H \rightarrow \gamma\gamma$ when the Higgs boson is produced in association with t quarks, W or Z bosons. ATL-PHYS-PUB-2014-012, 2014.
- [966] ATLAS Collaboration. Inclusive and differential fiducial cross sections of Higgs boson production measured in the $H \rightarrow ZZ^* \rightarrow 4\ell$ decay channel using $\sqrt{s} = 8$ TeV pp collision data recorded by the ATLAS detector. ATLAS-CONF-2014-044, 2014.
- [967] ATLAS Collaboration. Light-quark and gluon jet discrimination in pp collisions at $\sqrt{s} = 7$ TeV with the ATLAS detector. *Eur. Phys. J. C*, 74:3023, 2014.
- [968] ATLAS Collaboration. Limits on metastable gluinos from ATLAS SUSY searches at 8 TeV. ATLAS-CONF-2014-037, 2014.
- [969] ATLAS Collaboration. Measurement of χ_{c1} and χ_{c2} production with $\sqrt{s} = 7$ TeV pp collisions at ATLAS. *JHEP*, 07:154, 2014.

- [970] ATLAS Collaboration. Measurement of differential production cross-sections for a Z boson in association with b -jets in 7 TeV proton–proton collisions with the ATLAS detector. *JHEP*, 10:141, 2014.
- [971] ATLAS Collaboration. Measurement of dijet cross sections in $p\bar{p}$ collisions at 7 TeV centre-of-mass energy using the ATLAS detector. *JHEP*, 05:059, 2014.
- [972] ATLAS Collaboration. Measurement of distributions sensitive to the underlying event in inclusive Z -boson production in $p\bar{p}$ collisions at $\sqrt{s} = 7$ TeV with the ATLAS detector. *Eur. Phys. J. C*, 74:3195, 2014.
- [973] ATLAS Collaboration. Measurement of event-plane correlations in $\sqrt{s_{NN}} = 2.76$ TeV lead–lead collisions with the ATLAS detector. *Phys. Rev. C*, 90:024905, 2014.
- [974] ATLAS Collaboration. Measurement of flow harmonics with multi-particle cumulants in Pb+Pb collisions at $\sqrt{s_{NN}} = 2.76$ TeV with the ATLAS detector. ATLAS-CONF-2014-027, 2014.
- [975] ATLAS Collaboration. Measurement of flow harmonics with multi-particle cumulants in Pb+Pb collisions at $\sqrt{s_{NN}} = 2.76$ TeV with the ATLAS detector. *Eur. Phys. J. C*, 74:3157, 2014.
- [976] ATLAS Collaboration. Measurement of Higgs boson production in the diphoton decay channel in $p\bar{p}$ collisions at center-of-mass energies of 7 and 8 TeV with the ATLAS detector. *Phys. Rev. D*, 90:112015, 2014.
- [977] ATLAS Collaboration. Measurement of inclusive jet charged-particle fragmentation functions in Pb+Pb collisions at $\sqrt{s_{NN}} = 2.76$ TeV with the ATLAS detector. *Phys. Lett. B*, 739:320, 2014.
- [978] ATLAS Collaboration. Measurement of long-range pseudorapidity correlations and azimuthal harmonics in $\sqrt{s_{NN}} = 5.02$ TeV proton–lead collisions with the ATLAS detector. *Phys. Rev. C*, 90:044906, 2014.
- [979] ATLAS Collaboration. Measurement of long-range pseudorapidity correlations and azimuthal harmonics in $\sqrt{s_{NN}} = 5.02$ TeV proton–lead collisions with the ATLAS detector. ATLAS-CONF-2014-021, 2014.
- [980] ATLAS Collaboration. Measurement of spin correlation in top–antitop quark events and search for top squark pair production in proton–proton collisions at $\sqrt{s} = 8$ TeV using the ATLAS detector. ATLAS-CONF-2014-056, 2014.
- [981] ATLAS Collaboration. Measurement of the centrality and pseudorapidity dependence of the integrated elliptic flow in lead–lead collisions at $\sqrt{s_{NN}} = 2.76$ TeV with the ATLAS detector. *Eur. Phys. J. C*, 74:2982, 2014.

- [982] ATLAS Collaboration. Measurement of the correlation between elliptic flow and higher-order flow harmonics in lead–lead collisions at $\sqrt{s_{\text{NN}}} = 2.76$ TeV. ATLAS-CONF-2014-022, 2014.
- [983] ATLAS Collaboration. Measurement of the cross-section of high transverse momentum vector bosons reconstructed as single jets and studies of jet substructure in pp collisions at $\sqrt{s} = 7$ TeV with the ATLAS detector. *New J. Phys.*, 16:113013, 2014.
- [984] ATLAS Collaboration. Measurement of the cross section of high transverse momentum $Z \rightarrow b\bar{b}$ production in proton–proton collisions at $\sqrt{s} = 8$ TeV with the ATLAS Detector. *Phys. Lett. B*, 738:25, 2014.
- [985] ATLAS Collaboration. Measurement of the differential cross-section of highly boosted top quarks as a function of their transverse momentum using the ATLAS detector in $\sqrt{s} = 8$ TeV proton–proton collisions. ATLAS-CONF-2014-057, 2014.
- [986] ATLAS Collaboration. Measurement of the electroweak production of dijets in association with a Z-boson and distributions sensitive to vector boson fusion in proton–proton collisions at $\sqrt{s} = 8$ TeV using the ATLAS detector. *JHEP*, 04:031, 2014.
- [987] ATLAS Collaboration. Measurement of the Higgs boson mass from the $H \rightarrow \gamma\gamma$ and $H \rightarrow ZZ^* \rightarrow 4\ell$ channels in pp collisions at center-of-mass energies of 7 and 8 TeV with the ATLAS detector. *Phys. Rev. D*, 90:052004, 2014.
- [988] ATLAS Collaboration. Measurement of the Inclusive and Fiducial Cross-Section of Single Top-Quark t-Channel Events in pp Collisions at $\sqrt{s} = 8$ TeV. ATLAS-CONF-2014-007, 2014.
- [989] ATLAS Collaboration. Measurement of the inclusive isolated prompt photons cross section in pp collisions at $\sqrt{s} = 7$ TeV with the ATLAS detector using 4.6 fb^{-1} . *Phys. Rev. D*, 89:052004, 2014.
- [990] ATLAS Collaboration. Measurement of the low-mass Drell-Yan differential cross section at $\sqrt{s} = 7$ TeV using the ATLAS detector. *JHEP*, 06:112, 2014.
- [991] ATLAS Collaboration. Measurement of the mass difference between top and anti-top quarks in pp collisions at $\sqrt{s} = 7$ TeV using the ATLAS detector. *Phys. Lett. B*, 728:363, 2014.
- [992] ATLAS Collaboration. Measurement of the muon reconstruction performance of the ATLAS detector using 2011 and 2012 LHC proton–proton collision data. *Eur. Phys. J. C*, 74:3130, 2014.

- [993] ATLAS Collaboration. Measurement of the parity-violating asymmetry parameter α_b and the helicity amplitudes for the decay $\Lambda_b \rightarrow J/\psi + \Lambda$ with the ATLAS detector. *Phys. Rev. D*, 89:092009, 2014.
- [994] ATLAS Collaboration. Measurement of the production cross section of prompt J/ψ mesons in association with a W^\pm boson in $p\bar{p}$ collisions at $\sqrt{s} = 7$ TeV with the ATLAS detector. *JHEP*, 04:172, 2014.
- [995] ATLAS Collaboration. Measurement of the production cross-section of $\psi(2S) \rightarrow J/\psi(\rightarrow \mu^+\mu^-)\pi^+\pi^-$ in $p\bar{p}$ collisions at $\sqrt{s} = 7$ TeV at ATLAS. *JHEP*, 09:079, 2014.
- [996] ATLAS Collaboration. Measurement of the production of a W boson in association with a charm quark in $p\bar{p}$ collisions at $\sqrt{s} = 7$ TeV with the ATLAS detector. *JHEP*, 05:068, 2014.
- [997] ATLAS Collaboration. Measurement of the production of neighbouring jets in lead–lead collisions at $\sqrt{s_{NN}} = 2.76$ TeV with the ATLAS detector. ATLAS-CONF-2014-028, 2014.
- [998] ATLAS Collaboration. Measurement of the $t\bar{t}$ production cross-section using $e\mu$ events with b-tagged jets in $p\bar{p}$ collisions at $\sqrt{s} = 7$ and 8 TeV with the ATLAS detector. *Eur. Phys. J. C*, 74:3109, 2014.
- [999] ATLAS Collaboration. Measurement of the top quark mass in topologies enhanced with single top quarks produced in the t-channel at $\sqrt{s} = 8$ TeV using the ATLAS experiment. ATLAS-CONF-2014-055, 2014.
- [1000] ATLAS Collaboration. Measurement of the top quark pair production charge asymmetry in proton–proton collisions at $\sqrt{s} = 7$ TeV using the ATLAS detector. *JHEP*, 02:107, 2014.
- [1001] ATLAS Collaboration. Measurement of the total cross section from elastic scattering in $p\bar{p}$ collisions at $\sqrt{s} = 7$ TeV with the ATLAS detector. *Nucl. Phys. B*, 889:486, 2014.
- [1002] ATLAS Collaboration. Measurement of the total cross section from elastic scattering in $p\bar{p}$ collisions at $\sqrt{s} = 7$ TeV with the ATLAS detector. ATLAS-CONF-2014-040, 2014.
- [1003] ATLAS Collaboration. Measurement of the underlying event in jet events from 7 TeV proton–proton collisions with the ATLAS detector. *Eur. Phys. J. C*, 74:2965, 2014.
- [1004] ATLAS Collaboration. Measurement of the Z/γ^* boson transverse momentum distribution in $p\bar{p}$ collisions at $\sqrt{s} = 7$ TeV with the ATLAS detector. *JHEP*, 09:145, 2014.

- [1005] ATLAS Collaboration. Measurement of three-jet production cross-sections in pp collisions at 7 TeV centre-of-mass energy using the ATLAS detector. ATLAS-CONF-2014-045, 2014.
- [1006] ATLAS Collaboration. Measurement of W boson production and the lepton charge asymmetry in PbPb collisions at $\sqrt{s_{\text{NN}}} = 2.76$ TeV with the ATLAS detector. ATLAS-CONF-2014-023, 2014.
- [1007] ATLAS Collaboration. Measurement of W^+W^- production cross section in pp collisions at $\sqrt{s} = 8$ TeV with the ATLAS detector. ATLAS-CONF-2014-033, 2014.
- [1008] ATLAS Collaboration. Measurements of fiducial and differential cross sections for Higgs boson production in the diphoton decay channel at $\sqrt{s} = 8$ TeV with ATLAS. *JHEP*, 09:112, 2014.
- [1009] ATLAS Collaboration. Measurements of Four-Lepton Production at the Z Resonance in pp Collisions at $\sqrt{s} = 7$ and 8 TeV with ATLAS. *Phys. Rev. Lett.*, 112:231806, 2014.
- [1010] ATLAS Collaboration. Measurements of jet vetoes and azimuthal decorrelations in dijet events produced in pp collisions at $\sqrt{s} = 7$ TeV using the ATLAS detector. *Eur. Phys. J. C*, 74:3117, 2014.
- [1011] ATLAS Collaboration. Measurements of normalized differential cross-sections for $t\bar{t}$ production in pp collisions at $\sqrt{s} = 7$ TeV using the ATLAS detector. *Phys. Rev. D*, 90:072004, 2014.
- [1012] ATLAS Collaboration. Measurements of spin correlation in top–antitop quark events from proton–proton collisions at $\sqrt{s} = 7$ TeV using the ATLAS detector. *Phys. Rev. D*, 90:112016, 2014.
- [1013] ATLAS Collaboration. Measurements of the nuclear modification factor for jets in $\text{Pb}+\text{Pb}$ collisions at $\sqrt{s_{\text{NN}}} = 2.76$ TeV with the ATLAS detector. ATLAS-CONF-2014-025, 2014.
- [1014] ATLAS Collaboration. Measurements of the W production cross sections in association with jets with the ATLAS detector. ATLAS-CONF-2014-035, 2014.
- [1015] ATLAS Collaboration. Monitoring and data quality assessment of the ATLAS liquid argon calorimeter. *JINST*, 9:P07024, 2014.
- [1016] ATLAS Collaboration. Muon reconstruction efficiency and momentum resolution of the ATLAS experiment in proton–proton collisions at $\sqrt{s} = 7$ TeV in 2010. *Eur. Phys. J. C*, 74:3034, 2014.

- [1017] ATLAS Collaboration. Observation and measurement of Higgs boson decays to WW^* with ATLAS at the LHC. ATLAS-CONF-2014-060, 2014.
- [1018] ATLAS Collaboration. Observation of an Excited B_c^\pm Meson State with the ATLAS Detector. *Phys. Rev. Lett.*, 113:212004, 2014.
- [1019] ATLAS Collaboration. Operation and performance of the ATLAS semiconductor tracker. *JINST*, 9:P08009, 2014.
- [1020] ATLAS Collaboration. Performance of Boosted W Boson Identification with the ATLAS Detector. ATL-PHYS-PUB-2014-004, 2014.
- [1021] ATLAS Collaboration. Performance of shower deconstruction in ATLAS. ATLAS-CONF-2014-003, 2014.
- [1022] ATLAS Collaboration. Performance of the Fast ATLAS Tracking Simulation (FATRAS) and the ATLAS Fast Calorimeter Simulation (FastCaloSim) with single particles. ATL-SOFT-PUB-2014-01, 2014.
- [1023] ATLAS Collaboration. Pile-up Correction in Missing Transverse Momentum Reconstruction in the ATLAS Experiment in Proton–Proton Collisions at $\sqrt{s} = 8$ TeV. ATLAS-CONF-2014-019, 2014.
- [1024] ATLAS Collaboration. Projections for measurements of Higgs boson signal strengths and coupling parameters with the ATLAS detector at the HL-LHC. ATL-PHYS-PUB-2014-016, 2014.
- [1025] ATLAS Collaboration. Prospects for measuring Higgs pair production in the channel $H(\rightarrow \gamma\gamma)H(\rightarrow b\bar{b})$ using the ATLAS detector at the HL-LHC. ATL-PHYS-PUB-2014-019, 2014.
- [1026] ATLAS Collaboration. Prospects for New Physics in Higgs Couplings Studies with the ATLAS Detector at the HL-LHC. ATL-PHYS-PUB-2014-017, 2014.
- [1027] ATLAS Collaboration. Reconstruction and Modelling of Jet Pull with the ATLAS Detector. ATLAS-CONF-2014-048, 2014.
- [1028] ATLAS Collaboration. Search for a multi-Higgs-boson cascade in $W^+W^-b\bar{b}$ events with the ATLAS detector in $p\bar{p}$ collisions at $\sqrt{s} = 8$ TeV. *Phys. Rev. D*, 89:032002, 2014.
- [1029] ATLAS Collaboration. Search for a WZ resonance in the fully leptonic channel using $p\bar{p}$ collisions at $\sqrt{s} = 8$ TeV with the ATLAS detector. ATLAS-CONF-2014-015, 2014.

- [1030] ATLAS Collaboration. Search for charged Higgs bosons decaying via $H^\pm \rightarrow \tau^\pm \nu$ in hadronic final states using $p\bar{p}$ collision data at $\sqrt{s} = 8$ TeV with the ATLAS detector. ATLAS-CONF-2014-050, 2014.
- [1031] ATLAS Collaboration. Search for contact interactions and large extra dimensions in the dilepton channel using proton–proton collisions at $\sqrt{s} = 8$ TeV with the ATLAS detector. *Eur. Phys. J. C*, 74:3134, 2014.
- [1032] ATLAS Collaboration. Search for contact interactions and large extra dimensions in the dilepton channel using proton–proton collisions at $\sqrt{s} = 8$ TeV with the ATLAS detector. ATLAS-CONF-2014-030, 2014.
- [1033] ATLAS Collaboration. Search for dark matter in events with a hadronically decaying W or Z boson and missing transverse momentum in $p\bar{p}$ collisions at $\sqrt{s} = 8$ TeV with the ATLAS detector. *Phys. Rev. Lett.*, 112:041802, 2014.
- [1034] ATLAS Collaboration. Search for dark matter in events with a Z boson and missing transverse momentum in $p\bar{p}$ collisions at $\sqrt{s} = 8$ TeV with the ATLAS detector. *Phys. Rev. D*, 90:012004, 2014.
- [1035] ATLAS Collaboration. Search for direct pair production of the top squark in all-hadronic final states in proton–proton collisions at $\sqrt{s} = 8$ TeV with the ATLAS detector. *JHEP*, 09:015, 2014.
- [1036] ATLAS Collaboration. Search for direct production of charginos and neutralinos decaying via the 125 GeV Higgs boson in $\sqrt{s} = 8$ TeV $p\bar{p}$ collisions with the ATLAS detector. ATLAS-CONF-2014-062, 2014.
- [1037] ATLAS Collaboration. Search for direct production of charginos and neutralinos in events with three leptons and missing transverse momentum in $\sqrt{s} = 8$ TeV $p\bar{p}$ collisions with the ATLAS detector. *JHEP*, 04:169, 2014.
- [1038] ATLAS Collaboration. Search for direct production of charginos, neutralinos and sleptons in final states with two leptons and missing transverse momentum in $p\bar{p}$ collisions at $\sqrt{s} = 8$ TeV with the ATLAS detector. *JHEP*, 05:071, 2014.
- [1039] ATLAS Collaboration. Search for direct top squark pair production in events with a Z boson, b -jets and missing transverse momentum in $\sqrt{s} = 8$ TeV $p\bar{p}$ collisions with the ATLAS detector. *Eur. Phys. J. C*, 74:2883, 2014.
- [1040] ATLAS Collaboration. Search for direct top-squark pair production in final states with two leptons in $p\bar{p}$ collisions at $\sqrt{s} = 8$ TeV with the ATLAS detector. *JHEP*, 06:124, 2014.

- [1041] ATLAS Collaboration. Search for $H \rightarrow \gamma\gamma$ produced in association with top quarks and constraints on the top quark-Higgs boson Yukawa coupling using data taken at 7 TeV and 8 TeV with the ATLAS detector. ATLAS-CONF-2014-043, 2014.
- [1042] ATLAS Collaboration. Search for Higgs boson decays to a photon and a Z boson in pp collisions at $\sqrt{s} = 7$ and 8 TeV with the ATLAS detector. *Phys. Lett. B*, 732:8, 2014.
- [1043] ATLAS Collaboration. Search for high-mass dilepton resonances in pp collisions at $\sqrt{s} = 8$ TeV with the ATLAS detector. *Phys. Rev. D*, 90:052005, 2014.
- [1044] ATLAS Collaboration. Search for high-mass states with one lepton plus missing transverse momentum in pp collisions at $\sqrt{s} = 8$ TeV with the ATLAS detector. ATLAS-CONF-2014-017, 2014.
- [1045] ATLAS Collaboration. Search for Invisible Decays of a Higgs Boson Produced in Association with a Z Boson in ATLAS. *Phys. Rev. Lett.*, 112:201802, 2014.
- [1046] ATLAS Collaboration. Search for long-lived neutral particles decaying into lepton jets in proton-proton collisions at $\sqrt{s} = 8$ TeV with the ATLAS detector. *JHEP*, 11:088, 2014.
- [1047] ATLAS Collaboration. Search for microscopic black holes and string balls in final states with leptons and jets with the ATLAS detector at $\sqrt{s} = 8$ TeV. *JHEP*, 08:103, 2014.
- [1048] ATLAS Collaboration. Search for microscopic black holes and string balls in final states with leptons and jets with the ATLAS detector at $\sqrt{s} = 8$ TeV. ATLAS-CONF-2014-016, 2014.
- [1049] ATLAS Collaboration. Search for neutral Higgs bosons of the minimal supersymmetric standard model in pp collisions at $\sqrt{s} = 8$ TeV with the ATLAS detector. *JHEP*, 11:056, 2014.
- [1050] ATLAS Collaboration. Search for neutral Higgs bosons of the Minimal Supersymmetric Standard Model in pp collisions at $\sqrt{s} = 8$ TeV with the ATLAS detector. ATLAS-CONF-2014-049, 2014.
- [1051] ATLAS Collaboration. Search for new particles in events with one lepton and missing transverse momentum in pp collisions at $\sqrt{s} = 8$ TeV with the ATLAS detector. *JHEP*, 09:037, 2014.

- [1052] ATLAS Collaboration. Search for new phenomena in events with a photon and missing transverse momentum in pp collisions at $\sqrt{s} = 8$ TeV with the ATLAS detector. ATLAS-CONF-2014-051, 2014.
- [1053] ATLAS Collaboration. Search for new phenomena in photon+jet events collected in proton–proton collisions at $\sqrt{s} = 8$ TeV with the ATLAS detector. *Phys. Lett. B*, 728:562, 2014.
- [1054] ATLAS Collaboration. Search for new resonances in $W\gamma$ and $Z\gamma$ Final States in pp Collisions at $\sqrt{s} = 8$ TeV with the ATLAS Detector. *Phys. Lett. B*, 738:428, 2014.
- [1055] ATLAS Collaboration. Search for nonpointing and delayed photons in the diphoton and missing transverse momentum final state in 8 TeV pp collisions at the LHC using the ATLAS detector. *Phys. Rev. D*, 90:112005, 2014.
- [1056] ATLAS Collaboration. Search for pair and single production of new heavy quarks that decay to a Z boson and a third-generation quark in pp collisions at $\sqrt{s} = 8$ TeV with the ATLAS detector. *JHEP*, 11:104, 2014.
- [1057] ATLAS Collaboration. Search for pair produced long-lived neutral particles decaying in the ATLAS hadronic calorimeter in pp collisions at $\sqrt{s} = 8$ TeV. ATLAS-CONF-2014-041, 2014.
- [1058] ATLAS Collaboration. Search for pair-produced third-generation squarks decaying via charm quarks or in compressed supersymmetric scenarios in pp collisions at $\sqrt{s} = 8$ TeV with the ATLAS detector. *Phys. Rev. D*, 90:052008, 2014.
- [1059] ATLAS Collaboration. Search for pair production of new heavy quarks that decay to a Z boson and a third generation quark in pp collisions at $\sqrt{s} = 8$ TeV with the ATLAS detector. ATLAS-CONF-2014-036, 2014.
- [1060] ATLAS Collaboration. Search for Quantum Black Hole Production in High-Invariant-Mass Lepton+Jet Final States Using pp Collisions at $\sqrt{s} = 8$ TeV and the ATLAS Detector. *Phys. Rev. Lett.*, 112:091804, 2014.
- [1061] ATLAS Collaboration. Search for resonant diboson production in the $\ell^+\ell^-q\bar{q}$ final state in pp collisions at $\sqrt{s} = 8$ TeV with the ATLAS detector. ATLAS-CONF-2014-039, 2014.
- [1062] ATLAS Collaboration. Search for Scalar-Charm Pair-Production with the ATLAS Detector in pp Collisions at $\sqrt{s} = 8$ TeV. ATLAS-CONF-2014-063, 2014.

- [1063] ATLAS Collaboration. Search for Scalar Diphoton Resonances in the Mass Range 65–600 GeV with the ATLAS Detector in pp Collision Data at $\sqrt{s} = 8$ TeV. *Phys. Rev. Lett.*, 113:171801, 2014.
- [1064] ATLAS Collaboration. Search for scalar diphoton resonances in the mass range 65–600 GeV with the ATLAS detector in pp collision data at $\sqrt{s} = 8$ TeV. ATLAS-CONF-2014-031, 2014.
- [1065] ATLAS Collaboration. Search for squarks and gluinos with the ATLAS detector in final states with jets and missing transverse momentum using $\sqrt{s} = 8$ TeV proton–proton collision data. *JHEP*, 09:176, 2014.
- [1066] ATLAS Collaboration. Search for strong production of supersymmetric particles in final states with missing transverse momentum and at least three b-jets at $\sqrt{s} = 8$ TeV proton–proton collisions with the ATLAS detector. *JHEP*, 10:024, 2014.
- [1067] ATLAS Collaboration. Search for supersymmetry at $\sqrt{s} = 8$ TeV in final states with jets and two same-sign leptons or three leptons with the ATLAS detector. *JHEP*, 06:035, 2014.
- [1068] ATLAS Collaboration. Search for Supersymmetry at the high luminosity LHC with the ATLAS Detector. ATL-PHYS-PUB-2014-010, 2014.
- [1069] ATLAS Collaboration. Search for supersymmetry in events with four or more leptons in $\sqrt{s} = 8$ TeV pp collisions with the ATLAS detector. *Phys. Rev. D*, 90:052001, 2014.
- [1070] ATLAS Collaboration. Search for supersymmetry in events with large missing transverse momentum, jets, and at least one tau lepton in 20 fb^{-1} of $\sqrt{s} = 8$ TeV proton–proton collision data with the ATLAS detector. *JHEP*, 09:103, 2014.
- [1071] ATLAS Collaboration. Search for the direct pair production of top squarks decaying to a b-quark, a tau lepton, and weakly interacting particles in $\sqrt{s} = 8$ TeV pp collisions using 20 fb^{-1} of ATLAS data. ATLAS-CONF-2014-014, 2014.
- [1072] ATLAS Collaboration. Search for the direct production of charginos, neutralinos and staus in final states with at least two hadronically decaying taus and missing transverse momentum in pp collisions at $\sqrt{s} = 8$ TeV with the ATLAS detector. *JHEP*, 10:096, 2014.
- [1073] ATLAS Collaboration. Search for the lepton flavor violating decay $Z \rightarrow e\mu$ in pp collisions at $\sqrt{s} = 8$ TeV with the ATLAS detector. *Phys. Rev. D*, 90:072010, 2014.

- [1074] ATLAS Collaboration. Search for the Standard Model Higgs boson decay to $\mu^+\mu^-$ with the ATLAS detector. *Phys. Lett. B*, 738:68, 2014.
- [1075] ATLAS Collaboration. Search for the Standard Model Higgs boson produced in association with top quarks and decaying into $b\bar{b}$ in pp collisions at $\sqrt{s} = 8$ TeV with the ATLAS detector at the LHC. ATLAS-CONF-2014-011, 2014.
- [1076] ATLAS Collaboration. Search for top quark decays $t \rightarrow qH$ with $H \rightarrow \gamma\gamma$ using the ATLAS detector. *JHEP*, 06:008, 2014.
- [1077] ATLAS Collaboration. Search for top squark pair production in final states with one isolated lepton, jets, and missing transverse momentum in $\sqrt{s} = 8$ TeV pp collisions with the ATLAS detector. *JHEP*, 11:118, 2014.
- [1078] ATLAS Collaboration. Search for WZ resonances in the fully leptonic channel using pp collisions at $\sqrt{s} = 8$ TeV with the ATLAS detector. *Phys. Lett. B*, 737:223, 2014.
- [1079] ATLAS Collaboration. Sensitivity to WIMP Dark Matter in the Final States Containing Jets and Missing Transverse Momentum with the ATLAS Detector at 14 TeV LHC. ATL-PHYS-PUB-2014-007, 2014.
- [1080] ATLAS Collaboration. Standalone vertex finding in the ATLAS muon spectrometer. *JINST*, 9:P02001, 2014.
- [1081] ATLAS Collaboration. Studies of Monte Carlo generators in Higgs boson production for Run 2. ATL-PHYS-PUB-2014-022, 2014.
- [1082] ATLAS Collaboration. Studies of the VBF $H \rightarrow \tau_\ell \tau_{had}$ analysis at High Luminosity LHC conditions. ATL-PHYS-PUB-2014-018, 2014.
- [1083] ATLAS Collaboration. Studies of theoretical uncertainties on the measurement of the mass of the W boson at the LHC. ATL-PHYS-PUB-2014-015, 2014.
- [1084] ATLAS Collaboration. Study of heavy flavor quarks produced in association with top quark pairs at $\sqrt{s} = 7$ TeV using the ATLAS detector. *Phys. Rev. D*, 89:072012, 2014.
- [1085] ATLAS Collaboration. Tagging and suppression of pileup jets. ATL-PHYS-PUB-2014-001, 2014.
- [1086] ATLAS Collaboration. Tagging and suppression of pileup jets with the ATLAS detector. ATLAS-CONF-2014-018, 2014.
- [1087] ATLAS Collaboration. The ATLAS transverse-momentum trigger performance at the LHC in 2011. ATLAS-CONF-2014-002, 2014.

- [1088] ATLAS Collaboration. The differential production cross section of the $\phi(1020)$ meson in $\sqrt{s} = 7$ TeV pp collisions measured with the ATLAS detector. *Eur. Phys. J. C*, 74:2895, 2014.
- [1089] ATLAS Collaboration. Update of the prospects for the $H \rightarrow Z\gamma$ search at the High-Luminosity LHC. ATL-PHYS-PUB-2014-006, 2014.
- [1090] ATLAS Collaboration. Updated coupling measurements of the Higgs boson with the ATLAS detector using up to 25 fb^{-1} of proton–proton collision data. ATL-CONF-2014-009, 2014.
- [1091] ATLAS Collaboration. Using the size of clusters in the ATLAS pixel detector to reject spurious clusters and provide an initial estimate of track direction and position along the beam line. ATL-INDET-PUB-2014-005, 2014.
- [1092] ATLAS Collaboration. Z-boson production in p+Pb collisions at $\sqrt{s_{NN}} = 5.02$ TeV with the ATLAS detector at the LHC. ATL-CONF-2014-020, 2014.
- [1093] ATLAS Collaboration. *Phys. Rev. D*, 91:119901, 2015.
- [1094] ATLAS Collaboration. *Eur. Phys. J. C*, 75:370, 2015.
- [1095] ATLAS Collaboration. *Eur. Phys. J. C*, 75:408, 2015.
- [1096] ATLAS Collaboration. *JHEP*, 09:141, 2015.
- [1097] ATLAS Collaboration. *Phys. Rev. D*, 92:059903, 2015.
- [1098] ATLAS Collaboration. *Eur. Phys. J. C*, 75:463, 2015.
- [1099] ATLAS Collaboration. First look at pp collisions data at $\sqrt{s} = 13$ TeV in preparation for a search for squarks and gluinos in final states with jets and missing transverse momentum with the ATLAS detector. ATL-PHYS-PUB-2015-028, 2015.
- [1100] ATLAS Collaboration. A method for the construction of strongly reduced representations of ATLAS experimental uncertainties and the application thereof to the jet energy scale. ATL-PHYS-PUB-2015-014, 2015.
- [1101] ATLAS Collaboration. A morphing technique for signal modelling in a multi-dimensional space of coupling parameters. ATL-PHYS-PUB-2015-047, 2015.
- [1102] ATLAS Collaboration. A new tagger for the charge identification of b-jets. ATL-PHYS-PUB-2015-040, 2015.

- [1103] ATLAS Collaboration. A search for $t\bar{t}$ resonances using lepton-plus-jets events in proton–proton collisions at $\sqrt{s} = 8$ TeV with the ATLAS detector. *JHEP*, 08:148, 2015.
- [1104] ATLAS Collaboration. A search for B–L R-parity-violating scalar top decays in $\sqrt{s} = 8$ TeV pp collisions with the ATLAS experiment. ATLAS-CONF-2015-015, 2015.
- [1105] ATLAS Collaboration. A search for high-mass resonances decaying to $\tau^+\tau^-$ in pp collisions at $\sqrt{s} = 8$ TeV with the ATLAS detector. *JHEP*, 07:157, 2015.
- [1106] ATLAS Collaboration. A search for R-parity-violating scalar top decays in all-hadronic final states with the ATLAS detector in $\sqrt{s} = 8$ TeV pp collisions. ATLAS-CONF-2015-026, 2015.
- [1107] ATLAS Collaboration. A search for supersymmetry in events containing a leptonically decaying Z boson, jets and missing transverse momentum in $\sqrt{s} = 13$ TeV pp collisions with the ATLAS detector. ATLAS-CONF-2015-082, 2015.
- [1108] ATLAS Collaboration. A search for $t\bar{t}$ resonances using lepton plus jets events in proton–proton collisions at $\sqrt{s} = 8$ TeV with the ATLAS detector. ATLAS-CONF-2015-009, 2015.
- [1109] ATLAS Collaboration. A study of optimal parameter setting for MADGRAPH5_AMC@NLO + PYTHIA 8 matched setup. ATL-PHYS-PUB-2015-048, 2015.
- [1110] ATLAS Collaboration. A study of the sensitivity to the PYTHIA8 parton shower parameters of $t\bar{t}$ production measurements in pp collisions at $\sqrt{s} = 7$ TeV with the ATLAS experiment at the LHC. ATL-PHYS-PUB-2015-007, 2015.
- [1111] ATLAS Collaboration. Alignment of the ATLAS Inner Detector with the initial LHC data at $\sqrt{s} = 13$ TeV. ATL-PHYS-PUB-2015-031, 2015.
- [1112] ATLAS Collaboration. An imaging algorithm for vertex reconstruction for ATLAS Run-2. ATL-PHYS-PUB-2015-008, 2015.
- [1113] ATLAS Collaboration. Analysis of events with b-jets and a pair of leptons of the same charge in pp collisions at $\sqrt{s} = 8$ TeV with the ATLAS detector. *JHEP*, 10:150, 2015.
- [1114] ATLAS Collaboration. ATLAS Inner Detector Alignment Performance with February 2015 Cosmic Ray Data. ATL-PHYS-PUB-2015-009, 2015.

- [1115] ATLAS Collaboration. ATLAS Run 1 searches for direct pair production of third-generation squarks at the Large Hadron Collider. *Eur. Phys. J. C*, 75:510, 2015.
- [1116] ATLAS Collaboration. Boosted hadronic top identification at ATLAS for early 13 TeV data. ATL-PHYS-PUB-2015-053, 2015.
- [1117] ATLAS Collaboration. B^\pm mass reconstruction in $B^\pm \rightarrow J/\psi K^\pm$ decay at ATLAS at 13 TeV pp collisions at the LHC. ATLAS-CONF-2015-064, 2015.
- [1118] ATLAS Collaboration. Calibration of ATLAS b-tagging algorithms in dense jet environments. ATLAS-CONF-2016-001, 2015.
- [1119] ATLAS Collaboration. Centrality and rapidity dependence of inclusive jet production in $\sqrt{s_{NN}} = 5.02$ TeV proton-lead collisions with the ATLAS detector. *Phys. Lett. B*, 748:392, 2015.
- [1120] ATLAS Collaboration. Charged-particle distributions in $\sqrt{s} = 13$ TeV pp interactions measured with the ATLAS detector at the LHC. ATLAS-CONF-2015-028, 2015.
- [1121] ATLAS Collaboration. Classification of Events in the Combined ATLAS-LHCf Data Recorded During the p+Pb Collisions at $\sqrt{s_{NN}} = 5.02$ TeV. ATL-PHYS-PUB-2015-038, 2015.
- [1122] ATLAS Collaboration. Cluster Properties and Lorentz Angle Measurement in the 4-Layer Pixel Detector Using Cosmic Rays. ATL-PHYS-PUB-2015-012, 2015.
- [1123] ATLAS Collaboration. Combination of searches for strongly-produced supersymmetric particles with the ATLAS detector in proton-proton collisions at $\sqrt{s} = 8$ TeV. ATLAS-CONF-2015-011, 2015.
- [1124] ATLAS Collaboration. Combined searches for WW, WZ, and ZZ resonances in pp collisions at $\sqrt{s} = 8$ TeV with the ATLAS detector. ATLAS-CONF-2015-045, 2015.
- [1125] ATLAS Collaboration. Commissioning of the ATLAS b-tagging algorithms using t̄t events in early Run 2 data. ATL-PHYS-PUB-2015-039, 2015.
- [1126] ATLAS Collaboration. Commissioning of the reconstruction of hadronic tau lepton decays in ATLAS using pp collisions at $\sqrt{s} = 13$ TeV. ATL-PHYS-PUB-2015-025, 2015.
- [1127] ATLAS Collaboration. Comparison of Monte Carlo generator predictions from Powheg and Sherpa to ATLAS measurements of top pair production at 7 TeV. ATL-PHYS-PUB-2015-011, 2015.

- [1128] ATLAS Collaboration. Comparison of Monte Carlo generator predictions to ATLAS measurements of top pair production at 7 TeV. ATL-PHYS-PUB-2015-002, 2015.
- [1129] ATLAS Collaboration. Constraints on new phenomena via Higgs boson couplings and invisible decays with the ATLAS detector. *JHEP*, 11:206, 2015.
- [1130] ATLAS Collaboration. Constraints on promptly decaying supersymmetric particles with lepton-number- and R-parity-violating interactions using Run-1 ATLAS data. ATLAS-CONF-2015-018, 2015.
- [1131] ATLAS Collaboration. Constraints on the off-shell Higgs boson signal strength in the high-mass ZZ and WW final states with the ATLAS detector. *Eur. Phys. J. C*, 75:335, 2015.
- [1132] ATLAS Collaboration. Data-driven determination of the energy scale and resolution of jets reconstructed in the ATLAS calorimeters using dijet and multijet events at $\sqrt{s} = 8$ TeV. ATLAS-CONF-2015-017, 2015.
- [1133] ATLAS Collaboration. Detector level leading track underlying event distributions at 13 TeV measured in ATLAS. ATL-PHYS-PUB-2015-019, 2015.
- [1134] ATLAS Collaboration. Determination of spin and parity of the Higgs boson in the $WW^* \rightarrow e\nu\mu\nu$ decay channel with the ATLAS detector. *Eur. Phys. J. C*, 75:231, 2015.
- [1135] ATLAS Collaboration. Determination of the jet energy scale and resolution at ATLAS using Z/ γ -jet events in data at $\sqrt{s} = 8$ TeV. ATLAS-CONF-2015-057, 2015.
- [1136] ATLAS Collaboration. Determination of the Ratio of b-quark Fragmentation Fractions f_s/f_d in pp Collisions at $\sqrt{s} = 7$ TeV with the ATLAS Detector. *Phys. Rev. Lett.*, 115:262001, 2015.
- [1137] ATLAS Collaboration. Determination of the top-quark pole mass using $t\bar{t}$ + 1-jet events collected with the ATLAS experiment in 7 TeV pp collisions. *JHEP*, 10:121, 2015.
- [1138] ATLAS Collaboration. Differential top-antitop cross-section measurements as a function of observables constructed from final-state particles using pp collisions at $\sqrt{s} = 7$ TeV in the ATLAS detector. *JHEP*, 06:100, 2015.
- [1139] ATLAS Collaboration. Dijet resonance searches with the ATLAS detector at 14 TeV LHC. ATL-PHYS-PUB-2015-004, 2015.
- [1140] ATLAS Collaboration. Early Inner Detector Tracking Performance in the 2015 Data at $\sqrt{s} = 13$ TeV. ATL-PHYS-PUB-2015-051, 2015.

- [1141] ATLAS Collaboration. Electron identification measurements in ATLAS using $\sqrt{s} = 13$ TeV data with 50 ns bunch spacing. ATL-PHYS-PUB-2015-041, 2015.
- [1142] ATLAS Collaboration. Event Kinematic Distributions in Top-Quark Enriched Samples from $\sqrt{s} = 13$ TeV pp Collisions in the ATLAS Detector. ATL-PHYS-PUB-2015-017, 2015.
- [1143] ATLAS Collaboration. Evidence for single top-quark production in the s-channel in proton–proton collisions at $\sqrt{s} = 8$ TeV with the ATLAS detector using the Matrix Element Method. ATLAS-CONF-2015-047, 2015.
- [1144] ATLAS Collaboration. Evidence for the Higgs-boson Yukawa coupling to tau leptons with the ATLAS detector. *JHEP*, 04:117, 2015.
- [1145] ATLAS Collaboration. Evidence of $W\gamma\gamma$ Production in pp Collisions at $\sqrt{s} = 8$ TeV and Limits on Anomalous Quartic Gauge Couplings with the ATLAS Detector. *Phys. Rev. Lett.*, 115:031802, 2015.
- [1146] ATLAS Collaboration. Exclusive Jet Production with Forward Proton Tagging. Feasibility Studies for the AFP Project. ATL-PHYS-PUB-2015-003, 2015.
- [1147] ATLAS Collaboration. Expected Performance of Boosted Higgs ($\rightarrow b\bar{b}$) Boson Identification with the ATLAS Detector at $\sqrt{s} = 13$ TeV. ATL-PHYS-PUB-2015-035, 2015.
- [1148] ATLAS Collaboration. Expected performance of missing transverse momentum reconstruction for the ATLAS detector at $\sqrt{s} = 13$ TeV. ATL-PHYS-PUB-2015-023, 2015.
- [1149] ATLAS Collaboration. Expected performance of the ATLAS b-tagging algorithms in Run-2. ATL-PHYS-PUB-2015-022, 2015.
- [1150] ATLAS Collaboration. Expected sensitivity studies for gluino and squark searches using the early LHC 13 TeV Run-2 dataset with the ATLAS experiment. ATL-PHYS-PUB-2015-005, 2015.
- [1151] ATLAS Collaboration. Femtoscopy with identified charged pions in proton–lead collisions at $\sqrt{s_{NN}} = 5.02$ TeV with ATLAS. ATLAS-CONF-2015-054, 2015.
- [1152] ATLAS Collaboration. First look at proton–proton collision data at $\sqrt{s} = 13$ TeV in preparation for a search for squarks and gluinos in events with missing transverse energy, jets, and an isolated electron or muon. ATL-PHYS-PUB-2015-029, 2015.

- [1153] ATLAS Collaboration. First validation plots in preparation for a search for new phenomena in final states with large jet multiplicities and missing transverse momentum at $\sqrt{s} = 13$ TeV proton–proton collisions using the ATLAS experiment. ATL-PHYS-PUB-2015-030, 2015.
- [1154] ATLAS Collaboration. Forward Jet Vertex Tagging: A new technique for the identification and rejection of forward pileup jets. ATL-PHYS-PUB-2015-034, 2015.
- [1155] ATLAS Collaboration. Higgs Pair Production in the $H(\rightarrow \tau\tau)H(\rightarrow b\bar{b})$ Channel at the High-Luminosity LHC. ATL-PHYS-PUB-2015-046, 2015.
- [1156] ATLAS Collaboration. IBL Module Loading onto Stave and Quality Check. ATL-INDET-PUB-2015-003, 2015.
- [1157] ATLAS Collaboration. Identification and energy calibration of hadronically decaying tau leptons with the ATLAS experiment in $p\bar{p}$ collisions at $\sqrt{s} = 8$ TeV. *Eur. Phys. J. C*, 75:303, 2015.
- [1158] ATLAS Collaboration. Identification of Boosted, Hadronically-Decaying W and Z Bosons in $\sqrt{s} = 13$ TeV Monte Carlo Simulations for ATLAS. ATL-PHYS-PUB-2015-033, 2015.
- [1159] ATLAS Collaboration. Identification of high transverse momentum top quarks in $p\bar{p}$ collisions at $\sqrt{s} = 8$ TeV with the ATLAS detector. ATLAS-CONF-2015-036, 2015.
- [1160] ATLAS Collaboration. Impact of fragmentation modelling on the jet energy and the top-quark mass measurement using the ATLAS detector. ATL-PHYS-PUB-2015-042, 2015.
- [1161] ATLAS Collaboration. Inclusive spectra of isolated di-photon candidates using 6.4 pb^{-1} of $p\bar{p}$ collisions at $\sqrt{s} = 13$ TeV. ATL-PHYS-PUB-2015-020, 2015.
- [1162] ATLAS Collaboration. Internal structure of jets measured in Pb+Pb and $p\bar{p}$ collisions with the ATLAS detector at the LHC. ATLAS-CONF-2015-055, 2015.
- [1163] ATLAS Collaboration. Jet Calibration and Systematic Uncertainties for Jets Reconstructed in the ATLAS Detector at $\sqrt{s} = 13$ TeV. ATL-PHYS-PUB-2015-015, 2015.
- [1164] ATLAS Collaboration. Jet energy measurement and its systematic uncertainty in proton–proton collisions at $\sqrt{s} = 7$ TeV with the ATLAS detector. *Eur. Phys. J. C*, 75:17, 2015.

- [1165] ATLAS Collaboration. Jet energy scale and its uncertainty for jets reconstructed using the ATLAS heavy ion jet algorithm. ATLAS-CONF-2015-016, 2015.
- [1166] ATLAS Collaboration. Jet global sequential corrections with the ATLAS detector in proton–proton collisions at $\sqrt{s} = 8$ TeV. ATLAS-CONF-2015-002, 2015.
- [1167] ATLAS Collaboration. Kinematic distributions of $W \rightarrow l\nu$ and $Z \rightarrow ll$ production from $p\bar{p}$ collisions at $\sqrt{s} = 13$ TeV in the ATLAS detector. ATLAS-PHYS-PUB-2015-021, 2015.
- [1168] ATLAS Collaboration. Measurement of charged-particle spectra in Pb+Pb collisions at $\sqrt{s_{NN}} = 2.76$ TeV with the ATLAS detector at the LHC. *JHEP*, 09:050, 2015.
- [1169] ATLAS Collaboration. Measurement of colour flow with the jet pull angle in $t\bar{t}$ events using the ATLAS detector at $\sqrt{s} = 8$ TeV. *Phys. Lett. B*, 750:475, 2015.
- [1170] ATLAS Collaboration. Measurement of correlations between dijet-asymmetry and event-shape variables in Pb+Pb collisions at $\sqrt{s_{NN}} = 2.76$ TeV with the ATLAS detector at the LHC. ATLAS-CONF-2015-021, 2015.
- [1171] ATLAS Collaboration. Measurement of differential J/ψ production cross-sections and forward-backward ratios in $p + Pb$ collisions with the ATLAS detector. *Phys. Rev. C*, 92:034904, 2015.
- [1172] ATLAS Collaboration. Measurement of dijet p_T correlations in Pb+Pb and $p\bar{p}$ collisions at $\sqrt{s_{NN}} = 2.76$ TeV with the ATLAS detector. ATLAS-CONF-2015-052, 2015.
- [1173] ATLAS Collaboration. Measurement of exclusive $\gamma\gamma \rightarrow \ell^+\ell^-$ production in proton–proton collisions at $\sqrt{s} = 7$ TeV with the ATLAS detector. *Phys. Lett. B*, 749:242, 2015.
- [1174] ATLAS Collaboration. Measurement of forward-backward multiplicity correlations in lead–lead, proton–lead and proton–proton collisions with the ATLAS detector. ATLAS-CONF-2015-051, 2015.
- [1175] ATLAS Collaboration. Measurement of four-jet differential cross sections in $\sqrt{s} = 8$ TeV proton–proton collisions using the ATLAS detector. *JHEP*, 12:105, 2015.
- [1176] ATLAS Collaboration. Measurement of jet charge in dijet events from $\sqrt{s} = 8$ TeV $p\bar{p}$ collisions with the ATLAS detector. ATLAS-CONF-2015-025, 2015.

- [1177] ATLAS Collaboration. Measurement of jet fragmentation in 5.02 TeV proton–lead and 2.76 TeV proton–proton collisions with the ATLAS detector. ATLAS-CONF-2015-022, 2015.
- [1178] ATLAS Collaboration. Measurement of jets produced in top quark events using the di-lepton final state with 2 b-tagged jets in pp collisions at $\sqrt{s} = 13$ TeV with the ATLAS detector. ATLAS-CONF-2015-065, 2015.
- [1179] ATLAS Collaboration. Measurement of performance of the pixel neural network clustering algorithm of the ATLAS experiment at $\sqrt{s} = 13$ TeV. ATL-PHYS-PUB-2015-044, 2015.
- [1180] ATLAS Collaboration. Measurement of Spin Correlation in Top–Antitop Quark Events and Search for Top Squark Pair Production in pp Collisions at $\sqrt{s} = 8$ TeV Using the ATLAS Detector. *Phys. Rev. Lett.*, 114:142001, 2015.
- [1181] ATLAS Collaboration. Measurement of the branching ratio $\Gamma(\Lambda_b^0 \rightarrow \psi(2S)\Lambda^0)/\Gamma(\Lambda_b^0 \rightarrow J/\psi\Lambda^0)$ with the ATLAS detector. *Phys. Lett. B*, 751:63, 2015.
- [1182] ATLAS Collaboration. Measurement of the charge asymmetry in dileptonic decays of top quark pairs in pp collisions at $\sqrt{s} = 7$ TeV using the ATLAS detector. *JHEP*, 05:061, 2015.
- [1183] ATLAS Collaboration. Measurement of the charge asymmetry in highly boosted top-quark pair production in $\sqrt{s} = 8$ TeV pp collision data collected by the ATLAS experiment. ATLAS-CONF-2015-048, 2015.
- [1184] ATLAS Collaboration. Measurement of the correlation between flow harmonics of different order in lead–lead collisions at $\sqrt{s_{\text{NN}}} = 2.76$ TeV with the ATLAS detector. *Phys. Rev. C*, 92:034903, 2015.
- [1185] ATLAS Collaboration. Measurement of the dependence of transverse energy production at large pseudorapidity on the hard scattering kinematics of proton–proton collisions at $\sqrt{s} = 2.76$ TeV with ATLAS. ATLAS-CONF-2015-019, 2015.
- [1186] ATLAS Collaboration. Measurement of the differential cross-sections of prompt and non-prompt production of J/ψ and $\psi(2S)$ in pp collisions at $\sqrt{s} = 7$ and 8 TeV with the ATLAS detector. ATLAS-CONF-2015-024, 2015.
- [1187] ATLAS Collaboration. Measurement of the differential non-prompt J/ψ production fraction $\sqrt{s} = 13$ TeV pp collisions at the ATLAS experiment. ATLAS-CONF-2015-030, 2015.

- [1188] ATLAS Collaboration. Measurement of the forward-backward asymmetry of electron and muon pair-production in pp collisions at $\sqrt{s} = 7$ TeV with the ATLAS detector. *JHEP*, 09:049, 2015.
- [1189] ATLAS Collaboration. Measurement of the Higgs boson production cross section at 7, 8 and 13 TeV center-of-mass energies in the $H \rightarrow \gamma\gamma$ channel with the ATLAS detector. ATLAS-CONF-2015-060, 2015.
- [1190] ATLAS Collaboration. Measurement of the inclusive cross-section of single top-quark t-channel production in pp collisions at $\sqrt{s} = 13$ TeV. ATLAS-CONF-2015-079, 2015.
- [1191] ATLAS Collaboration. Measurement of the inclusive-jet cross section in proton–proton collisions at 13 TeV centre-of-mass energy with the ATLAS detector. ATLAS-CONF-2015-034, 2015.
- [1192] ATLAS Collaboration. Measurement of the inclusive jet cross-section in proton–proton collisions at $\sqrt{s} = 7$ TeV using 4.5 fb^{-1} of data with the ATLAS detector. *JHEP*, 02:153, 2015.
- [1193] ATLAS Collaboration. Measurement of the Inelastic Proton–Proton Cross-Section at $\sqrt{s} = 13$ TeV with the ATLAS Detector at the LHC. ATLAS-CONF-2015-038, 2015.
- [1194] ATLAS Collaboration. Measurement of the production and lepton charge asymmetry of W bosons in Pb+Pb collisions at $\sqrt{s_{\text{NN}}} = 2.76$ TeV with the ATLAS detector. *Eur. Phys. J. C*, 75:23, 2015.
- [1195] ATLAS Collaboration. Measurement of the Production Cross Sections of a Z Boson in Association with Jets in pp collisions at $\sqrt{s} = 13$ TeV with the ATLAS Detector. ATLAS-CONF-2015-041, 2015.
- [1196] ATLAS Collaboration. Measurement of the production of neighbouring jets in lead-lead collisions at $\sqrt{s_{\text{NN}}} = 2.76$ TeV with the ATLAS detector. *Phys. Lett. B*, 751:376, 2015.
- [1197] ATLAS Collaboration. Measurement of the suppression and elliptic anisotropy of heavy flavor muons in Pb+Pb collisions at $\sqrt{s_{\text{NN}}} = 2.76$ TeV with the ATLAS detector. ATLAS-CONF-2015-053, 2015.
- [1198] ATLAS Collaboration. Measurement of the $t\bar{t}$ production cross-section as a function of jet multiplicity and jet transverse momentum in 7 TeV proton–proton collisions with the ATLAS detector. *JHEP*, 01:020, 2015.
- [1199] ATLAS Collaboration. Measurement of the $t\bar{t}$ production cross-section in pp collisions at $\sqrt{s} = 13$ TeV using $e\mu$ events with b-tagged jets. ATLAS-CONF-2015-033, 2015.

- [1200] ATLAS Collaboration. Measurement of the $t\bar{t}W$ and $t\bar{t}Z$ production cross sections in pp collisions at $\sqrt{s} = 8$ TeV with the ATLAS detector. ATLAS-CONF-2015-032, 2015.
- [1201] ATLAS Collaboration. Measurement of the $t\bar{t}W$ and $t\bar{t}Z$ production cross sections in pp collisions at $\sqrt{s} = 8$ TeV with the ATLAS detector. *JHEP*, 11:172, 2015.
- [1202] ATLAS Collaboration. Measurement of the top pair production cross section in 8 TeV proton–proton collisions using kinematic information in the lepton+jets final state with ATLAS. *Phys. Rev. D*, 91:112013, 2015.
- [1203] ATLAS Collaboration. Measurement of the top quark branching ratios into channels with leptons and quarks with the ATLAS detector. *Phys. Rev. D*, 92:072005, 2015.
- [1204] ATLAS Collaboration. Measurement of the top-quark mass in the fully hadronic decay channel from ATLAS data at $\sqrt{s} = 7$ TeV. *Eur. Phys. J. C*, 75:158, 2015.
- [1205] ATLAS Collaboration. Measurement of the top quark mass in the $t\bar{t} \rightarrow$ lepton+jets and $t\bar{t} \rightarrow$ dilepton channels using $\sqrt{s} = 7$ TeV ATLAS data. *Eur. Phys. J. C*, 75:330, 2015.
- [1206] ATLAS Collaboration. Measurement of the $WW + WZ$ cross section and limits on anomalous triple gauge couplings using final states with one lepton, missing transverse momentum, and two jets with the ATLAS detector at $\sqrt{s} = 7$ TeV. *JHEP*, 01:049, 2015.
- [1207] ATLAS Collaboration. Measurement of three-jet production cross-sections in pp collisions at 7 TeV centre-of-mass energy using the ATLAS detector. *Eur. Phys. J. C*, 75:228, 2015.
- [1208] ATLAS Collaboration. Measurement of transverse energy–energy correlations in multi-jet events in pp collisions at $\sqrt{s} = 7$ TeV using the ATLAS detector and determination of the strong coupling constant $\alpha_s(m_Z)$. *Phys. Lett. B*, 750:427, 2015.
- [1209] ATLAS Collaboration. Measurement of two-particle correlations in $\sqrt{s} = 13$ TeV proton–proton collisions with the ATLAS detector at the LHC. ATLAS-CONF-2015-027, 2015.
- [1210] ATLAS Collaboration. Measurement of two-particle pseudorapidity correlations in lead–lead collisions at $\sqrt{s_{NN}} = 2.76$ TeV with the ATLAS detector. ATLAS-CONF-2015-020, 2015.

- [1211] ATLAS Collaboration. Measurement of $\Upsilon(nS)$ production with $p+Pb$ collisions at $\sqrt{s_{NN}} = 5.02$ TeV and $p\bar{p}$ collisions at $\sqrt{s} = 2.76$ TeV. ATLAS-CONF-2015-050, 2015.
- [1212] ATLAS Collaboration. Measurement of $W \rightarrow \mu\nu$ production in $p+Pb$ collisions at $\sqrt{s_{NN}} = 5.02$ TeV with the ATLAS Detector at the LHC. ATLAS-CONF-2015-056, 2015.
- [1213] ATLAS Collaboration. Measurement of W^\pm and Z Boson Production Cross Sections in $p\bar{p}$ Collisions at $\sqrt{s} = 13$ TeV with the ATLAS Detector. ATLAS-CONF-2015-039, 2015.
- [1214] ATLAS Collaboration. Measurements of four-lepton production in $p\bar{p}$ collisions at $\sqrt{s} = 8$ TeV with the ATLAS detector. ATLAS-CONF-2015-031, 2015.
- [1215] ATLAS Collaboration. Measurements of Higgs boson production and couplings in the four-lepton channel in $p\bar{p}$ collisions at center-of-mass energies of 7 and 8 TeV with the ATLAS detector. *Phys. Rev. D*, 91:012006, 2015.
- [1216] ATLAS Collaboration. Measurements of the Higgs boson production and decay rates and coupling strengths using $p\bar{p}$ collision data at $\sqrt{s} = 7$ and 8 TeV in the ATLAS experiment. ATLAS-CONF-2015-007, 2015.
- [1217] ATLAS Collaboration. Measurements of the Higgs boson production cross section at 7, 8 and 13 TeV centre-of-mass energies and search for new physics at 13 TeV in the $H \rightarrow ZZ^* \rightarrow \ell^+\ell^-\ell'^+\ell'^-$ final state with the ATLAS detector. ATLAS-CONF-2015-059, 2015.
- [1218] ATLAS Collaboration. Measurements of the Nuclear Modification Factor for Jets in $Pb+Pb$ Collisions at $\sqrt{s_{NN}} = 2.76$ TeV with the ATLAS Detector. *Phys. Rev. Lett.*, 114:072302, 2015.
- [1219] ATLAS Collaboration. Measurements of the $t\bar{t}$ production cross-section in the dilepton and lepton-plus-jets channels and of the ratio of the $t\bar{t}$ and Z boson cross-sections in $p\bar{p}$ collisions at $\sqrt{s} = 13$ TeV with the ATLAS detector. ATLAS-CONF-2015-049, 2015.
- [1220] ATLAS Collaboration. Measurements of the Total and Differential Higgs Boson Production Cross Sections Combining the $H \rightarrow \gamma\gamma$ and $H \rightarrow ZZ^* \rightarrow 4\ell$ Decay Channels at $\sqrt{s} = 8$ TeV with the ATLAS Detector. *Phys. Rev. Lett.*, 115:091801, 2015.
- [1221] ATLAS Collaboration. Measurements of the total cross sections for Higgs boson production combining the $H \rightarrow \gamma\gamma$ and $H \rightarrow ZZ^* \rightarrow 4\ell$ decay channels at 7, 8 and 13 TeV center-of-mass energies with the ATLAS detector. ATLAS-CONF-2015-069, 2015.

- [1222] ATLAS Collaboration. Measurements of the W production cross sections in association with jets with the ATLAS detector. *Eur. Phys. J. C*, 75:82, 2015.
- [1223] ATLAS Collaboration. Modelling $Z \rightarrow \tau\tau$ processes in ATLAS with τ -embedded $Z \rightarrow \mu\mu$ data. *JINST*, 10:P09018, 2015.
- [1224] ATLAS Collaboration. Monte Carlo Calibration and Combination of In-situ Measurements of Jet Energy Scale, Jet Energy Resolution and Jet Mass in ATLAS. ATLAS-CONF-2015-037, 2015.
- [1225] ATLAS Collaboration. Muon reconstruction performance in early $\sqrt{s} = 13$ TeV data. ATL-PHYS-PUB-2015-037, 2015.
- [1226] ATLAS Collaboration. Observation and measurement of Higgs boson decays to WW^* with the ATLAS detector. *Phys. Rev. D*, 92:012006, 2015.
- [1227] ATLAS Collaboration. Observation and measurements of the production of prompt and non-prompt J/ψ mesons in association with a Z boson in pp collisions at $\sqrt{s} = 8$ TeV with the ATLAS detector. *Eur. Phys. J. C*, 75:229, 2015.
- [1228] ATLAS Collaboration. Observation of top-quark pair production in association with a photon and measurement of the $t\bar{t}\gamma$ production cross section in pp collisions at $\sqrt{s} = 7$ TeV using the ATLAS detector. *Phys. Rev. D*, 91:072007, 2015.
- [1229] ATLAS Collaboration. Off-shell Higgs boson couplings measurement using $H \rightarrow ZZ \rightarrow 4\ell$ events at High Luminosity LHC . ATL-PHYS-PUB-2015-024, 2015.
- [1230] ATLAS Collaboration. Performance and Calibration of the JetFitterCharm Algorithm for c-Jet Identification. ATL-PHYS-PUB-2015-001, 2015.
- [1231] ATLAS Collaboration. Performance of jet substructure techniques in early $\sqrt{s} = 13$ TeV pp collisions with the ATLAS detector. ATLAS-CONF-2015-035, 2015.
- [1232] ATLAS Collaboration. Performance of missing transverse momentum reconstruction with the ATLAS detector in the first proton–proton collisions at $\sqrt{s} = 13$ TeV. ATL-PHYS-PUB-2015-027, 2015.
- [1233] ATLAS Collaboration. Performance of the ATLAS muon trigger in pp collisions at $\sqrt{s} = 8$ TeV. *Eur. Phys. J. C*, 75:120, 2015.

- [1234] ATLAS Collaboration. Properties of jets and inputs to jet reconstruction and calibration with the ATLAS detector using proton–proton collisions at $\sqrt{s} = 13$ TeV. ATL-PHYS-PUB-2015-036, 2015.
- [1235] ATLAS Collaboration. Proposal for particle-level object and observable definitions for use in physics measurements at the LHC. ATL-PHYS-PUB-2015-013, 2015.
- [1236] ATLAS Collaboration. Prospect for a search for direct pair production of a chargino and a neutralino decaying via aW boson and the lightest Higgs boson in final states with one lepton, two b-jets and missing transverse momentum at the high luminosity LHC with the ATLAS Detector. ATL-PHYS-PUB-2015-032, 2015.
- [1237] ATLAS Collaboration. Reconstruction, Energy Calibration, and Identification of Hadronically Decaying Tau Leptons in the ATLAS Experiment for Run-2 of the LHC. ATL-PHYS-PUB-2015-045, 2015.
- [1238] ATLAS Collaboration. Reconstruction of J/ ψ mesons in t \bar{t} final states in proton–proton collisions at $\sqrt{s} = 8$ TeV with the ATLAS detector. ATLAS-CONF-2015-040, 2015.
- [1239] ATLAS Collaboration. Robustness of the Artificial Neural Network Clustering Algorithm of the ATLAS experiment. ATL-PHYS-PUB-2015-052, 2015.
- [1240] ATLAS Collaboration. Search for a Charged Higgs Boson Produced in the Vector-Boson Fusion Mode with Decay H $^\pm \rightarrow W^\pm Z$ using pp Collisions at $\sqrt{s} = 8$ TeV with the ATLAS Experiment. *Phys. Rev. Lett.*, 114:231801, 2015.
- [1241] ATLAS Collaboration. Search for a CP-odd Higgs boson decaying to Zh in pp collisions at $\sqrt{s} = 8$ TeV with the ATLAS detector. *Phys. Lett. B*, 744:163, 2015.
- [1242] ATLAS Collaboration. Search for a Heavy Neutral Particle Decaying to e μ , e τ , or $\mu\tau$ in pp Collisions at $\sqrt{s} = 8$ TeV with the ATLAS Detector. *Phys. Rev. Lett.*, 115:031801, 2015.
- [1243] ATLAS Collaboration. Search for a new resonance decaying to a W or Z boson and a Higgs boson in the $\ell\ell/\ell\nu/\nu\nu + b\bar{b}$ final states with the ATLAS detector. *Eur. Phys. J. C*, 75:263, 2015.
- [1244] ATLAS Collaboration. Search for an Invisibly Decaying Higgs Boson Produced via Vector Boson Fusion in pp Collisions at $\sqrt{s} = 8$ TeV using the ATLAS Detector at the LHC. ATLAS-CONF-2015-004, 2015.

- [1245] ATLAS Collaboration. Search for anomalous production of prompt same-sign lepton pairs and pair-produced doubly charged Higgs bosons with $\sqrt{s} = 8$ TeV pp collisions using the ATLAS detector. *JHEP*, 03:041, 2015.
- [1246] ATLAS Collaboration. Search for beyond the Standard Model phenomena in $e\mu$ final states in pp collisions at $\sqrt{s} = 13$ TeV with the ATLAS detector. ATLAS-CONF-2015-072, 2015.
- [1247] ATLAS Collaboration. Search for Bottom Squark Pair Production with the ATLAS Detector in Proton–Proton Collisions at $\sqrt{s} = 13$ TeV. ATLAS-CONF-2015-066, 2015.
- [1248] ATLAS Collaboration. Search for charged Higgs bosons decaying via $H^\pm \rightarrow \tau^\pm \nu$ in fully hadronic final states using pp collision data at $\sqrt{s} = 8$ TeV with the ATLAS detector. *JHEP*, 03:088, 2015.
- [1249] ATLAS Collaboration. Search for dark matter in events with heavy quarks and missing transverse momentum in pp collisions with the ATLAS detector. *Eur. Phys. J. C*, 75:92, 2015.
- [1250] ATLAS Collaboration. Search for Dark Matter in Events with Missing Transverse Momentum and a Higgs Boson Decaying to Two Photons in pp Collisions at $\sqrt{s} = 8$ TeV with the ATLAS Detector. *Phys. Rev. Lett.*, 115:131801, 2015.
- [1251] ATLAS Collaboration. Search for dark matter produced in association with a hadronically decaying vector boson in pp collisions at $\sqrt{s} = 13$ TeV with the ATLAS detector at the LHC. ATLAS-CONF-2015-080, 2015.
- [1252] ATLAS Collaboration. Search for diboson resonances in the $\ell\ell qq$ final state in pp collisions at $\sqrt{s} = 13$ TeV with the ATLAS detector. ATLAS-CONF-2015-071, 2015.
- [1253] ATLAS Collaboration. Search for diboson resonances in the $\nu\nu qq$ final state in pp collisions at $\sqrt{s} = 13$ TeV with the ATLAS detector. ATLAS-CONF-2015-068, 2015.
- [1254] ATLAS Collaboration. Search for direct pair production of a chargino and a neutralino decaying to the 125 GeV Higgs boson in $\sqrt{s} = 8$ TeV pp collisions with the ATLAS detector. *Eur. Phys. J. C*, 75:208, 2015.
- [1255] ATLAS Collaboration. Search for evidence for strong gravity in jet final states produced in pp collisions at $\sqrt{s} = 13$ TeV using the ATLAS detector at the LHC. ATLAS-CONF-2015-043, 2015.

- [1256] ATLAS Collaboration. Search for exotic Higgs-boson decays in events with at least one photon, missing transverse momentum, and two forward jets produced in $\sqrt{s} = 8$ TeV $p\bar{p}$ collisions with the ATLAS detector. ATLAS-CONF-2015-001, 2015.
- [1257] ATLAS Collaboration. Search for flavour-changing neutral current top quark decays $t \rightarrow Hq$ in $p\bar{p}$ collisions at $\sqrt{s} = 8$ TeV with the ATLAS detector. *JHEP*, 12:061, 2015.
- [1258] ATLAS Collaboration. Search for gluinos in events with an isolated lepton, jets and missing transverse momentum at $\sqrt{s} = 13$ TeV with the ATLAS detector. ATLAS-CONF-2015-076, 2015.
- [1259] ATLAS Collaboration. Search for $H \rightarrow \gamma\gamma$ produced in association with top quarks and constraints on the Yukawa coupling between the top quark and the Higgs boson using data taken at 7 TeV and 8 TeV with the ATLAS detector. *Phys. Lett. B*, 740:222, 2015.
- [1260] ATLAS Collaboration. Search for heavy lepton resonances decaying to a Z boson and a lepton in $p\bar{p}$ collisions at $\sqrt{s} = 8$ TeV with the ATLAS detector. *JHEP*, 09:108, 2015.
- [1261] ATLAS Collaboration. Search for heavy long-lived multi-charged particles in $p\bar{p}$ collisions at $\sqrt{s} = 8$ TeV using the ATLAS detector. *Eur. Phys. J. C*, 75:362, 2015.
- [1262] ATLAS Collaboration. Search for heavy Majorana neutrinos with the ATLAS detector in $p\bar{p}$ collisions at $\sqrt{s} = 8$ TeV. *JHEP*, 07:162, 2015.
- [1263] ATLAS Collaboration. Search for Higgs and Z Boson Decays to $J/\psi\gamma$ and $\Upsilon(nS)\gamma$ with the ATLAS Detector. *Phys. Rev. Lett.*, 114:121801, 2015.
- [1264] ATLAS Collaboration. Search for Higgs boson pair production in the $b\bar{b}b\bar{b}$ final state from $p\bar{p}$ collisions at $\sqrt{s} = 8$ TeV with the ATLAS detector. *Eur. Phys. J. C*, 75:412, 2015.
- [1265] ATLAS Collaboration. Search for Higgs Boson Pair Production in the $\gamma\gamma b\bar{b}$ Final State Using $p\bar{p}$ Collision Data at $\sqrt{s} = 8$ TeV from the ATLAS Detector. *Phys. Rev. Lett.*, 114:081802, 2015.
- [1266] ATLAS Collaboration. Search for Higgs bosons decaying to $\alpha\alpha$ in the $\mu\mu\tau\tau$ final state in $p\bar{p}$ collisions at $\sqrt{s} = 8$ TeV with the ATLAS experiment. *Phys. Rev. D*, 92:052002, 2015.

- [1267] ATLAS Collaboration. Search for high-mass diboson resonances with boson-tagged jets in proton–proton collisions at $\sqrt{s} = 8$ TeV with the ATLAS detector. *JHEP*, 12:055, 2015.
- [1268] ATLAS Collaboration. Search for high-mass diphoton resonances in pp collisions at $\sqrt{s} = 8$ TeV with the ATLAS detector. *Phys. Rev. D*, 92:032004, 2015.
- [1269] ATLAS Collaboration. Search for invisible decays of the Higgs boson produced in association with a hadronically decaying vector boson in pp collisions at $\sqrt{s} = 8$ TeV with the ATLAS detector. *Eur. Phys. J. C*, 75:337, 2015.
- [1270] ATLAS Collaboration. Search for invisible particles produced in association with single-top-quarks in proton–proton collisions at $\sqrt{s} = 8$ TeV with the ATLAS detector. *Eur. Phys. J. C*, 75:79, 2015.
- [1271] ATLAS Collaboration. Search for lepton-flavour-violating $H \rightarrow \mu\tau$ decays of the Higgs boson with the ATLAS detector. *JHEP*, 11:211, 2015.
- [1272] ATLAS Collaboration. Search for long-lived, weakly interacting particles that decay to displaced hadronic jets in proton–proton collisions at $\sqrt{s} = 8$ TeV with the ATLAS detector. *Phys. Rev. D*, 92:012010, 2015.
- [1273] ATLAS Collaboration. Search for low-scale gravity signatures in multi-jet final states with the ATLAS detector at $\sqrt{s} = 8$ TeV. *JHEP*, 07:032, 2015.
- [1274] ATLAS Collaboration. Search for massive, long-lived particles using multitrack displaced vertices or displaced lepton pairs in pp collisions at $\sqrt{s} = 8$ TeV with the ATLAS detector. *Phys. Rev. D*, 92:072004, 2015.
- [1275] ATLAS Collaboration. Search for massive supersymmetric particles decaying to many jets using the ATLAS detector in pp collisions at $\sqrt{s} = 8$ TeV. *Phys. Rev. D*, 91:112016, 2015.
- [1276] ATLAS Collaboration. Search for metastable heavy charged particles with large ionisation energy loss in pp collisions at $\sqrt{s} = 8$ TeV using the ATLAS experiment. *Eur. Phys. J. C*, 75:407, 2015.
- [1277] ATLAS Collaboration. Search for metastable heavy charged particles with large ionisation energy loss in pp collisions at $\sqrt{s} = 8$ TeV using the ATLAS experiment. ATLAS-CONF-2015-013, 2015.
- [1278] ATLAS Collaboration. Search for Neutral Minimal Supersymmetric Standard Model Higgs Bosons $H/A \rightarrow \tau\tau$ produced in pp collisions at $\sqrt{s} = 18$ TeV with the ATLAS Detector. ATLAS-CONF-2015-061, 2015.

- [1279] ATLAS Collaboration. Search for new light gauge bosons in Higgs boson decays to four-lepton final states in pp collisions at $\sqrt{s} = 8$ TeV with the ATLAS detector at the LHC. *Phys. Rev. D*, 92:092001, 2015.
- [1280] ATLAS Collaboration. Search for new light gauge bosons in Higgs boson decays to four-lepton final states in pp collisions at $\sqrt{s} = 8$ TeV with the ATLAS detector at the LHC. ATLAS-CONF-2015-003, 2015.
- [1281] ATLAS Collaboration. Search for New Phenomena in Dijet Angular Distributions in Proton–Proton Collisions at $\sqrt{s} = 8$ TeV Measured with the ATLAS Detector. *Phys. Rev. Lett.*, 114:221802, 2015.
- [1282] ATLAS Collaboration. Search for New Phenomena in Dijet Mass and Angular Distributions with the ATLAS Detector at $\sqrt{s} = 13$ TeV. ATLAS-CONF-2015-042, 2015.
- [1283] ATLAS Collaboration. Search for new phenomena in events with a photon and missing transverse momentum in pp collisions at $\sqrt{s} = 8$ TeV with the ATLAS detector. *Phys. Rev. D*, 91:012008, 2015.
- [1284] ATLAS Collaboration. Search for new phenomena in events with three or more charged leptons in pp collisions at $\sqrt{s} = 8$ TeV with the ATLAS detector. *JHEP*, 08:138, 2015.
- [1285] ATLAS Collaboration. Search for new phenomena in final states with an energetic jet and large missing transverse momentum in pp collisions at $\sqrt{s} = 8$ TeV with the ATLAS detector. *Eur. Phys. J. C*, 75:299, 2015.
- [1286] ATLAS Collaboration. Search for new phenomena in final states with large jet multiplicities and missing transverse momentum with ATLAS using $\sqrt{s} = 13$ TeV proton–proton collisions. ATLAS-CONF-2015-077, 2015.
- [1287] ATLAS Collaboration. Search for new phenomena in the dijet mass distribution using pp collision data at $\sqrt{s} = 8$ TeV with the ATLAS detector. *Phys. Rev. D*, 91:052007, 2015.
- [1288] ATLAS Collaboration. Search for new phenomena in the dilepton final state using proton–proton collisions at $\sqrt{s} = 13$ TeV with the ATLAS detector. ATLAS-CONF-2015-070, 2015.
- [1289] ATLAS Collaboration. Search for new resonances decaying to a W or Z boson and a Higgs boson in the $\ell\ell b\bar{b}$, $\ell\nu b\bar{b}$, and $\nu\nu b\bar{b}$ channels in pp collisions at $\sqrt{s} = 13$ TeV with the ATLAS Detector. ATLAS-CONF-2015-074, 2015.

- [1290] ATLAS Collaboration. Search for new resonances in events with one lepton and missing transverse momentum in pp collisions at $\sqrt{s} = 13$ TeV with the ATLAS detector. ATLAS-CONF-2015-063, 2015.
- [1291] ATLAS Collaboration. Search for pair-produced long-lived neutral particles decaying to jets in the ATLAS hadronic calorimeter in pp collisions at $\sqrt{s} = 8$ TeV. *Phys. Lett. B*, 743:15, 2015.
- [1292] ATLAS Collaboration. Search for pair production of a new heavy quark that decays into a W boson and a light quark in pp collisions at $\sqrt{s} = 8$ TeV with the ATLAS detector. *Phys. Rev. D*, 92:112007, 2015.
- [1293] ATLAS Collaboration. Search for pair-production of gluinos decaying via stop and sbottom in events with b -jets and large missing transverse momentum in $\sqrt{s} = 13$ TeV pp collisions with the ATLAS detector. ATLAS-CONF-2015-067, 2015.
- [1294] ATLAS Collaboration. Search for photonic signatures of gauge-mediated supersymmetry in 8 TeV pp collisions with the ATLAS detector. *Phys. Rev. D*, 92:072001, 2015.
- [1295] ATLAS Collaboration. Search for production of vector-like quark pairs and of four top quarks in the lepton-plus-jets final state in pp collisions at $\sqrt{s} = 8$ TeV with the ATLAS detector. *JHEP*, 08:105, 2015.
- [1296] ATLAS Collaboration. Search for production of vector-like quark pairs and of four top quarks in the lepton plus jets final state in pp collisions at $\sqrt{s} = 8$ TeV with the ATLAS detector. ATLAS-CONF-2015-012, 2015.
- [1297] ATLAS Collaboration. Search for production of WW/WZ resonances decaying to a lepton, neutrino and jets in pp collisions at $\sqrt{s} = 8$ TeV with the ATLAS detector. *Eur. Phys. J. C*, 75:209, 2015.
- [1298] ATLAS Collaboration. Search for resonances decaying to photon pairs in 3.2 fb^{-1} of pp collisions at $\sqrt{s} = 13$ TeV with the ATLAS detector. ATLAS-CONF-2015-081, 2015.
- [1299] ATLAS Collaboration. Search for resonances with boson-tagged jets in 3.2 fb^{-1} of pp collisions at $\sqrt{s} = 13$ TeV collected with the ATLAS detector. ATLAS-CONF-2015-073, 2015.
- [1300] ATLAS Collaboration. Search for resonant diboson production in the $\ell\ell q\bar{q}$ final state in pp collisions at $\sqrt{s} = 8$ TeV with the ATLAS detector. *Eur. Phys. J. C*, 75:69, 2015.

- [1301] ATLAS Collaboration. Search for s -channel single top-quark production in proton–proton collisions at $\sqrt{s} = 8$ TeV with the ATLAS detector. *Phys. Lett. B*, 740:118, 2015.
- [1302] ATLAS Collaboration. Search for Scalar Charm Quark Pair Production in pp Collisions at $\sqrt{s} = 8$ TeV with the ATLAS Detector. *Phys. Rev. Lett.*, 114:161801, 2015.
- [1303] ATLAS Collaboration. Search for squarks and gluinos in events with isolated leptons, jets and missing transverse momentum at $\sqrt{s} = 8$ TeV with the ATLAS detector. *JHEP*, 04:116, 2015.
- [1304] ATLAS Collaboration. Search for squarks and gluinos in final states with jets and missing transverse momentum at $\sqrt{s} = 13$ TeV with the ATLAS detector. ATLAS-CONF-2015-062, 2015.
- [1305] ATLAS Collaboration. Search for supersymmetry at $\sqrt{s} = 13$ TeV in final states with jets and two same-sign leptons or three leptons with the ATLAS detector. ATLAS-CONF-2015-078, 2015.
- [1306] ATLAS Collaboration. Search for supersymmetry in events containing a same-flavour opposite-sign dilepton pair, jets, and large missing transverse momentum in $\sqrt{s} = 8$ TeV pp collisions with the ATLAS detector. *Eur. Phys. J. C*, 75:318, 2015.
- [1307] ATLAS Collaboration. Search for TeV-scale gravity signatures in high-mass final states with leptons and jets with the ATLAS detector at $\sqrt{s} = 13$ TeV. ATLAS-CONF-2015-046, 2015.
- [1308] ATLAS Collaboration. Search for the associated production of the Higgs boson with a top quark pair in multi-lepton final states with the ATLAS detector. ATLAS-CONF-2015-006, 2015.
- [1309] ATLAS Collaboration. Search for the associated production of the Higgs boson with a top quark pair in multilepton final states with the ATLAS detector. *Phys. Lett. B*, 749:519, 2015.
- [1310] ATLAS Collaboration. Search for the $b\bar{b}$ decay of the Standard Model Higgs boson in associated $(W/Z)H$ production with the ATLAS detector. *JHEP*, 01:069, 2015.
- [1311] ATLAS Collaboration. Search for the Standard Model Higgs and Z Boson decays to $J/\psi\gamma$: HL-LHC projections. ATL-PHYS-PUB-2015-043, 2015.
- [1312] ATLAS Collaboration. Search for the Standard Model Higgs boson produced in association with top quarks and decaying into $b\bar{b}$ in pp collisions at $\sqrt{s} = 8$ TeV with the ATLAS detector. *Eur. Phys. J. C*, 75:349, 2015.

- [1313] ATLAS Collaboration. Search for the X_b and other hidden-beauty states in the $\pi^+\pi^-\Upsilon(1S)$ channel at ATLAS. *Phys. Lett. B*, 740:199, 2015.
- [1314] ATLAS Collaboration. Search for type-III seesaw heavy leptons in pp collisions at $\sqrt{s} = 8$ TeV with the ATLAS Detector. *Phys. Rev. D*, 92:032001, 2015.
- [1315] ATLAS Collaboration. Search for vectorlike B quarks in events with one isolated lepton, missing transverse momentum, and jets at $\sqrt{s} = 8$ TeV with the ATLAS detector. *Phys. Rev. D*, 91:112011, 2015.
- [1316] ATLAS Collaboration. Search for $W' \rightarrow tb \rightarrow qqbb$ decays in pp collisions at $\sqrt{s} = 8$ TeV with the ATLAS detector. *Eur. Phys. J. C*, 75:165, 2015.
- [1317] ATLAS Collaboration. Search for $W' \rightarrow t\bar{b}$ in the lepton plus jets final state in proton–proton collisions at a centre-of-mass energy of $\sqrt{s} = 8$ TeV with the ATLAS detector. *Phys. Lett. B*, 743:235, 2015.
- [1318] ATLAS Collaboration. Search for WW/WZ resonance production in the $\ell\nu qq$ final state at $\sqrt{s} = 13$ TeV with the ATLAS detector at the LHC. ATLAS-CONF-2015-075, 2015.
- [1319] ATLAS Collaboration. Searches for heavy long-lived charged particles with the ATLAS detector in proton–proton collisions at $\sqrt{s} = 8$ TeV. *JHEP*, 01:068, 2015.
- [1320] ATLAS Collaboration. Searches for Higgs boson pair production in the $hh \rightarrow bb\tau\tau, \gamma\gamma WW^*, \gamma\gamma bb, bbbb$ channels with the ATLAS detector. *Phys. Rev. D*, 92:092004, 2015.
- [1321] ATLAS Collaboration. Selection of jets produced in 13 TeV proton–proton collisions with the ATLAS detector. ATLAS-CONF-2015-029, 2015.
- [1322] ATLAS Collaboration. Simultaneous measurements of the $t\bar{t}$, W^+W^- , and $Z/\gamma^* \rightarrow \tau\tau$ production cross-sections in pp collisions at $\sqrt{s} = 7$ TeV with the ATLAS detector. *Phys. Rev. D*, 91:052005, 2015.
- [1323] ATLAS Collaboration. Statistical combination of all-hadronic and one-lepton analyses targeting scalar top pair production using proton–proton collisions at $\sqrt{s} = 8$ TeV with the ATLAS detector. ATLAS-CONF-2015-010, 2015.
- [1324] ATLAS Collaboration. Stereo Information in Micromegas Detectors. ATL-MUON-PUB-2015-001, 2015.
- [1325] ATLAS Collaboration. Studies of the ATLAS Inner Detector material using $\sqrt{s} = 13$ TeV pp collision data. ATL-PHYS-PUB-2015-050, 2015.

- [1326] ATLAS Collaboration. Study of correlation of PDF uncertainty in single top and top pair production at the LHC. ATL-PHYS-PUB-2015-010, 2015.
- [1327] ATLAS Collaboration. Study of hard double parton scattering in four-jet events in pp collisions at $\sqrt{s} = 7$ TeV with the ATLAS experiment at the LHC. ATLAS-CONF-2015-058, 2015.
- [1328] ATLAS Collaboration. Study of inclusive isolated-photon production in pp collisions at $\sqrt{s} = 13$ TeV with the ATLAS detector. ATL-PHYS-PUB-2015-016, 2015.
- [1329] ATLAS Collaboration. Study of J/ψ and $\psi(2S)$ production in $\sqrt{s_{\text{NN}}} = 5.02$ TeV p+Pb and $\sqrt{s} = 2.76$ TeV pp collisions with the ATLAS detector. ATLAS-CONF-2015-023, 2015.
- [1330] ATLAS Collaboration. Study of the $B_c^+ \rightarrow J/\psi D_s^+$ and $B_c^+ \rightarrow J/\psi D_s^{*+}$ decays with the ATLAS detector. ATLAS-CONF-2015-014, 2015.
- [1331] ATLAS Collaboration. Study of the Higgs boson decaying to WW^* produced in association with a weak boson with the ATLAS detector at the LHC. ATLAS-CONF-2015-005, 2015.
- [1332] ATLAS Collaboration. Study of the mechanical stability of the ATLAS Insertable B-Layer. ATL-INDET-PUB-2015-001, 2015.
- [1333] ATLAS Collaboration. Study of the spin and parity of the Higgs boson in di-boson decays with the ATLAS detector. ATLAS-CONF-2015-008, 2015.
- [1334] ATLAS Collaboration. Study of the spin and parity of the Higgs boson in diboson decays with the ATLAS detector. *Eur. Phys. J. C*, 75:476, 2015.
- [1335] ATLAS Collaboration. Study of $(W/Z)H$ production and Higgs boson couplings using $H \rightarrow WW^*$ decays with the ATLAS detector. *JHEP*, 08:137, 2015.
- [1336] ATLAS Collaboration. Summary of the ATLAS experiment's sensitivity to supersymmetry after LHC Run 1 — interpreted in the phenomenological MSSM. *JHEP*, 10:134, 2015.
- [1337] ATLAS Collaboration. Summary of the searches for squarks and gluinos using $\sqrt{s} = 8$ TeV pp collisions with the ATLAS experiment at the LHC. *JHEP*, 10:054, 2015.
- [1338] ATLAS Collaboration. Texas Instruments TPS7H1101-SP Fast Neutron Irradiation Results. ATL-MUON-PUB-2015-002, 2015.

- [1339] ATLAS Collaboration. The Optimization of ATLAS Track Reconstruction in Dense Environments. ATL-PHYS-PUB-2015-006, 2015.
- [1340] ATLAS Collaboration. Track Reconstruction Performance of the ATLAS Inner Detector at $\sqrt{s} = 13$ TeV. ATL-PHYS-PUB-2015-018, 2015.
- [1341] ATLAS Collaboration. Two-particle Bose-Einstein correlations in $p\bar{p}$ collisions at $\sqrt{s} = 0.9$ and 7 TeV measured with the ATLAS detector. *Eur. Phys. J. C*, 75:466, 2015.
- [1342] ATLAS Collaboration. Upgrade plans for the Hadronic Endcap Calorimeter of ATLAS for the high luminosity stage of the LHC. ATL-LARG-PUB-2015-001, 2015.
- [1343] ATLAS Collaboration. Vertex Reconstruction Performance of the ATLAS Detector at $\sqrt{s} = 13$ TeV. ATL-PHYS-PUB-2015-026, 2015.
- [1344] ATLAS Collaboration. Z boson production in $p + Pb$ collisions at $\sqrt{s_{NN}} = 5.02$ TeV measured with the ATLAS detector. *Phys. Rev. C*, 92:044915, 2015.
- [1345] ATLAS Collaboration. *Eur. Phys. J. C*, 76:152, 2016.
- [1346] ATLAS Collaboration. *Phys. Rev. D*, 93:039901, 2016.
- [1347] ATLAS Collaboration. 2015 start-up trigger menu and initial performance assessment of the ATLAS trigger using Run-2 data. ATL-DAQ-PUB-2016-001, 2016.
- [1348] ATLAS Collaboration. A measurement of material in the ATLAS tracker using secondary hadronic interactions in 7 TeV $p\bar{p}$ collisions. 2016.
- [1349] ATLAS Collaboration. A new method to distinguish hadronically decaying boosted Z bosons from W bosons using the ATLAS detector. *Eur. Phys. J. C*, 76:238, 2016.
- [1350] ATLAS Collaboration. A re-interpretation of $\sqrt{s} = 8$ TeV ATLAS results on electroweak supersymmetry production to explore general gauge mediated models. ATLAS-CONF-2016-033, 2016.
- [1351] ATLAS Collaboration. A search for an excited muon decaying to a muon and two jets in $p\bar{p}$ collisions at $\sqrt{s} = 8$ TeV with the ATLAS detector. *New J. Phys.*, 18:073021, 2016.
- [1352] ATLAS Collaboration. A search for new phenomena in events with missing transverse momentum and a Higgs boson decaying to two photons in a 13.3 fb^{-1} $p\bar{p}$ collision dataset at $\sqrt{s} = 13$ TeV with the ATLAS detector. ATLAS-CONF-2016-087, 2016.

- [1353] ATLAS Collaboration. A search for pair produced resonances in four-jet final states in proton–proton collisions at $\sqrt{s} = 13$ TeV with the ATLAS experiment. ATLAS-CONF-2016-084, 2016.
- [1354] ATLAS Collaboration. A search for prompt lepton-jets in pp collisions at $\sqrt{s} = 8$ TeV with the ATLAS detector. *JHEP*, 02:062, 2016.
- [1355] ATLAS Collaboration. A Search for Resonances Decaying to a W or Z Boson and a Higgs Boson in the $q\bar{q}^{(\prime)}b\bar{b}$ Final State. ATLAS-CONF-2016-083, 2016.
- [1356] ATLAS Collaboration. A search for top squarks with R-parity-violating decays to all-hadronic final states with the ATLAS detector in $\sqrt{s} = 8$ TeV proton–proton collisions. *JHEP*, 06:067, 2016.
- [1357] ATLAS Collaboration. Beam-induced and cosmic-ray backgrounds observed in the ATLAS detector during the LHC 2012 proton–proton running period. *JINST*, 11:P05013, 2016.
- [1358] ATLAS Collaboration. Boosted Higgs ($\rightarrow b\bar{b}$) Boson Identification with the ATLAS Detector at $\sqrt{s} = 13$ TeV. ATLAS-CONF-2016-039, 2016.
- [1359] ATLAS Collaboration. Boosted Object Tagging with Variable-R Jets in the ATLAS Detector. ATL-PHYS-PUB-2016-013, 2016.
- [1360] ATLAS Collaboration. Centrality, rapidity and transverse momentum dependence of isolated prompt photon production in lead–lead collisions at $\sqrt{s_{\text{NN}}} = 2.76$ TeV measured with the ATLAS detector. *Phys. Rev. C*, 93:034914, 2016.
- [1361] ATLAS Collaboration. Charged-particle distributions at low transverse momentum in $\sqrt{s} = 13$ TeV pp interactions measured with the ATLAS detector at the LHC. *Eur. Phys. J. C*, 76:502, 2016.
- [1362] ATLAS Collaboration. Charged-particle distributions in pp interactions at $\sqrt{s} = 8$ TeV measured with the ATLAS detector. *Eur. Phys. J. C*, 76:403, 2016.
- [1363] ATLAS Collaboration. Charged-particle distributions in $\sqrt{s} = 13$ TeV pp interactions measured with the ATLAS detector at the LHC. *Phys. Lett. B*, 758:67, 2016.
- [1364] ATLAS Collaboration. Combination of searches for WW , WZ , and ZZ resonances in pp collisions at $\sqrt{s} = 8$ TeV with the ATLAS detector. *Phys. Lett. B*, 755:285, 2016.

- [1365] ATLAS Collaboration. Combination of the searches for Higgs boson production in association with top quarks in the $\gamma\gamma$, multilepton, and $b\bar{b}$ decay channels at $\sqrt{s} = 13$ TeV with the ATLAS Detector. ATLAS-CONF-2016-068, 2016.
- [1366] ATLAS Collaboration. Combined measurements of the Higgs boson production and decay rates in $H \rightarrow ZZ^* \rightarrow 4\ell$ and $H \rightarrow \gamma\gamma$ final states using pp collision data at $\sqrt{s} = 13$ TeV in the ATLAS experiment. ATLAS-CONF-2016-081, 2016.
- [1367] ATLAS Collaboration. Constraints on non-Standard Model Higgs boson interactions in an effective Lagrangian using differential cross sections measured in the $H \rightarrow \gamma\gamma$ decay channel at $\sqrt{s} = 8$ TeV with the ATLAS detector. *Phys. Lett. B*, 753:69, 2016.
- [1368] ATLAS Collaboration. Dark matter interpretations of ATLAS searches for the electroweak production of supersymmetric particles in $\sqrt{s} = 8$ TeV proton–proton collisions. *JHEP*, 09:175, 2016.
- [1369] ATLAS Collaboration. Dijet production in $\sqrt{s} = 7$ TeV pp collisions with large rapidity gaps at the ATLAS experiment. *Phys. Lett. B*, 754:214, 2016.
- [1370] ATLAS Collaboration. Discrimination between Light Quark and Gluon Jets in pp collisions at $\sqrt{s} = 8$ TeV with the ATLAS Detector. ATLAS-CONF-2016-034, 2016.
- [1371] ATLAS Collaboration. Efficiency and Hit Spatial Resolution of ATLAS IBL Sensors in LHC Run 2 Collision Events. ATL-INDET-PUB-2016-001, 2016.
- [1372] ATLAS Collaboration. Electron and photon energy calibration with the ATLAS detector using data collected in 2015 at $\sqrt{s} = 13$ TeV. ATL-PHYS-PUB-2016-015, 2016.
- [1373] ATLAS Collaboration. Electron efficiency measurements with the ATLAS detector using the 2015 LHC proton–proton collision data. ATLAS-CONF-2016-024, 2016.
- [1374] ATLAS Collaboration. Estimate of the m_H shift due to interference between signal and background processes in the $H \rightarrow \gamma\gamma$ channel, for the $\sqrt{s} = 8$ TeV dataset recorded by ATLAS. ATL-PHYS-PUB-2016-009, 2016.
- [1375] ATLAS Collaboration. Evidence for single top-quark production in the s-channel in proton–proton collisions at $\sqrt{s} = 8$ TeV with the ATLAS detector using the Matrix Element Method. *Phys. Lett. B*, 756:228, 2016.

- [1376] ATLAS Collaboration. Expected performance for an upgraded ATLAS detector at High-Luminosity LHC. ATL-PHYS-PUB-2016-026, 2016.
- [1377] ATLAS Collaboration. Expected performance for displaced Lepton Jets: ATLAS trigger and reconstruction efficiency in LHC 2015 run. ATL-PHYS-PUB-2016-010, 2016.
- [1378] ATLAS Collaboration. Expected Performance of the ATLAS Inner Tracker at the High-Luminosity LHC. ATL-PHYS-PUB-2016-025, 2016.
- [1379] ATLAS Collaboration. Expected sensitivity of ATLAS to FCNC top quark decays $t \rightarrow Zq$ and $t \rightarrow Hq$ at the High Luminosity LHC. ATL-PHYS-PUB-2016-019, 2016.
- [1380] ATLAS Collaboration. Femtoscopy with identified charged pions in proton-lead collisions at $\sqrt{s_{NN}} = 5.02$ TeV with ATLAS. ATLAS-CONF-2016-027, 2016.
- [1381] ATLAS Collaboration. Further searches for squarks and gluinos in final states with jets and missing transverse momentum at $\sqrt{s} = 13$ TeV with the ATLAS detector. ATLAS-CONF-2016-078, 2016.
- [1382] ATLAS Collaboration. Further studies on simulation of top-quark production for the ATLAS experiment at $\sqrt{s} = 13$ TeV. ATL-PHYS-PUB-2016-016, 2016.
- [1383] ATLAS Collaboration. Identification of Boosted, Hadronically Decaying W Bosons and Comparisons with ATLAS Data Taken at $\sqrt{s} = 8$ TeV. *Eur. Phys. J. C*, 76:154, 2016.
- [1384] ATLAS Collaboration. Identification of high transverse momentum top quarks in $p\bar{p}$ collisions at $\sqrt{s} = 8$ TeV with the ATLAS detector. *JHEP*, 06:093, 2016.
- [1385] ATLAS Collaboration. Jet mass reconstruction with the ATLAS Detector in early Run 2 data. ATLAS-CONF-2016-035, 2016.
- [1386] ATLAS Collaboration. Light-by-light scattering in ultra-peripheral Pb+Pb collisions at $\sqrt{s_{NN}} = 5.02$ TeV with the ATLAS detector at the LHC. ATLAS-CONF-2016-111, 2016.
- [1387] ATLAS Collaboration. Luminosity determination in $p\bar{p}$ collisions at $\sqrt{s} = 8$ TeV using the ATLAS detector at the LHC. *Eur. Phys. J. C*, 76:653, 2016.
- [1388] ATLAS Collaboration. Measurement of charged particle spectra in $p\bar{p}$ collisions and nuclear modification factor R_{pPb} at $\sqrt{s_{NN}} = 5.02$ TeV with the ATLAS detector at the LHC. ATLAS-CONF-2016-108, 2016.

- [1389] ATLAS Collaboration. Measurement of $D^{*\pm}$, D^\pm and D_s^\pm meson production cross sections in $p\bar{p}$ collisions at $\sqrt{s} = 7$ TeV with the ATLAS detector. *Nucl. Phys. B*, 907:717, 2016.
- [1390] ATLAS Collaboration. Measurement of event-shape observables in $Z \rightarrow \ell^+\ell^-$ events in $p\bar{p}$ collisions at $\sqrt{s} = 7$ TeV with the ATLAS detector at the LHC. *Eur. Phys. J. C*, 76:375, 2016.
- [1391] ATLAS Collaboration. Measurement of exclusive $\gamma\gamma \rightarrow W^+W^-$ production and search for exclusive Higgs boson production in $p\bar{p}$ collisions at $\sqrt{s} = 8$ TeV using the ATLAS detector. *Phys. Rev. D*, 94:032011, 2016.
- [1392] ATLAS Collaboration. Measurement of fiducial, differential and production cross sections in the $H \rightarrow \gamma\gamma$ decay channel with 13.3 fb^{-1} of 13 TeV proton-proton collision data with the ATLAS detector. ATLAS-CONF-2016-067, 2016.
- [1393] ATLAS Collaboration. Measurement of fiducial differential cross sections of gluon-fusion production of Higgs bosons decaying to $WW^* \rightarrow e\nu\mu\nu$ with the ATLAS detector at $\sqrt{s} = 8$ TeV. *JHEP*, 08:104, 2016.
- [1394] ATLAS Collaboration. Measurement of high-mass dimuon pairs in ultra-peripheral lead-lead collisions at $\sqrt{s_{NN}} = 5.02$ TeV with the ATLAS detector at the LHC. ATLAS-CONF-2016-025, 2016.
- [1395] ATLAS Collaboration. Measurement of inclusive-jet cross-sections in proton-proton collisions at $\sqrt{s} = 13$ TeV centre-of-mass energy with the ATLAS detector. ATLAS-CONF-2016-092, 2016.
- [1396] ATLAS Collaboration. Measurement of jet activity in top quark events using the $e\mu$ final state with two b -tagged jets in $p\bar{p}$ collisions at $\sqrt{s} = 8$ TeV with the ATLAS detector. *JHEP*, 09:074, 2016.
- [1397] ATLAS Collaboration. Measurement of jet charge in dijet events from $\sqrt{s} = 8$ TeV $p\bar{p}$ collisions with the ATLAS detector. *Phys. Rev. D*, 93:052003, 2016.
- [1398] ATLAS Collaboration. Measurement of large radius jet mass reconstruction performance at $\sqrt{s} = 8$ TeV using the ATLAS detector. ATLAS-CONF-2016-008, 2016.
- [1399] ATLAS Collaboration. Measurement of multi-particle azimuthal correlations in $p\bar{p}$ collisions at $\sqrt{s} = 5.02$ and 13 TeV with the ATLAS detector. ATLAS-CONF-2016-106, 2016.

- [1400] ATLAS Collaboration. Measurement of the angular coefficients in Z -boson events using electron and muon pairs from data taken at $\sqrt{s} = 8$ TeV with the ATLAS detector. *JHEP*, 08:159, 2016.
- [1401] ATLAS Collaboration. Measurement of the azimuthal anisotropy of charged particles in 5.02 TeV Pb+Pb collisions with the ATLAS detector. ATLAS-CONF-2016-105, 2016.
- [1402] ATLAS Collaboration. Measurement of the $b\bar{b}$ dijet cross section in $p\bar{p}$ collisions at $\sqrt{s} = 7$ TeV with the ATLAS detector. *Eur. Phys. J. C*, 76:670, 2016.
- [1403] ATLAS Collaboration. Measurement of the centrality dependence of the charged-particle pseudorapidity distribution in proton–lead collisions at $\sqrt{s_{NN}} = 5.02$ TeV with the ATLAS detector. *Eur. Phys. J. C*, 76:199, 2016.
- [1404] ATLAS Collaboration. Measurement of the charge asymmetry in highly boosted top-quark pair production in $\sqrt{s} = 8$ TeV $p\bar{p}$ collision data collected by the ATLAS experiment. *Phys. Lett. B*, 756:52, 2016.
- [1405] ATLAS Collaboration. Measurement of the charge asymmetry in top-quark pair production in the lepton-plus-jets final state in $p\bar{p}$ collision data at $\sqrt{s} = 8$ TeV with the ATLAS detector. *Eur. Phys. J. C*, 76:87, 2016.
- [1406] ATLAS Collaboration. Measurement of the charged-particle multiplicity inside jets from $\sqrt{s} = 8$ TeV $p\bar{p}$ collisions with the ATLAS detector. *Eur. Phys. J. C*, 76:322, 2016.
- [1407] ATLAS Collaboration. Measurement of the correlation between the polar angles of leptons from top quark decays in the helicity basis at $\sqrt{s} = 7$ TeV using the ATLAS detector. *Phys. Rev. D*, 93:012002, 2016.
- [1408] ATLAS Collaboration. Measurement of the CP-violating phase ϕ_s and the B_s^0 meson decay width difference with $B_s^0 \rightarrow J/\psi \phi$ decays in ATLAS. *JHEP*, 08:147, 2016.
- [1409] ATLAS Collaboration. Measurement of the cross-section for producing a W boson in association with a single top quark in $p\bar{p}$ collisions at $\sqrt{s} = 13$ TeV with ATLAS. 2016.
- [1410] ATLAS Collaboration. Measurement of the cross-section of the production of a W boson in association with a single top quark with ATLAS at $\sqrt{s} = 13$ TeV. ATLAS-CONF-2016-065, 2016.

- [1411] ATLAS Collaboration. Measurement of the dependence of transverse energy production at large pseudorapidity on the hard-scattering kinematics of proton–proton collisions at $\sqrt{s} = 2.76$ TeV with ATLAS. *Phys. Lett. B*, 756:10, 2016.
- [1412] ATLAS Collaboration. Measurement of the differential cross-section of highly boosted top quarks as a function of their transverse momentum in $\sqrt{s} = 8$ TeV proton–proton collisions using the ATLAS detector. *Phys. Rev. D*, 93:032009, 2016.
- [1413] ATLAS Collaboration. Measurement of the differential cross-sections of prompt and non-prompt production of J/ψ and $\psi(2S)$ in $p\bar{p}$ collisions at $\sqrt{s} = 7$ and 8 TeV with the ATLAS detector. *Eur. Phys. J. C*, 76:283, 2016.
- [1414] ATLAS Collaboration. Measurement of the double-differential high-mass Drell-Yan cross section in $p\bar{p}$ collisions at $\sqrt{s} = 8$ TeV with the ATLAS detector. *JHEP*, 08:009, 2016.
- [1415] ATLAS Collaboration. Measurement of the inclusive isolated prompt photon cross section in $p\bar{p}$ collisions at $\sqrt{s} = 8$ TeV with the ATLAS detector. *JHEP*, 08:005, 2016.
- [1416] ATLAS Collaboration. Measurement of the Inelastic Proton–Proton Cross Section at $\sqrt{s} = 13$ TeV with the ATLAS Detector at the LHC. *Phys. Rev. Lett.*, 117:182002, 2016.
- [1417] ATLAS Collaboration. Measurement of the photon identification efficiencies with the ATLAS detector using LHC Run-1 data. 2016.
- [1418] ATLAS Collaboration. Measurement of the production cross-section of a single top quark in association with a W boson at 8 TeV with the ATLAS experiment. *JHEP*, 01:064, 2016.
- [1419] ATLAS Collaboration. Measurement of the prompt J/ψ pair production cross-section in $p\bar{p}$ collisions at $\sqrt{s} = 8$ TeV with the ATLAS detector. ATLAS-CONF-2016-047, 2016.
- [1420] ATLAS Collaboration. Measurement of the relative width difference of the B^0 - \bar{B}^0 system with the ATLAS detector. *JHEP*, 06:081, 2016.
- [1421] ATLAS Collaboration. Measurement of the $t\bar{t}$ production cross-section using $e\mu$ events with b -tagged jets in $p\bar{p}$ collisions at $\sqrt{s} = 13$ TeV with the ATLAS detector. ATLAS-CONF-2016-005, 2016.
- [1422] ATLAS Collaboration. Measurement of the $t\bar{t}$ production cross-section using $e\mu$ events with b -tagged jets in $p\bar{p}$ collisions at $\sqrt{s} = 13$ TeV with the ATLAS detector. *Phys. Lett. B*, 761:136, 2016.

- [1423] ATLAS Collaboration. Measurement of the $t\bar{t}Z$ and $t\bar{t}W$ production cross sections in multilepton final states using 3.2 fb^{-1} of pp collisions at 13 TeV at the LHC. ATLAS-CONF-2016-003, 2016.
- [1424] ATLAS Collaboration. Measurement of the top quark mass in the $t\bar{t} \rightarrow$ dilepton channel from $\sqrt{s} = 8 \text{ TeV}$ ATLAS data. *Phys. Lett. B*, 761:350, 2016.
- [1425] ATLAS Collaboration. Measurement of the total cross section from elastic scattering in pp collisions at $\sqrt{s} = 8 \text{ TeV}$ with the ATLAS detector. *Phys. Lett. B*, 761:158, 2016.
- [1426] ATLAS Collaboration. Measurement of the transverse momentum and ϕ_η^* distributions of Drell-Yan lepton pairs in proton–proton collisions at $\sqrt{s} = 8 \text{ TeV}$ with the ATLAS detector. *Eur. Phys. J. C*, 76:291, 2016.
- [1427] ATLAS Collaboration. Measurement of the W -boson mass in pp collisions at $\sqrt{s} = 7 \text{ TeV}$ with the ATLAS detector. ATLAS-CONF-2016-113, 2016.
- [1428] ATLAS Collaboration. Measurement of the $W^\pm Z$ boson pair-production cross section in pp collisions at $\sqrt{s} = 13 \text{ TeV}$ with the ATLAS Detector. *Phys. Lett. B*, 762:1, 2016.
- [1429] ATLAS Collaboration. Measurement of the W^+W^- production cross section in pp collisions at a centre-of-mass energy of $\sqrt{s} = 13 \text{ TeV}$ with the ATLAS experiment. ATLAS-CONF-2016-090, 2016.
- [1430] ATLAS Collaboration. Measurement of the ZZ Production Cross Section in pp Collisions at $\sqrt{s} = 13 \text{ TeV}$ with the ATLAS Detector. *Phys. Rev. Lett.*, 116:101801, 2016.
- [1431] ATLAS Collaboration. Measurement of top quark pair differential cross sections in the dilepton channel in pp collisions at $\sqrt{s} = 7$ and 8 TeV with ATLAS. *Phys. Rev. D*, 94:092003, 2016.
- [1432] ATLAS Collaboration. Measurement of total and differential W^+W^- production cross sections in proton–proton collisions at $\sqrt{s} = 8 \text{ TeV}$ with the ATLAS detector and limits on anomalous triple-gauge-boson couplings. *JHEP*, 09:029, 2016.
- [1433] ATLAS Collaboration. Measurement of track reconstruction inefficiencies in the core of jets via pixel dE/dx with the ATLAS experiment using $\sqrt{s} = 13 \text{ TeV}$ pp collision data. ATL-PHYS-PUB-2016-007, 2016.

- [1434] ATLAS Collaboration. Measurement of W^\pm and Z-boson production cross sections in pp collisions at $\sqrt{s} = 13$ TeV with the ATLAS detector. *Phys. Lett. B*, 759:601, 2016.
- [1435] ATLAS Collaboration. Measurement of $W^\pm Z$ boson pair-production in pp collisions at $\sqrt{s} = 13$ TeV with the ATLAS Detector and confidence intervals for anomalous triple gauge boson couplings. ATLAS-CONF-2016-043, 2016.
- [1436] ATLAS Collaboration. Measurement of W^+W^- production in association with one jet in proton–proton collisions at $\sqrt{s} = 8$ TeV with the ATLAS detector. *Phys. Lett. B*, 763:114, 2016.
- [1437] ATLAS Collaboration. Measurement Prospects for VBF $H \rightarrow WW^* \rightarrow e\nu\mu\nu$ production with 3 ab^{-1} of HL-LHC pp -collisions. ATL-PHYS-PUB-2016-018, 2016.
- [1438] ATLAS Collaboration. Measurements of fiducial cross-sections for $t\bar{t}$ production with one or two additional b-jets in pp collisions at $\sqrt{s} = 8$ TeV using the ATLAS detector. *Eur. Phys. J. C*, 76:11, 2016.
- [1439] ATLAS Collaboration. Measurements of four-lepton production in pp collisions at $\sqrt{s} = 8$ TeV with the ATLAS detector. *Phys. Lett. B*, 753:552, 2016.
- [1440] ATLAS Collaboration. Measurements of long-range azimuthal anisotropies and associated Fourier coefficients in pp collisions at 5.02 and 13 TeV and $\text{p}+\text{Pb}$ collisions at $\sqrt{s_{\text{NN}}} = 5.02$ TeV with the ATLAS detector. ATLAS-CONF-2016-026, 2016.
- [1441] ATLAS Collaboration. Measurements of $t\bar{t}$ differential cross-sections in the all-hadronic channel with the ATLAS detector using highly boosted top quarks in pp collisions at $\sqrt{s} = 13$ TeV. ATLAS-CONF-2016-100, 2016.
- [1442] ATLAS Collaboration. Measurements of the charge asymmetry in top-quark pair production in the dilepton final state at $\sqrt{s} = 8$ TeV with the ATLAS detector. *Phys. Rev. D*, 94:032006, 2016.
- [1443] ATLAS Collaboration. Measurements of the Higgs boson production and decay rates and coupling strengths using pp collision data at $\sqrt{s} = 7$ and 8 TeV in the ATLAS experiment. *Eur. Phys. J. C*, 76:6, 2016.
- [1444] ATLAS Collaboration. Measurements of the Higgs boson production cross section via Vector Boson Fusion and associated WH production in the $WW^* \rightarrow \ell\nu\ell\nu$ decay mode with the ATLAS detector at $\sqrt{s} = 13$ TeV. ATLAS-CONF-2016-112, 2016.

- [1445] ATLAS Collaboration. Measurements of the Production Cross Section of a Z Boson in Association with Jets in pp Collisions at $\sqrt{s} = 13$ TeV with the ATLAS Detector. ATLAS-CONF-2016-046, 2016.
- [1446] ATLAS Collaboration. Measurements of top-quark pair differential cross-sections in the lepton+jets channel in pp collisions at $\sqrt{s} = 13$ TeV using the ATLAS detector. ATLAS-CONF-2016-040, 2016.
- [1447] ATLAS Collaboration. Measurements of top-quark pair differential cross-sections in the lepton+jets channel in pp collisions at $\sqrt{s} = 8$ TeV using the ATLAS detector. *Eur. Phys. J. C*, 76:538, 2016.
- [1448] ATLAS Collaboration. Measurements of top quark spin observables in $t\bar{t}$ events using dilepton final states at $\sqrt{s} = 8$ TeV with the ATLAS detector. ATLAS-CONF-2016-099, 2016.
- [1449] ATLAS Collaboration. Measurements of $W^\pm Z$ production cross sections in pp collisions at $\sqrt{s} = 8$ TeV with the ATLAS detector and limits on anomalous gauge boson self-couplings. *Phys. Rev. D*, 93:092004, 2016.
- [1450] ATLAS Collaboration. Measurements of $Z\gamma$ and $Z\gamma\gamma$ production in pp collisions at $\sqrt{s} = 8$ TeV with the ATLAS detector. *Phys. Rev. D*, 93:112002, 2016.
- [1451] ATLAS Collaboration. Modelling of the $t\bar{t}H$ and $t\bar{t}V(V = W, Z)$ processes for $\sqrt{s} = 13$ TeV ATLAS analyses. ATL-PHYS-PUB-2016-005, 2016.
- [1452] ATLAS Collaboration. Monte Carlo Generators for the Production of a W or Z/γ^* Boson in Association with Jets at ATLAS in Run 2. ATL-PHYS-PUB-2016-003, 2016.
- [1453] ATLAS Collaboration. Multi-boson simulation for 13 TeV ATLAS analyses. ATL-PHYS-PUB-2016-002, 2016.
- [1454] ATLAS Collaboration. Muon reconstruction performance of the ATLAS detector in proton–proton collision data at $\sqrt{s} = 13$ TeV. *Eur. Phys. J. C*, 76:292, 2016.
- [1455] ATLAS Collaboration. Observation of Long-Range Elliptic Azimuthal Anisotropies in $\sqrt{s} = 13$ and 2.76 TeV pp Collisions with the ATLAS Detector. *Phys. Rev. Lett.*, 116:172301, 2016.
- [1456] ATLAS Collaboration. Optimisation of the ATLAS b-tagging performance for the 2016 LHC Run. ATL-PHYS-PUB-2016-012, 2016.

- [1457] ATLAS Collaboration. Performance of b -jet identification in the atlas experiment. *Journal of Instrumentation*, 11(04):P04008, 2016.
- [1458] ATLAS Collaboration. Performance of b-jet identification in the ATLAS experiment. *JINST*, 11:P04008, 2016.
- [1459] ATLAS Collaboration. Performance of pile-up mitigation techniques for jets in pp collisions at $\sqrt{s} = 8$ TeV using the ATLAS detector. *Eur. Phys. J. C*, 76:581, 2016.
- [1460] ATLAS Collaboration. Photon identification in 2015 ATLAS data. ATL-PHYS-PUB-2016-014, 2016.
- [1461] ATLAS Collaboration. Probing lepton flavour violation via neutrinoless $\tau \rightarrow 3\mu$ decays with the ATLAS detector. *Eur. Phys. J. C*, 76:232, 2016.
- [1462] ATLAS Collaboration. Probing the Wtb vertex structure with t-channel single top-quark events in pp collisions at $\sqrt{s} = 13$ TeV with the ATLAS detector. ATLAS-CONF-2016-097, 2016.
- [1463] ATLAS Collaboration. Production measurements of $\psi(2S)$ and $X(3872) \rightarrow J/\psi\pi^+\pi^-$ at $\sqrt{s} = 8$ TeV with the ATLAS detector. ATLAS-CONF-2016-028, 2016.
- [1464] ATLAS Collaboration. Projected sensitivity to Higgs boson pair production in the $b\bar{b}b\bar{b}$ final state using proton–proton collisions at HL-LHC with the ATLAS detector. ATL-PHYS-PUB-2016-024, 2016.
- [1465] ATLAS Collaboration. Prospect for a search for direct stau production in events with at least two hadronic taus and missing transverse momentum at the High Luminosity LHC with the ATLAS Detector. ATL-PHYS-PUB-2016-021, 2016.
- [1466] ATLAS Collaboration. Prospective results for vector-boson fusion-mediated Higgs boson searches in the four lepton final state at the High Luminosity Large Hadron Collider. ATL-PHYS-PUB-2016-008, 2016.
- [1467] ATLAS Collaboration. Prospects for a search for direct pair production of top squarks in scenarios with compressed mass spectra at the high luminosity LHC with the ATLAS Detector. ATL-PHYS-PUB-2016-022, 2016.
- [1468] ATLAS Collaboration. Prospects for Observing $t\bar{t}HH$ Production with the ATLAS Experiment at the HL-LHC. ATL-PHYS-PUB-2016-023, 2016.
- [1469] ATLAS Collaboration. Pursuit of new phenomena in final states with high jet multiplicity, high jet masses and missing transverse momentum with ATLAS at $\sqrt{s} = 13$ TeV. ATLAS-CONF-2016-095, 2016.

- [1470] ATLAS Collaboration. Reconstruction of hadronic decay products of tau leptons with the ATLAS experiment. *Eur. Phys. J. C*, 76:295, 2016.
- [1471] ATLAS Collaboration. Review of the ATLAS Open Data Dataset. ATL-OREACH-PUB-2016-001, 2016.
- [1472] ATLAS Collaboration. Search for a CP-odd Higgs boson decaying to Zh in pp collisions at $\sqrt{s} = 13$ TeV with the ATLAS detector. ATLAS-CONF-2016-015, 2016.
- [1473] ATLAS Collaboration. Search for a high-mass Higgs boson decaying to a pair of W bosons in pp collisions at $\sqrt{s} = 13$ TeV with the ATLAS detector. ATLAS-CONF-2016-021, 2016.
- [1474] ATLAS Collaboration. Search for a high-mass Higgs boson decaying to a pair of W bosons in pp collisions at $\sqrt{s} = 13$ TeV with the ATLAS detector. ATLAS-CONF-2016-074, 2016.
- [1475] ATLAS Collaboration. Search for a high-mass Higgs boson decaying to a W boson pair in pp collisions at $\sqrt{s} = 8$ TeV with the ATLAS detector. *JHEP*, 01:032, 2016.
- [1476] ATLAS Collaboration. Search for a Scalar Partner of the Top Quark in the Jets+ E_T^{miss} Final State at $\sqrt{s} = 13$ TeV with the ATLAS detector. ATLAS-CONF-2016-077, 2016.
- [1477] ATLAS Collaboration. Search for an additional, heavy Higgs boson in the $H \rightarrow ZZ$ decay channel at $\sqrt{s} = 8$ TeV in pp collision data with the ATLAS detector. *Eur. Phys. J. C*, 76:45, 2016.
- [1478] ATLAS Collaboration. Search for anomalous couplings in the Wtb vertex from the measurement of double differential angular decay rates of single top quarks produced in the t-channel with the ATLAS detector. *JHEP*, 04:023, 2016.
- [1479] ATLAS Collaboration. Search for bottom squark pair production in proton–proton collisions at $\sqrt{s} = 13$ TeV with the ATLAS detector. *Eur. Phys. J. C*, 76:547, 2016.
- [1480] ATLAS Collaboration. Search for charged Higgs bosons in the $H^\pm \rightarrow tb$ decay channel in pp collisions at $\sqrt{s} = 13$ TeV using the ATLAS detector. ATLAS-CONF-2016-089, 2016.
- [1481] ATLAS Collaboration. Search for charged Higgs bosons in the $H^\pm \rightarrow tb$ decay channel in pp collisions at $\sqrt{s} = 8$ TeV using the ATLAS detector. *JHEP*, 03:127, 2016.

- [1482] ATLAS Collaboration. Search for charged Higgs bosons in the τ +jets final state with 14.7 fb^{-1} of pp collision data recorded at $\sqrt{s} = 13 \text{ TeV}$ with the ATLAS experiment. ATLAS-CONF-2016-088, 2016.
- [1483] ATLAS Collaboration. Search for charged Higgs bosons produced in association with a top quark and decaying via $H^\pm \rightarrow \tau\nu$ using pp collision data recorded at $\sqrt{s} = 13 \text{ TeV}$ by the ATLAS detector. *Phys. Lett. B*, 759:555, 2016.
- [1484] ATLAS Collaboration. Search for Dark Matter in association with a Higgs boson decaying to b-quarks in pp collisions at $\sqrt{s} = 13 \text{ TeV}$ with the ATLAS detector. ATLAS-CONF-2016-019, 2016.
- [1485] ATLAS Collaboration. Search for dark matter produced in association with a hadronically decaying vector boson in pp collisions at $\sqrt{s} = 13 \text{ TeV}$ with the ATLAS detector. *Phys. Lett. B*, 763:251, 2016.
- [1486] ATLAS Collaboration. Search for dark matter produced in association with a Higgs boson decaying to two bottom quarks in pp collisions at $\sqrt{s} = 8 \text{ TeV}$ with the ATLAS detector. *Phys. Rev. D*, 93:072007, 2016.
- [1487] ATLAS Collaboration. Search for Dark Matter production associated with bottom quarks in 13.3 fb^{-1} of pp collisions at $\sqrt{s} = 13 \text{ TeV}$ with the ATLAS detector at the LHC. ATLAS-CONF-2016-086, 2016.
- [1488] ATLAS Collaboration. Search for diboson resonance production in the $\ell\nu qq$ final state using pp collisions at $\sqrt{s} = 13 \text{ TeV}$ with the ATLAS detector at the LHC. ATLAS-CONF-2016-062, 2016.
- [1489] ATLAS Collaboration. Search for direct top squark pair production and dark matter production in final states with two leptons in $\sqrt{s} = 13 \text{ TeV}$ pp collisions using 13.3 fb^{-1} of ATLAS data. ATLAS-CONF-2016-076, 2016.
- [1490] ATLAS Collaboration. Search for direct top squark pair production in events with a Z boson, b-jets and missing transverse momentum in $\sqrt{s} = 13 \text{ TeV}$ pp collisions with the ATLAS detector. ATLAS-CONF-2016-038, 2016.
- [1491] ATLAS Collaboration. Search for direct top squark pair production in final states with two leptons in $\sqrt{s} = 13 \text{ TeV}$ pp collisions using 3.2 fb^{-1} of ATLAS data. ATLAS-CONF-2016-009, 2016.
- [1492] ATLAS Collaboration. Search for direct top squark pair production in final states with two tau leptons in pp collisions at $\sqrt{s} = 8 \text{ TeV}$ with the ATLAS detector. *Eur. Phys. J. C*, 76:81, 2016.

- [1493] ATLAS Collaboration. Search for doubly-charged Higgs bosons in same-charge electron pair final states using proton–proton collisions at $\sqrt{s} = 13$ TeV with the ATLAS detector. ATLAS-CONF-2016-051, 2016.
- [1494] ATLAS Collaboration. Search for electroweak production of supersymmetric particles in final states with tau leptons in $\sqrt{s} = 13$ TeV $p\bar{p}$ collisions with the ATLAS detector. ATLAS-CONF-2016-093, 2016.
- [1495] ATLAS Collaboration. Search for flavour-changing neutral current top-quark decays to qZ in $p\bar{p}$ collision data collected with the ATLAS detector at $\sqrt{s} = 8$ TeV. *Eur. Phys. J. C*, 76:12, 2016.
- [1496] ATLAS Collaboration. Search for four-top-quark production in final states with one charged lepton and multiple jets using 3.2 fb^{-1} of proton–proton collisions at $\sqrt{s} = 13$ TeV with the ATLAS detector at the LHC. ATLAS-CONF-2016-020, 2016.
- [1497] ATLAS Collaboration. Search for gluinos in events with an isolated lepton, jets and missing transverse momentum at $\sqrt{s} = 13$ TeV with the ATLAS detector. *Eur. Phys. J. C*, 76:565, 2016.
- [1498] ATLAS Collaboration. Search for heavy Higgs bosons A/H decaying to a top-quark pair in $p\bar{p}$ collisions at $\sqrt{s} = 8$ TeV with the ATLAS detector. ATLAS-CONF-2016-073, 2016.
- [1499] ATLAS Collaboration. Search for heavy long-lived charged R-hadrons with the ATLAS detector in 3.2 fb^{-1} of proton–proton collision data at $\sqrt{s} = 13$ TeV. *Phys. Lett. B*, 760:647, 2016.
- [1500] ATLAS Collaboration. Search for heavy neutral resonances in vector boson fusion in $p\bar{p}$ collisions at $\sqrt{s} = 13$ TeV with the ATLAS detector at the Large Hadron Collider. ATLAS-CONF-2016-053, 2016.
- [1501] ATLAS Collaboration. Search for heavy particles decaying to pairs of highly-boosted top quarks using lepton-plus-jets events in proton–proton collisions at $\sqrt{s} = 13$ TeV with the ATLAS detector. ATLAS-CONF-2016-014, 2016.
- [1502] ATLAS Collaboration. Search for heavy resonances decaying to a Z boson and a photon in $p\bar{p}$ collisions at $\sqrt{s} = 13$ TeV with the ATLAS detector. ATLAS-CONF-2016-010, 2016.
- [1503] ATLAS Collaboration. Search for Higgs and Z Boson Decays to $\phi\gamma$ with the ATLAS Detector. *Phys. Rev. Lett.*, 117:111802, 2016.

- [1504] ATLAS Collaboration. Search for Higgs boson pair production in the $b\bar{b}\gamma\gamma$ final state using pp collision data at $\sqrt{s} = 13$ TeV with the ATLAS detector. ATLAS-CONF-2016-004, 2016.
- [1505] ATLAS Collaboration. Search for Higgs boson pair production in the final state of $\gamma\gamma WW^*(\rightarrow l\nu jj)$ using 13.3 fb^{-1} of pp collision data recorded at 13 TeV with the ATLAS detector. ATLAS-CONF-2016-071, 2016.
- [1506] ATLAS Collaboration. Search for Higgs boson production via weak boson fusion and decaying to $b\bar{b}$ in association with a high-energy photon using the ATLAS detector. ATLAS-CONF-2016-063, 2016.
- [1507] ATLAS Collaboration. Search for Higgs bosons decaying into di-muon in pp collisions at $\sqrt{s} = 13$ TeV with the ATLAS detector. ATLAS-CONF-2016-041, 2016.
- [1508] ATLAS Collaboration. Search for high-mass new phenomena in the dilepton final state using proton–proton collisions at $\sqrt{s} = 13$ TeV with the ATLAS detector. *Phys. Lett. B*, 761:372, 2016.
- [1509] ATLAS Collaboration. Search for high-mass resonances decaying into a Z boson pair in the $\ell\ell\nu\nu$ final state in pp collisions at $\sqrt{s} = 13$ TeV with the ATLAS detector. ATLAS-CONF-2016-012, 2016.
- [1510] ATLAS Collaboration. Search for invisible decays of a Higgs boson using vector-boson fusion in pp collisions at $\sqrt{s} = 8$ TeV with the ATLAS detector. *JHEP*, 01:172, 2016.
- [1511] ATLAS Collaboration. Search for light dijet resonances with the ATLAS detector using a Trigger-object Level Analysis in LHC pp collisions at $\sqrt{s} = 13$ TeV. ATLAS-CONF-2016-030, 2016.
- [1512] ATLAS Collaboration. Search for long-lived neutral particles decaying in the hadronic calorimeter of ATLAS at $\sqrt{s} = 13$ TeV in 3.2 fb^{-1} of data. ATLAS-CONF-2016-103, 2016.
- [1513] ATLAS Collaboration. Search for long-lived neutral particles decaying into displaced lepton-jets in proton–proton collisions at $\sqrt{s} = 13$ TeV with the ATLAS detector. ATLAS-CONF-2016-042, 2016.
- [1514] ATLAS Collaboration. Search for magnetic monopoles and stable particles with high electric charges in 8 TeV pp collisions with the ATLAS detector. *Phys. Rev. D*, 93:052009, 2016.

- [1515] ATLAS Collaboration. Search for massive supersymmetric particles in multi-jet final states produced in pp collisions at $\sqrt{s} = 13$ TeV using the ATLAS detector at the LHC. ATLAS-CONF-2016-057, 2016.
- [1516] ATLAS Collaboration. Search for metastable heavy charged particles with large ionization energy loss in pp collisions at $\sqrt{s} = 13$ TeV using the ATLAS experiment. *Phys. Rev. D*, 93:112015, 2016.
- [1517] ATLAS Collaboration. Search for Minimal Supersymmetric Standard Model Higgs bosons H/A and for a Z' boson in the $\tau\tau$ final state produced in pp collisions at $\sqrt{s} = 13$ TeV with the ATLAS Detector. *Eur. Phys. J. C*, 76:585, 2016.
- [1518] ATLAS Collaboration. Search for new high-mass resonances in the dilepton final state using proton–proton collisions at $\sqrt{s} = 13$ TeV with the ATLAS detector. ATLAS-CONF-2016-045, 2016.
- [1519] ATLAS Collaboration. Search for new light resonances decaying to jet pairs and produced in association with a photon in proton–proton collisions at $\sqrt{s} = 13$ TeV with the ATLAS detector. ATLAS-CONF-2016-029, 2016.
- [1520] ATLAS Collaboration. Search for new light resonances decaying to jet pairs and produced in association with a photon or a jet in proton–proton collisions at $\sqrt{s} = 13$ TeV with the ATLAS detector. ATLAS-CONF-2016-070, 2016.
- [1521] ATLAS Collaboration. Search for new phenomena in a lepton plus high jet multiplicity final state with the ATLAS experiment using $\sqrt{s} = 13$ TeV proton–proton collision data. ATLAS-CONF-2016-094, 2016.
- [1522] ATLAS Collaboration. Search for new phenomena in different-flavour high-mass dilepton final states in pp collisions at $\sqrt{s} = 13$ TeV with the ATLAS detector. *Eur. Phys. J. C*, 76:541, 2016.
- [1523] ATLAS Collaboration. Search for new phenomena in dijet events collected in 2015 and 2016 pp collisions with the ATLAS detector at $\sqrt{s} = 13$ TeV. ATLAS-CONF-2016-069, 2016.
- [1524] ATLAS Collaboration. Search for New Phenomena in Dijet Mass and Angular Distributions from pp Collisions at $\sqrt{s} = 13$ TeV with the ATLAS Detector. *Phys. Lett. B*, 754:302, 2016.
- [1525] ATLAS Collaboration. Search for new phenomena in events containing a same-flavour opposite-sign dilepton pair, jets, and large missing transverse momentum in $\sqrt{s} = 13$ TeV pp collisions with the ATLAS detector. ATLAS-CONF-2016-098, 2016.

- [1526] ATLAS Collaboration. Search for new phenomena in events with a photon and missing transverse momentum in pp collisions at $\sqrt{s} = 13$ TeV with the ATLAS detector. *JHEP*, 06:059, 2016.
- [1527] ATLAS Collaboration. Search for new phenomena in events with at least three photons collected in pp collisions at $\sqrt{s} = 8$ TeV with the ATLAS detector. *Eur. Phys. J. C*, 76:210, 2016.
- [1528] ATLAS Collaboration. Search for new phenomena in events with missing transverse momentum and a Higgs boson decaying to two photons in pp collisions at $\sqrt{s} = 13$ TeV with the ATLAS detector. ATLAS-CONF-2016-011, 2016.
- [1529] ATLAS Collaboration. Search for new phenomena in final states with an energetic jet and large missing transverse momentum in pp collisions at $\sqrt{s} = 13$ TeV using the ATLAS detector. *Phys. Rev. D*, 94:032005, 2016.
- [1530] ATLAS Collaboration. Search for new phenomena in final states with large jet multiplicities and missing transverse momentum with ATLAS using $\sqrt{s} = 13$ TeV proton–proton collisions. *Phys. Lett. B*, 757:334, 2016.
- [1531] ATLAS Collaboration. Search for new phenomena in $t\bar{t}$ final states with additional heavy-flavour jets in 3.2 fb^{-1} of pp collisions at $\sqrt{s} = 13$ TeV with the ATLAS detector. ATLAS-CONF-2016-104, 2016.
- [1532] ATLAS Collaboration. Search for new phenomena in the $Z(\rightarrow \ell\ell) + E_T^{\text{miss}}$ final state at $\sqrt{s} = 13$ TeV with the ATLAS detector. ATLAS-CONF-2016-056, 2016.
- [1533] ATLAS Collaboration. Search for new phenomena using events with b-jets and a pair of same-charge leptons in 3.2 fb^{-1} of pp collisions at $\sqrt{s} = 13$ TeV with the ATLAS detector. ATLAS-CONF-2016-032, 2016.
- [1534] ATLAS Collaboration. Search for new phenomena with photon+jet events in proton–proton collisions at $\sqrt{s} = 13$ TeV with the ATLAS detector. *JHEP*, 03:041, 2016.
- [1535] ATLAS Collaboration. Search for new resonances decaying to a charged lepton and a neutrino in pp collisions at $\sqrt{s} = 13$ TeV with the ATLAS detector. ATLAS-CONF-2016-061, 2016.
- [1536] ATLAS Collaboration. Search for new resonances decaying to a Z boson and a photon in 13.3 fb^{-1} of pp collisions at $\sqrt{s} = 13$ TeV with the ATLAS detector. ATLAS-CONF-2016-044, 2016.

- [1537] ATLAS Collaboration. Search for new resonances in events with one lepton and missing transverse momentum in pp collisions at $\sqrt{s} = 13$ TeV with the ATLAS detector. *Phys. Lett. B*, 762:334, 2016.
- [1538] ATLAS Collaboration. Search for pair production of a heavy vector-like quark decaying to a high- p_{T} W boson and b quarks in the lepton plus jets final state in pp collisions at $\sqrt{s} = 13$ TeV with the ATLAS detector. ATLAS-CONF-2016-102, 2016.
- [1539] ATLAS Collaboration. Search for pair production of gluinos decaying via stop and sbottom in events with b -jets and large missing transverse momentum in pp collisions at $\sqrt{s} = 13$ TeV with the ATLAS detector. *Phys. Rev. D*, 94:032003, 2016.
- [1540] ATLAS Collaboration. Search for pair production of gluinos decaying via top or bottom squarks in events with b -jets and large missing transverse momentum in pp collisions at $\sqrt{s} = 13$ TeV with the ATLAS detector. ATLAS-CONF-2016-052, 2016.
- [1541] ATLAS Collaboration. Search for pair production of Higgs bosons in the $b\bar{b}b\bar{b}$ final state using proton–proton collisions at $\sqrt{s} = 13$ TeV with the ATLAS detector. ATLAS-CONF-2016-049, 2016.
- [1542] ATLAS Collaboration. Search for pair production of Higgs bosons in the $b\bar{b}b\bar{b}$ final state using proton–proton collisions at $\sqrt{s} = 13$ TeV with the ATLAS detector. *Phys. Rev. D*, 94:052002, 2016.
- [1543] ATLAS Collaboration. Search for pair production of Higgs bosons in the $b\bar{b}b\bar{b}$ final state using proton–proton collisions at $\sqrt{s} = 13$ TeV with the ATLAS detector. ATLAS-CONF-2016-017, 2016.
- [1544] ATLAS Collaboration. Search for pair production of vector-like top partners in events with exactly one lepton and large missing transverse momentum in $\sqrt{s} = 13$ TeV pp collisions with the ATLAS detector. ATLAS-CONF-2016-101, 2016.
- [1545] ATLAS Collaboration. Search for production of vector-like top quark pairs and of four top quarks in the lepton-plus-jets final state in pp collisions at $\sqrt{s} = 13$ TeV with the ATLAS detector. ATLAS-CONF-2016-013, 2016.
- [1546] ATLAS Collaboration. Search for resonances below 1.2 TeV from the mass distribution of b -jet pairs in proton–proton collisions at $\sqrt{s} = 13$ TeV with the ATLAS detector. ATLAS-CONF-2016-031, 2016.
- [1547] ATLAS Collaboration. Search for resonances in diphoton events at $\sqrt{s} = 13$ TeV with the ATLAS detector. *JHEP*, 09:001, 2016.

- [1548] ATLAS Collaboration. Search for resonances in diphoton events with the ATLAS detector at $\sqrt{s} = 13$ TeV. ATLAS-CONF-2016-018, 2016.
- [1549] ATLAS Collaboration. Search for resonances in the mass distribution of jet pairs with one or two jets identified as b-jets in proton–proton collisions at $\sqrt{s} = 13$ TeV with the ATLAS detector. *Phys. Lett. B*, 759:229, 2016.
- [1550] ATLAS Collaboration. Search for resonances in the mass distribution of jet pairs with one or two jets identified as b-jets with the ATLAS detector with 2015 and 2016 data. ATLAS-CONF-2016-060, 2016.
- [1551] ATLAS Collaboration. Search for resonances with boson-tagged jets in 15.5 fb^{-1} of pp collisions at $\sqrt{s} = 13$ TeV collected with the ATLAS detector. ATLAS-CONF-2016-055, 2016.
- [1552] ATLAS Collaboration. Search for scalar diphoton resonances with 15.4 fb^{-1} of data collected at $\sqrt{s} = 13$ TeV in 2015 and 2016 with the ATLAS detector. ATLAS-CONF-2016-059, 2016.
- [1553] ATLAS Collaboration. Search for scalar leptoquarks in pp collisions at $\sqrt{s} = 13$ TeV with the ATLAS experiment. *New J. Phys.*, 18:093016, 2016.
- [1554] ATLAS Collaboration. Search for single production of a vector-like quark via a heavy gluon in the 4b final state with the ATLAS detector in pp collisions at $\sqrt{s} = 8$ TeV. *Phys. Lett. B*, 758:249, 2016.
- [1555] ATLAS Collaboration. Search for single production of vector-like quarks decaying into Wb in pp collisions at $\sqrt{s} = 13$ TeV with the ATLAS detector. ATLAS-CONF-2016-072, 2016.
- [1556] ATLAS Collaboration. Search for single production of vector-like quarks decaying into Wb in pp collisions at $\sqrt{s} = 8$ TeV with the ATLAS detector. *Eur. Phys. J. C*, 76:442, 2016.
- [1557] ATLAS Collaboration. Search for single top-quark production via flavour-changing neutral currents at 8 TeV with the ATLAS detector. *Eur. Phys. J. C*, 76:55, 2016.
- [1558] ATLAS Collaboration. Search for squarks and gluinos in events with an isolated lepton, jets and missing transverse momentum at $\sqrt{s} = 13$ TeV with the ATLAS detector. ATLAS-CONF-2016-054, 2016.
- [1559] ATLAS Collaboration. Search for squarks and gluinos in events with hadronically decaying tau leptons, jets and missing transverse momentum in proton–proton collisions at $\sqrt{s} = 13$ TeV recorded with the ATLAS detector. *Eur. Phys. J. C*, 76:683, 2016.

- [1560] ATLAS Collaboration. Search for squarks and gluinos in final states with jets and missing transverse momentum at $\sqrt{s} = 13$ TeV with the ATLAS detector. *Eur. Phys. J. C*, 76:392, 2016.
- [1561] ATLAS Collaboration. Search for strong gravity in multijet final states produced in pp collisions at $\sqrt{s} = 13$ TeV using the ATLAS detector at the LHC. *JHEP*, 03:026, 2016.
- [1562] ATLAS Collaboration. Search for supersymmetry at $\sqrt{s} = 13$ TeV in final states with jets and two same-sign leptons or three leptons with the ATLAS detector. *Eur. Phys. J. C*, 76:259, 2016.
- [1563] ATLAS Collaboration. Search for supersymmetry in a final state containing two photons and missing transverse momentum in $\sqrt{s} = 13$ TeV pp collisions at the LHC using the ATLAS detector. *Eur. Phys. J. C*, 76:517, 2016.
- [1564] ATLAS Collaboration. Search for supersymmetry in events with four or more leptons in $\sqrt{s} = 13$ TeV pp collisions using 13.3 fb^{-1} of ATLAS data. ATLAS-CONF-2016-075, 2016.
- [1565] ATLAS Collaboration. Search for Supersymmetry in events with photons, jets and missing transverse energy with the ATLAS detector in 13 TeV pp collisions. ATLAS-CONF-2016-066, 2016.
- [1566] ATLAS Collaboration. Search for supersymmetry with two same-sign leptons or three leptons using 13.2 fb^{-1} of $\sqrt{s} = 13$ TeV pp collision data collected by the ATLAS detector. ATLAS-CONF-2016-037, 2016.
- [1567] ATLAS Collaboration. Search for TeV-scale gravity signatures in high-mass final states with leptons and jets with the ATLAS detector at $\sqrt{s} = 13$ TeV. *Phys. Lett. B*, 760:520, 2016.
- [1568] ATLAS Collaboration. Search for TeV-scale gravity signatures in high-mass final states with leptons and jets with the ATLAS detector at $\sqrt{s} = 13$ TeV. ATLAS-CONF-2016-006, 2016.
- [1569] ATLAS Collaboration. Search for the Associated Production of a Higgs Boson and a Top Quark Pair in Multilepton Final States with the ATLAS Detector. ATLAS-CONF-2016-058, 2016.
- [1570] ATLAS Collaboration. Search for the electroweak production of charginos and neutralinos in multilepton final states at $\sqrt{s} = 13$ TeV with the ATLAS detector. ATLAS-CONF-2016-096, 2016.

- [1571] ATLAS Collaboration. Search for the electroweak production of supersymmetric particles in $\sqrt{s} = 8$ TeV $p\bar{p}$ collisions with the ATLAS detector. *Phys. Rev. D*, 93:052002, 2016.
- [1572] ATLAS Collaboration. Search for the Higgs boson produced in association with a W boson and decaying to four b -quarks via two spin-zero particles in $p\bar{p}$ collisions at 13 TeV with the ATLAS detector. *Eur. Phys. J. C*, 76:605, 2016.
- [1573] ATLAS Collaboration. Search for the Minimal Supersymmetric Standard Model Higgs bosons H/A in the $\tau\tau$ final state in up to 13.3 fb^{-1} of $p\bar{p}$ collision data at $\sqrt{s} = 13$ TeV with the ATLAS detector. ATLAS-CONF-2016-085, 2016.
- [1574] ATLAS Collaboration. Search for the production of single vector-like and excited quarks in the Wt final state in $p\bar{p}$ collisions at $\sqrt{s} = 8$ TeV with the ATLAS detector. *JHEP*, 02:110, 2016.
- [1575] ATLAS Collaboration. Search for the Standard Model Higgs boson decaying into $b\bar{b}$ produced in association with top quarks decaying hadronically in $p\bar{p}$ collisions at $\sqrt{s} = 8$ TeV with the ATLAS detector. *JHEP*, 05:160, 2016.
- [1576] ATLAS Collaboration. Search for the Standard Model Higgs boson produced by vector-boson fusion and decaying to bottom quarks in $\sqrt{s} = 8$ TeV $p\bar{p}$ collisions with the ATLAS detector. *JHEP*, 11:112, 2016.
- [1577] ATLAS Collaboration. Search for the Standard Model Higgs boson produced in association with a vector boson and decaying to a $b\bar{b}$ pair in $p\bar{p}$ collisions at 13 TeV using the ATLAS detector. ATLAS-CONF-2016-091, 2016.
- [1578] ATLAS Collaboration. Search for the Standard Model Higgs boson produced in association with top quarks and decaying into a $b\bar{b}$ pair in $p\bar{p}$ collisions at $\sqrt{s} = 13$ TeV with the ATLAS detector. ATLAS-CONF-2016-080, 2016.
- [1579] ATLAS Collaboration. Search for top-squark pair production in final states with two tau leptons, jets, and missing transverse momentum in $\sqrt{s} = 13$ TeV $p\bar{p}$ collisions with the ATLAS detector. ATLAS-CONF-2016-048, 2016.
- [1580] ATLAS Collaboration. Search for top squarks in final states with one isolated lepton, jets, and missing transverse momentum in $\sqrt{s} = 13$ TeV $p\bar{p}$ collisions of ATLAS data. ATLAS-CONF-2016-007, 2016.
- [1581] ATLAS Collaboration. Search for top squarks in final states with one isolated lepton, jets, and missing transverse momentum in $\sqrt{s} = 13$ TeV $p\bar{p}$ collisions with the ATLAS detector. *Phys. Rev. D*, 94:052009, 2016.

- [1582] ATLAS Collaboration. Search for top squarks in final states with one isolated lepton, jets, and missing transverse momentum in $\sqrt{s} = 13$ TeV pp collisions with the ATLAS detector. ATLAS-CONF-2016-050, 2016.
- [1583] ATLAS Collaboration. Search for ZZ resonances in the $\ell\ell qq$ final state in pp collisions at $\sqrt{s} = 13$ TeV with the ATLAS detector. ATLAS-CONF-2016-016, 2016.
- [1584] ATLAS Collaboration. Searches for heavy diboson resonances in pp collisions at $\sqrt{s} = 13$ TeV with the ATLAS detector. *JHEP*, 09:173, 2016.
- [1585] ATLAS Collaboration. Searches for heavy ZZ and ZW resonances in the $\ell\ell qq$ and $\nu\nu qq$ final states in pp collisions at $\sqrt{s} = 13$ TeV with the ATLAS detector. ATLAS-CONF-2016-082, 2016.
- [1586] ATLAS Collaboration. Searches for scalar leptoquarks in pp collisions at $\sqrt{s} = 8$ TeV with the ATLAS detector. *Eur. Phys. J. C*, 76:5, 2016.
- [1587] ATLAS Collaboration. Simulation of top-quark production for the ATLAS experiment at $\sqrt{s} = 13$ TeV. ATL-PHYS-PUB-2016-004, 2016.
- [1588] ATLAS Collaboration. Studies of b-tagging performance and jet substructure in a high p_T $g \rightarrow b\bar{b}$ rich sample of large-R jets from pp collisions at $\sqrt{s} = 8$ TeV with the ATLAS detector. ATLAS-CONF-2016-002, 2016.
- [1589] ATLAS Collaboration. Studies of $t\bar{t}c\bar{c}$ production with MADGRAPH5_AMC@NLO and HERWIG++ for the ATLAS experiment. ATL-PHYS-PUB-2016-011, 2016.
- [1590] ATLAS Collaboration. Studies on top-quark Monte Carlo modelling for Top2016. ATL-PHYS-PUB-2016-020, 2016.
- [1591] ATLAS Collaboration. Studies related to gender and geographic diversity in the ATLAS Collaboration. ATL-GEN-PUB-2016-001, 2016.
- [1592] ATLAS Collaboration. Study of hard double-parton scattering in four-jet events in pp collisions at $\sqrt{s} = 7$ TeV with the ATLAS experiment. 2016.
- [1593] ATLAS Collaboration. Study of higher-order QCD corrections in the $gg \rightarrow H \rightarrow WW$ process. ATL-PHYS-PUB-2016-006, 2016.
- [1594] ATLAS Collaboration. Study of $J/\psi \rightarrow \mu^+\mu^-$ and $\psi(2S) \rightarrow \mu^+\mu^-$ production with 2015 Pb+Pb data at $\sqrt{s_{\text{NN}}} = 5.02$ TeV and pp data at $\sqrt{s} = 5.02$ TeV with the ATLAS detector. ATLAS-CONF-2016-109, 2016.

- [1595] ATLAS Collaboration. Study of photon-jet momentum correlations in Pb+Pb and pp collisions at $\sqrt{s_{\text{NN}}} = 5.02$ TeV with ATLAS. ATLAS-CONF-2016-110, 2016.
- [1596] ATLAS Collaboration. Study of the $B_c^+ \rightarrow J/\psi D_s^+$ and $B_c^+ \rightarrow J/\psi D_s^{*+}$ decays with the ATLAS detector. *Eur. Phys. J. C*, 76:4, 2016.
- [1597] ATLAS Collaboration. Study of the Higgs boson properties and search for high-mass scalar resonances in the $H \rightarrow ZZ^* \rightarrow 4\ell$ decay channel at $\sqrt{s} = 13$ TeV with the ATLAS detector. ATLAS-CONF-2016-079, 2016.
- [1598] ATLAS Collaboration. Study of the rare decays of B_s^0 and B^0 into muon pairs from data collected during the LHC Run 1 with the ATLAS detector. *Eur. Phys. J. C*, 76:513, 2016.
- [1599] ATLAS Collaboration. Test of CP Invariance in vector-boson fusion production of the Higgs boson using the *Optimal Observable* method in the ditau decay channel with the ATLAS detector. *Eur. Phys. J. C*, 76:658, 2016.
- [1600] ATLAS Collaboration. The performance of the jet trigger for the ATLAS detector during 2011 data taking. *Eur. Phys. J. C*, 76:526, 2016.
- [1601] ATLAS Collaboration. The Pythia 8 A3 tune description of ATLAS minimum bias and inelastic measurements incorporating the Donnachie-Landshoff diffractive model. ATL-PHYS-PUB-2016-017, 2016.
- [1602] ATLAS Collaboration. Top-quark mass measurement in the all-hadronic $t\bar{t}$ decay channel at $\sqrt{s} = 8$ TeV with the ATLAS detector. ATLAS-CONF-2016-064, 2016.
- [1603] ATLAS Collaboration. Transverse momentum, rapidity, and centrality dependence of inclusive charged-particle production in $\sqrt{s_{\text{NN}}} = 5.02$ TeV p+Pb collisions measured by the ATLAS experiment. *Phys. Lett. B*, 763:313, 2016.
- [1604] ATLAS Collaboration. Trigger monitoring and rate predictions using Enhanced Bias data from the ATLAS Detector at the LHC. ATL-DAQ-PUB-2016-002, 2016.
- [1605] ATLAS Collaboration. Validation of Monte Carlo event generators in the ATLAS Collaboration for LHC Run 2. ATL-PHYS-PUB-2016-001, 2016.
- [1606] ATLAS Collaboration. Z Boson Production in pp Collisions at $\sqrt{s} = 5.02$ with the ATLAS detector at the LHC. ATLAS-CONF-2016-107, 2016.
- [1607] ATLAS Collaboration. *Eur. Phys. J. C*, 77:712, 2017.

- [1608] ATLAS Collaboration. A measurement of the calorimeter response to single hadrons and determination of the jet energy scale uncertainty using LHC Run-1 pp -collision data with the ATLAS detector. *Eur. Phys. J. C*, 77:26, 2017.
- [1609] ATLAS Collaboration. A measurement of the soft-drop jet mass in pp collisions at $\sqrt{s} = 13 \text{ TeV}$ with the ATLAS detector. 2017.
- [1610] ATLAS Collaboration. A model-independent general search for new phenomena with the ATLAS detector at $\sqrt{s} = 13 \text{ TeV}$. ATLAS-CONF-2017-001, 2017.
- [1611] ATLAS Collaboration. A search for B-L R-parity-violating scalar top in $\sqrt{s} = 13 \text{ TeV} \text{ pp}$ collisions with the ATLAS experiment. ATLAS-CONF-2017-036, 2017.
- [1612] ATLAS Collaboration. A search for B – L R-parity-violating top squarks in $\sqrt{s} = 13 \text{ TeV} \text{ pp}$ collisions with the ATLAS experiment. 2017.
- [1613] ATLAS Collaboration. A search for pair-produced resonances in four-jet final states at $\sqrt{s} = 13 \text{ TeV}$ with the ATLAS detector. 2017.
- [1614] ATLAS Collaboration. A search for pair-produced resonances in four-jet final states at $\sqrt{s} = 13 \text{ TeV}$ with the ATLAS detector. ATLAS-CONF-2017-025, 2017.
- [1615] ATLAS Collaboration. A search for resonances decaying into a Higgs boson and a new particle X in the $XH \rightarrow q\bar{q}bb$ final state with the ATLAS detector. 2017.
- [1616] ATLAS Collaboration. A study of different colour reconnection settings for Pythia8 generator using underlying event observables. ATL-PHYS-PUB-2017-008, 2017.
- [1617] ATLAS Collaboration. Analysis of the Wtb vertex from the measurement of triple-differential angular decay rates of single top quarks produced in the t-channel at $\sqrt{s} = 8 \text{ TeV}$ with the ATLAS detector. *JHEP*, 12:017, 2017.
- [1618] ATLAS Collaboration. Analytical description of missing transverse-momentum trigger rates in ATLAS with $\sqrt{s} = 7$ and 8 TeV data. ATL-DAQ-PUB-2017-002, 2017.
- [1619] ATLAS Collaboration. Angular analysis of $B_d^0 \rightarrow K^*\mu^+\mu^-$ decays in pp collisions at $\sqrt{s} = 13 \text{ TeV}$ with the ATLAS detector. ATLAS-CONF-2017-023, 2017.

- [1620] ATLAS Collaboration. ATLAS simulation of boson plus jets processes in Run 2. ATL-PHYS-PUB-2017-006, 2017.
- [1621] ATLAS Collaboration. Azimuthal femtoscopy in central p +Pb collisions at $\sqrt{s_{NN}} = 5.02$ TeV with ATLAS. ATLAS-CONF-2017-008, 2017.
- [1622] ATLAS Collaboration. Beam backgrounds in the ATLAS detector during LHC loss map tests at $\beta^* = 40$ cm and $\beta^* = 80$ cm at $E_{beam} = 6.5$ TeV. ATL-DAPR-PUB-2017-001, 2017.
- [1623] ATLAS Collaboration. Combined measurements of Higgs boson production and decay in the $H \rightarrow ZZ^* \rightarrow 4\ell$ and $H \rightarrow \gamma\gamma$ channels using $\sqrt{s} = 13$ TeV proton-proton collision data collected with the ATLAS experiment. ATLAS-CONF-2017-047, 2017.
- [1624] ATLAS Collaboration. Constituent-level pile-up mitigation techniques in ATLAS. ATLAS-CONF-2017-065, 2017.
- [1625] ATLAS Collaboration. Constraints on an effective Lagrangian from the combined $H \rightarrow ZZ^* \rightarrow 4\ell$ and $H \rightarrow \gamma\gamma$ channels using 36.1 fb^{-1} of $\sqrt{s} = 13$ TeV pp collision data collected with the ATLAS detector. ATL-PHYS-PUB-2017-018, 2017.
- [1626] ATLAS Collaboration. D meson production and long-range azimuthal correlation in 8.16 TeV p+Pb collisions with ATLAS. ATLAS-CONF-2017-073, 2017.
- [1627] ATLAS Collaboration. Determination of the strong coupling constant α_s from transverse energy-energy correlations in multijet events at $\sqrt{s} = 8$ TeV using the ATLAS detector. *Eur. Phys. J. C*, 77:872, 2017.
- [1628] ATLAS Collaboration. Differential $ZZ \rightarrow \ell^+\ell^-\ell'^+\ell'^-$ cross section measurements and a TGC search in 13 TeV pp collisions with the ATLAS detector. ATLAS-CONF-2017-031, 2017.
- [1629] ATLAS Collaboration. Direct top-quark decay width measurement in the $t\bar{t}$ lepton+jets channel at $\sqrt{s} = 8$ TeV with the ATLAS experiment. 2017.
- [1630] ATLAS Collaboration. Direct top-quark decay width measurement in the $t\bar{t}$ lepton+jets channel at $\sqrt{s} = 8$ TeV with the ATLAS experiment. ATLAS-CONF-2017-056, 2017.
- [1631] ATLAS Collaboration. Electron and photon reconstruction and performance in ATLAS using a dynamical, topological cell clustering-based approach. ATL-PHYS-PUB-2017-022, 2017.

- [1632] ATLAS Collaboration. Electron efficiency measurements with the ATLAS detector using 2012 LHC proton–proton collision data. *Eur. Phys. J. C*, 77:195, 2017.
- [1633] ATLAS Collaboration. Evidence for light-by-light scattering in heavy-ion collisions with the ATLAS detector at the LHC. *Nature Phys.*, 2017.
- [1634] ATLAS Collaboration. Evidence for the associated production of the Higgs boson and a top quark pair with the ATLAS detector. 2017.
- [1635] ATLAS Collaboration. Evidence for the associated production of the Higgs boson and a top quark pair with the ATLAS detector. ATLAS-CONF-2017-077, 2017.
- [1636] ATLAS Collaboration. Evidence for the $H \rightarrow b\bar{b}$ decay with the ATLAS detector. *JHEP*, 12:024, 2017.
- [1637] ATLAS Collaboration. Evidence for the $H \rightarrow b\bar{b}$ decay with the ATLAS detector. ATLAS-CONF-2017-041, 2017.
- [1638] ATLAS Collaboration. Femtoscopy with identified charged pions in proton–lead collisions at $\sqrt{s_{NN}} = 5.02$ TeV with ATLAS. *Phys. Rev. C*, 96:064908, 2017.
- [1639] ATLAS Collaboration. Fiducial, total and differential cross-section measurements of t-channel single top-quark production in $p\bar{p}$ collisions at 8 TeV using data collected by the ATLAS detector. *Eur. Phys. J. C*, 77:531, 2017.
- [1640] ATLAS Collaboration. Flow fluctuations using four-particle cumulants in Pb+Pb collisions at $\sqrt{s_{NN}} = 5.02$ TeV with the ATLAS detector. ATLAS-CONF-2017-066, 2017.
- [1641] ATLAS Collaboration. High- E_T isolated-photon plus jets production in $p\bar{p}$ collisions at $\sqrt{s} = 8$ TeV with the ATLAS detector. *Nucl. Phys. B*, 918:257, 2017.
- [1642] ATLAS Collaboration. Identification and rejection of pile-up jets at high pseudorapidity with the ATLAS detector. *Eur. Phys. J. C*, 77:580, 2017.
- [1643] ATLAS Collaboration. Identification of Hadronically-Decaying W Bosons and Top Quarks Using High-Level Features as Input to Boosted Decision Trees and Deep Neural Networks in ATLAS at $\sqrt{s} = 13$ TeV. ATL-PHYS-PUB-2017-004, 2017.
- [1644] ATLAS Collaboration. Identification of Jets Containing b-Hadrons with Recurrent Neural Networks at the ATLAS Experiment. ATL-PHYS-PUB-2017-003, 2017.

- [1645] ATLAS Collaboration. Impact of Alternative Inputs and Grooming Methods on Large-R Jet Reconstruction in ATLAS. ATL-PHYS-PUB-2017-020, 2017.
- [1646] ATLAS Collaboration. Improving jet substructure performance in ATLAS using Track-Calorimeters. ATL-PHYS-PUB-2017-015, 2017.
- [1647] ATLAS Collaboration. In-situ measurements of the ATLAS large-radius jet response in 13 TeV pp collisions. ATLAS-CONF-2017-063, 2017.
- [1648] ATLAS Collaboration. Jet energy scale measurements and their systematic uncertainties in proton–proton collisions at $\sqrt{s} = 13$ TeV with the ATLAS detector. *Phys. Rev. D*, 96:072002, 2017.
- [1649] ATLAS Collaboration. Jet reclustering and close-by effects in ATLAS Run 2. ATLAS-CONF-2017-062, 2017.
- [1650] ATLAS Collaboration. Jet reconstruction and performance using particle flow with the ATLAS Detector. *Eur. Phys. J. C*, 77:466, 2017.
- [1651] ATLAS Collaboration. Measurement of b-hadron pair production with the ATLAS detector in proton–proton collisions at $\sqrt{s} = 8$ TeV. *JHEP*, 11:062, 2017.
- [1652] ATLAS Collaboration. Measurement of charged-particle distributions sensitive to the underlying event in $\sqrt{s} = 13$ TeV proton–proton collisions with the ATLAS detector at the LHC. *JHEP*, 03:157, 2017.
- [1653] ATLAS Collaboration. Measurement of colour flow using jet-pull observables in $t\bar{t}$ events with the ATLAS experiment at $\sqrt{s} = 13$ TeV. ATLAS-CONF-2017-069, 2017.
- [1654] ATLAS Collaboration. Measurement of contributions of diffractive processes to forward photon spectra in pp collisions at $\sqrt{s} = 13$ TeV. ATLAS-CONF-2017-075, 2017.
- [1655] ATLAS Collaboration. Measurement of detector-corrected observables sensitive to the anomalous production of events with jets and large missing transverse momentum in pp collisions at $\sqrt{s} = 13$ TeV using the ATLAS detector. *Eur. Phys. J. C*, 77:765, 2017.
- [1656] ATLAS Collaboration. Measurement of differential cross sections and W^+/W^- cross-section ratios for W boson production in association with jets at $\sqrt{s} = 8$ TeV with the ATLAS detector. 2017.
- [1657] ATLAS Collaboration. Measurement of differential cross-sections of a single top quark produced in association with a W boson at $\sqrt{s} = 13$ TeV with ATLAS. 2017.

- [1658] ATLAS Collaboration. Measurement of forward-backward multiplicity correlations in lead–lead, proton–lead and proton–proton collisions with the ATLAS detector. *Phys. Rev. C*, 95:064914, 2017.
- [1659] ATLAS Collaboration. Measurement of inclusive and differential cross sections in the $H \rightarrow ZZ^* \rightarrow 4\ell$ decay channel at 13 TeV with the ATLAS detector. ATLAS-CONF-2017-032, 2017.
- [1660] ATLAS Collaboration. Measurement of inclusive and differential cross sections in the $H \rightarrow ZZ^* \rightarrow 4\ell$ decay channel in pp collisions at $\sqrt{s} = 13$ TeV with the ATLAS detector. *JHEP*, 10:132, 2017.
- [1661] ATLAS Collaboration. Measurement of inclusive jet and dijet cross-sections in proton–proton collisions at $\sqrt{s} = 13$ TeV with the ATLAS detector. 2017.
- [1662] ATLAS Collaboration. Measurement of inclusive jet and dijet cross-sections in proton–proton collisions at $\sqrt{s} = 13$ TeV with the ATLAS detector. ATLAS-CONF-2017-048, 2017.
- [1663] ATLAS Collaboration. Measurement of jet activity produced in top-quark events with an electron, a muon and two b -tagged jets in the final state in pp collisions at $\sqrt{s} = 13$ TeV with the ATLAS detector. *Eur. Phys. J. C*, 77:220, 2017.
- [1664] ATLAS Collaboration. Measurement of jet fragmentation in 5.02 TeV lead–lead and proton–proton collisions with the ATLAS detector. ATLAS-CONF-2017-005, 2017.
- [1665] ATLAS Collaboration. Measurement of jet fragmentation in 5.02 TeV proton–lead and proton–proton collisions with the ATLAS detector. 2017.
- [1666] ATLAS Collaboration. Measurement of jet fragmentation in 5.02 TeV proton–lead and proton–proton collisions with the ATLAS detector. ATLAS-CONF-2017-004, 2017.
- [1667] ATLAS Collaboration. Measurement of jet fragmentation in Pb+Pb and pp collisions at $\sqrt{s_{NN}} = 2.76$ TeV with the ATLAS detector at the LHC. *Eur. Phys. J. C*, 77:379, 2017.
- [1668] ATLAS Collaboration. Measurement of jet p_T correlations in Pb+Pb and pp collisions at $\sqrt{s_{NN}} = 2.76$ TeV with the ATLAS detector. *Phys. Lett. B*, 774:379, 2017.
- [1669] ATLAS Collaboration. Measurement of lepton differential distributions and the top quark mass in $t\bar{t}$ production in pp collisions at $\sqrt{s} = 8$ TeV with the ATLAS detector. *Eur. Phys. J. C*, 77:804, 2017.

- [1670] ATLAS Collaboration. Measurement of lepton differential distributions and the top quark mass in $t\bar{t}$ production in $p\bar{p}$ collisions at $\sqrt{s} = 8$ TeV with the ATLAS detector. ATLAS-CONF-2017-044, 2017.
- [1671] ATLAS Collaboration. Measurement of long-range azimuthal correlations in Z -boson tagged $p\bar{p}$ collisions at $\sqrt{s} = 8$ TeV. ATLAS-CONF-2017-068, 2017.
- [1672] ATLAS Collaboration. Measurement of longitudinal flow correlations in $Pb+Pb$ collisions at $\sqrt{s_{NN}} = 2.76$ TeV and 5.02 TeV with the ATLAS detector. ATLAS-CONF-2017-003, 2017.
- [1673] ATLAS Collaboration. Measurement of longitudinal flow de-correlations in $Pb+Pb$ collisions at $\sqrt{s_{NN}} = 2.76$ and 5.02 TeV with the ATLAS detector. 2017.
- [1674] ATLAS Collaboration. Measurement of multi-particle azimuthal correlations in $p\bar{p}$, $p+Pb$ and low-multiplicity $Pb+Pb$ collisions with the ATLAS detector. *Eur. Phys. J. C*, 77:428, 2017.
- [1675] ATLAS Collaboration. Measurement of multi-particle azimuthal correlations in $p\bar{p}$, $p+Pb$ and low-multiplicity $Pb+Pb$ collisions with the ATLAS detector. ATLAS-CONF-2017-007, 2017.
- [1676] ATLAS Collaboration. Measurement of multi-particle azimuthal correlations with the subevent cumulant method in $p\bar{p}$ and $p+Pb$ collisions with the ATLAS detector. ATLAS-CONF-2017-002, 2017.
- [1677] ATLAS Collaboration. Measurement of multi-particle azimuthal correlations with the subevent cumulant method in $p\bar{p}$ and $p+Pb$ collisions with the ATLAS detector at the LHC. 2017.
- [1678] ATLAS Collaboration. Measurement of nuclear modification factor R_{AA} in $Pb+Pb$ collisions at $\sqrt{s_{NN}} = 5.02$ TeV with the ATLAS detector at the LHC. ATLAS-CONF-2017-012, 2017.
- [1679] ATLAS Collaboration. Measurement of quarkonium production in proton–lead and proton–proton collisions at 5.02 TeV with the ATLAS detector. 2017.
- [1680] ATLAS Collaboration. Measurement of Tau Polarisation in $Z/\gamma^* \rightarrow \tau\tau$ Decays in Proton–Proton Collisions at $\sqrt{s} = 8$ TeV with the ATLAS Detector. ATLAS-CONF-2017-049, 2017.
- [1681] ATLAS Collaboration. Measurement of τ polarisation in $Z/\gamma^* \rightarrow \tau\tau$ decays in proton–proton collisions at $\sqrt{s} = 8$ TeV with the ATLAS detector. 2017.

- [1682] ATLAS Collaboration. Measurement of the cross-section for electroweak production of dijets in association with a Z boson in pp collisions at $\sqrt{s} = 13$ TeV with the ATLAS detector. *Phys. Lett. B*, 775:206, 2017.
- [1683] ATLAS Collaboration. Measurement of the cross section for inclusive isolated-photon production in pp collisions at $\sqrt{s} = 13$ TeV using the ATLAS detector. *Phys. Lett. B*, 770:473, 2017.
- [1684] ATLAS Collaboration. Measurement of the cross section for isolated-photon plus jet production in pp collisions at $\sqrt{s} = 13$ TeV using the ATLAS detector. ATLAS-CONF-2017-059, 2017.
- [1685] ATLAS Collaboration. Measurement of the Drell–Yan triple-differential cross section in pp collisions at $\sqrt{s} = 8$ TeV. *JHEP*, 12:059, 2017.
- [1686] ATLAS Collaboration. Measurement of the fragmentation function for photon-tagged jets in $\sqrt{s_{\text{NN}}} = 5.02$ TeV Pb+Pb and pp collisions with the ATLAS detector. ATLAS-CONF-2017-074, 2017.
- [1687] ATLAS Collaboration. Measurement of the Higgs boson coupling properties in the $H \rightarrow ZZ^* \rightarrow 4\ell$ decay channel at $\sqrt{s} = 13$ TeV with the ATLAS detector. 2017.
- [1688] ATLAS Collaboration. Measurement of the Higgs boson coupling properties in the $H \rightarrow ZZ^* \rightarrow 4\ell$ decay channel at $\sqrt{s} = 13$ TeV with the ATLAS detector. ATLAS-CONF-2017-043, 2017.
- [1689] ATLAS Collaboration. Measurement of the Higgs boson mass in the $H \rightarrow ZZ^* \rightarrow 4\ell$ and $H \rightarrow \gamma\gamma$ channels with $\sqrt{s} = 13$ TeV pp collisions using the ATLAS detector. ATLAS-CONF-2017-046, 2017.
- [1690] ATLAS Collaboration. Measurement of the inclusive and fiducial $t\bar{t}$ production cross-sections in the lepton+jets channel in pp collisions at $\sqrt{s} = 8$ TeV with the ATLAS detector. 2017.
- [1691] ATLAS Collaboration. Measurement of the inclusive cross-sections of single top-quark and top-antiquark t-channel production in pp collisions at $\sqrt{s} = 13$ TeV with the ATLAS detector. *JHEP*, 04:086, 2017.
- [1692] ATLAS Collaboration. Measurement of the inclusive jet cross-sections in proton–proton collisions at $\sqrt{s} = 8$ TeV with the ATLAS detector. *JHEP*, 09:020, 2017.
- [1693] ATLAS Collaboration. Measurement of the inclusive $t\bar{t}$ cross-section in the lepton+jets channel in pp collisions at $\sqrt{s} = 8$ TeV at the ATLAS detector. ATLAS-CONF-2017-054, 2017.

- [1694] ATLAS Collaboration. Measurement of the k_t splitting scales in $Z \rightarrow ll$ events in $p\bar{p}$ collisions at $\sqrt{s} = 8$ TeV with the ATLAS detector. *JHEP*, 08:026, 2017.
- [1695] ATLAS Collaboration. Measurement of the long-range pseudorapidity correlations between muons and charged particles in $\sqrt{s_{NN}} = 8.16$ TeV proton–lead collisions with the ATLAS detector. ATLAS-CONF-2017-006, 2017.
- [1696] ATLAS Collaboration. Measurement of the production cross-section of a single top quark in association with a Z boson in proton–proton collisions at 13 TeV with the ATLAS detector. 2017.
- [1697] ATLAS Collaboration. Measurement of the production cross-section of a single top quark in association with a Z boson in proton–proton collisions at 13 TeV with the ATLAS detector. ATLAS-CONF-2017-052, 2017.
- [1698] ATLAS Collaboration. Measurement of the production cross section of three isolated photons in $p\bar{p}$ collisions at $\sqrt{s} = 8$ TeV using the ATLAS detector. 2017.
- [1699] ATLAS Collaboration. Measurement of the prompt J/ψ pair production cross-section in $p\bar{p}$ collisions at $\sqrt{s} = 8$ TeV with the ATLAS detector. *Eur. Phys. J. C*, 77:76, 2017.
- [1700] ATLAS Collaboration. Measurement of the tau lepton reconstruction and identification performance in the ATLAS experiment using $p\bar{p}$ collisions at $\sqrt{s} = 13$ TeV. ATLAS-CONF-2017-029, 2017.
- [1701] ATLAS Collaboration. Measurement of the $t\bar{t}$ production cross section in the $\tau + \text{jets}$ final state in $p\bar{p}$ collisions at $\sqrt{s} = 8$ TeV using the ATLAS detector. *Phys. Rev. D*, 95:072003, 2017.
- [1702] ATLAS Collaboration. Measurement of the $t\bar{t}\gamma$ production cross section in proton–proton collisions at $\sqrt{s} = 8$ TeV with the ATLAS detector. *JHEP*, 11:086, 2017.
- [1703] ATLAS Collaboration. Measurement of the $t\bar{t}Z$ and $t\bar{t}W$ production cross sections in multilepton final states using 3.2 fb^{-1} of $p\bar{p}$ collisions at $\sqrt{s} = 13$ TeV with the ATLAS detector. *Eur. Phys. J. C*, 77:40, 2017.
- [1704] ATLAS Collaboration. Measurement of the top quark mass in the $t\bar{t} \rightarrow \text{lepton+jets}$ channel from $\sqrt{s} = 8$ TeV ATLAS data. ATLAS-CONF-2017-071, 2017.
- [1705] ATLAS Collaboration. Measurement of the W -boson mass in $p\bar{p}$ collisions at $\sqrt{s} = 7$ TeV with the ATLAS detector. 2017.

- [1706] ATLAS Collaboration. Measurement of the W boson polarisation in $t\bar{t}$ events from pp collisions at $\sqrt{s} = 8$ TeV in the lepton+jets channel with ATLAS. *Eur. Phys. J. C*, 77:264, 2017.
- [1707] ATLAS Collaboration. Measurement of the W^+W^- production cross section in pp collisions at a centre-of-mass energy of $\sqrt{s} = 13$ TeV with the ATLAS experiment. 2017.
- [1708] ATLAS Collaboration. Measurement of the ZZ production cross section in proton-proton collisions at $\sqrt{s} = 8$ TeV using the $ZZ \rightarrow \ell^-\ell^+\ell^-\ell^+$ and $ZZ \rightarrow \ell^-\ell^+\nu\bar{\nu}$ decay channels with the ATLAS detector. *JHEP*, 01:099, 2017.
- [1709] ATLAS Collaboration. Measurement of W boson angular distributions in events with high transverse momentum jets at $\sqrt{s} = 8$ TeV using the ATLAS detector. *Phys. Lett. B*, 765:132, 2017.
- [1710] ATLAS Collaboration. Measurement of W boson production in the muon channel in $Pb+Pb$ collisions at $\sqrt{s_{NN}} = 5.02$ TeV. ATLAS-CONF-2017-067, 2017.
- [1711] ATLAS Collaboration. Measurement of $W^\pm W^\pm$ vector-boson scattering and limits on anomalous quartic gauge couplings with the ATLAS detector. *Phys. Rev. D*, 96:012007, 2017.
- [1712] ATLAS Collaboration. Measurement of $WW/WZ \rightarrow \ell\nu qq'$ production with the hadronically decaying boson reconstructed as one or two jets in pp collisions at $\sqrt{s} = 8$ TeV with ATLAS, and constraints on anomalous gauge couplings. *Eur. Phys. J. C*, 77:563, 2017.
- [1713] ATLAS Collaboration. Measurements of charge and CP asymmetries in b -hadron decays using top-quark events collected by the ATLAS detector in pp collisions at $\sqrt{s} = 8$ TeV. *JHEP*, 02:071, 2017.
- [1714] ATLAS Collaboration. Measurements of electroweak Wjj production and constraints on anomalous gauge couplings with the ATLAS detector. *Eur. Phys. J. C*, 77:474, 2017.
- [1715] ATLAS Collaboration. Measurements of Higgs boson properties in the diphoton decay channel with 36.1 fb^{-1} pp collision data at the center-of-mass energy of 13 TeV with the ATLAS detector. ATLAS-CONF-2017-045, 2017.
- [1716] ATLAS Collaboration. Measurements of integrated and differential cross sections for isolated photon pair production in pp collisions at $\sqrt{s} = 8$ TeV with the ATLAS detector. *Phys. Rev. D*, 95:112005, 2017.

- [1717] ATLAS Collaboration. Measurements of long-range azimuthal anisotropies and associated Fourier coefficients for pp collisions at $\sqrt{s} = 5.02$ and 13 TeV and p+Pb collisions at $\sqrt{s_{\text{NN}}} = 5.02$ TeV with the ATLAS detector. *Phys. Rev. C*, 96:024908, 2017.
- [1718] ATLAS Collaboration. Measurements of $\psi(2S)$ and $X(3872) \rightarrow J/\psi \pi^+ \pi^-$ production in pp collisions at $\sqrt{s} = 8$ TeV with the ATLAS detector. *JHEP*, 01:117, 2017.
- [1719] ATLAS Collaboration. Measurements of the production cross section of a Z boson in association with jets in pp collisions at $\sqrt{s} = 13$ TeV with the ATLAS detector. *Eur. Phys. J. C*, 77:361, 2017.
- [1720] ATLAS Collaboration. Measurements of top-quark pair differential cross-sections in the $e\mu$ channel in pp collisions at $\sqrt{s} = 13$ TeV using the ATLAS detector. *Eur. Phys. J. C*, 77:292, 2017.
- [1721] ATLAS Collaboration. Measurements of top-quark pair differential cross-sections in the lepton+jets channel in pp collisions at $\sqrt{s} = 13$ TeV using the ATLAS detector. *JHEP*, 11:191, 2017.
- [1722] ATLAS Collaboration. Measurements of top-quark pair to Z -boson cross-section ratios at $\sqrt{s} = 13, 8, 7$ TeV with the ATLAS detector. *JHEP*, 02:117, 2017.
- [1723] ATLAS Collaboration. Measurements of top quark spin observables in $t\bar{t}$ events using dilepton final states in $\sqrt{s} = 8$ TeV pp collisions with the ATLAS detector. *JHEP*, 03:113, 2017.
- [1724] ATLAS Collaboration. Modelling of Track Reconstruction Inside Jets with the 2016 ATLAS $\sqrt{s} = 13$ TeV pp Dataset. ATL-PHYS-PUB-2017-016, 2017.
- [1725] ATLAS Collaboration. Multi-Boson Simulation for 13 TeV ATLAS Analyses. ATL-PHYS-PUB-2017-005, 2017.
- [1726] ATLAS Collaboration. Optimisation and performance studies of the ATLAS b-tagging algorithms for the 2017-18 LHC run. ATL-PHYS-PUB-2017-013, 2017.
- [1727] ATLAS Collaboration. Performance of algorithms that reconstruct missing transverse momentum in $\sqrt{s} = 8$ TeV proton–proton collisions in the ATLAS detector. *Eur. Phys. J. C*, 77:241, 2017.
- [1728] ATLAS Collaboration. Performance of the ATLAS track reconstruction algorithms in dense environments in LHC Run 2. *Eur. Phys. J. C*, 77:673, 2017.

- [1729] ATLAS Collaboration. Performance of the ATLAS Transition Radiation Tracker in Run 1 of the LHC: tracker properties. *JINST*, 12:P05002, 2017.
- [1730] ATLAS Collaboration. Performance of the ATLAS Trigger System in 2015. *Eur. Phys. J. C*, 77:317, 2017.
- [1731] ATLAS Collaboration. Performance of the reconstruction of large impact parameter tracks in the inner detector of ATLAS. ATL-PHYS-PUB-2017-014, 2017.
- [1732] ATLAS Collaboration. Performance of Top Quark and W Boson Tagging in Run 2 with ATLAS. ATLAS-CONF-2017-064, 2017.
- [1733] ATLAS Collaboration. Photo-nuclear dijet production in ultra-peripheral $\text{Pb}+\text{Pb}$ collisions. ATLAS-CONF-2017-011, 2017.
- [1734] ATLAS Collaboration. Precision measurement and interpretation of inclusive W^+ , W^- and Z/γ^* production cross sections with the ATLAS detector. *Eur. Phys. J. C*, 77:367, 2017.
- [1735] ATLAS Collaboration. Probing the Wtb vertex structure in t-channel single-top-quark production and decay in pp collisions at $\sqrt{s} = 8$ TeV with the ATLAS detector. *JHEP*, 04:124, 2017.
- [1736] ATLAS Collaboration. Prompt photon production in $\sqrt{s_{\text{NN}}} = 8.16$ TeV $\text{p}+\text{Pb}$ collisions with ATLAS. ATLAS-CONF-2017-072, 2017.
- [1737] ATLAS Collaboration. Prospects for the measurement of the W -boson transverse momentum with a low pileup data sample at $\sqrt{s} = 13$ TeV with the ATLAS detector. ATL-PHYS-PUB-2017-021, 2017.
- [1738] ATLAS Collaboration. Proton tagging with the one arm AFP detector. ATL-PHYS-PUB-2017-012, 2017.
- [1739] ATLAS Collaboration. Quark versus Gluon Jet Tagging Using Charged-Particle Constituent Multiplicity with the ATLAS Detector. ATL-PHYS-PUB-2017-009, 2017.
- [1740] ATLAS Collaboration. Quark versus Gluon Jet Tagging Using Jet Images with the ATLAS Detector. ATL-PHYS-PUB-2017-017, 2017.
- [1741] ATLAS Collaboration. Radiation induced effects in the ATLAS Insertable B-Layer readout chip. ATL-INDET-PUB-2017-001, 2017.
- [1742] ATLAS Collaboration. Reconstruction of primary vertices at the ATLAS experiment in Run 1 proton–proton collisions at the LHC. *Eur. Phys. J. C*, 77:332, 2017.

- [1743] ATLAS Collaboration. Search for a new heavy gauge boson resonance decaying into a lepton and missing transverse momentum in 36 fb^{-1} of pp collisions at $\sqrt{s} = 13 \text{ TeV}$ with the ATLAS experiment. 2017.
- [1744] ATLAS Collaboration. Search for a new heavy gauge boson resonance decaying into a lepton and missing transverse momentum in 36 fb^{-1} of pp collisions at $\sqrt{s} = 13 \text{ TeV}$ with the ATLAS experiment. ATLAS-CONF-2017-016, 2017.
- [1745] ATLAS Collaboration. Search for a Scalar Partner of the Top Quark in the E_T^{miss} Final State at $\sqrt{s} = 13 \text{ TeV}$ with the ATLAS detector. ATLAS-CONF-2017-020, 2017.
- [1746] ATLAS Collaboration. Search for a scalar partner of the top quark in the jets plus missing transverse momentum final state at $\sqrt{s} = 13 \text{ TeV}$ with the ATLAS detector. *JHEP*, 12:085, 2017.
- [1747] ATLAS Collaboration. Search for additional heavy neutral Higgs and gauge bosons in the ditau final state produced in 36.1 fb^{-1} of pp collisions at $\sqrt{s} = 13 \text{ TeV}$ with the ATLAS detector. ATLAS-CONF-2017-050, 2017.
- [1748] ATLAS Collaboration. Search for an invisibly decaying Higgs boson or dark matter candidates produced in association with a Z boson in pp collisions at $\sqrt{s} = 13 \text{ TeV}$ with the ATLAS detector. ATLAS-CONF-2017-040, 2017.
- [1749] ATLAS Collaboration. Search for anomalous electroweak production of WW/WZ in association with a high-mass dijet system in pp collisions at $\sqrt{s} = 8 \text{ TeV}$ with the ATLAS detector. *Phys. Rev. D*, 95:032001, 2017.
- [1750] ATLAS Collaboration. Search for dark matter and other new phenomena in events with an energetic jet and large missing transverse momentum using the ATLAS detector. 2017.
- [1751] ATLAS Collaboration. Search for dark matter and other new phenomena in events with an energetic jet and large missing transverse momentum using the ATLAS detector. ATLAS-CONF-2017-060, 2017.
- [1752] ATLAS Collaboration. Search for dark matter at $\sqrt{s} = 13 \text{ TeV}$ in final states containing an energetic photon and large missing transverse momentum with the ATLAS detector. *Eur. Phys. J. C*, 77:393, 2017.
- [1753] ATLAS Collaboration. Search for dark matter in association with a Higgs boson decaying to b -quarks in pp collisions at $\sqrt{s} = 13 \text{ TeV}$ with the ATLAS detector. *Phys. Lett. B*, 765:11, 2017.

- [1754] ATLAS Collaboration. Search for dark matter in association with a Higgs boson decaying to two photons at $\sqrt{s} = 13$ TeV with the ATLAS detector. *Phys. Rev. D*, 96:112004, 2017.
- [1755] ATLAS Collaboration. Search for Dark Matter Produced in Association with a Higgs Boson Decaying to $b\bar{b}$ at $\sqrt{s} = 13$ TeV with the ATLAS Detector. ATLAS-CONF-2017-028, 2017.
- [1756] ATLAS Collaboration. Search for Dark Matter Produced in Association with a Higgs Boson Decaying to $b\bar{b}$ using 36 fb^{-1} of $p\bar{p}$ collisions at $\sqrt{s} = 13$ TeV with the ATLAS Detector. *Phys. Rev. Lett.*, 119:181804, 2017.
- [1757] ATLAS Collaboration. Search for direct pair production of higgsinos by reinterpretation of the disappearing track analysis with 36.1 fb^{-1} of $\sqrt{s} = 13$ TeV data collected with the ATLAS experiment. ATL-PHYS-PUB-2017-019, 2017.
- [1758] ATLAS Collaboration. Search for direct top squark pair production in events with a Higgs or Z boson, and missing transverse momentum in $p\bar{p}$ collisions at $\sqrt{s} = 13$ TeV with the ATLAS detector. ATLAS-CONF-2017-019, 2017.
- [1759] ATLAS Collaboration. Search for direct top squark pair production in events with a Higgs or Z boson, and missing transverse momentum in $\sqrt{s} = 13$ TeV $p\bar{p}$ collisions with the ATLAS detector. *JHEP*, 08:006, 2017.
- [1760] ATLAS Collaboration. Search for direct top squark pair production in final states with two leptons in $\sqrt{s} = 13$ TeV $p\bar{p}$ collisions with the ATLAS detector. *Eur. Phys. J. C*, 77:898, 2017.
- [1761] ATLAS Collaboration. Search for direct top squark pair production in final states with two leptons in $\sqrt{s} = 13$ TeV $p\bar{p}$ collisions with the ATLAS detector. ATLAS-CONF-2017-034, 2017.
- [1762] ATLAS Collaboration. Search for doubly charged Higgs boson production in multi-lepton final states with the ATLAS detector using proton–proton collisions at $\sqrt{s} = 13$ TeV. 2017.
- [1763] ATLAS Collaboration. Search for doubly-charged Higgs boson production in multi-lepton final states with the ATLAS detector using proton–proton collisions at $\sqrt{s} = 13$ TeV. ATLAS-CONF-2017-053, 2017.
- [1764] ATLAS Collaboration. Search for electroweak production of supersymmetric particles in the two and three lepton final state at $\sqrt{s} = 13$ TeV with the ATLAS detector. ATLAS-CONF-2017-039, 2017.

- [1765] ATLAS Collaboration. Search for electroweak production of supersymmetric states in scenarios with compressed mass spectra at $\sqrt{s} = 13$ TeV with the ATLAS detector. 2017.
- [1766] ATLAS Collaboration. Search for exclusive Higgs and Z boson decays to $\phi\gamma$ and $\rho\gamma$ with the ATLAS Detector. ATLAS-CONF-2017-057, 2017.
- [1767] ATLAS Collaboration. Search for exclusive Higgs and Z boson decays to $\phi\gamma$ and $\rho\gamma$ with the ATLAS detector. 2017.
- [1768] ATLAS Collaboration. Search for flavour-changing neutral current $t \rightarrow qZ$ top quark decays in proton–proton collisions at $\sqrt{s} = 13$ TeV with the ATLAS Detector. ATLAS-CONF-2017-070, 2017.
- [1769] ATLAS Collaboration. Search for heavy Higgs bosons A/H decaying to a top quark pair in pp collisions at $\sqrt{s} = 8$ TeV with the ATLAS detector. *Phys. Rev. Lett.*, 119:191803, 2017.
- [1770] ATLAS Collaboration. Search for heavy resonances decaying into a W or Z boson and a Higgs boson in final states with leptons and b-jets in 36 fb^{-1} of $\sqrt{s} = 13$ TeV pp collisions with the ATLAS detector. 2017.
- [1771] ATLAS Collaboration. Search for heavy resonances decaying to a W or Z boson and a Higgs boson in final states with leptons and b-jets in 36.1 fb^{-1} of pp collision data at $\sqrt{s} = 13$ TeV with the ATLAS detector. ATLAS-CONF-2017-055, 2017.
- [1772] ATLAS Collaboration. Search for heavy resonances decaying to a W or Z boson and a Higgs boson in the $q\bar{q}^{(\prime)}b\bar{b}$ final state in pp collisions at $\sqrt{s} = 13$ TeV with the ATLAS detector. *Phys. Lett. B*, 774:494, 2017.
- [1773] ATLAS Collaboration. Search for Heavy Resonances Decaying to a W or Z Boson and a Higgs Boson in the $q\bar{q}^{(\prime)}b\bar{b}$ Final State in pp Collisions at $\sqrt{s} = 13$ TeV with the ATLAS Detector. ATLAS-CONF-2017-018, 2017.
- [1774] ATLAS Collaboration. Search for heavy resonances decaying to a Z boson and a photon in pp collisions at $\sqrt{s} = 13$ TeV with the ATLAS detector. *Phys. Lett. B*, 764:11, 2017.
- [1775] ATLAS Collaboration. Search for heavy ZZ resonances in the $\ell^+\ell^-\ell^+\ell^-$ and $\ell^+\ell^-\nu\bar{\nu}$ final states using proton–proton collisions at $\sqrt{s} = 13$ TeV with the ATLAS detector. ATLAS-CONF-2017-058, 2017.
- [1776] ATLAS Collaboration. Search for heavy ZZ resonances in the $\ell^+\ell^-\ell^+\ell^-$ and $\ell^+\ell^-\nu\bar{\nu}$ final states using proton proton collisions at $\sqrt{s} = 13$ TeV with the ATLAS detector. 2017.

- [1777] ATLAS Collaboration. Search for Higgs boson decays to Beyond-the-Standard-Model light bosons in four-lepton events with the ATLAS detector at $\sqrt{s} = 13$ TeV. ATLAS-CONF-2017-042, 2017.
- [1778] ATLAS Collaboration. Search for lepton-flavour-violating decays of the Higgs and Z bosons with the ATLAS detector. *Eur. Phys. J. C*, 77:70, 2017.
- [1779] ATLAS Collaboration. Search for long-lived charginos based on a disappearing-track signature in pp collisions at $\sqrt{s} = 13$ TeV with the ATLAS detector. 2017.
- [1780] ATLAS Collaboration. Search for long-lived charginos based on a disappearing-track signature in pp collisions at $\sqrt{s} = 13$ TeV with the ATLAS detector. ATLAS-CONF-2017-017, 2017.
- [1781] ATLAS Collaboration. Search for long-lived, massive particles in events with displaced vertices and missing transverse momentum in $\sqrt{s} = 13$ TeV pp collisions with the ATLAS detector. 2017.
- [1782] ATLAS Collaboration. Search for long-lived, massive particles in events with displaced vertices and missing transverse momentum in $\sqrt{s} = 13$ TeV pp collisions with the ATLAS detector. ATLAS-CONF-2017-026, 2017.
- [1783] ATLAS Collaboration. Search for new high-mass phenomena in the dilepton final state using 36.1 fb^{-1} of proton–proton collision data at $\sqrt{s} = 13$ TeV with the ATLAS detector. ATLAS-CONF-2017-027, 2017.
- [1784] ATLAS Collaboration. Search for new high-mass phenomena in the dilepton final state using 36 fb^{-1} of proton–proton collision data at $\sqrt{s} = 13$ TeV with the ATLAS detector. *JHEP*, 10:182, 2017.
- [1785] ATLAS Collaboration. Search for new phenomena in a lepton plus high jet multiplicity final state with the ATLAS experiment using $\sqrt{s} = 13$ TeV proton–proton collision data. *JHEP*, 09:088, 2017.
- [1786] ATLAS Collaboration. Search for new phenomena in a lepton plus high jet multiplicity final state with the ATLAS experiment using $\sqrt{s} = 13$ TeV proton–proton collision data. ATLAS-CONF-2017-013, 2017.
- [1787] ATLAS Collaboration. Search for new phenomena in dijet events using 37 fb^{-1} of pp collision data collected at $\sqrt{s} = 13$ TeV with the ATLAS detector. *Phys. Rev. D*, 96:052004, 2017.

- [1788] ATLAS Collaboration. Search for new phenomena in events containing a same-flavour opposite-sign dilepton pair, jets, and large missing transverse momentum in $\sqrt{s} = 13$ TeV pp collisions with the ATLAS detector. *Eur. Phys. J. C*, 77:144, 2017.
- [1789] ATLAS Collaboration. Search for new phenomena in events with missing transverse momentum and a Higgs boson decaying into two photons at $\sqrt{s} = 13$ TeV with the ATLAS detector. ATLAS-CONF-2017-024, 2017.
- [1790] ATLAS Collaboration. Search for new phenomena in high-mass diphoton final states using 37 fb^{-1} of proton–proton collisions collected at $\sqrt{s} = 13$ TeV with the ATLAS detector. *Phys. Lett. B*, 775:105, 2017.
- [1791] ATLAS Collaboration. Search for new phenomena in high-mass final states with a photon and a jet from pp collisions at $\sqrt{s} = 13$ TeV with the ATLAS detector. 2017.
- [1792] ATLAS Collaboration. Search for new phenomena with large jet multiplicities and missing transverse momentum using large-radius jets and flavour-tagging at ATLAS in 13 TeV pp collisions. *JHEP*, 12:034, 2017.
- [1793] ATLAS Collaboration. Search for new phenomena with large jet multiplicities and missing transverse momentum using large-radius jets and flavour-tagging at ATLAS in 13 TeV pp collisions. ATLAS-CONF-2017-033, 2017.
- [1794] ATLAS Collaboration. Search for new resonances decaying to a W or Z boson and a Higgs boson in the $\ell^+\ell^- b\bar{b}$, $\ell\nu b\bar{b}$, and $\nu\bar{\nu} b\bar{b}$ channels with pp collisions at $\sqrt{s} = 13$ TeV with the ATLAS detector. *Phys. Lett. B*, 765:32, 2017.
- [1795] ATLAS Collaboration. Search for pair production of heavy vector-like quarks decaying to high- $\text{p}_T W$ bosons and b quarks in the lepton-plus-jets final state in pp collisions at $\sqrt{s} = 13$ TeV with the ATLAS detector. *JHEP*, 10:141, 2017.
- [1796] ATLAS Collaboration. Search for pair production of higgsinos in final states with at least three b -tagged jets using the ATLAS detector in $\sqrt{s} = 13$ TeV pp collisions. ATLAS-CONF-2017-081, 2017.
- [1797] ATLAS Collaboration. Search for pair production of vector-like top quarks in events with one lepton and an invisibly decaying Z boson in $\sqrt{s} = 13$ TeV pp collisions at the ATLAS detector. ATLAS-CONF-2017-015, 2017.
- [1798] ATLAS Collaboration. Search for pair production of vector-like top quarks in events with one lepton, jets, and missing transverse momentum in $\sqrt{s} = 13$ TeV pp collisions with the ATLAS detector. *JHEP*, 08:052, 2017.

- [1799] ATLAS Collaboration. Search for photonic signatures of gauge-mediated supersymmetry in 13 TeV pp collisions with the ATLAS detector. ATLAS-CONF-2017-080, 2017.
- [1800] ATLAS Collaboration. Search for production of supersymmetric particles in final states with missing transverse momentum and multiple b -jets at $\sqrt{s} = 13$ TeV proton-proton collisions with the ATLAS detector. ATLAS-CONF-2017-021, 2017.
- [1801] ATLAS Collaboration. Search for squarks and gluinos in events with an isolated lepton, jets, and missing transverse momentum at $\sqrt{s} = 13$ TeV with the ATLAS detector. *Phys. Rev. D*, 96:112010, 2017.
- [1802] ATLAS Collaboration. Search for squarks and gluinos in final states with jets and missing transverse momentum using 36 fb^{-1} of $\sqrt{s} = 13$ TeV pp collision data with the ATLAS detector. 2017.
- [1803] ATLAS Collaboration. Search for squarks and gluinos in final states with jets and missing transverse momentum using 36 fb^{-1} of $\sqrt{s} = 13$ TeV pp collision data with the ATLAS detector. ATLAS-CONF-2017-022, 2017.
- [1804] ATLAS Collaboration. Search for supersymmetry in events with b -tagged jets and missing transverse momentum in pp collisions at $\sqrt{s} = 13$ TeV with the ATLAS detector. *JHEP*, 11:195, 2017.
- [1805] ATLAS Collaboration. Search for supersymmetry in events with b -tagged jets and missing transverse momentum in pp collisions at $\sqrt{s} = 13$ TeV with the ATLAS detector. ATLAS-CONF-2017-038, 2017.
- [1806] ATLAS Collaboration. Search for Supersymmetry in final states with missing transverse momentum and multiple b -jets in proton–proton collisions at $\sqrt{s} = 13$ TeV with the ATLAS detector. 2017.
- [1807] ATLAS Collaboration. Search for supersymmetry in final states with two same-sign or three leptons and jets using 36 fb^{-1} of $\sqrt{s} = 13$ TeV pp collision data with the ATLAS detector. *JHEP*, 09:084, 2017.
- [1808] ATLAS Collaboration. Search for supersymmetry in final states with two same-sign or three leptons and jets using 36 fb^{-1} of $\sqrt{s} = 13$ TeV pp collision data with the ATLAS detector. ATLAS-CONF-2017-030, 2017.
- [1809] ATLAS Collaboration. Search for the decay of the Higgs boson to charm quarks with the ATLAS experiment. ATLAS-CONF-2017-078, 2017.

- [1810] ATLAS Collaboration. Search for the Dimuon Decay of the Higgs Boson in pp Collisions at $\sqrt{s} = 13$ TeV with the ATLAS Detector. *Phys. Rev. Lett.*, 119:051802, 2017.
- [1811] ATLAS Collaboration. Search for the dimuon decay of the Higgs boson in pp collisions at $\sqrt{s} = 13$ TeV with the ATLAS detector. ATLAS-CONF-2017-014, 2017.
- [1812] ATLAS Collaboration. Search for the direct production of charginos and neutralinos in final states with tau leptons in $\sqrt{s} = 13$ TeV pp collisions with the ATLAS detector. 2017.
- [1813] ATLAS Collaboration. Search for the direct production of charginos and neutralinos in final states with tau leptons in $\sqrt{s} = 13$ TeV pp collisions with the ATLAS detector. ATLAS-CONF-2017-035, 2017.
- [1814] ATLAS Collaboration. Search for the Standard Model Higgs boson produced in association with top quarks and decaying into a $b\bar{b}$ pair in pp collisions at $\sqrt{s} = 13$ TeV with the ATLAS detector. 2017.
- [1815] ATLAS Collaboration. Search for the Standard Model Higgs boson produced in association with top quarks and decaying into a $b\bar{b}$ pair in pp collisions at $\sqrt{s} = 13$ TeV with the ATLAS detector. ATLAS-CONF-2017-076, 2017.
- [1816] ATLAS Collaboration. Search for top squark pair production in final states with one isolated lepton, jets, and missing transverse momentum using 36 fb^{-1} of $\sqrt{s} = 13$ TeV pp collision data with the ATLAS detector. ATLAS-CONF-2017-037, 2017.
- [1817] ATLAS Collaboration. Search for top-squark pair production in final states with one lepton, jets, and missing transverse momentum using 36 fb^{-1} of $\sqrt{s} = 13$ TeV pp collision data with the ATLAS detector. 2017.
- [1818] ATLAS Collaboration. Search for top squarks decaying to tau sleptons in pp collisions at $\sqrt{s} = 13$ TeV with the ATLAS detector. ATLAS-CONF-2017-079, 2017.
- [1819] ATLAS Collaboration. Search for $W' \rightarrow tb$ in the hadronic final state with the ATLAS detector in $\sqrt{s} = 13$ TeV pp collisions. ATLAS-CONF-2017-082, 2017.
- [1820] ATLAS Collaboration. Search for WW/WZ resonance production in $\ell\nu qq$ final states in pp collisions at $\sqrt{s} = 13$ TeV with the ATLAS detector. 2017.

- [1821] ATLAS Collaboration. Search for WW/WZ resonance production in $\ell\nu qq$ final states in pp collisions at $\sqrt{s} = 13$ TeV with the ATLAS detector. ATLAS-CONF-2017-051, 2017.
- [1822] ATLAS Collaboration. Searches for heavy ZZ and ZW resonances in the $\ell\ell qq$ and $\nu\nu qq$ final states in pp collisions at $\sqrt{s} = 13$ TeV with the ATLAS detector. 2017.
- [1823] ATLAS Collaboration. Searches for the $Z\gamma$ decay mode of the Higgs boson and for new high-mass resonances in pp collisions at $\sqrt{s} = 13$ TeV with the ATLAS detector. *JHEP*, 10:112, 2017.
- [1824] ATLAS Collaboration. Secondary vertex finding for jet flavour identification with the ATLAS detector. ATL-PHYS-PUB-2017-011, 2017.
- [1825] ATLAS Collaboration. Studies of $Z\gamma$ production in association with a high-mass dijet system in pp collisions at $\sqrt{s} = 8$ TeV with the ATLAS detector. 2017.
- [1826] ATLAS Collaboration. Studies on the impact of an extended Inner Detector tracker and a forward muon tagger on $W^\pm W^\pm$ scattering in pp collisions at the High-Luminosity LHC with the ATLAS experiment. ATL-PHYS-PUB-2017-023, 2017.
- [1827] ATLAS Collaboration. Studies on top-quark Monte Carlo modelling with Sherpa and MG5_aMC@NLO. ATL-PHYS-PUB-2017-007, 2017.
- [1828] ATLAS Collaboration. Study of inclusive jet yields in $Pb+Pb$ collisions at $\sqrt{s_{NN}} = 5.02$ TeV . ATLAS-CONF-2017-009, 2017.
- [1829] ATLAS Collaboration. Study of ordered hadron chains with the ATLAS detector. *Phys. Rev. D*, 96:092008, 2017.
- [1830] ATLAS Collaboration. Study of the double Higgs production channel $H(\rightarrow b\bar{b})H(\rightarrow \gamma\gamma)$ with the ATLAS experiment at HL-LHC. ATL-PHYS-PUB-2017-001, 2017.
- [1831] ATLAS Collaboration. Study of the material of the ATLAS inner detector for Run 2 of the LHC. *JINST*, 12:P12009, 2017.
- [1832] ATLAS Collaboration. Study of $WW\gamma$ and $WZ\gamma$ production in pp collisions at $\sqrt{s} = 8$ TeV and search for anomalous quartic gauge couplings with the ATLAS experiment. *Eur. Phys. J. C*, 77:646, 2017.
- [1833] ATLAS Collaboration. Study on the prospects of a $t\bar{t}$ resonance search in events with one lepton at a High Luminosity LHC. ATL-PHYS-PUB-2017-002, 2017.

- [1834] ATLAS Collaboration. The ATLAS Tau Trigger in Run 2. ATLAS-CONF-2017-061, 2017.
- [1835] ATLAS Collaboration. Top-quark mass measurement in the all-hadronic $t\bar{t}$ decay channel at $\sqrt{s} = 8$ TeV with the ATLAS detector. *JHEP*, 09:118, 2017.
- [1836] ATLAS Collaboration. Topological cell clustering in the ATLAS calorimeters and its performance in LHC Run 1. *Eur. Phys. J. C*, 77:490, 2017.
- [1837] ATLAS Collaboration. Trigger Menu in 2016. ATL-DAQ-PUB-2017-001, 2017.
- [1838] ATLAS Collaboration. Trigger-object Level Analysis with the ATLAS detector at the Large Hadron Collider: summary and perspectives. ATL-DAQ-PUB-2017-003, 2017.
- [1839] ATLAS Collaboration. Variable Radius, Exclusive- k_T , and Center-of-Mass Subjet Reconstruction for Higgs($\rightarrow b\bar{b}$) Tagging in ATLAS. ATL-PHYS-PUB-2017-010, 2017.
- [1840] ATLAS Collaboration. Z boson production in Pb+Pb collisions at $\sqrt{s_{NN}} = 5.02$ TeV with the ATLAS detector at the LHC. ATLAS-CONF-2017-010, 2017.
- [1841] ATLAS Collaboration. $ZZ \rightarrow \ell^+\ell^-\ell'^+\ell'^-$ cross-section measurements and search for anomalous triple gauge couplings in 13 TeV pp collisions with the ATLAS detector. 2017.
- [1842] ATLAS Collaboration. Measurement of differential cross sections of isolated-photon plus heavy-flavour jet production in pp collisions at $\sqrt{s} = 8$ TeV using the ATLAS detector. *Phys. Lett. B*, 776:295, 2018.
- [1843] ATLAS Collaboration. Measurement of the exclusive $\gamma\gamma \rightarrow \mu^+\mu^-$ process in proton-proton collisions at $\sqrt{s} = 13$ TeV with the ATLAS detector. *Phys. Lett. B*, 777:303, 2018.
- [1844] ATLAS Collaboration. Measurements of b-jet tagging efficiency with the atlas detector using $t\bar{t}$ events at $\sqrt{s} = 13$ tev. *Journal of High Energy Physics*, 2018(8), Aug 2018.
- [1845] ATLAS Collaboration. The new lucid-2 detector for luminosity measurement and monitoring in atlas. *JINST*, 13(07):P07017, 2018.
- [1846] ATLAS Collaboration. Search for additional heavy neutral Higgs and gauge bosons in the ditau final state produced in 36 fb^{-1} of pp collisions at $\sqrt{s} = 13$ TeV with the ATLAS detector. *JHEP*, 01:055, 2018.

- [1847] ATLAS Collaboration. Search for an invisibly decaying Higgs boson or dark matter candidates produced in association with a Z boson in pp collisions at $\sqrt{s} = 13$ TeV with the ATLAS detector. *Phys. Lett. B*, 776:318, 2018.
- [1848] ATLAS Collaboration. Search for dark matter produced in association with bottom or top quarks in $\sqrt{s} = 13$ TeV pp collisions with the ATLAS detector. *Eur. Phys. J. C*, 78:18, 2018.
- [1849] ATLAS Collaboration. Search for diboson resonances with boson-tagged jets in pp collisions at $\sqrt{s} = 13$ TeV with the ATLAS detector. *Phys. Lett. B*, 777:91, 2018.
- [1850] ATLAS Collaboration. Search for heavy resonances decaying into WW in the $e\nu\mu\nu$ final state in pp collisions at $\sqrt{s} = 13$ TeV with the ATLAS detector. *Eur. Phys. J. C*, 78:24, 2018.
- [1851] ATLAS Collaboration. Measurement of the fiducial and differential cross-section of a top quark pair in association with a Z boson at 13 TeV with the ATLAS detector. (ATL-COM-PHYS-2019-334), Apr 2019.
- [1852] ATLAS Collaboration. Observation of electroweak $W^\pm Z$ boson pair production in association with two jets in pp collisions at $\sqrt{s} = 13$ TeV with the ATLAS detector. *Phys. Lett.*, B793:469–492, 2019.
- [1853] ATLAS Collaboration. Observation of the associated production of a top quark and a z boson in pp collisions at $\sqrt{s}= 13$ tev with the atlas detector. *Journal of High Energy Physics*, 2020(7), Jul 2020.
- [1854] ATLAS Collaboration. Observation of the Higgs boson production in association with a tt pair with the ATLAS detector. *PoS*, EPS-HEP2019:325, 2020.
- [1855] M. Bahr et al. Herwig++ physics and manual. *Eur. Phys. J. C*, 58:639, 2008.
- [1856] Richard D. Ball et al. Parton distributions with LHC data. *Nuclear Physics B*, 867, 2013.
- [1857] Richard D. Ball et al. Parton distributions for the LHC Run II. *JHEP*, 04:040, 2015.
- [1858] Shankha Banerjee, Satyanarayan Mukhopadhyay, and Biswarup Mukhopadhyaya. Higher dimensional operators and the lhc higgs data: The role of modified kinematics. *Physical Review D*, 89(5), Mar 2014.

- [1859] Rene Brun and Fons Rademakers. ROOT - An Object Oriented Data Analysis Framework. *Proceedings AIHENP 96 Workshop, Lausanne, Sep. 1996, Nucl. Inst. and Meth. in Phys. Res. A* 389 (1997) 81-86.
- [1860] Matteo Cacciari, Gavin P Salam, and Gregory Soyez. The anti k_t jet clustering algorithm. *Journal of High Energy Physics*, 2008(04), Apr 2008.
- [1861] Tianqi Chen and Carlos Guestrin. XGBoost: A scalable tree boosting system. In *Proceedings of the 22nd ACM SIGKDD International Conference on Knowledge Discovery and Data Mining*, KDD '16, pages 785–794, New York, NY, USA, 2016. ACM.
- [1862] CMS Collaboration. CMS Physics Technical Design Report, Volume II: Physics Performance. *J. Phys. G*, 34:995, 2007.
- [1863] CMS Collaboration. The CMS experiment at the CERN LHC. *JINST*, 3:S08004, 2008.
- [1864] CMS Collaboration. Aligning the CMS Muon Chambers with the Muon Alignment System during an Extended Cosmic Ray Run. *JINST*, 5:T03019, 2010.
- [1865] CMS Collaboration. Alignment of the CMS Muon System with Cosmic-Ray and Beam-Halo Muons. *JINST*, 5:T03020, 2010.
- [1866] CMS Collaboration. Alignment of the CMS Silicon Tracker during Commissioning with Cosmic Rays. *JINST*, 5:T03009, 2010.
- [1867] CMS Collaboration. Calibration of the CMS Drift Tube Chambers and Measurement of the Drift Velocity with Cosmic Rays. *JINST*, 5:T03016, 2010.
- [1868] CMS Collaboration. CMS Data Processing Workflows during an Extended Cosmic Ray Run. *JINST*, 5:T03006, 2010.
- [1869] CMS Collaboration. CMS Tracking Performance Results from early LHC Operation. *Eur. Phys. J. C*, 70:1165, 2010.
- [1870] CMS Collaboration. Commissioning and Performance of the CMS Pixel Tracker with Cosmic Ray Muons. *JINST*, 5:T03007, 2010.
- [1871] CMS Collaboration. Commissioning and Performance of the CMS Silicon Strip Tracker with Cosmic Ray Muons. *JINST*, 5:T03008, 2010.
- [1872] CMS Collaboration. Commissioning of the CMS Experiment and the Cosmic Run at Four Tesla. *JINST*, 5:T03001, 2010.
- [1873] CMS Collaboration. Commissioning of the CMS High-Level Trigger with Cosmic Rays. *JINST*, 5:T03005, 2010.

- [1874] CMS Collaboration. Fine Synchronization of the CMS Muon Drift-Tube Local Trigger using Cosmic Rays. *JINST*, 5:T03004, 2010.
- [1875] CMS Collaboration. First Measurement of Bose-Einstein Correlations in Proton–Proton Collisions at $\sqrt{s} = 0.9$ and 2.36 TeV at the LHC. *Phys. Rev. Lett.*, 105:032001, 2010.
- [1876] CMS Collaboration. First Measurement of the Underlying Event Activity at the LHC with $\sqrt{s} = 0.9$ TeV. *Eur. Phys. J. C*, 70:555, 2010.
- [1877] CMS Collaboration. Identification and Filtering of Uncharacteristic Noise in the CMS Hadron Calorimeter. *JINST*, 5:T03014, 2010.
- [1878] CMS Collaboration. Measurement of the charge ratio of atmospheric muons with the CMS detector. *Phys. Lett. B*, 692:83, 2010.
- [1879] CMS Collaboration. Measurement of the Muon Stopping Power in Lead Tungstate. *JINST*, 5:P03007, 2010.
- [1880] CMS Collaboration. Observation of long-range, near-side angular correlations in proton–proton collisions at the LHC. *JHEP*, 09:091, 2010.
- [1881] CMS Collaboration. Performance and Operation of the CMS Electromagnetic Calorimeter. *JINST*, 5:T03010, 2010.
- [1882] CMS Collaboration. Performance of CMS Hadron Calorimeter Timing and Synchronization using Test Beam, Cosmic Ray, and LHC Beam Data. *JINST*, 5:T03013, 2010.
- [1883] CMS Collaboration. Performance of CMS Muon Reconstruction in Cosmic-Ray Events. *JINST*, 5:T03022, 2010.
- [1884] CMS Collaboration. Performance of the CMS Cathode Strip Chambers with Cosmic Rays. *JINST*, 5:T03018, 2010.
- [1885] CMS Collaboration. Performance of the CMS Drift-Tube Chamber Local Trigger with Cosmic Rays. *JINST*, 5:T03003, 2010.
- [1886] CMS Collaboration. Performance of the CMS Drift Tube Chambers with Cosmic Rays. *JINST*, 5:T03015, 2010.
- [1887] CMS Collaboration. Performance of the CMS Hadron Calorimeter with Cosmic Ray Muons and LHC Beam Data. *JINST*, 5:T03012, 2010.
- [1888] CMS Collaboration. Performance of the CMS Level-1 Trigger during Commissioning with Cosmic Ray Muons and LHC beams. *JINST*, 5:T03002, 2010.

- [1889] CMS Collaboration. Performance Study of the CMS Barrel Resistive Plate Chambers with Cosmic Rays. *JINST*, 5:T03017, 2010.
- [1890] CMS Collaboration. Precise Mapping of the Magnetic Field in the CMS Barrel Yoke using Cosmic Rays. *JINST*, 5:T03021, 2010.
- [1891] CMS Collaboration. Search for Dijet Resonances in 7 TeV pp Collisions at CMS. *Phys. Rev. Lett.*, 105:211801, 2010.
- [1892] CMS Collaboration. Search for Quark Compositeness with the Dijet Centrality Ratio in pp Collisions at $\sqrt{s} = 7$ TeV. *Phys. Rev. Lett.*, 105:262001, 2010.
- [1893] CMS Collaboration. Time Reconstruction and Performance of the CMS Electromagnetic Calorimeter. *JINST*, 5:T03011, 2010.
- [1894] CMS Collaboration. Transverse momentum and pseudorapidity distributions of charged hadrons in pp collisions at $\sqrt{s} = 0.9$ and 2.36 TeV. *JHEP*, 02:041, 2010.
- [1895] CMS Collaboration. Transverse-Momentum and Pseudorapidity Distributions of Charged Hadrons in pp Collisions at $\sqrt{s} = 7$ TeV. *Phys. Rev. Lett.*, 105:022002, 2010.
- [1896] CMS Collaboration. A search for excited leptons in pp collisions at $\sqrt{s} = 7$ TeV. *Phys. Lett. B*, 704:143, 2011.
- [1897] CMS Collaboration. Charged particle multiplicities in pp interactions at $\sqrt{s} = 0.9$, 2.36, and 7 TeV. *JHEP*, 01:079, 2011.
- [1898] CMS Collaboration. Charged particle transverse momentum spectra in pp collisions at $\sqrt{s} = 0.9$ and 7 TeV. *JHEP*, 08:086, 2011.
- [1899] CMS Collaboration. Dependence on pseudorapidity and on centrality of charged hadron production in PbPb collisions at $\sqrt{s_{\text{NN}}} = 2.76$ TeV. *JHEP*, 08:141, 2011.
- [1900] CMS Collaboration. Determination of Jet Energy Calibration and Transverse Momentum Resolution in CMS. *JINST*, 6:P11002, 2011.
- [1901] CMS Collaboration. Dijet Azimuthal Decorrelations in pp Collisions at $\sqrt{s} = 7$ TeV. *Phys. Rev. Lett.*, 106:122003, 2011.
- [1902] CMS Collaboration. First Measurement of Hadronic Event Shapes in pp Collisions at $\sqrt{s} = 7$ TeV. *Phys. Lett. B*, 699:48, 2011.

- [1903] CMS Collaboration. First measurement of the cross section for top-quark pair production in proton–proton collisions at $\sqrt{s} = 7$ TeV. *Phys. Lett. B*, 695:424, 2011.
- [1904] CMS Collaboration. Inclusive b-hadron production cross section with muons in pp collisions at $\sqrt{s} = 7$ TeV. *JHEP*, 03:090, 2011.
- [1905] CMS Collaboration. Indications of suppression of excited Υ states in PbPb collisions at $\sqrt{s_{\text{NN}}} = 2.76$ TeV. *Phys. Rev. Lett.*, 107:052302, 2011.
- [1906] CMS Collaboration. Long-range and short-range dihadron angular correlations in central PbPb collisions at $\sqrt{s_{\text{NN}}} = 2.76$ TeV. *JHEP*, 07:076, 2011.
- [1907] CMS Collaboration. Measurement of $B\bar{B}$ Angular Correlations based on Secondary Vertex Reconstruction at $\sqrt{s} = 7$ TeV. *JHEP*, 03:136, 2011.
- [1908] CMS Collaboration. Measurement of Bose-Einstein Correlations in pp Collisions at $\sqrt{s} = 0.9$ and 7 TeV. *JHEP*, 05:029, 2011.
- [1909] CMS Collaboration. Measurement of Dijet Angular Distributions and Search for Quark Compositeness in pp Collisions at $\sqrt{s} = 7$ TeV. *Phys. Rev. Lett.*, 106:201804, 2011.
- [1910] CMS Collaboration. Measurement of energy flow at large pseudorapidities in pp collisions at $\sqrt{s} = 0.9$ and 7 TeV. *JHEP*, 11:148, 2011.
- [1911] CMS Collaboration. Measurement of the B^+ Production Cross Section in pp Collisions at $\sqrt{s} = 7$ TeV. *Phys. Rev. Lett.*, 106:112001, 2011.
- [1912] CMS Collaboration. Measurement of the B^0 Production Cross Section in pp Collisions at $\sqrt{s} = 7$ TeV. *Phys. Rev. Lett.*, 106:252001, 2011.
- [1913] CMS Collaboration. Measurement of the B_s^0 Production Cross Section with $B_s^0 \rightarrow J/\psi\phi$ Decays in pp Collisions at $\sqrt{s} = 7$ TeV. *Phys. Rev. D*, 84:052008, 2011.
- [1914] CMS Collaboration. Measurement of the Differential Cross Section for Isolated Prompt Photon Production in pp Collisions at 7 TeV. *Phys. Rev. D*, 84:052011, 2011.
- [1915] CMS Collaboration. Measurement of the differential dijet production cross section in proton–proton collisions at $\sqrt{s} = 7$ TeV. *Phys. Lett. B*, 700:187, 2011.
- [1916] CMS Collaboration. Measurement of the Drell-Yan Cross Section in pp Collisions at $\sqrt{s} = 7$ TeV. *JHEP*, 10:007, 2011.

- [1917] CMS Collaboration. Measurement of the Inclusive Jet Cross Section in pp Collisions at $\sqrt{s} = 7$ TeV. *Phys. Rev. Lett.*, 107:132001, 2011.
- [1918] CMS Collaboration. Measurement of the inclusive W and Z production cross sections in pp collisions at $\sqrt{s} = 7$ TeV with the CMS experiment. *JHEP*, 10:132, 2011.
- [1919] CMS Collaboration. Measurement of the Inclusive Z Cross Section via Decays to Tau Pairs in pp Collisions at $\sqrt{s} = 7$ TeV. *JHEP*, 08:117, 2011.
- [1920] CMS Collaboration. Measurement of the Isolated Prompt Photon Production Cross Section in pp Collisions at $\sqrt{s} = 7$ TeV. *Phys. Rev. Lett.*, 106:082001, 2011.
- [1921] CMS Collaboration. Measurement of the lepton charge asymmetry in inclusive W production in pp collisions at $\sqrt{s} = 7$ TeV. *JHEP*, 04:050, 2011.
- [1922] CMS Collaboration. Measurement of the Polarization of W Bosons with Large Transverse Momenta in $W + \text{Jets}$ Events at the LHC. *Phys. Rev. Lett.*, 107:021802, 2011.
- [1923] CMS Collaboration. Measurement of the Ratio of the 3-jet to 2-jet Cross Sections in pp Collisions at $\sqrt{s} = 7$ TeV. *Phys. Lett. B*, 702:336, 2011.
- [1924] CMS Collaboration. Measurement of the $t\bar{t}$ Production Cross Section in pp Collisions at 7 TeV in Lepton + Jets Events Using b -quark Jet Identification. *Phys. Rev. D*, 84:092004, 2011.
- [1925] CMS Collaboration. Measurement of the t -channel single top quark production cross section in pp collisions at $\sqrt{s} = 7$ TeV. *Phys. Rev. Lett.*, 107:091802, 2011.
- [1926] CMS Collaboration. Measurement of the $t\bar{t}$ production cross section and the top quark mass in the dilepton channel in pp collisions at $\sqrt{s} = 7$ TeV. *JHEP*, 07:049, 2011.
- [1927] CMS Collaboration. Measurement of the $t\bar{t}$ production cross section in pp collisions at $\sqrt{s} = 7$ TeV using the kinematic properties of events with leptons and jets. *Eur. Phys. J. C*, 71:1721, 2011.
- [1928] CMS Collaboration. Measurement of the Underlying Event Activity at the LHC with $\sqrt{s} = 7$ TeV and Comparison with $\sqrt{s} = 0.9$ TeV. *JHEP*, 09:109, 2011.
- [1929] CMS Collaboration. Measurement of the weak mixing angle with the Drell-Yan process in proton–proton collisions at the LHC. *Phys. Rev. D*, 84:112002, 2011.

- [1930] CMS Collaboration. Measurement of W^+W^- Production and Search for the Higgs Boson in pp Collisions at $\sqrt{s} = 7 \text{ TeV}$. *Phys. Lett. B*, 699:25, 2011.
- [1931] CMS Collaboration. Measurement of $W\gamma$ and $Z\gamma$ production in pp collisions at $\sqrt{s} = 7 \text{ TeV}$. *Phys. Lett. B*, 701:535, 2011.
- [1932] CMS Collaboration. Measurements of Inclusive W and Z Cross Sections in pp Collisions at $\sqrt{s} = 7 \text{ TeV}$. *JHEP*, 01:080, 2011.
- [1933] CMS Collaboration. Missing transverse energy performance of the CMS detector. *JINST*, 6:P09001, 2011.
- [1934] CMS Collaboration. Observation and studies of jet quenching in PbPb collisions at $\sqrt{s_{\text{NN}}} = 2.76 \text{ TeV}$. *Phys. Rev. C*, 84:024906, 2011.
- [1935] CMS Collaboration. Prompt and non-prompt J/ψ production in pp collisions at $\sqrt{s} = 7 \text{ TeV}$. *Eur. Phys. J. C*, 71:1575, 2011.
- [1936] CMS Collaboration. Search for a Heavy Bottom-like Quark in pp Collisions at $\sqrt{s} = 7 \text{ TeV}$. *Phys. Lett. B*, 701:204, 2011.
- [1937] CMS Collaboration. Search for a heavy gauge boson W' in the final state with an electron and large missing transverse energy in pp collisions at $\sqrt{s} = 7 \text{ TeV}$. *Phys. Lett. B*, 698:21, 2011.
- [1938] CMS Collaboration. Search for a Vectorlike Quark with Charge 2/3 in $t + Z$ Events from pp Collisions at $\sqrt{s} = 7 \text{ TeV}$. *Phys. Rev. Lett.*, 107:271802, 2011.
- [1939] CMS Collaboration. Search for a W' boson decaying to a muon and a neutrino in pp collisions at $\sqrt{s} = 7 \text{ TeV}$. *Phys. Lett. B*, 701:160, 2011.
- [1940] CMS Collaboration. Search for $B_s^0 \rightarrow \mu^+\mu^-$ and $B^0 \rightarrow \mu^+\mu^-$ Decays in pp Collisions at $\sqrt{s} = 7 \text{ TeV}$. *Phys. Rev. Lett.*, 107:191802, 2011.
- [1941] CMS Collaboration. Search for First Generation Scalar Leptoquarks in the $e\nu jj$ channel in pp collisions at $\sqrt{s} = 7 \text{ TeV}$. *Phys. Lett. B*, 703:246, 2011.
- [1942] CMS Collaboration. Search for Heavy Stable Charged Particles in pp collisions at $\sqrt{s} = 7 \text{ TeV}$. *JHEP*, 03:024, 2011.
- [1943] CMS Collaboration. Search for Large Extra Dimensions in the Diphoton Final State at the Large Hadron Collider. *JHEP*, 05:085, 2011.
- [1944] CMS Collaboration. Search for light resonances decaying into pairs of muons as a signal of new physics. *JHEP*, 07:098, 2011.

- [1945] CMS Collaboration. Search for Microscopic Black Hole Signatures at the Large Hadron Collider. *Phys. Lett. B*, 697:434, 2011.
- [1946] CMS Collaboration. Search for Neutral Minimal Supersymmetric Standard Model Higgs Bosons Decaying to Tau Pairs in pp Collisions at $\sqrt{s} = 7 \text{ TeV}$. *Phys. Rev. Lett.*, 106:231801, 2011.
- [1947] CMS Collaboration. Search for New Physics with a Monojet and Missing Transverse Energy in pp Collisions at $\sqrt{s} = 7 \text{ TeV}$. *Phys. Rev. Lett.*, 107:201804, 2011.
- [1948] CMS Collaboration. Search for New Physics with Jets and Missing Transverse Momentum in pp collisions at $\sqrt{s} = 7 \text{ TeV}$. *JHEP*, 08:155, 2011.
- [1949] CMS Collaboration. Search for new physics with same-sign isolated dilepton events with jets and missing transverse energy at the LHC. *JHEP*, 06:077, 2011.
- [1950] CMS Collaboration. Search for Pair Production of First-Generation Scalar Leptoquarks in pp Collisions at $\sqrt{s} = 7 \text{ TeV}$. *Phys. Rev. Lett.*, 106:201802, 2011.
- [1951] CMS Collaboration. Search for Pair Production of Second-Generation Scalar Leptoquarks in pp Collisions at $\sqrt{s} = 7 \text{ TeV}$. *Phys. Rev. Lett.*, 106:201803, 2011.
- [1952] CMS Collaboration. Search for Physics Beyond the Standard Model in Opposite-Sign Dilepton Events at $\sqrt{s} = 7 \text{ TeV}$. *JHEP*, 06:026, 2011.
- [1953] CMS Collaboration. Search for Physics Beyond the Standard Model Using Multilepton Signatures in pp Collisions at $\sqrt{s} = 7 \text{ TeV}$. *Phys. Lett. B*, 704:411, 2011.
- [1954] CMS Collaboration. Search for Resonances in the Dijet Mass Spectrum from 7 TeV pp Collisions at CMS. *Phys. Lett. B*, 704:123, 2011.
- [1955] CMS Collaboration. Search for Resonances in the Dilepton Mass Distribution in pp Collisions at $\sqrt{s} = 7 \text{ TeV}$. *JHEP*, 05:093, 2011.
- [1956] CMS Collaboration. Search for same-sign top-quark pair production at $\sqrt{s} = 7 \text{ TeV}$ and limits on flavour changing neutral currents in the top sector. *JHEP*, 08:005, 2011.
- [1957] CMS Collaboration. Search for Stopped Gluinos in pp Collisions at $\sqrt{s} = 7 \text{ TeV}$. *Phys. Rev. Lett.*, 106:011801, 2011.

- [1958] CMS Collaboration. Search for Supersymmetry at the LHC in Events with Jets and Missing Transverse Energy. *Phys. Rev. Lett.*, 107:221804, 2011.
- [1959] CMS Collaboration. Search for supersymmetry in events with a lepton, a photon, and large missing transverse energy in pp collisions at $\sqrt{s} = 7 \text{ TeV}$. *JHEP*, 06:093, 2011.
- [1960] CMS Collaboration. Search for Supersymmetry in Events with b Jets and Missing Transverse Momentum at the LHC. *JHEP*, 07:113, 2011.
- [1961] CMS Collaboration. Search for Supersymmetry in pp Collisions at 7 TeV in Events with Jets and Missing Transverse Energy. *Phys. Lett. B*, 698:196, 2011.
- [1962] CMS Collaboration. Search for supersymmetry in pp collisions at $\sqrt{s} = 7 \text{ TeV}$ in events with a single lepton, jets, and missing transverse momentum. *JHEP*, 08:156, 2011.
- [1963] CMS Collaboration. Search for Supersymmetry in pp Collisions at $\sqrt{s} = 7 \text{ TeV}$ in Events with Two Photons and Missing Transverse Energy. *Phys. Rev. Lett.*, 106:211802, 2011.
- [1964] CMS Collaboration. Search for Three-Jet Resonances in pp Collisions at $\sqrt{s} = 7 \text{ TeV}$. *Phys. Rev. Lett.*, 107:101801, 2011.
- [1965] CMS Collaboration. Strange Particle Production in pp Collisions at $\sqrt{s} = 0.9$ and 7 TeV. *JHEP*, 05:064, 2011.
- [1966] CMS Collaboration. Study of Z Boson Production in PbPb Collisions at $\sqrt{s_{\text{NN}}} = 2.76 \text{ TeV}$. *Phys. Rev. Lett.*, 106:212301, 2011.
- [1967] CMS Collaboration. Upsilon production cross-section in pp collisions at $\sqrt{s} = 7 \text{ TeV}$. *Phys. Rev. D*, 83:112004, 2011.
- [1968] CMS Collaboration. A search for a doubly-charged Higgs boson in pp collisions at $\sqrt{s} = 7 \text{ TeV}$. *Eur. Phys. J. C*, 72:2189, 2012.
- [1969] CMS Collaboration. Azimuthal anisotropy of charged particles at high transverse momenta in PbPb collisions at $\sqrt{s_{\text{NN}}} = 2.76 \text{ TeV}$. *Phys. Rev. Lett.*, 109:022301, 2012.
- [1970] CMS Collaboration. Centrality dependence of dihadron correlations and azimuthal anisotropy harmonics in PbPb collisions at $\sqrt{s_{\text{NN}}} = 2.76 \text{ TeV}$. *Eur. Phys. J. C*, 72:2012, 2012.
- [1971] CMS Collaboration. Combined results of searches for the standard model Higgs boson in pp collisions at $\sqrt{s} = 7 \text{ TeV}$. *Phys. Lett. B*, 710:26, 2012.

- [1972] CMS Collaboration. Combined search for the quarks of a sequential fourth generation. *Phys. Rev. D*, 86:112003, 2012.
- [1973] CMS Collaboration. Exclusive $\gamma\gamma \rightarrow \mu^+\mu^-$ production in proton–proton collisions at $\sqrt{s} = 7$ TeV. *JHEP*, 01:052, 2012.
- [1974] CMS Collaboration. Forward Energy Flow, Central Charged-Particle Multiplicities, and Pseudorapidity Gaps in W and Z Boson Events from pp Collisions at $\sqrt{s} = 7$ TeV. *Eur. Phys. J. C*, 72:1839, 2012.
- [1975] CMS Collaboration. Inclusive and differential measurements of the $t\bar{t}$ charge asymmetry in proton–proton collisions at $\sqrt{s} = 7$ TeV. *Phys. Lett. B*, 717:129, 2012.
- [1976] CMS Collaboration. Inclusive b -jet production in pp collisions at $\sqrt{s} = 7$ TeV. *JHEP*, 04:084, 2012.
- [1977] CMS Collaboration. Inclusive search for squarks and gluinos in pp collisions at $\sqrt{s} = 7$ TeV. *Phys. Rev. D*, 85:012004, 2012.
- [1978] CMS Collaboration. Jet momentum dependence of jet quenching in PbPb collisions at $\sqrt{s_{\text{NN}}} = 2.76$ TeV. *Phys. Lett. B*, 712:176, 2012.
- [1979] CMS Collaboration. Jet Production Rates in Association with W and Z Bosons in pp Collisions at $\sqrt{s} = 7$ TeV. *JHEP*, 01:010, 2012.
- [1980] CMS Collaboration. J/ψ and $\psi(2S)$ production in pp collisions at $\sqrt{s} = 7$ TeV. *JHEP*, 02:011, 2012.
- [1981] CMS Collaboration. Measurement of isolated photon production in pp and PbPb collisions at $\sqrt{s_{\text{NN}}} = 2.76$ TeV. *Phys. Lett. B*, 710:256, 2012.
- [1982] CMS Collaboration. Measurement of jet fragmentation into charged particles in pp and PbPb collisions at $\sqrt{s_{\text{NN}}} = 2.76$ TeV. *JHEP*, 10:087, 2012.
- [1983] CMS Collaboration. Measurement of the charge asymmetry in top-quark pair production in proton–proton collisions at $\sqrt{s} = 7$ TeV. *Phys. Lett. B*, 709:28, 2012.
- [1984] CMS Collaboration. Measurement of the cross section for production of $b\bar{b}X$ decaying to muons in pp collisions at $\sqrt{s} = 7$ TeV. *JHEP*, 06:110, 2012.
- [1985] CMS Collaboration. Measurement of the electron charge asymmetry in inclusive W production in pp collisions at $\sqrt{s} = 7$ TeV. *Phys. Rev. Lett.*, 109:111806, 2012.

- [1986] CMS Collaboration. Measurement of the inclusive production cross sections for forward jets and for dijet events with one forward and one central jet in pp collisions at $\sqrt{s} = 7$ TeV. *JHEP*, 06:036, 2012.
- [1987] CMS Collaboration. Measurement of the Λ_b cross section and the $\bar{\Lambda}_b$ to Λ_b ratio with $J/\psi\Lambda$ decays in pp collisions at $\sqrt{s} = 7$ TeV. *Phys. Lett. B*, 714:136, 2012.
- [1988] CMS Collaboration. Measurement of the mass difference between top and antitop quarks. *JHEP*, 06:109, 2012.
- [1989] CMS Collaboration. Measurement of the Production Cross Section for Pairs of Isolated Photons in pp collisions at $\sqrt{s} = 7$ TeV. *JHEP*, 01:133, 2012.
- [1990] CMS Collaboration. Measurement of the pseudorapidity and centrality dependence of the transverse energy density in PbPb collisions at $\sqrt{s_{\text{NN}}} = 2.76$ TeV. *Phys. Rev. Lett.*, 109:152303, 2012.
- [1991] CMS Collaboration. Measurement of the Rapidity and Transverse Momentum Distributions of Z Bosons in pp Collisions at $\sqrt{s} = 7$ TeV. *Phys. Rev. D*, 85:032002, 2012.
- [1992] CMS Collaboration. Measurement of the relative prompt production rate of χ_{c2} and χ_{c1} in pp collisions at $\sqrt{s} = 7$ TeV. *Eur. Phys. J. C*, 72:2251, 2012.
- [1993] CMS Collaboration. Measurement of the single-top-quark t -channel cross section in pp collisions at $\sqrt{s} = 7$ TeV. *JHEP*, 12:035, 2012.
- [1994] CMS Collaboration. Measurement of the $t\bar{t}$ production cross section in pp collisions at $\sqrt{s} = 7$ TeV in dilepton final states containing a τ . *Phys. Rev. D*, 85:112007, 2012.
- [1995] CMS Collaboration. Measurement of the $t\bar{t}$ production cross section in the dilepton channel in pp collisions at $\sqrt{s} = 7$ TeV. *JHEP*, 11:067, 2012.
- [1996] CMS Collaboration. Measurement of the top-quark mass in $t\bar{t}$ events with dilepton final states in pp collisions at $\sqrt{s} = 7$ TeV. *Eur. Phys. J. C*, 72:2202, 2012.
- [1997] CMS Collaboration. Measurement of the top-quark mass in $t\bar{t}$ events with lepton+jets final states in pp collisions at $\sqrt{s} = 7$ TeV. *JHEP*, 12:105, 2012.
- [1998] CMS Collaboration. Measurement of the underlying event activity in pp collisions at $\sqrt{s} = 0.9$ and 7 TeV with the novel jet-area/median approach. *JHEP*, 08:130, 2012.

- [1999] CMS Collaboration. Measurement of the underlying event in the Drell-Yan process in proton–proton collisions at $\sqrt{s} = 7$ TeV. *Eur. Phys. J. C*, 72:2080, 2012.
- [2000] CMS Collaboration. Measurement of the $Z/\gamma^* + b$ -jet cross section in $p\bar{p}$ collisions at 7 TeV. *JHEP*, 06:126, 2012.
- [2001] CMS Collaboration. Observation of a new boson at a mass of 125 GeV with the CMS experiment at the LHC. *Phys. Lett. B*, 716:30, 2012.
- [2002] CMS Collaboration. Observation of a new Ξ_b baryon. *Phys. Rev. Lett.*, 108:252002, 2012.
- [2003] CMS Collaboration. Observation of sequential Υ suppression in PbPb collisions. *Phys. Rev. Lett.*, 109:222301, 2012.
- [2004] CMS Collaboration. Observation of Z decays to four leptons with the CMS detector at the LHC. *JHEP*, 12:034, 2012.
- [2005] CMS Collaboration. Performance of CMS muon reconstruction in $p\bar{p}$ collision events at $\sqrt{s} = 7$ TeV. *JINST*, 7:P10002, 2012.
- [2006] CMS Collaboration. Performance of τ -lepton reconstruction and identification in CMS. *JINST*, 7:P01001, 2012.
- [2007] CMS Collaboration. Ratios of dijet production cross sections as a function of the absolute difference in rapidity between jets in proton–proton collisions at $\sqrt{s} = 7$ TeV. *Eur. Phys. J. C*, 72:2216, 2012.
- [2008] CMS Collaboration. Search for a fermiophobic Higgs boson in $p\bar{p}$ collisions at $\sqrt{s} = 7$ TeV. *JHEP*, 09:111, 2012.
- [2009] CMS Collaboration. Search for a Higgs boson in the decay channel $H \rightarrow ZZ^{(*)} \rightarrow q\bar{q}\ell^-\ell^+$ in $p\bar{p}$ collisions at $\sqrt{s} = 7$ TeV. *JHEP*, 04:036, 2012.
- [2010] CMS Collaboration. Search for a light charged Higgs boson in top quark decays in $p\bar{p}$ collisions at $\sqrt{s} = 7$ TeV. *JHEP*, 07:143, 2012.
- [2011] CMS Collaboration. Search for a light pseudoscalar Higgs boson in the dimuon decay channel in $p\bar{p}$ collisions at $\sqrt{s} = 7$ TeV. *Phys. Rev. Lett.*, 109:121801, 2012.
- [2012] CMS Collaboration. Search for a W' or Techni- ρ Decaying into WZ in $p\bar{p}$ Collisions at $\sqrt{s} = 7$ TeV. *Phys. Rev. Lett.*, 109:141801, 2012.
- [2013] CMS Collaboration. Search for anomalous production of multilepton events in $p\bar{p}$ collisions at $\sqrt{s} = 7$ TeV. *JHEP*, 06:169, 2012.

- [2014] CMS Collaboration. Search for anomalous $t\bar{t}$ production in the highly-boosted all-hadronic final state. *JHEP*, 09:029, 2012.
- [2015] CMS Collaboration. Search for $B_s^0 \rightarrow \mu^+ \mu^-$ and $B^0 \rightarrow \mu^+ \mu^-$ decays. *JHEP*, 04:033, 2012.
- [2016] CMS Collaboration. Search for charge-asymmetric production of W' bosons in $t\bar{t} + \text{jet}$ events from pp collisions at $\sqrt{s} = 7 \text{ TeV}$. *Phys. Lett. B*, 717:351, 2012.
- [2017] CMS Collaboration. Search for dark matter and large extra dimensions in monojet events in pp collisions at $\sqrt{s} = 7 \text{ TeV}$. *JHEP*, 09:094, 2012.
- [2018] CMS Collaboration. Search for Dark Matter and Large Extra Dimensions in pp Collisions Yielding a Photon and Missing Transverse Energy. *Phys. Rev. Lett.*, 108:261803, 2012.
- [2019] CMS Collaboration. Search for electroweak production of charginos and neutralinos using leptonic final states in pp collisions at $\sqrt{s} = 7 \text{ TeV}$. *JHEP*, 11:147, 2012.
- [2020] CMS Collaboration. Search for exclusive or semi-exclusive $\gamma\gamma$ production and observation of exclusive and semi-exclusive $e^+ e^-$ production in pp collisions at $\sqrt{s} = 7 \text{ TeV}$. *JHEP*, 11:080, 2012.
- [2021] CMS Collaboration. Search for heavy bottom-like quarks in 4.9 fb^{-1} of pp collisions at $\sqrt{s} = 7 \text{ TeV}$. *JHEP*, 05:123, 2012.
- [2022] CMS Collaboration. Search for heavy lepton partners of neutrinos in proton–proton collisions in the context of the type III seesaw mechanism. *Phys. Lett. B*, 718:348, 2012.
- [2023] CMS Collaboration. Search for heavy long-lived charged particles in pp collisions at $\sqrt{s} = 7 \text{ TeV}$. *Phys. Lett. B*, 713:408, 2012.
- [2024] CMS Collaboration. Search for heavy Majorana neutrinos in $\mu^\pm \mu^\pm + \text{jets}$ and $e^\pm e^\pm + \text{jets}$ events in pp collisions at $\sqrt{s} = 7 \text{ TeV}$. *Phys. Lett. B*, 717:109, 2012.
- [2025] CMS Collaboration. Search for heavy neutrinos and W_R bosons with right-handed couplings in a left-right symmetric model in pp collisions at $\sqrt{s} = 7 \text{ TeV}$. *Phys. Rev. Lett.*, 109:261802, 2012.
- [2026] CMS Collaboration. Search for heavy, top-like quark pair production in the dilepton final state in pp collisions at $\sqrt{s} = 7 \text{ TeV}$. *Phys. Lett. B*, 716:103, 2012.

- [2027] CMS Collaboration. Search for high mass resonances decaying into τ -lepton pairs in pp collisions at $\sqrt{s} = 7 \text{ TeV}$. *Phys. Lett. B*, 716:82, 2012.
- [2028] CMS Collaboration. Search for large extra dimensions in dimuon and di-electron events in pp collisions at $\sqrt{s} = 7 \text{ TeV}$. *Phys. Lett. B*, 711:15, 2012.
- [2029] CMS Collaboration. Search for leptonic decays of W' bosons in pp collisions at $\sqrt{s} = 7 \text{ TeV}$. *JHEP*, 08:023, 2012.
- [2030] CMS Collaboration. Search for microscopic black holes in pp collisions at $\sqrt{s} = 7 \text{ TeV}$. *JHEP*, 04:061, 2012.
- [2031] CMS Collaboration. Search for narrow resonances in dilepton mass spectra in pp collisions at $\sqrt{s} = 7 \text{ TeV}$. *Phys. Lett. B*, 714:158, 2012.
- [2032] CMS Collaboration. Search for neutral Higgs bosons decaying to tau pairs in pp collisions at $\sqrt{s} = 7 \text{ TeV}$. *Phys. Lett. B*, 713:68, 2012.
- [2033] CMS Collaboration. Search for new physics in events with same-sign dileptons and b -tagged jets in pp collisions at $\sqrt{s} = 7 \text{ TeV}$. *JHEP*, 08:110, 2012.
- [2034] CMS Collaboration. Search for new physics in the multijet and missing transverse momentum final state in proton–proton collisions at $\sqrt{s} = 7 \text{ TeV}$. *Phys. Rev. Lett.*, 109:171803, 2012.
- [2035] CMS Collaboration. Search for new physics with long-lived particles decaying to photons and missing energy in pp collisions at $\sqrt{s} = 7 \text{ TeV}$. *JHEP*, 11:172, 2012.
- [2036] CMS Collaboration. Search for new physics with same-sign isolated dilepton events with jets and missing transverse energy. *Phys. Rev. Lett.*, 109:071803, 2012.
- [2037] CMS Collaboration. Search for pair produced fourth-generation up-type quarks in pp collisions at $\sqrt{s} = 7 \text{ TeV}$ with a lepton in the final state. *Phys. Lett. B*, 718:307, 2012.
- [2038] CMS Collaboration. Search for pair production of first- and second-generation scalar leptoquarks in pp collisions at $\sqrt{s} = 7 \text{ TeV}$. *Phys. Rev. D*, 86:052013, 2012.
- [2039] CMS Collaboration. Search for physics beyond the standard model in events with a Z boson, jets, and missing transverse energy in pp collisions at $\sqrt{s} = 7 \text{ TeV}$. *Phys. Lett. B*, 716:260, 2012.

- [2040] CMS Collaboration. Search for quark compositeness in dijet angular distributions from pp collisions at $\sqrt{s} = 7$ TeV. *JHEP*, 05:055, 2012.
- [2041] CMS Collaboration. Search for resonant $t\bar{t}$ production in lepton+jets events in pp collisions at $\sqrt{s} = 7$ TeV. *JHEP*, 12:015, 2012.
- [2042] CMS Collaboration. Search for signatures of extra dimensions in the diphoton mass spectrum at the Large Hadron Collider. *Phys. Rev. Lett.*, 108:111801, 2012.
- [2043] CMS Collaboration. Search for stopped long-lived particles produced in pp collisions at $\sqrt{s} = 7$ TeV. *JHEP*, 08:026, 2012.
- [2044] CMS Collaboration. Search for supersymmetry in events with b -quark jets and missing transverse energy in pp collisions at 7 TeV. *Phys. Rev. D*, 86:072010, 2012.
- [2045] CMS Collaboration. Search for supersymmetry in hadronic final states using M_{T2} in pp collisions at $\sqrt{s} = 7$ TeV. *JHEP*, 10:018, 2012.
- [2046] CMS Collaboration. Search for the standard model Higgs boson decaying into two photons in pp collisions at $\sqrt{s} = 7$ TeV. *Phys. Lett. B*, 710:403, 2012.
- [2047] CMS Collaboration. Search for the standard model Higgs boson decaying to bottom quarks in pp collisions at $\sqrt{s} = 7$ TeV. *Phys. Lett. B*, 710:284, 2012.
- [2048] CMS Collaboration. Search for the standard model Higgs boson decaying to W^+W^- in the fully leptonic final state in pp collisions at $\sqrt{s} = 7$ TeV. *Phys. Lett. B*, 710:91, 2012.
- [2049] CMS Collaboration. Search for the Standard Model Higgs Boson in the Decay Channel $H \rightarrow ZZ \rightarrow 4\ell$ in pp Collisions at $\sqrt{s} = 7$ TeV. *Phys. Rev. Lett.*, 108:111804, 2012.
- [2050] CMS Collaboration. Search for the standard model Higgs boson in the $H \rightarrow ZZ \rightarrow 2\ell 2\nu$ channel in pp collisions at $\sqrt{s} = 7$ TeV. *JHEP*, 03:040, 2012.
- [2051] CMS Collaboration. Search for the standard model Higgs boson in the $H \rightarrow ZZ \rightarrow \ell^+\ell^-\tau^+\tau^-$ decay channel in pp collisions at $\sqrt{s} = 7$ TeV. *JHEP*, 03:081, 2012.
- [2052] CMS Collaboration. Search for the standard model Higgs boson produced in association with W and Z bosons in pp collisions at $\sqrt{s} = 7$ TeV. *JHEP*, 11:088, 2012.

- [2053] CMS Collaboration. Search for third-generation leptoquarks and scalar bottom quarks in pp collisions at $\sqrt{s} = 7 \text{ TeV}$. *JHEP*, 12:055, 2012.
- [2054] CMS Collaboration. Search for three-jet resonances in pp collisions at $\sqrt{s} = 7 \text{ TeV}$. *Phys. Lett. B*, 718:329, 2012.
- [2055] CMS Collaboration. Shape, transverse size, and charged hadron multiplicity of jets in pp collisions at 7 TeV . *JHEP*, 06:160, 2012.
- [2056] CMS Collaboration. Study of high- p_T charged particle suppression in PbPb compared to pp collisions at $\sqrt{s_{\text{NN}}} = 2.76 \text{ TeV}$. *Eur. Phys. J. C*, 72:1945, 2012.
- [2057] CMS Collaboration. Study of the dijet mass spectrum in $\text{pp} \rightarrow W + \text{jets}$ events at $\sqrt{s} = 7 \text{ TeV}$. *Phys. Rev. Lett.*, 109:251801, 2012.
- [2058] CMS Collaboration. Study of the inclusive production of charged pions, kaons, and protons in pp collisions at $\sqrt{s} = 0.9, 2.76$, and 7 TeV . *Eur. Phys. J. C*, 72:2164, 2012.
- [2059] CMS Collaboration. Study of W boson production in PbPb and pp collisions at $\sqrt{s_{\text{NN}}} = 2.76 \text{ TeV}$. *Phys. Lett. B*, 715:66, 2012.
- [2060] CMS Collaboration. Suppression of non-prompt J/ψ , prompt J/ψ , and $\Upsilon(1S)$ in PbPb collisions at $\sqrt{s_{\text{NN}}} = 2.76 \text{ TeV}$. *JHEP*, 05:063, 2012.
- [2061] CMS Collaboration. Angular analysis and branching fraction measurement of the decay $\text{B}^0 \rightarrow \text{K}^{*0}\mu^+\mu^-$. *Phys. Lett. B*, 727:77, 2013.
- [2062] CMS Collaboration. Energy calibration and resolution of the CMS electromagnetic calorimeter in pp collisions at $\sqrt{s} = 7 \text{ TeV}$. *JINST*, 8:P09009, 2013.
- [2063] CMS Collaboration. Event shapes and azimuthal correlations in $Z + \text{jets}$ events in pp collisions at $\sqrt{s} = 7 \text{ TeV}$. *Phys. Lett. B*, 722:238, 2013.
- [2064] CMS Collaboration. Evidence for associated production of a single top quark and W boson in pp collisions at $\sqrt{s} = 7 \text{ TeV}$. *Phys. Rev. Lett.*, 110:022003, 2013.
- [2065] CMS Collaboration. Forward-backward asymmetry of Drell-Yan lepton pairs in pp collisions at $\sqrt{s} = 7 \text{ TeV}$. *Phys. Lett. B*, 718:752, 2013.
- [2066] CMS Collaboration. Identification of b -quark jets with the CMS experiment. *JINST*, 8:P04013, 2013.

- [2067] CMS Collaboration. Inclusive search for supersymmetry using razor variables in pp collisions at $\sqrt{s} = 7 \text{ TeV}$. *Phys. Rev. Lett.*, 111:081802, 2013.
- [2068] CMS Collaboration. Interpretation of searches for supersymmetry with simplified models. *Phys. Rev. D*, 88:052017, 2013.
- [2069] CMS Collaboration. Jet and underlying event properties as a function of charged-particle multiplicity in proton–proton collisions at $\sqrt{s} = 7 \text{ TeV}$. *Eur. Phys. J. C*, 73:2674, 2013.
- [2070] CMS Collaboration. Measurement of associated production of vector bosons and top quark–antiquark pairs in pp collisions at $\sqrt{s} = 7 \text{ TeV}$. *Phys. Rev. Lett.*, 110:172002, 2013.
- [2071] CMS Collaboration. Measurement of differential top-quark-pair production cross sections in pp collisions at $\sqrt{s} = 7 \text{ TeV}$. *Eur. Phys. J. C*, 73:2339, 2013.
- [2072] CMS Collaboration. Measurement of masses in the $t\bar{t}$ system by kinematic endpoints in pp collisions at $\sqrt{s} = 7 \text{ TeV}$. *Eur. Phys. J. C*, 73:2494, 2013.
- [2073] CMS Collaboration. Measurement of neutral strange particle production in the underlying event in proton–proton collisions at $\sqrt{s} = 7 \text{ TeV}$. *Phys. Rev. D*, 88:052001, 2013.
- [2074] CMS Collaboration. Measurement of the azimuthal anisotropy of neutral pions in PbPb collisions at $\sqrt{s_{\text{NN}}} = 2.76 \text{ TeV}$. *Phys. Rev. Lett.*, 110:042301, 2013.
- [2075] CMS Collaboration. Measurement of the $B_s^0 \rightarrow \mu^+ \mu^-$ Branching Fraction and Search for $B^0 \rightarrow \mu^+ \mu^-$ with the CMS Experiment. *Phys. Rev. Lett.*, 111:101804, 2013.
- [2076] CMS Collaboration. Measurement of the cross section and angular correlations for associated production of a Z boson with b hadrons in pp collisions at $\sqrt{s} = 7 \text{ TeV}$. *JHEP*, 12:039, 2013.
- [2077] CMS Collaboration. Measurement of the differential and double-differential Drell-Yan cross sections in proton–proton collisions at $\sqrt{s} = 7 \text{ TeV}$. *JHEP*, 12:030, 2013.
- [2078] CMS Collaboration. Measurement of the elliptic anisotropy of charged particles produced in PbPb collisions at $\sqrt{s_{\text{NN}}} = 2.76 \text{ TeV}$. *Phys. Rev. C*, 87:014902, 2013.

- [2079] CMS Collaboration. Measurement of the hadronic activity in events with a Z and two jets and extraction of the cross section for the electroweak production of a Z with two jets in pp collisions at $\sqrt{s} = 7 \text{ TeV}$. *JHEP*, 10:062, 2013.
- [2080] CMS Collaboration. Measurement of the inelastic proton–proton cross section at $\sqrt{s} = 7 \text{ TeV}$. *Phys. Lett. B*, 722:5, 2013.
- [2081] CMS Collaboration. Measurement of the Λ_b^0 lifetime in pp collisions at $\sqrt{s} = 7 \text{ TeV}$. *JHEP*, 07:163, 2013.
- [2082] CMS Collaboration. Measurement of the production cross section for $Z\gamma \rightarrow v\bar{v}\gamma$ in pp collisions at $\sqrt{s} = 7 \text{ TeV}$ and limits on $ZZ\gamma$ and $Z\gamma\gamma$ triple gauge boson couplings. *JHEP*, 10:164, 2013.
- [2083] CMS Collaboration. Measurement of the prompt J/ψ and $\psi(2S)$ polarizations in pp collisions at $\sqrt{s} = 7 \text{ TeV}$. *Phys. Lett. B*, 727:381, 2013.
- [2084] CMS Collaboration. Measurement of the ratio of the inclusive 3-jet cross section to the inclusive 2-jet cross section in pp collisions at $\sqrt{s} = 7 \text{ TeV}$ and first determination of the strong coupling constant in the TeV range. *Eur. Phys. J. C*, 73:2604, 2013.
- [2085] CMS Collaboration. Measurement of the sum of WW and WZ production with W +dijet events in pp collisions at $\sqrt{s} = 7 \text{ TeV}$. *Eur. Phys. J. C*, 73:2283, 2013.
- [2086] CMS Collaboration. Measurement of the $t\bar{t}$ production cross section in pp collisions at $\sqrt{s} = 7 \text{ TeV}$ with lepton + jets final states. *Phys. Lett. B*, 720:83, 2013.
- [2087] CMS Collaboration. Measurement of the $t\bar{t}$ production cross section in the all-jet final state in pp collisions at $\sqrt{s} = 7 \text{ TeV}$. *JHEP*, 05:065, 2013.
- [2088] CMS Collaboration. Measurement of the $t\bar{t}$ production cross section in the $\tau+\text{jets}$ channel in pp collisions at $\sqrt{s} = 7 \text{ TeV}$. *Eur. Phys. J. C*, 73:2386, 2013.
- [2089] CMS Collaboration. Measurement of the $\Upsilon(1S)$, $\Upsilon(2S)$, and $\Upsilon(3S)$ cross sections in pp collisions at $\sqrt{s} = 7 \text{ TeV}$. *Phys. Lett. B*, 727:101, 2013.
- [2090] CMS Collaboration. Measurement of the $\Upsilon(1S)$, $\Upsilon(2S)$ and $\Upsilon(3S)$ Polarizations in pp Collisions at $\sqrt{s} = 7 \text{ TeV}$. *Phys. Rev. Lett.*, 110:081802, 2013.

- [2091] CMS Collaboration. Measurement of the W -boson helicity in top-quark decays from $t\bar{t}$ production in lepton+jets events in pp collisions at $\sqrt{s} = 7 \text{ TeV}$. *JHEP*, 10:167, 2013.
- [2092] CMS Collaboration. Measurement of the W^+W^- cross section in pp collisions at $\sqrt{s} = 7 \text{ TeV}$ and limits on anomalous $WW\gamma$ and WWZ couplings. *Eur. Phys. J. C*, 73:2610, 2013.
- [2093] CMS Collaboration. Measurement of the $X(3872)$ production cross section via decays to $J/\psi\pi^+\pi^-$ in pp collisions at $\sqrt{s} = 7 \text{ TeV}$. *JHEP*, 04:154, 2013.
- [2094] CMS Collaboration. Measurement of the ZZ production cross section and search for anomalous couplings in $2\ell 2\ell'$ final states in pp collisions at $\sqrt{s} = 7 \text{ TeV}$. *JHEP*, 01:063, 2013.
- [2095] CMS Collaboration. Measurement of W^+W^- and ZZ production cross sections in pp collisions at $\sqrt{s} = 8 \text{ TeV}$. *Phys. Lett. B*, 721:190, 2013.
- [2096] CMS Collaboration. Measurements of differential jet cross sections in proton–proton collisions at $\sqrt{s} = 7 \text{ TeV}$ with the CMS detector. *Phys. Rev. D*, 87:112002, 2013.
- [2097] CMS Collaboration. Multiplicity and transverse momentum dependence of two- and four-particle correlations in pPb and PbPb collisions. *Phys. Lett. B*, 724:213, 2013.
- [2098] CMS Collaboration. Observation of a diffractive contribution to dijet production in proton–proton collisions at $\sqrt{s} = 7 \text{ TeV}$. *Phys. Rev. D*, 87:012006, 2013.
- [2099] CMS Collaboration. Observation of a new boson with mass near 125 GeV in pp collisions at $\sqrt{s} = 7$ and 8 TeV . *JHEP*, 06:081, 2013.
- [2100] CMS Collaboration. Observation of long-range, near-side angular correlations in pPb collisions at the LHC. *Phys. Lett. B*, 718:795, 2013.
- [2101] CMS Collaboration. Rapidity distributions in exclusive $Z + \text{jet}$ and $\gamma + \text{jet}$ events in pp collisions at $\sqrt{s} = 7 \text{ TeV}$. *Phys. Rev. D*, 88:112009, 2013.
- [2102] CMS Collaboration. Search for a Higgs boson decaying into a b -quark pair and produced in association with b quarks in proton–proton collisions at 7 TeV . *Phys. Lett. B*, 722:207, 2013.
- [2103] CMS Collaboration. Search for a Higgs boson decaying into a Z and a photon in pp collisions at $\sqrt{s} = 7$ and 8 TeV . *Phys. Lett. B*, 726:587, 2013.

- [2104] CMS Collaboration. Search for a narrow, spin-2 resonance decaying to a pair of Z bosons in the $q\bar{q}\ell^+\ell^-$ final state. *Phys. Lett. B*, 718:1208, 2013.
- [2105] CMS Collaboration. Search for a new bottomonium state decaying to $\Upsilon(1S)\pi^+\pi^-$ in $p\bar{p}$ collisions at $\sqrt{s} = 8$ TeV. *Phys. Lett. B*, 727:57, 2013.
- [2106] CMS Collaboration. Search for a non-standard-model Higgs boson decaying to a pair of new light bosons in four-muon final states. *Phys. Lett. B*, 726:564, 2013.
- [2107] CMS Collaboration. Search for a standard-model-like Higgs boson with a mass in the range 145 to 1000 GeV at the LHC. *Eur. Phys. J. C*, 73:2469, 2013.
- [2108] CMS Collaboration. Search for a W' boson decaying to a bottom quark and a top quark in $p\bar{p}$ collisions at $\sqrt{s} = 7$ TeV. *Phys. Lett. B*, 718:1229, 2013.
- [2109] CMS Collaboration. Search for anomalous production of highly boosted Z bosons decaying to $\mu^+\mu^-$ in proton–proton collisions at $\sqrt{s} = 7$ TeV. *Phys. Lett. B*, 722:28, 2013.
- [2110] CMS Collaboration. Search for contact interactions in $\mu^+\mu^-$ events in $p\bar{p}$ collisions at $\sqrt{s} = 7$ TeV. *Phys. Rev. D*, 87:032001, 2013.
- [2111] CMS Collaboration. Search for contact interactions using the inclusive jet p_T spectrum in $p\bar{p}$ collisions at $\sqrt{s} = 7$ TeV. *Phys. Rev. D*, 87:052017, 2013.
- [2112] CMS Collaboration. Search for excited leptons in $p\bar{p}$ collisions at $\sqrt{s} = 7$ TeV. *Phys. Lett. B*, 720:309, 2013.
- [2113] CMS Collaboration. Search for exotic resonances decaying into WZ/ZZ in $p\bar{p}$ collisions at $\sqrt{s} = 7$ TeV. *JHEP*, 02:036, 2013.
- [2114] CMS Collaboration. Search for flavor changing neutral currents in top quark decays in $p\bar{p}$ collisions at 7 TeV. *Phys. Lett. B*, 718:1252, 2013.
- [2115] CMS Collaboration. Search for fractionally charged particles in $p\bar{p}$ collisions at $\sqrt{s} = 7$ TeV. *Phys. Rev. D*, 87:092008, 2013.
- [2116] CMS Collaboration. Search for gluino mediated bottom- and top-squark production in multijet final states in $p\bar{p}$ collisions at 8 TeV. *Phys. Lett. B*, 725:243, 2013.
- [2117] CMS Collaboration. Search for heavy narrow dilepton resonances in $p\bar{p}$ collisions at $\sqrt{s} = 7$ TeV and $\sqrt{s} = 8$ TeV. *Phys. Lett. B*, 720:63, 2013.

- [2118] CMS Collaboration. Search for heavy quarks decaying into a top quark and a W or Z boson using lepton + jets events in pp collisions at $\sqrt{s} = 7 \text{ TeV}$. *JHEP*, 01:154, 2013.
- [2119] CMS Collaboration. Search for heavy resonances in the W/Z -tagged dijet mass spectrum in pp collisions at 7 TeV . *Phys. Lett. B*, 723:280, 2013.
- [2120] CMS Collaboration. Search for long-lived particles in events with photons and missing energy in proton–proton collisions at $\sqrt{s} = 7 \text{ TeV}$. *Phys. Lett. B*, 722:273, 2013.
- [2121] CMS Collaboration. Search for microscopic black holes in pp collisions at $\sqrt{s} = 8 \text{ TeV}$. *JHEP*, 07:178, 2013.
- [2122] CMS Collaboration. Search for narrow resonances and quantum black holes in inclusive and b -tagged dijet mass spectra from pp collisions at $\sqrt{s} = 7 \text{ TeV}$. *JHEP*, 01:013, 2013.
- [2123] CMS Collaboration. Search for narrow resonances using the dijet mass spectrum in pp collisions at $\sqrt{s} = 8 \text{ TeV}$. *Phys. Rev. D*, 87:114015, 2013.
- [2124] CMS Collaboration. Search for new physics in events with opposite-sign leptons, jets, and missing transverse energy in pp collisions at $\sqrt{s} = 7 \text{ TeV}$. *Phys. Lett. B*, 718:815, 2013.
- [2125] CMS Collaboration. Search for new physics in events with photons, jets, and missing transverse energy in pp collisions at $\sqrt{s} = 7 \text{ TeV}$. *JHEP*, 03:111, 2013.
- [2126] CMS Collaboration. Search for new physics in events with same-sign dileptons and b jets in pp collisions at $\sqrt{s} = 8 \text{ TeV}$. *JHEP*, 03:037, 2013.
- [2127] CMS Collaboration. Search for new physics in final states with a lepton and missing transverse energy in pp collisions at the LHC. *Phys. Rev. D*, 87:072005, 2013.
- [2128] CMS Collaboration. Search for pair-produced dijet resonances in four-jet final states in pp collisions at $\sqrt{s} = 7 \text{ TeV}$. *Phys. Rev. Lett.*, 110:141802, 2013.
- [2129] CMS Collaboration. Search for pair production of third-generation leptons and top squarks in pp collisions at $\sqrt{s} = 7 \text{ TeV}$. *Phys. Rev. Lett.*, 110:081801, 2013.
- [2130] CMS Collaboration. Search for physics beyond the standard model in events with τ leptons, jets, and large transverse momentum imbalance in pp collisions at $\sqrt{s} = 7 \text{ TeV}$. *Eur. Phys. J. C*, 73:2493, 2013.

- [2131] CMS Collaboration. Search for supersymmetry in events with opposite-sign dileptons and missing transverse energy using an artificial neural network. *Phys. Rev. D*, 87:072001, 2013.
- [2132] CMS Collaboration. Search for supersymmetry in events with photons and low missing transverse energy in pp collisions at $\sqrt{s} = 7 \text{ TeV}$. *Phys. Lett. B*, 719:42, 2013.
- [2133] CMS Collaboration. Search for supersymmetry in final states with a single lepton, b-quark jets, and missing transverse energy in proton–proton collisions at $\sqrt{s} = 7 \text{ TeV}$. *Phys. Rev. D*, 87:052006, 2013.
- [2134] CMS Collaboration. Search for supersymmetry in final states with missing transverse energy and 0, 1, 2, or ≥ 3 b-quark jets in 7 TeV pp collisions using the variable α_T . *JHEP*, 01:077, 2013.
- [2135] CMS Collaboration. Search for supersymmetry in hadronic final states with missing transverse energy using the variables α_T and b-quark multiplicity in pp collisions at $\sqrt{s} = 8 \text{ TeV}$. *Eur. Phys. J. C*, 73:2568, 2013.
- [2136] CMS Collaboration. Search for supersymmetry in pp collisions at $\sqrt{s} = 7 \text{ TeV}$ in events with a single lepton, jets, and missing transverse momentum. *Eur. Phys. J. C*, 73:2404, 2013.
- [2137] CMS Collaboration. Search for the standard model Higgs boson produced in association with a top-quark pair in pp collisions at the LHC. *JHEP*, 05:145, 2013.
- [2138] CMS Collaboration. Search for top-squark pair production in the single-lepton final state in pp collisions at $\sqrt{s} = 8 \text{ TeV}$. *Eur. Phys. J. C*, 73:2677, 2013.
- [2139] CMS Collaboration. Search for top squarks in R-parity-violating supersymmetry using three or more leptons and b-tagged jets. *Phys. Rev. Lett.*, 111:221801, 2013.
- [2140] CMS Collaboration. Search for Z' resonances decaying to $t\bar{t}$ in dilepton+jets final states in pp collisions at $\sqrt{s} = 7 \text{ TeV}$. *Phys. Rev. D*, 87:072002, 2013.
- [2141] CMS Collaboration. Search in leptonic channels for heavy resonances decaying to long-lived neutral particles. *JHEP*, 02:085, 2013.
- [2142] CMS Collaboration. Searches for Higgs bosons in pp collisions at $\sqrt{s} = 7$ and 8 TeV in the context of four-generation and fermiophobic models. *Phys. Lett. B*, 725:36, 2013.

- [2143] CMS Collaboration. Searches for long-lived charged particles in pp collisions at $\sqrt{s} = 7$ and 8 TeV. *JHEP*, 07:122, 2013.
- [2144] CMS Collaboration. Searches for new physics using the $t\bar{t}$ invariant mass distribution in pp collisions at $\sqrt{s} = 8$ TeV. *Phys. Rev. Lett.*, 111:211804, 2013.
- [2145] CMS Collaboration. Studies of jet mass in dijet and $W/Z + \text{jet}$ events. *JHEP*, 05:090, 2013.
- [2146] CMS Collaboration. Studies of jet quenching using isolated-photon+jet correlations in PbPb and pp collisions at $\sqrt{s_{\text{NN}}} = 2.76$ TeV. *Phys. Lett. B*, 718:773, 2013.
- [2147] CMS Collaboration. Study of exclusive two-photon production of W^+W^- in pp collisions at $\sqrt{s} = 7$ TeV and constraints on anomalous quartic gauge couplings. *JHEP*, 07:116, 2013.
- [2148] CMS Collaboration. Study of the Mass and Spin-Parity of the Higgs Boson Candidate Via Its Decays to Z Boson Pairs. *Phys. Rev. Lett.*, 110:081803, 2013.
- [2149] CMS Collaboration. Study of the underlying event at forward rapidity in pp collisions at $\sqrt{s} = 0.9, 2.76$, and 7 TeV. *JHEP*, 04:072, 2013.
- [2150] CMS Collaboration. The performance of the CMS muon detector in proton-proton collisions at $\sqrt{s} = 7$ TeV at the LHC. *JINST*, 8:P11002, 2013.
- [2151] CMS Collaboration. A search for $WW\gamma$ and $WZ\gamma$ production and constraints on anomalous quartic gauge couplings in pp collisions at $\sqrt{s} = 8$ TeV. *Phys. Rev. D*, 90:032008, 2014.
- [2152] CMS Collaboration. Alignment of the CMS tracker with LHC and cosmic ray data. *JINST*, 9:P06009, 2014.
- [2153] CMS Collaboration. Constraints on the Higgs boson width from off-shell production and decay to Z -boson pairs. *Phys. Lett. B*, 736:64, 2014.
- [2154] CMS Collaboration. Description and performance of track and primary-vertex reconstruction with the CMS tracker. *JINST*, 9:P10009, 2014.
- [2155] CMS Collaboration. Determination of the top-quark pole mass and strong coupling constant from the $t\bar{t}$ production cross section in pp collisions at $\sqrt{s} = 7$ TeV. *Phys. Lett. B*, 728:496, 2014.

- [2156] CMS Collaboration. Event activity dependence of $\Upsilon(nS)$ production in $\sqrt{s_{NN}} = 5.02$ TeV pPb and $\sqrt{s} = 2.76$ TeV pp collisions. *JHEP*, 04:103, 2014.
- [2157] CMS Collaboration. Evidence for the 125 GeV Higgs boson decaying to a pair of τ leptons. *JHEP*, 05:104, 2014.
- [2158] CMS Collaboration. Evidence for the direct decay of the 125 GeV Higgs boson to fermions. *Nature Phys.*, 10:557, 2014.
- [2159] CMS Collaboration. Evidence of b-Jet Quenching in PbPb Collisions at $\sqrt{s_{NN}} = 2.76$ TeV. *Phys. Rev. Lett.*, 113:132301, 2014.
- [2160] CMS Collaboration. Identification techniques for highly boosted W bosons that decay into hadrons. *JHEP*, 12:017, 2014.
- [2161] CMS Collaboration. Inclusive search for a vector-like T quark with charge $\frac{2}{3}$ in pp collisions at $\sqrt{s} = 8$ TeV. *Phys. Lett. B*, 729:149, 2014.
- [2162] CMS Collaboration. Measurement of associated $W +$ charm production in pp collisions at $\sqrt{s} = 7$ TeV. *JHEP*, 02:013, 2014.
- [2163] CMS Collaboration. Measurement of differential cross sections for the production of a pair of isolated photons in pp collisions at $\sqrt{s} = 7$ TeV. *Eur. Phys. J. C*, 74:3129, 2014.
- [2164] CMS Collaboration. Measurement of four-jet production in proton–proton collisions at $\sqrt{s} = 7$ TeV. *Phys. Rev. D*, 89:092010, 2014.
- [2165] CMS Collaboration. Measurement of Higgs boson production and properties in the WW decay channel with leptonic final states. *JHEP*, 01:096, 2014.
- [2166] CMS Collaboration. Measurement of higher-order harmonic azimuthal anisotropy in PbPb collisions at $\sqrt{s_{NN}} = 2.76$ TeV. *Phys. Rev. C*, 89:044906, 2014.
- [2167] CMS Collaboration. Measurement of inclusive W and Z boson production cross sections in pp collisions at $\sqrt{s} = 8$ TeV. *Phys. Rev. Lett.*, 112:191802, 2014.
- [2168] CMS Collaboration. Measurement of jet fragmentation in PbPb and pp collisions at $\sqrt{s_{NN}} = 2.76$ TeV. *Phys. Rev. C*, 90:024908, 2014.
- [2169] CMS Collaboration. Measurement of prompt J/ψ pair production in pp collisions at $\sqrt{s} = 7$ TeV. *JHEP*, 09:094, 2014.

- [2170] CMS Collaboration. Measurement of prompt $\psi(2S)$ to J/ψ yield ratios in PbPb and $p\bar{p}$ collisions at $\sqrt{s_{NN}} = 2.76$ TeV. *Phys. Rev. Lett.*, 113:262301, 2014.
- [2171] CMS Collaboration. Measurement of pseudorapidity distributions of charged particles in proton–proton collisions at $\sqrt{s} = 8$ TeV by the CMS and TOTEM experiments. *Eur. Phys. J. C*, 74:3053, 2014.
- [2172] CMS Collaboration. Measurement of the muon charge asymmetry in inclusive $p\bar{p} \rightarrow W + X$ production at $\sqrt{s} = 7$ TeV and an improved determination of light parton distribution functions. *Phys. Rev. D*, 90:032004, 2014.
- [2173] CMS Collaboration. Measurement of the production cross section for a W boson and two b jets in $p\bar{p}$ collisions at $\sqrt{s} = 7$ TeV. *Phys. Lett. B*, 735:204, 2014.
- [2174] CMS Collaboration. Measurement of the production cross sections for a Z boson and one or more b jets in $p\bar{p}$ collisions at $\sqrt{s} = 7$ TeV. *JHEP*, 06:120, 2014.
- [2175] CMS Collaboration. Measurement of the properties of a Higgs boson in the four-lepton final state. *Phys. Rev. D*, 89:092007, 2014.
- [2176] CMS Collaboration. Measurement of the ratio $\mathcal{B}(t \rightarrow Wb)/\mathcal{B}(t \rightarrow Wq)$ in $p\bar{p}$ collisions at $\sqrt{s} = 8$ TeV. *Phys. Lett. B*, 736:33, 2014.
- [2177] CMS Collaboration. Measurement of the ratio of inclusive jet cross sections using the anti- k_T algorithm with radius parameters $R = 0.5$ and 0.7 in $p\bar{p}$ collisions at $\sqrt{s} = 7$ TeV. *Phys. Rev. D*, 90:072006, 2014.
- [2178] CMS Collaboration. Measurement of the $t\bar{t}$ production cross section in the dilepton channel in $p\bar{p}$ collisions at $\sqrt{s} = 8$ TeV. *JHEP*, 02:024, 2014.
- [2179] CMS Collaboration. Measurement of the t -channel single-top-quark production cross section and of the $|V_{tb}|$ CKM matrix element in $p\bar{p}$ collisions at $\sqrt{s} = 8$ TeV. *JHEP*, 06:090, 2014.
- [2180] CMS Collaboration. Measurement of the $t\bar{t}$ production cross section in $p\bar{p}$ collisions at $\sqrt{s} = 8$ TeV in dilepton final states containing one τ lepton. *Phys. Lett. B*, 739:23, 2014.
- [2181] CMS Collaboration. Measurement of the top-quark mass in all-jets $t\bar{t}$ events in $p\bar{p}$ collisions at $\sqrt{s} = 7$ TeV. *Eur. Phys. J. C*, 74:2758, 2014.
- [2182] CMS Collaboration. Measurement of the triple-differential cross section for photon+jets production in proton–proton collisions at $\sqrt{s} = 7$ TeV. *JHEP*, 06:009, 2014.

- [2183] CMS Collaboration. Measurement of the $W\gamma$ and $Z\gamma$ inclusive cross sections in pp collisions at $\sqrt{s} = 7 \text{ TeV}$ and limits on anomalous triple gauge boson couplings. *Phys. Rev. D*, 89:092005, 2014.
- [2184] CMS Collaboration. Measurement of top quark–antiquark pair production in association with a W or Z boson in pp collisions at $\sqrt{s} = 8 \text{ TeV}$. *Eur. Phys. J. C*, 74:3060, 2014.
- [2185] CMS Collaboration. Measurement of WZ and ZZ production in pp collisions at $\sqrt{s} = 8 \text{ TeV}$ in final states with b -tagged jets. *Eur. Phys. J. C*, 74:2973, 2014.
- [2186] CMS Collaboration. Measurements of $t\bar{t}$ spin correlations and top-quark polarization using dilepton final states in pp collisions at $\sqrt{s} = 7 \text{ TeV}$. *Phys. Rev. Lett.*, 112:182001, 2014.
- [2187] CMS Collaboration. Measurements of the $t\bar{t}$ charge asymmetry using the dilepton decay channel in pp collisions at $\sqrt{s} = 7 \text{ TeV}$. *JHEP*, 04:191, 2014.
- [2188] CMS Collaboration. Modification of jet shapes in PbPb collisions at $\sqrt{s_{\text{NN}}} = 2.76 \text{ TeV}$. *Phys. Lett. B*, 730:243, 2014.
- [2189] CMS Collaboration. Observation of a peaking structure in the $J/\psi\phi$ mass spectrum from $B^\pm \rightarrow J/\psi\phi K^\pm$ decays. *Phys. Lett. B*, 734:261, 2014.
- [2190] CMS Collaboration. Observation of the associated production of a single top quark and a W boson in pp collisions at $\sqrt{s} = 8 \text{ TeV}$. *Phys. Rev. Lett.*, 112:231802, 2014.
- [2191] CMS Collaboration. Observation of the diphoton decay of the Higgs boson and measurement of its properties. *Eur. Phys. J. C*, 74:3076, 2014.
- [2192] CMS Collaboration. Probing color coherence effects in pp collisions at $\sqrt{s} = 7 \text{ TeV}$. *Eur. Phys. J. C*, 74:2901, 2014.
- [2193] CMS Collaboration. Search for anomalous production of events with three or more leptons in pp collisions at $\sqrt{s} = 8 \text{ TeV}$. *Phys. Rev. D*, 90:032006, 2014.
- [2194] CMS Collaboration. Search for baryon number violation in top-quark decays. *Phys. Lett. B*, 731:173, 2014.
- [2195] CMS Collaboration. Search for excited quarks in the $\gamma+\text{jet}$ final state in proton–proton collisions at $\sqrt{s} = 8 \text{ TeV}$. *Phys. Lett. B*, 738:274, 2014.

- [2196] CMS Collaboration. Search for flavor-changing neutral currents in top-quark decays $t \rightarrow Zq$ in pp collisions at $\sqrt{s} = 8$ TeV. *Phys. Rev. Lett.*, 112:171802, 2014.
- [2197] CMS Collaboration. Search for heavy neutrinos and W bosons with right-handed couplings in proton–proton collisions at $\sqrt{s} = 8$ TeV. *Eur. Phys. J. C*, 74:3149, 2014.
- [2198] CMS Collaboration. Search for invisible decays of Higgs bosons in the vector boson fusion and associated ZH production modes. *Eur. Phys. J. C*, 74:2980, 2014.
- [2199] CMS Collaboration. Search for jet extinction in the inclusive jet- p_T spectrum from proton–proton collisions at $\sqrt{s} = 8$ TeV. *Phys. Rev. D*, 90:032005, 2014.
- [2200] CMS Collaboration. Search for massive resonances decaying into pairs of boosted bosons in semi-leptonic final states at $\sqrt{s} = 8$ TeV. *JHEP*, 08:174, 2014.
- [2201] CMS Collaboration. Search for massive resonances in dijet systems containing jets tagged as W or Z boson decays in pp collisions at $\sqrt{s} = 8$ TeV. *JHEP*, 08:173, 2014.
- [2202] CMS Collaboration. Search for neutral MSSM Higgs bosons decaying to a pair of tau leptons in pp collisions. *JHEP*, 10:160, 2014.
- [2203] CMS Collaboration. Search for new physics in the multijet and missing transverse momentum final state in proton–proton collisions at $\sqrt{s} = 8$ TeV. *JHEP*, 06:055, 2014.
- [2204] CMS Collaboration. Search for pair production of excited top quarks in the lepton+jets final state. *JHEP*, 06:125, 2014.
- [2205] CMS Collaboration. Search for pair production of third-generation scalar leptoquarks and top squarks in proton–proton collisions at $\sqrt{s} = 8$ TeV. *Phys. Lett. B*, 739:229, 2014.
- [2206] CMS Collaboration. Search for standard model production of four top quarks in the lepton + jets channel in pp collisions at $\sqrt{s} = 8$ TeV. *JHEP*, 11:154, 2014.
- [2207] CMS Collaboration. Search for supersymmetry in pp collisions at $\sqrt{s} = 8$ TeV in events with a single lepton, large jet multiplicity, and multiple b jets. *Phys. Lett. B*, 733:328, 2014.

- [2208] CMS Collaboration. Search for supersymmetry with razor variables in pp collisions at $\sqrt{s} = 7 \text{ TeV}$. *Phys. Rev. D*, 90:112001, 2014.
- [2209] CMS Collaboration. Search for the associated production of the Higgs boson with a top-quark pair. *JHEP*, 09:087, 2014.
- [2210] CMS Collaboration. Search for the standard model Higgs boson produced in association with a W or a Z boson and decaying to bottom quarks. *Phys. Rev. D*, 89:012003, 2014.
- [2211] CMS Collaboration. Search for top-quark partners with charge $5/3$ in the same-sign dilepton final state. *Phys. Rev. Lett.*, 112:171801, 2014.
- [2212] CMS Collaboration. Search for top squark and higgsino production using diphoton Higgs boson decays. *Phys. Rev. Lett.*, 112:161802, 2014.
- [2213] CMS Collaboration. Search for top-squark pairs decaying into Higgs or Z bosons in pp collisions at $\sqrt{s} = 8 \text{ TeV}$. *Phys. Lett. B*, 736:371, 2014.
- [2214] CMS Collaboration. Search for $W' \rightarrow tb$ decays in the lepton + jets final state in pp collisions at $\sqrt{s} = 8 \text{ TeV}$. *JHEP*, 05:108, 2014.
- [2215] CMS Collaboration. Searches for electroweak neutralino and chargino production in channels with Higgs, Z , and W bosons in pp collisions at 8 TeV . *Phys. Rev. D*, 90:092007, 2014.
- [2216] CMS Collaboration. Searches for electroweak production of charginos, neutralinos, and sleptons decaying to leptons and W , Z , and Higgs bosons in pp collisions at 8 TeV . *Eur. Phys. J. C*, 74:3036, 2014.
- [2217] CMS Collaboration. Searches for heavy Higgs bosons in two-Higgs-doublet models and for $t \rightarrow ch$ decay using multilepton and diphoton final states in pp collisions at $\sqrt{s} = 8 \text{ TeV}$. *Phys. Rev. D*, 90:112013, 2014.
- [2218] CMS Collaboration. Searches for light- and heavy-flavour three-jet resonances in pp collisions at $\sqrt{s} = 8 \text{ TeV}$. *Phys. Lett. B*, 730:193, 2014.
- [2219] CMS Collaboration. Studies of azimuthal dihadron correlations in ultra-central PbPb collisions at $\sqrt{s_{\text{NN}}} = 2.76 \text{ TeV}$. *JHEP*, 02:088, 2014.
- [2220] CMS Collaboration. Studies of dijet transverse momentum balance and pseudorapidity distributions in pPb collisions at $\sqrt{s_{\text{NN}}} = 5.02 \text{ TeV}$. *Eur. Phys. J. C*, 74:2951, 2014.
- [2221] CMS Collaboration. Study of double parton scattering using $W + 2$ -jet events in proton–proton collisions at $\sqrt{s} = 7 \text{ TeV}$. *JHEP*, 03:032, 2014.

- [2222] CMS Collaboration. Study of hadronic event-shape variables in multijet final states in pp collisions at $\sqrt{s} = 7$ TeV. *JHEP*, 10:87, 2014.
- [2223] CMS Collaboration. Study of the production of charged pions, kaons, and protons in pPb collisions at $\sqrt{s_{\text{NN}}} = 5.02$ TeV. *Eur. Phys. J. C*, 74:2847, 2014.
- [2224] CMS Collaboration. Angular coefficients of Z bosons produced in pp collisions at $\sqrt{s} = 8$ TeV and decaying to $\mu^+\mu^-$ as a function of transverse momentum and rapidity. *Phys. Lett. B*, 750:154, 2015.
- [2225] CMS Collaboration. Comparison of the $Z/\gamma^* + \text{jets}$ to $\gamma + \text{jets}$ cross sections in pp collisions at $\sqrt{s} = 8$ TeV. *JHEP*, 10:128, 2015.
- [2226] CMS Collaboration. Constraints on parton distribution functions and extraction of the strong coupling constant from the inclusive jet cross section in pp collisions at $\sqrt{s} = 7$ TeV. *Eur. Phys. J. C*, 75:288, 2015.
- [2227] CMS Collaboration. Constraints on the pMSSM, AMSB model and on other models from the search for long-lived charged particles in proton–proton collisions at $\sqrt{s} = 8$ TeV. *Eur. Phys. J. C*, 75:325, 2015.
- [2228] CMS Collaboration. Constraints on the spin-parity and anomalous HVV couplings of the Higgs boson in proton collisions at 7 and 8 TeV. *Phys. Rev. D*, 92:012004, 2015.
- [2229] CMS Collaboration. Differential cross section measurements for the production of a W boson in association with jets in proton–proton collisions at $\sqrt{s} = 7$ TeV. *Phys. Lett. B*, 741:12, 2015.
- [2230] CMS Collaboration. Distributions of topological observables in inclusive three- and four-jet events in pp collisions at $\sqrt{s} = 7$ TeV. *Eur. Phys. J. C*, 75:302, 2015.
- [2231] CMS Collaboration. Evidence for Collective Multiparticle Correlations in pPb Collisions. *Phys. Rev. Lett.*, 115:012301, 2015.
- [2232] CMS Collaboration. Evidence for transverse-momentum- and pseudorapidity-dependent event-plane fluctuations in PbPb and pPb collisions. *Phys. Rev. C*, 92:034911, 2015.
- [2233] CMS Collaboration. Limits on the Higgs boson lifetime and width from its decay to four charged leptons. *Phys. Rev. D*, 92:072010, 2015.
- [2234] CMS Collaboration. Long-range two-particle correlations of strange hadrons with charged particles in pPb and PbPb collisions at LHC energies. *Phys. Lett. B*, 742:200, 2015.

- [2235] CMS Collaboration. Measurement of diffractive dissociation cross sections in pp collisions at $\sqrt{s} = 7$ TeV. *Phys. Rev. D*, 92:012003, 2015.
- [2236] CMS Collaboration. Measurement of electroweak production of two jets in association with a Z boson in proton–proton collisions at $\sqrt{s} = 8$ TeV. *Eur. Phys. J. C*, 75:66, 2015.
- [2237] CMS Collaboration. Measurement of jet multiplicity distributions in $t\bar{t}$ production in pp collisions at $\sqrt{s} = 7$ TeV. *Eur. Phys. J. C*, 74:3014, 2015.
- [2238] CMS Collaboration. Measurement of J/ψ and $\psi(2S)$ Prompt Double-Differential Cross Sections in pp Collisions at $\sqrt{s} = 7$ TeV. *Phys. Rev. Lett.*, 114:191802, 2015.
- [2239] CMS Collaboration. Measurement of the cross section ratio $\sigma_{t\bar{t}b\bar{b}}/\sigma_{t\bar{t}jj}$ in pp collisions at $\sqrt{s} = 8$ TeV. *Phys. Lett. B*, 746:132, 2015.
- [2240] CMS Collaboration. Measurement of the differential cross section for top quark pair production in pp collisions at $\sqrt{s} = 8$ TeV. *Eur. Phys. J. C*, 75:542, 2015.
- [2241] CMS Collaboration. Measurement of the inclusive 3-jet production differential cross section in proton–proton collisions at 7 TeV and determination of the strong coupling constant in the TeV range. *Eur. Phys. J. C*, 75:186, 2015.
- [2242] CMS Collaboration. Measurement of the $\text{pp} \rightarrow ZZ$ production cross section and constraints on anomalous triple gauge couplings in four-lepton final states at $\sqrt{s} = 8$ TeV. *Phys. Lett. B*, 740:250, 2015.
- [2243] CMS Collaboration. Measurement of the production cross section ratio $\sigma(\chi_{b2}(1P))/\sigma(\chi_{b1}(1P))$ in pp collisions at $\sqrt{s} = 8$ TeV. *Phys. Lett. B*, 743:383, 2015.
- [2244] CMS Collaboration. Measurement of the ratio of the production cross sections times branching fractions of $B_c^\pm \rightarrow J/\psi \pi^\pm$ and $B^\pm \rightarrow J/\psi K^\pm$ and $\mathcal{B}(B_c^\pm \rightarrow J/\psi \pi^\pm \pi^\pm \pi^\mp)/\mathcal{B}(B_c^\pm \rightarrow J/\psi \pi^\pm)$ in pp collisions at $\sqrt{s} = 7$ TeV. *JHEP*, 01:063, 2015.
- [2245] CMS Collaboration. Measurement of the underlying event activity using charged-particle jets in proton–proton collisions at $\sqrt{s} = 2.76$ TeV. *JHEP*, 09:137, 2015.
- [2246] CMS Collaboration. Measurement of the W boson helicity in events with a single reconstructed top quark in pp collisions at $\sqrt{s} = 8$ TeV. *JHEP*, 01:053, 2015.

- [2247] CMS Collaboration. Measurement of the Z boson differential cross section in transverse momentum and rapidity in proton–proton collisions at 8 TeV. *Phys. Lett. B*, 749:187, 2015.
- [2248] CMS Collaboration. Measurement of the $Z\gamma$ production cross section in pp collisions at 8 TeV and search for anomalous triple gauge boson couplings. *JHEP*, 04:164, 2015.
- [2249] CMS Collaboration. Measurements of differential and double-differential Drell-Yan cross sections in proton–proton collisions at 8 TeV. *Eur. Phys. J. C*, 75:147, 2015.
- [2250] CMS Collaboration. Measurements of jet multiplicity and differential production cross sections of $Z + \text{jets}$ events in proton–proton collisions at $\sqrt{s} = 7$ TeV. *Phys. Rev. D*, 91:052008, 2015.
- [2251] CMS Collaboration. Measurements of the $\Upsilon(1S)$, $\Upsilon(2S)$, and $\Upsilon(3S)$ differential cross sections in pp collisions at $\sqrt{s} = 7$ TeV. *Phys. Lett. B*, 749:14, 2015.
- [2252] CMS Collaboration. Measurements of the ZZ production cross sections in the $2\ell 2\nu$ channel in proton–proton collisions at $\sqrt{s} = 7$ and 8 TeV and combined constraints on triple gauge couplings. *Eur. Phys. J. C*, 75:511, 2015.
- [2253] CMS Collaboration. Nuclear effects on the transverse momentum spectra of charged particles in pPb collisions at $\sqrt{s_{\text{NN}}} = 5.02$ TeV. *Eur. Phys. J. C*, 75:237, 2015.
- [2254] CMS Collaboration. Observation of the rare $B_s^0 \rightarrow \mu^+\mu^-$ decay from the combined analysis of CMS and LHCb data. *Nature*, 522:68, 2015.
- [2255] CMS Collaboration. Performance of electron reconstruction and selection with the CMS detector in proton–proton collisions at $\sqrt{s} = 8$ TeV. *JINST*, 10:P06005, 2015.
- [2256] CMS Collaboration. Performance of photon reconstruction and identification with the CMS detector in proton–proton collisions at $\sqrt{s} = 8$ TeV. *JINST*, 10:P08010, 2015.
- [2257] CMS Collaboration. Performance of the CMS missing transverse momentum reconstruction in pp data at $\sqrt{s} = 8$ TeV. *JINST*, 10:P02006, 2015.
- [2258] CMS Collaboration. Precise determination of the mass of the Higgs boson and tests of compatibility of its couplings with the standard model predictions using proton collisions at 7 and 8 TeV. *Eur. Phys. J. C*, 75:212, 2015.

- [2259] CMS Collaboration. Production of leading charged particles and leading charged-particle jets at small transverse momenta in pp collisions at $\sqrt{s} = 8$ TeV. *Phys. Rev. D*, 92:112001, 2015.
- [2260] CMS Collaboration. Pseudorapidity distribution of charged hadrons in proton–proton collisions at $\sqrt{s} = 13$ TeV. *Phys. Lett. B*, 751:143, 2015.
- [2261] CMS Collaboration. Search for a charged Higgs boson in pp collisions at $\sqrt{s} = 8$ TeV. *JHEP*, 11:018, 2015.
- [2262] CMS Collaboration. Search for a Higgs boson in the mass range from 145 to 1000 GeV decaying to a pair of W or Z bosons. *JHEP*, 10:144, 2015.
- [2263] CMS Collaboration. Search for a light charged Higgs boson decaying to $c\bar{s}$ in pp collisions at $\sqrt{s} = 8$ TeV. *JHEP*, 12:178, 2015.
- [2264] CMS Collaboration. Search for a pseudoscalar boson decaying into a Z boson and the 125 GeV Higgs boson in $\ell^+\ell^-b\bar{b}$ final states. *Phys. Lett. B*, 748:221, 2015.
- [2265] CMS Collaboration. Search for a standard model Higgs boson produced in association with a top-quark pair and decaying to bottom quarks using a matrix element method. *Eur. Phys. J. C*, 75:251, 2015.
- [2266] CMS Collaboration. Search for a standard model-like Higgs boson in the $\mu^+\mu^-$ and e^+e^- decay channels at the LHC. *Phys. Lett. B*, 744:184, 2015.
- [2267] CMS Collaboration. Search for dark matter, extra dimensions, and unparticles in monojet events in proton–proton collisions at $\sqrt{s} = 8$ TeV. *Eur. Phys. J. C*, 75:235, 2015.
- [2268] CMS Collaboration. Search for decays of stopped long-lived particles produced in proton–proton collisions at $\sqrt{s} = 8$ TeV. *Eur. Phys. J. C*, 75:151, 2015.
- [2269] CMS Collaboration. Search for diphoton resonances in the mass range from 150 to 850 GeV in pp collisions at $\sqrt{s} = 8$ TeV. *Phys. Lett. B*, 750:494, 2015.
- [2270] CMS Collaboration. Search for disappearing tracks in proton–proton collisions at $\sqrt{s} = 8$ TeV. *JHEP*, 01:096, 2015.
- [2271] CMS Collaboration. Search for Displaced Supersymmetry in Events with an Electron and a Muon with Large Impact Parameters. *Phys. Rev. Lett.*, 114:061801, 2015.

- [2272] CMS Collaboration. Search for heavy Majorana neutrinos in $\mu^\pm\mu^\pm + \text{jets}$ events in proton–proton collisions at $\sqrt{s} = 8$ TeV. *Phys. Lett. B*, 748:144, 2015.
- [2273] CMS Collaboration. Search for lepton-flavour-violating decays of the Higgs boson. *Phys. Lett. B*, 749:337, 2015.
- [2274] CMS Collaboration. Search for long-lived neutral particles decaying to quark–antiquark pairs in proton–proton collisions at $\sqrt{s} = 8$ TeV. *Phys. Rev. D*, 91:012007, 2015.
- [2275] CMS Collaboration. Search for long-lived particles that decay into final states containing two electrons or two muons in proton–proton collisions at $\sqrt{s} = 8$ TeV. *Phys. Rev. D*, 91:052012, 2015.
- [2276] CMS Collaboration. Search for monotop signatures in proton–proton collisions at $\sqrt{s} = 8$ TeV. *Phys. Rev. Lett.*, 114:101801, 2015.
- [2277] CMS Collaboration. Search for narrow high-mass resonances in proton–proton collisions at $\sqrt{s} = 8$ TeV decaying to a Z and a Higgs boson. *Phys. Lett. B*, 748:255, 2015.
- [2278] CMS Collaboration. Search for neutral color-octet weak-triplet scalar particles in proton–proton collisions at $\sqrt{s} = 8$ TeV. *JHEP*, 09:201, 2015.
- [2279] CMS Collaboration. Search for neutral MSSM Higgs bosons decaying into a pair of bottom quarks. *JHEP*, 11:071, 2015.
- [2280] CMS Collaboration. Search for new resonances decaying via WZ to leptons in proton–proton collisions at $\sqrt{s} = 8$ TeV. *Phys. Lett. B*, 740:83, 2015.
- [2281] CMS Collaboration. Search for pair-produced resonances decaying to jet pairs in proton–proton collisions at $\sqrt{s} = 8$ TeV. *Phys. Lett. B*, 747:98, 2015.
- [2282] CMS Collaboration. Search for physics beyond the standard model in dilepton mass spectra in proton–proton collisions at $\sqrt{s} = 8$ TeV. *JHEP*, 04:025, 2015.
- [2283] CMS Collaboration. Search for physics beyond the standard model in events with two leptons, jets, and missing transverse momentum in pp collisions at $\sqrt{s} = 8$ TeV. *JHEP*, 04:124, 2015.
- [2284] CMS Collaboration. Search for physics beyond the standard model in final states with a lepton and missing transverse energy in proton–proton collisions at $\sqrt{s} = 8$ TeV. *Phys. Rev. D*, 91:092005, 2015.

- [2285] CMS Collaboration. Search for quark contact interactions and extra spatial dimensions using dijet angular distributions in proton–proton collisions at $\sqrt{s} = 8$ TeV. *Phys. Lett. B*, 746:79, 2015.
- [2286] CMS Collaboration. Search for resonances and quantum black holes using dijet mass spectra in proton–proton collisions at $\sqrt{s} = 8$ TeV. *Phys. Rev. D*, 91:052009, 2015.
- [2287] CMS Collaboration. Search for resonant pair production of Higgs bosons decaying to two bottom quark–antiquark pairs in proton–proton collisions at 8 TeV. *Phys. Lett. B*, 749:560, 2015.
- [2288] CMS Collaboration. Search for stealth supersymmetry in events with jets, either photons or leptons, and low missing transverse momentum in pp collisions at 8 TeV. *Phys. Lett. B*, 743:503, 2015.
- [2289] CMS Collaboration. Search for supersymmetry in the vector-boson fusion topology in proton–proton collisions at $\sqrt{s} = 8$ TeV. *JHEP*, 11:189, 2015.
- [2290] CMS Collaboration. Search for supersymmetry using razor variables in events with b -tagged jets in pp collisions at $\sqrt{s} = 8$ TeV. *Phys. Rev. D*, 91:052018, 2015.
- [2291] CMS Collaboration. Search for supersymmetry with photons in pp collisions at $\sqrt{s} = 8$ TeV. *Phys. Rev. D*, 92:072006, 2015.
- [2292] CMS Collaboration. Search for the production of dark matter in association with top-quark pairs in the single-lepton final state in proton–proton collisions at $\sqrt{s} = 8$ TeV. *JHEP*, 06:121, 2015.
- [2293] CMS Collaboration. Search for the standard model Higgs boson produced through vector boson fusion and decaying to $b\bar{b}$. *Phys. Rev. D*, 92:032008, 2015.
- [2294] CMS Collaboration. Search for third-generation scalar leptoquarks in the $t\tau$ channel in proton–proton collisions at $\sqrt{s} = 8$ TeV. *JHEP*, 07:042, 2015.
- [2295] CMS Collaboration. Search for vector-like T quarks decaying to top quarks and Higgs bosons in the all-hadronic channel using jet substructure. *JHEP*, 06:080, 2015.
- [2296] CMS Collaboration. Searches for supersymmetry based on events with b jets and four W bosons in pp collisions at 8 TeV. *Phys. Lett. B*, 745:5, 2015.
- [2297] CMS Collaboration. Searches for supersymmetry using the M_{T2} variable in hadronic events produced in pp collisions at 8 TeV. *JHEP*, 05:078, 2015.

- [2298] CMS Collaboration. Searches for third-generation squark production in fully hadronic final states in proton–proton collisions at $\sqrt{s} = 8$ TeV. *JHEP*, 06:116, 2015.
- [2299] CMS Collaboration. Study of final-state radiation in decays of Z bosons produced in pp collisions at 7 TeV. *Phys. Rev. D*, 91:092012, 2015.
- [2300] CMS Collaboration. Study of vector boson scattering and search for new physics in events with two same-sign leptons and two jets. *Phys. Rev. Lett.*, 114:051801, 2015.
- [2301] CMS Collaboration. Study of W boson production in pPb collisions at $\sqrt{s_{\text{NN}}} = 5.02$ TeV. *Phys. Lett. B*, 750:565, 2015.
- [2302] CMS Collaboration. Study of Z production in PbPb and pp collisions at $\sqrt{s_{\text{NN}}} = 2.76$ TeV in the dimuon and dielectron decay channels. *JHEP*, 03:022, 2015.
- [2303] CMS Collaboration. A search for pair production of new light bosons decaying into muons. *Phys. Lett. B*, 752:146, 2016.
- [2304] CMS Collaboration. Angular analysis of the decay $B^0 \rightarrow K^{*0}\mu^+\mu^-$ from pp collisions at $\sqrt{s} = 8$ TeV. *Phys. Lett. B*, 753:424, 2016.
- [2305] CMS Collaboration. Azimuthal decorrelation of jets widely separated in rapidity in pp collisions at $\sqrt{s} = 7$ TeV. *JHEP*, 08:139, 2016.
- [2306] CMS Collaboration. Combined search for anomalous pseudoscalar HVV couplings in VH($H \rightarrow b\bar{b}$) production and $H \rightarrow VV$ decay. *Phys. Lett. B*, 759:672, 2016.
- [2307] CMS Collaboration. Correlations between jets and charged particles in PbPb and pp collisions at $\sqrt{s_{\text{NN}}} = 2.76$ TeV. *JHEP*, 02:156, 2016.
- [2308] CMS Collaboration. Decomposing transverse momentum balance contributions for quenched jets in PbPb collisions at $\sqrt{s_{\text{NN}}} = 2.76$ TeV. *JHEP*, 11:055, 2016.
- [2309] CMS Collaboration. Event generator tunes obtained from underlying event and multiparton scattering measurements. *Eur. Phys. J. C*, 76:155, 2016.
- [2310] CMS Collaboration. Evidence for exclusive $\gamma\gamma \rightarrow W^+W^-$ production and constraints on anomalous quartic gauge couplings in pp collisions at $\sqrt{s} = 7$ and 8 TeV. *JHEP*, 08:119, 2016.
- [2311] CMS Collaboration. Forward-backward asymmetry of Drell-Yan lepton pairs in pp collisions at $\sqrt{s} = 8$ TeV. *Eur. Phys. J. C*, 76:325, 2016.

- [2312] CMS Collaboration. Inclusive and differential measurements of the $t\bar{t}$ charge asymmetry in pp collisions at $\sqrt{s} = 8$ TeV. *Phys. Lett. B*, 757:154, 2016.
- [2313] CMS Collaboration. Measurement of differential and integrated fiducial cross sections for Higgs boson production in the four-lepton decay channel in pp collisions at $\sqrt{s} = 7$ and 8 TeV. *JHEP*, 04:005, 2016.
- [2314] CMS Collaboration. Measurement of differential cross sections for Higgs boson production in the diphoton decay channel in pp collisions at $\sqrt{s} = 8$ TeV. *Eur. Phys. J. C*, 76:13, 2016.
- [2315] CMS Collaboration. Measurement of dijet azimuthal decorrelation in pp collisions at $\sqrt{s} = 8$ TeV. *Eur. Phys. J. C*, 76:536, 2016.
- [2316] CMS Collaboration. Measurement of electroweak production of a W boson and two forward jets in proton–proton collisions at $\sqrt{s} = 8$ TeV. *JHEP*, 11:147, 2016.
- [2317] CMS Collaboration. Measurement of inclusive jet production and nuclear modifications in pPb collisions at $\sqrt{s_{\text{NN}}} = 5.02$ TeV. *Eur. Phys. J. C*, 76:372, 2016.
- [2318] CMS Collaboration. Measurement of long-range near-side two-particle angular correlations in pp collisions at $\sqrt{s} = 13$ TeV. *Phys. Rev. Lett.*, 116:172302, 2016.
- [2319] CMS Collaboration. Measurement of spin correlations in $t\bar{t}$ production using the matrix element method in the muon+jets final state in pp collisions at $\sqrt{s} = 8$ TeV. *Phys. Lett. B*, 758:321, 2016.
- [2320] CMS Collaboration. Measurement of $t\bar{t}$ production with additional jet activity, including b quark jets, in the dilepton decay channel using pp collisions at $\sqrt{s} = 8$ TeV. *Eur. Phys. J. C*, 76:379, 2016.
- [2321] CMS Collaboration. Measurement of the charge asymmetry in top quark pair production in pp collisions at $\sqrt{s} = 8$ TeV using a template method. *Phys. Rev. D*, 93:034014, 2016.
- [2322] CMS Collaboration. Measurement of the CP-violating weak phase ϕ_s and the decay width difference $\Delta\Gamma_s$ using the $B_s^0 \rightarrow J/\psi\phi(1020)$ decay channel in pp collisions at $\sqrt{s} = 8$ TeV. *Phys. Lett. B*, 757:97, 2016.
- [2323] CMS Collaboration. Measurement of the differential cross section and charge asymmetry for inclusive $\text{pp} \rightarrow W^\pm + X$ production at $\sqrt{s} = 8$ TeV. *Eur. Phys. J. C*, 76:469, 2016.

- [2324] CMS Collaboration. Measurement of the differential cross sections for top quark pair production as a function of kinematic event variables in pp collisions at $\sqrt{s} = 7$ and 8 TeV. *Phys. Rev. D*, 94:052006, 2016.
- [2325] CMS Collaboration. Measurement of the double-differential inclusive jet cross section in proton–proton collisions at $\sqrt{s} = 13$ TeV. *Eur. Phys. J. C*, 76:451, 2016.
- [2326] CMS Collaboration. Measurement of the inclusive jet cross section in pp collisions at $\sqrt{s} = 2.76$ TeV. *Eur. Phys. J. C*, 76:265, 2016.
- [2327] CMS Collaboration. Measurement of the inelastic cross section in proton–lead collisions at $\sqrt{s_{\text{NN}}} = 5.02$ TeV. *Phys. Lett. B*, 759:641, 2016.
- [2328] CMS Collaboration. Measurement of the integrated and differential $t\bar{t}$ production cross sections for high- p_{T} top quarks in pp collisions at $\sqrt{s} = 8$ TeV. *Phys. Rev. D*, 94:072002, 2016.
- [2329] CMS Collaboration. Measurement of the mass of the top quark in decays with a J/ψ meson in pp collisions at 8 TeV. *JHEP*, 12:123, 2016.
- [2330] CMS Collaboration. Measurement of the ratio $\mathcal{B}(B_s^0 \rightarrow J/\psi f_0(980))/\mathcal{B}(B_s^0 \rightarrow J/\psi \phi(1020))$ in pp collisions at $\sqrt{s} = 7$ TeV. *Phys. Lett. B*, 756:84, 2016.
- [2331] CMS Collaboration. Measurement of the $t\bar{t}$ production cross section in the all-jets final state in pp collisions at $\sqrt{s} = 8$ TeV. *Eur. Phys. J. C*, 76:128, 2016.
- [2332] CMS Collaboration. Measurement of the $t\bar{t}$ production cross section in the $e\mu$ channel in proton–proton collisions at $\sqrt{s} = 7$ and 8 TeV. *JHEP*, 08:029, 2016.
- [2333] CMS Collaboration. Measurement of the top quark mass using charged particles in pp collisions at $\sqrt{s} = 8$ TeV. *Phys. Rev. D*, 93:092006, 2016.
- [2334] CMS Collaboration. Measurement of the top quark mass using proton–proton data at $\sqrt{s} = 7$ and 8 TeV. *Phys. Rev. D*, 93:072004, 2016.
- [2335] CMS Collaboration. Measurement of the top quark pair production cross section in proton–proton collisions at $\sqrt{s} = 13$ TeV. *Phys. Rev. Lett.*, 116:052002, 2016.
- [2336] CMS Collaboration. Measurement of the W boson helicity fractions in the decays of top quark pairs to lepton+jets final states produced in pp collisions at $\sqrt{s} = 8$ TeV. *Phys. Lett. B*, 762:512, 2016.

- [2337] CMS Collaboration. Measurement of the W^+W^- cross section in pp collisions at $\sqrt{s} = 8$ TeV and limits on anomalous gauge couplings. *Eur. Phys. J. C*, 76:401, 2016.
- [2338] CMS Collaboration. Measurement of the $Z\gamma \rightarrow \nu\bar{\nu}\gamma$ production cross section in pp collisions at $\sqrt{s} = 8$ TeV and limits on anomalous $ZZ\gamma$ and $Z\gamma\gamma$ trilinear gauge boson couplings. *Phys. Lett. B*, 760:448, 2016.
- [2339] CMS Collaboration. Measurement of the ZZ production cross section and $Z \rightarrow \ell^+\ell^-\ell'^+\ell'^-$ branching fraction in pp collisions at $\sqrt{s} = 13$ TeV. *Phys. Lett. B*, 763:280, 2016.
- [2340] CMS Collaboration. Measurement of top quark polarisation in t-channel single top quark production. *JHEP*, 04:073, 2016.
- [2341] CMS Collaboration. Measurement of transverse momentum relative to dijet systems in PbPb and pp collisions at $\sqrt{s_{\text{NN}}} = 2.76$ TeV. *JHEP*, 01:006, 2016.
- [2342] CMS Collaboration. Measurements of $t\bar{t}$ charge asymmetry using dilepton final states in pp collisions at $\sqrt{s} = 8$ TeV. *Phys. Lett. B*, 760:365, 2016.
- [2343] CMS Collaboration. Measurements of $t\bar{t}$ spin correlations and top quark polarization using dilepton final states in pp collisions at $\sqrt{s} = 8$ TeV. *Phys. Rev. D*, 93:052007, 2016.
- [2344] CMS Collaboration. Observation of top quark pairs produced in association with a vector boson in pp collisions at $\sqrt{s} = 8$ TeV. *JHEP*, 01:096, 2016.
- [2345] CMS Collaboration. Phenomenological MSSM interpretation of CMS searches in pp collisions at $\sqrt{s} = 7$ and 8 TeV. *JHEP*, 10:129, 2016.
- [2346] CMS Collaboration. Reconstruction and identification of τ lepton decays to hadrons and ν_τ at CMS. *JINST*, 11:P01019, 2016.
- [2347] CMS Collaboration. Search for a Higgs boson decaying into $\gamma^*\gamma \rightarrow \ell\ell\gamma$ with low dilepton mass in pp collisions at $\sqrt{s} = 8$ TeV. *Phys. Lett. B*, 753:341, 2016.
- [2348] CMS Collaboration. Search for a low-mass pseudoscalar Higgs boson produced in association with a $b\bar{b}$ pair in pp collisions at $\sqrt{s} = 8$ TeV. *Phys. Lett. B*, 758:296, 2016.
- [2349] CMS Collaboration. Search for a massive resonance decaying into a Higgs boson and a W or Z boson in hadronic final states in proton–proton collisions at $\sqrt{s} = 8$ TeV. *JHEP*, 02:145, 2016.

- [2350] CMS Collaboration. Search for a very light NMSSM Higgs boson produced in decays of the 125 GeV scalar boson and decaying into τ leptons in pp collisions at $\sqrt{s} = 8$ TeV. *JHEP*, 01:079, 2016.
- [2351] CMS Collaboration. Search for anomalous single top quark production in association with a photon in pp collisions at $\sqrt{s} = 8$ TeV. *JHEP*, 04:035, 2016.
- [2352] CMS Collaboration. Search for dark matter and unparticles produced in association with a Z boson in proton–proton collisions at $\sqrt{s} = 8$ TeV. *Phys. Rev. D*, 93:052011, 2016.
- [2353] CMS Collaboration. Search for dark matter in proton–proton collisions at 8 TeV with missing transverse momentum and vector boson tagged jets. *JHEP*, 12:083, 2016.
- [2354] CMS Collaboration. Search for dark matter particles in proton–proton collisions at $\sqrt{s} = 8$ TeV using the razor variables. *JHEP*, 12:088, 2016.
- [2355] CMS Collaboration. Search for direct pair production of scalar top quarks in the single- and dilepton channels in proton–proton collisions at $\sqrt{s} = 8$ TeV. *JHEP*, 07:027, 2016.
- [2356] CMS Collaboration. Search for direct pair production of supersymmetric top quarks decaying to all-hadronic final states in pp collisions at $\sqrt{s} = 8$ TeV. *Eur. Phys. J. C*, 76:460, 2016.
- [2357] CMS Collaboration. Search for excited leptons in proton–proton collisions at $\sqrt{s} = 8$ TeV. *JHEP*, 03:125, 2016.
- [2358] CMS Collaboration. Search for exotic decays of a Higgs boson into undetectable particles and one or more photons. *Phys. Lett. B*, 753:363, 2016.
- [2359] CMS Collaboration. Search for heavy Majorana neutrinos in $e^\pm e^\pm + \text{jets}$ and $e^\pm \mu^\pm + \text{jets}$ events in proton–proton collisions at $\sqrt{s} = 8$ TeV. *JHEP*, 04:169, 2016.
- [2360] CMS Collaboration. Search for heavy resonances decaying to two Higgs bosons in final states containing four b quarks. *Eur. Phys. J. C*, 76:371, 2016.
- [2361] CMS Collaboration. Search for Higgs boson off-shell production in proton–proton collisions at 7 and 8 TeV and derivation of constraints on its total decay width. *JHEP*, 09:051, 2016.

- [2362] CMS Collaboration. Search for lepton flavour violating decays of heavy resonances and quantum black holes to an $e\mu$ pair in proton–proton collisions at $\sqrt{s} = 8$ TeV. *Eur. Phys. J. C*, 76:317, 2016.
- [2363] CMS Collaboration. Search for lepton flavour violating decays of the Higgs boson to $e\tau$ and $e\mu$ in proton–proton collisions at $\sqrt{s} = 8$ TeV. *Phys. Lett. B*, 763:472, 2016.
- [2364] CMS Collaboration. Search for long-lived charged particles in proton–proton collisions at $\sqrt{s} = 13$ TeV. *Phys. Rev. D*, 94:112004, 2016.
- [2365] CMS Collaboration. Search for massive $W\text{H}$ resonances decaying into the $\ell\nu b\bar{b}$ final state at $\sqrt{s} = 8$ TeV. *Eur. Phys. J. C*, 76:237, 2016.
- [2366] CMS Collaboration. Search for narrow resonances decaying to dijets in proton–proton collisions at $\sqrt{s} = 13$ TeV. *Phys. Rev. Lett.*, 116:071801, 2016.
- [2367] CMS Collaboration. Search for Narrow Resonances in Dijet Final States at $\sqrt{s} = 8$ TeV with the Novel CMS Technique of Data Scouting. *Phys. Rev. Lett.*, 117:031802, 2016.
- [2368] CMS Collaboration. Search for neutral MSSM Higgs bosons decaying to $\mu^+\mu^-$ in $p\bar{p}$ collisions at $\sqrt{s} = 7$ and 8 TeV. *Phys. Lett. B*, 752:221, 2016.
- [2369] CMS Collaboration. Search for neutral resonances decaying into a Z boson and a pair of b jets or τ leptons. *Phys. Lett. B*, 759:369, 2016.
- [2370] CMS Collaboration. Search for new phenomena in monophoton final states in proton–proton collisions at $\sqrt{s} = 8$ TeV. *Phys. Lett. B*, 755:102, 2016.
- [2371] CMS Collaboration. Search for new physics in final states with two opposite-sign, same-flavor leptons, jets, and missing transverse momentum in $p\bar{p}$ collisions at $\sqrt{s} = 13$ TeV. *JHEP*, 12:013, 2016.
- [2372] CMS Collaboration. Search for new physics in same-sign dilepton events in proton–proton collisions at $\sqrt{s} = 13$ TeV. *Eur. Phys. J. C*, 76:439, 2016.
- [2373] CMS Collaboration. Search for new physics with the M_{T2} variable in all-jets final states produced in $p\bar{p}$ collisions at $\sqrt{s} = 13$ TeV. *JHEP*, 10:006, 2016.
- [2374] CMS Collaboration. Search for pair-produced vectorlike B quarks in proton–proton collisions at $\sqrt{s} = 8$ TeV. *Phys. Rev. D*, 93:112009, 2016.

- [2375] CMS Collaboration. Search for pair production of first and second generation leptoquarks in proton–proton collisions at $\sqrt{s} = 8$ TeV. *Phys. Rev. D*, 93:032004, 2016.
- [2376] CMS Collaboration. Search for R-parity violating decays of a top squark in proton–proton collisions at $\sqrt{s} = 8$ TeV. *Phys. Lett. B*, 760:178, 2016.
- [2377] CMS Collaboration. Search for Resonant Production of High-Mass Photon Pairs in Proton–Proton Collisions at $\sqrt{s} = 8$ and 13 TeV. *Phys. Rev. Lett.*, 117:051802, 2016.
- [2378] CMS Collaboration. Search for resonant $t\bar{t}$ production in proton–proton collisions at $\sqrt{s} = 8$ TeV. *Phys. Rev. D*, 93:012001, 2016.
- [2379] CMS Collaboration. Search for s channel single top quark production in $p\bar{p}$ collisions at $\sqrt{s} = 7$ and 8 TeV. *JHEP*, 09:027, 2016.
- [2380] CMS Collaboration. Search for single production of scalar leptoquarks in proton–proton collisions at $\sqrt{s} = 8$ TeV. *Phys. Rev. D*, 93:032005, 2016.
- [2381] CMS Collaboration. Search for supersymmetry in electroweak production with photons and large missing transverse energy in $p\bar{p}$ collisions at $\sqrt{s} = 8$ TeV. *Phys. Lett. B*, 759:479, 2016.
- [2382] CMS Collaboration. Search for supersymmetry in events with a photon, a lepton, and missing transverse momentum in $p\bar{p}$ collisions at $\sqrt{s} = 8$ TeV. *Phys. Lett. B*, 757:6, 2016.
- [2383] CMS Collaboration. Search for supersymmetry in events with soft leptons, low jet multiplicity, and missing transverse energy in proton–proton collisions at $\sqrt{s} = 8$ TeV. *Phys. Lett. B*, 759:9, 2016.
- [2384] CMS Collaboration. Search for supersymmetry in $p\bar{p}$ collisions at $\sqrt{s} = 13$ TeV in the single-lepton final state using the sum of masses of large-radius jets. *JHEP*, 08:122, 2016.
- [2385] CMS Collaboration. Search for supersymmetry in $p\bar{p}$ collisions at $\sqrt{s} = 8$ TeV in final states with boosted W bosons and b jets using razor variables. *Phys. Rev. D*, 93:092009, 2016.
- [2386] CMS Collaboration. Search for supersymmetry in the multijet and missing transverse momentum final state in $p\bar{p}$ collisions at 13 TeV. *Phys. Lett. B*, 758:152, 2016.

- [2387] CMS Collaboration. Search for the associated production of a Higgs boson with a single top quark in proton–proton collisions at $\sqrt{s} = 8$ TeV. *JHEP*, 06:177, 2016.
- [2388] CMS Collaboration. Search for the production of an excited bottom quark decaying to tW in proton–proton collisions at $\sqrt{s} = 8$ TeV. *JHEP*, 01:166, 2016.
- [2389] CMS Collaboration. Search for two Higgs bosons in final states containing two photons and two bottom quarks in proton–proton collisions at 8 TeV. *Phys. Rev. D*, 94:052012, 2016.
- [2390] CMS Collaboration. Search for vectorlike charge 2/3 T quarks in proton–proton collisions at $\sqrt{(s)} = 8$ TeV. *Phys. Rev. D*, 93:012003, 2016.
- [2391] CMS Collaboration. Search for W' decaying to tau lepton and neutrino in proton–proton collisions at $\sqrt{s} = 8$ TeV. *Phys. Lett. B*, 755:196, 2016.
- [2392] CMS Collaboration. Search for $W' \rightarrow tb$ in proton–proton collisions at $\sqrt{s} = 8$ TeV. *JHEP*, 02:122, 2016.
- [2393] CMS Collaboration. Searches for a heavy scalar boson H decaying to a pair of 125 GeV Higgs bosons hh or for a heavy pseudoscalar boson A decaying to Zh , in the final states with $h \rightarrow \tau\tau$. *Phys. Lett. B*, 755:217, 2016.
- [2394] CMS Collaboration. Searches for R-parity-violating supersymmetry in pp collisions at $\sqrt{s} = 8$ TeV in final states with 0–4 leptons. *Phys. Rev. D*, 94:112009, 2016.
- [2395] CMS Collaboration. Studies of inclusive four-jet production with two b-tagged jets in proton–proton collisions at 7 TeV. *Phys. Rev. D*, 94:112005, 2016.
- [2396] CMS Collaboration. Study of B meson production in pPb collisions at $\sqrt{s_{NN}} = 5.02$ TeV using exclusive hadronic decays. *Phys. Rev. Lett.*, 116:032301, 2016.
- [2397] CMS Collaboration. Study of Z boson production in pPb collisions at $\sqrt{s_{NN}} = 5.02$ TeV. *Phys. Lett. B*, 759:36, 2016.
- [2398] CMS Collaboration. Transverse momentum spectra of inclusive b jets in pPb collisions at $\sqrt{s_{NN}} = 5.02$ TeV. *Phys. Lett. B*, 754:59, 2016.
- [2399] CMS Collaboration. $\Upsilon(nS)$ polarizations versus particle multiplicity in pp collisions at $\sqrt{s} = 7$ TeV. *Phys. Lett. B*, 761:31, 2016.

- [2400] CMS Collaboration. A search for Higgs boson pair production in the $b\bar{b}\tau\tau$ final state in proton–proton collisions at $\sqrt{s} = 8$ TeV. *Phys. Rev. D*, 96:072004, 2017.
- [2401] CMS Collaboration. A search for new phenomena in $p\bar{p}$ collisions at $\sqrt{s} = 13$ TeV in final states with missing transverse momentum and at least one jet using the α_T variable. *Eur. Phys. J. C*, 77:294, 2017.
- [2402] CMS Collaboration. Azimuthal correlations for inclusive 2-jet, 3-jet, and 4-jet events in $p\bar{p}$ collisions at $\sqrt{s} = 13$ TeV. 2017.
- [2403] CMS Collaboration. Challenges to the chiral magnetic wave using charge-dependent azimuthal anisotropies in $p\text{Pb}$ and PbPb collisions at $\sqrt{s_{\text{NN}}} = 5.02$ TeV. 2017.
- [2404] CMS Collaboration. Charged-particle nuclear modification factors in PbPb and pPb collisions at $\sqrt{s_{\text{NN}}} = 5.02$ TeV. *JHEP*, 04:039, 2017.
- [2405] CMS Collaboration. Coherent J/ψ photoproduction in ultra-peripheral PbPb collisions at $\sqrt{s_{\text{NN}}} = 2.76$ TeV with the CMS experiment. *Phys. Lett. B*, 772:489, 2017.
- [2406] CMS Collaboration. Combination of searches for heavy resonances decaying to WW , WZ , ZZ , WH , and ZH boson pairs in proton–proton collisions at $\sqrt{s} = 8$ TeV and 13 TeV. *Phys. Lett. B*, 774:533, 2017.
- [2407] CMS Collaboration. Constraints on anomalous Higgs boson couplings using production and decay information in the four-lepton final state. *Phys. Lett. B*, 775:1, 2017.
- [2408] CMS Collaboration. Constraints on the chiral magnetic effect using charge-dependent azimuthal correlations in pPb and PbPb collisions at the LHC. 2017.
- [2409] CMS Collaboration. Constraints on the double-parton scattering cross section from same-sign W boson pair production in proton–proton collisions at $\sqrt{s} = 8$ TeV. 2017.
- [2410] CMS Collaboration. Cross section measurement of t-channel single top quark production in $p\bar{p}$ collisions at $\sqrt{s} = 13$ TeV. *Phys. Lett. B*, 772:752, 2017.
- [2411] CMS Collaboration. Electroweak production of two jets in association with a Z boson in proton–proton collisions at $\sqrt{s} = 13$ TeV. 2017.
- [2412] CMS Collaboration. Evidence for collectivity in $p\bar{p}$ collisions at the LHC. *Phys. Lett. B*, 765:193, 2017.

- [2413] CMS Collaboration. Evidence for the Higgs boson decay to a bottom quark-antiquark pair. 2017.
- [2414] CMS Collaboration. Exclusive and semi-exclusive $\pi^+\pi^-$ production in proton–proton collisions at $\sqrt{s} = 7$ TeV. 2017.
- [2415] CMS Collaboration. Identification of heavy-flavour jets with the CMS detector in pp collisions at 13 TeV. 2017.
- [2416] CMS Collaboration. Inclusive search for a highly boosted Higgs boson decaying to a bottom quark-antiquark pair. 2017.
- [2417] CMS Collaboration. Inclusive search for supersymmetry using razor variables in pp collisions at $\sqrt{s} = 13$ TeV. *Phys. Rev. D*, 95:012003, 2017.
- [2418] CMS Collaboration. Jet energy scale and resolution in the CMS experiment in pp collisions at 8 TeV. *JINST*, 12:P02014, 2017.
- [2419] CMS Collaboration. Measurement and QCD analysis of double-differential inclusive jet cross sections in pp collisions at $\sqrt{s} = 8$ TeV and cross section ratios to 2.76 and 7 TeV. *JHEP*, 03:156, 2017.
- [2420] CMS Collaboration. Measurement of angular parameters from the decay $B^0 \rightarrow K^{*0}\mu^+\mu^-$ in proton–proton collisions at $\sqrt{s} = 8$ TeV. 2017.
- [2421] CMS Collaboration. Measurement of associated Z + charm production in proton–proton collisions at $\sqrt{s} = 8$ TeV. 2017.
- [2422] CMS Collaboration. Measurement of b hadron lifetimes in pp collisions at $\sqrt{s} = 8$ TeV. 2017.
- [2423] CMS Collaboration. Measurement of B^\pm Meson Nuclear Modification Factor in PbPb collisions at $\sqrt{s_{\text{NN}}} = 5.02$ TeV. *Phys. Rev. Lett.*, 119:152301, 2017.
- [2424] CMS Collaboration. Measurement of charged pion, kaon, and proton production in proton–proton collisions at $\sqrt{s} = 13$ TeV. *Phys. Rev. D*, 96:112003, 2017.
- [2425] CMS Collaboration. Measurement of differential cross sections for top quark pair production using the lepton+jets final state in proton–proton collisions at 13 TeV. *Phys. Rev. D*, 95:092001, 2017.
- [2426] CMS Collaboration. Measurement of differential cross sections in the ϕ^* variable for inclusive Z boson production in pp collisions at $\sqrt{s} = 8$ TeV. 2017.

- [2427] CMS Collaboration. Measurement of double-differential cross sections for top quark pair production in pp collisions at $\sqrt{s} = 8$ TeV and impact on parton distribution functions. *Eur. Phys. J. C*, 77:459, 2017.
- [2428] CMS Collaboration. Measurement of electroweak-induced production of $W\gamma$ with two jets in pp collisions at $\sqrt{s} = 8$ TeV and constraints on anomalous quartic gauge couplings. *JHEP*, 06:106, 2017.
- [2429] CMS Collaboration. Measurement of inclusive jet cross-sections in pp and PbPb collisions at $\sqrt{s_{\text{NN}}} = 2.76$ TeV. *Phys. Rev. C*, 96:015202, 2017.
- [2430] CMS Collaboration. Measurement of normalized differential $t\bar{t}$ cross sections in the dilepton channel from pp collisions at $\sqrt{s} = 13$ TeV. 2017.
- [2431] CMS Collaboration. Measurement of prompt and nonprompt charmonium suppression in PbPb collisions at 5.02 TeV. 2017.
- [2432] CMS Collaboration. Measurement of prompt and nonprompt J/ψ production in pp and pPb collisions at $\sqrt{s_{\text{NN}}} = 5.02$ TeV. *Eur. Phys. J. C*, 77:269, 2017.
- [2433] CMS Collaboration. Measurement of prompt D^0 meson azimuthal anisotropy in PbPb collisions at $\sqrt{s_{\text{NN}}} = 5.02$ TeV. 2017.
- [2434] CMS Collaboration. Measurement of quarkonium production cross sections in pp collisions at $\sqrt{s} = 13$ TeV. 2017.
- [2435] CMS Collaboration. Measurement of the associated production of a single top quark and a Z boson in pp collisions at $\sqrt{s} = 13$ TeV. 2017.
- [2436] CMS Collaboration. Measurement of the cross section for electroweak production of $Z\gamma$ in association with two jets and constraints on anomalous quartic gauge couplings in proton–proton collisions at $\sqrt{s} = 8$ TeV. *Phys. Lett. B*, 770:380, 2017.
- [2437] CMS Collaboration. Measurement of the cross section for top quark pair production in association with a W or Z boson in proton–proton collisions at $\sqrt{s} = 13$ TeV. 2017.
- [2438] CMS Collaboration. Measurement of the differential cross sections for the associated production of a W boson and jets in proton–proton collisions at $\sqrt{s} = 13$ TeV. *Phys. Rev. D*, 96:072005, 2017.
- [2439] CMS Collaboration. Measurement of the inclusive energy spectrum in the very forward direction in proton–proton collisions at $\sqrt{s} = 13$ TeV. *JHEP*, 08:046, 2017.

- [2440] CMS Collaboration. Measurement of the jet mass in highly boosted $t\bar{t}$ events from $p\bar{p}$ collisions at $\sqrt{s} = 8$ TeV. *Eur. Phys. J. C*, 77:467, 2017.
- [2441] CMS Collaboration. Measurement of the mass difference between top quark and antiquark in $p\bar{p}$ collisions at $\sqrt{s} = 8$ TeV. *Phys. Lett. B*, 770:50, 2017.
- [2442] CMS Collaboration. Measurement of the production cross section of a W boson in association with two b jets in $p\bar{p}$ collisions at $\sqrt{s} = 8$ TeV. *Eur. Phys. J. C*, 77:92, 2017.
- [2443] CMS Collaboration. Measurement of the semileptonic $t\bar{t} + \gamma$ production cross section in $p\bar{p}$ collisions at $\sqrt{s} = 8$ TeV. *JHEP*, 10:006, 2017.
- [2444] CMS Collaboration. Measurement of the splitting function in $p\bar{p}$ and $PbPb$ collisions at $\sqrt{s_{NN}} = 5.02$ TeV. 2017.
- [2445] CMS Collaboration. Measurement of the $t\bar{t}$ production cross section using events in the $e\mu$ final state in $p\bar{p}$ collisions at $\sqrt{s} = 13$ TeV. *Eur. Phys. J. C*, 77:172, 2017.
- [2446] CMS Collaboration. Measurement of the $t\bar{t}$ production cross section using events with one lepton and at least one jet in $p\bar{p}$ collisions at $\sqrt{s} = 13$ TeV. *JHEP*, 09:051, 2017.
- [2447] CMS Collaboration. Measurement of the top quark mass in the dileptonic $t\bar{t}$ decay channel using the mass observables $M_{b\ell}$, M_{T2} , and $M_{b\ell\nu}$ in $p\bar{p}$ collisions at $\sqrt{s} = 8$ TeV. *Phys. Rev. D*, 96:032002, 2017.
- [2448] CMS Collaboration. Measurement of the top quark mass using single top quark events in proton–proton collisions at $\sqrt{s} = 8$ TeV. *Eur. Phys. J. C*, 77:354, 2017.
- [2449] CMS Collaboration. Measurement of the total and differential inclusive B^+ hadron cross sections in $p\bar{p}$ collisions at $\sqrt{s} = 13$ TeV. *Phys. Lett. B*, 771:435, 2017.
- [2450] CMS Collaboration. Measurement of the transverse momentum spectra of weak vector bosons produced in proton–proton collisions at $\sqrt{s} = 8$ TeV. *JHEP*, 02:096, 2017.
- [2451] CMS Collaboration. Measurement of the transverse momentum spectrum of the Higgs boson produced in $p\bar{p}$ collisions at $\sqrt{s} = 8$ TeV using $H \rightarrow WW$ decays. *JHEP*, 03:032, 2017.

- [2452] CMS Collaboration. Measurement of the triple-differential dijet cross section in proton–proton collisions at $\sqrt{s} = 8$ TeV and constraints on parton distribution functions. *Eur. Phys. J. C*, 77:746, 2017.
- [2453] CMS Collaboration. Measurement of the underlying event activity in inclusive Z boson production in proton–proton collisions at $\sqrt{s} = 13$ TeV. 2017.
- [2454] CMS Collaboration. Measurement of the WZ production cross section in pp collisions at $\sqrt{s} = 13$ TeV. *Phys. Lett. B*, 766:268, 2017.
- [2455] CMS Collaboration. Measurement of the WZ production cross section in pp collisions at $\sqrt{s} = 7$ and 8 TeV and search for anomalous triple gauge couplings at $\sqrt{s} = 8$ TeV. *Eur. Phys. J. C*, 77:236, 2017.
- [2456] CMS Collaboration. Measurement of vector boson scattering and constraints on anomalous quartic couplings from events with four leptons and two jets in proton–proton collisions at $\sqrt{s} = 13$ TeV. *Phys. Lett. B*, 774:682, 2017.
- [2457] CMS Collaboration. Measurements of differential cross sections for associated production of a W boson and jets in proton–proton collisions at $\sqrt{s} = 8$ TeV. *Phys. Rev. D*, 95:052002, 2017.
- [2458] CMS Collaboration. Measurements of jet charge with dijet events in pp collisions at $\sqrt{s} = 8$ TeV. *JHEP*, 10:131, 2017.
- [2459] CMS Collaboration. Measurements of properties of the Higgs boson decaying into the four-lepton final state in pp collisions at $\sqrt{s} = 13$ TeV. *JHEP*, 11:047, 2017.
- [2460] CMS Collaboration. Measurements of the associated production of a Z boson and b jets in pp collisions at $\sqrt{s} = 8$ TeV. *Eur. Phys. J. C*, 77:751, 2017.
- [2461] CMS Collaboration. Measurements of the charm jet cross section and nuclear modification factor in pPb collisions at $\sqrt{s_{\text{NN}}} = 5.02$ TeV. *Phys. Lett. B*, 772:306, 2017.
- [2462] CMS Collaboration. Measurements of the differential production cross sections for a Z boson in association with jets in pp collisions at $\sqrt{s} = 8$ TeV. *JHEP*, 04:022, 2017.
- [2463] CMS Collaboration. Measurements of the $\text{pp} \rightarrow W\gamma\gamma$ and $\text{pp} \rightarrow Z\gamma\gamma$ cross sections and limits on anomalous quartic gauge couplings at $\sqrt{s} = 8$ TeV. *JHEP*, 10:072, 2017.

- [2464] CMS Collaboration. Measurements of the $\text{pp} \rightarrow ZZ$ production cross section and the $Z \rightarrow 4\ell$ branching fraction, and constraints on anomalous triple gauge couplings at $\sqrt{s} = 13$ TeV. 2017.
- [2465] CMS Collaboration. Measurements of the $t\bar{t}$ production cross section in lepton+jets final states in pp collisions at 8 TeV and ratio of 8 to 7 TeV cross sections. *Eur. Phys. J. C*, 77:15, 2017.
- [2466] CMS Collaboration. Mechanical stability of the CMS strip tracker measured with a laser alignment system. *JINST*, 12:P04023, 2017.
- [2467] CMS Collaboration. Multiplicity and rapidity dependence of strange hadron production in pp , pPb , and PbPb collisions at the LHC. *Phys. Lett. B*, 768:103, 2017.
- [2468] CMS Collaboration. Non-Gaussian elliptic-flow fluctuations in PbPb collisions at $\sqrt{s_{\text{NN}}} = 5.02$ TeV. 2017.
- [2469] CMS Collaboration. Nuclear modification factor of D^0 mesons in PbPb collisions at $\sqrt{s_{\text{NN}}} = 5.02$ TeV. 2017.
- [2470] CMS Collaboration. Observation of Charge-Dependent Azimuthal Correlations in p-Pb Collisions and its Implication for the Search for the Chiral Magnetic Effect. *Phys. Rev. Lett.*, 118:122301, 2017.
- [2471] CMS Collaboration. Observation of correlated azimuthal anisotropy Fourier harmonics in pp and pPb collisions at the LHC. 2017.
- [2472] CMS Collaboration. Observation of electroweak production of same-sign W boson pairs in the two jet and two same-sign lepton final state in proton–proton collisions at 13 TeV. 2017.
- [2473] CMS Collaboration. Observation of the decay $B^+ \rightarrow \psi(2S)\phi(1020)K^+$ in pp collisions at $\sqrt{s} = 8$ TeV. *Phys. Lett. B*, 764:66, 2017.
- [2474] CMS Collaboration. Observation of the Higgs boson decay to a pair of τ leptons. 2017.
- [2475] CMS Collaboration. Observation of Top Quark Production in Proton–Nucleus Collisions. *Phys. Rev. Lett.*, 119:242001, 2017.
- [2476] CMS Collaboration. Observation of $\Upsilon(1S)$ pair production in proton–proton collisions at $\sqrt{s} = 8$ TeV. *JHEP*, 05:013, 2017.
- [2477] CMS Collaboration. Particle-flow reconstruction and global event description with the CMS detector. *JINST*, 12:P10003, 2017.

- [2478] CMS Collaboration. Principal-component analysis of two-particle azimuthal correlations in PbPb and pPb collisions at CMS. *Phys. Rev. C*, 96:064902, 2017.
- [2479] CMS Collaboration. Pseudorapidity and transverse momentum dependence of flow harmonics in pPb and PbPb collisions. 2017.
- [2480] CMS Collaboration. Pseudorapidity dependence of long-range two-particle correlations in pPb collisions at $\sqrt{s_{\text{NN}}} = 5.02$ TeV. *Phys. Rev. C*, 96:014915, 2017.
- [2481] CMS Collaboration. Pseudorapidity distributions of charged hadrons in proton–lead collisions at $\sqrt{s_{\text{NN}}} = 5.02$ and 8.16 TeV. 2017.
- [2482] CMS Collaboration. Relative Modification of Prompt $\psi(2S)$ and J/ψ Yields from pp to PbPb Collisions at $\sqrt{s_{\text{NN}}} = 5.02$ TeV. *Phys. Rev. Lett.*, 118:162301, 2017.
- [2483] CMS Collaboration. Search for a heavy composite Majorana neutrino in the final state with two leptons and two quarks at $\sqrt{s} = 13$ TeV. *Phys. Lett. B*, 775:315, 2017.
- [2484] CMS Collaboration. Search for a heavy resonance decaying to a top quark and a vector-like top quark at $\sqrt{s} = 13$ TeV. *JHEP*, 09:053, 2017.
- [2485] CMS Collaboration. Search for a light pseudoscalar Higgs boson produced in association with bottom quarks in pp collisions at $\sqrt{s} = 8$ TeV. *JHEP*, 11:010, 2017.
- [2486] CMS Collaboration. Search for a massive resonance decaying to a pair of Higgs bosons in the four b quark final state in proton–proton collisions at $\sqrt{s} = 13$ TeV. 2017.
- [2487] CMS Collaboration. Search for anomalous couplings in boosted $WW/WZ \rightarrow \ell\nu q\bar{q}$ production in proton–proton collisions at $\sqrt{s} = 8$ TeV. *Phys. Lett. B*, 772:21, 2017.
- [2488] CMS Collaboration. Search for anomalous Wtb couplings and flavour-changing neutral currents in t-channel single top quark production in pp collisions at $\sqrt{s} = 7$ and 8 TeV. *JHEP*, 02:028, 2017.
- [2489] CMS Collaboration. Search for associated production of a Z boson with a single top quark and for tZ flavour-changing interactions in pp collisions at $\sqrt{s} = 8$ TeV. *JHEP*, 07:003, 2017.
- [2490] CMS Collaboration. Search for associated production of dark matter with a Higgs boson decaying to $b\bar{b}$ or $\gamma\gamma$ at $\sqrt{s} = 13$ TeV. *JHEP*, 10:180, 2017.

- [2491] CMS Collaboration. Search for black holes and other new phenomena in high multiplicity final states in proton–proton collisions at $\sqrt{s} = 13$ TeV. *Phys. Lett. B*, 774:279, 2017.
- [2492] CMS Collaboration. Search for charged Higgs bosons produced via vector boson fusion and decaying into a pair of W and Z bosons using $p\bar{p}$ collisions at $\sqrt{s} = 13$ TeV. *Phys. Rev. Lett.*, 119:141802, 2017.
- [2493] CMS Collaboration. Search for CP violation in $t\bar{t}$ production and decay in proton–proton collisions at $\sqrt{s} = 8$ TeV. *JHEP*, 03:101, 2017.
- [2494] CMS Collaboration. Search for Dark Matter and Supersymmetry with a Compressed Mass Spectrum in the Vector Boson Fusion Topology in Proton–Proton Collisions at $\sqrt{s} = 8$ TeV. *Phys. Rev. Lett.*, 118:021802, 2017.
- [2495] CMS Collaboration. Search for dark matter and unparticles in events with a Z boson and missing transverse momentum in proton–proton collisions at $\sqrt{s} = 13$ TeV. *JHEP*, 03:061, 2017.
- [2496] CMS Collaboration. Search for dark matter produced in association with heavy-flavor quark pairs in proton–proton collisions at $\sqrt{s} = 13$ TeV. *Eur. Phys. J. C*, 77:845, 2017.
- [2497] CMS Collaboration. Search for dark matter produced with an energetic jet or a hadronically decaying W or Z boson at $\sqrt{s} = 13$ TeV. *JHEP*, 07:014, 2017.
- [2498] CMS Collaboration. Search for dijet resonances in proton–proton collisions at $\sqrt{s} = 13$ TeV and constraints on dark matter and other models. *Phys. Lett. B*, 769:520, 2017.
- [2499] CMS Collaboration. Search for direct production of supersymmetric partners of the top quark in the all-jets final state in proton–proton collisions at $\sqrt{s} = 13$ TeV. *JHEP*, 10:005, 2017.
- [2500] CMS Collaboration. Search for electroweak production of a vector-like quark decaying to a top quark and a Higgs boson using boosted topologies in fully hadronic final states. *JHEP*, 04:136, 2017.
- [2501] CMS Collaboration. Search for electroweak production of charginos and neutralinos in multilepton final states in proton–proton collisions at $\sqrt{s} = 13$ TeV. 2017.
- [2502] CMS Collaboration. Search for electroweak production of charginos and neutralinos in WH events in proton–proton collisions at $\sqrt{s} = 13$ TeV. *JHEP*, 11:029, 2017.

- [2503] CMS Collaboration. Search for electroweak production of charginos in final states with two τ leptons in pp collisions at $\sqrt{s} = 8$ TeV. *JHEP*, 04:018, 2017.
- [2504] CMS Collaboration. Search for Evidence of the Type-III Seesaw Mechanism in Multilepton Final States in Proton–Proton Collisions at $\sqrt{s} = 13$ TeV. *Phys. Rev. Lett.*, 119:221802, 2017.
- [2505] CMS Collaboration. Search for excited quarks of light and heavy flavor in $\gamma + \text{jet}$ final states in proton–proton collisions at $\sqrt{s} = 13$ TeV. 2017.
- [2506] CMS Collaboration. Search for gauge-mediated supersymmetry in events with at least one photon and missing transverse momentum in pp collisions at $\sqrt{s} = 13$ TeV. 2017.
- [2507] CMS Collaboration. Search for heavy gauge W' boson in events with an energetic lepton and large missing transverse momentum at $\sqrt{s} = 13$ TeV. *Phys. Lett. B*, 770:278, 2017.
- [2508] CMS Collaboration. Search for heavy neutrinos or third-generation leptoquarks in final states with two hadronically decaying τ leptons and two jets in proton–proton collisions at $\sqrt{s} = 13$ TeV. *JHEP*, 03:077, 2017.
- [2509] CMS Collaboration. Search for heavy resonances decaying into a vector boson and a Higgs boson in final states with charged leptons, neutrinos, and b quarks. *Phys. Lett. B*, 768:137, 2017.
- [2510] CMS Collaboration. Search for heavy resonances decaying to tau lepton pairs in proton–proton collisions at $\sqrt{s} = 13$ TeV. *JHEP*, 02:048, 2017.
- [2511] CMS Collaboration. Search for heavy resonances that decay into a vector boson and a Higgs boson in hadronic final states at $\sqrt{s} = 13$ TeV. *Eur. Phys. J. C*, 77:636, 2017.
- [2512] CMS Collaboration. Search for Higgs boson pair production in events with two bottom quarks and two tau leptons in proton–proton collisions at $\sqrt{s} = 13$ TeV. 2017.
- [2513] CMS Collaboration. Search for higgsino pair production in pp collisions at $\sqrt{s} = 13$ TeV in final states with large missing transverse momentum and two Higgs bosons decaying via $H \rightarrow b\bar{b}$. 2017.
- [2514] CMS Collaboration. Search for high-mass diphoton resonances in proton–proton collisions at 13 TeV and combination with 8 TeV search. *Phys. Lett. B*, 767:147, 2017.

- [2515] CMS Collaboration. Search for high-mass $Z\gamma$ resonances in $e^+e^-\gamma$ and $\mu^+\mu^-\gamma$ final states in proton–proton collisions at $\sqrt{s} = 8$ and 13 TeV. *JHEP*, 01:076, 2017.
- [2516] CMS Collaboration. Search for high-mass $Z\gamma$ resonances in proton–proton collisions at $\sqrt{s} = 8$ and 13 TeV using jet substructure techniques. *Phys. Lett. B*, 772:363, 2017.
- [2517] CMS Collaboration. Search for lepton flavour violating decays of the Higgs boson to $\mu\tau$ and $e\tau$ in proton–proton collisions at $\sqrt{s} = 13$ TeV. 2017.
- [2518] CMS Collaboration. Search for leptophobic Z' bosons decaying into four-lepton final states in proton–proton collisions at $\sqrt{s} = 8$ TeV. *Phys. Lett. B*, 773:563, 2017.
- [2519] CMS Collaboration. Search for light bosons in decays of the 125 GeV Higgs boson in proton–proton collisions at $\sqrt{s} = 8$ TeV. *JHEP*, 10:076, 2017.
- [2520] CMS Collaboration. Search for low mass vector resonances decaying into quark-antiquark pairs in proton–proton collisions at $\sqrt{s} = 13$ TeV. 2017.
- [2521] CMS Collaboration. Search for low mass vector resonances decaying to quark-antiquark pairs in proton–proton collisions at $\sqrt{s} = 13$ TeV. *Phys. Rev. Lett.*, 119:111802, 2017.
- [2522] CMS Collaboration. Search for massive resonances decaying into WW , WZ or ZZ bosons in proton–proton collisions at $\sqrt{s} = 13$ TeV. *JHEP*, 03:162, 2017.
- [2523] CMS Collaboration. Search for massive resonances decaying into WW , WZ , ZZ , qW , and qZ with dijet final states at $\sqrt{s} = 13$ TeV. 2017.
- [2524] CMS Collaboration. Search for narrow resonances in dilepton mass spectra in proton–proton collisions at $\sqrt{s} = 13$ TeV and combination with 8 TeV data. *Phys. Lett. B*, 768:57, 2017.
- [2525] CMS Collaboration. Search for natural supersymmetry in events with top quark pairs and photons in $p\bar{p}$ collisions at $\sqrt{s} = 8$ TeV. 2017.
- [2526] CMS Collaboration. Search for new long-lived particles at $\sqrt{s} = 13$ TeV. 2017.
- [2527] CMS Collaboration. Search for new phenomena in events with high jet multiplicity and low missing transverse momentum in proton–proton collisions at $\sqrt{s} = 8$ TeV. *Phys. Lett. B*, 770:257, 2017.

- [2528] CMS Collaboration. Search for new phenomena in final states with two opposite-charge, same-flavor leptons, jets, and missing transverse momentum in pp collisions at $\sqrt{s} = 13$ TeV. 2017.
- [2529] CMS Collaboration. Search for new phenomena with multiple charged leptons in proton–proton collisions at $\sqrt{s} = 13$ TeV. *Eur. Phys. J. C*, 77:635, 2017.
- [2530] CMS Collaboration. Search for new phenomena with the M_{T2} variable in the all-hadronic final state produced in proton–proton collisions at $\sqrt{s} = 13$ TeV. *Eur. Phys. J. C*, 77:710, 2017.
- [2531] CMS Collaboration. Search for new physics in events with a leptonically decaying Z boson and a large transverse momentum imbalance in proton–proton collisions at $\sqrt{s} = 13$ TeV. 2017.
- [2532] CMS Collaboration. Search for new physics in final states with an energetic jet or a hadronically decaying W or Z boson and transverse momentum imbalance at $\sqrt{s} = 13$ TeV. 2017.
- [2533] CMS Collaboration. Search for new physics in the monophoton final state in proton–proton collisions at $\sqrt{s} = 13$ TeV. *JHEP*, 10:073, 2017.
- [2534] CMS Collaboration. Search for new physics with dijet angular distributions in proton–proton collisions at $\sqrt{s} = 13$ TeV. *JHEP*, 07:013, 2017.
- [2535] CMS Collaboration. Search for pair production of excited top quarks in the lepton+jets final state. 2017.
- [2536] CMS Collaboration. Search for pair production of vector-like quarks in the $bW\bar{b}W$ channel from proton–proton collisions at $\sqrt{s} = 13$ TeV. 2017.
- [2537] CMS Collaboration. Search for pair production of vector-like T and B quarks in single-lepton final states using boosted jet substructure techniques at $\sqrt{s} = 13$ TeV. *JHEP*, 11:085, 2017.
- [2538] CMS Collaboration. Search for physics beyond the standard model in events with high-momentum Higgs bosons and missing transverse momentum in proton–proton collisions at 13 TeV. 2017.
- [2539] CMS Collaboration. Search for physics beyond the standard model in events with two leptons of same sign, missing transverse momentum, and jets in proton–proton collisions at $\sqrt{s} = 13$ TeV. *Eur. Phys. J. C*, 77:578, 2017.
- [2540] CMS Collaboration. Search for R-parity violating supersymmetry in pp collisions at $\sqrt{s} = 13$ TeV using b jets in a final state with a single lepton, many jets, and high sum of large-radius jet masses. 2017.

- [2541] CMS Collaboration. Search for R-parity violating supersymmetry with displaced vertices in proton–proton collisions at $\sqrt{s} = 8$ TeV. *Phys. Rev. D*, 95:012009, 2017.
- [2542] CMS Collaboration. Search for resonant and nonresonant Higgs boson pair production in the $b\bar{b}\ell\nu\ell\nu$ final state in proton–proton collisions at $\sqrt{s} = 13$ TeV. 2017.
- [2543] CMS Collaboration. Search for single production of a heavy vector-like T quark decaying to a Higgs boson and a top quark with a lepton and jets in the final state. *Phys. Lett. B*, 771:80, 2017.
- [2544] CMS Collaboration. Search for single production of a vector-like T quark decaying to a Z boson and a top quark in proton–proton collisions at $\sqrt{s} = 13$ TeV. 2017.
- [2545] CMS Collaboration. Search for single production of vector-like quarks decaying into a b quark and a W boson in proton–proton collisions at $\sqrt{s} = 13$ TeV. *Phys. Lett. B*, 772:634, 2017.
- [2546] CMS Collaboration. Search for single production of vector-like quarks decaying to a Z boson and a top or a bottom quark in proton–proton collisions at $\sqrt{s} = 13$ TeV. *JHEP*, 05:029, 2017.
- [2547] CMS Collaboration. Search for standard model production of four top quarks in proton–proton collisions at $\sqrt{s} = 13$ TeV. *Phys. Lett. B*, 772:336, 2017.
- [2548] CMS Collaboration. Search for standard model production of four top quarks with same-sign and multilepton final states in proton–proton collisions at $\sqrt{s} = 13$ TeV. 2017.
- [2549] CMS Collaboration. Search for supersymmetry in events with at least one photon, missing transverse momentum, and large transverse event activity in proton–proton collisions at $\sqrt{s} = 13$ TeV. 2017.
- [2550] CMS Collaboration. Search for supersymmetry in events with at least three electrons or muons, jets, and missing transverse momentum in proton–proton collisions at $\sqrt{s} = 13$ TeV. 2017.
- [2551] CMS Collaboration. Search for supersymmetry in events with one lepton and multiple jets exploiting the angular correlation between the lepton and the missing transverse momentum in proton–proton collisions at $\sqrt{s} = 13$ TeV. 2017.
- [2552] CMS Collaboration. Search for supersymmetry in events with one lepton and multiple jets in proton–proton collisions at $\sqrt{s} = 13$ TeV. *Phys. Rev. D*, 95:012011, 2017.

- [2553] CMS Collaboration. Search for supersymmetry in events with photons and missing transverse energy in pp collisions at 13 TeV. *Phys. Lett. B*, 769:391, 2017.
- [2554] CMS Collaboration. Search for supersymmetry in multijet events with missing transverse momentum in proton–proton collisions at 13 TeV. *Phys. Rev. D*, 96:032003, 2017.
- [2555] CMS Collaboration. Search for supersymmetry in pp collisions at $\sqrt{s} = 13$ TeV in the single-lepton final state using the sum of masses of large-radius jets. *Phys. Rev. Lett.*, 119:151802, 2017.
- [2556] CMS Collaboration. Search for supersymmetry in proton–proton collisions at 13 TeV using identified top quarks. 2017.
- [2557] CMS Collaboration. Search for supersymmetry in the all-hadronic final state using top quark tagging in pp collisions at $\sqrt{s} = 13$ TeV. *Phys. Rev. D*, 96:012004, 2017.
- [2558] CMS Collaboration. Search for supersymmetry with Higgs boson to diphoton decays using the razor variables at $\sqrt{s} = 13$ TeV. 2017.
- [2559] CMS Collaboration. Search for $t\bar{t}$ resonances in highly-boosted lepton+jets and fully hadronic final states in proton–proton collisions at $\sqrt{s} = 13$ TeV. *JHEP*, 07:001, 2017.
- [2560] CMS Collaboration. Search for the flavor-changing neutral current interactions of the top quark and the Higgs boson which decays into a pair of b quarks at $\sqrt{s} = 13$ TeV. 2017.
- [2561] CMS Collaboration. Search for the pair production of third-generation squarks with two-body decays to a bottom or charm quark and a neutralino in proton–proton collisions at $\sqrt{s} = 13$ TeV. 2017.
- [2562] CMS Collaboration. Search for the $X(5568)$ state decaying into $B_s^0\pi^\pm$ in proton–proton collisions at $\sqrt{s} = 8$ TeV. 2017.
- [2563] CMS Collaboration. Search for third-generation scalar leptoquarks and heavy right-handed neutrinos in final states with two tau leptons and two jets in proton–proton collisions at $\sqrt{s} = 13$ TeV. *JHEP*, 07:121, 2017.
- [2564] CMS Collaboration. Search for top quark decays via Higgs-boson-mediated flavor-changing neutral currents in pp collisions at $\sqrt{s} = 8$ TeV. *JHEP*, 02:079, 2017.

- [2565] CMS Collaboration. Search for top quark partners with charge 5/3 in proton–proton collisions at $\sqrt{s} = 13$ TeV. *JHEP*, 08:073, 2017.
- [2566] CMS Collaboration. Search for top squark pair production in compressed-mass-spectrum scenarios in proton–proton collisions at $\sqrt{s} = 8$ TeV using the α_T variable. *Phys. Lett. B*, 767:403, 2017.
- [2567] CMS Collaboration. Search for top squark pair production in $p\bar{p}$ collisions at $\sqrt{s} = 13$ TeV using single lepton events. *JHEP*, 10:019, 2017.
- [2568] CMS Collaboration. Search for top squarks and dark matter particles in opposite-charge dilepton final states at $\sqrt{s} = 13$ TeV. 2017.
- [2569] CMS Collaboration. Search for vector-like light-flavor quark partners in proton–proton collisions at $\sqrt{s} = 8$ TeV. 2017.
- [2570] CMS Collaboration. Search for $Z\gamma$ resonances using leptonic and hadronic final states in proton–proton collisions at $\sqrt{s} = 13$ TeV. 2017.
- [2571] CMS Collaboration. Search for ZZ resonances in the $2\ell 2\nu$ final state in proton-proton collisions at 13 TeV. 2017.
- [2572] CMS Collaboration. Searches for invisible decays of the Higgs boson in $p\bar{p}$ collisions at $\sqrt{s} = 7, 8$, and 13 TeV. *JHEP*, 02:135, 2017.
- [2573] CMS Collaboration. Searches for pair production of third-generation squarks in $\sqrt{s} = 13$ TeV $p\bar{p}$ collisions. *Eur. Phys. J. C*, 77:327, 2017.
- [2574] CMS Collaboration. Searches for W' bosons decaying to a top quark and a bottom quark in proton–proton collisions at 13 TeV. *JHEP*, 08:029, 2017.
- [2575] CMS Collaboration. Study of Bose–Einstein correlations in $p\bar{p}$, pPb , and $PbPb$ collisions at the LHC. 2017.
- [2576] CMS Collaboration. Study of dijet events with a large rapidity gap between the two leading jets in $p\bar{p}$ collisions at $\sqrt{s} = 7$ TeV. 2017.
- [2577] CMS Collaboration. Study of jet quenching with isolated-photon+jet correlations in $PbPb$ and $p\bar{p}$ collisions at $\sqrt{s_{NN}} = 5.02$ TeV. 2017.
- [2578] CMS Collaboration. Study of jet quenching with Z +jet correlations in $PbPb$ and $p\bar{p}$ collisions at $\sqrt{s_{NN}} = 5.02$ TeV. *Phys. Rev. Lett.*, 119:082301, 2017.
- [2579] CMS Collaboration. Suppression and azimuthal anisotropy of prompt and nonprompt J/ψ production in $PbPb$ collisions at $\sqrt{s_{NN}} = 2.76$ TeV. *Eur. Phys. J. C*, 77:252, 2017.

- [2580] CMS Collaboration. Suppression of excited Υ states relative to the ground state in PbPb collisions at $\sqrt{s_{\text{NN}}} = 5.02$ TeV. 2017.
- [2581] CMS Collaboration. Suppression of $\Upsilon(1S)$, $\Upsilon(2S)$ and $\Upsilon(3S)$ quarkonium states in PbPb collisions at $\sqrt{s_{\text{NN}}} = 2.76$ TeV. *Phys. Lett. B*, 770:357, 2017.
- [2582] CMS Collaboration. The CMS trigger system. *JINST*, 12:P01020, 2017.
- [2583] CMS Collaboration. Azimuthal anisotropy of charged particles with transverse momentum up to 100 GeV/c in PbPb collisions at $\sqrt{s_{\text{NN}}} = 5.02$ TeV. *Phys. Lett. B*, 776:195, 2018.
- [2584] CMS Collaboration. Measurements of $t\bar{t}$ cross sections in association with b jets and inclusive jets and their ratio using dilepton final states in pp collisions at $\sqrt{s} = 13$ TeV. *Phys. Lett. B*, 776:355, 2018.
- [2585] CMS Collaboration. Search for heavy resonances decaying to a top quark and a bottom quark in the lepton+jets final state in proton–proton collisions at 13 TeV. *Phys. Lett. B*, 777:39, 2018.
- [2586] ATLAS Collaboration. Electron reconstruction and identification in the atlas experiment using the 2015 and 2016 lhc proton proton collision data at $\sqrt{s} = 13$ TeV. *The European Physical Journal C*, 79(8), Aug 2019.
- [2587] The ATLAS Collaboration. Observation of higgs boson production in association with a top quark pair at the lhc with the atlas detector. *Physics Letters B*, 784:173–191, 2018.
- [2588] Beranger Dumont, Sylvain Fichet, and Gero von Gersdorff. A bayesian view of the higgs sector with higher dimensional operators. *Journal of High Energy Physics*, 2013(7), Jul 2013.
- [2589] John Ellis. Higgs Physics. (KCL-PH-TH-2013-49. KCL-PH-TH-2013-49. LCTS-2013-36. CERN-PH-TH-2013-315):117–168. 52 p, Dec 2013. 52 pages, 45 figures, Lectures presented at the ESHEP 2013 School of High-Energy Physics, to appear as part of the proceedings in a CERN Yellow Report.
- [2590] R. Frederix, S. Frixione, V. Hirschi, D. Pagani, H.-S. Shao, and M. Zaro. The automation of next-to-leading order electroweak calculations. *Journal of High Energy Physics*, 2018(7), Jul 2018.
- [2591] S. Frixione, G. Ridolfi, and P. Nason. A positive-weight next-to-leading-order monte carlo for heavy flavour hadroproduction. *JHEP*, 09:126, 2007.
- [2592] T. Gleisberg, Stefan. Hoeche, F. Krauss, M. Schonherr, S. Schumann, F. Siegert, and J. Winter. Event generation with SHERPA 1.1. *JHEP*, 02:007, 2009.

- [2593] Jeffrey Goldstone, Abdus Salam, and Steven Weinberg. Broken symmetries. *Phys. Rev.*, 127:965–970, Aug 1962.
- [2594] David Griffiths. *Introduction to Elementary Particles*. 1987.
- [2595] The LHC Study Group. LHC, The Large Hadron Collider, Conceptual Design. *CERN AC 95-05 (LHC)*, 1995.
- [2596] P. W. Higgs. Broken Symmetries and the Masses of Gauge Bosons. *Phys. Rev. Lett.* 13 (Oct, 1964) 508-509.
- [2597] F. Maltoni O. Mattelaer J. Alwall, M. Herquet and T. Stelzer. MadGraph 5 : Going Beyond. *JHEP* 1106, 128 *arXiv:1106.0522 [hep-ph]*, 2011.
- [2598] H.-L. Lai et al. New parton distributions for collider physics. *Phys. Rev. D*, 82:074024, 2010.
- [2599] Walter Lampl et al. Calorimeter Clustering Algorithms: Description and Performance. ATL-LARG-PUB-2008-002, 2008.
- [2600] Marija Marjanovic. Atlas tile calorimeter calibration and monitoring systems, 06 2018.
- [2601] Paul Barham Martin Abadi, Ashish Agarwal and et al. Tensorflow: Large-scale machine learning on heterogeneous systems. 2015. Software available from tensorflow.org.
- [2602] Rohin Narayan, Joshua Angus Mcfayden, Allison McCarn Deiana, Andre Sopczak, Andreas Hoecker, Antonio Policicchio, Arthur Rene Chomont, Aurelio Juste Rozas, Chen Jia, Chenliang Wang, Djamel Eddine Boumediene, Merve Nazlim Agaras, Nello Bruscino, Jose Manuel Clavijo Columbie, Michael Duehrssen, Peter Johannes Falke, Simonetta Gentile, Kirill Grevtsov, Jun Guo, Fudong He, Nazim Huseynov, Judith Katzy, Stergios Kazakos, Matthew Henry Klein, Kun Liu, LianLiang Ma, Marcos Miralles Lopez, Santu Mondal, Emmanuel Monnier, Maria Moreno Llacer, Rustem Ospanov, Marcel Niemeyer, Peter Onyisi, Thomas Peiffer, Richard Polifka, Jianming Qian, Stefan Richter, Meng-ju Tsai, Tamara Vazquez Schroeder, Zhi Zheng, Li Zhi, Nihal Brahimi, and Weiming Yao. Measurement of the total and differential cross sections of a top-quark-antiquark pair in association with a W boson in proton-proton collisions at a centre-of-mass energy of 13 TeV with ATLAS detector at the Large Hadron Collider. Technical Report ATL-COM-PHYS-2020-217, CERN, Geneva, Mar 2020.
- [2603] Robert Oerter. *The theory of almost everything : the Standard Model, the unsung triumph of modern physics*. Pi Press, New York, 2006.
- [2604] Giampiero Passarino. WW Scattering and Perturbative Unitarity. *Nuclear Physics B*, 343:31–59, 1990.

- [2605] E. Re. Single-top wt-channel production matched with parton showers using the powheg method. *Eur. Phys. J. C*, 71:1547, 2011.
- [2606] A.M. Sirunyan, A. Tumasyan, W. Adam, F. Ambrogi, E. Asilar, T. Bergauer, J. Brandstetter, M. Dragicevic, J. Ero, A. Escalante Del Valle, and et al. Observation of $t\bar{t}h$ production. *Physical Review Letters*, 120(23), Jun 2018.
- [2607] F. Cuypers S. Dawson D. Errede T. Barklow, U. Baur. Anomalous Gauge Boson Couplings. *arXiv:hep-ph/9611454 [hep-ph]*, 1996.
- [2608] The ATLAS Collaboration. Performance of missing transverse momentum reconstruction with the atlas detector using proton proton collisions at $\sqrt{s} = 13\text{tev}$. *The European Physical Journal C*, (11), Nov 2018.
- [2609] Markus Zinser. *The Large Hadron Collider*, pages 47–51. Springer International Publishing, Cham, 2018.